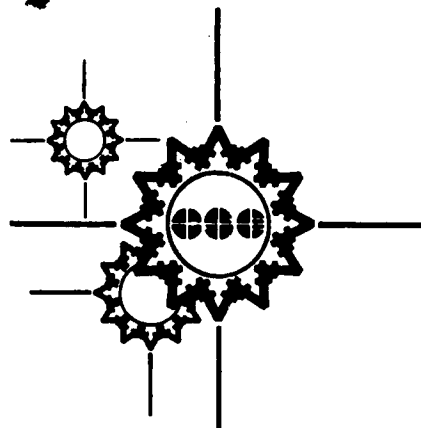


CSE/87-056



**DIRBE
External Calibrator (DEC)**

by

Clair L. Wyatt, V. Alan Thurgood, and Glenn D. Allred

Center for Space Engineering
Utah State University
Logan, Utah 84322 4140

Final Report

18 August 1987

NASA Contract No. NAS5-28185

Prepared for

NASA-Goddard Space Flight Center
Greenbelt, Maryland 20771

CENTER FOR SPACE ENGINEERING

UTAH STATE UNIVERSITY UMC 4140 LOGAN, UTAH 84322



(NASA-CR-180761) DIRBE EXTERNAL CALIBRATOR
(DEC) Final Report (Utah State Univ.)
558 p CSCL 14B

N88-19760

Unclas
G3/35 0133306

CSE/87-056

DIRBE
External Calibrator (DEC)

by

Clair L. Wyatt, V. Alan Thurgood, and Glenn D. Allred

Center for Space Engineering
Utah State University
Logan, Utah 84322 4140

Final Report
NASA Contract No. NAS5-28185

Prepared for
NASA-Goddard Space Flight Center
Greenbelt, Maryland 20771

Note to the printer:

With the exception of Appendix D, this entire text is layed out to be printed on both sides of the page. Appendix D should be printed on one side of the page only. Throughout the remainder of the text odd numbered pages are right hand, even numbered pages are left hand pages.

ABSTRACT

Under NASA Contract No. NAS5-28185, the Center for Space Engineering at Utah State University has produced a calibration instrument for the Diffuse Infrared Background Experiment (DIRBE). DIRBE is one of the instruments aboard the Cosmic Background Experiment Observatory (COBE). The calibration instrument is referred to as the DEC (DIRBE External Calibrator). DEC produces a steerable, infrared beam of controlled spectral content and intensity and with selectable point source or diffuse source characteristics, that can be directed into the DIRBE to map fields and determine response characteristics.

This report details the design of the DEC instrument, its operation and characteristics and provides an analysis of the systems capabilities and performance.

~~PRECEDING PAGE BLANK NOT FILMED~~

TABLE OF CONTENTS

	<u>Page No.</u>
ABSTRACT	iii
LIST OF ILLUSTRATIONS	ix
LIST OF TABLES	xix
ACRONYMS	xxi
1. INTRODUCTION	1
2. DIRBE EXTERNAL CALIBRATOR - CONCEPT	3
3. SYSTEM DISCUSSION	9
3.1 Integrating Sphere Module	9
3.1.1 IR Sources	9
3.1.2 First Integrating Sphere	11
3.1.3 Aperture Wheel	12
3.1.4 Integrating Sphere Module Filter Wheel	13
3.1.5 Second Integrating Sphere	13
3.1.6 Winston Cones	14
3.1.7 Mode Selector Wheel	15
3.2 Collimating Mirror Module	31
3.2.1 Collimating Mirror	31
3.3 Pointing Mirror Module	37
3.3.1 Pointing Mirror	37
3.3.2 2-Axis Gimbal (Pointing Mirror)	37
3.3.3 Pointing Mirror Calibration	38
3.4 Sample Mirror Module	43
3.4.1 Sample Mirror	43
3.5 Absolute Radiometer Module	47
3.5.1 Collecting (Primary) Mirror	47
3.5.2 Folding (Secondary) Mirror	47
3.5.3 Absolute Radiometer Filter Wheel	47
3.5.4 Chopper	48
3.5.5 Condensing Cone	48
3.5.6 Bolometer Detector/Preamp Submodule	48
3.6 Full-Time Monitor Module	57
3.7 DEC Temperature Monitors	58

TABLE OF CONTENTS (Cont.)

3.8 Internal Surface Treatment 60

3.9 Control and Monitor Unit 62

4. TESTING AND RESULTS 65

4.1 Preliminary Testing 65

4.2 Source Stability Tests 72

4.3 Photometer Calibration 73

4.4 Beam Uniformity Test 77

4.5 Absolute Radiometer Calibration 103

4.6 System Cold Tests 105

4.6.1 System Dewar Test, 1 March 1985 105

4.6.2 First System Cold Test, 4 April 1985 105

4.6.3 Second System Cold Test, 14 June 1985 106

4.6.4 Third System Cold Test, 25 July 1985 106

4.6.5 Fourth System Cold Test, 3 Sept 1985 106

4.7 Beam Linearity Tests 109

4.8 Beam Power 124

APPENDIX A Filter Spectral Transmittance: Tabulations
and Graphic Plots A-1

APPENDIX B Description of CMU Electronics and Operation . B-1

Electronics B-5

Std Buss B-5

Digital Electronics in Std Box B-7

Analog Electronics B-9

Bolometer Battery Postamps B-14

Wiring Scheme Used in DEC B-15

Description of CMU Operation B-17

Wheel Moves B-17

Wheel Position Requests B-18

Beam Sample Mirror Move B-19

Beam Sample Mirror Position Requests B-20

Pointing Mirror Moves B-20

Pointing Mirror Position Requests B-22

LVDT Control B-23

Bolometer Signal Requests B-23

~~PRECEDING PAGE BLANK NOT FILMED~~

TABLE OF CONTENTS (Cont.)

Chopper Monitors and Control	B-25
Preamp Monitors and Control	B-25
Bias Monitors and Control	B-26
Temperature Monitor Request	B-27
Source Control	B-28
APPENDIX C Operating Instructions	C-1
Power Up Procedure	C-5
Software Organization	C-5
Definitions of Variables -	C-6
Position Data Request	C-6
Temperature Data Request	C-7
Monitor Signal Data Request	C-7
Motor Move Commands	C-8
Source Set Commands	C-11
System Control Commands	C-12
System Initialize Command	C-13
Raw A/D Data Request	C-14
Raw PIO Data Request	C-16
Definitions of Data Variables	C-17
Variable Position Data	C-17
Variable Temperature Data	C-18
Variable Monitor Signal Data -	C-19
Variable Raw A/D Data -	C-21
Variable Raw PIO Data -	C-23
Definition of Status Codes Returned	C-24
PC Status Codes	C-25
Error Codes Returned by Std Buss	C-25
APPENDIX D Source Stability Report	D-1
Note: Appendix D is a reproduction of a Master of Science thesis completed at USU. Hence, its page and figure numbers are independent from the numbering sequence used throughout the remainder of this report.	
APPENDIX E Absolute Radiometer Calibration Report	E-1
Introduction	E-3
Gain Normalized Response	E-6
Detector Response vs. Detector Temperature	E-7
Bolometer Temperature vs. Bolometer DC	E-9
Field-of-View Calibration	E-10
Field-of-View Analysis and Complete Data Set	E-11
Linearity Calibration	E-12
Extended-area Calibration	E-13

TABLE OF CONTENTS (Cont.)

AR Voltage Response	E-14
Data Consistency	E-15
Radiometric Analysis	E-17
Sterance [radiance] Calibration	E-18
Band Sterance [radiance] Calibration	E-18
Noise Equivalent Sterance [radiance]	E-20
Point Source Calibration	E-22
Beam Uniformity and Spectral Band Corrections	E-25
Calibration Uncertainties	E-27
APPENDIX F Cold Test Data	F-1
Introduction	F-3
Test Section Descriptions	F-4
Cold Test Data	F-34
APPENDIX G Bolometer Data	G-1
Full-time Monitor Bolometer Data	G-3
General Description	G-13
Cooling the Dewar	G-14
Pumping the Dewar	G-15
Recommended Test Procedures	G-17
Frequency Response	G-18
Response vs. Bias Current	G-19
Absolute Noise Measurement	G-19
Symbols, Units, and Formulae	G-22
APPENDIX H Absolute Calibration Fixtures	H-1
APPENDIX J DEC Beam Uniformity Tests	J-1

LIST OF ILLUSTRATIONS

<u>Figure</u>	<u>Title</u>	<u>Page No.</u>
1. . . .	A conceptual block diagram of the DIRBE External Calibrator.	6
2. . . .	A design layout of the DEC instrument.	7
3. . . .	Integrating sphere module.	21
4. . . .	Tungsten bulb IR source with glass envelope removed.	22
5. . . .	Large area infrared source and mounting.	23
6. . . .	Mechanical details of sphere no. 1	24
7. . . .	Aperture/Filter wheel design	25
8. . . .	Photograph illustrating Aperture/Filter wheel design	26
9. . . .	Mechanical details of sphere no. 2	27
10. . . .	Winston cones design	28
11. . . .	Photograph of integrating sphere module showing IR sources and aperture and filter wheels.	29
12. . . .	Photograph of integrating sphere module showing Winston cones and filter wheel	30
13. . . .	The DEC optical path downstream from the Winston cones.	33
14. . . .	NASA drawing detailing the DEC Collimating mirror	34
15. . . .	Collimating mirror and baffle in the partially assembled DEC instrument	35
16. . . .	A rear view of the collimating mirror, baffle, and temperature sensor	36
17. . . .	Detail drawing of the DEC pointing mirror.	40
18. . . .	Drawing of the pointing mirror gimbal and drivers.	41
19. . . .	Photograph of the pointing mirror gimbal drive mechanism.	42
20. . . .	Sample mirror assembly	44
21. . . .	Sample mirror details.	45
22. . . .	A photograph of the sample mirror in the DEC instrument	46
23. . . .	Mechanical details of the absolute radiometer collecting (primary) mirror	53
24. . . .	Mechanical details of the absolute radiometer folding (secondary) mirror.	54
25. . . .	Absolute radiometer configuration.	55

LIST OF ILLUSTRATIONS (Cont)

<u>Figure</u>	<u>Title</u>	<u>Page No.</u>
26	A photograph of the absolute radiometer mounted in the DEC instrument	56
27	Photometric reflectance spectra of six optical-black coatings	61
28	Photo of test dewar and vacuum pumps	67
29	Assembly drawing of the DEC test dewar	68
30	Test dewar with DEC in place	69
31	DEC cold finger with copper cooling inserts	70
32	A photograph of the pointing mirror showing the copper straps and inlays which provide a low thermal resistance path to the DEC test dewar cold finger	71
33	Photometer field of view as a cross-section for the small field stop. The full-angle half-power field of view is approximately 0.2°	74
34	Photometer Field of view as a cross-section for the large field stop. The full-angle half-power field of view is approximately 6.5°	75
35	Photometer linearity data. The merged linearity data are plotted with linear least squares best-fit equation superimposed. The rms error for equally weighted points is 2.03%	76
36	Beam areance [irradiance] (Φ/cm^2) as a horizontal cross-section for the double cones mounted on the integrating sphere exit aperture. The point source mode aperture is flat	81
37	Beam areance [irradiance] (Φ/cm^2) as a horizontal cross-section for the double cones mounted on the integrating sphere exit aperture. The point source mode aperture is canted	82
38	Beam areance [irradiance] (Φ/cm^2) as a vertical cross-section for the double cones mounted on the integrating sphere exit aperture. The point source mode aperture is canted	83
39	Uniformity of blackbody pointance [intensity] (Φ/sr) as a function of the off-axis angle for a 0.785-inch diameter aperture	84
40	Uniformity of blackbody pointance [intensity] (Φ/sr) as a function of the off-axis angle for a 0.017-inch diameter aperture	85

LIST OF ILLUSTRATIONS (Cont)

<u>Figure</u>	<u>Title</u>	<u>Page No.</u>
41 . . .	Uniformity of double-cone pointance [intensity] (Φ /sr) as a function of off-axis angle for a 0.785-inch diameter aperture86
42 . . .	Uniformity of double-cone pointance [intensity] (Φ /sr) as a function of off-axis angle for a 0.017-inch diameter aperture87
43 . . .	Uniformity of integrating sphere exit aperture pointance [intensity] (Φ /sr) as a function of off-axis angle for a 0.785-inch diameter aperture88
44 . . .	Uniformity of plexiglass exit pointance [intensity] (Φ /sr) as a function of off-axis angle for a 0.017-inch diameter aperture. Plexiglass rod mounted on the integrating sphere exit aperture89
45 . . .	Uniformity of plexiglass exit pointance [intensity] (Φ /sr) as a function of off-axis angle for a 0.785-inch diameter aperture. Plexiglass rod mounted on the integrating sphere exit aperture90
46 . . .	Beam areance [irradiance] (Φ /cm ²) as a horizontal cross-section for the double cones mounted on the integrating sphere exit aperture. The point source mode aperture is flat91
47 . . .	Beam areance [irradiance] (Φ /cm ²) as a horizontal cross-section for the double cones mounted on the integration sphere exit aperture. The point source mode aperture is canted92
48 . . .	Beam areance [irradiance] (Φ /cm ²) as a 45° cross-section for the double cones mounted on the integrating sphere exit aperture. The point source mode aperture is canted93
49 . . .	Beam areance [irradiance] (Φ /cm ²) as a horizontal cross-section for the plexiglass cylinder mounted on the integrating sphere exit port. The point source mode aperture is flat94
50 . . .	Beam areance [irradiance] (Φ /cm ²) as a horizontal cross-section for the gold cylinder mounted on the integrating sphere exit aperture. The point source mode aperture is canted95
51 . . .	Beam areance [irradiance] (Φ /cm ²) as a horizontal cross-section for the gold cylinder mounted on the integrating sphere exit aperture. The point source mode aperture is canted96
52 . . .	Beam areance [irradiance] (Φ /cm ²) as a 45° cross-section for the gold cylinder mounted on the integrating sphere exit aperture. The point source mode aperture is canted97

LIST OF ILLUSTRATIONS (Cont)

<u>Figure</u>	<u>Title</u>	<u>Page No.</u>
53	Beam areance [irradiance] (Φ/cm^2) as a vertical cross-section for the gold cylinder mounted on the integrating sphere exit aperture. The point source mode aperture is canted	98
54	Beam areance [irradiance] (Φ/cm^2) as a horizontal cross-section for the double cones mounted on the integrating sphere exit aperture. The point source mode aperture is flat. This is a replot in different format of the data given in Figure 46 and is used for comparison with Figures 55 and 56	99
55	Beam areance [irradiance] (Φ/cm^2) as a horizontal cross-section for the recoated double cones mounted to the USU blackbody and using a 0.0158-inch aperture	100
56	Beam areance [irradiance] (Φ/cm^2) as a horizontal cross-section for the recoated double cones mounted to the USU blackbody and using a 0.085-inch aperture	101
57	Sketch of the test setup used to obtain the data in Figures 55 and 56	102
58	Beam linearity data obtained using the photometer to sample the beam power for 6 sets in which the source level was incremented from low to high flux levels. For each temperature the aperture wheel was sequenced through all positions. The data exhibit high background levels for small apertures and nonlinearity for large apertures	119
59	AR response for 9 sets of data in which the source power level was varied from zero to full-on. For each source level the aperture wheel was sequenced through all positions. The data exhibit non-linearity for all levels	120
60	AR response for the 9th set of Figure 59. An offset correction of 0.12 volts was made in an attempt to correct for the background. The data for this graph is tabulated in Table 17, where the non-linearity is reported at 48.92%	121
61	AR response for the 3rd set of Figure 59. An offset correction of 0.0115 volts was made in an attempt to correct for the background. The data for this graph is tabulated in Table 18, where the non-linearity is reported at 27.34%	122
62	Plot of data from Table 19 and the computer report in Table 20. These data were obtained by setting Source S2 (bulb with envelope) at 1.917 volts and rotating the aperture wheel through all positions	123

LIST OF ILLUSTRATIONS (Cont)

<u>Figure</u>	<u>Title</u>	<u>Page No.</u>
A-1 . . .	Band 1, AG 1.11, Temperature 2°K, Wavelength vs. Transmittance	A-21
A-2 . . .	Band 2, AG 2.11, Temperature 2°K, Wavelength vs. Transmittance	A-22
A-3 . . .	Band 3, AG 3.11, Temperature 2°K, Wavelength vs. Transmittance	A-23
A-4 . . .	Band 4, AG 4.6, Temperature 2°K, Wavelength vs. Transmittance	A-24
A-5 . . .	Band 5, BA 5.1 and BA 5.1A, Temperature 2°K, Wavelength vs. Transmittance	A-25
A-6 . . .	Band 6, OCLI 6.4 and OCLI 6.4A, Temperature 2°K, Wavelength vs. Transmittance	A-26
A-7 . . .	Band 7, OCLI 7.3, Temperature 2°K, Wavelength vs. Transmittance	A-27
A-8 . . .	Band 8, OCLI 8.3, Temperature 2°K, Wavelength vs. Transmittance	A-28
A-9 . . .	Band 9, PE 9.1, Temperature 2°K, Wavelength vs. Transmittance	A-29
A-10 . . .	Band 10, PE 10.1, Temperature 2°K, Wavelength vs. Transmittance	A-30
E-1 . . .	A block diagram of the voltage gain configuration of the AR electronics	E-65
E-2 . . .	Bolometer dc vs. bolometer response data points with a least squares best-fit superimposed	E-66
E-3 . . .	Bolometer dc vs. bolometer temperature data points with a least squares best-fit superimposed	E-67
E-4 . . .	Contour analysis of the AR field of view obtained with the 0.007-inch diameter cold pinhole mounted in the entrance aperture	E-68
E-5 . . .	Three dimensional representation of the AR field of view obtained with a 0.007-inch diameter cold pinhole mounted in the entrance aperture	E-69
E-6 . . .	Contour analysis of the AR field of view obtained with full entrance aperture	E-70
E-7 . . .	Three dimensional representation of the AR field of view obtained with full entrance aperture	E-71
E-8 . . .	The field of view as a cross-section is obtained with a 0.3579-inch diameter cold pinhole mounted in the entrance aperture	E-72

LIST OF ILLUSTRATIONS (Cont)

<u>Figure</u>	<u>Title</u>	<u>Page No.</u>
E-9 . . .	Two linearity data sets obtained in the USU Cold Collimator. Note that the nonlinearity is a function of absolute signal but not of aperture area . . .	E-73
E-10 . . .	A plot of extended-area calibration for band 5 (See data points listed in Table E-4)	E-74
E-11 . . .	The absolute calibration data total sterance [radiance] vs. output voltage data points for band #6	E-75
E-12 . . .	The absolute calibration data total sterance [radiance] vs. output voltage data points for band #7	E-76
E-13 . . .	The absolute calibration data total sterance [radiance] vs. output voltage data points for band #8	E-77
E-14 . . .	The absolute calibration data sterance [radiance] vs. output voltage data points for the "open" position with a least squares best-fit superimposed. The data exhibit 39.2% full-scale nonlinearity and an rms error of 7.22% . . .	E-78
E-15 . . .	Ten second dark noise scan. Top curve FTM, bottom curve AR. Note: Short term rms noise = STD (standard deviation) . . .	E-79
E-16 . . .	One hundred-fifty second dark noise scan. Top curve FTM, bottom curve AR. Note: Long term rms noise = STD (standard deviation)	E-80
E-17 . . .	Graphic plot of point source calibration for Band 1	E-81
E-18 . . .	Graphic plot of point source calibration for Band 2	E-82
E-19 . . .	Graphic plot of point source calibration for Band 3	E-83
E-20 . . .	Graphic plot of point source calibration for Band 4	E-84
E-21 . . .	Graphic plot of point source calibration for Band 5	E-85
E-22 . . .	Graphic plot of point source calibration for Band 6	E-86
E-23 . . .	Graphic plot of point source calibration for Band 7	E-87
E-24 . . .	Graphic plot of point source calibration for Band 8	E-88
E-25 . . .	Graphic plot of point source calibration for Band 9	E-89
E-26 . . .	Graphic plot of point source calibration for Band 10	E-90

LIST OF ILLUSTRATIONS (Cont)

<u>Figure</u>	<u>Title</u>	<u>Page No.</u>
G-1 . . .	Wiring diagram for DEC bolometer module . . .	G-6
G-2 . . .	DEC bolometer preamplifier schematic	G-7
G-3 . . .	DC load curve, 1.5K, Unit No. 904	G-8
G-4 . . .	DC load curve, 2.0K, Unit No. 904	G-9
G-5 . . .	Frequency response, Unit No. 904	G-10
G-6 . . .	Pumping system	G-16
G-7 . . .	Load curve setup	G-17
G-8 . . .	Load curve	G-17
G-9 . . .	Frequency response setup	G-18
G-10a . .	Frequency response, single τ	G-18
G-10b . .	Frequency response, double τ	G-18
G-11 . . .	Noise measurement setup	G-20
G-12 . . .	Noise calibration	G-20
G-13 . . .	DC load curve, 1.5K, Unit No. 906	G-28
G-14 . . .	DC load curve, 2.0K, Unit No. 906	G-29.
G-15 . . .	Frequency response, Unit No. 906	G-30
G-16 . . .	DC load curve, 1.5K, Unit No. 905	G-34
G-17 . . .	DC load curve, 2.0K, Unit No. 905	G-35
G-18 . . .	Frequency response, Unit No. 905	G-36
H-1 . . .	Layout sketch of the Infrared Laboratories test Dewar. The AR was mounted in this Dewar for calibration	H-4
H-2 . . .	Layout sketch of the USU Cold Collimator. This cryogenic device contains a precision aperture and a filter wheel, and motors to scan the beam	H-5
H-3 . . .	Optical sketch of the USU Cold Collimator . .	H-6..
H-4 . . .	Optical Schematic of the USU Cold Collimator showing details of the filter and aperture wheels, window, and external blackbody source	H-7
H-5 . . .	Layout sketch of the special test Dewar interfaced to the USU cold collimator. Note that vacuum, radiation shield, and cold shield continuity are maintained in the interface. The AR baffle is fitted with a photon-tight non-contact baffle . . .	H-8

LIST OF ILLUSTRATIONS (Cont)

<u>Figure</u>	<u>Title</u>	<u>Page No.</u>
H-6 . . .	Layout sketch of the special test Dewar interfaced to the USU cold collimator. Note that vacuum, radiation shield, and cold shield continuity are maintained in the interface. The temperature controlled blackbody simulator is honeycombed, blackened, and coupled to the AR baffle with a photon-tight non-contact baffle.	H-9
H-7 . . .	A diagram of the Absolute Radiometer showing the precision off-axis pinhole used for calibration the AR.	H-10
J-1 . . .	DEC beam uniformity test setup	J-11
J-2 . . .	Cutaway view of DEC beam uniformity detector/baffle assembly	J-12
J-3 . . .	Dec beam detector response	J-13
J-4 . . .	DEC beam uniformity detector preamp schematic.	J-14
J-5 . . .	DEC beam uniformity X-axis field-of-view.	J-15
J-6 . . .	DEC beam univormity Y-axis field-of-view.	J-16
J-7 . . .	Linear response versus actual response	J-17
J-8 . . .	DEC beam uniformity amplifier schematic.	J-18
J-9 . . .	DEC beam mapping file #1 - contour every 0.2V	J-19
J-10 . . .	DEC beam mapping file #1 - Tilt: 0 - Rotation: 0.	J-20
J-11 . . .	DEC beam mapping file #1 - Tilt: 0 - Rotation: 270.	J-21
J-12 . . .	DEC beam mapping file #1 - Tilt: 25 - Rotation: 25.	J-22
J-13 . . .	DEC beam mapping file #1 - Tilt: 25 - Rotation: 115.	J-23
J-14 . . .	DEC beam mapping file #1 - Tilt: 25 - Rotation: 205.	J-24
J-15 . . .	DEC beam mapping file #1 - Tilt: 25 - Rotation: 205.	J-25
J-16 . . .	DEC beam mapping File #2 - contour every 0.2V	J-26
J-17 . . .	DEC beam mapping file #2 - Tilt: 0 - Rotation: 0.	J-27
J-18 . . .	DEC beam mapping file #2 - Tilt: 0 - Rotation: 270.	J-28
J-19 . . .	DEC beam mapping file #2 - Tilt: 25 - Rotation: 25.	J-29

LIST OF ILLUSTRATIONS (Cont)

<u>Figure</u>	<u>Title</u>	<u>Page No.</u>
J-20	DEC beam mapping file #2 - Tilt: 25 - Rotation: 115	J-30
J-21	DEC beam mapping file #2 - Tilt: 25 - Rotation: 205	J-31
J-22	DEC beam mapping file #2 - Tilt: 25 - Rotation: 295	J-32
J-23	DEC beam mapping file #3 - contour every 0.2V	J-33
J-24	DEC beam mapping file #3 - Tilt: 25 - Rotation: 115	J-34
J-25	DEC beam mapping file #4 - contour every 0.2V	J-35
J-26	DEC beam mapping file #4 - Tilt: 0 - Rotation: 0	J-36
J-27	DEC beam mapping file #4 - Tilt: 0 - Rotation: 270	J-37
J-28	DEC beam mapping file #4 - Tilt: 25 - Rotation: 25	J-38
J-29	DEC beam mapping file #4 - Tilt: 25 - Rotation: 115	J-39
J-30	DEC beam mapping file #4 - Tilt: 25 - Rotation: 205	J-40
J-31	DEC beam mapping file #4 - Tilt: 25 - Rotation: 295	J-41
J-32	DEC beam mapping file #5 - contour every 0.2V	J-42
J-33	DEC beam mapping file #5 - Tilt: 0 - Rotation: 0	J-43
J-34	DEC beam mapping file #5 - Tilt: 0 - Rotation: 270	J-44
J-35	DEC beam mapping file #5 - Tilt: 25 - Rotation: 25	J-45
J-36	DEC beam mapping file #5 - Tilt: 25 - Rotation: 115	J-46
J-37	DEC beam mapping file #5 - Tilt: 25 - Rotation: 205	J-47
J-38	DEC beam mapping file #5 - Tilt: 25 - Rotation: 295	J-48
J-39	DEC beam mapping file #2 - contour every 0.02 - corrected and normalized	J-49
J-40	DEC beam mapping file #2 - Tilt: 0 - Rotation: 0. Normalized and corrected	J-50

LIST OF ILLUSTRATIONS (Cont)

<u>Figure</u>	<u>Title</u>	<u>Page No.</u>
J-41	. . . DEC beam mapping file #2 - Tilt: 0 - Rotation: 270. Normalized and corrected	. . . J-51
J-42	. . . DEC beam mapping file #2 - Tilt: 25 - Rotation: 25. Normalized and corrected	. . . J-52
J-43	. . . DEC beam mapping file #2 - Tilt: 25 - Rotation: 115. Normalized and corrected	. . . J-53
J-44	. . . DEC beam mapping file #2 - Tilt: 25 - Rotation: 205. Normalized and corrected	. . . J-54
J-45	. . . DEC beam mapping file #2 - Tilt: 25 - Rotation: 295. Normalized and corrected	. . . J-55
J-46	. . . DEC software demonstration - Tilt: 25 - Rotation: 115. J-56
J-47	. . . DEC software demopnstration - contour every 0.2V J-57

LIST OF TABLES

<u>Table No.</u>	<u>Page No.</u>
1 • Values Utilized in Solution of (E-1) for Tungsten Bulb Source	18
2 • Values Utilized in Solution of (E-1) for Large-Area IR Source	18
3 • Filter/Aperture/Mode Select Wheels Specifications	19
4 • Aperture vs. Position and Aperture Set Information for Aperture Wheel	19
5 • Filter vs. Wheel Position for Integrating Spheres Module Filter Wheel	20
6 • Filters/Apertures vs. Position for Mode Selector Wheel	20
7 • Collimating Mirror Specifications	32
8 • Pointing Mirror Specifications	39
9 • Sample Mirror Specifications	43
10 • Collecting and Folding Mirror Specifications, Absolute Radiometer	51
11 • Absolute Radiometer Filter Wheel - Filter vs. Wheel Position	51
12 • Absolute Radiometer Specifications	52
13 • DEC Temperature Sensors	59
14 • Summary of Lamp Performance	72
15 • Aperture Wheel Position, Aperture, Relative Energy, and Area	113
16 • Integrating Sphere Linearity Data Obtained Using Photometer to Sample Beam Power	114
17 • Computer Report of Best-Fit Linearity Analysis for Data Given in Figure 60	115
18 • Computer Report of Best-Fit Linearity Analysis for Data Given in Figure 61	116
19 • Data from 2 September 1985 Test Number 1402	117
20 • Computer Report of Linearity Analysis for Data Given in Table 19 and Figure 62	118
E-1 • Computer Report Corresponding to the Best-Fit Analysis of Figure E-2	E-32
E-2 • Computer Report Corresponding to the Best-Fit Analysis of Figure E-3	E-33
E-3 • Near Field of View Analysis	E-34
E-4 • DEC AR Extended-Area Source Calibration for Band 5	E-49
E-5 • DEC AR Extended-Area Source Calibration for Band 6	E-50

LIST OF TABLES (Cont)

E-6	DEC AR Extended-Area Source Calibration for Band 7	E-51
E-7	DEC AR Extended-Area Source Calibration for Band 8	E-52
E-8	DEC AR Extended-Area Source Calibration for Band 10	E-53
E-9	Linearity Analysis of DEC AR Band 10 (open)	E-54
E-10	Point Source Calibration Data for Band 1	E-55
E-11	Point Source Calibration Data for Band 2	E-56
E-12	Point Source Calibration Data for Band 3	E-57
E-13	Point Source Calibration Data for Band 4	E-58
E-14	Point Source Calibration Data for Band 5	E-59
E-15	Point Source Calibration Data for Band 6	E-60
E-16	Point Source Calibration Data for Band 7	E-61
E-17	Point Source Calibration Data for Band 8	E-62
E-18	Point Source Calibration Data for Band 9	E-62
E-19	Point Source Calibration Data for Band 10	E-63

LIST OF ACRONYMS

AR	Absolute Radiometer
AW	Aperture Wheel
BV	Black Velvet (3-M)
CMU	Command and Monitor Unit
COBE	Cosmic Background Experiment Observatory
CSE	Center for Space Engineering, USU
CVF	Circular Variable Filter
DEC	DIRBE External Calibrator
DSM	Diffuse Source Mode
FTM	Full-time Monitor
FW	Filter Wheel
GaAs	Galium Arsenide
GFE	Government Furnished Equipment
GSFC	Goddard Space Flight Center
IR	Infrared
IRI	Infrared Industries
ITD	Instrument Test Dewar
LAS	Large Area Source (IR)
LHe	Liquid Helium
LN2	Liquid Nitrogen
LMSC	Lockheed Missile and Space Company
LSB	Least Significant Bit
LVDT	Linear Variable Differential Transformer
MSB	Most Significant Bit
NEP	Noise Equivalent Power
NES	Noise Equivalent Sterance [Radiance]
PM	Pointing Mirror
PSM	Point Source Mode
PIO	Parallel Input/Output
rms	Root Mean Squared
SDL	Space Dynamics Laboratory (now CSE)
STD	Standard
USU	Utah State University, Logan, Utah

This page intentionally left blank.

1 . INTRODUCTION

NASA's Cosmic Background Experiment Observatory (COBE) is a sky mapping mission designed to measure the cosmic background radiation believed to be a remnant of early processes which occurred during the formation of the universe. From these measurements COBE will obtain data on a variety of infrared sources and thus, cosmological questions may be answered. During its mission COBE will map the entire celestial sphere two times in the wavelength region of from 1 μm to 1.3 cm.

One of the three COBE instruments used to accomplish the mapping is the Diffuse Infrared Background Experiment (DIRBE), which will provide spectral measurements in the 1 to 300 μm range. DIRBE is a superfluid helium cooled, ten-band radiometer, using an off-axis Gregorian telescope design with multiple pupils and bandpass filters for wavelength definition. It has a 19-cm diameter aperture with a nominal 1° field-of-view, and is designed for high straylight rejection.

Utah State University's Center for Space Engineering, under contract to NASA, has designed, fabricated, and tested the DIRBE External Calibrator (DEC), which is the primary source of ground based (preflight) calibration for DIRBE. This report provides a description of the DEC system design, its testing, capabilities and operating instructions.

In the report that follows Tables and Figures have been placed at the end of the section that contains the first reference to them. This has been done to maintain continuity in the text.

This page intentionally left blank.

2 . DIRBE EXTERNAL CALIBRATOR

-CONCEPT-

The DEC is designed to project radiation beams of known spectral and intensity characteristics into the DIRBE entrance pupil during ground based testing and calibration of the DIRBE. These beams may be diffuse, full-field beams used for calibration of the DIRBE, or steered beams of low divergence. A steered radiation beam permits determination of DIRBE's beam response, or field-of-view. Calibration of DIRBE with the DEC will provide performance verification and calibration in order that flight data may be analyzed.

The DEC is designed to operate at superfluid helium temperatures. During operation DEC and the DIRBE instrument will be enclosed in an Instrument Test Dewar (ITD). The DEC will receive its cryogenic cooling from that source.

Figure 1 is a conceptual block diagram describing the DEC and its operating principles. The illustration is for conceptual purposes only and does not attempt to show the actual physical configuration of the DEC.

In operation, light from any of five sources is injected into the first integrating sphere. This sphere serves to make all of the sources look similarly diffuse. Light exiting from the first integrating sphere passes into the second integrating sphere through changeable apertures and bandpass filters, which are mounted in separate wheels between the first and second integrating spheres. These apertures and filters serve to vary the spectral quality and intensity of the light entering the second integrating sphere.

The second integrating sphere receives the light and spreads it uniformly over the sphere surface, thereby providing a diffuse source of light for the downstream system. Light is coupled from the second integrating sphere via a pair of mouth-to-mouth Winston cones and a mode selector wheel. The mouth-to-mouth cones serve the dual purpose of limiting stray light and ensuring

that the emitted light comes from a portion of the second integrating sphere wall that is diffusely illuminated. The mode selector wheel includes apertures for operation in either a point source mode or a diffuse source mode. Additionally, the mode selector wheel has other apertures and polarizing filters which can be selected and these affect the divergence and polarization of the output beam. The light exiting via the Winston cones impinges upon the collimating mirror, thence, exiting DEC via a steerable pointing mirror which directs the exiting light beam into DIRBE.

At the second integrating sphere the system is equipped with a full-time monitor which samples the power being scattered off a portion of the sphere wall as an indicator of relative beam band power.

Additionally, a sample mirror is located such that it may be inserted into the beam between the collimating mirror and the pointing mirror. The purpose of this moveable mirror is to deflect a portion (center 25%) of the DEC output beam into the absolute radiometer.

The absolute radiometer is equipped with a filter wheel that holds ten band defining filters (NASA furnished) that are identical to the ten bands of DIRBE, and thus, the output from the absolute radiometer defines the input to the DIRBE instrument.

The instrument baseplate serves the functions of providing support for the DEC components and providing the interface between DEC and the DIRBE instrument test dewar. The entire DEC assembly is contained within a thin-wall aluminum enclosure, which attaches to the DEC baseplate. The cover serves as a thermal and optical shield and prevents contamination of the unit.

The DEC uses stepper motors to accomplish the tasks of moving and positioning the mechanical parts of the assembly such as aperture and filter wheels, mode selector wheels, and mirrors. The motors are controlled from the control and monitor unit which

runs programs to execute commands, stores the data for future analysis, and displays the status of the system. In addition, the control and monitor unit controls the level of the 5 sources at integrating sphere number 1 and the choppers in the absolute radiometer and full-time monitor. It monitors temperatures from temperature sensors throughout the system, beam angle, beam intensity, wheel positions, sample mirror position, voltages and power being sent to each source in the system. The CMU employs an IBM PC as the basic tool for accomplishing its functions.

The discussion above presents the basic concepts of the DEC in greatly simplified form for first familiarization with the system. The following paragraphs delve more deeply into the design precepts and operating concepts of the instrument. As can be seen in Figure 2, a design layout of the DEC instrument, the DEC is divided into several subsystem modules. These modular subsystems evolved from performance and design requirements. The following discussions conform to the modular aspects of the DEC system.

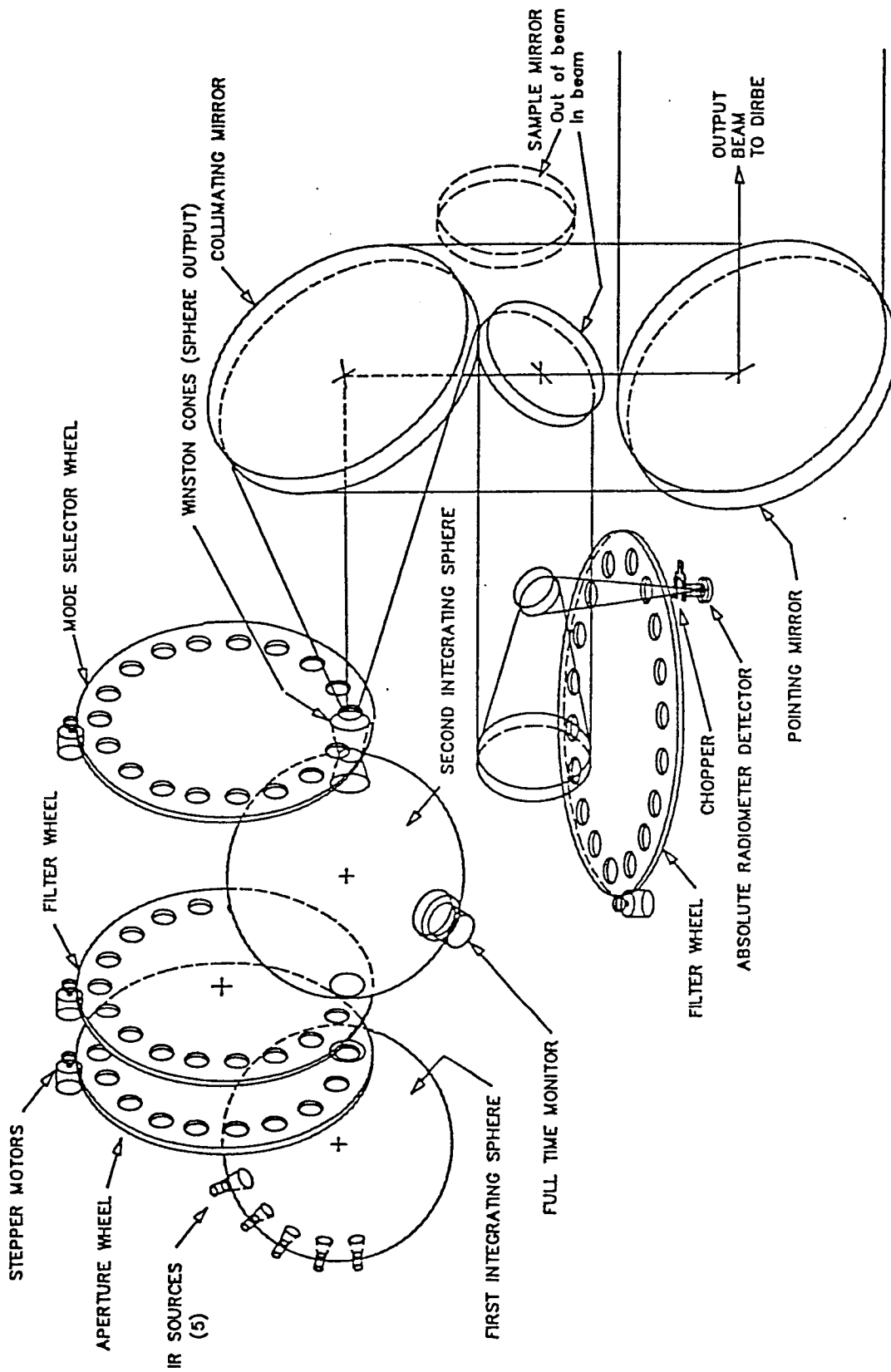
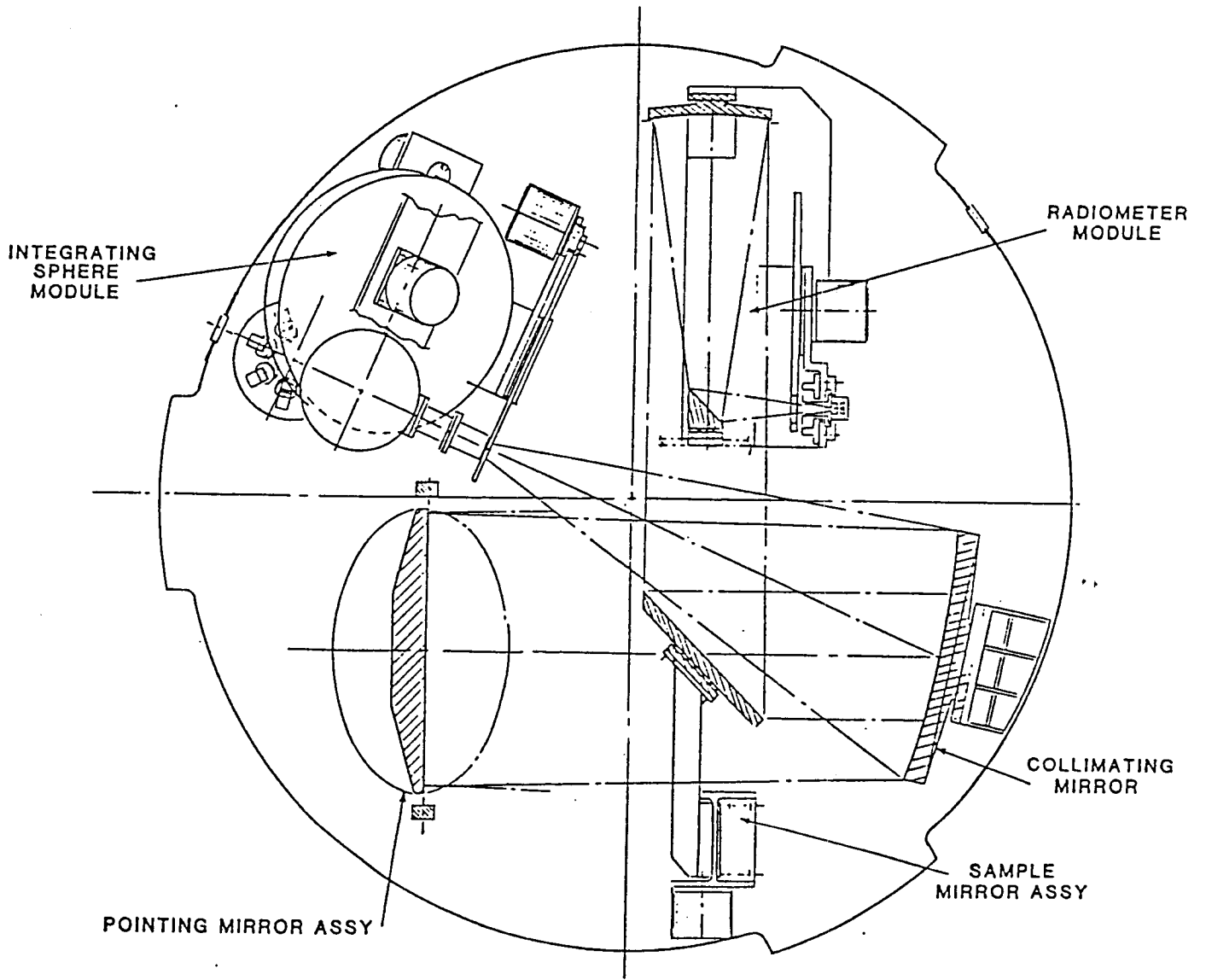


Figure 1. A conceptual block diagram of the DIRBE External Calibrator.



DIRBE CALIBRATOR ASSEMBLY

Figure 2. A design layout of the DEC instrument.

This page intentionally left blank.

3. SYSTEM DISCUSSION

3.1 Integrating Sphere Module

The integrating sphere module serves to provide a uniform Lambertian source at controlled flux levels within 10 bands that correspond to the spectral bands of DIRBE. In order of sequence the integrating sphere module contains the following elements as shown in Figure 3:

5 IR Sources	1 large-area source 4 tungsten bulb sources
First Integrating Sphere . .	4-inch diameter, interfaces with the five sources noted above. Output from the sphere goes to the aperture wheel.
Aperture Wheel	18 position device, position 1 is open, positions 2-15 contain apertures of increasing diameter, positions 16 and 17 are open, position 18 is opaque. Apertures at positions 2-15 provide relative beam energy with limits of 0.000122 and 1. Input is from first integrating sphere, output goes to filter wheel.
Filter Wheel	18 position device, position 1 is opaque, positions 2-11 are filtered (bands 1-10), 12 through 18 are open. Input is from the aperture wheel, output goes to second integrating sphere.
Second Integrating Sphere .	4-inch diameter, interfaces with Filter Wheel (input), full-time monitor, and mouth-to mouth Winston cones (output).
Mouth-to Mouth Winston Cones	Interface between second integrating sphere and mode selector wheel.
Mode Selector Wheel	18 position device, position 1 is opaque, positions 2-18 contain apertures or polarizers. Basic function is to provide point source mode and diffuse source mode. Some IR polarizers are provided for diffuse source mode.

3.1.1 IR Sources

Five infrared sources provide the radiation for the output beam from the DEC. These sources can be controlled separately or in any combination desired. They are located at the first integrating sphere. The sources are of three types as outlined below:

1. Shorter wavelengths are provided by two Chicago Miniature lamps with tungsten filaments and envelopes. These are mounted to the first integrating sphere with source cones as shown in Figure 3.

2. Medium wavelengths are provided by two Chicago Miniature lamps with tungsten filaments, identical to those in 1. (above), but on these lamps the glass envelopes have been removed. These bulbs are also mounted to the first integrating sphere with cones as shown in Figure 3.

Figure 4 illustrates the tungsten bulb with envelope removed.

3. Longer wavelengths are provided from an IR blackbody source (Large Area Source, LAS). Figure 5 illustrates the large area source and its mounting.

Equation 1 (E-1), the beam flux equation, gives the integrated beam flux as a function of source temperature, area, and emissivity; sphere size and reflectivity; and various geometrical coupling coefficients.

$$\Phi_{out} = \Phi_s C_1 F_1 C_2 F_2 C_3 F_3 k \quad \text{Watts} \quad (E-1)$$

where

Φ_s = source band flux in watts

C_1 = source to sphere loss factor

F_1 = first sphere loss

C_2 = sphere to sphere loss factor

F_2 = second sphere loss

C_3 = coupling to collimator loss factor

F_3 = filter loss

k = solid angle loss

$\Delta\phi$ = uncertainty, percent/degree

This equation, useful in parametric design, provides for trade-off analysis and determined the source size and temperature (with the predetermined sphere size) to achieve the specified beam power of 1×10^{-9} W in each band.

The difficulty in achieving the 1×10^{-9} W led to a compromise when NASA GSFC personnel agreed to accept 3×10^{-10} W in Bands 1 and 10. Note that the tungsten source, which operates at a higher temperature, is optimum for bands 1 through 6 and the large-area source is optimum for bands 3 through 10. This provides some overlap in the center.

Tables 1 and 2 tabulate all the values utilized in the solution of the equation for each source in each band. These data determined the major aspects of the DEC design.

3.1.2 First Integrating Sphere

The first integrating sphere provides a means of coupling the radiation from any, or any combination of, the IR sources into the DEC optical train without the necessity for using moving mechanical parts. It also assures that the source is a uniform, diffuse Lambertian radiator. Prior to the award of the DEC contract to USU, multiple considerations were made by NASA to determine the optimum size spheres to use in the DEC application. These considerations involved allowed volume, existing component sizes, and operational requirements for DEC. They indicated that the maximum practical sphere size for the DEC application should be about 4-inches diameter. This is the diameter of the integrating spheres used in DEC (both spheres 1 and 2). In order for a sphere to work effectively as an integrating sphere, its interior surface must be coated with a highly reflective non-specular coating. The design for DEC uses an integrating sphere with its interior surface sandblasted to an rms surface roughness of 10 micrometers and coated with evaporated gold. The selection of interior surface roughness is a key decision in the design of the integrating sphere. If the surface is too smooth, it will be specular at long wavelengths, while if it is too rough, the roughness may show through as source granularity at the short wavelengths.

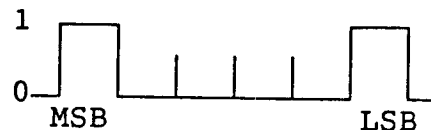
Integrating Sphere No. 1 has six ports, i.e., five for the IR sources and one exit port for output radiation. Both integrating spheres were manufactured by Labsphere. Figure 6

provides mechanical details concerning the no. 1 sphere, its ports and their positioning.

3.1.3 Aperture Wheel

As illustrated in the conceptual block diagram (Figure 1), four motor-driven wheels are employed in the DEC, i.e., the aperture wheel, filter wheel, mode selector wheel, and absolute radiometer filter wheel. The position of each of the wheels is controlled from the DEC Command and Monitor Unit. The basic mechanical design of each of these wheels is identical. Each wheel is an eighteen position device, rim driven by a stepper motor drive and geneva mechanism. The design of the wheels is illustrated in Figures 7 and 8. Wheel position in each case is monitored by six switches which together generate a unique binary code related to each of the 18 possible wheel positions. One of the switches is located at the geneva mechanism on each wheel, and the other five are located near the wheel centers. Switch openings/closures are initiated by lobes machined into the mechanism/wheel. Since the geneva mechanisms for moving the wheels are situated at the wheel edge, it is necessary to employ two geneva mechanism rotations for each complete change of wheel position (change of aperture/filter), i.e., one geneva mechanism rotation moves the wheel halfway to the next position; the second geneva rotation places the wheel on the position. To eliminate the possibility of stopping a wheel between positions one of the switches is dedicated to determining whether the wheel is on or between positions. The other five switches define which position the wheel is at in accordance with the following example.

Example of parallel binary output from wheel switches



The most significant bit (MSB) as illustrated shows a 1 if the geneva mechanism is "on" a position, the other 4 bits then indicate the binary number for the position. If the MSB is at 0

the wheel is between positions and the remaining 4 digits are ignored.

When the wheels are commanded to new positions, the controlling software is designed to achieve this using the shortest route to the new position. This is to keep heat generated by the stepper motors at a minimum.

Table 3 lists details pertaining to the wheels in general.

The aperture wheel provides a means of attenuating radiation exiting the first integrating sphere with a maximum possible attenuation of 10,000, thereby controlling the energy to the Filter Wheel, the downstream DEC system and DIRBE (See Figure 1). The wheel contains 14 apertures plus three open and one opaque position as delineated in Table 4.

3.1.4 Integrating Sphere Module Filter Wheel

The mechanical design of the Filter Wheel is identical with that of the Aperture Wheel (discussed above). The filters used in both the filter wheel at the output of the first integrating sphere and the filter wheel for the absolute radiometer (discussed later) were provided by NASA to USU for installation in the DEC. All of these filters, with the exception of the bands 9 and 10 filters in the absolute radiometer wheel, were delivered to USU and installed prior to delivery of DEC to NASA. Filters for bands 9 and 10 of the absolute radiometer were not available until September 1986 and USU personnel installed those filters at Goddard Space Flight Center at that time. NASA also provided specifications for wavelength and transmittance for the filters. These are included in this report as Appendix A. Table 5 describes which filters are assigned to each position for the Integrating Spheres Module Filter Wheel.

3.1.5 Second Integrating Sphere

The second integrating sphere receives input energy from the first sphere via the aperture wheel and filter wheel. The purpose of the second sphere is to provide a constant area

geometry, independent of the configuration of the upstream parts of the system. Hence, even though the IR band and intensity exiting the second integrating sphere may change depending upon source(s) selected and their temperatures, aperture selected, and filter selected, the output geometry from the second integrating sphere remains constant. Mechanical details of size and interior surface finishes and coatings are identical with sphere 1. Details of ports, their sizes and placements are included in Figure 9.

The Full-Time Monitor interfaces with the second integrating sphere. That part of the system will be discussed later in this report.

The output of the second integrating sphere is accomplished via mouth-to-mouth Winston cones.

3.1.6 Winston Cones

Mouth-to-mouth Winston cones are used to bring light out of the second integrating sphere and project it onto the collimating mirror (via the mode selector wheel). Mouth-to-mouth Winston cones were recommended for this purpose by NASA and were used because they accept radiation from a defined area (the sphere wall) and make it appear as a diffuse source at the other end. Design considerations indicated that putting them mouth-to-mouth would create a projected diffuse source output within a defined angle with some rolloff at the edges. This would allow the output (from the second integrating sphere) to be selected from a particular area of the sphere wall that was evenly illuminated and free of ports or apertures, and then essentially project the output onto the collimating mirror, thereby producing much less scattering than would be encountered had the output simply been taken from an exit aperture. Both calculated and measured Winston cone performance was evaluated and with this information in mind the cones were designed as follows:

Cone large diameter. 0.75 inches
Cone F/# 1.663
Cone small diameter. 0.216 inches
Cone length. 1.60 inches

Figure 10 details the Winston cones as they were produced for the DEC. Two sets of cones were fabricated and their interiors were gold plated to provide high reflectance to the IR radiation.

Subsequent testing of the cones at the system level proved that they did not function as anticipated. The cones produce nonuniformities in beam output intensity across the field of the output beam. This aspect system will be discussed later in this report.

The second set of cones was subsequently cleaned and recoated with gold by another company that felt that they could provide a coating which would increase the uniformity of the output from the cones. This indeed proved to be the case, but as of this writing NASA has not elected to allow replacement of the original cones with the second set.

3.1.7 Mode Selector Wheel

The output beam from the Winston Cones to the collimating mirror first passes through the Mode Selector Wheel. This device has two primary functions, i.e., to provide either a point source mode or a diffuse source mode to the collimating/pointing output optics and thence, to DIRBE. This is achieved by providing a set of apertures which control beam power and divergence. In addition, IR polarizing filters are included at some positions of the wheel. These will allow the response of the DIRBE to various polarizations to be measured in the first (short wavelength) bands in the diffuse source mode.

Mechanical design of the mode selector wheel and geneva drive mechanism is identical with the other wheels in the system (see filter wheel discussion, above). Table 6 defines the

characteristics of the apertures/filters vs. position for the mode selector wheel.

To provide an absolute calibration on DIRBE it is important to provide a beam of uniform and known radiance which overfills the fields-of-view of the DIRBE radiometers. The larger apertures in the mode selector wheel are used to accomplish this. Correspondingly, the mode selector wheel with its set of apertures and filters was placed at the focus of the collimating mirror. This necessarily placed the downstream end of the Winston cone coupling pair approximately 0.4 inches behind the collimating mirror focal plane. Even with this degree of defocus, with the larger apertures of the mode selector wheel the 0.75-inch diameter of the Winston cone exit should provide a beam which is uniformly bright within an angle of 2° full angle. This will serve to uniformly illuminate the DIRBE radiometers which have a field-of-view on the order of 0.75°

The requirements for mapping the DIRBE fields-of-view are quite different from those associated with absolute calibration. In the case of field-of-view mapping, what is needed is a well collimated beam providing uniform irradiance; that is to say that the exact shape of the beam divergence is not important as long as it is small ($<0.1^\circ$) and the total amount of power per unit area of the beam is constant. To this end the small apertures are placed in the mode selector wheel at the focus of the collimating mirror. One of these apertures (position 2) is tilted so that it makes a 46° angle with the collimating mirror optical axis. Design considerations indicated that tilting this aperture would distort the beam divergence, but would act to keep the beam power uniform. System testing later proved that there was essentially no advantage to tilting the aperture because beam nonuniformities mask the effects of tilting and that the aperture provided in position 15 (untilted) was as effective as the tilted one in position 2. The wheel included in the photograph in Figure 8 is the Mode Select Wheel.

The integrating sphere module of the DEC instrument is

illustrated in Figures 11 and 12. Figure 11 shows the IR sources mounted to the first integrating sphere. Also visible in this illustration are the side by side aperture and filter wheels between spheres 1 and 2, and the stepper motors used to drive the wheels. Figure 11 also shows two of the eleven temperature sensors included in the DEC assembly, i.e., Integrating Sphere No. 1 Temperature Sensor (shown on the near side of the sphere 1 mounting flange) and the Baseplate No. 1 Temperature Sensor (visible slightly to the left of sphere 1). Figure 12 is a view of the integrating sphere module showing the Winston Cones exit port. Also visible in Figure 12 are the grooves and lobes on the filter wheel. These are used for monitoring wheel position.

TABLE 1
Values Utilized in Solution of (E-1)
for Tungsten Bulb Source

TUNGSTEN BULB SOURCE

BAND NO.	λ_1 (μm)	λ_2 (μm)	ρ	ϕ_s	C_1	F_1	C_2	F_2	C_3	F_3	k	ϕ_{out} (W)	$\Delta\phi$ %
1	1.1	1.4	0.93	1.7E-4	0.5	9.5E-2	7.6E-2	9.5E-2	6.3E-2	0.7	1.2E-1	3.0E-10	0.7
2	2.2	2.6	0.94	7.2E-4	0.5	1.1E-1	7.6E-2	1.1E-1	6.3E-2	0.7	1.2E-1	1.8E-9	0.4
3	2.9	4.0	0.94	1.5E-3	0.5	1.1E-1	7.6E-2	1.1E-1	6.3E-2	0.7	1.2E-1	3.6E-9	0.3
4	4.5	5.1	0.94	4.2E-4	0.5	1.1E-1	7.6E-2	1.1E-1	6.3E-2	0.7	1.2E-1	1.0E-9	0.2
5	8.0	15.0	0.95	4.5E-4	0.5	1.3E-1	7.6E-2	1.3E-1	6.3E-2	0.7	1.2E-1	1.5E-9	0.1
6	15.0	30.0	0.95	9.6E-5	0.5	1.3E-1	7.6E-2	1.3E-1	6.3E-2	0.7	1.2E-1	3.3E-10	0.1
7	40.0	80.0	0.95	6.2E-6	0.5	1.3E-1	7.6E-2	1.3E-1	6.3E-2	0.7	1.2E-1	2.1E-11	0.1
8	80.0	120.0	0.95	6.7E-7	0.5	1.3E-1	7.6E-2	1.3E-1	6.3E-2	0.7	1.2E-1	2.3E-12	0.1
9	120.0	200.0	0.95	2.2E-7	0.5	1.3E-1	7.6E-2	1.3E-1	6.3E-2	0.7	1.2E-1	1.5E-13	0.1
10	200.0	300.0	0.95	4.4E-7	0.5	1.3E-1	7.6E-2	1.3E-1	6.3E-2	0.7	1.2E-1	1.5E-12	0.1

T = 1240K
 $A_s = 1.6E-3 \text{ cm}^2$ (0.001x0.050 in.)
 $E = 0.3$

TABLE 2
Values Utilized in the Solution of (E-1)
for Large-Area IR Source

IR SOURCE BAND FLUX

BAND NO.	λ_1 (μm)	λ_2 (μm)	ρ	ϕ_s	C_1	F_1	C_2	F_2	C_3	F_3	k	ϕ_{out} (W)	$\Delta\phi$ %
1	1.1	1.4	0.93	2.4E-14	1	9.5E-2	7.6E-2	9.5E-2	6.3E-2	0.7	1.2E-1	8.7E-20	16
2	2.2	2.6	0.94	1.6E-7	1	1.1E-1	7.6E-2	1.1E-1	6.3E-2	0.7	1.2E-1	7.8E-13	8.2
3	2.9	4.0	0.94	6.0E-7	1	1.1E-1	7.6E-2	1.1E-1	6.3E-2	0.7	1.2E-1	2.9E-10	5.5
4	4.5	5.1	0.94	3.6E-4	1	1.1E-1	7.6E-2	1.1E-1	6.3E-2	0.7	1.2E-1	1.8E-9	4.2
5	8.0	15.0	0.95	3.1E-2	1	1.3E-1	7.6E-2	1.3E-1	6.3E-2	0.7	1.2E-1	2.1E-7	1.8
6	15.0	30.0	0.95	2.9E-2	1	1.3E-1	7.6E-2	1.3E-1	6.3E-2	0.7	1.2E-1	2.0E-7	1.0
7	40.0	80.0	0.95	4.6E-3	1	1.3E-1	7.6E-2	1.3E-1	6.3E-2	0.7	1.2E-1	3.1E-8	0.6
8	80.0	120.0	0.95	6.1E-4	1	1.3E-1	7.6E-2	1.3E-1	6.3E-2	0.7	1.2E-1	4.15E-9	0.5
9	120.0	200.0	0.95	2.3E-4	1	1.3E-1	7.6E-2	1.3E-1	6.3E-2	0.7	1.2E-1	1.6E-9	0.4
10	200.0	300.0	0.95	4.7E-5	1	1.3E-1	7.6E-2	1.3E-1	6.3E-2	0.7	1.2E-1	3.2E-10	0.4

T = 270K
 $A = 2.85 \text{ cm}^2$
 $E = 0.9$

Table 3
Filter/Aperture/Mode Select Wheels Specifications

Parameter	Value/Notes
Motor Resolution	400 steps to move to adjacent position.
Slew Rate	400 steps/second, 1 second to nearest position, 9.0 seconds to farthest position.
Positioning Accuracy	Aperture positioned within 0.010", this equates to 2.04 arc minutes error in the beam going to DIRBE.

Table 4.
Aperture vs. Position,
and Aperture Set Information for Aperture Wheel

Wheel Position	Aperture Diameter (Inches)	Relative Beam Energy	Aperture Mat'l	Aperture Thickness (Inches)
1	Open			
2	0.00838	0.000122	Electroform Nickel	0.001
3	0.01185	0.000244	Electroform Nickel	0.001
4	0.01676	0.000488	Electroform Nickel	0.001
5	0.0237	0.000977	Electroform Nickel	0.001
6	0.0335	0.00195	Stainless Steel	0.007
7	0.0474	0.00391	Stainless Steel	0.007
8	0.067	0.00781	Stainless Steel	0.007
9	0.0948	0.0156	Stainless Steel	0.007
10	0.134	0.0313	Stainless Steel	0.007
11	0.1896	0.0625	Stainless Steel	0.007
12	0.268	0.125	Stainless Steel	0.007
13	0.3792	0.25	Stainless Steel	0.007
14	0.536	0.5	Stainless Steel	0.007
15	0.7584	1.0	Stainless Steel	0.007
16	Open			
17	Open			
18	Opaque			

Table 5
Filter vs. Wheel Position for Integrating Spheres Module
Filter Wheel

Wheel Position	Filter	Wheel Position	Filter
1	Opaque	10	Band 9
2	Band 1	11	Band 10
3	Band 2	12	Open
4	Band 3	13	Open
5	Band 4	14	Open
6	Band 5	15	Open
7	Band 6	16	Open
8	Band 7	17	Open
9	Band 8	18	Open

Table 6
Filters/Apertures vs. Position for Mode Selector Wheel

Position	Filter/Aperture	Position	Filter/Aperture
1	Opaque	10	Open*
2	0.017" tilted	11	Open*
3	Open	12	Open*
4	Polarizer 0°	13	0.008"
5	Polarizer 45°	14	0.012"
6	Polarizer 90°	15	0.017"
7	Polarizer 130°	16	0.047"
8	Open	17	0.134"
9	Open	18	0.379"

* Positions reserved for Cambridge Polarizers at NASA request.

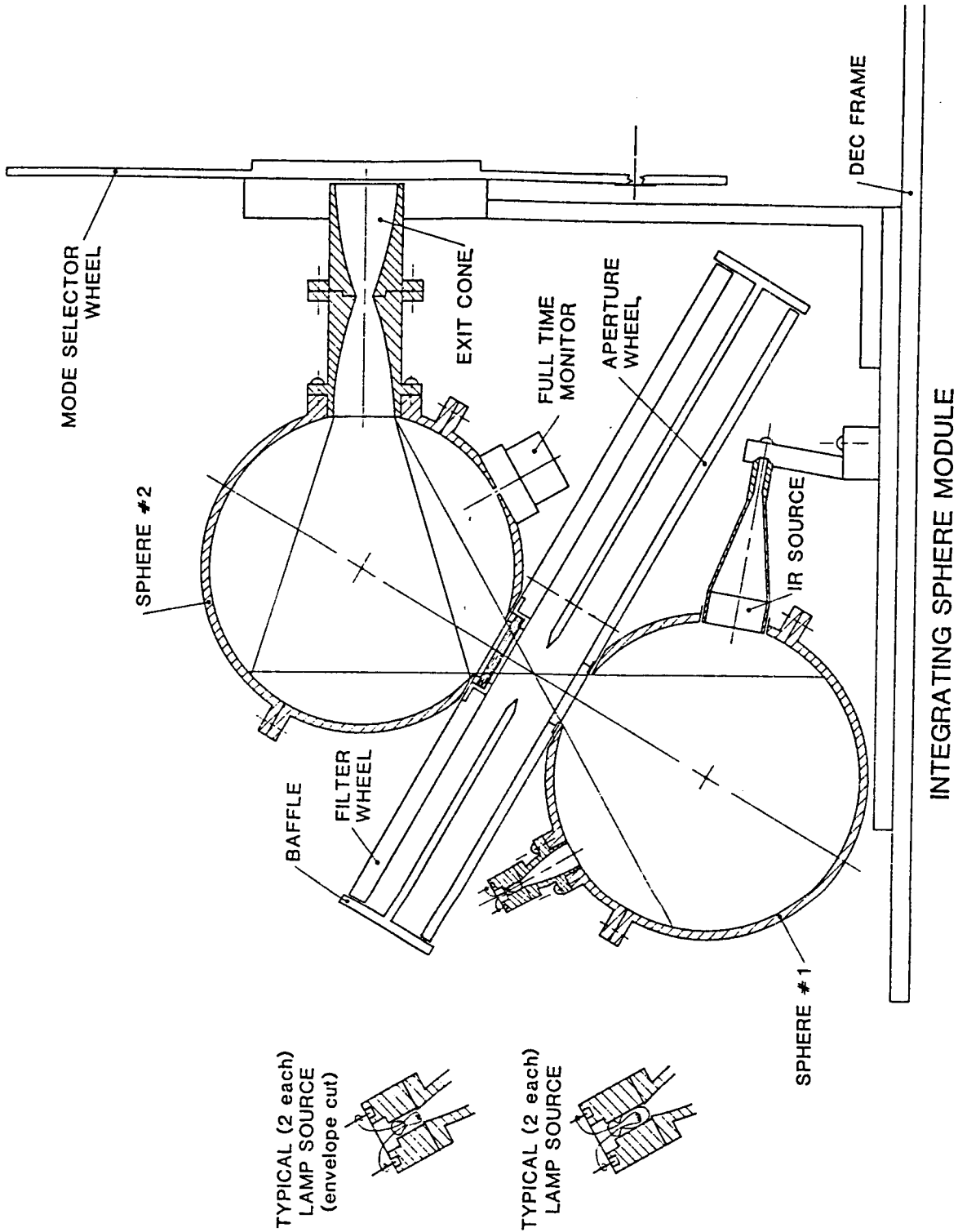


Figure 3. Integrating sphere module.

ORIGINAL PAGE IS
OF POOR QUALITY

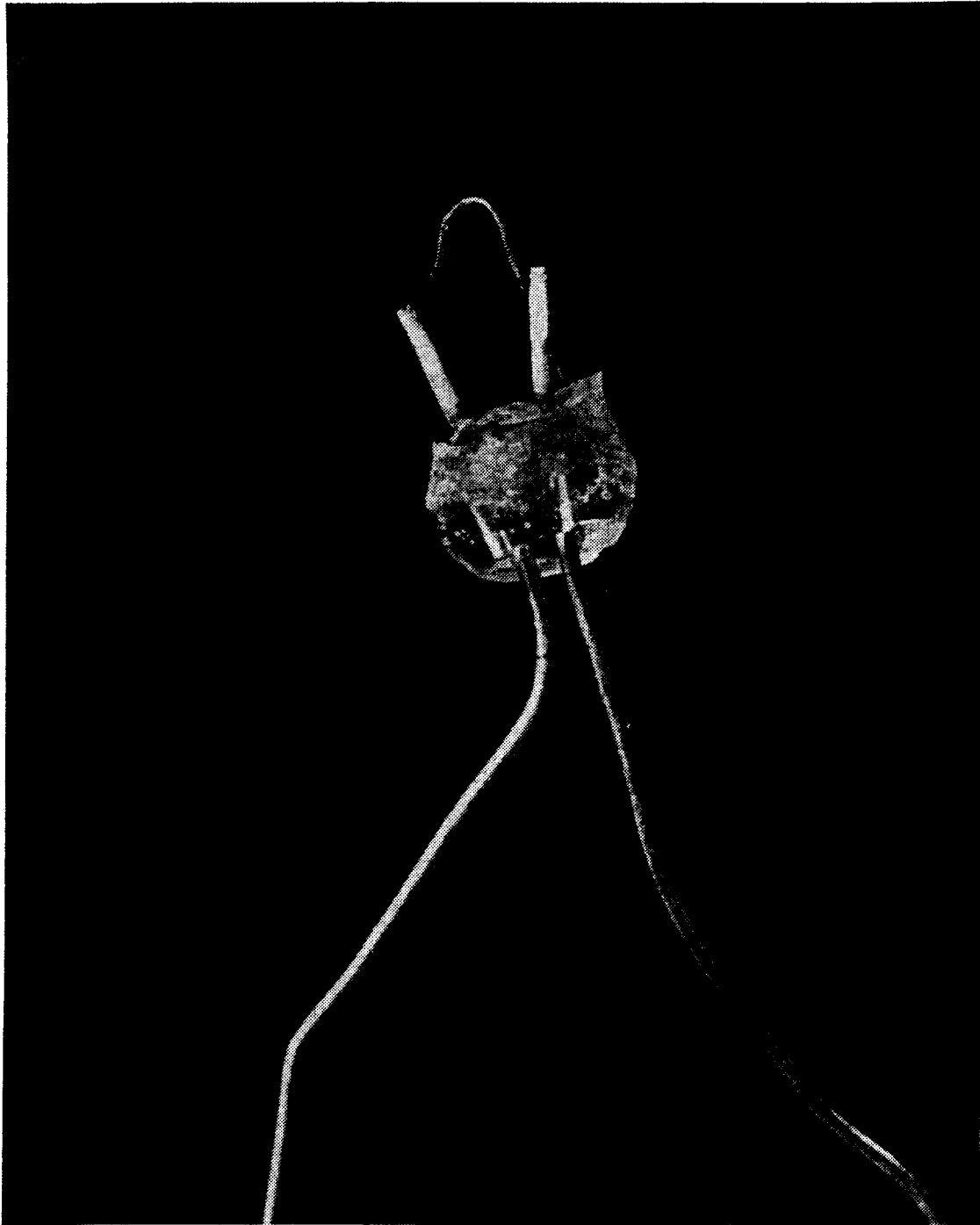


Figure 4. Tungsten bulb infrared source with glass envelop removed.

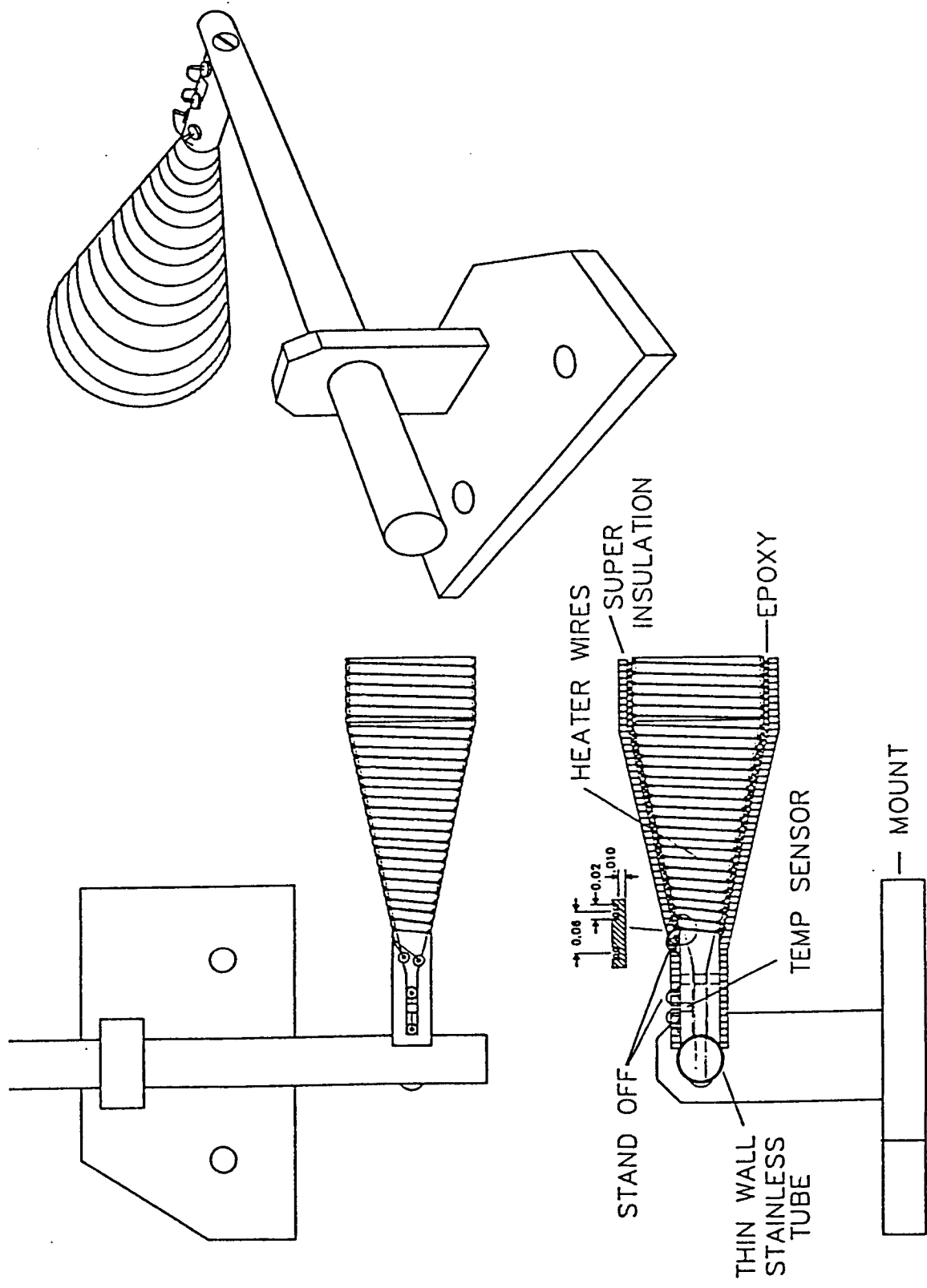
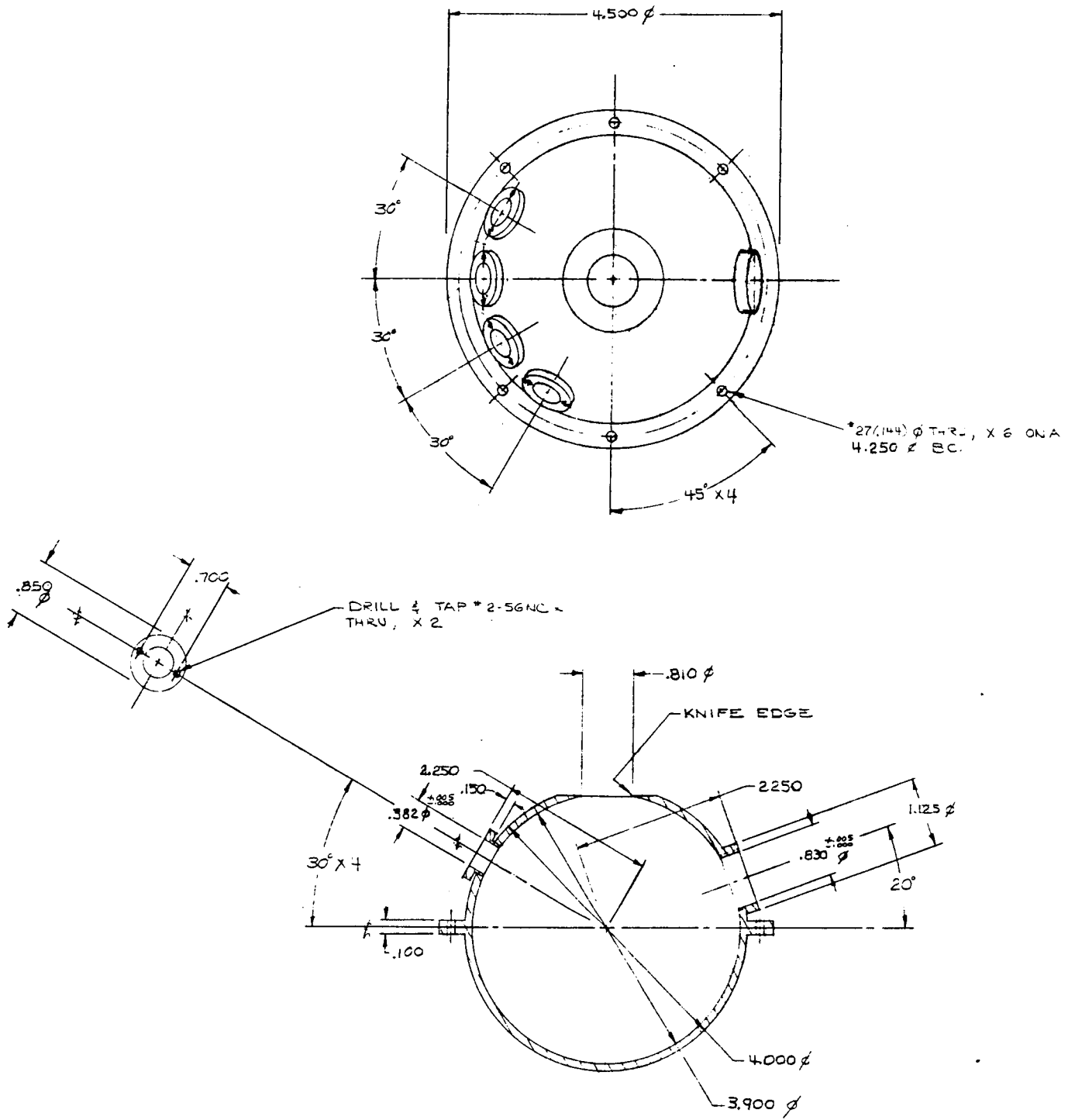
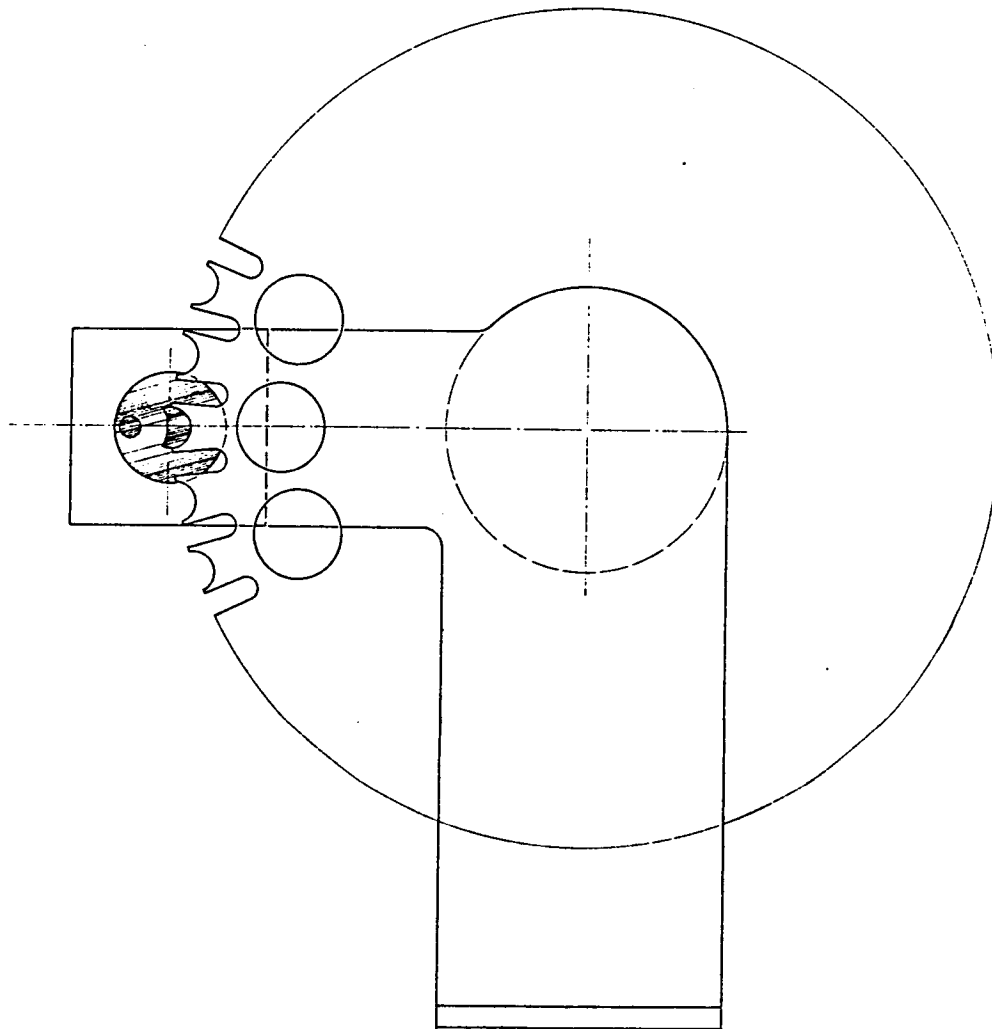
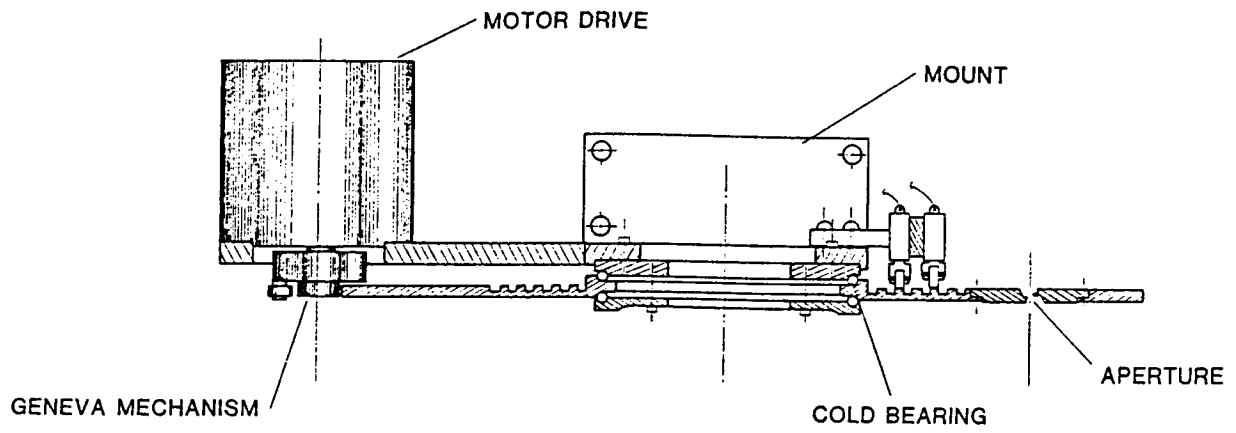


Figure 5. Large area infrared source and mounting.



CSE DRAWING #D1-2289

Figure 6. Mechanical details of sphere no. 1.



APERTURE DRIVE

Figure 7. Aperture/filter wheel design.

ORIGINAL PAGE IS
OF POOR QUALITY

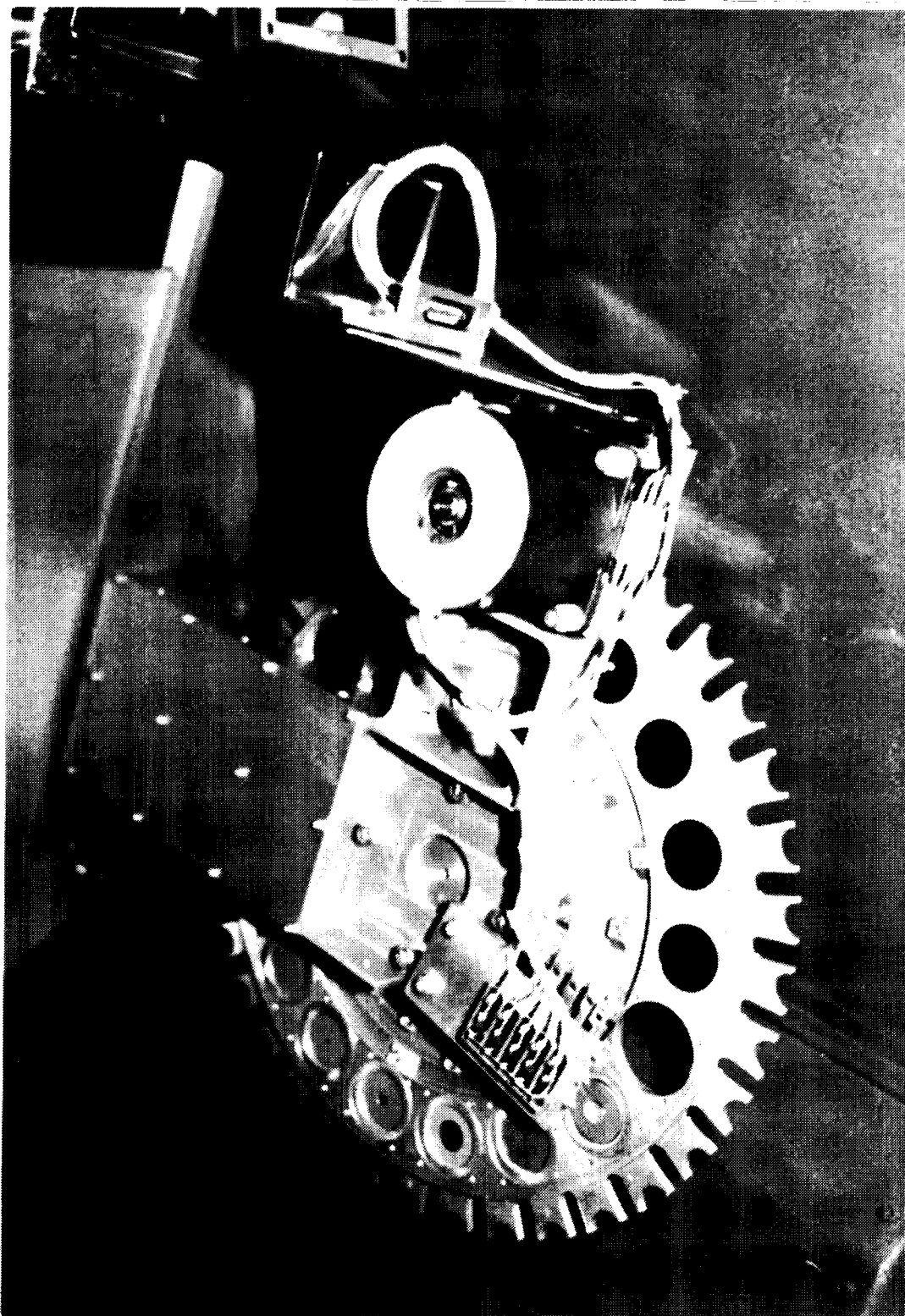


Figure 8. Photograph illustrating Aperture/Filter wheel design.

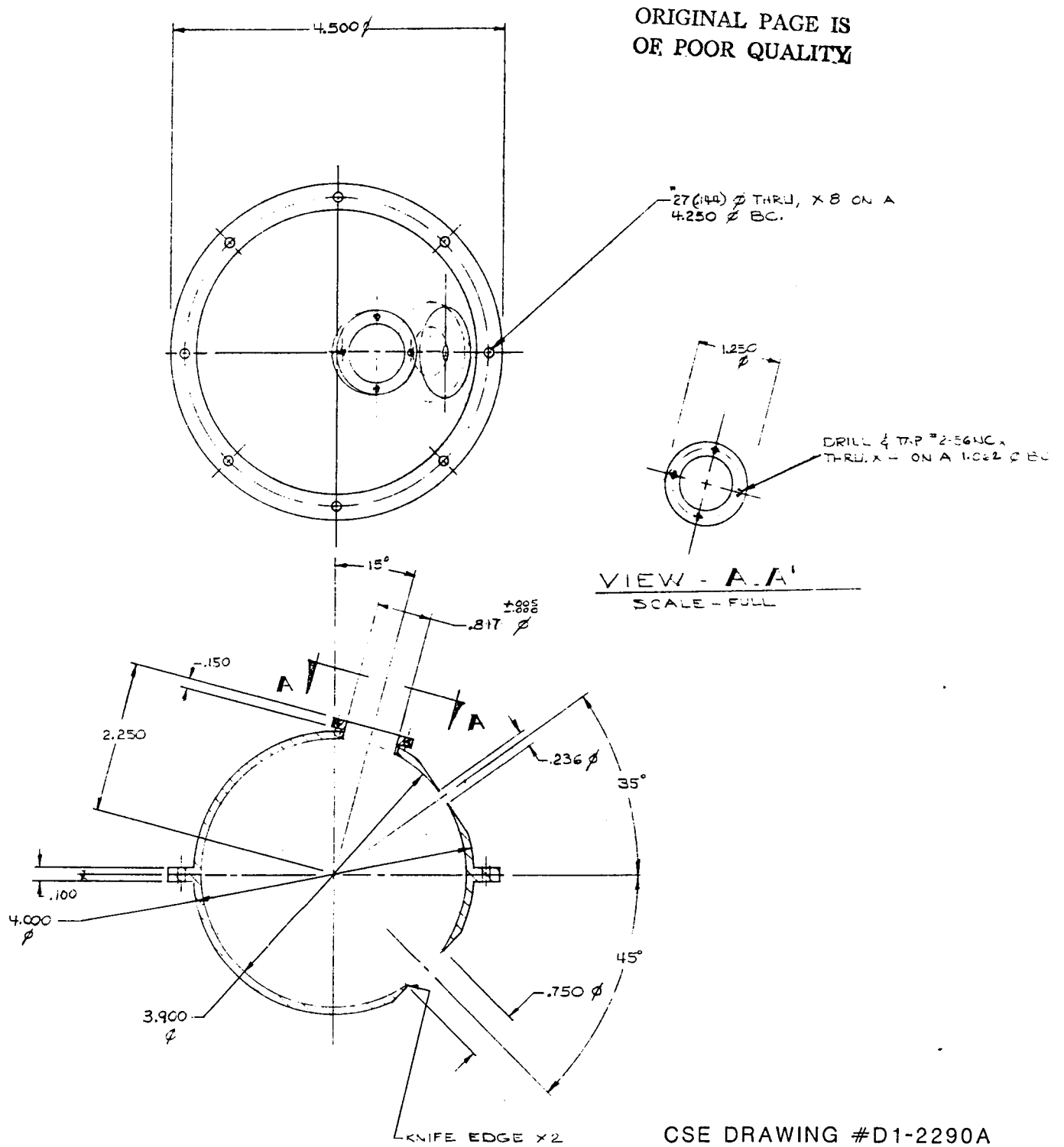
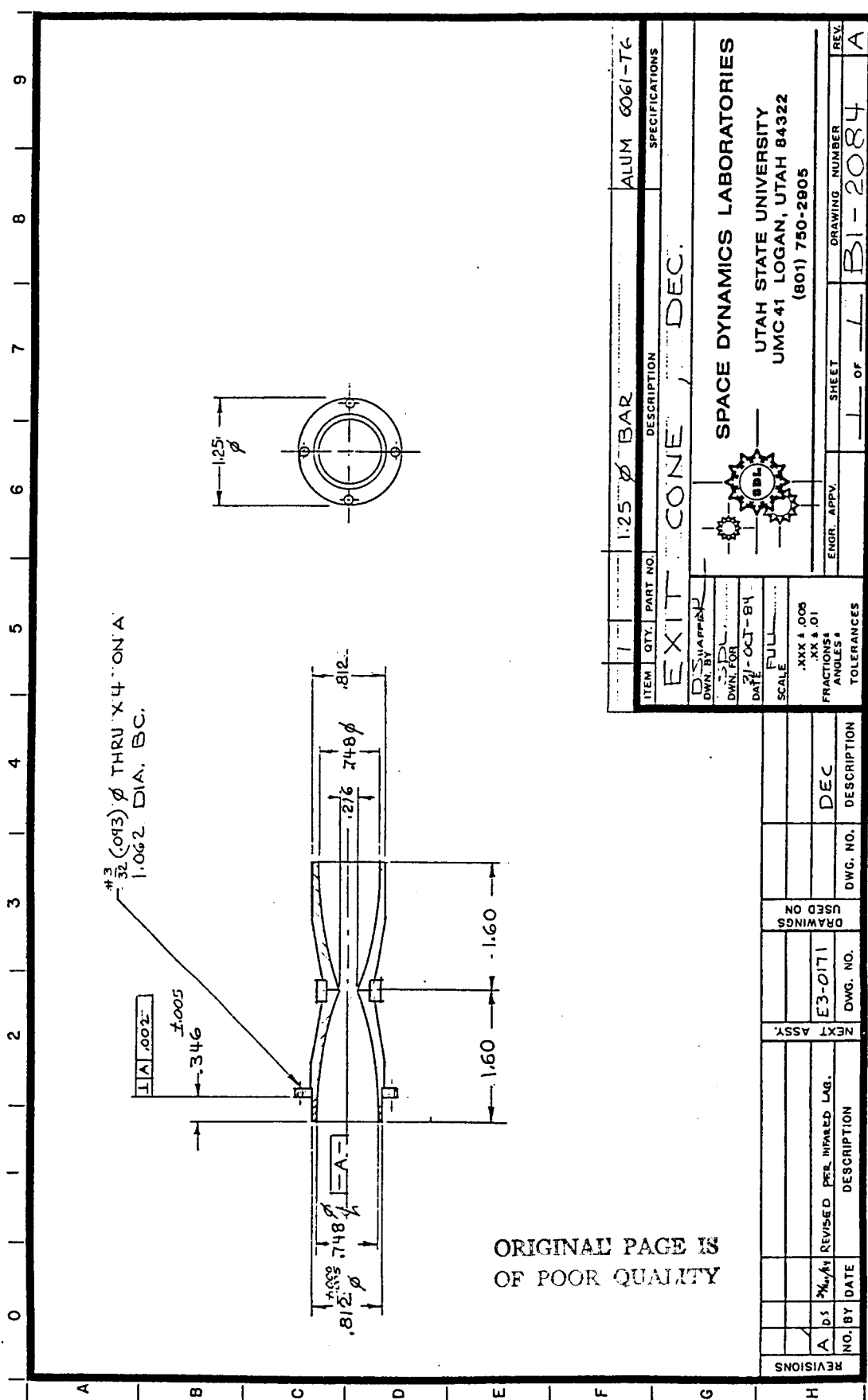


Figure 9. Mechanical details of integrating sphere no. 2.



ORIGINAL PAGE IS
OF POOR QUALITY

Figure 10. The Winston cones used as the exit port from integrating sphere no. 2.

ORIGINAL PAGE IS
OF POOR QUALITY

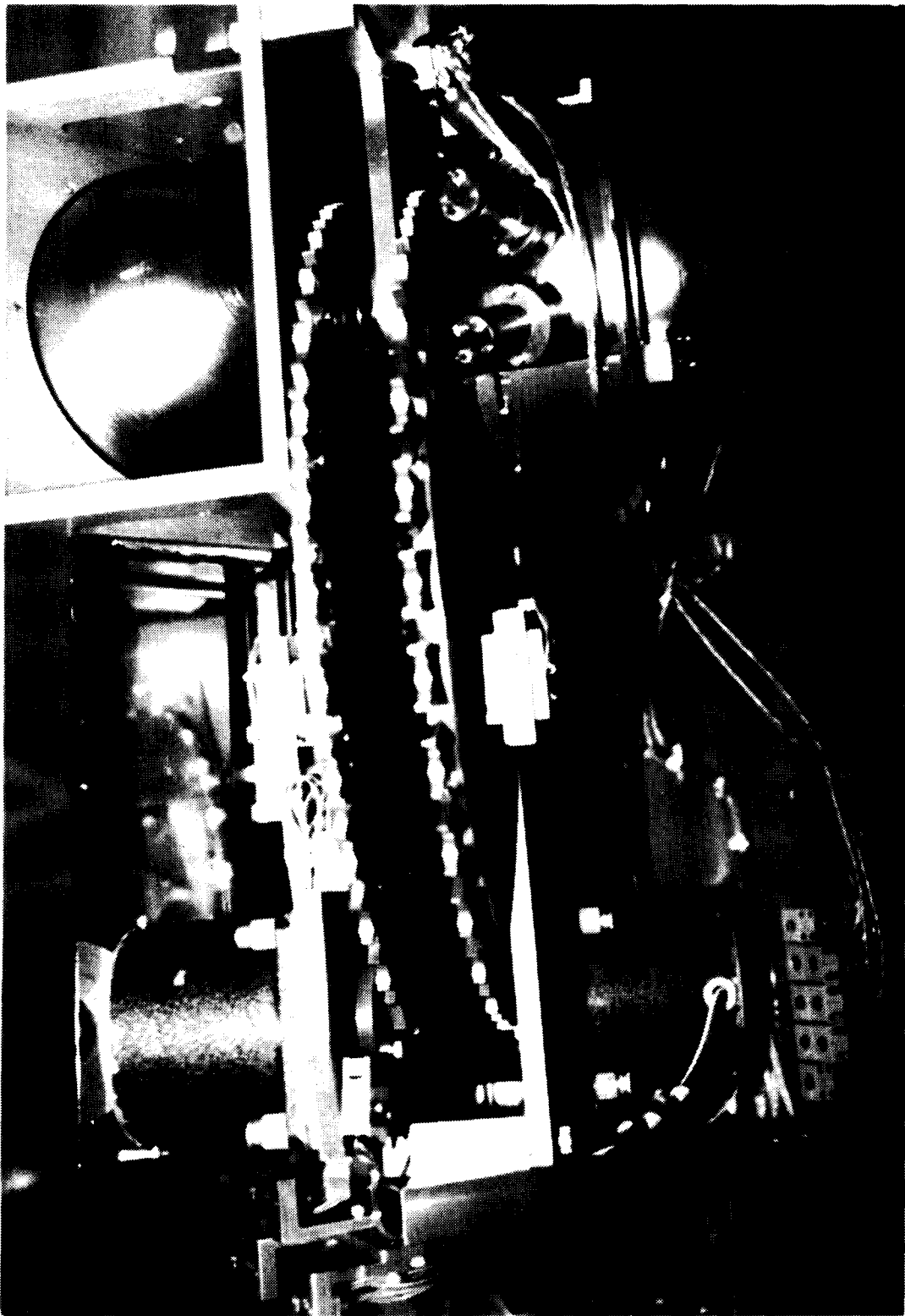


Figure 11. Photograph of integrating sphere module showing IR sources and aperture and filter wheels.



Figure 12. Photograph of integrating sphere module showing Winston cones and filter wheel.

3.2 Collimating Mirror Module

Figure 13 shows the optical path in the DEC downstream from the mouth-to-mouth Winston Cones and is included as reference for the following discussions.

3.2.1 Collimating Mirror

NASA provided the collimating mirror as GFE for the DEC instrument. It receives the light from the Winston cones via the mode selector wheel, collimates it into a beam of parallel rays and reflects them to the pointing mirror. The collimating mirror is a diamond turned, off-axis parabola made of aluminum with a polished nickel plating. The parent blank from which the off-axis section was taken was $f/0.74$. The optical surface is coated with evaporated gold. Image quality from the collimating mirror is much better than required for the point source mode. Table 7 contains specifications for the collimating mirror and Figure 14 provides further information on physical configuration.

Figure 15 shows the DEC instrument in a partially assembled configuration. The collimating mirror is clearly seen at the top right of the illustration. Note that the mirror itself is partially surrounded by a modified hemispherical baffle. The baffle is designed to trap any light which overfills the collimating mirror. Figure 16 shows the back of the collimating mirror as seen through the back end of the baffle. The ribbed mounting structure for the mirror works with the reflective inner baffle surface to trap and absorb light that overfills the mirror. Also shown in Figure 16 is the Collimating Mirror Temperature Sensor, mounted to the back of the mirror mount.

Table 7
Collimating Mirror Specifications

Parameter	Value
Diameter	9.0 inches
Focal Length	16.831 inches
f/#	1.87

Note: All mirrors supplied by USU for the DEC instrument have surface quality equivalent to that of the Collimating mirror.

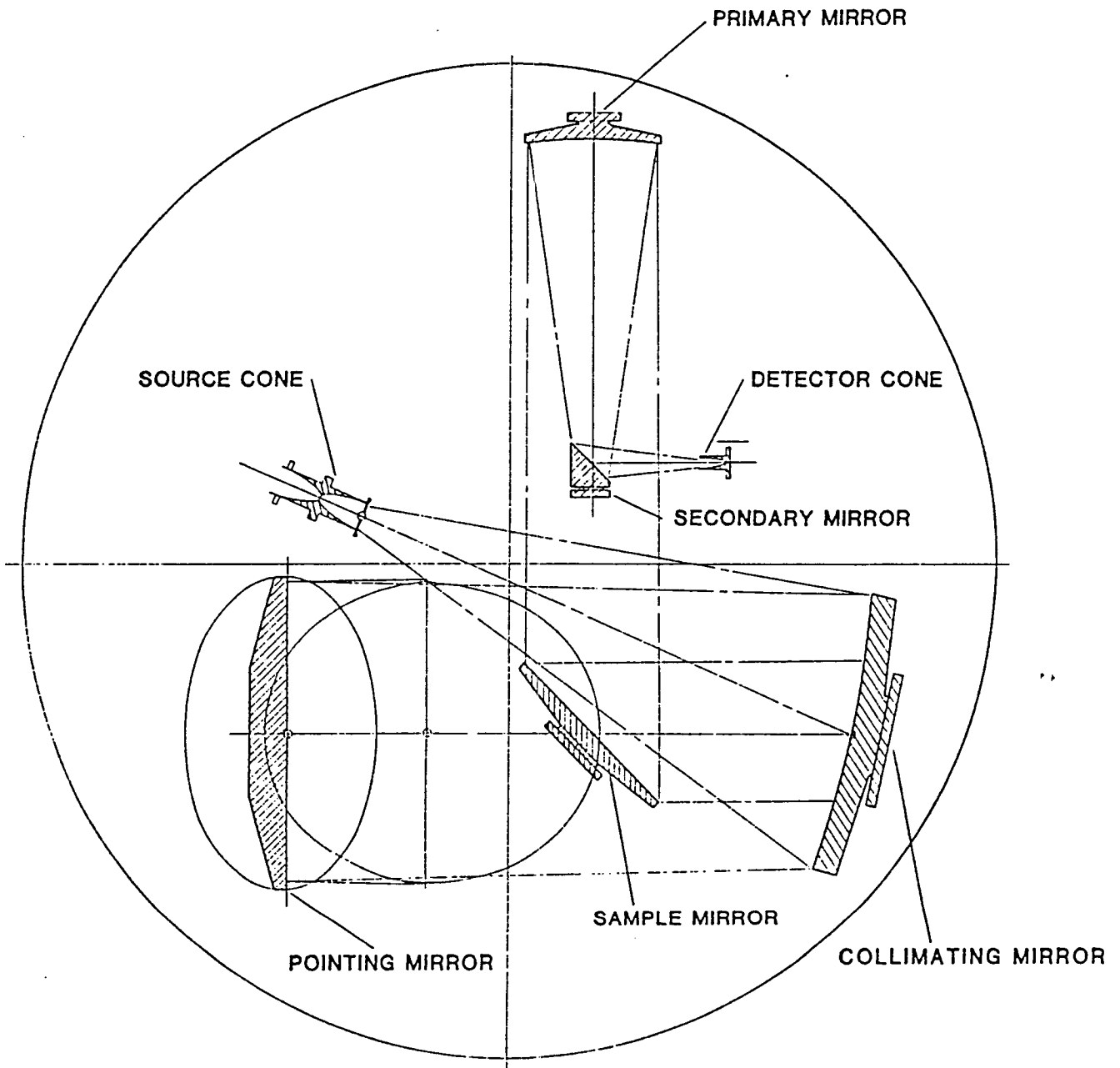


Figure 13. The DEC optical path downstream from the Winston cones.

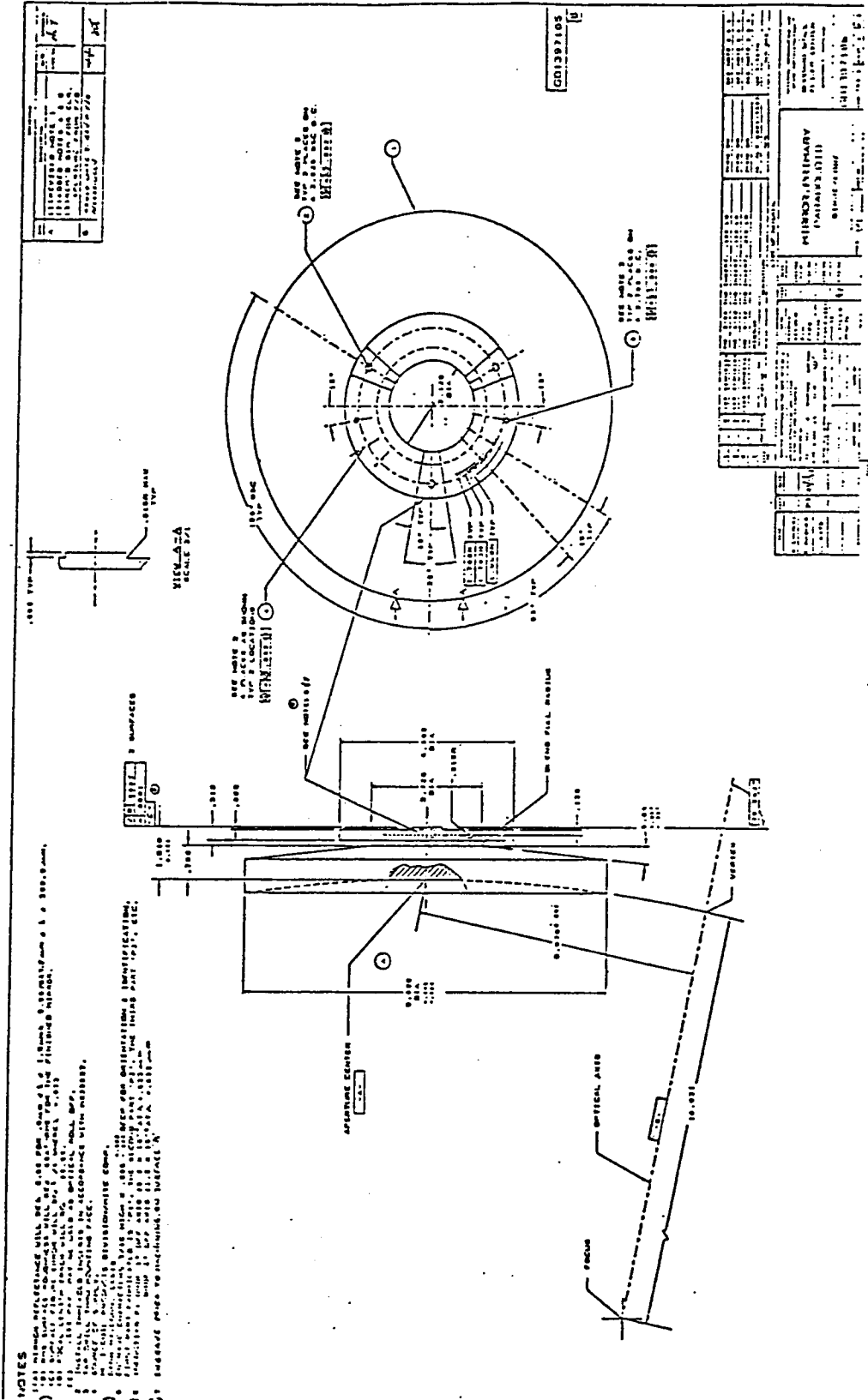


Figure 14. NASA drawing detailing the DEC Collimating mirror. Note: This is the most legible drawing existing at USU as of this writing. If further details are required this drawing was included as Figure 2-8 in NASA's RFP No. 5-28723/234, the reader is referred to that source.

ORIGINAL PAGE IS
OF POOR QUALITY

ORIGINAL PAGE IS
OF POOR QUALITY

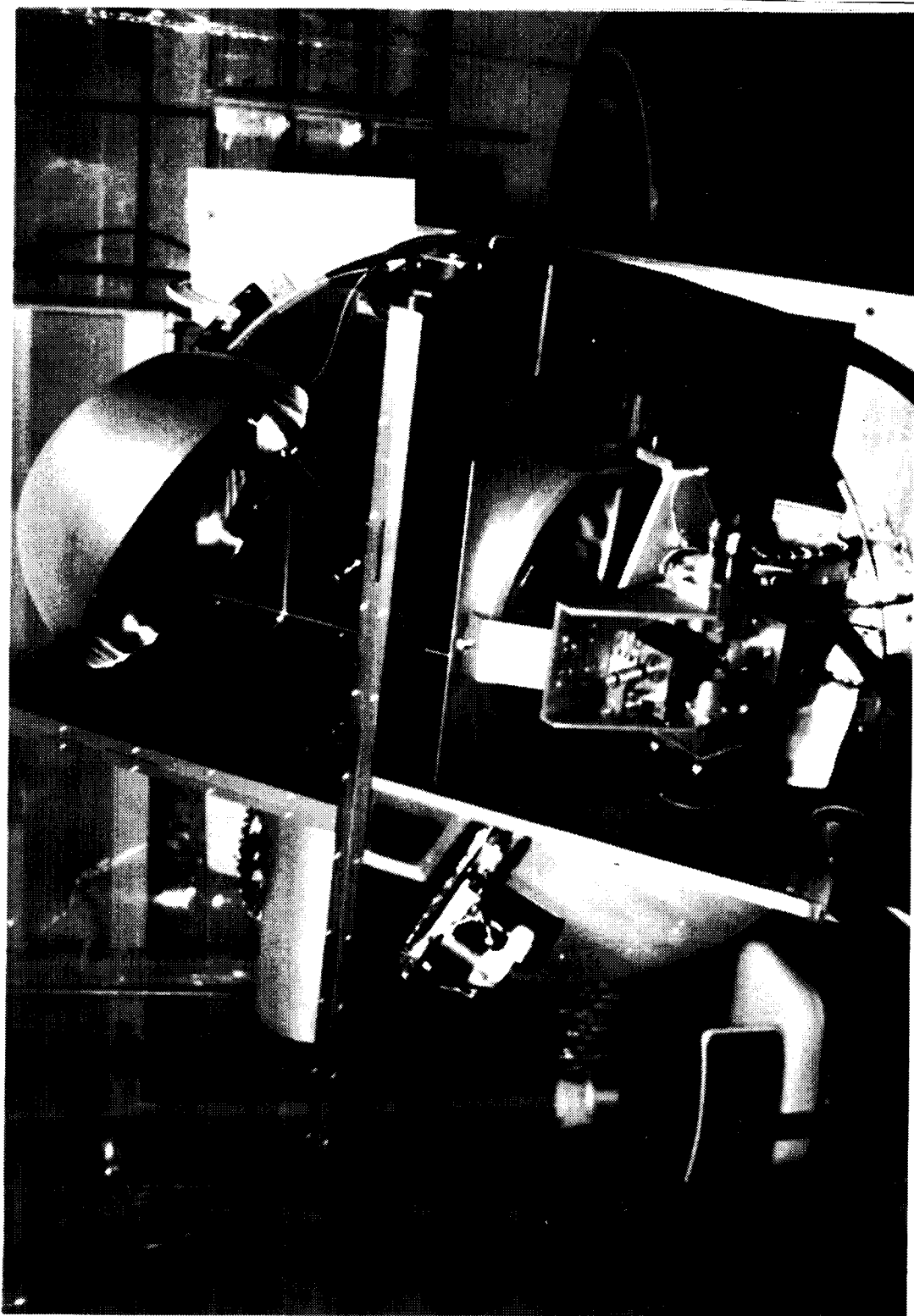


Figure 15. Collimating mirror and baffle in the partially assembled DEC instrument.

ORIGINAL PAGE IS
OF POOR QUALITY

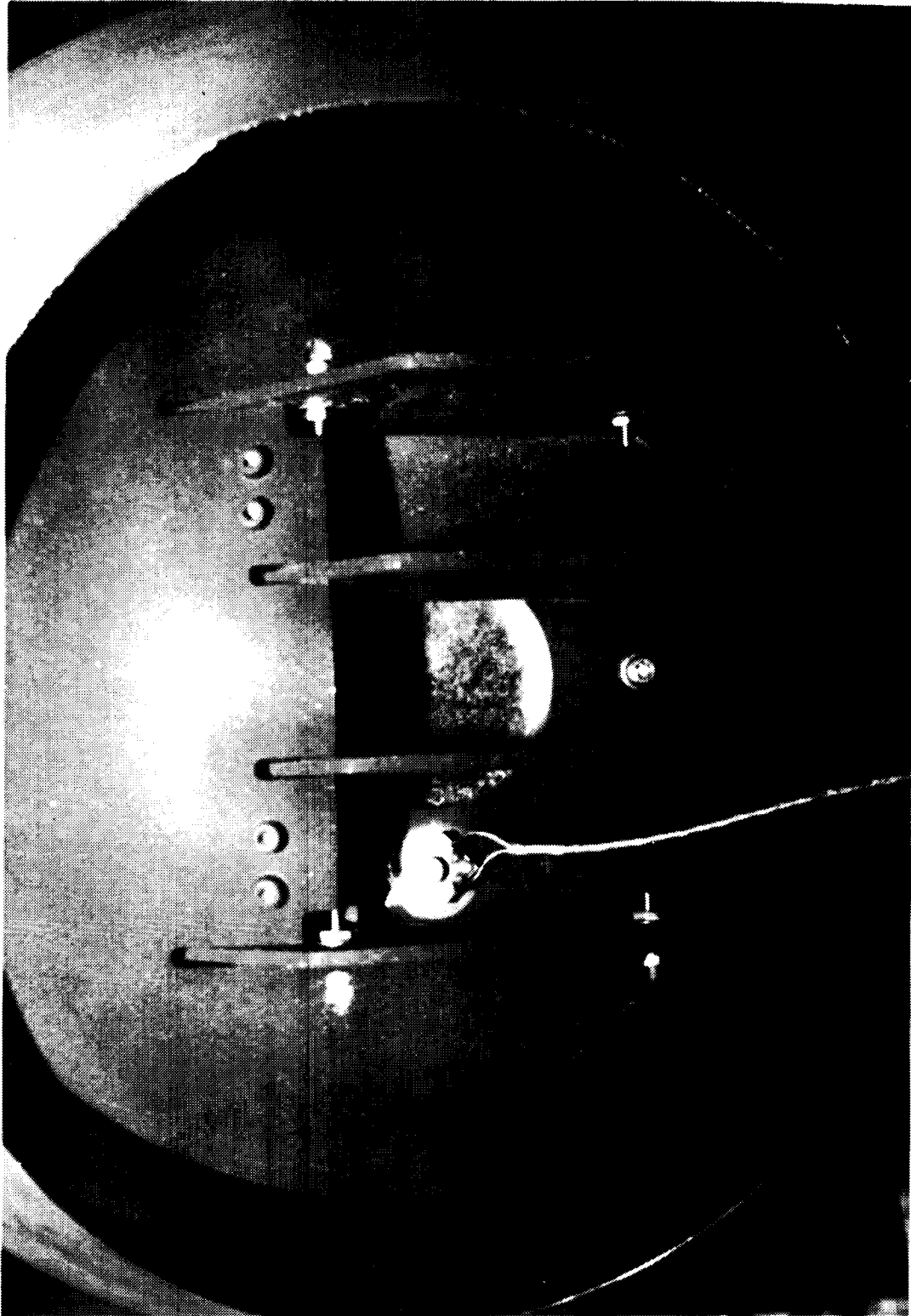


Figure 16. A rear view of the collimating mirror, baffle, and temperature sensor.

3.3 Pointing Mirror Module

3.3.1 Pointing Mirror

The pointing mirror is the final optical component in the DEC light path. It is an optical flat placed to receive the light from the collimating mirror and direct it into the DIRBE instrument. The mirror is of an elliptical shape and is sized so that it does not vignette the radiation from the collimating mirror. Table 8 gives specifications for the pointing mirror and Figure 17 details its configuration.

3.3.2 2-Axis Gimbal (Pointing Mirror)

The light beam reflected from the pointing mirror is used for mapping the spatial response of the DIRBE when the DEC is in the point source mode. To achieve this function, we equipped the pointing mirror with a 2-axis gimbal by which the exiting light beam from the DEC instrument can be pointed to desired positions within the specified $2^\circ \times 2^\circ$ limits. Two stepper motors accomplish the movement of the gimbal, two LVDTs (linear variable differential transformers) monitor the position for control of the steppers and for position indications. In essence, movement of the pointing mirror is accomplished using a joystick design. The stepper motors operate on the joystick at right angles to each other such that through the gimbal system the mirror is moved in either the X- or Y-axis with pivoting occurring at the front surface of the mirror. Spring loading on two sides (opposite the stepper motors) keeps the joystick in solid contact with the stepper motor drivers, and maintains the connection to the LVDTs cores. Figures 18 and 19 show the gimbal and drive mechanism for the pointing mirror. In addition the pointing mirror can be clearly seen in the lower right area of the photo shown as Figure 15.

Two movement modes are used for the pointing mirror. In both modes the output from the LVDTs are A/D converted into an twelve-bit parallel number. This number is compared with a lookup table and if the difference is >255 , the stepper motors

are moved 80 steps in the proper direction. This procedure is repeated until the difference between the A/D output and the lookup table is <255. When this occurs the motors are driven 4 steps in the proper direction and this procedure is repeated until the mirror is in position. Movement capabilities exceed the specified $\pm 2^\circ$ in each axis. Initially, our goal was to achieve a movement capability of $\pm 4^\circ$, but some difficulties were encountered with reliability when the mirror was commanded beyond $\pm 3^\circ$. A patch in the software of the computer now limits movement to $\pm 3^\circ$. Mirror positioning accuracy is $\pm 0.02^\circ$ about the zero position in each of the two axes.

One of the eleven DEC temperature sensors is mounted on the back of the inner gimbal of the pointing mirror.

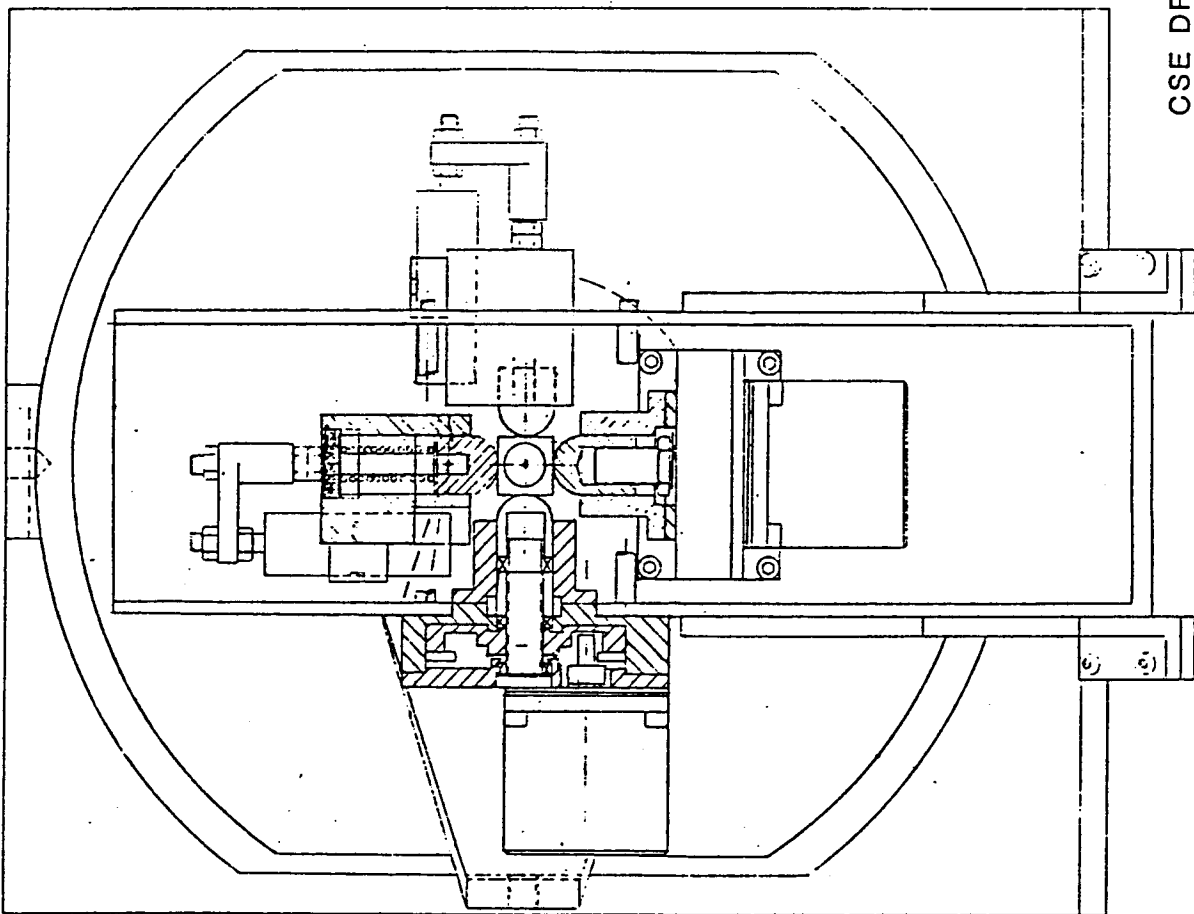
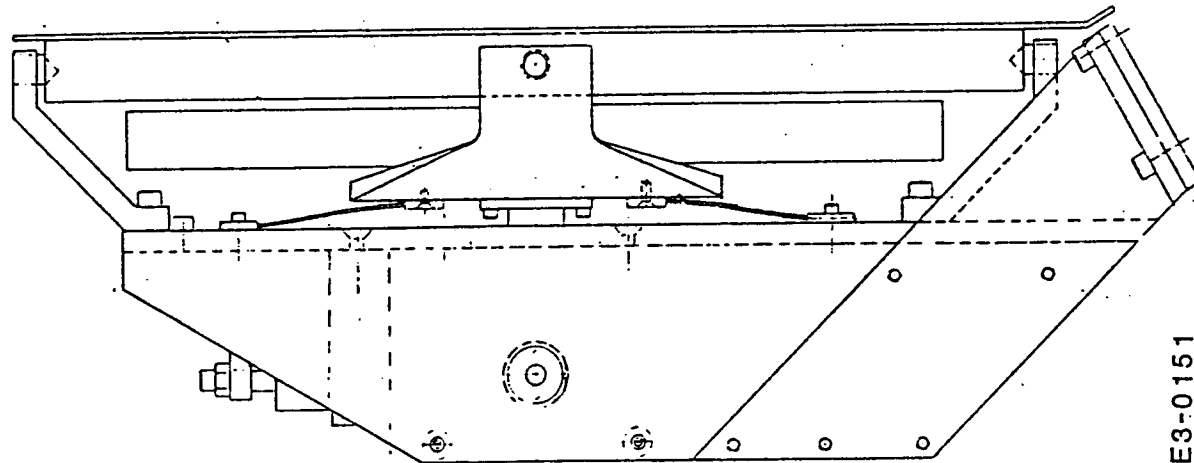
3.3.3 Pointing Mirror Calibration

The pointing mirror mechanism was calibrated to obtain the relationship between the angle at which the output beam exits DEC and the count from the A/D converter that reads the outputs of the LVDTs (see section 3.3.2). This data is used to generate the lookup tables used by the microprocessor in the STD BUSS in the DEC Control and Monitor Unit.

In retrospect, we believe that the pointing mirror calibrations accomplished at USU on 19 July 1985 may be in error by as much as 20% due to the method used for calibration. The recently discovered problem is that a crosshair target was used for the calibration rather than a collimated source and the distance from the pointing mirror to the crosshairs target was not recorded. Worst case indicates a probable error of 20%. The error is uniform and repeatable across the field. Readouts should not be used for absolute measurements, they can be used to indicate uniform increments of movement. GSFC personnel have been notified of the probable error. These calibrations should be rechecked at GSFC.

Table 8
Pointing Mirror Specifications

Parameter	Value
Material	Aluminum
Coating	Nickel - Gold Electroplate
Major Axis	11.800 inches
Minor Axis	10.000 inches
Figure	$\lambda/4$ at 0.633 μm (flat)
RMS Surface Roughness	<60Å
Clear Aperture Edge Effects	<0.50 inches



CSE DRAWING #E3-0151

Figure 18. Drawing of the pointing mirror gimbal and drivers.

ORIGINAL PAGE IS
OF POOR QUALITY

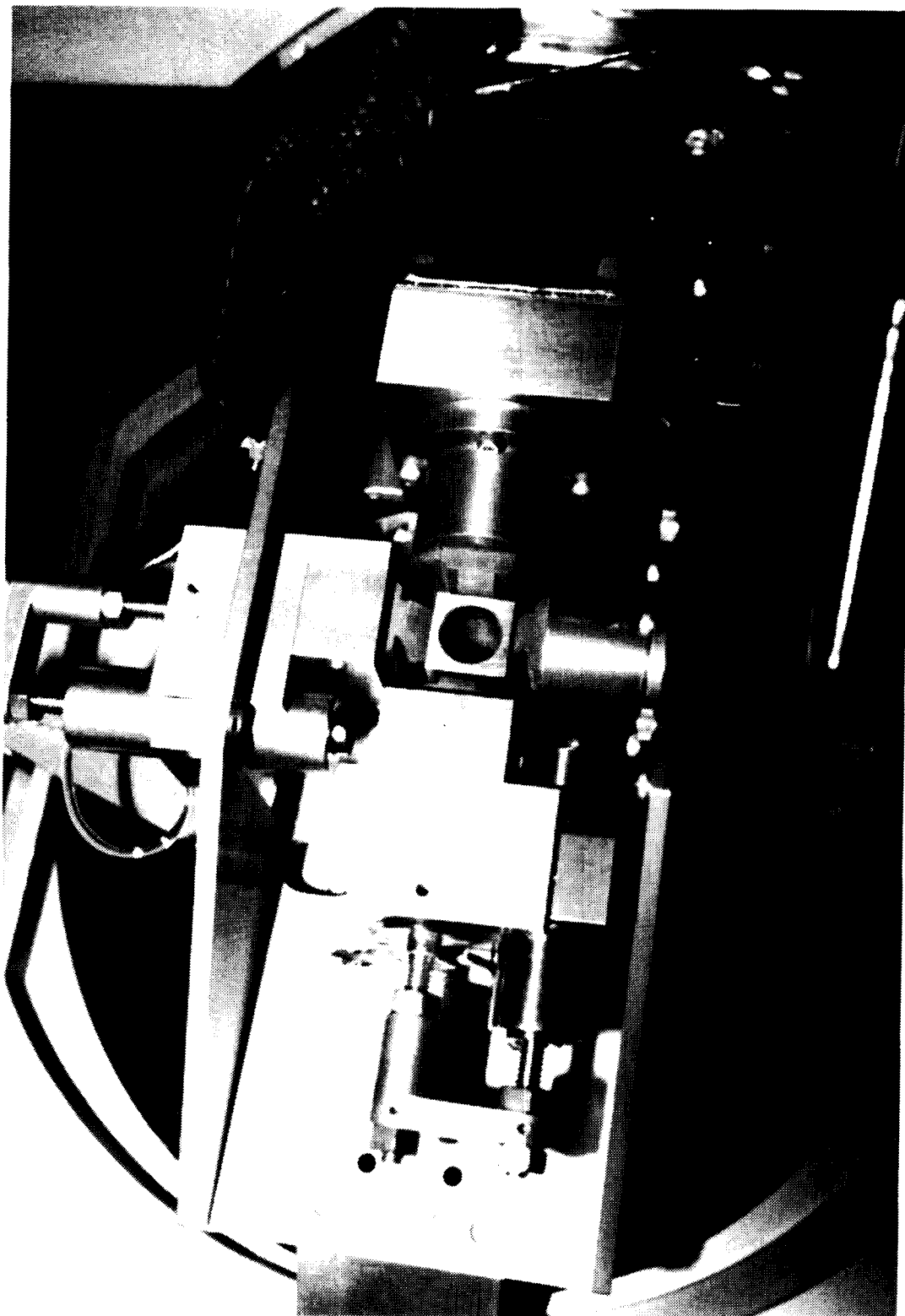


Figure 19. Photograph of the pointing mirror gimbal drive mechanism.

3.4 Sample Mirror Module

The Sample Mirror Module works in conjunction with the Absolute Radiometer Module (see following pages) to provide absolute measurements of the DEC output beam band radiance.

3.4.1 Sample Mirror

The sampling mirror (see Figure 1) is a two-position device that can be used to deflect the center 25% of the DEC beam into the absolute radiometer for measurements. When these measurements are completed the sampling mirror is withdrawn from the DEC beam, allowing the entire beam to be sent to DIRBE. Figure 20 details the sampling mirror assembly, and Table 9 and Figure 21 provide specifications for the sample mirror.

As shown in Figure 20 the sample mirror is rotated in and out of the DEC beam by a stepping motor. Control of the stepper is via the DEC Command and Monitor Unit. Limit switches at both extremes of the rotation stop the stepper drive motor. The mirror arm is then driven a small additional amount to spring load the arm against the mechanical stops. Position of the sample mirror is monitored at the CMU and indicates whether the sample mirror is fully into the beam, between positions, or fully out of the beam. Figure 22 is a photograph showing the sample mirror mounted in the DEC. The temperature monitor mounted on the sample mirror arm near the mirror is plainly visible.

Table 9
Sample Mirror Specifications

Parameter	Value
Material	Aluminum
Major Axis	6.365 inches
Minor Axis	4.500 inches
Coating	Nickel - Gold Electroplate
RMS Surface Roughness . .	<60Å
Figure	$\lambda/4$ at 0.633 μ m (flat)
Clear Aperture Edge Effects	<0.005 inches

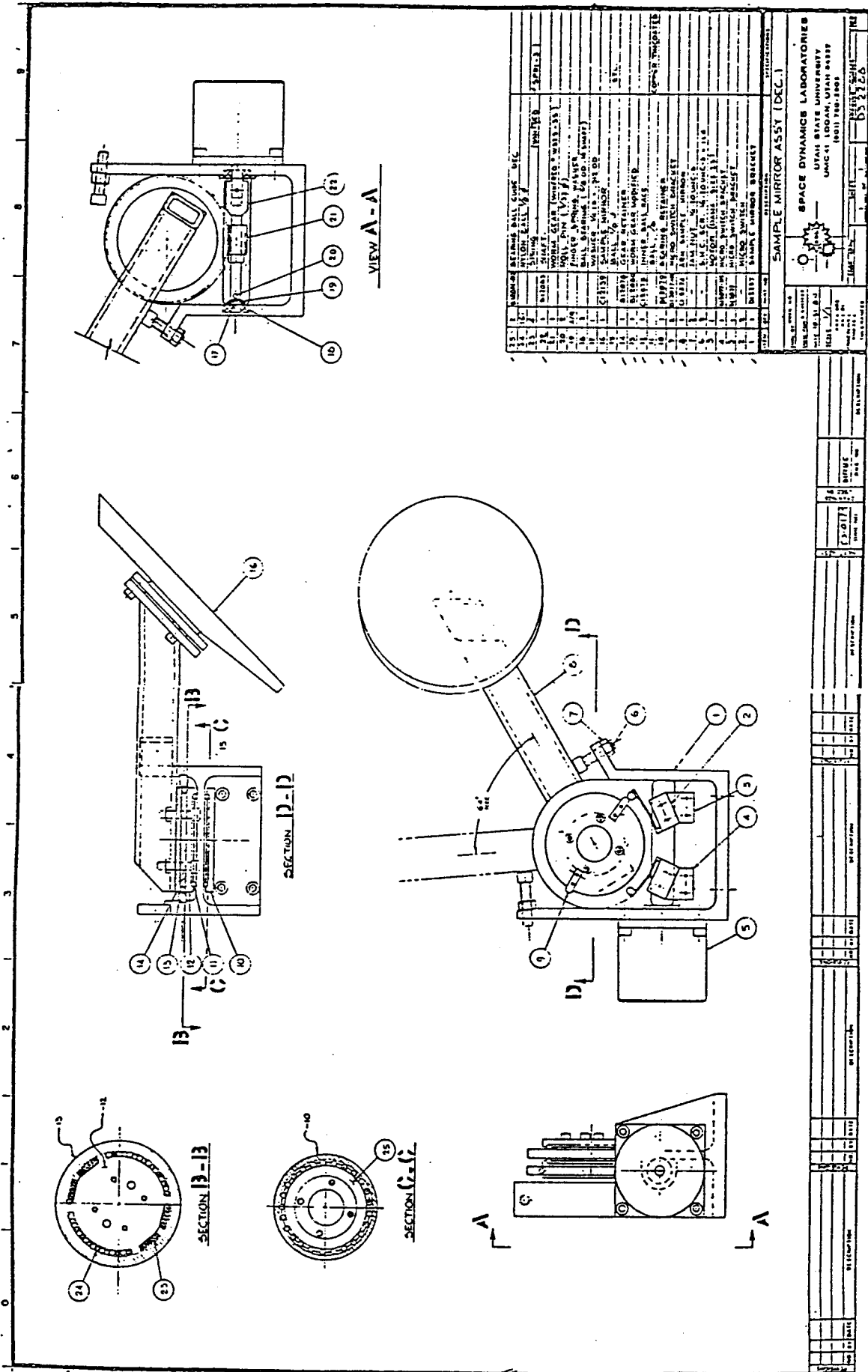


Figure 20: Sample mirror assembly.

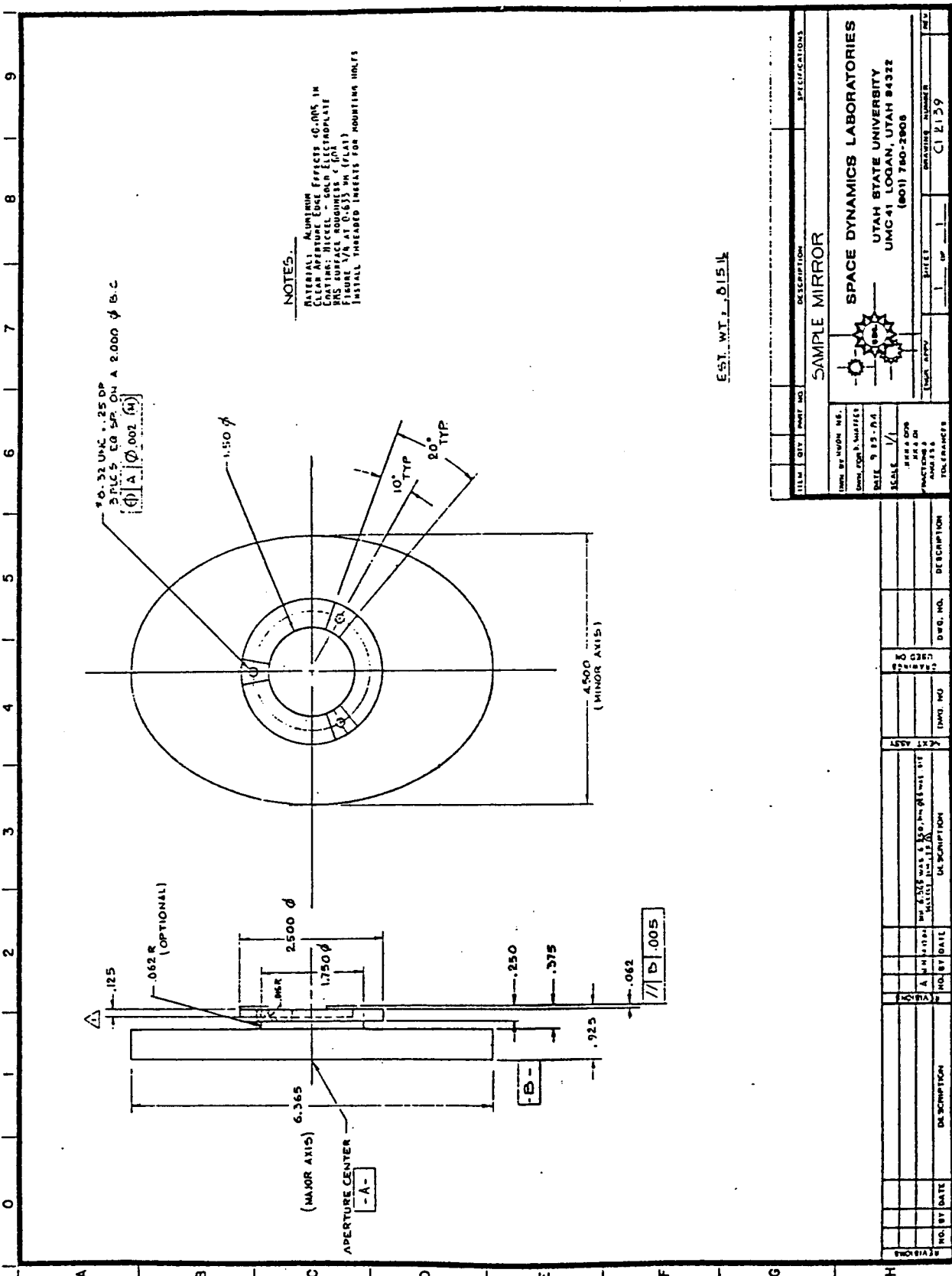


Figure 21. Sample mirror details.

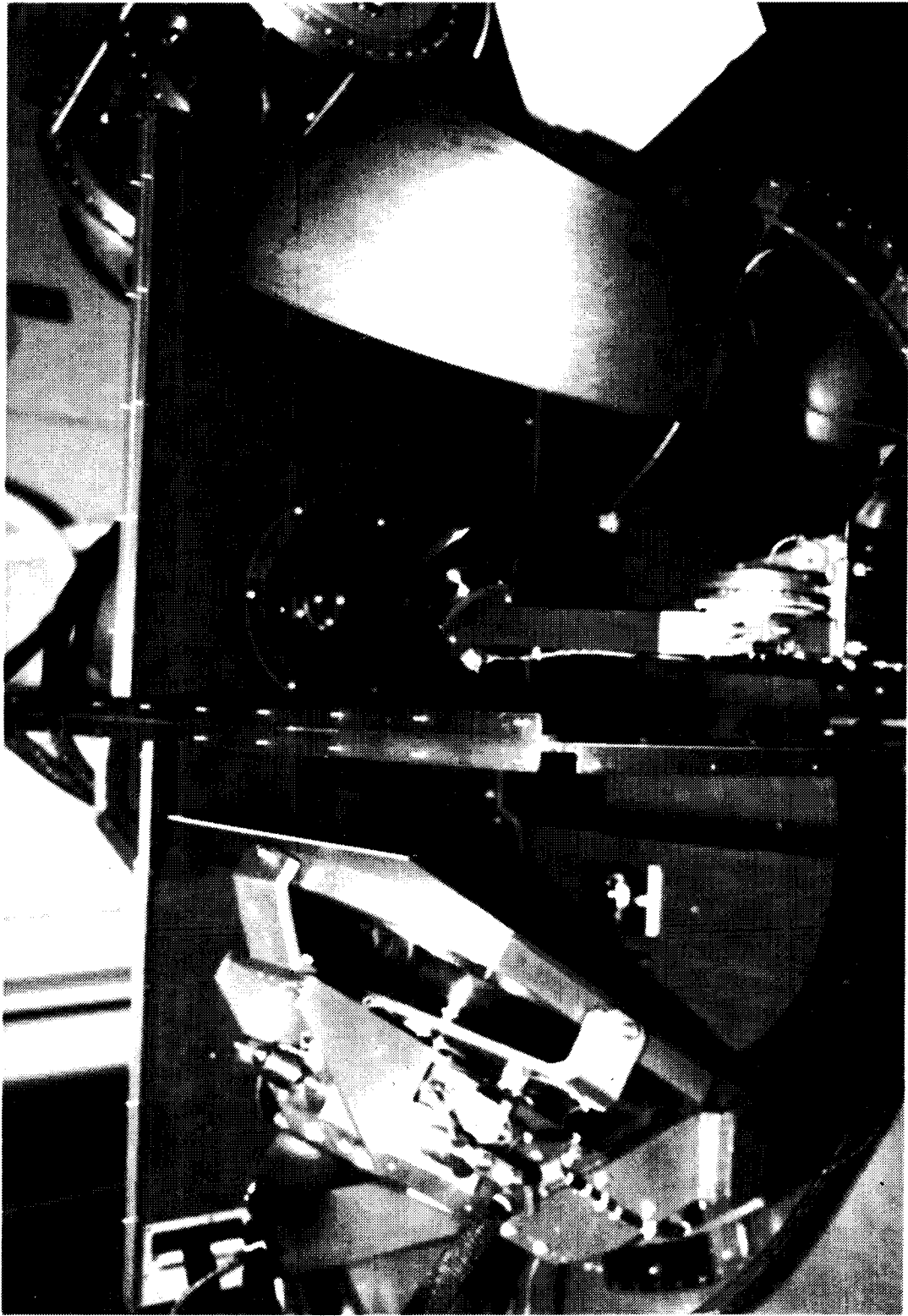


Figure 22. A photograph of the sample mirror in the DEC instrument.

3.5 Absolute Radiometer Module

The absolute radiometer provides absolute measurements of the beam band radiance into the DIRBE from the DEC instrument. To achieve these measurements the AR was designed to match the DIRBE field-of-view and remain independent of the DEC geometry.

Measurements from the Absolute Radiometer are achieved when the DEC sampling mirror is inserted into the DEC light beam thereby directing the center 25% of the beam into the absolute radiometer for measurements (see Figure 1).

The module is made up of a collecting (primary) mirror, folding (secondary) mirror, filter wheel assembly, vibrating reed light chopper, parabolic cone condenser, and bolometer detector/preamplifier sub-module. These components of the assembly are described below.

3.5.1 Collecting (Primary) Mirror

In operation, energy from the main light beam is diverted to the collecting mirror by the sample mirror. The collecting mirror has a focal length of 12.5" and collects the light from the sample mirror, focuses and directs it back along the optical axis to the folding (secondary) mirror. Table 10 includes the specifications for the collecting mirror and Figure 23 details the mirror.

3.5.2 Folding (Secondary) Mirror

Light from the collecting mirror falls upon the folding mirror, which is placed well ahead of the collecting mirror focal plane, and is diverted along the optical axis of the filter wheel and chopper, to the condensing cone and bolometer detector. The folding mirror is an optical flat, its specifications are also included in Table 10. Figure 24 details the mirror.

3.5.3 Absolute Radiometer Filter Wheel

Energy diverted to the absolute radiometer bolometer detector passes first through the Absolute Radiometer Filter

Wheel as shown in Figure 1. This filter wheel is identical in mechanical design to the other wheels in the DEC system. It holds 10 band-defining filters and 4 polarizers which were provided for this application by NASA. The 10 filters match the wavelengths in the 10 DIRBE bands. In addition to the filters and polarizers some of the filter wheel positions are open or opaque. Table 11 defines the filters/polarizers vs. wheel position for the absolute radiometer filter wheel. Position control for the wheel is via the Command and Monitor Unit.

3.5.4 Chopper

The absolute radiometer light chopper is a 2-blade, vibrating reed-type chopper. It operates at 25 Hz. It is incorporated in the absolute radiometer in order to accommodate signal processing techniques which largely eliminate errors due to DC drift and inherent preamp noise. The chopper is designed to operate from ambient to cryogenic temperatures. Table 12 contains additional details concerning the chopper.

3.5.5 Condensing Cone

The condensing cone provides for efficient coupling of incoming energy from the chopper to the bolometer detector. It is used to minimize the area of the bolometer detector and thus maximize detector NEP. The cones are described further in Table 12.

3.5.6 Bolometer Detector/Preamplifier Submodule

The absolute radiometer detector/preamplifier sub-module contains a Class A bolometer with its associated load resistor and JFET. The detector DC level is preserved and monitored along with the chopped, rectified and filtered signal from the bolometer detector. The preamplifier associated with the detector is connected in the source follower mode, and thus provides the impedance transformation required to interface the high impedance bolometer to the signal conditioning amplifier

which is located outside of the instrument test dewar.

The detector/preamp submodule includes a sensitive temperature sensor which operates in the 1.5 to 5°K range. This device provides a backup to the bolometer for indications of the submodule temperature.

The configuration of the Absolute Radiometer Module is shown in Figure 25. It should be noted that the detector/preamplifier sub-module is thermally isolated from the main Absolute Radiometer structure and is heat sunked separately to insure an operational temperature of approximately 1.8°K.

The design of the AR is based on the following requirements:

- 1.) Calibration - Independent of DEC geometry
- 2.) Ability to interface with USU point and extended calibration sources
- 3.) Self-contained
- 4.) Uniform field-of-view.

In the diffuse source mode, independence from the DEC geometry is provided by making the AR collector both the limiting aperture and field stop in the system. In this mode, the calibration of the AR is related to the DEC in terms of beam sterance [radiance] (W/cm^2 sr).

In the point source mode, the AR collector is still the limiting aperture stop in the system, but is not being overfilled by the DEC beam. Therefore, in this case the calibration of the AR is related to the DEC in terms of areance [irradiance] (W/cm^2).

Calibration of the AR is performed by installing the self-contained radiometer module into a test dewar and interfacing it first to the USU extended-area source calibration unit and then to the USU cold collimator unit. Data from these two series of tests are then combined to generate the calibration transfer functions.

Field-of-view uniformity is an important design parameter because of its relationship to the uncertainty of the calibration equations. Field-of-view uniformity is determined by the spatial

uniformity of the responsivity of the detector/condensing cone coupling, the convolution of the blur circle with the field stop, and the convolution of the field stop with the chopper aperture.

A figure of merit for the blur circle factor is the ratio of the field stop diameter to blur circle diameter. In the case of the AR this ratio is $6/0.064 = 93.8$. A typical ratio of 10 for this figure of merit is a good minimum.

A vibrating reed chopper generates a modulated signal having various degrees of non-symmetry from zero to some maximum value as a point source image is moved about within the bounds of the field stop. These spatially related variations cause variations in the apparent gain of the signal conditioning amplifier. The results of these gain variations are the presence of undulations in the field-of-view response curve. A figure of merit for this chopping factor is the ratio (RC) of the signal on-time to signal off-time, given by:

$$RC = (2AT - DAP)/(2AT + DAP) = 0.7$$

where

AT = Amplitude of the chopper tines (MAX) = 19mm

DAP = Diameter of the field stop aperture = 6mm

Empirical measurements of the effect of non-symmetry as related to RC have demonstrated that for RC = 0.7 the gain errors are less than or equal to 4.5%.

Specifications for the Absolute Radiometer are included in Table 12. In Figure 25 (top view) the light path from the collecting mirror to the detector/preamp subassembly has been added for clarity.

Figure 26 shows the absolute radiometer installed in the DEC instrument. Particularly well shown in the photo is the module's filter wheel and position monitors. A temperature sensor is mounted slightly to the left of the wheel axle.

Table 10
Collecting and Folding Mirror Specifications
Absolute Radiometer

Parameter	Collecting Mirror Value	Folding Mirror Value
Material	Aluminum	Aluminum
Size	4.5 inches (Dia)	1.766 inches Major Axis 1.250 inches Minor Axis
Coating	Nickel	Nickel
Figure	Gold Electroplate $\lambda/4$ at 0.633 μm (spherical)	Gold Electroplate $\lambda/4$ at 0.633 μm (flat)
RMS Surface Roughness	<60Å	<60Å
Focal Length	12.5 \pm 0.05 inches	N/A
Clear Aperture Edge Effects	<0.005 inches	<0.005 inches

Table 11
Absolute Radiometer Filter Wheel - Filter vs. Wheel Position

Wheel Position	Filter	Wheel Position	Filter
1	Opaque	10	Band 9
2	Band 1	11	Band 10
3	Band 2	12	0° Polarizer
4	Band 3	13	45° Polarizer
5	Band 4	14	90° Polarizer
6	Band 5	15	135° Polarizer
7	Band 6	16	Open
8	Band 7	17	Open
9	Band 8	18	Open

Appendix A contains filter specifications for Bands 1-10.

Table 12
Absolute Radiometer Specifications

Item	Detail	Parameter
Collector		
	Clear Aperture	10.6 cm
	F Number	3.25
	Focal Length	34.4 cm
	Blur Circle	0.064 mm
Folding Mirror		
	Diameter	3.18 cm
	Obscuration	9%
Chopper		
	At Rest Aperture	3 mm
	Maximum Aperture	19 mm
	Blade Width	11 mm
	Frequency	25 Hz
Filter Wheel		
	Apertures	18
Condensing Cone		
	Entrance Aperture	6 mm
	Exit Aperture	1 mm
	F Number	3.0
Detector/Preamp		
	Detector	1.75 mm (octagonal)
Operating Temperature 1.8°K		
	Calibrated Temperature Range	1.5 to 3.0°K
	Responsivity	1 - 2 x 10 ⁶ V/W
	NEP (20Hz, 1 sec)	9 x 10 ⁻¹⁵ Watts (1σ)
	V (Noise) (20Hz)	2.48 x 10 ⁻⁸ V/Hz ^{1/2}
AR System		
	Effective Aperture	88.24 cm ²
	Field-of-View (Full)	0.938° (2.105 x 10 ⁻⁴ sr)

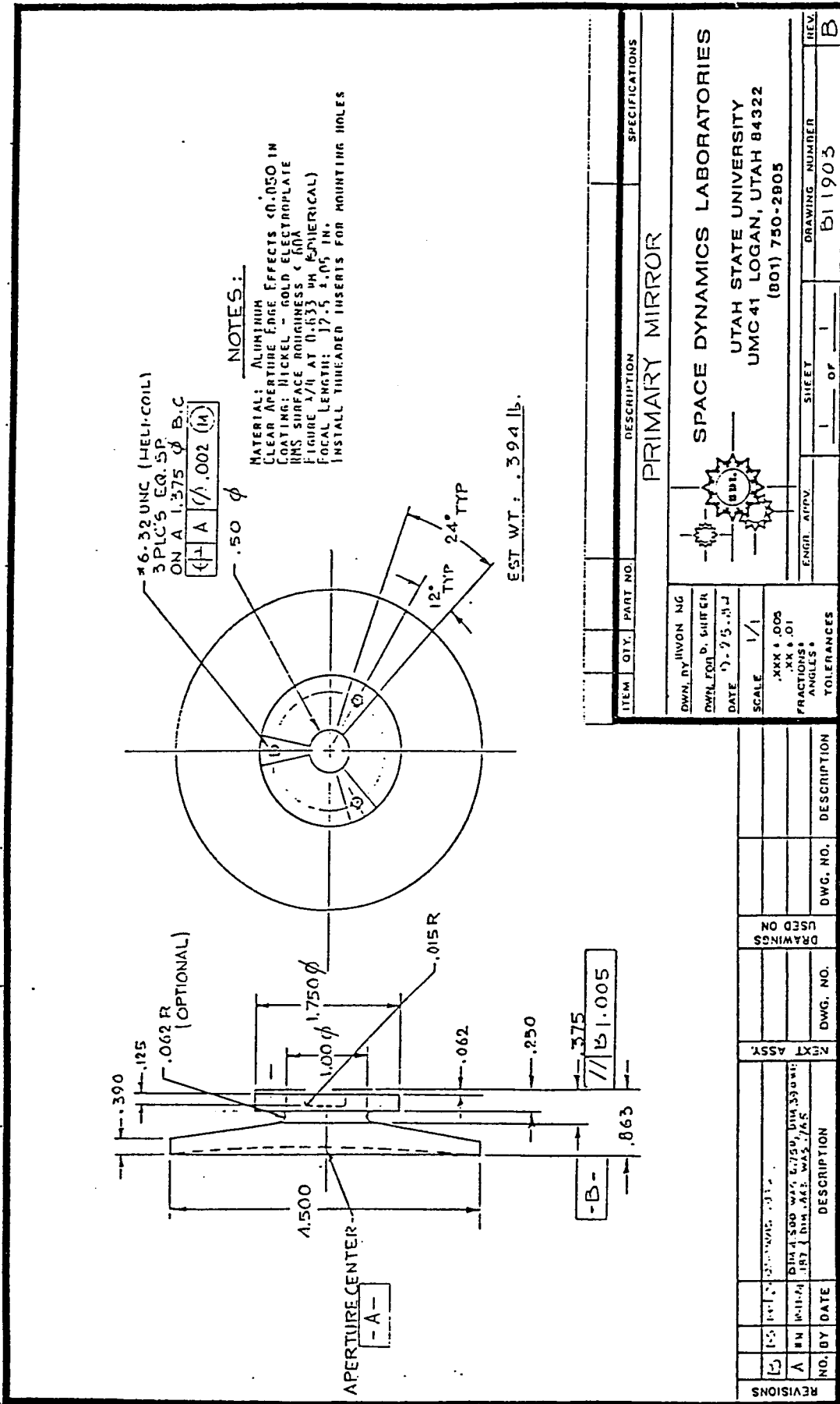
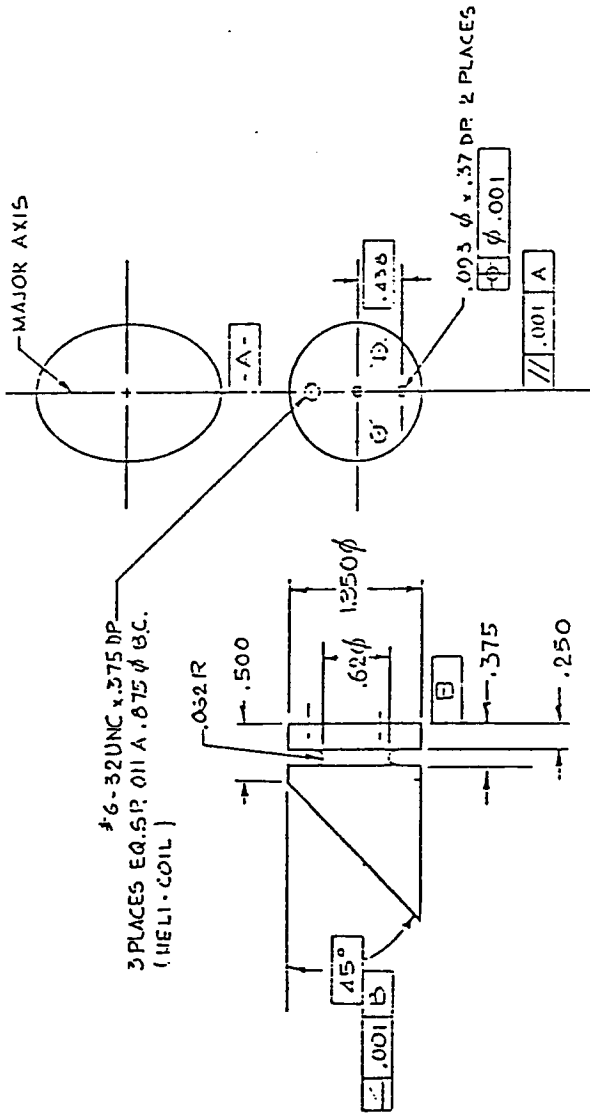


Figure 23: Mechanical details of the absolute radiometer collecting (primary) mirror.

FOR THIS PART BY
OR FOUR QUANTITY



NOTES

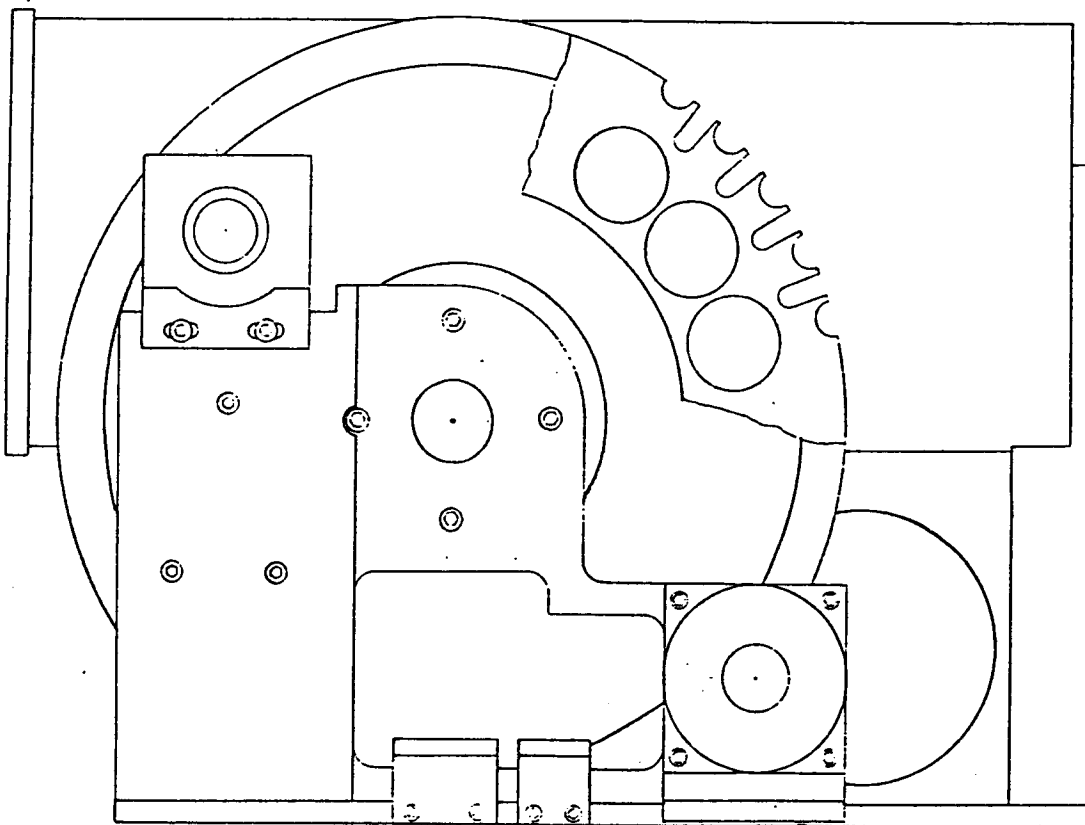
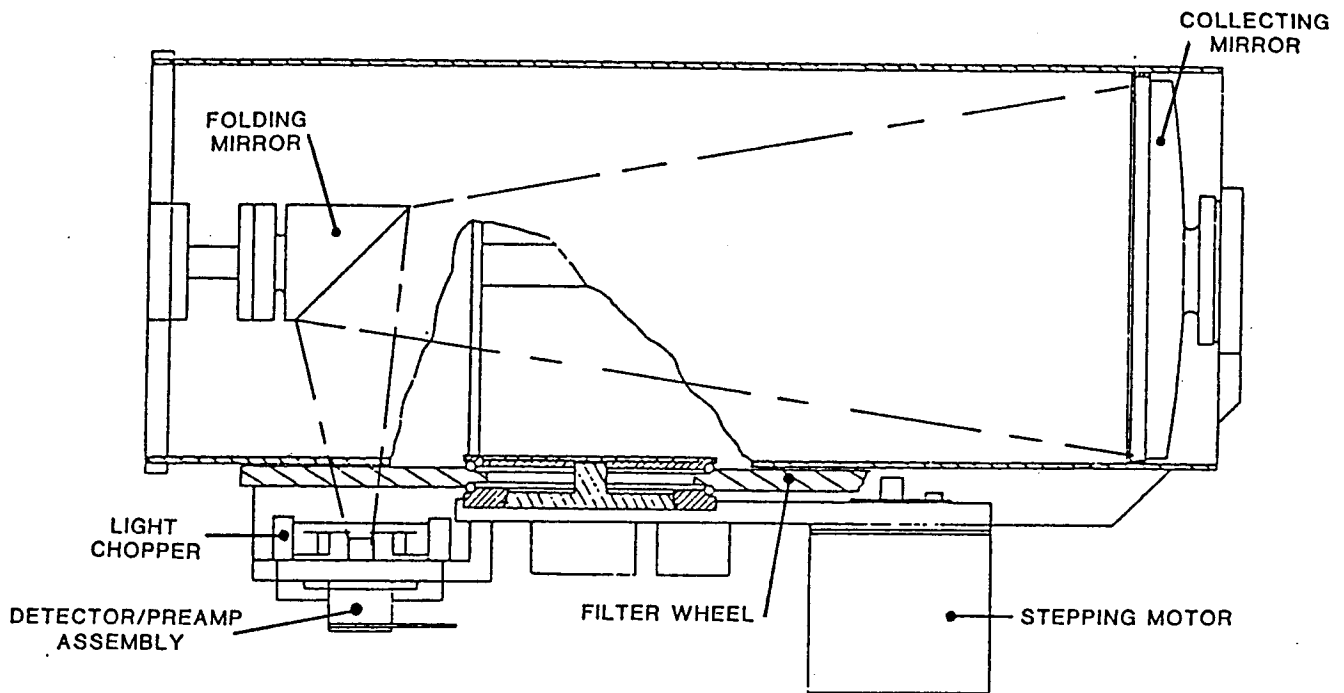
MATERIAL: ALUMINUM
CLEAR APERTURE EDGE EFFECTS < 0.050 IN.
COATING: NICKEL - GOLD ELECTROPLATE
RMS SURFACE ROUGHNESS < 100A
FIGURE 1/4 AT 0.633 μ M (FLAT)
INSTALL THREADED INSERTS FOR MOUNTING HOLES

EST. WT. .108 lb.

NO.	BY	DATE	DESCRIPTION	DWG. NO. 1	DWG. NO.	DESCRIPTION
1	D.S.	12/1	REVISED TO .075 DIA. HELI-COIL			

ITEM	QTY.	PART NO.	DESCRIPTION	SPECIFICATIONS
SECONDARY MIRROR				
SPACE DYNAMICS LABORATORIES UTAH STATE UNIVERSITY UMC 41 LOGAN, UTAH 84322 (801) 750-2905				
DWN. BY UM011 HIG.			ENGR. APPV. _____	
DWG. FOR D. SWABER			SHEET 1 OF 1	
DATE 9-25-64			DRAWING NUMBER B11904	
SCALE 1/1			REV. D	
XXX .005				
XX .01				
FRACTIONS				
ANGLES				
TOLERANCES				

Figure 24. Mechanical details of the absolute radiometer folding (secondary) mirror.



CSE DRAWING #E3-0175

Figure 25. Absolute radiometer configuration.



Figure 26. A photograph of the absolute radiometer mounted in the DEC instrument.

3.6 Full-Time Monitor Module

The Full-Time Monitor Module interfaces with the second integrating sphere as shown in Figure 1, and samples the power scattered from a portion of the sphere wall. The power measured is related to the flux density from the sphere wall. Thus, the module provides for continuous measurements of the relative DEC output beam band power.

The full-time monitor consists of a condensing cone, a chopper, and bolometer detector/preamp submodule with remotely located signal conditioning amplifiers and a temperature sensor which operates in the 1.5 to 5°K range. The full-time monitor chopper, bolometer detector/preamplifier assembly is identical to that of the absolute radiometer.

3.7 DEC Temperature Monitors

The DEC assembly incorporates temperature sensors in various locations to monitor important system temperatures and ascertain that the assembly is properly cooled to cryogenic operational temperatures. A total of eleven sensors are included as detailed in Table 13.

As noted in the Table, germanium resistor temperature sensors are used in the Absolute Radiometer and Full-time monitors. They were calibrated by Lake Shore Cryotronics, Inc., from 1.4 to 6°K. Each of these sensors has a look-up table in the Control and Monitor Unit STD buss to give the temperature in degrees Kelvin.

All of the other temperature sensors in DEC are Lake Shore silicon diode sensors. We purchased these as a matched set ($\pm 0.1^\circ\text{K}$ at 4.2°K , $\pm 1^\circ\text{K}$ at 77°K , and $\pm 1^\circ\text{K}$ at 300°K). One of the sensors was calibrated by Lake Shore Cryotronics, Inc., from 1.4°K to 330°K . This calibration curve is used in the STD buss to convert the voltage to temperature in degrees Kelvin.

The silicon diode sensors have a change in sensitivity at approximately 25°K , and another small change below 4.2°K . These changes are not repeatable between sensors to the accuracy NASA-GSFC personnel felt was desirable, so, to improve accuracy, USU set up a calibration test for the silicon sensors. The sensors were mounted together on a large copper block and were placed in a cryogenic dewar. We measured the temperature being read out from the STD buss system vs. the actual temperature. From these data curves were generated which showed the error vs. temperature. We used straight lines over smaller temperature ranges to approximate the errors. Some software was added in the SDL Primitives on the PC (CMU) to make these corrections to the temperatures before passing the results on to the user software.

The calibrations on the temperature sensors have been provided previously to NASA GSFC under separate cover and therefore they are not included again in this report.

Table 13
DEC Temperature Sensors

Sensor	Type	Location
Integrating sphere module	Silicon diode	Mounting flange of sphere no. 1 (see Figure 11)
Large Area Source	Silicon diode	Throat of source (see Figure 5)
Collimating Mirror	Silicon diode	Back of mirror mount (see Figure 16)
Beam Sample Mirror	Silicon diode	Back of mirror mount (see Figure 22)
Pointing Mirror	Silicon diode	Back of crossbar on inner gimbal
Absolute Radiometer Module	Silicon diode	Back of chopper mount near bolometer (see Figure 26)
Absolute Radiometer Detector	Germanium	Back of bolometer mounting block
Full-time Monitor Detector	Germanium	Back of bolometer mounting block
Baseplate No. 1	Silicon diode	Baseplate in integrating sphere module (see Figure 11)
Baseplate No. 2	Silicon diode	Baseplate in absolute radiometer module (see Figure 26)
Baseplate No. 3	Silicon diode	Baseplate between DEC beam exit port and collimating mirror (see Figure 22)

3.8 Internal Surface Treatment

It was necessary to treat the internal surfaces of the DEC assembly to provide for absorption of stray radiation and avoid the possibility of contaminating the output signal from such sources. The design goal was to have a one-bounce absorbing material as the internal coating. Figure 27 shows the photometric reflectance spectra of six optical-black coatings. The specular reflectance at 6° incidence angle was measured with a detector that subtended 9.02×10^{-4} sr at the substrate. The principal absorption bands of amorphous silicate material are shown schematically in the lower left corner. Coating roughness and thickness are given in parentheses (σ, d) with each curve. These data were taken from Smith,¹

The Cornell coating is essentially identical to the 3M BV (black velvet) coating with the addition of grit to increase absorption. However, the 3M BV coating is no longer available, hence, both of these coatings were inappropriate. Access to the IITRI, Martin, and LMSC coatings was extremely difficult. As a result, the coating used on the interior of the DEC instrument was a composite made up of Chemglaze Z306 with the addition of silicon carbide grit (#180). A Chemglaze primer (#9924) was applied, then the Chemglaze Z306 was applied, coated with the silicon carbide grit, and then lightly repainted with the Chemglaze to reblacken the surface. After application, the coating was allowed to cure in an environmentally controlled enclosure at -100°F for several days.

1. Smith, S.M., *Specular reflectance of optical-black coatings in the far infrared*, Applied Optics, 23, 2311, 15 July 1984.

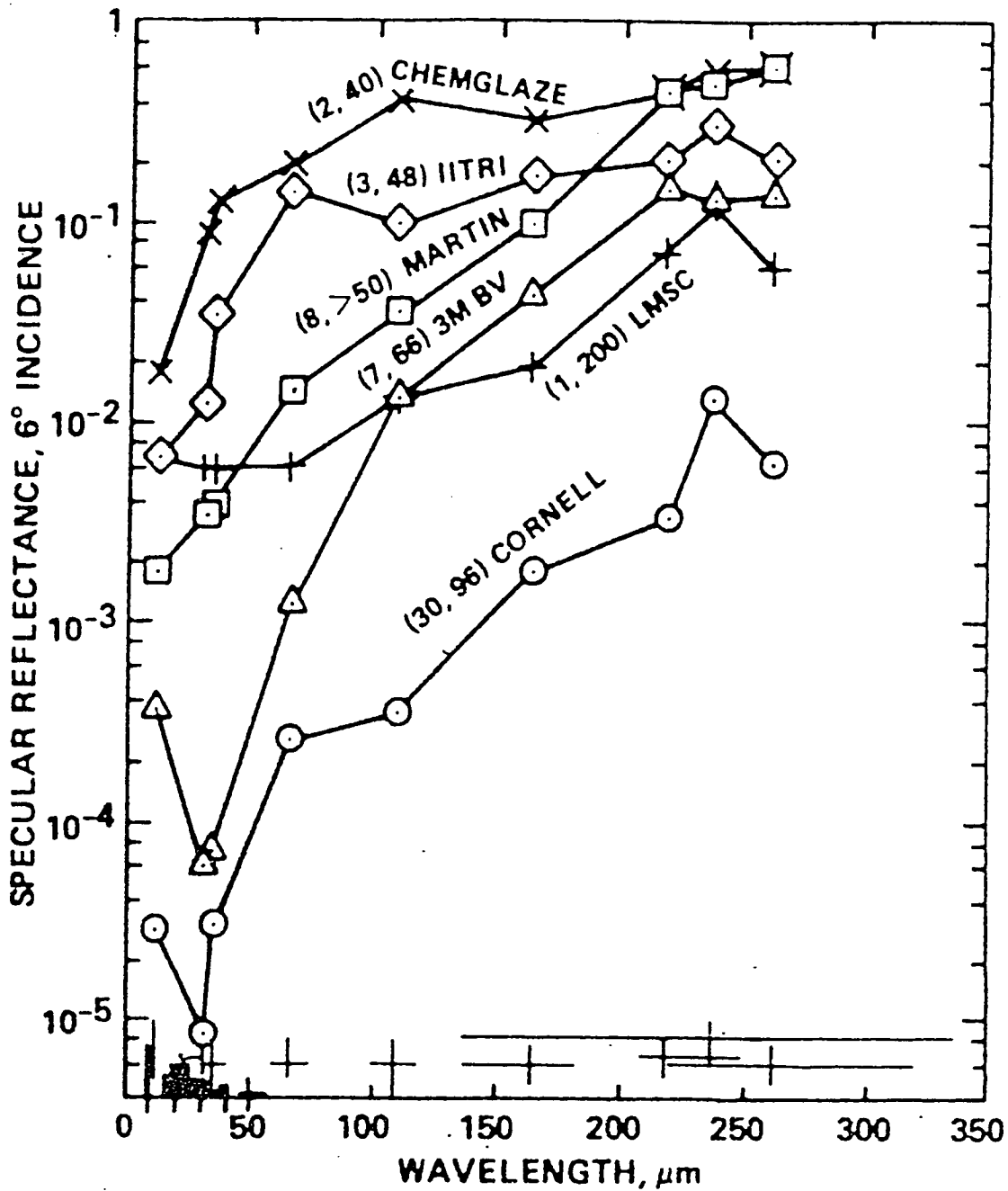


Figure 27. Photometric reflectance spectra of six optical-black coatings. (From Smith¹)

3.9 Control and Monitor Unit

The Control and Monitor Unit (CMU) allows an IBM PC to control and monitor all of the functions of the DEC. These functions include positioning and monitoring the position of the four wheels in the system, positioning the Beam Sample Mirror and monitoring its position, and positioning the Pointing Mirror to steer the angle of the output beam into DIRBE and monitoring the mirror's position. Also controlled are the level of the 5 IR sources at integrating sphere no. 1, control of choppers in the Absolute Radiometer and Full-time Monitor, control of LVDTs, preamp batteries, and bias batteries. The CMU monitors temperatures, beam angle, beam intensity, wheel positions, Beam sample mirror position, battery voltages and power being sent to each source in the system.

During the design stage of the DEC, one of the objectives was to provide flexibility to monitor and command in any order. With this objective in mind, the system has been designed to handle requests for data and commands in a serial fashion. Each request for data causes the data to be sampled and converted to the units to return to the user. A status is also returned from each data request to indicate if the data is valid, or if problems were encountered in obtaining the result. All commands sent to the CMU are completed before the status is returned to the user, with the exception of the Large Area IR source temperature set command. This command sets the desired new temperature in the processor, and then control returns to the user while the temperature is being changed to the new level. This allows the user to monitor the temperature and set other mechanisms for the next phase of the test. Appendices B and C contain the description of the CMU and discuss the operation of the unit, including definitions of interface variables used to send commands or request data, and definitions of status error codes. The user should also be aware that a number of manuals and documents have been delivered to NASA and these give details which cannot practically be included here. These include copies

of the operations manuals for all commercial boards used in the STD BUSS, temperature sensor calibrations, bolometer manuals, wire lists, schematics and parts lists of boards built by USU, and software listings.

This page intentionally left blank.

4 . TESTING AND RESULTS

4 . 1 Preliminary Testing

For testing of the DEC instrument, USU designed and fabricated a cryogenic dewar to house and cool the assembly, thereby simulating the cooling that would normally occur when the DEC and DIRBE are mounted in the instrument test dewar. Figure 28 is a photograph of the finished and closed dewar attached to vacuum pumps at USU. An assembly drawing of the dewar is included as Figure 29. Figure 30 illustrates the dewar with the top cover removed and the DEC instrument in place (the DEC top cover is removed in the photograph).

Preliminary thermal testing indicated two problems, i.e., (1) the test dewar cold-finger, the large flat plate shown in Figure 31, could not be maintained at a cold enough temperature when thermal energy was introduced in amounts comparable to those predicted for DEC; and (2) those modules in DEC that consumed energy (motors and optical sources) produced temperatures higher than could be tolerated within the unit.

This problem was solved by including copper heat straps in both the dewar and the DEC instrument itself. The dewar was provided with copper pads mounted on the cold finger to interface with the DEC feet. These pads can be seen as the larger, stepped copper blocks (3) in Figure 31. Each pad was put into thermal contact with the liquid helium contained within the dewar by soldering copper straps to the pads and allowing the straps to extend to the bottom of the helium vessel as shown in Figure 29. This provided a direct, high thermal conductance path directly to the DEC feet.

The DEC baseplate was inlaid with copper straps that provided low thermal resistance from each heat producing module to the copper pads. In addition, the copper conduction paths within the DEC instrument were extended to enable motors to be directly mounted to the copper. Figure 32 illustrates this approach for the pointing mirror module. As can be seen in the

Figure, both of the pointing mirror drive motors are mounted to the copper straps which then connect with the base inlay that interfaces with the pads on the cold finger.

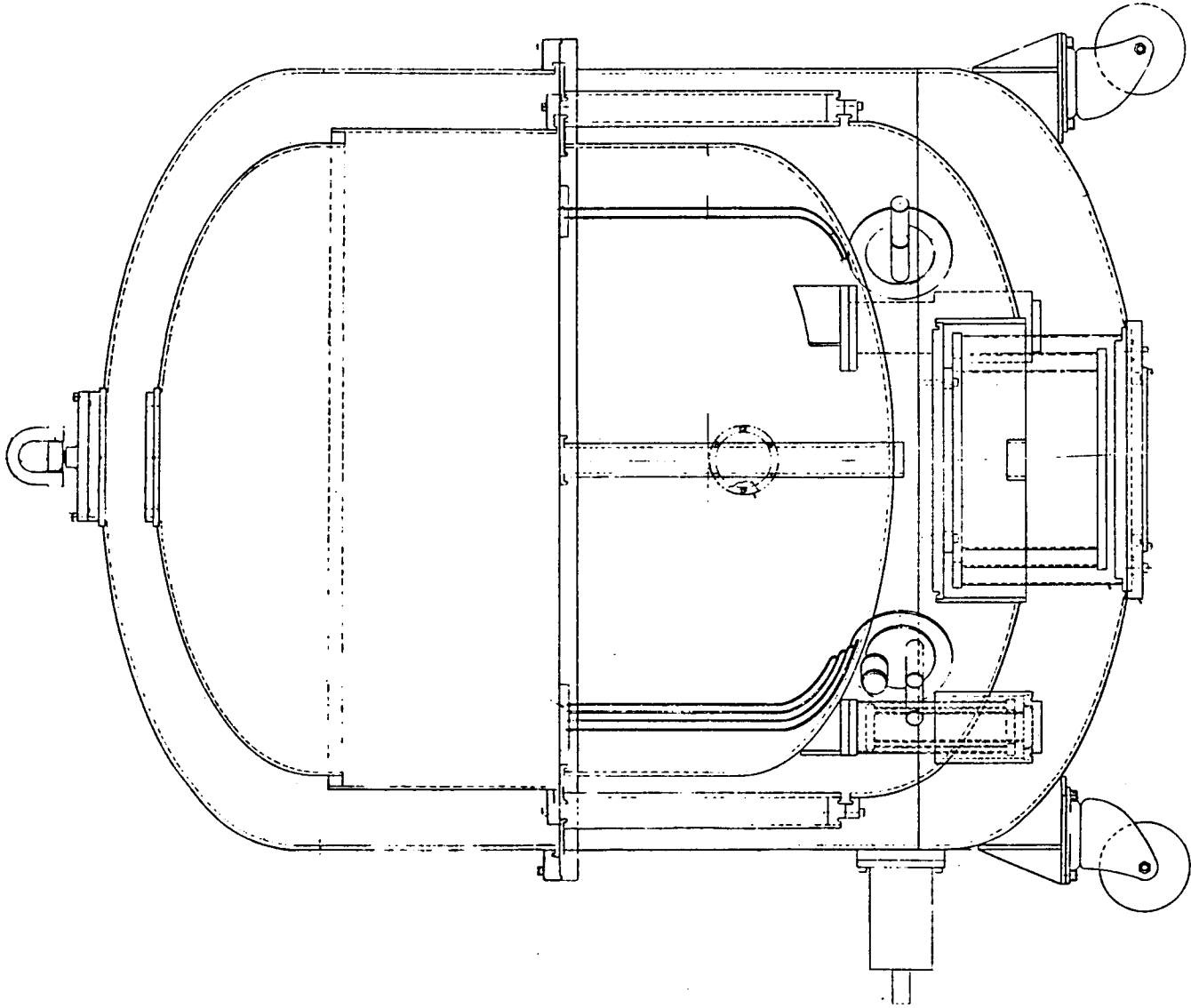
In addition, the bolometers in both the full-time monitor and the absolute radiometer were provided with low resistance thermal paths to the cold finger by attaching copper straps to the bolometer mountings. These copper paths directly exit the DEC enclosure through copper contacts placed in thin stainless-steel disks mounted in the side walls of the DEC. Additional (external) copper straps run down to the smaller copper pads on the dewar cold finger (see Figure 31) and are attached there. As with the larger pads, which interface with the mounting feet, these smaller pads are also placed in direct contact with the liquid helium by copper straps internal to the test dewar (see Figure 29).

The second problem encountered during the preliminary testing was that of an excessive radiant background in the DEC beam. This resulted from two factors, i.e., 1.) optical leaks between the integrating spheres module and the downstream part of the system, and 2.) scattered radiation actually entering sphere no. 2 and thence adding this unwanted component to the output from the sphere. The problem was more severe when the smallest aperture in the aperture wheel was utilized (or when the aperture wheel was in the closed position) since in that condition, the ratio of energy in the first sphere to the second sphere is largest. Only the first part of this problem was recognized prior to the delivery of DEC. A baffle placed around the double cone eliminated the first part of the problem by trapping and absorbing the stray energy and sealing it within the integrating sphere module compartment, thus eliminating it from the general volume of DEC. The second part of the background problem was not dealt with at USU, but GSFC personnel have made some modifications to reduce its effects.



Figure 28. A photograph of the DEC test dewar attached to vacuum pumps at USU.

ORIGINAL PAGE IS
OF POOR QUALITY



DATE	12/15/53
BY	W. H. ...
DEWAR ASSY. DRAWING	21252
SPENCE BYNUMBERS LABORATORIES	
STATE STATE UNIVERSITY	
MADISON, WISCONSIN	
MADISON 6, WISCONSIN	

Figure 29. An assembly drawing of the DEC test dewar.

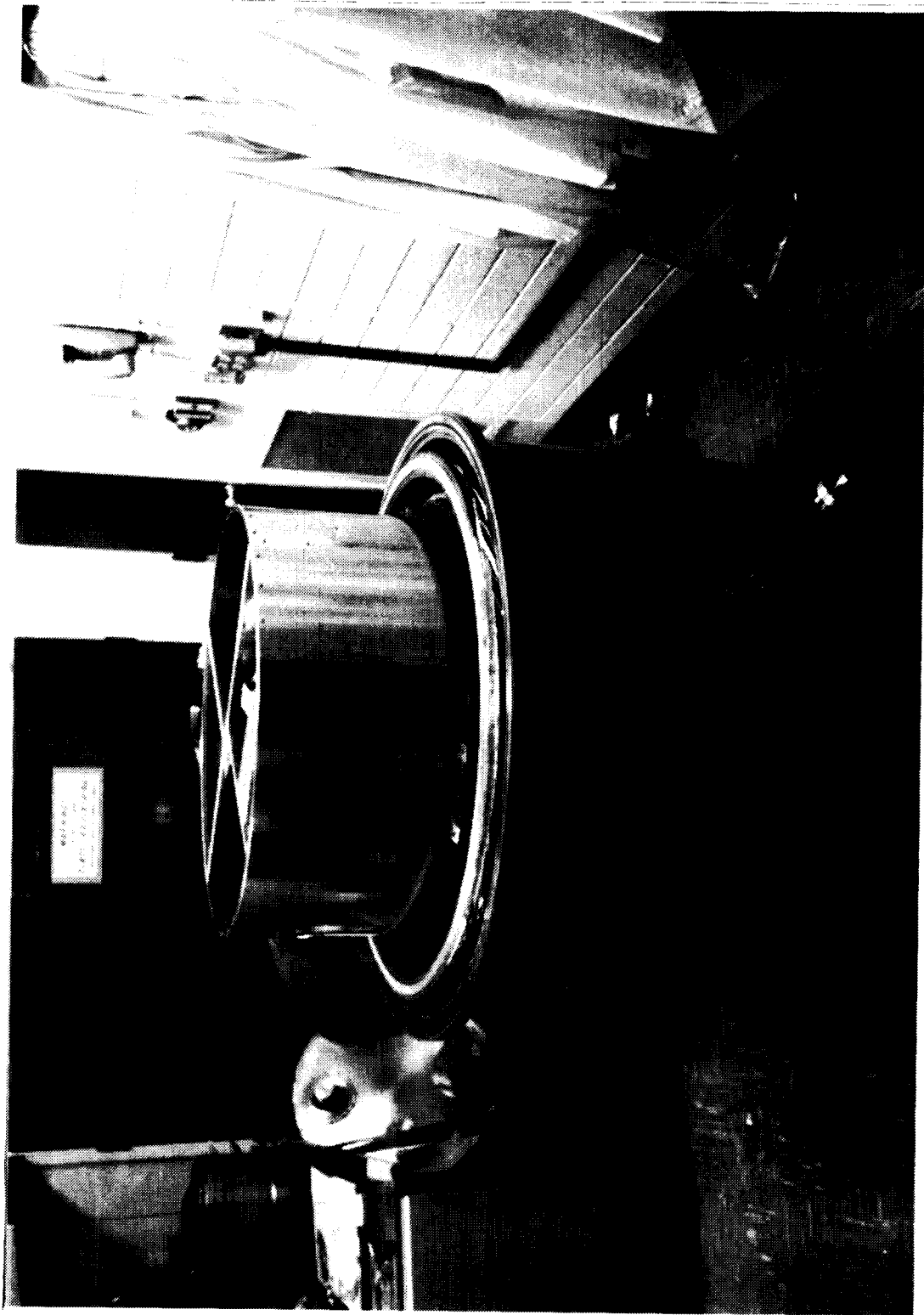


Figure 30. A photograph of the DEC test dewar with top cover removed and the DEC instrument in place. The top cover plate of DEC is removed in this photograph.

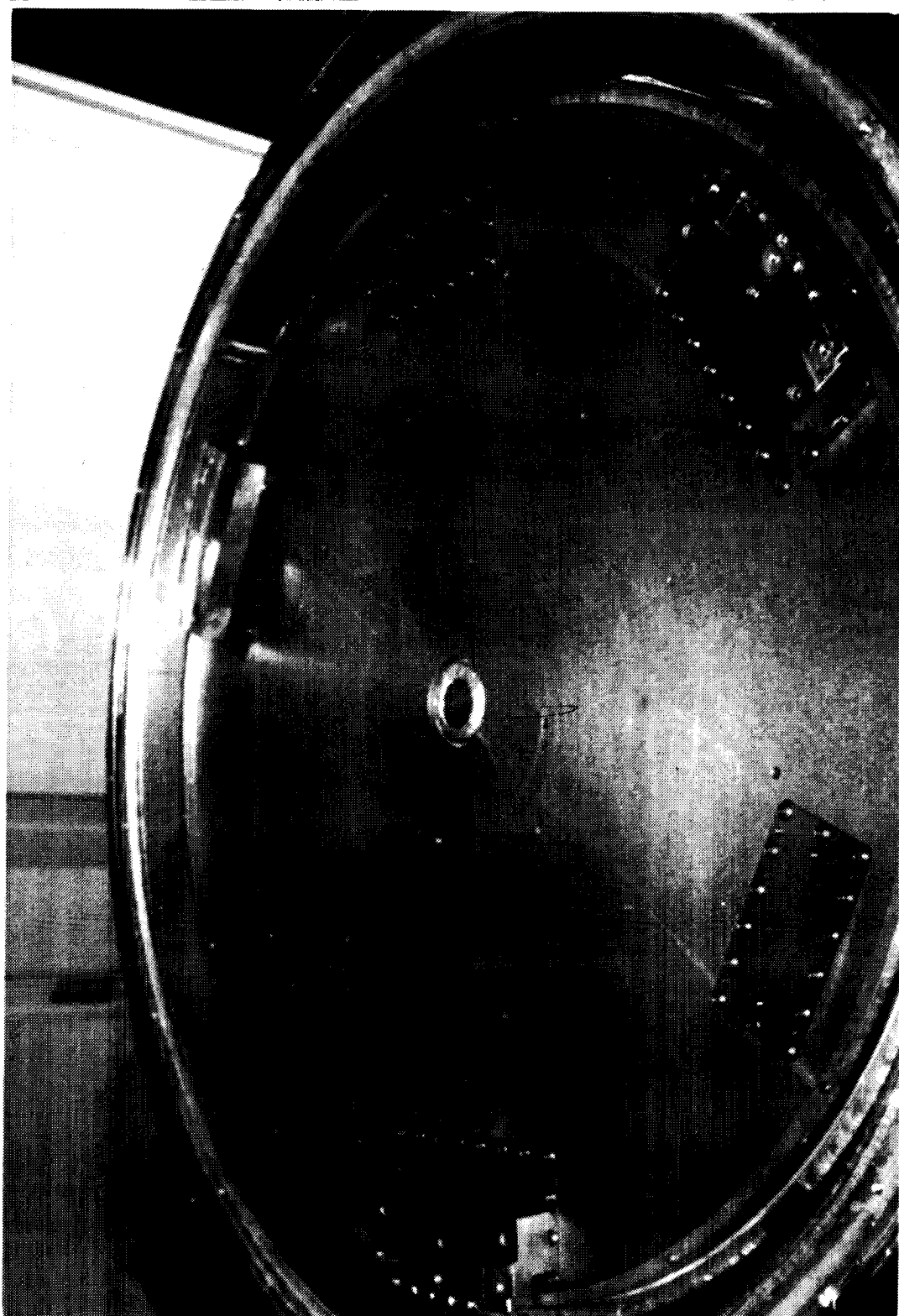


Figure 31. A photograph of the DEC test dewar showing the cold finger with copper inserts for cooling.

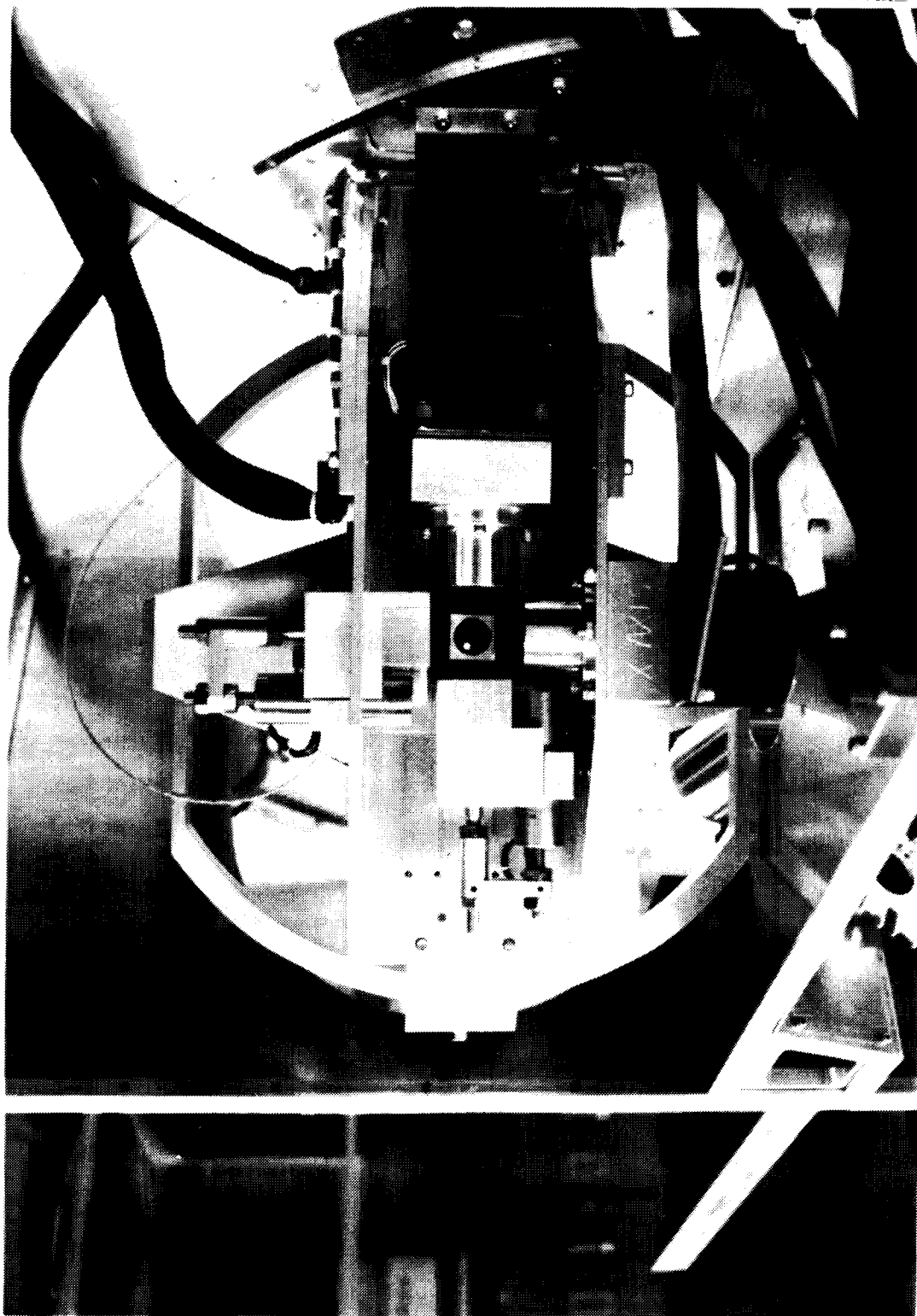


Figure 32. A photograph of the DEC pointing mirror showing the copper straps and inlays for cooling the pointing mirror X- and Y-axis motors.

4.2 Source Stability Tests

As discussed previously, Chicago Miniature Lamps with and without the glass envelopes were proposed for use as blackbody simulators in the first integrating sphere. The source stability was the subject of a Master of Science thesis entitled

Blackbody Source Evaluation Utilizing a Comparitor Radiometer, by Hasan Niaz, Utah State University, 1984.

The thesis is included in its entirety as Appendix D in this report, and deals primarily with the development of the comparitor radiometer. The results of the source tests were reported in the September 1984 Monthly Technical and Schedule progress Report as shown in Table 14.

TABLE 14
Summary of Lamp Performance

Parameter	Value
Lamp long-term stability (3.5 hrs)	0.75°C
Lamp short-term stability (<5 sec)	0.25°C
Short Term repeatability (rms)	0.32
Primary voltage 10%	No change
Temperature range 0° to 75°F	No change
Reference source at	T = 900°K
Detector peak response at	$\lambda = 3.22 \mu\text{m}$
Detector bandwidth	$\Delta\lambda = 1.4 \mu\text{m}$

4.3 Photometer Calibration

A photometer was utilized to measure the beam uniformity in the point source mode using a 2-cm diameter sample area. At the request of NASA personnel the spot diameter was reduced to 0.5 cm to increase the resolution. Beam uniformity depends upon the gold reflectivity in the spheres and exit cones, therefore, it is necessary to make the measurements above $0.75 \mu\text{m}$. A GaAs Hamamatsu multiplier phototube, type R636 was chosen for this measurement because of its uniform response in the $0.75 \mu\text{m}$ to $0.9 \mu\text{m}$ region. Calculations indicated that a 1000 Watt tungsten-halogen lamp (mounted in place of the large-area source at sphere #1) would provide adequate signal-to-noise ratio.

The photometer was designed with a replaceable field stop. With a small field stop the full-angle field-of-view is 0.2° and is marginally useful for measuring the uniformity of beam divergence (W/sr). The field-of-view is illustrated as a normalized cross section plot in Figure 33.

The field-of-view obtained with the large field stop is over 7° full-angle and is illustrated in Figure 34. The large field-of-view is useful for measuring the beam irradiance (W/cm^2) uniformity. In this case the incident power per unit area can be measured independent of the beam divergence.

The photometer linearity was measured using the USU cold collimator (warm) precision aperture set. Figure 35, is a plot of the merged data with a superimposed linear least squares, best fit equation. The rms error for equally weighted points is 2.03%.

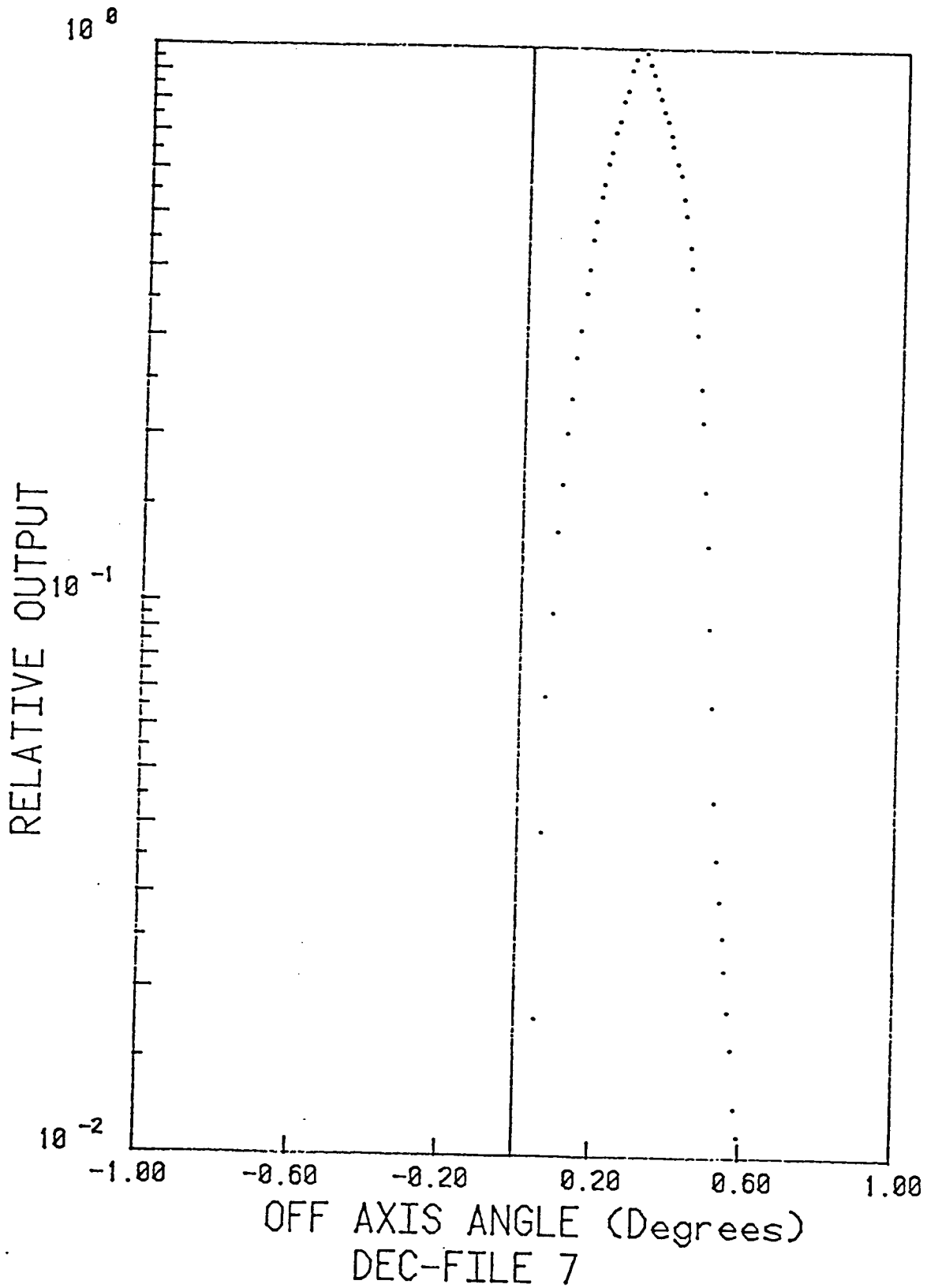


Figure 33. Photometer field of view as a cross-section for the small field stop. The full-angle half-power field of view is approximately 0.2°.

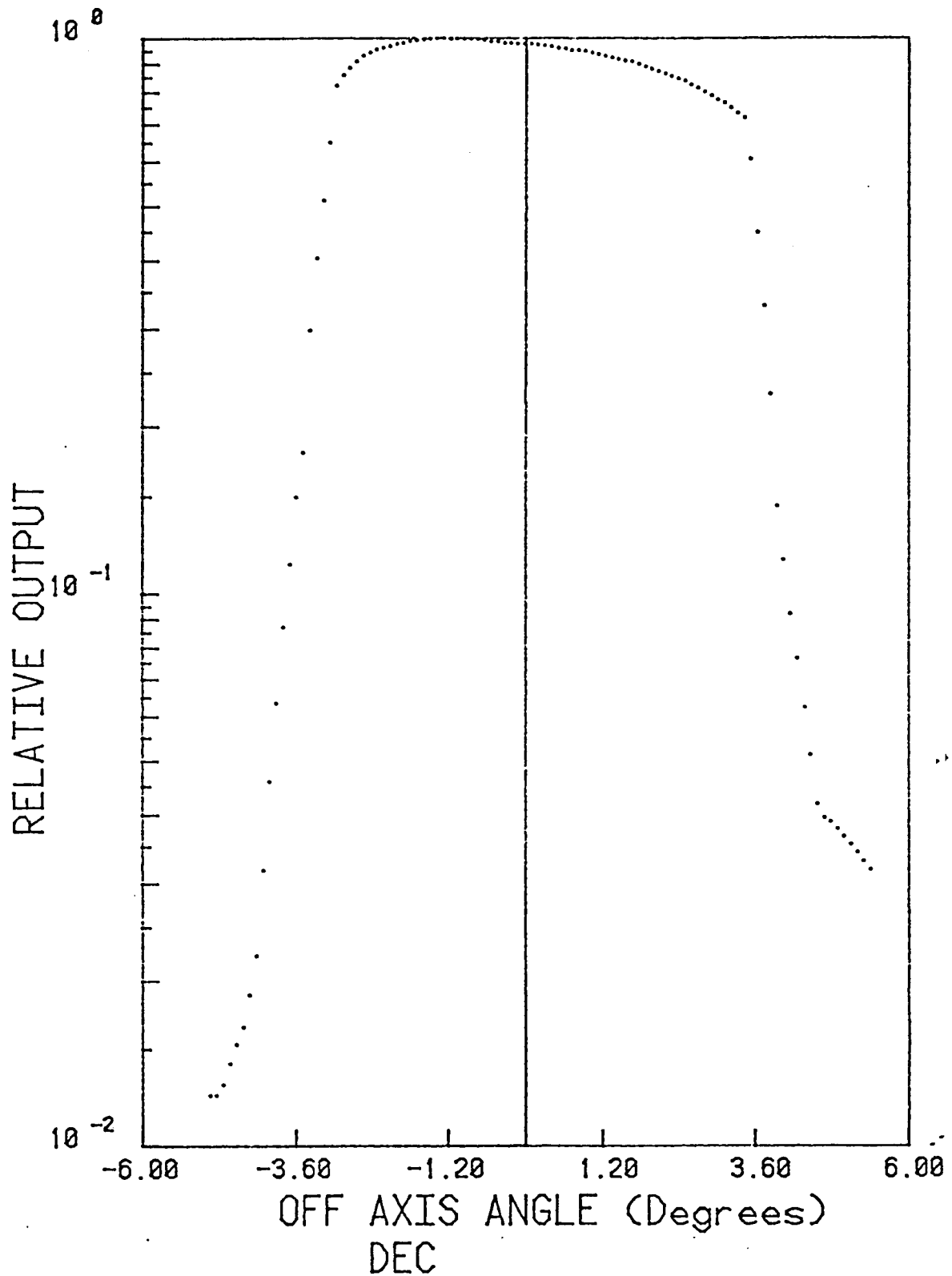


Figure 34. Photometer field of view as a cross-section for the large field stop. The full-angle half-power field of view is approximately 6.5°.

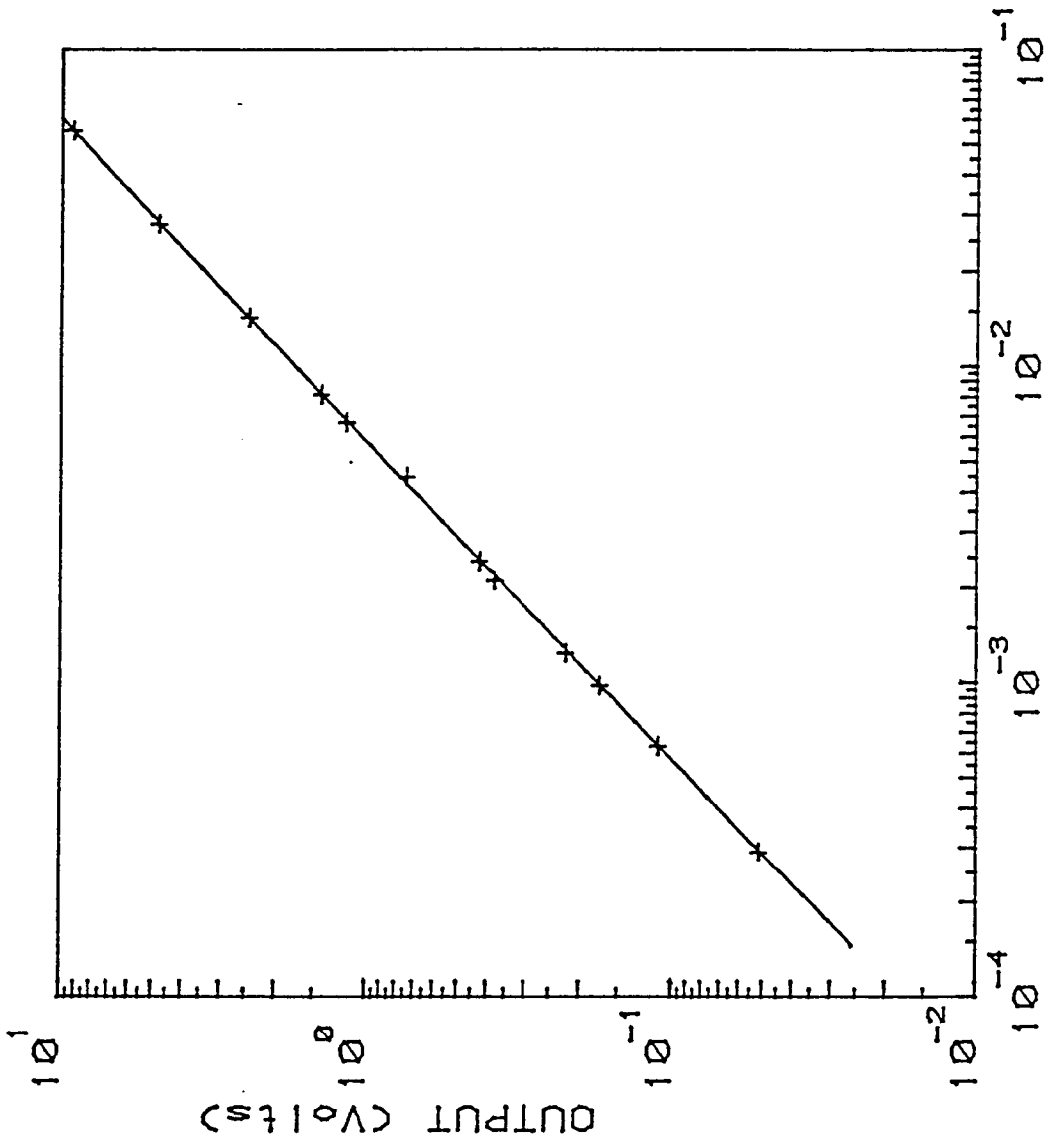


Figure 35. Photometer linearity data. The merged linearity data are plotted with linear least squares best-fit equation super-imposed. The rms error for equally weighted points is 2.03%.

4.4 Beam Uniformity Tests

The beam uniformity tests were initially conducted, in accordance with the contractual requirements, with a circular sample size of 2-cm diameter. In essence these tests provided a highly undersampled scenario and were not a complete verification of the specification on beam uniformity. When it became apparent that the beam exhibited considerable nonuniformity, NASA personnel requested that the resolution be increased by a factor of 4. This was accomplished by reducing the sample diameter to 0.5 cm.

The tests described below, were all taken with the mode select wheel in the point source mode. As previously noted, the mode select wheel contains two point source apertures; the first is "flat" mounted with its normal lying along the collimating mirror central ray, the second is the "canted mode" with its normal canted some 23° with respect to the collimating mirror central ray. the 23° cant provides for uniform beam irradiance (Φ/cm^2) by compensating for the variable distance to the mirror edges (inherent in an off-axis system) by varying projected area.

The first test was conducted on 7 June 1985. The test was designed to measure the areance [irradiance] (W/cm^2) of the beam at a position corresponding roughly to the DIRBE entrance aperture. This was accomplished by supporting the photometer in the beam. The photometer was stepped across the beam both horizontally and vertically in 2-cm increments.

The results for a horizontal scan are given in Figure 36 for the flat mounted point source mode aperture and in Figure 37 for the canted point source mode aperture. Figure 38 provides a vertical scan of the beam with the canted aperture. In all cases the beam exhibits a central bright spot corresponding to the integrating sphere wall as viewed directly through the hole in the exit cones, and a darker surround corresponding to the surface of the cone. The nonuniformity of the skirts in the horizontal scan, appears to overcompensate for the canted aperture. The extent of nonuniformity in the beam probably

precludes drawing any valid conclusions as to the value of the canted aperture.

The second test, conducted on 21 June 1985 was designed to evaluate the performance of the cones independent of the integrating spheres. This test was performed using an IRI Model 463 Radiation Source. The source was rotated and the pointance [intensity] (Φ/sr) measured as a function of off-axis angle. (Note: The edge of the collimating mirror is approximately 15° off axis.) Figures 39 and 40 give the pointance of the blackbody with a 0.785" aperture (full-field divergence of 2.67° (specification $>2^\circ$) which closely simulates the diffuse mode) and with a 0.017 inch aperture (full-field divergence of 0.058° (specification 0.1°) which closely simulates the point source mode) respectively. The blackbody exhibits Lambertian radiation over only a few degrees near the axis; however, the cones should reproduce whatever they see. Figures 41 and 42 give the pointance of the double cone output for the same apertures. Figures 41 and 42 indicate that the cones are imperfect.

The third test, conducted on 5 July 1985, was designed to evaluate the Lambertian properties of the integrating sphere exit aperture (without the cones). The integrating sphere module was mounted upon a rotary table and the pointance measured as a function of angle as in test two. The results given in Figure 43 indicate the following:

- 1.) There are some irregularities in the near-axis pointance,
- 2.) The general distribution is far from Lambertian.

The fourth test was conducted on 8 July 1985 and was designed to confirm that poor reflectivity was the reason for the malfunctioning of the cones. This was accomplished by an experiment in which a plexiglass cylinder was used on the integrating sphere exit port in place of the cones. The reflection on the inner surface of a solid cylinder is near 100%, and although a plexiglass rod would not be satisfactory in the infrared, it should give valid results in the range of $0.75\mu\text{m}$ to $0.9\mu\text{m}$. The results are given in Figures 44 and 45 for the small

and large apertures respectively: the uniformity is greatly improved over the cones.

The fifth test, which was conducted on 11 July 1985, was a repeat of some of the above tests with the increased resolution indicated above. Figures 46 and 47 give the horizontal beam areance for the flat and canted point source mode apertures respectively. Figure 48 gives a 45° scan. The nonuniformity is not circularly symmetrical and suggests that extensive mapping is required.

Figures 49 and 50 provide data from the testing of the solid plexiglass cylinder mounted on the integrating sphere exit port. The resulting improvement suggests, as predicted, that the malfunction of the cones results from poor gold reflectivity.

The sixth and final test was accomplished on 19 July after a frantic effort to fabricate a gold coated cylinder. The objective was to replace the solid plexiglass cylinder with a gold coated pipe. The results given in Figures 51, 52, and 53 are as follows: The reflectivity of the gold is about the same as that obtained with the cones, as evidenced by the approximately 60% level of the beam in the wings. In addition, the wider diameter cylinder produces a larger central bright spot and reveals an integrating sphere nonuniformity of about 8%.

The general conclusions to the beam uniformity tests are that nonuniformity is a severe problem which requires further attention. The problem appears to result from poor reflectivity of the gold surface in both the integrating spheres and the exit cones.

As noted earlier in this report (ref. page 15), one set of cones was cleaned and recoated with gold by a different company than the one which initially gold coated the interior of the cones. Tests conducted at USU in September of 1986 indicate that this coating is superior. This is illustrated by comparing Figure 54 with Figures 55 and 56. Figure 54 is a replot of the data given in Figure 42 (Uniformity of double cone pointance as a function of off-axis angle for a 0.017- inch diameter aperture)

in a different format for ease of comparison. Figures 55 and 56 are the data taken in September 1986 after the second set of cones were recoated. Notice that the intensity in the wings has significantly increased in the recoated cones. Figure 57 is a sketch of the test setup that produced the data in Figures 55 and 56.

From 8 September 1986 through 20 September 1986, USU personnel worked on-site at NASA GSFC to make final measurements of the DEC output beam uniformity. These measurements and the method used to procure the data are fully described in Appendix J.

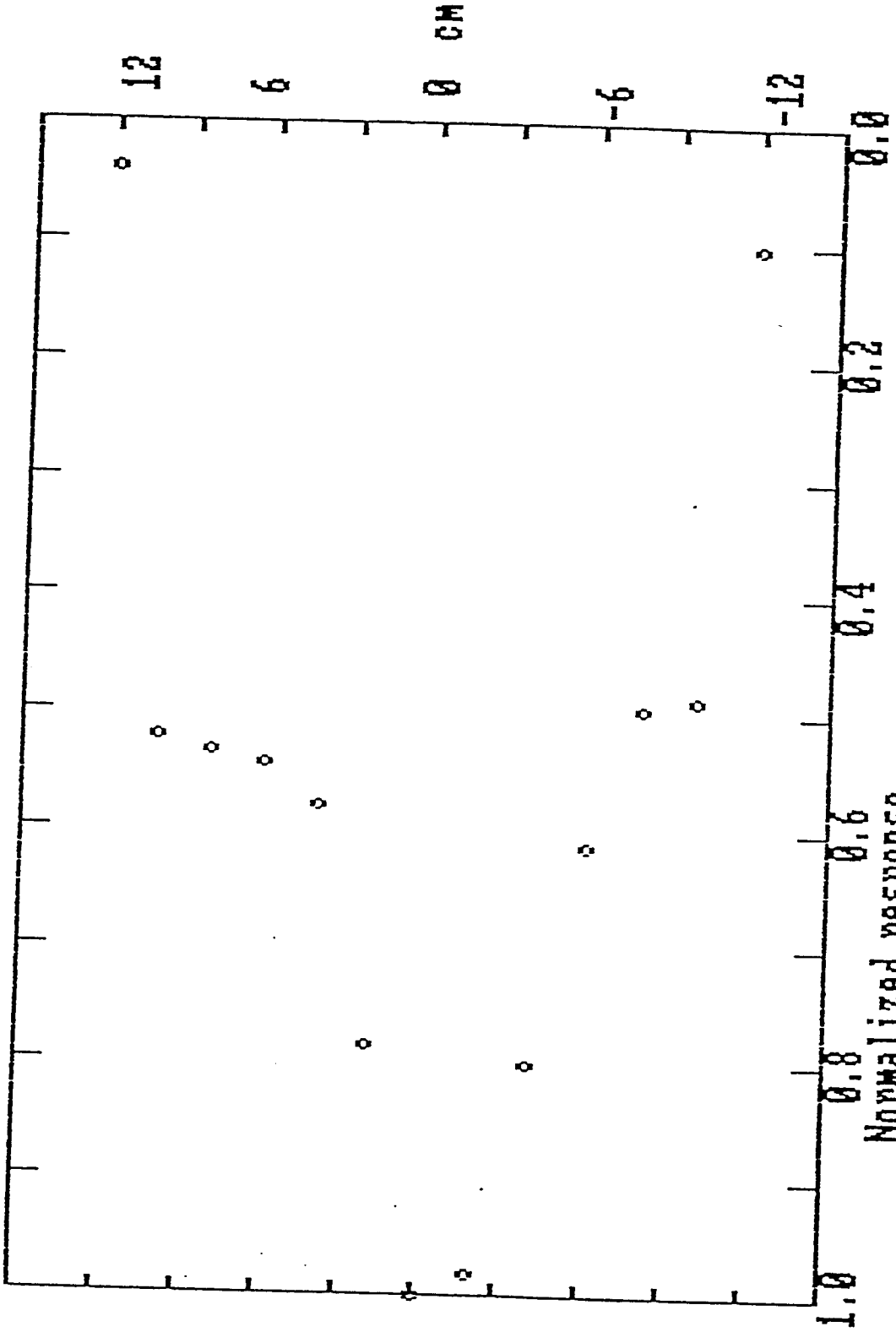


Figure 36. Beam areance [irradiance] (ϕ/cm^2) as a horizontal cross-section for the double cones mounted on the integrating sphere exit aperture. The point source mode aperture is flat.

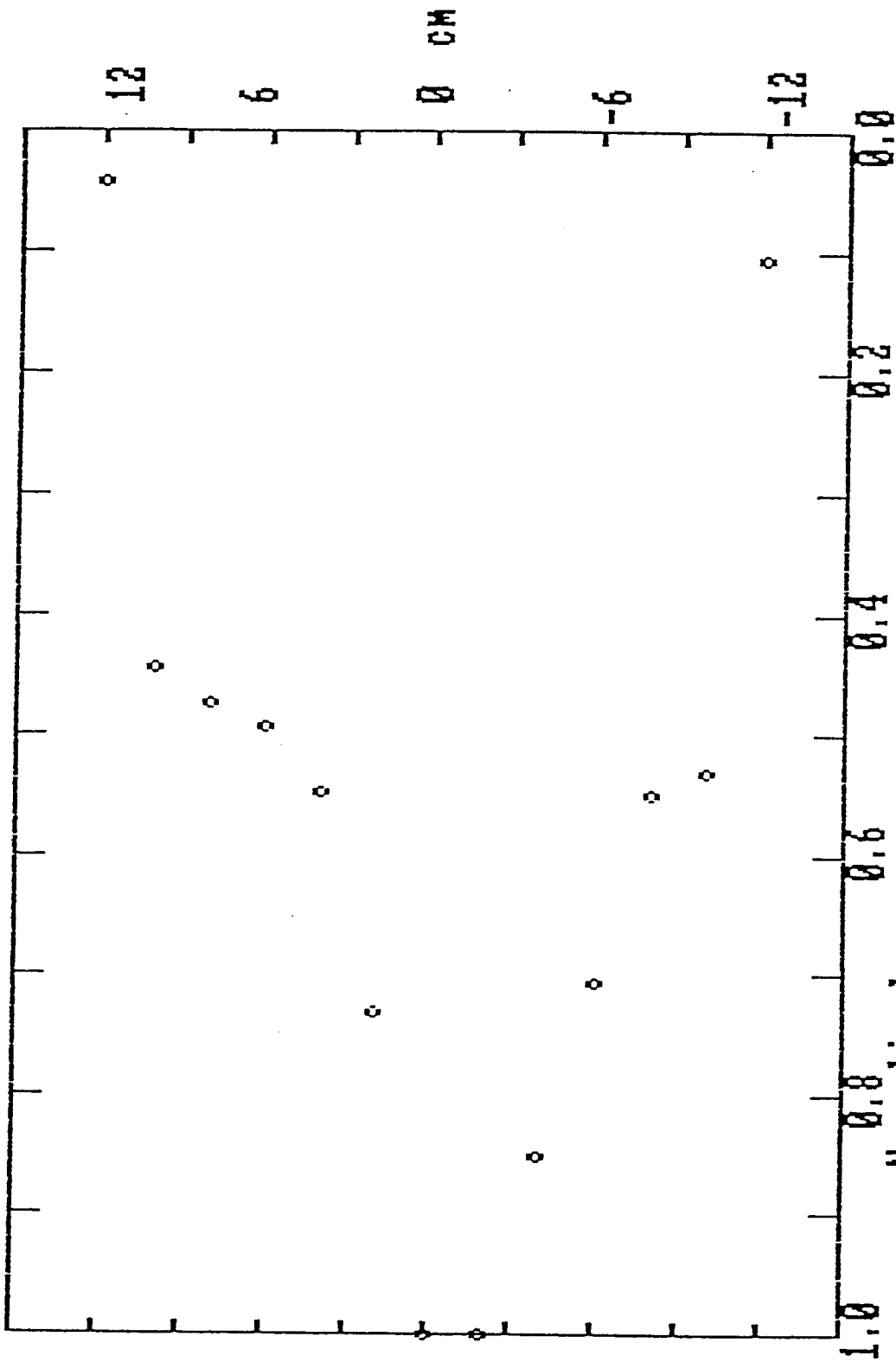
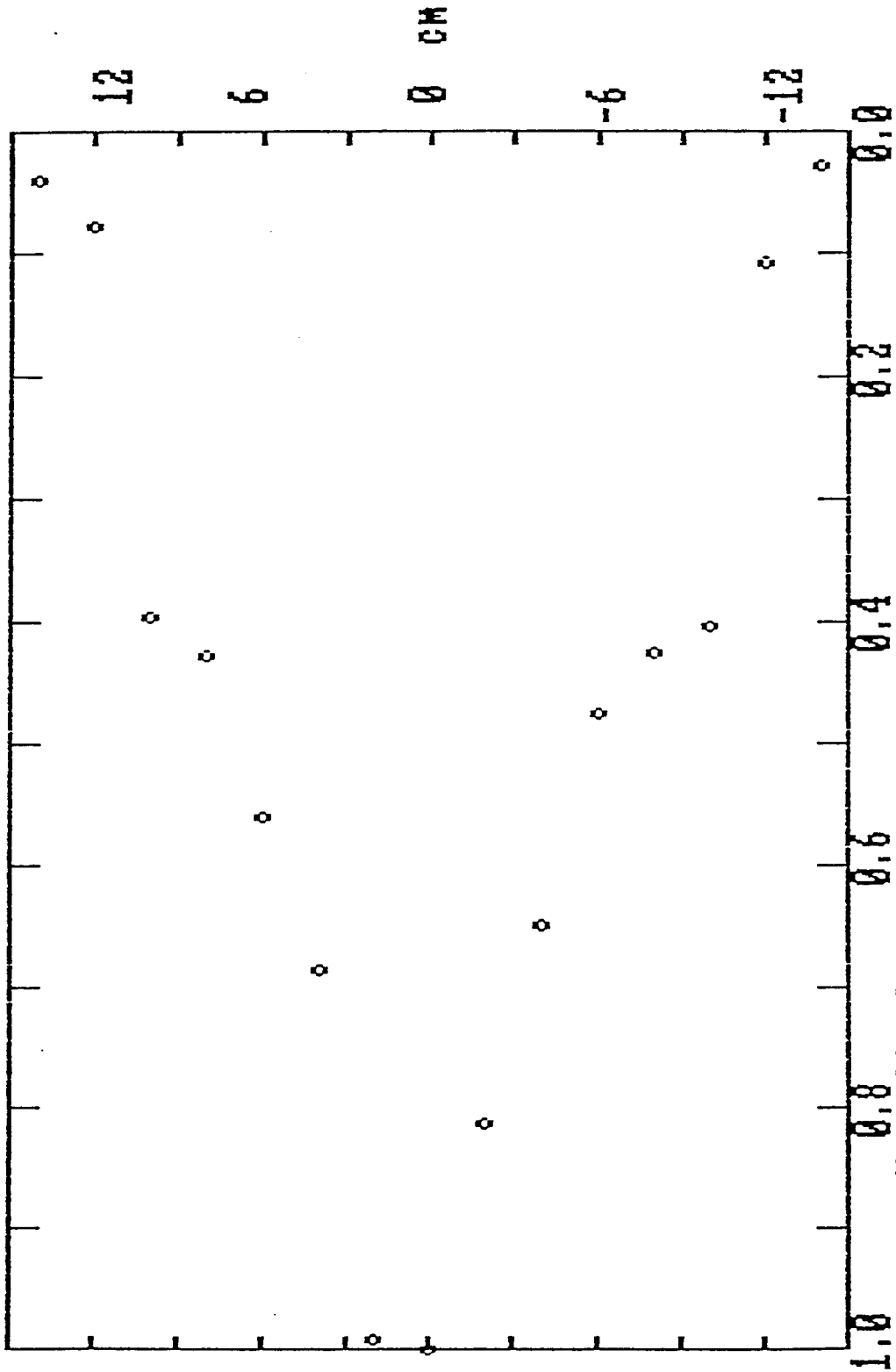
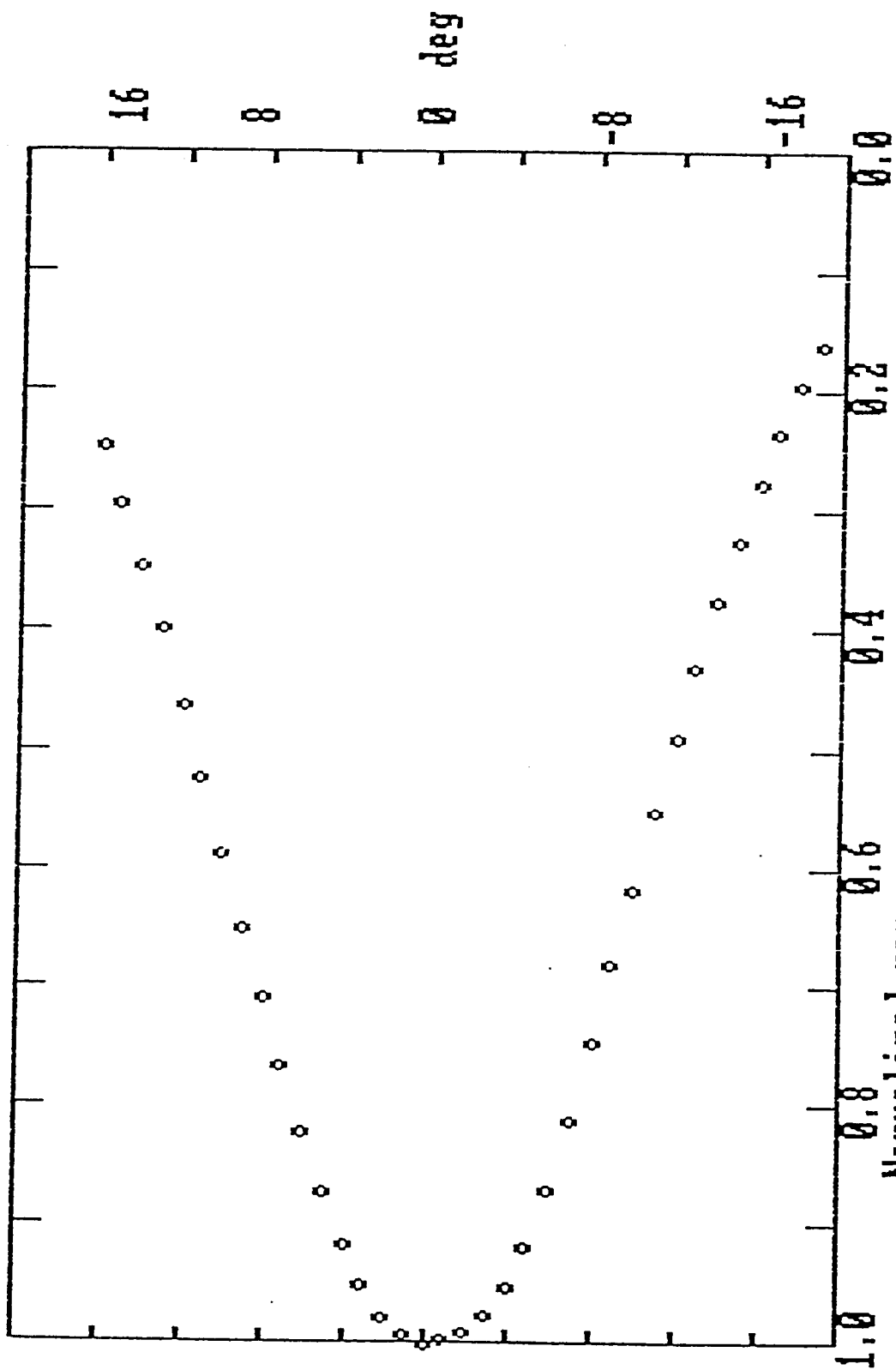


Figure 37: Beam areance [irradiance] (Φ/cm^2) as a horizontal cross-section for the double cones mounted on the integrating sphere exit aperture. The point source mode aperture is canted.



Normalized response
 Double Cones-int sph, 7 June 1985, E(W/cm²), C-PSM, var, res/L.

Figure 38. Beam areance [irradiance] (ϕ/cm^2) as a vertical cross-section for the double cones mounted on the integrating sphere exit aperture. The point source mode aperture is canted.



Normalized response
 Blackbody I (W/sr), 21 May 1987, aperture 0.785

Figure 39: Uniformity of blackbody pointance [intensity] (ϕ /sr) as a function of the off-axis angle for a 0.785-inch diameter aperture.

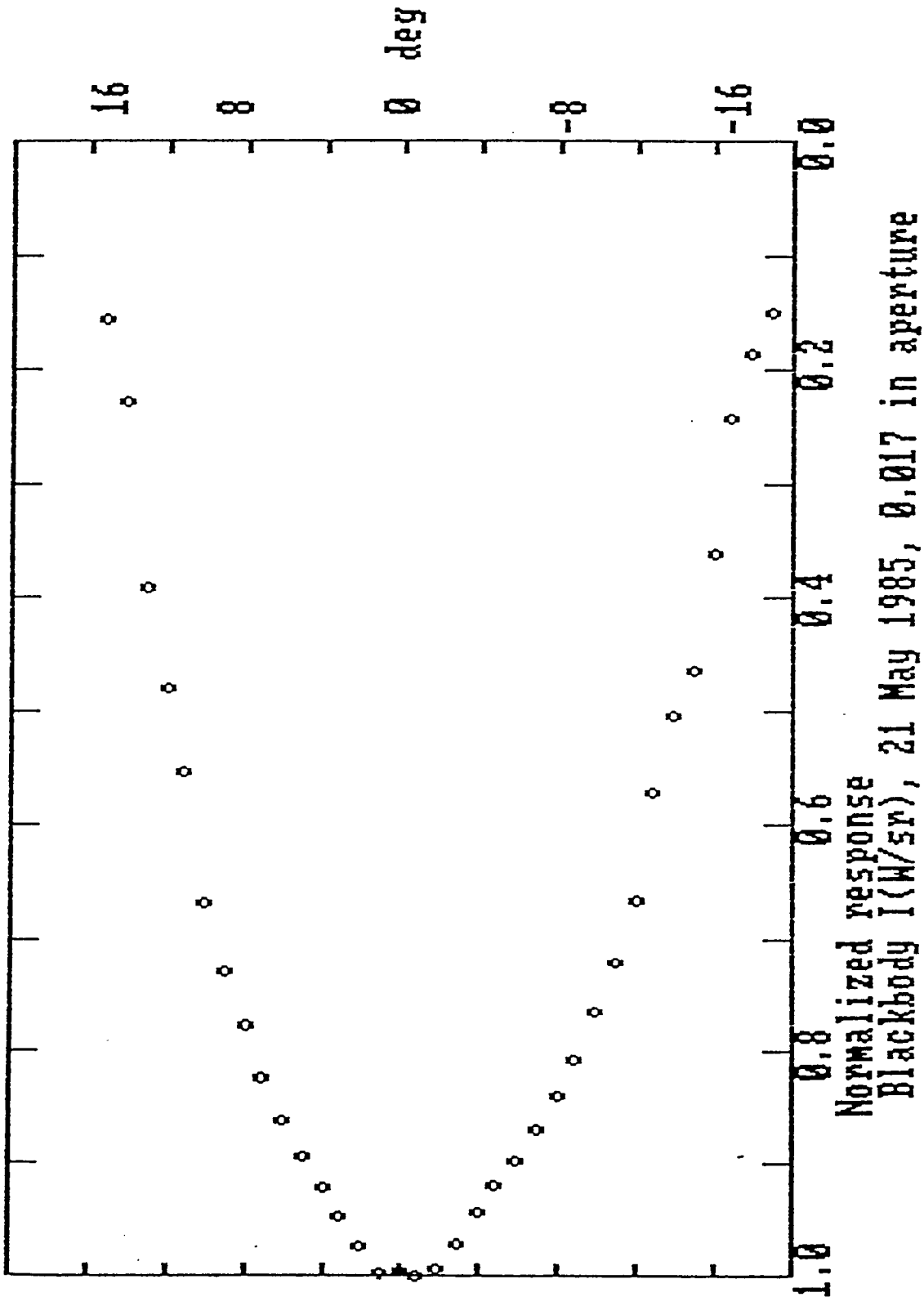


Figure 40: Uniformity of blackbody pointance [intensity] (ϕ /sr) as a function of the off-axis angle for a 0.017-inch diameter aperture.

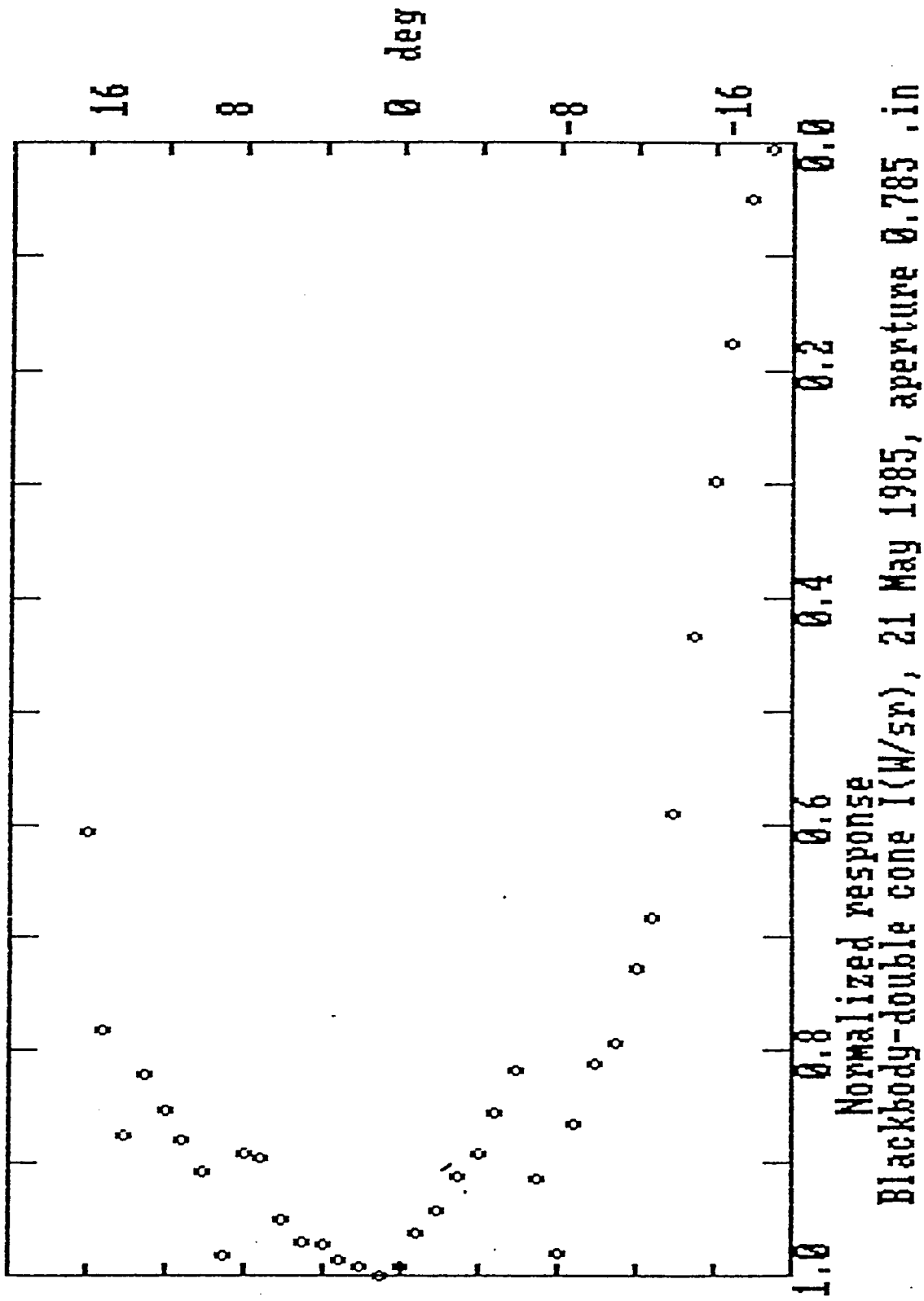
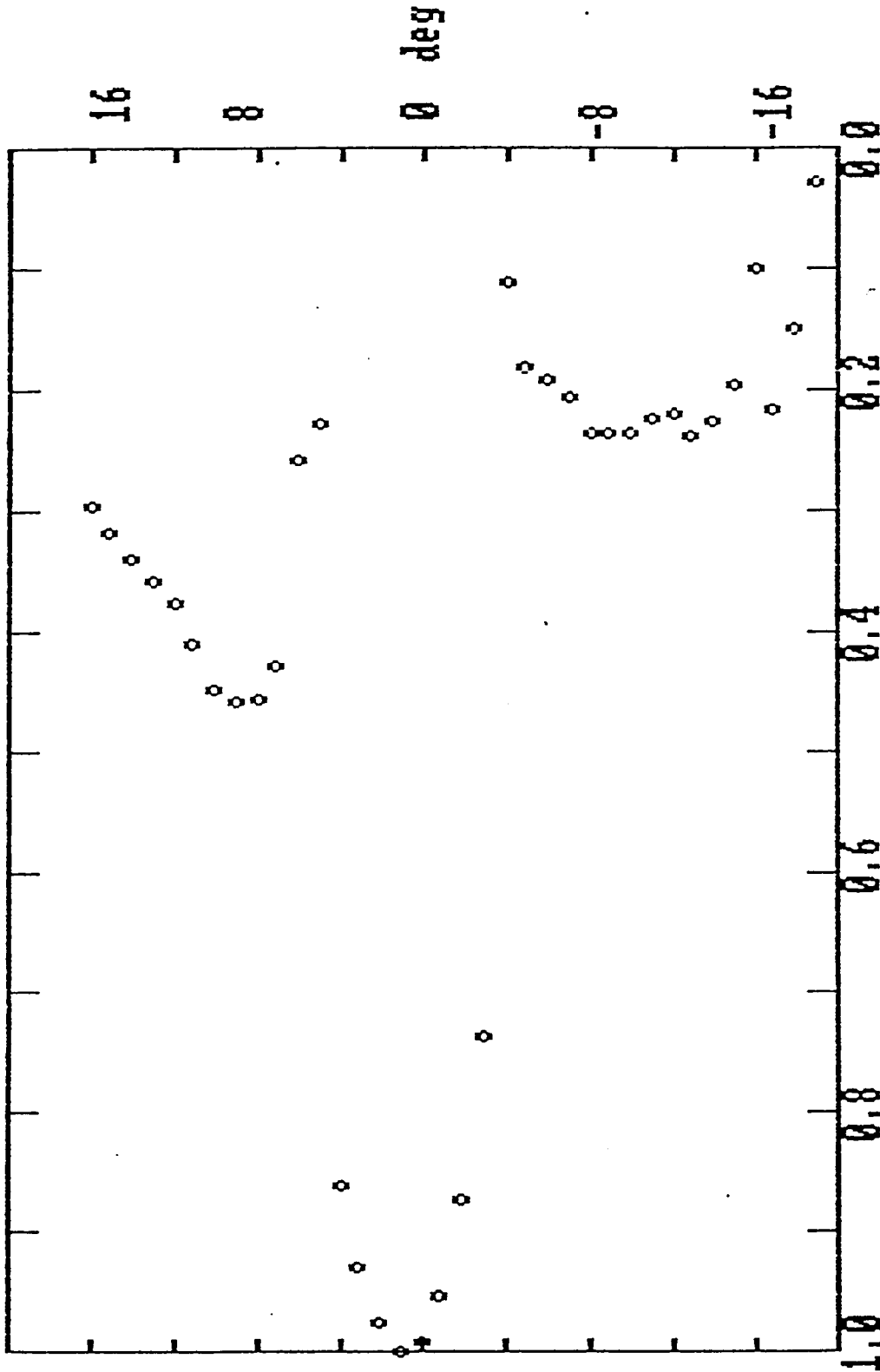
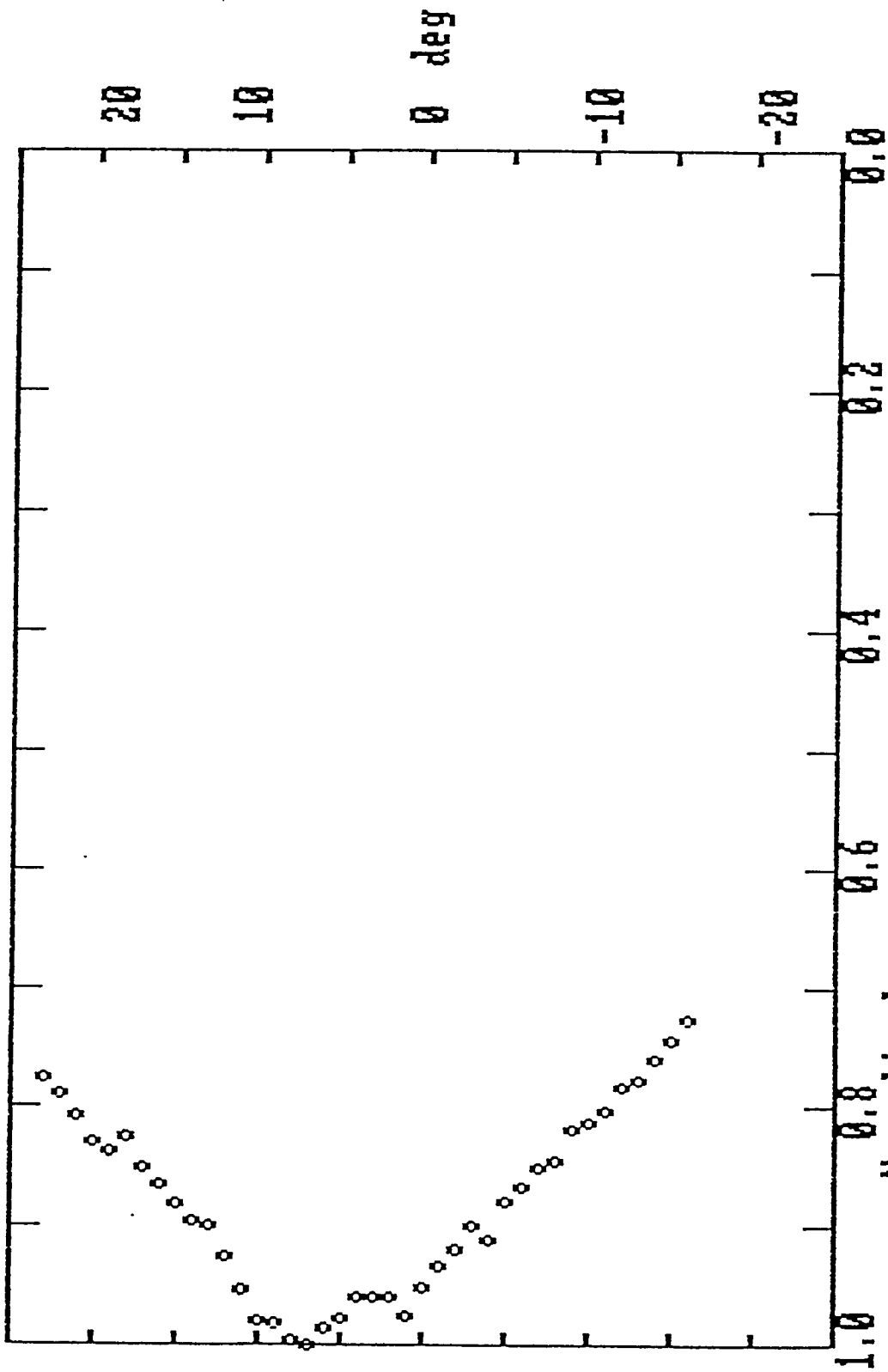


Figure 41: Uniformity of double-cone pointance [intensity] (ϕ /sr) as a function of off-axis angle for a 0.785-inch diameter aperture (simulates diffuse source mode).



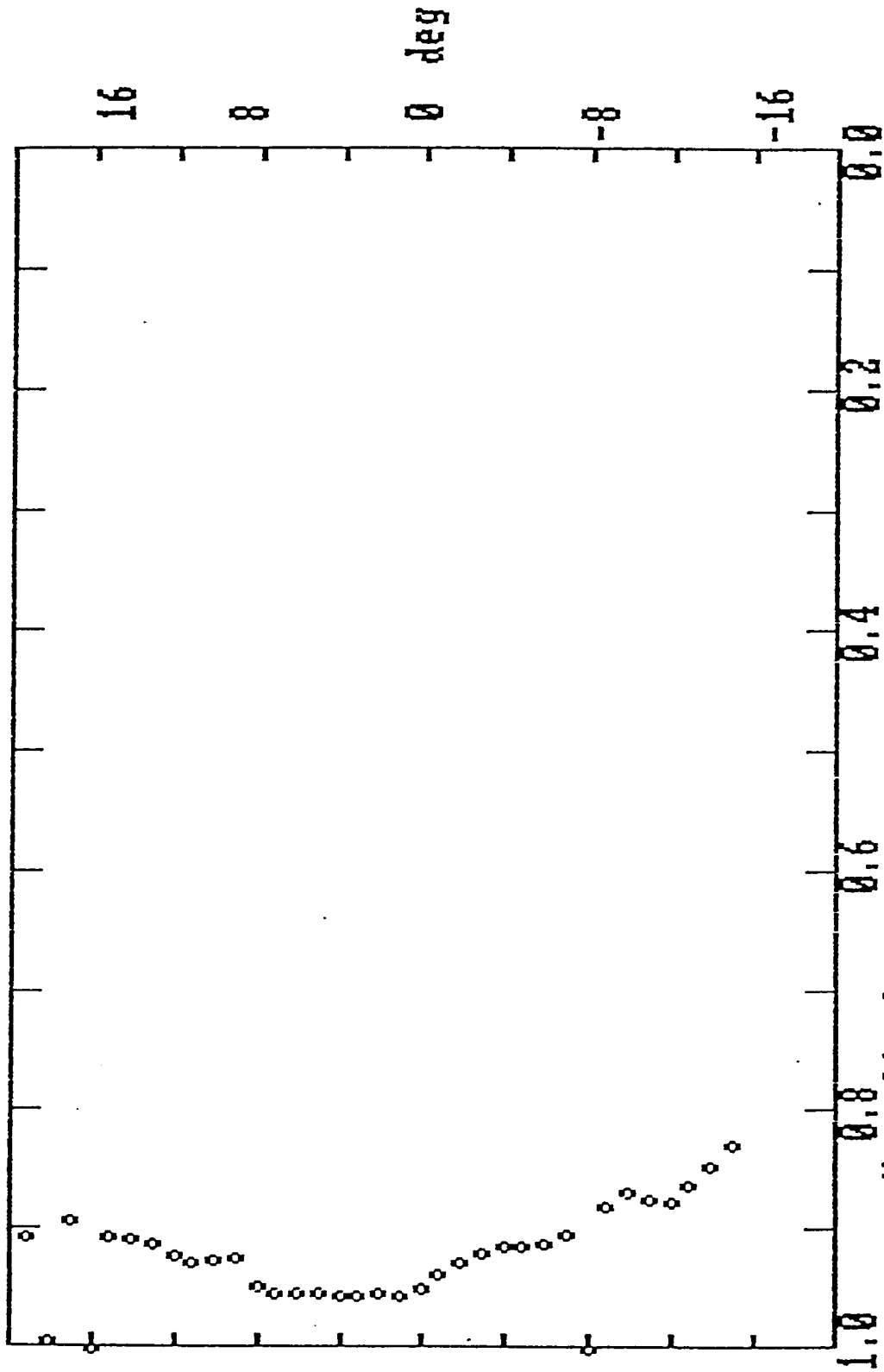
Normalized response
 Blackbody-double cone I(W/sr), 21 June 1985, aperture 0.017 in.

Figure 42: Uniformity of double-cone pointance [intensity] (ϕ/sr) as a function of off-axis angle for a 0.017-inch diameter aperture (simulates point source mode).



Normalized response
Integrating sphere I(W/sr), 5 July 1985, aperture 0.785 in.

Figure 43. Uniformity of integrating sphere exit aperture pointance [intensity] (ϕ /sr) as a function of off-axis angle for a 0.785-inch diameter aperture.



Normalized response
 Plexiglass rod on int sphs, I(W/sr), 8 July 1985, ap 0.017 in.

Figure 44: Uniformity of plexiglass exit pointance [intensity] (ϕ /sr) as a function of off-axis angle for a 0.017-inch diameter aperture. Plexiglass rod mounted on the integrating sphere exit aperture.

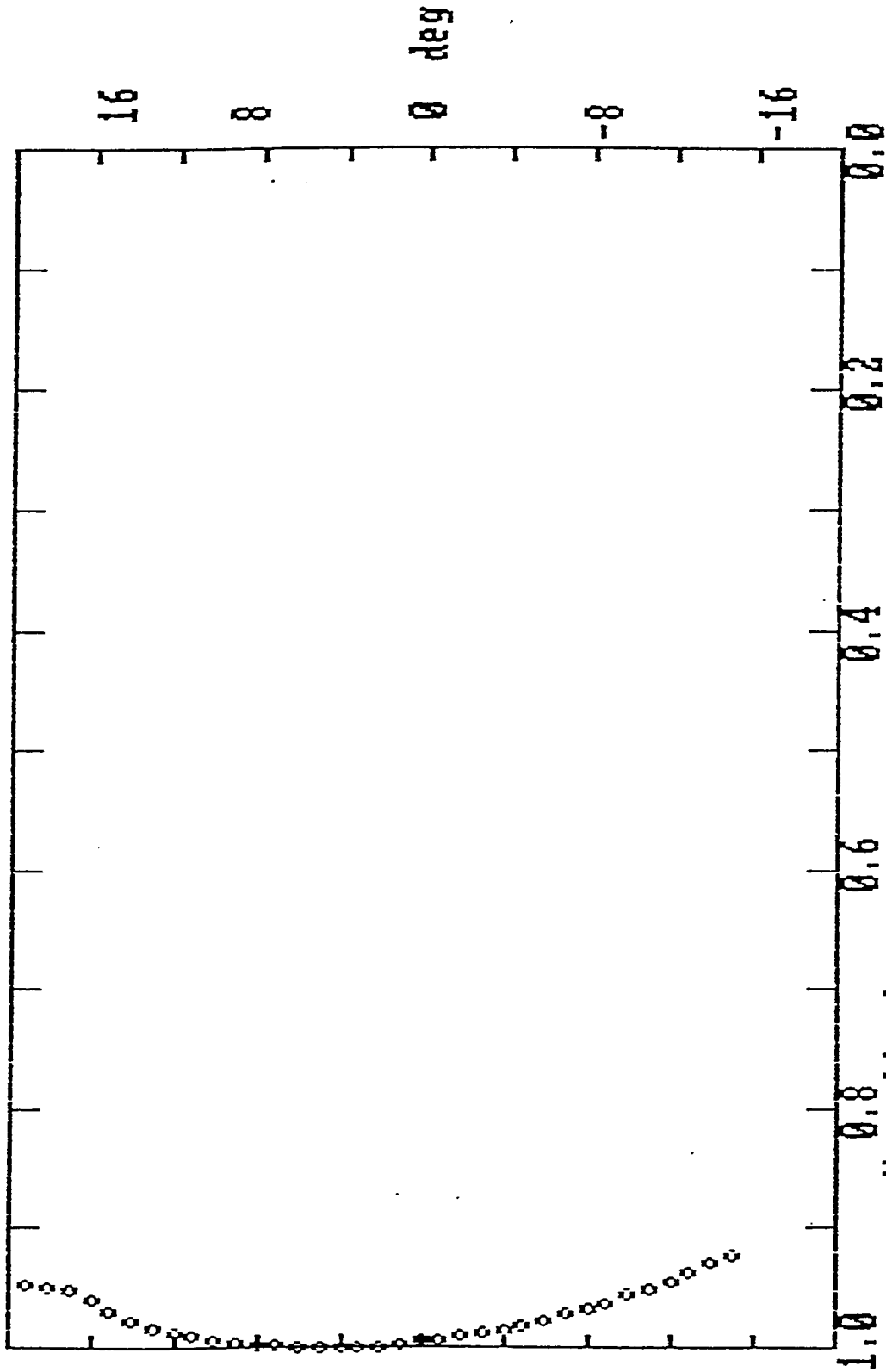
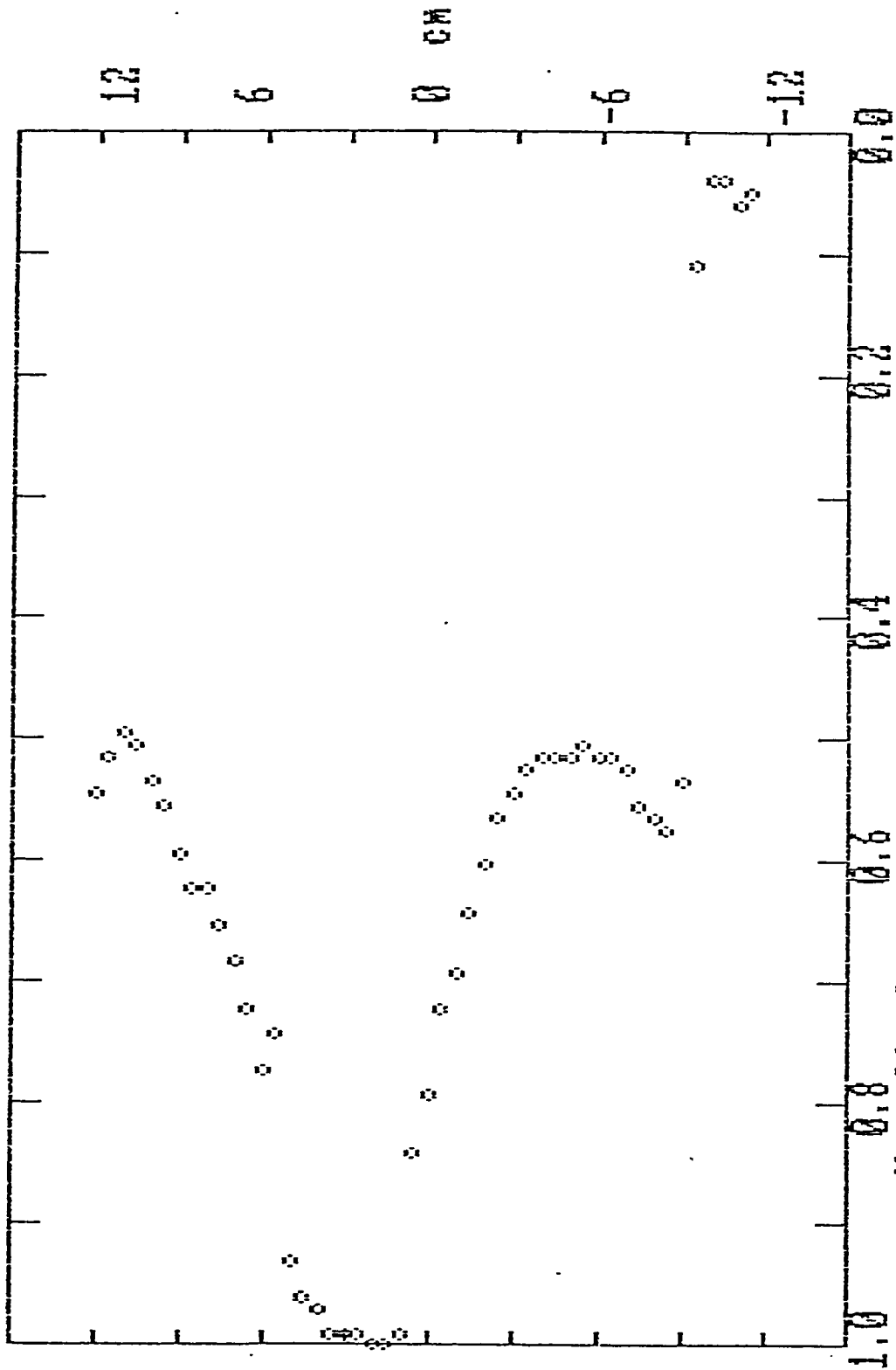
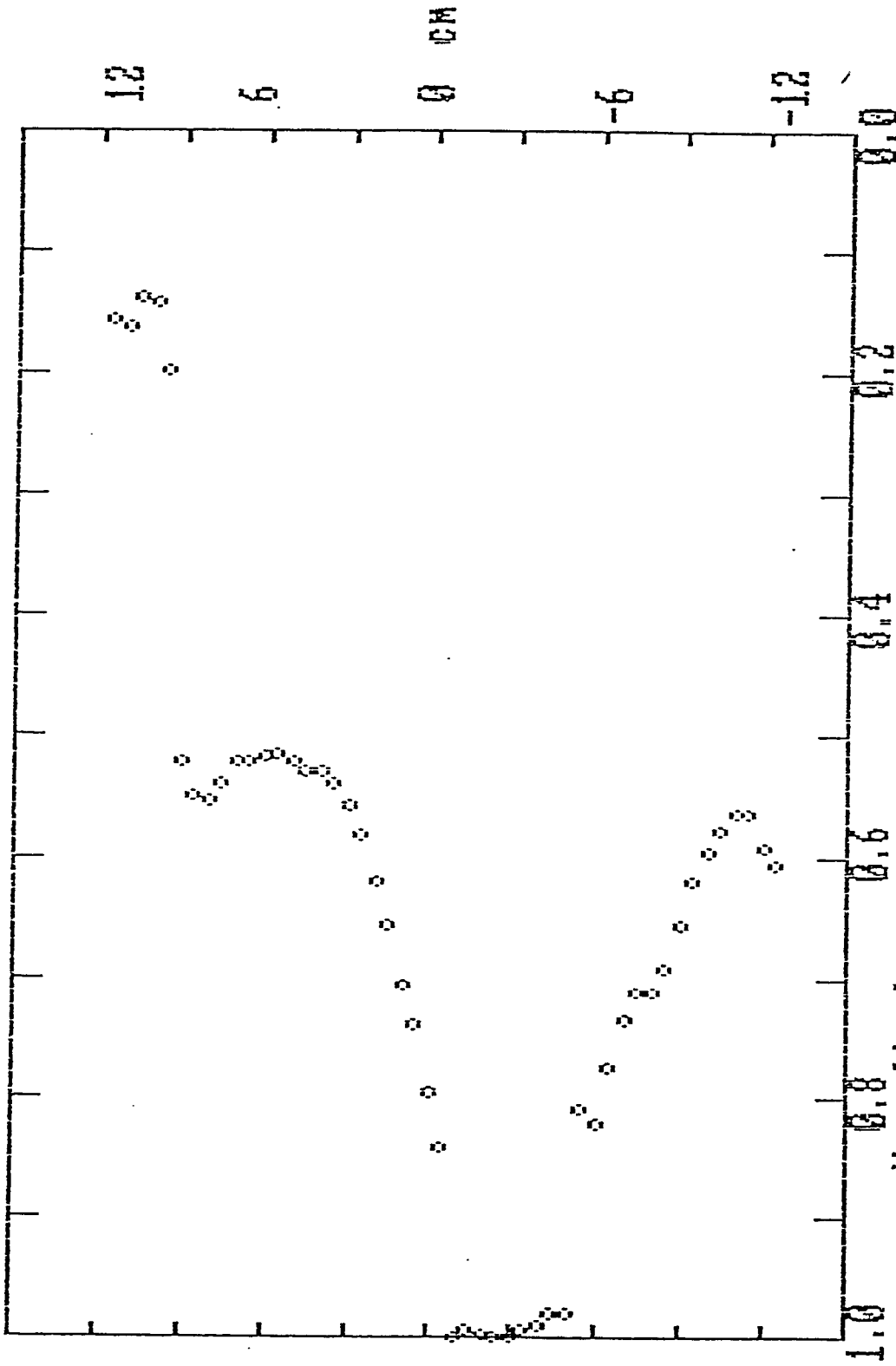


Figure 45: Uniformity of plexiglass exit pointance [intensity] (ϕ/sr) as a function of off-axis angle for a 0.785-inch diameter aperture. Plexiglass rod mounted on the integrating sphere exit aperture.



Double cones-int sphs, 11 July 1985, E(W/cm+2), F-psm, hor, res/H

Figure 46.: Beam areance [irradiance] (ϕ/cm^2) as a horizontal cross-section for the double cones mounted on the integrating sphere exit aperture. The point source mode aperture is flat.



Normalized response
 Double cones-int sphs, 11 July 1985, E(W/cm+2), C-PSM, hor, res/H

Figure 47. Beam areance [irradiance] (ϕ/cm^2) as a horizontal cross-section for the double cones mounted on the integration sphere exit aperture. The point source mode aperture is canted.

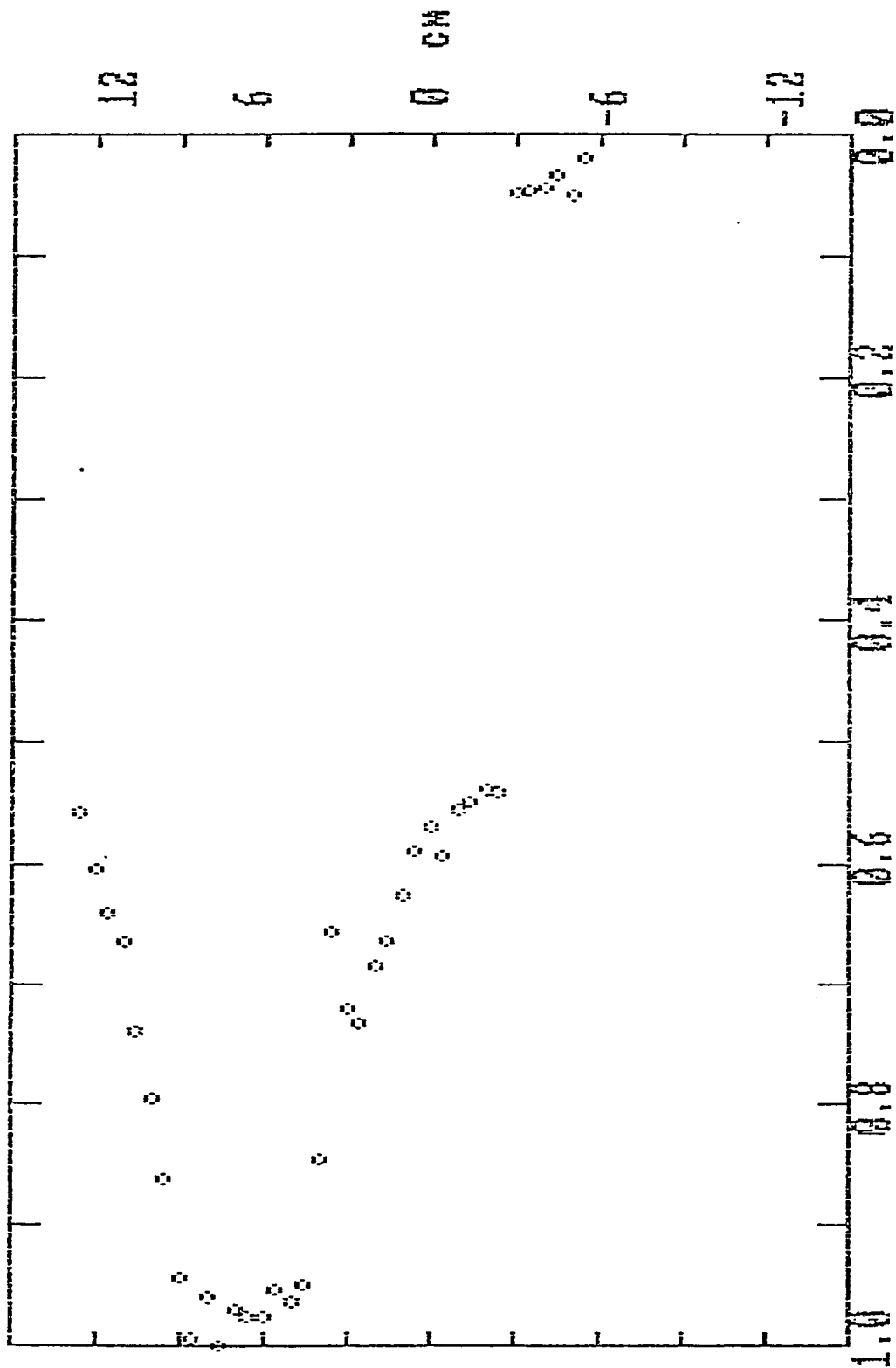


Figure 48: Beam areance [irradiance] (ϕ/cm^2) as a 45° cross-section for the double cones mounted on the integrating sphere exit aperture. The point source mode aperture is canted.

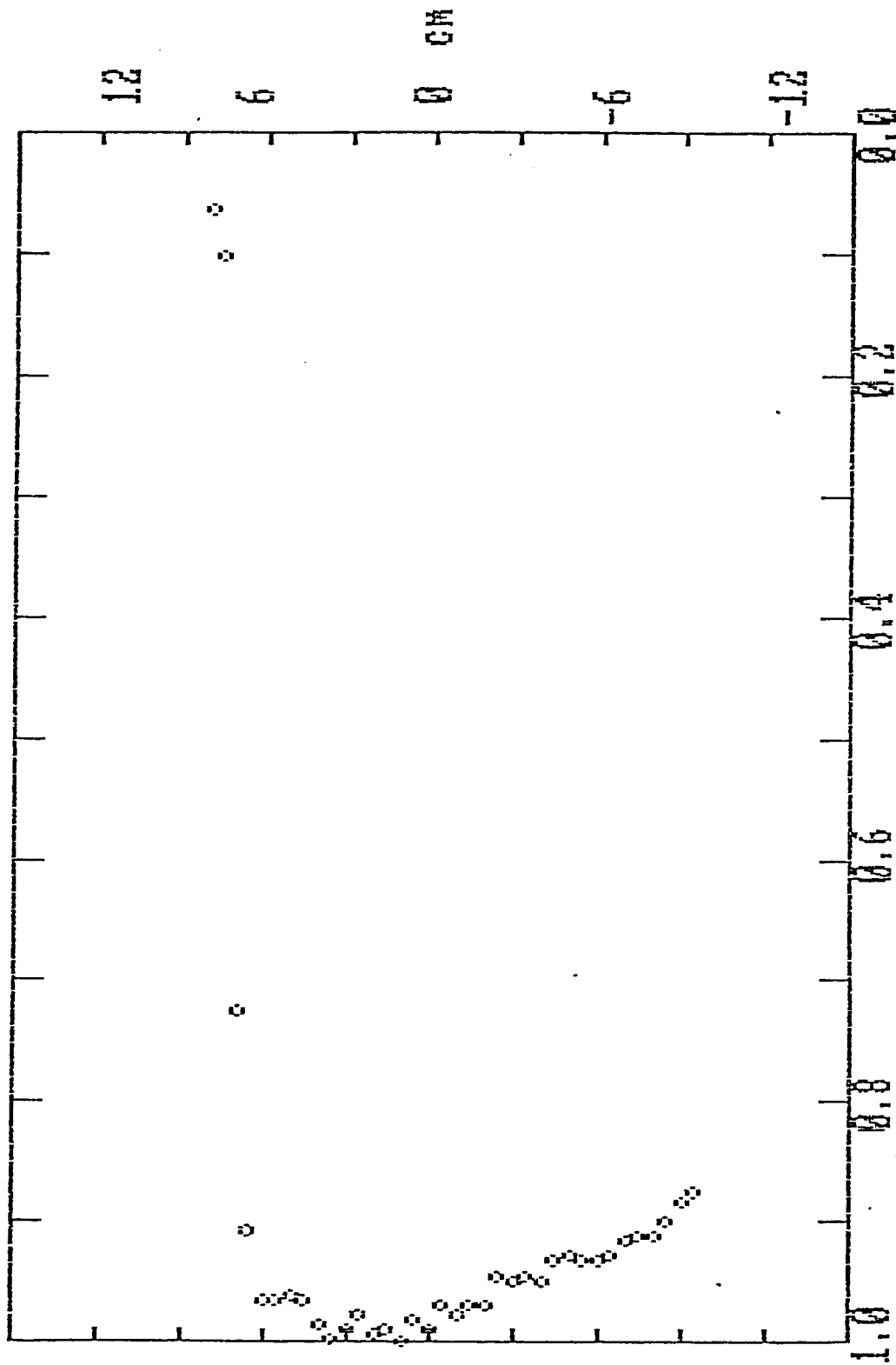


Figure 49. Beam areance [irradiance] (Φ/cm^2) as a horizontal cross-section for the plexiglass cylinder mounted on the integrating sphere exit port. The point source mode aperture is flat.

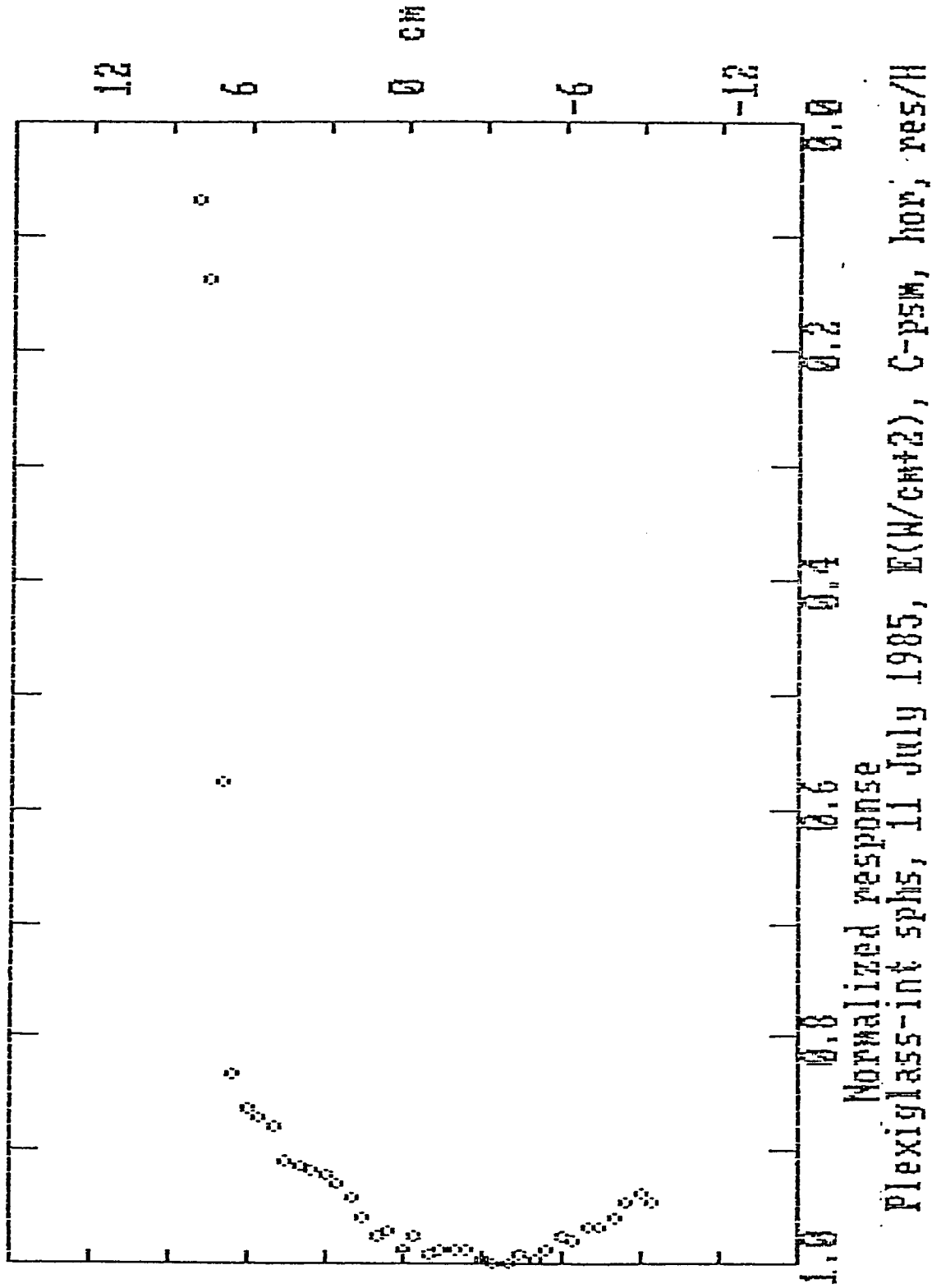


Figure 50: Beam areance [irradiance] (ϕ/cm^2) as a horizontal cross-section for the gold cylinder mounted on the integrating sphere exit aperture. The point source mode aperture is canted.

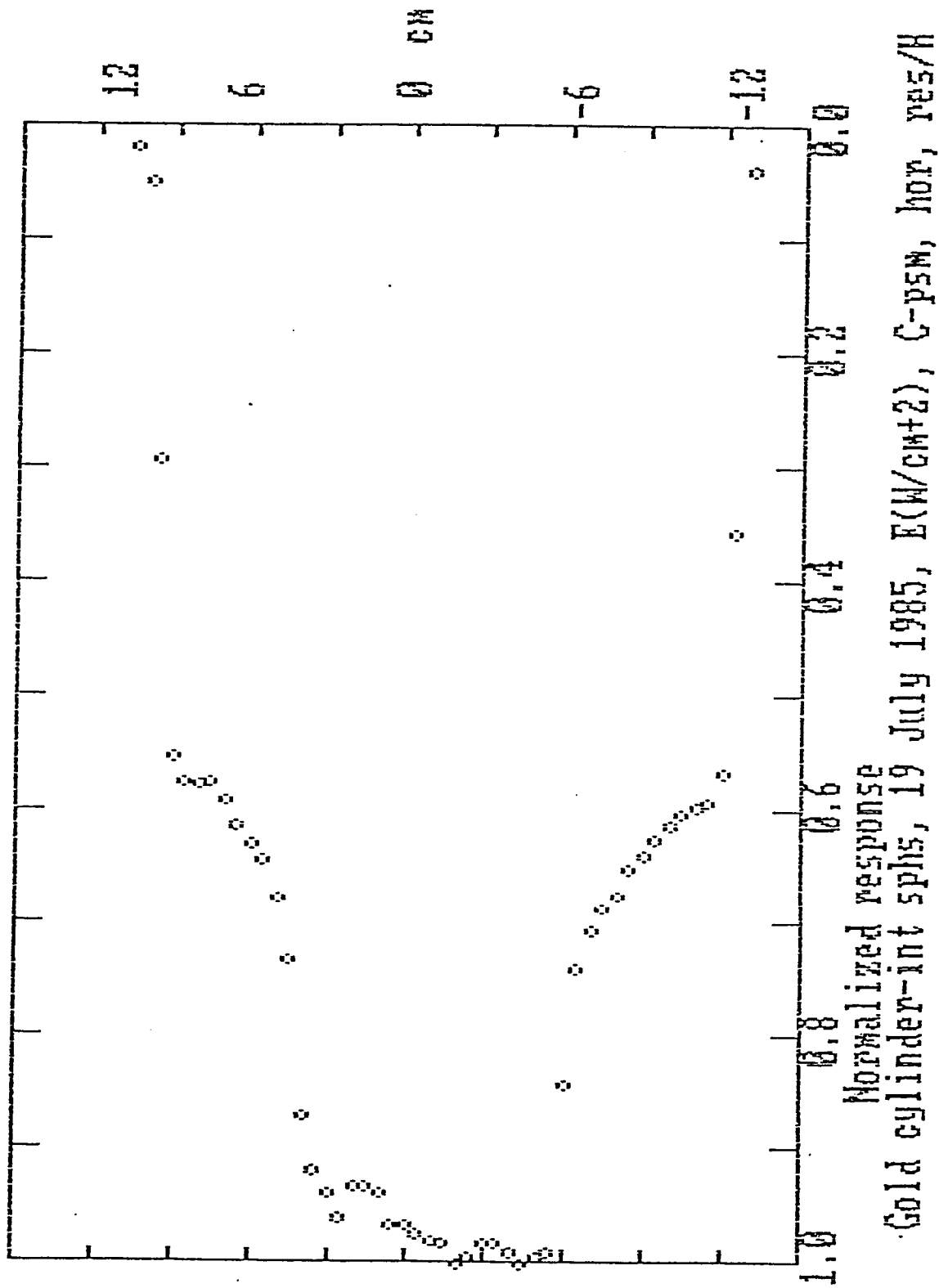
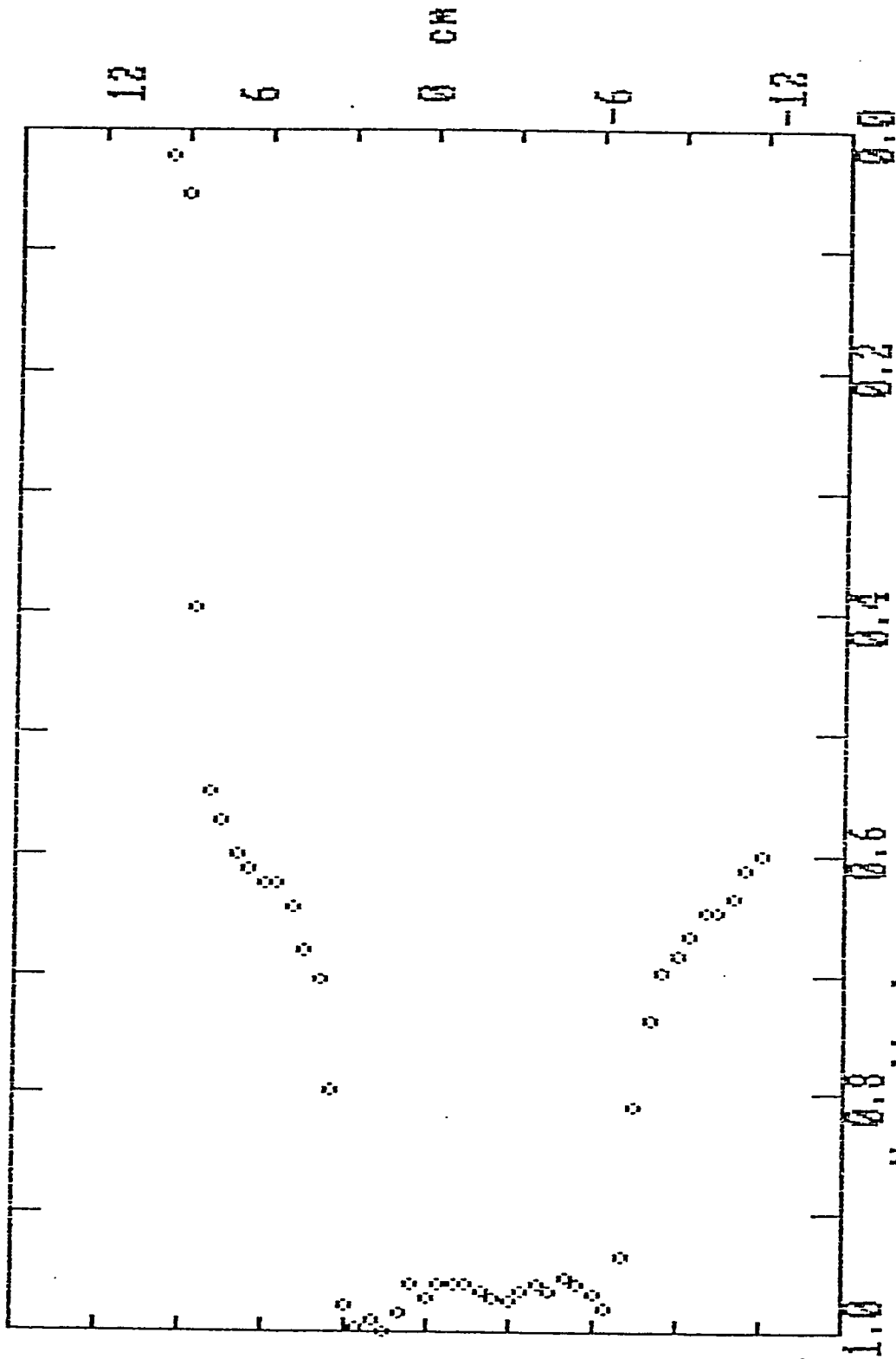


Figure 51: Beam areance [irradiance] (Φ/cm^2) as a horizontal cross-section for the gold cylinder mounted on the integrating sphere exit aperture. The point source mode aperture is canted.



Normalized response
 Gold cylinder-int sphs, 19 July 1985, E(W/cm²), C-PSM 45 deg, res/H

Figure 52. Beam areance [irradiance] (ϕ/cm^2) as a 45° cross-section for the gold cylinder mounted on the integrating sphere exit aperture. The point source mode aperture is canted.

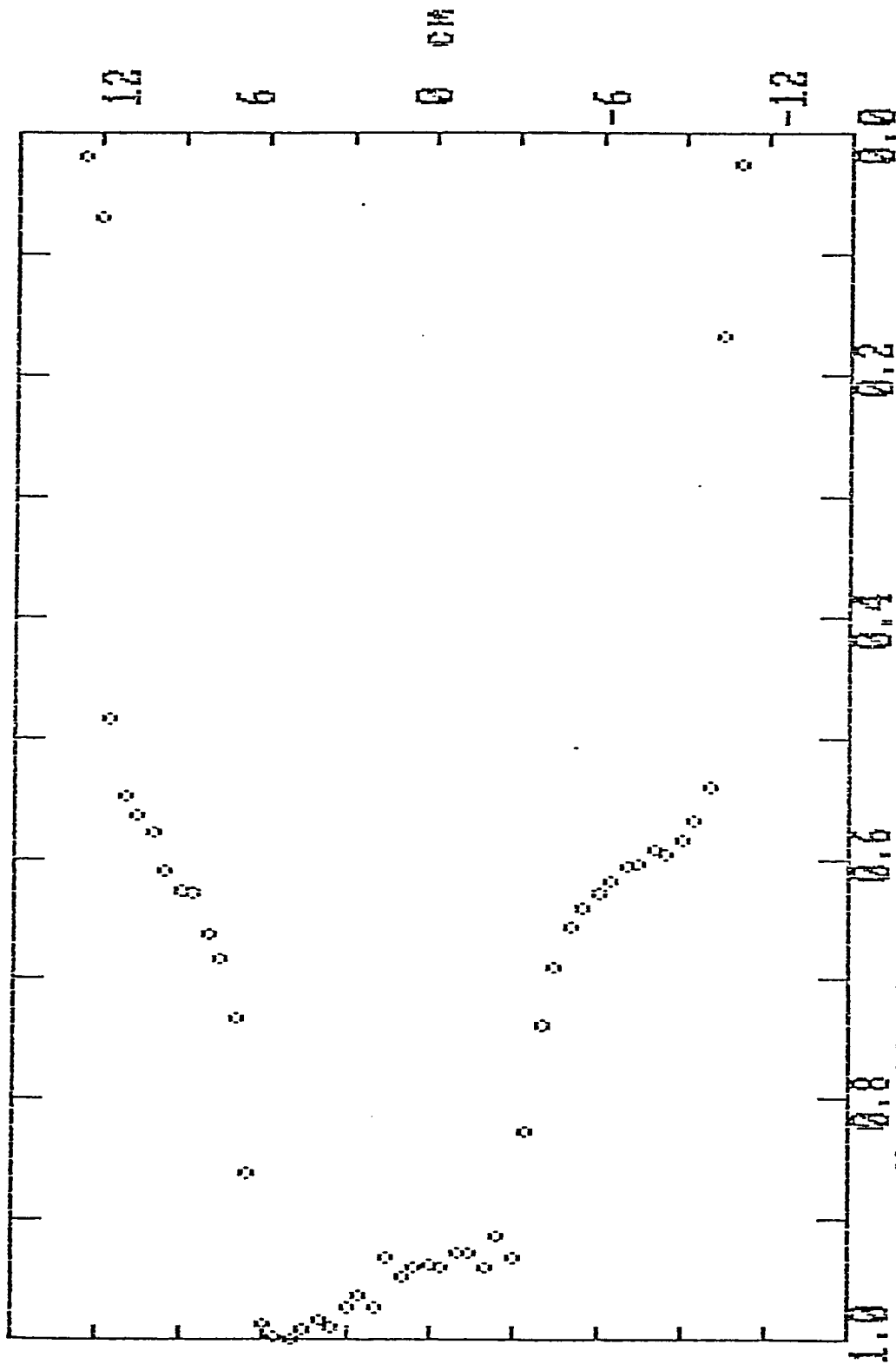


Figure 53. Beam areance [irradiance] (Φ/cm^2) as a vertical cross-section for the gold cylinder mounted on the integrating sphere exit aperture. The point source mode aperture is canted.

21 June 1985 - Aperture .017 in.

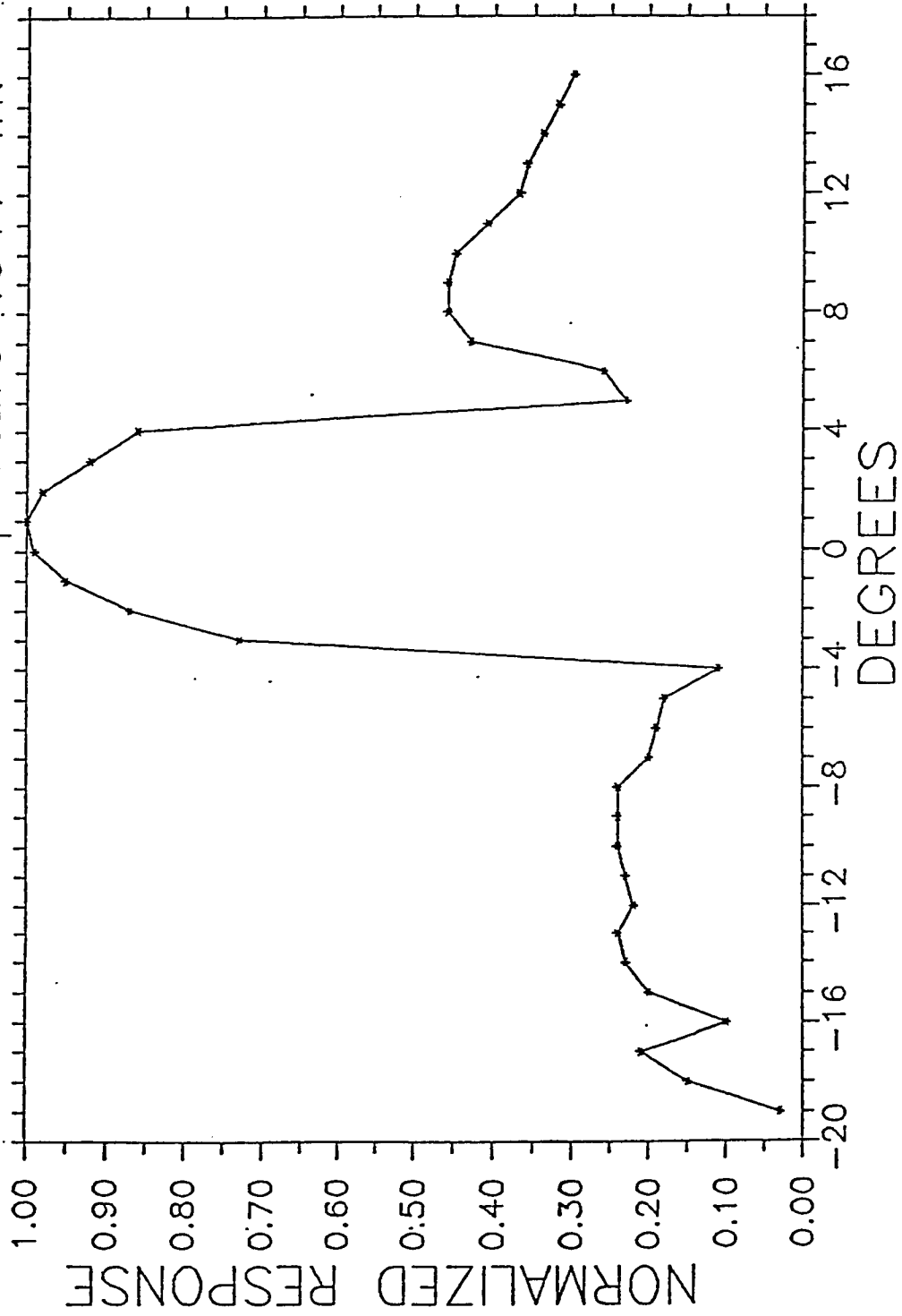


Figure 54. Uniformity of double-cone pointance [intensity] (Φ/sr) as a function of off-axis angle for a 0.017-inch diameter aperture (simulated point source mode). This data is the same as that in Figure 42, but has been replotted for easy comparison with Figures 55 & 56.

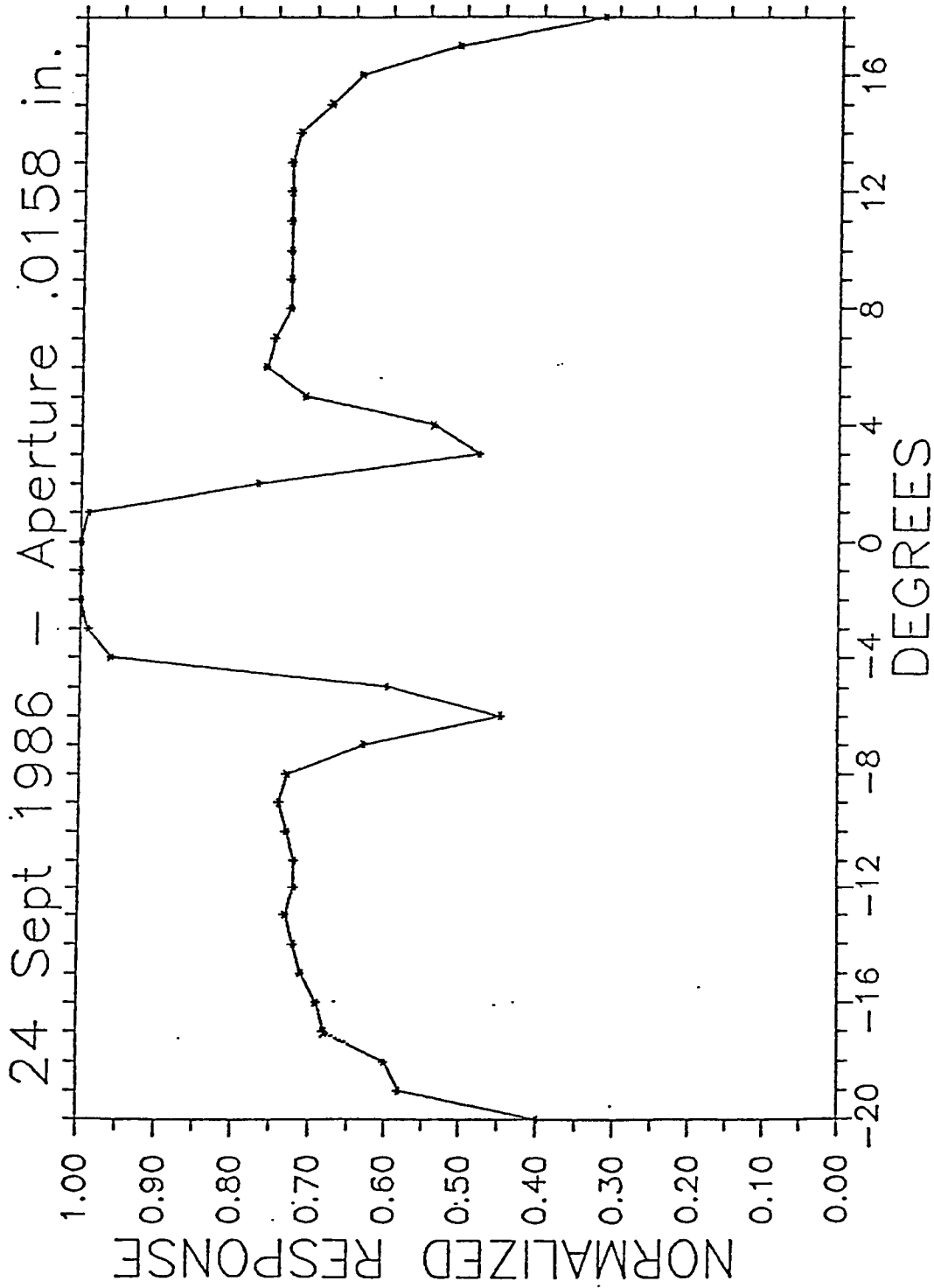


Figure 55. Beam areance [irradiance] (ψ/cm^2) as a horizontal cross-section for the recoated double cones mounted to the USU blackbody and using a 0.0158-inch aperture.

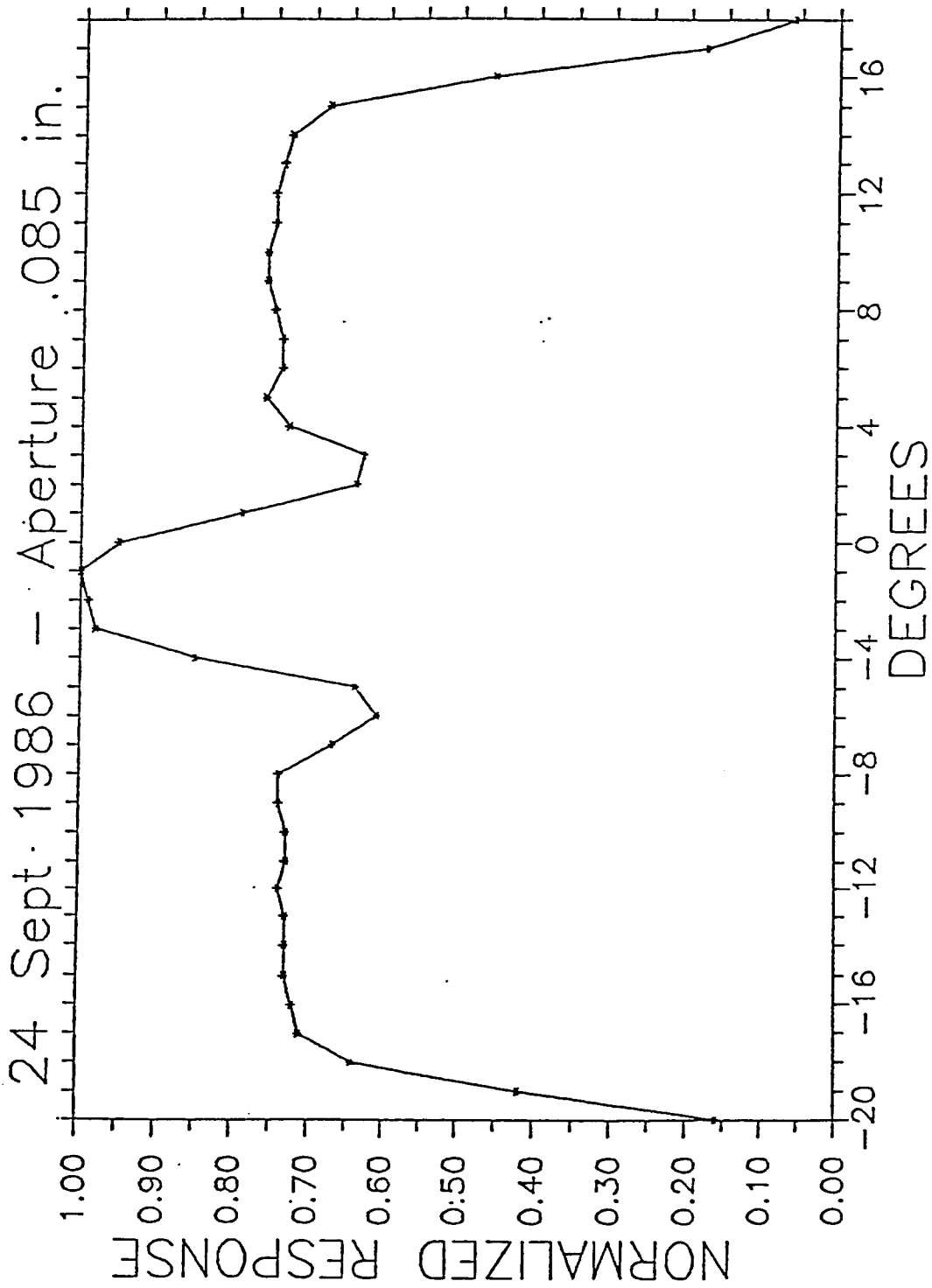


Figure 56. Beam areance [irradiance] (ϕ/cm^2) as a horizontal cross-section for the recoated double cones mounted to the USU blackbody and using a 0.085-inch aperture.

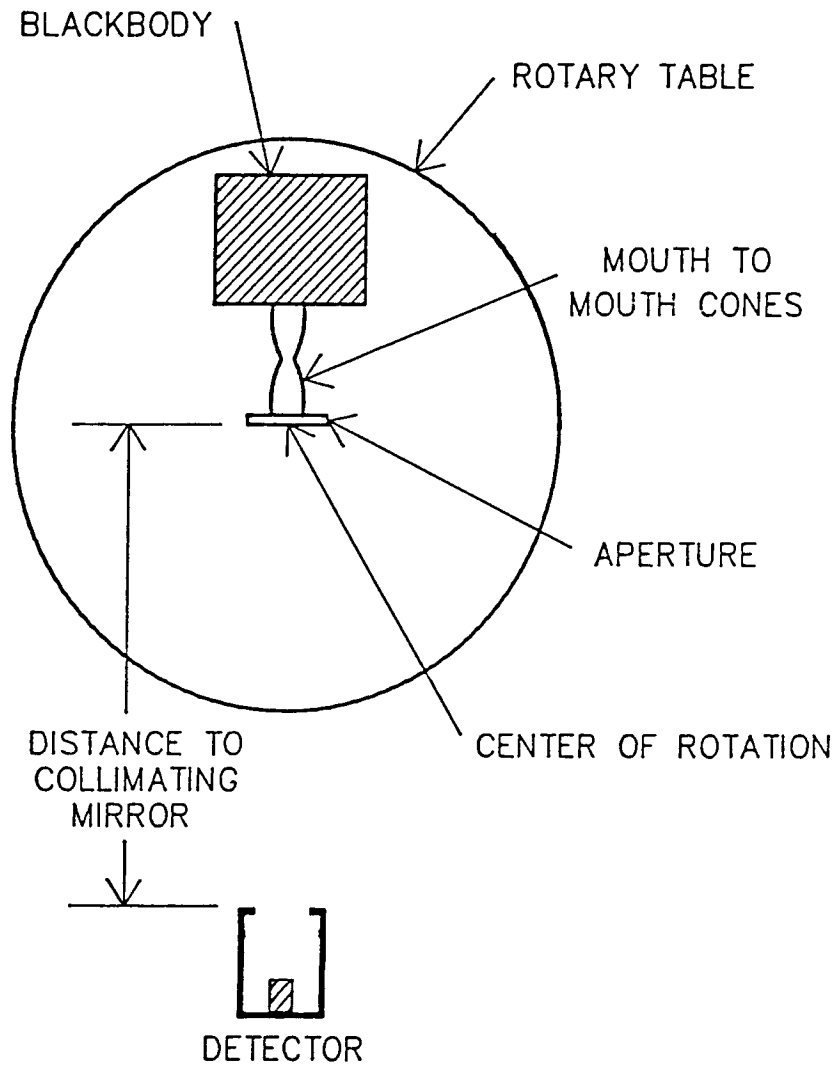


Figure 57. Sketch of the test setup used for the 24 September 1986 tests that yielded the data in Figures 55 and 56.

4.5 AR Calibration

Radiation exiting the integrating sphere is likely to exhibit some spectral dependence due to variations in sphere reflectance. Contamination of sphere surfaces may cause the spectral dependence to change with time. Utilization of bandpass filters in the absolute radiometer provides a measure of the band flux in the DEC beam that is independent of sphere spectral dependence provided the bandpass characteristics of the integrating sphere module and the Absolute Radiometer module match those in DIRBE.

At a 1 March 1985 meeting at NASA Goddard, it was revealed that the DIRBE filters exhibit long wavelength leaks; and that blocking in DIRBE is obtained by using multiple detectors which exhibit wavelength cutoff to compliment the filters. However, the detector utilized in DEC is a bolometer that responds to wavelengths up to and greater than 1000 μm . Thus, the bandpass of the Absolute Radiometer is not matched to that of DIRBE. An absolute calibration of the DEC beam is still possible if the DIRBE spectral response function is well known (including the leak regions where any significant beam energy is present) for DEC and DIRBE. The spectral response curves do not yield calculated effective flux values that are consistent with the measured response. In every case the filter transmission in the leak region appears to be greater than the filter data indicates. This can be explained based upon the fact that the filter curves were obtained at a temperature of about 10°K but are operated at a temperature of about 1.5°K in the DEC. At these lower temperatures the leak transmittance increases. Thus, the filters in DEC are of questionable value. The ideal solution to this problem is to measure the system spectral response function at the proper operating temperature.

In principle it is possible to determine the band-power based upon the DIRBE spectral bandpass function using the open position as indicated in Appendix E.

The Absolute Radiometer calibration report is a self-contained document included in this report as Appendix E. The following is a summary of significant Absolute Radiometer parameters from that report:

1. The CMU reports data that have been corrected for the low-gain output which means that it can range from the noise level (approximately 1 mV) to 10 V full-scale. All data must be preprocessed to account for changes in the operating temperatures of the bolometer. The algorithm for making this correction is given from Appendix E as

$$V_c = \frac{V \times 0.6532}{(-0.1175 + 2.569 \times V_{dc})} \quad (E-3)$$

where V_{dc} is the bolometer dc

$$V_{dc} = \text{ARBODC}|_{\text{biason}} - \text{ARBODC}|_{\text{biasoff}}$$

where ARBODC is the AR Bolometer DC and where V is the output reported by the CMU.

2. The beam sterance [radiance] measured for the "open" position is given by

$$L = 9.281 \times 10^{-9} \times V_c + 5.984 \times 10^{-9} \times V_c^2 \quad \text{W cm}^{-2} \text{ sr}^{-1} \quad (E-9)$$

where V_c is the voltage preprocessed by Eq. (E-3). It is important to note that the system exhibits some nonlinearity. This nonlinearity is significant above 1.0 Volt. Equation (E-9) provides for "linearization of the data" as well as providing the basis for calculating beam power.

3. The beam areance [irradiance] measured for the open position is given by

$$E = 1.95 \times 10^{-11} V + 1.26 \times 10^{-12} V^2 \quad \text{W/cm}^2. \quad (E-14)$$

4.6 System Cold Tests

The following is a summary of the significant tests that were performed as part of the DEC development. Also given are the problems encountered and the action taken to correct each problem.

4.6.1 System Dewar Test, 1 March 1985

CONDITIONS: A heater was placed on the cold finger at a point midway between the center and the outer edge. The cold finger temperature was measured on the edge and at the center.

RESULTS: Without heat injection, the dewar cold finger temperature achieved about 1.5°K operation. With 4 watts injected into the cold finger, the edge temperature varied from 2° to 5°K; the center temperature varied from 2° to 11°K. With 9 watts injected into the cold finger, the temperature went as high as 17°.

ACTION: Copper pads were installed on the dewar cold finger and copper straps were soldered to the pads that extended to the bottom of the liquid helium vessel (See pages 65 and 66).

4.6.2 First System Cold Test, 4 April 1985

CONDITIONS: No mirror or spheres installed. Objective was to test for mechanical movement and contamination of test mirrors.

RESULTS: No contamination observed. Excessive heating of DEC base plate was observed when the Beam Sample Mirror was actuated. Pointing Mirror mechanism froze up so the mirror could not be moved. Temperature sensor variation in response was excessive. Some encoder switches failed. There appeared to be a thermal short in the large area source.

ACTION: A heat strap was added to the Beam Sample Mirror to reduce the temperature buildup. Modifications were made in the Pointing Mirror system that included using TORLON on the driver threads. The temperature probes were individually calibrated and lookup tables generated to provide accurate temperature readings of all test points. All the switch encoder levers were discarded

and a new design fabricated and installed. The insulating rod on the Large Area Source was lengthened to reduce the thermal conduction to the DEC baseplate.

4.6.3 Second System Cold Test, 14 June 1985

CONDITIONS: All optics installed, objective was to test the entire system for acceptance.

RESULTS: The Large Area Source exhibited a thermal short. Pointing Mirror froze up and could not be moved. Some of the encoder switches were inoperative.

ACTION: A positional adjustment was made to the Large Area Source to eliminate the thermal short as it was in contact with the integrating sphere when cold. Gears were added to Pointing Mirror motors to increase torque. Adjustments were made in the encoder switch levers.

4.6.4 Third System Cold Test, 25 July 1985

CONDITIONS: All-up systems acceptance test.

RESULTS: Considerable data were obtained on all mechanical and optical systems. All mechanical systems functioned except as follows: The Pointing Mirror stuck in the negative X direction-- it was possible to loosen it by driving the motors with a larger current. Some switch encoders failed. The detector response indicated that a large background was present in DEC. There appeared to be some software problems regarding the analog gains used to preprocess the detector data.

ACTION: The Pointing Mirror Rulon bearing was loosened and alignment pins were added to provide repeatable performance. The encoder switch levers were completely redesigned, fabricated, and installed. The software was modified to correct the gain problem.

4.6.5 Fourth System Cold Test, 3 September 1985

CONDITIONS: All-up systems acceptance test.

RESULTS: Considerable data were obtained on the functioning of

all mechanical and optical systems. All mechanical systems worked except the Pointing Mirror stuck in the negative X direction (beyond -3°). The Full-Time Monitor preamplifier became inoperative midway through the test.

ACTION: Replace the Full-Time Monitor preamplifier.

NASA decided to accept the DEC based upon the results of the fourth system cold test. As to the Pointing Mirror problem, the specifications called for the mirror to operate over a 2° range which this test satisfied (See pages 37 and 38). It was also necessary to replace the Full-Time Monitor preamplifier.

Appendix F contains a detailed description and graphic presentation of the fourth and final cold test. A complete and exhaustive analysis of this data is not provided here. The details of the test were prescribed by NASA personnel and we have assumed that they would do most of the analysis in accordance with their measurement goals. However, temperature variations with motor usage, and light leak problems are addressed here in order to verify system performance in those areas and to illustrate the use of Appendix F.

Tests 201 through 205 (See pages F-5, F-6, and F-36 through F-37) moved all the wheels in the DEC system. The graphic data on page F-36 and F-37 shows appropriate outputs. The left and right columns provide scale calibrations and can be used with a straight-edge to read an intermediate data point. The traces show all 4 wheels moving through all their positions (these graphs resolve 19 positions, position zero indicates a nonvalid position and is the lowest graphic value; positions 1 through 18 correspond to wheel positions).

The traces also show the base plate #3 temperature (p.F-37). This graph covers a range of 0°K to 5°K with a 0.5° resolution. During test 200 (reference point), a 2° reading is indicated, and shows no change throughout the above referenced wheel tests.

Test 211 (Page F-38 and F-39) shows that when the bulb w/envelope is driven to 2.0 volts that the integrating sphere temperature does not change, but the large area source (LAS)

warms up and goes off scale (greater than 10°K). This is interesting because it seems that the LAS is absorbing radiant energy from the bulb.

Test 301 shows the LAS cooling some time later from the above bulb test. This test also shows the movement of the pointing mirror (PM) in both x and y axes. The PM temperature indicates temperatures fluctuating between 4 and 5°K .

Tests 500 through 511 move the beam sample mirror (BSM). in response to these movements the BSM temperature immediately rises from 2.5°K to about 6°K and levels off at about 10°K . Tests 600 through 602 show the BSM cooling down.

That concludes the discussion about motor use and the resulting temperature effects. Next we look at light leaks.

Test 1402 (page F-30 and F-94 through F-95) has source 2 on half power, open all wheels and run aperture wheel through all positions, and is the data reported below for beam linearity. A measure of light leaks can be obtained from this data also, since the aperture wheel was put in the closed position. The graphic data on page F-94 shows that the AR chopper, preamplifier, and bias are on, that the wheels are in the open position, and the AR response can be resolved to 1 volt as the aperture wheel passes through its positions. The AR response to the closed position is indicated as zero in the graphic data resolved to 1.0 volt. The same data are listed in Table 19 (below) to full resolution, where the AR response to the closed position is given as 0.020. Note that for very small apertures (positions 2 through 5) that the AR response varies from 13 to 24 mV. According to Appendix E, the AR noise varies from 1.36 to 2.90 mV rms; thus, the peak to peak variations are expected to be a factor of 3 to 5 times the rms value, possibly as great as 15 mV. It appears, for the data given in Table 19, that any light leaks are negligible.

4.7 Beam Linearity Tests

The beam linearity was measured in connection with the above described beam uniformity tests. The objective of this test was to verify that the beam power is proportional to the integrating sphere aperture area. By way of review: the aperture wheel contains 14 apertures whose area varies over a range of 8000. The DEC beam power is supposed to be a linear function of aperture area as described earlier. Table 15 describes the apertures, dimensions and relative beam energy.

The GaAs photometer was used to sample the beam power while the apertures were cycled through all 14 positions. The source was held constant so that the beam power should be a linear function of aperture area. The full dynamic range could not be covered in a single source setting; thus, the source was incremented and the apertures repeatedly cycled for a total of 6 independent data sets. The linearity of the photometer was established as reported above. Thus, the photometer output voltage should also be a linear function of aperture area. The data are given in Table 16, and a plot of the 6 data sets is given in Figure 58 where construction lines have been added to illustrate linear response. The data given in Table 16 and in Figure 58 are interpreted as follows:

- 1.) Each data set exhibits a background level for small apertures. This resulted from the fact that the ratio of flux in the first sphere to beam power is greater for small apertures. This background is to be expected since the integrating sphere module was not mounted in its DEC photon-tight compartment and the intersphere baffle had not been installed at the time of the measurement.
- 2.) With the exception of the low-level background, the response appears linear for apertures of area less than about 0.1 cm^2 and somewhat nonlinear for larger apertures. The exact amount of nonlinearity is difficult to determine from the data of Table 16 and Figure 58 because of the high background.

There exists a basis in theory for nonlinear performance in the integrating sphere module as follows: The first sphere loss factor F_1 (see equation (E-1)) is given by

$$F_1 = (r_o/2r_s)^2 \rho_w \{1 - \rho_w [1 - (r_1^2 + r_o^2)/4r_s]\}^{-1}$$

where

r_o = exit port radius (the aperture set)

r_1 = entrance port radius (the source)

r_s = sphere radius

ρ = wall reflectivity

Notice that the first term $(r_o/2r_s)^2$ is proportional to the exit port area (or precision aperture radius-squared). The second term also contains the exit aperture radius and results in the indicated nonlinear relationship between F_1 and r_o . The onset of nonlinearity occurs when the quantity r_o^2 is no longer negligibly small compared to r_1^2 , or in fact when the area of the exit port is about 0.03 of the entrance port (see Table 15).

The theoretical ratio of aperture area to sphere loss differs by 11.5% over the range of the aperture set for $\rho = 0.93$ as follows:

The ratio of aperture area to sphere loss for the 0.008-inch diameter aperture is 2.70, while the ratio for the 0.758-inch diameter aperture is 3.01. This is interpreted as indicating that the flux for the large aperture is 11.5% low.

The conclusions given here concerning beam nonlinearity are supported in the 25 July 1985 system cold test and the 2 September 1985 final cold test.

In the 25 July 1985 cold test, the Absolute Radiometer response was recorded for 9 sets of data in which the source level was varied from zero to full-on. Each set was obtained by recording the absolute radiometer response for each aperture set and for a particular source setting. This resulted in a family of curves as illustrated in Figure 59 (the construction lines represent linear response). The data in Figure 59 exhibit a

large background and nonlinear response for large-signal-levels.

The 3rd (from the bottom) and 9th (top) data sets of Figure 59 were subjected to best-fit linearity analysis. The 9th set is illustrated in Figure 60 and the computer report is given in Table 17. The background was compensated for by subtracting off 0.12 volts. The data, which ranges from 0.011 to 8.85 volts, exhibits a nonlinearity of 48.92% at 10 volts output; however, the onset of nonlinearity occurs at a relative beam power of about 0.03 or at 0.6 volts (see construction lines on the Figure). Note that a relative beam power of 0.03 corresponds to an aperture area of about 0.1 cm^2 as shown in Table 15.

The 3rd set is illustrated in Figure 61 and the computer report is given in Table 18. In this case the background was compensated for by subtracting off 0.0115 volts. The data, which ranges from 0.001 to 0.718 volts exhibits a nonlinearity of 27.3% at 1.0 volts output. Here again, the onset of nonlinearity occurs at an aperture area of about 0.1 cm^2 , but in this case it corresponds to 0.03 volts.

The 2 September data (see Appendix F, Test 1402) were obtained by setting Source S2 (bulb with envelope) at 1.917 volts and rotating the aperture wheel through all positions. These data are given in Table 19. The first column (V) is the AR rectified output voltage reported by the CMU for each aperture position. The second column is the bolometer V_{dc} with bias voltage reported by the CMU. The third column is the corrected AR rectified output voltage; this correction is made using Equation (E-3) (Appendix E). In order to make this correction it is necessary to know the V_{dc} without bias; the data for test 1401 and 1402 showed that V_{dc} without bias was stable at 0.566 volts. The fourth column is the AR rectified output corrected for offset V_o which appears to vary from 0.014 to 0.21 during the test; a value of 0.021 was used in the correction, indicating some negative (unreal) outputs for small apertures. The fifth, sixth and seventh columns give aperture position, aperture number, and relative beam power.

The data given in Table 19 were also subjected to linearity analysis. Only the data for aperture positions 8 through 15 are useful. The results are illustrated in Figure 62 and the computer report is given in Table 20. The AR response ranges from 0.033 to 3.684 and exhibits a nonlinearity of 37.15% for 10 volts. Once again, we see the onset of nonlinearity occurring at an aperture area of about 0.1 cm², but in this case it corresponds to an output of 0.05 volts.

The nonlinearity appears to be a function of aperture area rather than absolute output voltage and consequently is probably real but not of great consequence. The percent nonlinearity predicted by the computer program (Tables 17 and 18) for the cold-test data reported above is based upon an extrapolation of the data set to the indicated full-scale output and is subject to some error especially when the end-points contain some noise.

According to Appendix E, the Absolute Radiometer exhibits nonlinearity that is a function of absolute output voltage and is limited to signal levels above 1.0 volt (See Appendix E, Figure E-8) and could contribute to some of the nonlinearity observed in the above system tests. It is likely that the aperture position #14 nonlinearity is as predicted; namely about 10 to 12%.

The nonlinear relationship observed between the precision aperture and the beam power can be ignored provided the beam power is determined by the AR for any given aperture setting.

TABLE 15
Aperture Wheel Position, Aperture, Relative Energy and Area

Wheel Position	Aperture Diameter (Inches)	Relative Beam Energy	Area (cm ²)
1	Open	--	--
2	0.008	0.000111	0.000324
3	0.012	0.000251	0.00073
4	0.017	0.000502	0.00146
5	0.024	0.00100	0.00292
6	0.034	0.00201	0.00586
7	0.047	0.00384	0.0112
8	0.067	0.00781	0.0228
9	0.095	0.0157	0.0457
10	0.134	0.0313	0.091
11	0.190	0.0629	0.183
12	0.268	0.125	0.364
13	0.379	0.25	0.728
14	0.536	0.5	1.46
15	0.758	1.0	2.91
16	Open		
17	Open		
18	Opaque		

TABLE 16

Integrating Sphere linearity data obtained using the photometer to sample the beam power for 6 sets in which the source level was incremented from low to high flux levels. For each temperature the aperture wheel was sequenced through all positions.

Aperture Wheel Pos.	Area (cm ₂)	V = Photometer Output Increasing Source Density ▶▶▶▶▶▶					
		V ₁	V ₂	V ₃	V ₄	V ₅	V ₆
15	2.91x10 ⁰	4.95					
14	1.46x10 ⁰	2.62					
13	7.28x10 ⁻¹	1.38	5.13				
12	3.64x10 ⁻¹	0.75	2.93				
11	1.83x10 ⁻¹		1.46	7.95			
10	9.10x10 ⁻²		0.72	4.21			
9	4.57x10 ⁻²		0.36	2.17	7.30		
8	2.28x10 ⁻²			1.02	3.60		
7	1.12x10 ⁻²			0.48	1.79		
6	5.86x10 ⁻³				0.97	6.58	
5	2.92x10 ⁻³				0.49	3.58	8.89
4	1.46x10 ⁻³					1.69	4.43
3	7.30x10 ⁻⁴					0.87	2.24
2	3.24x10 ⁻⁴						

TABLE 17
 Computer Report of Best-Fit Linearity Analysis
 for Data Given in Figure 60

L I N E A R I T Y A N A L Y S I S

TABLE

MODEL DEC AR, 1 CHANNEL DEC
 SOURCE SELF DATE: 7/25/85

LINEARITY DATA SET (VOLTAGES ADJUSTED TO CH-HI)

SIGNAL (V)	AREA (SQ-CM)	SIGNAL (V)	AREA (SQ-CM)
8.850	1.000E+000	6.870	5.000E-001
4.158	2.500E-001	2.298	1.250E-001
1.194	6.290E-002	0.594	3.130E-002
0.308	1.570E-002	0.149	7.810E-003
0.075	3.840E-003	0.044	2.010E-003
0.021	1.000E-003	0.011	5.020E-004

FULL SCALE VOLTAGE REFERRED TO CH HI IS 10 VOLTS

CHANNEL GAINS

CHANNEL	GAIN
PRE	1.000

TRANSFER FUNCTION* (NO INTERCEPT TERM)

TERM NO.	TERM
1	4.760E-002
2	4.559E-003

QUALITY OF FIT AND NONLINEARITY*

STANDARD DEVIATION (PERCENT)	FULL-SCALE NONLINEARITY (PERCENT)
9.50	48.92

* REFERRED TO THE HIGH-GAIN CHANNEL

TABLE 18

Computer Report of Best-Fit Linearity Analysis
for Data Given in Figure 61

L I N E A R I T Y A N A L Y S I S

TABLE

MODEL DEC AR, 1 CHANNEL DEC
SOURCE SELF DATE: 7/25/85

LINEARITY DATA SET (VOLTAGES ADJUSTED TO CH-HI)

SIGNAL (V)	AREA (SQ-CM)	SIGNAL (V)	AREA (SQ-CM)
0.001	1.000E-003	0.002	2.010E-003
0.003	3.840E-003	0.007	7.810E-003
0.014	1.570E-002	0.029	3.130E-002
0.057	6.290E-002	0.114	1.250E-001
0.216	2.500E-001	0.410	5.000E-001
0.718	1.000E+000		

FULL SCALE VOLTAGE REFERRED TO CH HI IS 1 VOLTS

CHANNEL GAINS

CHANNEL	GAIN
PRE	1.000

TRANSFER FUNCTION* (NO INTERCEPT TERM)

TERM NO.	TERM
1	1.077E+000
2	4.052E-001

QUALITY OF FIT AND NONLINEARITY*

STANDARD DEVIATION (PERCENT)	FULL-SCALE NONLINEARITY (PERCENT)
6.64	27.34

* REFERRED TO THE HIGH-GAIN CHANNEL

TABLE 19

2 September 1985 Test Number 1402 (See Appendix F)

Source 2 on half-power
 All Filter Wheels Open
 Cycle Aperture Wheel

V	V _{dc}	V _c	V _c -V _o	Aperture Position	Aperture Number	Relative Beam Power
4.196	0.877	4.022	4.001	1	Open	-
0.015	0.879	0.014	-0.006	2	14	0.000111
0.014	0.879	0.013	-.007	3	13	0.000251
0.015	0.880	0.014	-0.006	4	12	0.000502
0.018	0.880	0.017	-.004	5	11	0.00100
0.024	0.880	0.023	0.002	6	10	0.00201
0.034	0.880	0.032	0.011	7	9	0.00384
0.057	0.880	0.054	0.033	8	8	0.00781
0.102	0.880	0.097	0.076	9	7	0.0157
0.182	0.880	0.173	0.152	10	6	0.0313
0.350	0.881	0.332	0.311	11	5	0.0629
0.677	0.881	0.642	0.621	12	4	0.125
1.265	0.880	1.199	1.178	13	3	0.25
2.354	0.881	2.231	2.209	14	2	0.5
3.909	0.880	3.705	3.684	15	1	1.0
4.227	0.879	4.021	4.000	16	Open	-
4.235	0.878	4.044	4.023	17	Open	-
0.021	0.881	0.020	-	18	Closed	-

TABLE 20

Computer Report of Linearity Analysis for Data
Given in Table 19 and Figure 62

L I N E A R I T Y A N A L Y S I S

TABLE

MODEL DEC AR , 1 CHANNEL DEC
SOURCE SELF DATE: 2 SEP 1985

LINEARITY DATA SET (VOLTAGES ADJUSTED TO CH-HI)

SIGNAL (V)	AREA (SQ-CM)	SIGNAL (V)	AREA (SQ-CM)
0.033	7.810E-003	0.076	1.560E-002
0.152	3.500E-002	0.311	6.250E-002
0.621	1.250E-001	1.178	2.500E-001
2.209	5.000E-001	3.684	1.000E+000

FULL SCALE VOLTAGE REFERRED TO CH HI IS 10 VOLTS

CHANNEL GAINS

CHANNEL	GAIN
PRE	1.000

TRANSFER FUNCTION* (NO INTERCEPT TERM)

TERM NO.	TERM
1	2.081E-001
2	1.230E-002

QUALITY OF FIT AND NONLINEARITY*

STANDARD DEVIATION (PERCENT)	FULL-SCALE NONLINEARITY (PERCENT)
8.04	37.15

* REFERRED TO THE HIGH-GAIN CHANNEL

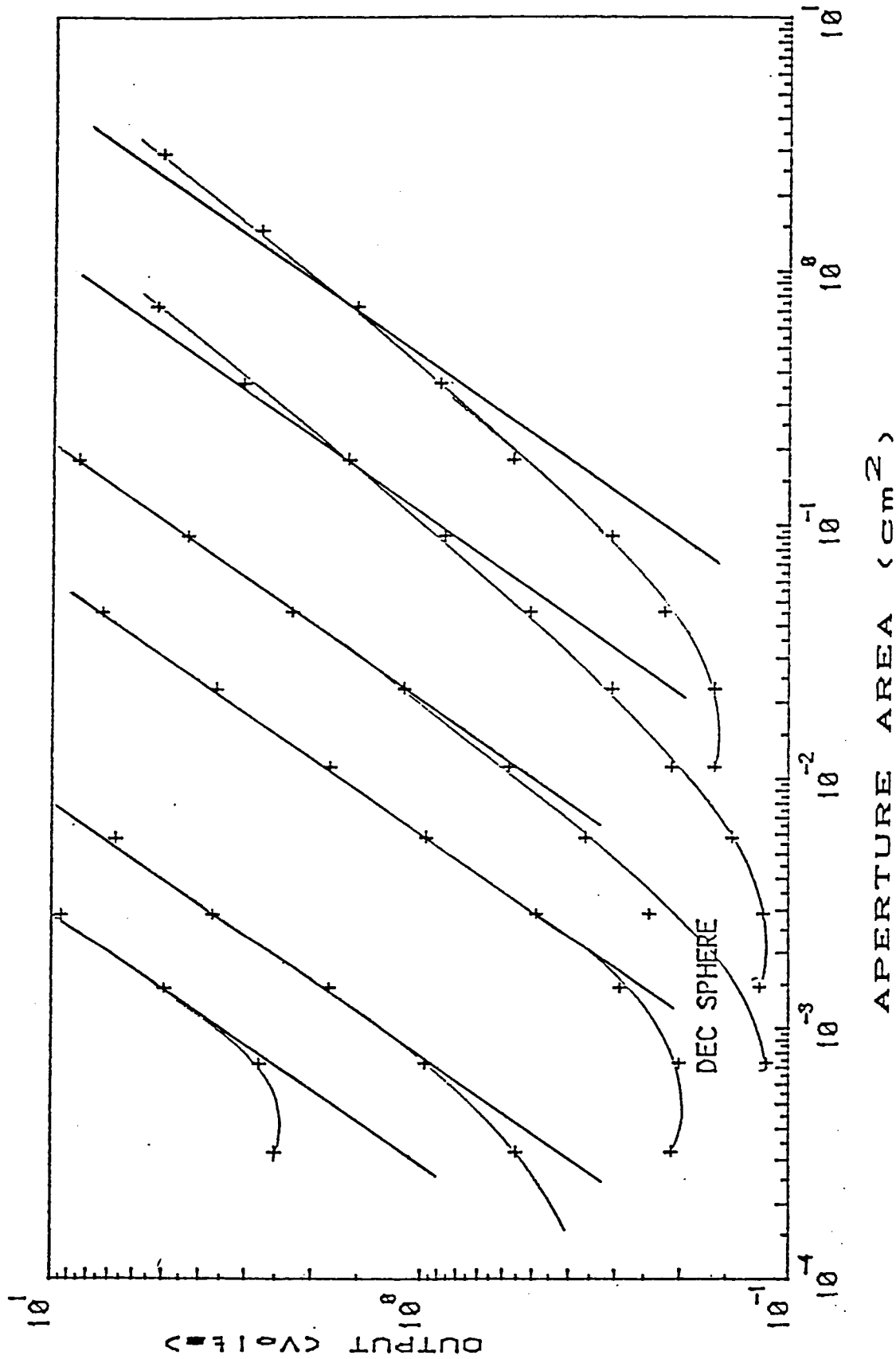
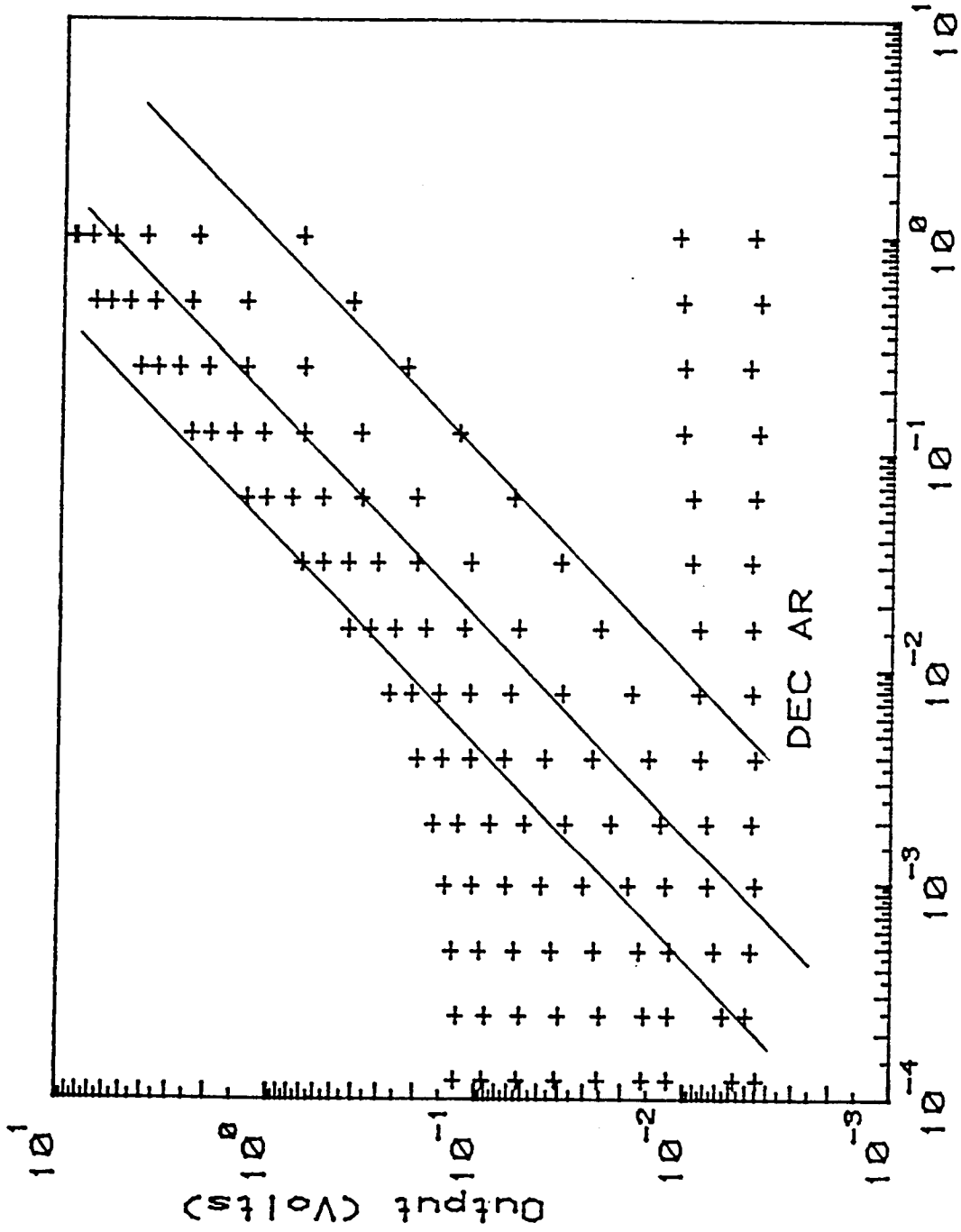


Figure 58. Beam linearity data obtained using the photometer to sample the beam power for 6 sets in which the source level was incremented from low to high flux levels. For each temperature the aperture wheel was sequenced through all positions. The data exhibit high background levels for small apertures and nonlinearity for large apertures.



RELATIVE BEAM ENERGY

Figure 59. Composite plot of the data given in Figure 58. The data sets were merged vertically discarding those points corrupted with background. The data exhibit about 65% nonlinearity at the largest aperture position.

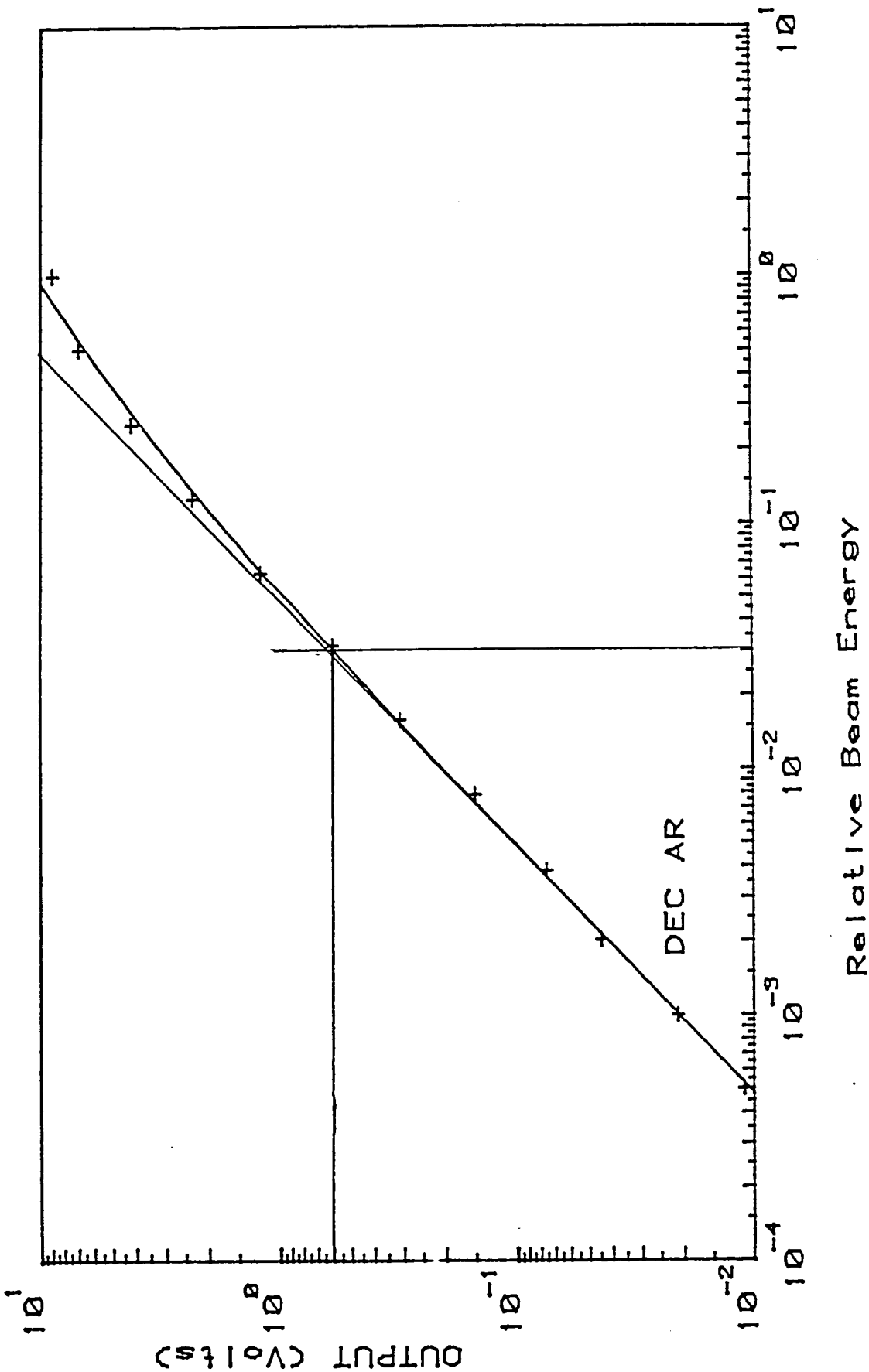


Figure 60; AR response for 9 sets of data in which the source power level was varied from zero to full-on. For each source level the aperture wheel was sequenced through all positions. The data exhibit non-linearity for all levels.

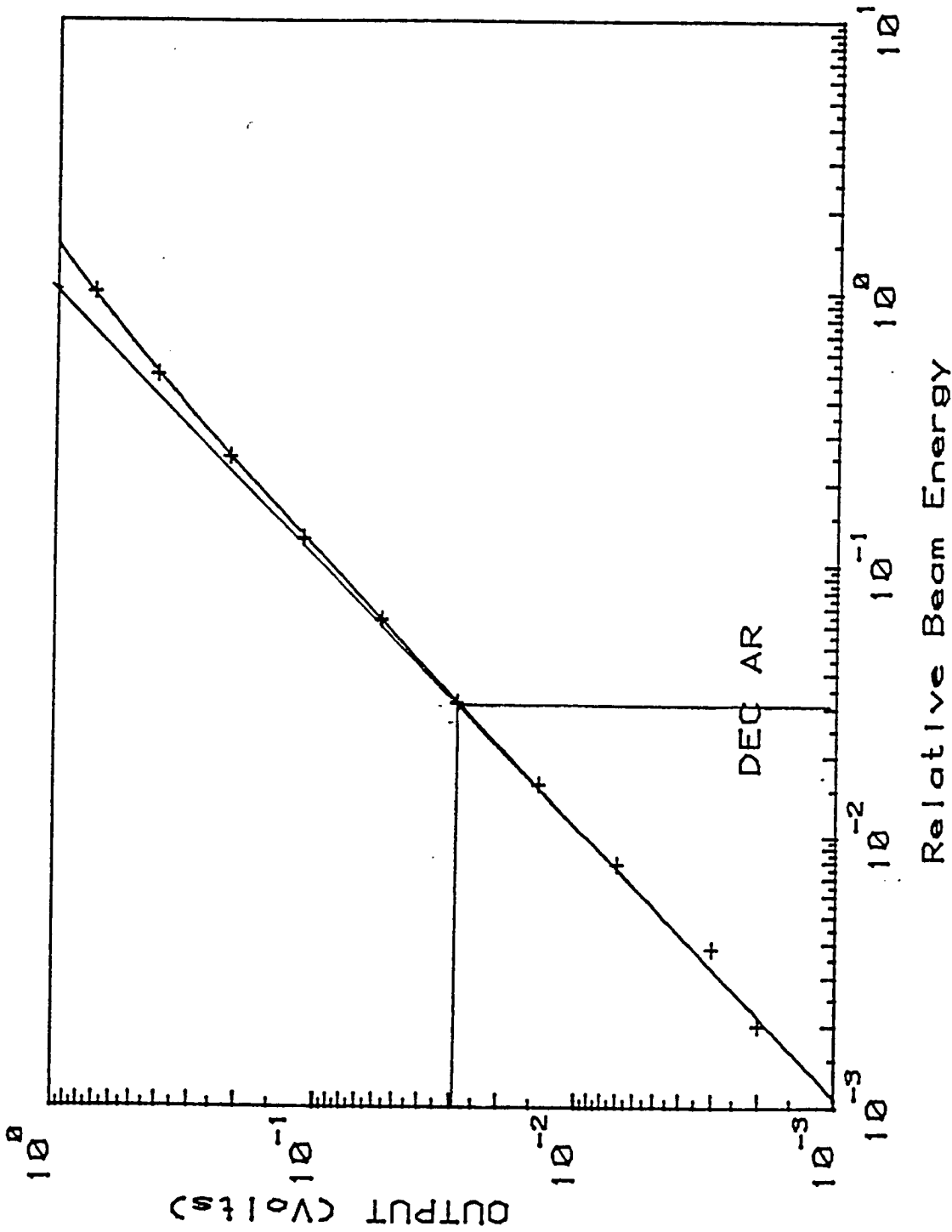


Figure 61. AR response for the 9th set of Figure 60. An offset correction of 0.12 volts was made in an attempt to correct for the background. The data for this graph is tabulated in Table 14, where the non-linearity is reported at 47.2% for 10 V.

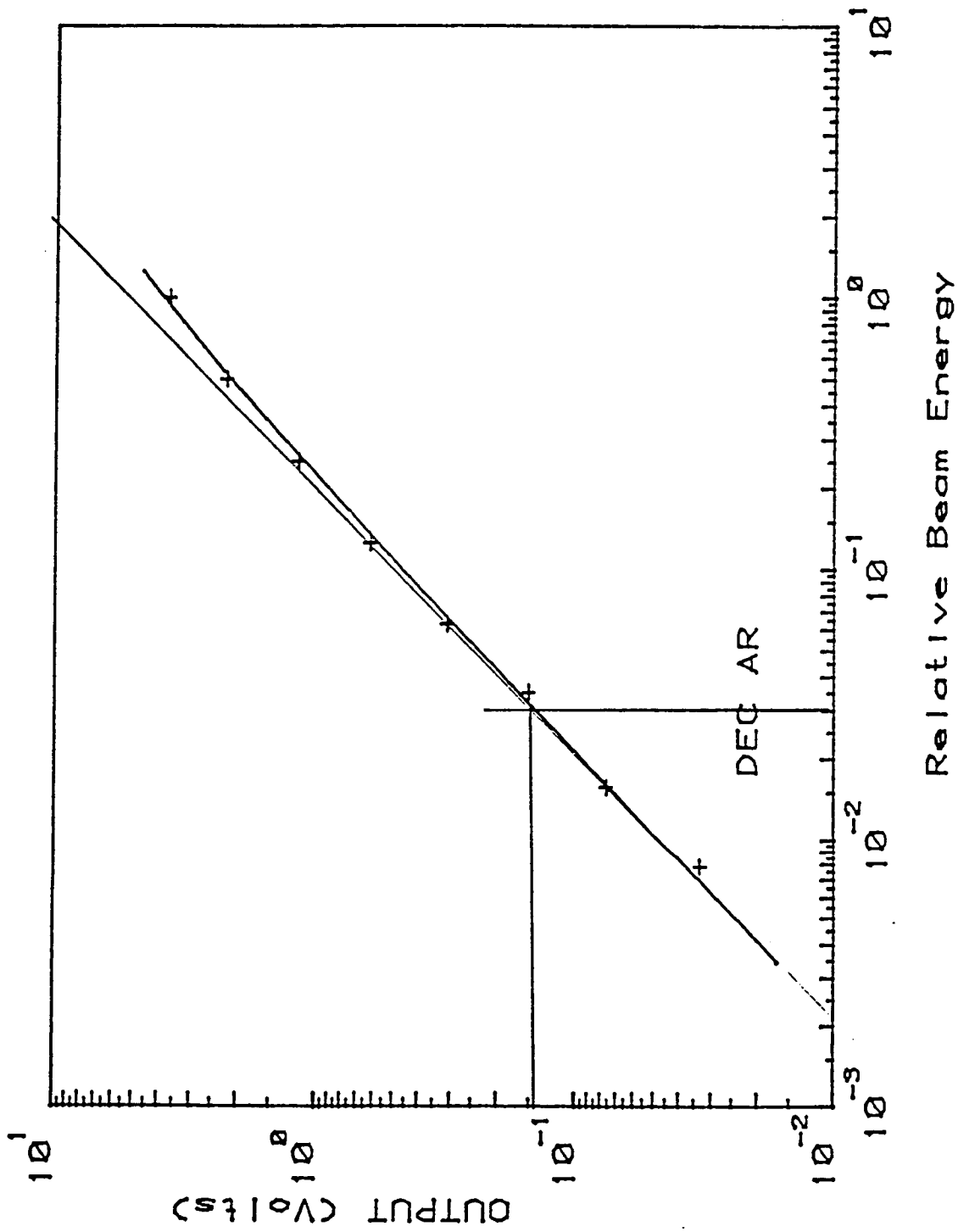


Figure 62. AR response for the 3rd set of Figure 60. An offset correction of 0.0115 volts was made in an attempt to correct for the background. The data for this graph is tabulated in Table 18, where the non-linearity is reported at 47%.

4.8 Beam Power

This section describes the procedure that must be used to calculate the effective beam power in a specific DIRBE band. The same (diffuse source mode) data given in section 4.7 (Beam Linearity Tests (25 July 1985 system cold test)) is used as an example. This is accomplished by examining the AR response and utilizing the AR calibration to find the beam sterance [radiance] in units of $W\text{ cm}^{-2}\text{ sr}^{-1}$. The beam power is given by the product of the beam sterance [radiance] and the DIRBE throughput.

Based upon the data for the 9th set (see Figures 60 and Table 17) we have for Source 2, aperture position 15, a maximum of 8.85 volts output for the open filter position. Using Equation (E-9) we have

$$9.193 \times 10^{-9} \times 8.9 + 6.134 \times 10^{-9} \times 8.9^2 = 1.30 \times 10^{-6} \quad W\text{ cm}^{-2}\text{ sr}^{-1}$$

The above calculation gives the average sterance [radiance] over that portion of the DEC beam that is sampled by the sample mirror.

The beam power (over the sampled region) is given by

$$L \times A \Omega = 8.87 \times 10^{-8} \quad W$$

where the DIRBE throughput is given by

$$A \Omega = \pi(D)^2 \times \text{Sine}^2 \delta = 6.82 \times 10^{-2} \quad \text{cm}^2 \text{sr}$$

where

the DIRBE aperture is $D = 19$ cm diameter and

the half-angle (square) field-of-view is 0.4443° .

The lamp voltage for the 9th data set was 3.84 volts (Note, the bulb is rated at 5.0 volts), and the mode selector wheel was set in the DSM position. Note: We have heard rumors that the DIRBE field-of-view has been, or may be changed from the specified value. However, the above calculation is typical and can be used

as an example of how the beam power calculation can be done for a specific DEC aperture and DIRBE throughput.

Corrections must be made, as detailed in Appendix E and repeated here, for the beam nonuniformity and for the DIRBE spectral band. The corrections for beam nonuniformity are accomplished by finding a factor F_{BEAM} which is used to correct the beam power as calculated from an AR calibration. The beam flux is given as a fraction F_{BEAM} of the total flux measured by the AR, where

$$F_{\text{BEAM}} = \frac{\frac{1}{N} \sum_{i=1}^N \Phi_i \text{ (DIRBE beam)}}{\frac{1}{M} \sum_{i=1}^M \Phi_i \text{ (BSM beam)}}$$

where the numerator is the average relative beam intensity over that portion of the beam sampled by DIRBE and N is the number of sample points in that set; where the denominator is the average of the relative beam intensity sampled by the beam sample mirror (the central 4 inches), and where Φ is taken from the beam uniformity measurement data, Appendix J.

The best that can be done to determine the DIRBE data subset is to assume a concentric 19-cm diameter region in the center of the DEC beam. A similar argument applies to the beam sample mirror subset, namely, assume a concentric 4-inch diameter (10.16 cm) region centered on the DEC beam. The exact locations depend upon the machine tolerance build-up and are not known. Perhaps they can be measured at NASA.

The corrections for a specific DEC band are also made by calculating a correction factor F_{BAND} which is used to correct the beam power as calculated from an AR calibration. The band flux is given as a fraction F_{BAND} of the total flux measured by

the AR in the open filter position, where

$$F_{\text{BAND}} = \frac{\int_{\text{DIRBE spectral band}} L(\lambda) R(\lambda) d\lambda}{\sigma T^4 / \pi}$$

where the integration is carried out over the DIRBE spectral bandpass function $R(\lambda)$, and the denominator gives the total sterance [radiance] for the open position. We do not believe the filters installed in the DEC are useful in this calibration for 2 reasons:

1. Their response function in the leak region is not presently known.
2. Even if the response function in the leak region was known to a high degree of accuracy, the leak is so enormous that the response with the filter in place is generally within an order of magnitude of the open response.

The only clear-cut solution to this problem is based upon the original premise that the DEC AR spectral response be matched to the DIRBE response.

The band corrections detailed above also require a knowledge of the spectral characteristics of the source and the integrating spheres. This should be straight-forward for the large-area source. This source should be an excellent blackbody simulator. However, the spectral properties of the lamps and the spheres poses more of a problem inasmuch as they have not been characterized in the spectral domain.

The answer to the question "how nearly does the AR large-area source approximate an ideal blackbody over the range of 1 to 1000 μm " is not known. We do not know of any data obtained in the system tests that can be applied to this problem because the factors that determine beam power (see Tables 1 and 2) are not well known.

APPENDIX A

Filter Spectral Transmittance:
Tabulations and Graphic Plots

This page intentionally left blank.

BAND 1 FILTER DATA

LAMBDA(μM)	t(LAMBDA)	R(LAMBDA)	LAMBDA(μM)	t(LAMBDA)	R(LAMBDA)
.500	.500E-03	.526E-03	7.600	.250E-03	.263E-03
.650	.500E-03	.526E-03	10.000	.250E-03	.263E-03
.800	.500E-03	.526E-03	13.000	.250E-03	.263E-03
.900	.500E-03	.526E-03	16.000	.370E-03	.389E-03
1.000	.500E-03	.526E-03	18.000	.550E-03	.579E-03
1.050	.500E-03	.526E-03	19.800	.800E-03	.842E-03
1.075	.500E-03	.526E-03	23.000	.800E-03	.842E-03
1.081	.250E-01	.263E-01	30.000	.800E-03	.842E-03
1.087	.600E-01	.632E-01	40.000	.800E-03	.842E-03
1.093	.900E-01	.947E-01	50.000	.800E-03	.842E-03
1.099	.210	.221	60.000	.800E-03	.842E-03
1.105	.390	.411	70.000	.800E-03	.842E-03
1.111	.500	.526	80.000	.800E-03	.842E-03
1.117	.600	.632	100.000	.800E-03	.842E-03
1.124	.640	.674	130.000	.350E-03	.368E-03
1.136	.860	.905	140.000	.150E-03	.158E-03
1.149	.950	1.00	200.000	.150E-03	.158E-03
1.163	.910	.958	300.000	.150E-03	.158E-03
1.176	.890	.937	340.000	.180E-02	.189E-02
1.190	.910	.958	360.000	.550E-02	.579E-02
1.205	.920	.968	390.000	.260E-01	.274E-01
1.220	.850	.895	410.000	.400E-01	.421E-01
1.235	.820	.863	435.000	.550E-01	.579E-01
1.250	.840	.884	464.000	.100	.105
1.266	.840	.884	500.000	.140	.147
1.282	.800	.842	555.000	.240	.253
1.299	.810	.853	625.000	.330	.347
1.316	.880	.926	667.000	.405	.426
1.333	.850	.895	689.000	.395	.416
1.351	.730	.768	741.000	.490	.516
1.370	.710	.747	800.000	.480	.505
1.389	.725	.763	870.000	.610	.642
1.408	.820	.863	904.000	.570	.600
1.418	.880	.926	1000.000	.720	.758
1.429	.660	.695			
1.449	.110	.116			
1.471	.250E-01	.263E-01			
1.493	.100E-01	.105E-01			
1.520	.500E-03	.526E-03			
1.950	.500E-03	.526E-03			
2.100	.500E-03	.526E-03			
2.200	.400E-03	.421E-03			
2.300	.350E-03	.368E-03			
2.600	.300E-03	.316E-03			
2.800	.250E-03	.263E-03			
3.000	.220E-03	.232E-03			
3.450	.200E-03	.211E-03			
3.900	.200E-03	.211E-03			
5.100	.250E-03	.263E-03			

PRECEDING PAGE BLANK NOT FILMED

BAND 1 FILTER DATA

LAMBDA(um)	t(LAMBDA)	R(LAMBDA)	LAMBDA(um)	t(LAMBDA)	R(LAMBDA)
.500	.500E-03	.526E-03	3.600	.150E-03	.158E-03
.650	.500E-03	.526E-03	3.900	.200E-03	.211E-03
.800	.500E-03	.526E-03	4.000	.120E-03	.126E-03
.900	.500E-03	.526E-03	5.100	.250E-03	.263E-03
1.000	.500E-03	.526E-03	7.600	.250E-03	.263E-03
1.050	.500E-03	.526E-03	10.000	.250E-03	.263E-03
1.075	.500E-03	.526E-03	13.000	.250E-03	.263E-03
1.081	.250E-01	.263E-01	16.000	.370E-03	.389E-03
1.087	.600E-01	.632E-01	18.000	.550E-03	.579E-03
1.093	.900E-01	.947E-01	19.800	.800E-03	.842E-03
1.099	.210	.221	23.000	.800E-03	.842E-03
1.105	.390	.411	30.000	.800E-03	.842E-03
1.111	.500	.526	40.000	.800E-03	.842E-03
1.117	.600	.632	50.000	.800E-03	.842E-03
1.124	.640	.674	60.000	.800E-03	.842E-03
1.136	.860	.905	70.000	.800E-03	.842E-03
1.149	.950	1.00	80.000	.800E-03	.842E-03
1.163	.910	.958	100.000	.800E-03	.842E-03
1.176	.890	.937	130.000	.350E-03	.368E-03
1.190	.910	.958	140.000	.150E-03	.158E-03
1.205	.920	.968	200.000	.150E-03	.158E-03
1.220	.850	.895	300.000	.150E-03	.158E-03
1.235	.820	.863			
1.250	.840	.884			
1.266	.840	.884			
1.282	.800	.842			
1.299	.810	.853			
1.316	.880	.926			
1.333	.850	.895			
1.351	.730	.768			
1.370	.710	.747			
1.389	.725	.763			
1.408	.820	.863			
1.418	.880	.926			
1.429	.660	.695			
1.449	.110	.116			
1.471	.250E-01	.263E-01			
1.493	.100E-01	.105E-01			
1.520	.500E-03	.526E-03			
1.950	.500E-03	.526E-03			
2.100	.500E-03	.526E-03			
2.200	.400E-03	.421E-03			
2.300	.350E-03	.368E-03			
2.600	.300E-03	.316E-03			
2.800	.250E-03	.263E-03			
3.000	.220E-03	.232E-03			
3.200	.200E-03	.211E-03			
3.400	.180E-03	.189E-03			
3.450	.200E-03	.211E-03			

BAND 2 FILTER DATA

LAMBDA(μM)	t(LAMBDA)	R(LAMBDA)	LAMBDA(μM)	t(LAMBDA)	R(LAMBDA)
.500	.500E-03	.610E-03	17.800	.100E-02	.122E-02
.650	.500E-03	.610E-03	22.800	.900E-03	.110E-02
.800	.500E-03	.610E-03	25.500	.900E-03	.110E-02
.950	.500E-03	.610E-03	26.700	.800E-03	.976E-03
1.100	.500E-03	.610E-03	29.000	.500E-03	.610E-03
1.250	.500E-03	.610E-03	68.000	.150E-02	.183E-02
1.400	.500E-03	.610E-03	80.000	.150E-02	.183E-02
1.650	.500E-03	.610E-03	100.000	.550E-03	.671E-03
1.930	.150E-03	.183E-03	130.000	.200E-03	.244E-03
1.940	.500E-02	.610E-02	150.000	.150E-03	.183E-03
1.960	.200E-01	.244E-01	200.000	.150E-03	.183E-03
1.970	.300E-01	.366E-01	250.000	.150E-03	.183E-03
1.980	.400E-01	.488E-01	285.000	.150E-03	.183E-03
1.990	.500E-01	.610E-01	290.000	.150E-03	.183E-03
2.000	.700E-01	.854E-01	300.000	.500E-03	.610E-03
2.010	.110	.134	330.000	.350E-02	.427E-02
2.020	.180	.220	350.000	.850E-02	.104E-01
2.030	.300	.366	380.000	.250E-01	.305E-01
2.060	.760	.927	400.000	.430E-01	.524E-01
2.070	.820	1.00	430.000	.650E-01	.793E-01
2.090	.790	.963	435.000	.750E-01	.915E-01
2.110	.770	.939	500.000	.180	.220
2.150	.760	.927	571.000	.365	.445
2.190	.770	.939	588.000	.365	.445
2.300	.750	.915	667.000	.460	.561
2.360	.740	.902	714.000	.450	.549
2.380	.750	.915	769.000	.560	.683
2.390	.670	.817	833.000	.520	.634
2.410	.400	.488	909.000	.680	.829
2.420	.160	.195	1000.000	.590	.720
2.440	.700E-01	.854E-01			
2.450	.300E-01	.366E-01			
2.470	.200E-01	.244E-01			
2.490	.100E-01	.122E-01			
2.510	.500E-02	.610E-02			
2.530	.100E-02	.122E-02			
2.540	.150E-03	.183E-03			
2.700	.150E-03	.183E-03			
2.850	.300E-03	.366E-03			
3.300	.400E-03	.488E-03			
3.450	.300E-03	.366E-03			
3.600	.250E-03	.305E-03			
4.000	.130E-03	.159E-03			
5.000	.120E-03	.146E-03			
6.200	.330E-03	.402E-03			
7.500	.230E-03	.280E-03			
10.000	.180E-03	.220E-03			
14.500	.180E-03	.220E-03			
16.300	.400E-03	.488E-03			

BAND 3 FILTER DATA

LAMBDA(μM)	t(LAMBDA)	R(LAMBDA)	LAMBDA(μM)	t(LAMBDA)	R(LAMBDA)
.400	.500E-03	.510E-03	4.348	.150E-03	.153E-03
.550	.500E-03	.510E-03	4.500	.500E-03	.510E-03
.700	.500E-03	.510E-03	5.300	.500E-03	.510E-03
.850	.500E-03	.510E-03	6.500	.400E-02	.408E-02
.950	.600E-03	.612E-03	6.757	.400E-02	.408E-02
1.000	.900E-03	.918E-03	6.780	.150	.153
1.100	.100E-02	.102E-02	6.849	.630	.643
1.200	.900E-03	.918E-03	6.897	.470	.480
1.300	.600E-03	.612E-03	7.018	.180	.184
1.400	.550E-03	.561E-03	7.067	.160	.163
1.600	.500E-03	.510E-03	7.143	.180	.184
1.750	.400E-03	.408E-03	7.273	.350	.357
1.900	.250E-03	.255E-03	7.463	.710	.724
2.050	.200E-03	.204E-03	7.547	.500	.510
2.200	.180E-03	.184E-03	7.692	.340	.347
2.500	.140E-03	.143E-03	7.843	.290	.296
2.778	.150E-03	.153E-03	8.000	.360	.367
2.857	.150E-03	.153E-03	8.097	.400	.408
2.941	.500E-02	.510E-02	8.333	.140	.143
2.963	.100E-01	.102E-01	8.511	.500E-01	.510E-01
2.985	.200E-01	.204E-01	8.803	.230E-02	.235E-02
3.008	.500E-01	.510E-01	9.500	.230E-02	.235E-02
3.030	.160	.163	10.500	.230E-02	.235E-02
3.053	.480	.490	10.707	.100E-02	.102E-02
3.077	.900	.918	11.001	.400E-01	.408E-01
3.101	.960	.980	11.111	.700E-01	.714E-01
3.125	.940	.959	11.364	.230	.235
3.175	.980	1.00	11.494	.340	.347
3.226	.895	.913	11.628	.410	.418
3.279	.870	.888	11.765	.430	.439
3.333	.900	.918	12.195	.270	.276
3.390	.915	.934	12.500	.170	.173
3.448	.885	.903	12.821	.130	.133
3.509	.880	.898	12.987	.118	.120
3.571	.940	.959	13.333	.110	.112
3.636	.960	.980	13.889	.120	.122
3.704	.920	.939	14.286	.110	.112
3.774	.880	.898	14.706	.900E-01	.918E-01
3.846	.890	.908	15.152	.800E-01	.816E-01
3.883	.910	.929	15.748	.100	.102
3.922	.940	.959	16.667	.190	.194
3.960	.980	1.00	17.094	.240	.245
4.000	.800	.816	17.857	.200	.204
4.040	.290	.296	18.519	.130	.133
4.082	.600E-01	.612E-01	19.231	.600E-01	.612E-01
4.124	.150E-01	.153E-01	20.000	.600E-01	.612E-01
4.167	.100E-01	.102E-01	21.008	.400E-01	.408E-01
4.211	.500E-02	.510E-02	21.978	.250E-01	.255E-01
4.255	.100E-02	.102E-02	22.400	.210E-01	.214E-01

BAND 3 FILTER DATA

LAMBDA(um)	t(LAMBDA)	R(LAMBDA)	LAMBDA(um)	t(LAMBDA)	R(LAMBDA)
22.700	.280E-01	.286E-01	122.000	.520	.531
22.800	.250E-01	.255E-01	123.500	.505	.515
23.200	.350E-01	.357E-01	124.200	.520	.531
23.800	.250E-01	.255E-01	125.000	.500	.510
24.200	.320E-01	.327E-01	126.600	.510	.520
25.000	.250E-01	.255E-01	127.400	.495	.505
26.200	.380E-01	.388E-01	129.000	.510	.520
27.400	.380E-01	.388E-01	129.900	.490	.500
28.000	.280E-01	.286E-01	133.300	.500	.510
28.800	.330E-01	.337E-01	134.600	.485	.495
30.600	.650E-01	.663E-01	135.500	.500	.510
31.500	.900E-01	.918E-01	137.000	.485	.495
33.300	.160	.163	137.400	.500	.510
33.900	.160	.163	139.900	.478	.488
36.400	.200	.204	140.800	.490	.500
37.700	.260	.265	142.900	.470	.480
40.000	.270	.276	143.900	.480	.490
42.500	.300	.306	145.400	.465	.474
44.400	.280	.286	146.400	.480	.490
45.900	.310	.316	148.200	.460	.469
47.200	.290	.296	149.300	.475	.485
49.300	.320	.327	151.500	.458	.467
50.800	.300	.306	152.700	.470	.480
52.600	.320	.327	153.900	.460	.469
54.100	.310	.316	156.000	.470	.480
55.600	.360	.367	157.500	.440	.449
58.200	.330	.337	159.200	.460	.469
64.500	.440	.449	161.300	.440	.449
69.000	.420	.429	162.600	.458	.467
80.000	.540	.551	165.300	.435	.444
80.700	.530	.541	166.700	.450	.459
81.300	.550	.561	168.900	.430	.439
84.000	.530	.541	169.800	.450	.459
86.200	.550	.561	172.400	.420	.429
87.000	.530	.541	174.800	.450	.459
100.500	.520	.531	176.100	.420	.429
101.200	.510	.520	178.600	.440	.449
102.000	.520	.531	180.200	.420	.429
102.800	.515	.526	183.500	.430	.439
103.000	.530	.541	185.200	.410	.418
104.000	.520	.531	188.700	.430	.439
109.900	.520	.531	190.500	.410	.418
110.500	.510	.520	192.300	.440	.449
111.100	.520	.531	196.100	.400	.408
114.900	.520	.531	198.000	.430	.439
118.300	.520	.531	200.000	.400	.408
119.300	.510	.520	204.100	.430	.439
120.500	.520	.531	206.200	.400	.408
121.200	.500	.510	208.330	.420	.429

BAND 3 FILTER DATA

LAMBDA(μM)	t(LAMBDA)	R(LAMBDA)	LAMBDA(μM)	t(LAMBDA)	R(LAMBDA)
212.800	.390	.398	740.700	.370	.378
215.100	.410	.418	769.200	.340	.347
217.400	.380	.388	833.300	.370	.378
222.200	.410	.418	869.600	.350	.357
224.700	.380	.388	909.100	.400	.408
227.300	.405	.413	1000.000	.340	.347
232.600	.375	.383			
235.300	.400	.408			
241.000	.370	.378			
243.900	.400	.408			
246.900	.370	.378			
253.200	.390	.398			
256.400	.360	.367			
263.200	.380	.388			
266.700	.350	.357			
270.300	.380	.388			
277.800	.350	.357			
281.700	.380	.388			
285.700	.345	.352			
294.100	.380	.388			
298.500	.350	.357			
303.000	.380	.388			
312.500	.350	.357			
317.500	.370	.378			
322.600	.335	.342			
333.300	.360	.367			
341.300	.335	.342			
344.800	.370	.378			
357.100	.340	.347			
363.600	.370	.378			
377.400	.340	.347			
384.600	.370	.378			
400.000	.340	.347			
408.200	.385	.393			
416.700	.340	.347			
434.800	.375	.383			
444.400	.333	.340			
465.100	.350	.357			
476.200	.340	.347			
487.800	.380	.388			
512.800	.345	.352			
526.300	.380	.388			
555.600	.330	.337			
561.800	.365	.372			
588.200	.340	.347			
625.000	.390	.398			
645.200	.360	.367			
666.700	.385	.393			
714.300	.330	.337			

BAND 4 FILTER DATA

LAMBDA(μM)	t(LAMBDA)	R(LAMBDA)	LAMBDA(μM)	t(LAMBDA)	R(LAMBDA)
.450	.500E-03	.588E-03	8.403	.200E-01	.235E-01
.600	.500E-03	.588E-03	8.475	.150E-01	.176E-01
.750	.500E-03	.588E-03	9.001	.100E-02	.118E-02
.900	.600E-03	.706E-03	9.597	.130E-02	.153E-02
1.000	.100E-02	.118E-02	10.000	.500E-03	.588E-03
1.100	.800E-03	.941E-03	10.604	.130E-02	.153E-02
1.250	.700E-03	.824E-03	11.001	.600E-02	.706E-02
1.400	.600E-03	.706E-03	11.111	.100E-01	.118E-01
1.650	.450E-03	.529E-03	11.364	.100	.118
1.800	.430E-03	.506E-03	11.494	.200	.235
2.250	.330E-03	.388E-03	11.628	.300	.353
2.700	.270E-03	.318E-03	11.834	.400	.471
3.000	.220E-03	.259E-03	12.048	.340	.400
3.450	.150E-03	.176E-03	12.346	.180	.212
4.000	.150E-03	.176E-03	12.500	.130	.153
4.258	.150E-03	.176E-03	12.821	.800E-01	.941E-01
4.286	.100E-02	.118E-02	12.987	.700E-01	.824E-01
4.310	.500E-02	.588E-02	13.514	.800E-01	.941E-01
4.310	.500E-02	.588E-02	13.986	.950E-01	.112
4.348	.130E-01	.153E-01	14.286	.900E-01	.106
4.484	.250E-01	.294E-01	14.706	.600E-01	.706E-01
4.494	.550E-01	.647E-01	15.267	.550E-01	.647E-01
4.545	.250	.294	16.129	.100	.118
4.598	.640	.753	16.667	.165	.194
4.619	.795	.935	17.391	.230	.271
4.706	.800	.941	17.857	.200	.235
4.762	.830	.976	18.519	.110	.129
4.819	.850	1.00	19.231	.700E-01	.824E-01
4.938	.830	.976	20.000	.600E-01	.706E-01
5.063	.820	.965	21.277	.550E-01	.647E-01
5.195	.800	.941	22.220	.450E-01	.529E-01
5.263	.680	.800	22.222	.450E-01	.529E-01
5.333	.300	.353	23.000	.380E-01	.447E-01
5.405	.600E-01	.706E-01	23.600	.320E-01	.376E-01
5.602	.100E-02	.118E-02	24.600	.330E-01	.388E-01
6.000	.100E-02	.118E-02	25.200	.230E-01	.271E-01
6.500	.100E-02	.118E-02	27.600	.230E-01	.271E-01
7.200	.900E-03	.106E-02	27.850	.900E-02	.106E-01
7.502	.600E-03	.706E-03	28.400	.200E-01	.235E-01
7.599	.120E-02	.141E-02	28.500	.200E-01	.235E-01
7.905	.200E-01	.235E-01	29.800	.420E-01	.494E-01
7.937	.350E-01	.412E-01	30.600	.380E-01	.447E-01
8.000	.110	.129	30.769	.400E-01	.471E-01
8.065	.400	.471	30.770	.400E-01	.471E-01
8.097	.535	.629	37.700	.600E-01	.706E-01
8.130	.370	.435	44.400	.260	.306
8.197	.150	.176	50.000	.370	.435
8.264	.700E-01	.824E-01	51.300	.390	.459
8.333	.400E-01	.471E-01	53.500	.400	.471

BAND 4 FILTER DATA

LAMBDA(μM)	t(LAMBDA)	R(LAMBDA)	LAMBDA(μM)	t(LAMBDA)	R(LAMBDA)
56.800	.440	.518	588.000	.540	.635
58.800	.430	.506	606.000	.520	.612
61.300	.445	.524	625.000	.570	.671
64.500	.430	.506	645.000	.485	.571
66.700	.440	.518	690.000	.565	.665
69.000	.420	.494	714.000	.440	.518
71.400	.440	.518	741.000	.580	.682
74.100	.420	.494	800.000	.575	.676
76.900	.455	.535	832.000	.580	.682
80.000	.420	.494	870.000	.390	.459
83.300	.440	.518	952.000	.570	.671
87.000	.415	.488	1000.000	.370	.435
90.900	.460	.541			
95.200	.460	.541			
100.000	.445	.524			
107.500	.515	.606			
111.100	.515	.606			
116.300	.545	.641			
120.500	.545	.641			
125.000	.620	.729			
133.300	.610	.718			
137.000	.630	.741			
142.900	.615	.724			
153.800	.610	.718			
156.700	.620	.729			
181.800	.610	.718			
200.000	.620	.729			
222.200	.600	.706			
247.000	.580	.682			
253.000	.590	.694			
256.000	.565	.665			
260.000	.580	.682			
263.000	.565	.665			
270.000	.585	.688			
274.000	.560	.659			
278.000	.570	.671			
286.000	.545	.641			
294.000	.560	.659			
303.000	.540	.635			
333.000	.560	.659			
345.000	.535	.629			
357.000	.550	.647			
370.000	.570	.671			
385.000	.540	.635			
435.000	.540	.635			
476.000	.550	.647			
488.000	.520	.612			
556.000	.520	.612			
562.000	.490	.576			

BAND 5 FILTER DATA

LAMBDA(μM)	t(LAMBDA)	R(LAMBDA)	LAMBDA(μM)	t(LAMBDA)	R(LAMBDA)
1.500	.800E-03	.920E-03	31.000	.350E-02	.402E-02
2.000	.500E-03	.575E-03	32.000	.130E-02	.149E-02
2.500	.300E-03	.345E-03	32.400	.650E-03	.747E-03
3.000	.230E-03	.264E-03	34.500	.800E-03	.920E-03
3.300	.150E-03	.172E-03	46.000	.800E-03	.920E-03
4.000	.150E-03	.172E-03	53.000	.800E-03	.920E-03
5.100	.150E-03	.172E-03	54.000	.800E-03	.920E-03
5.250	.330E-03	.379E-03	55.000	.170E-02	.195E-02
5.600	.330E-02	.379E-02	56.000	.650E-02	.747E-02
6.000	.300E-02	.345E-02	57.500	.180E-02	.207E-02
6.500	.300E-02	.345E-02	59.200	.700E-03	.805E-03
7.000	.300E-02	.345E-02	63.000	.350E-02	.402E-02
7.402	.100E-02	.115E-02	65.000	.800E-02	.920E-02
7.500	.200E-02	.230E-02	68.000	.100E-01	.115E-01
7.502	.500E-03	.575E-03	72.000	.250E-01	.287E-01
7.599	.500E-03	.575E-03	74.100	.350E-01	.402E-01
8.000	.200E-01	.230E-01	80.000	.830E-01	.954E-01
8.097	.375	.431	83.300	.115	.132
8.264	.585	.672	87.000	.165	.190
8.439	.675	.776	89.300	.173	.199
8.696	.705	.810	95.200	.125	.144
8.889	.825	.948	100.000	.850E-01	.977E-01
8.969	.810	.931	103.100	.750E-01	.862E-01
9.050	.850	.977	106.400	.780E-01	.897E-01
9.524	.730	.839	111.000	.630E-01	.724E-01
9.756	.800	.920	111.100	.630E-01	.724E-01
10.000	.760	.874	117.647	.200E-01	.230E-01
10.256	.850	.977	125.000	.100E-01	.115E-01
11.111	.570	.655	140.000	.200E-03	.230E-03
11.765	.870	1.00	220.000	.150E-03	.172E-03
12.500	.630	.724	290.000	.150E-03	.172E-03
12.903	.740	.851	370.000	.200E-03	.230E-03
13.423	.620	.713	435.000	.200E-03	.230E-03
13.889	.700	.805	478.000	.500E-03	.575E-03
14.815	.460	.529	552.000	.900E-03	.103E-02
16.000	.260	.299	678.000	.110E-02	.126E-02
16.393	.220	.253	840.000	.190E-02	.218E-02
16.667	.300	.345			
17.090	.300E-01	.345E-01			
17.094	.300E-01	.345E-01			
17.513	.200E-03	.230E-03			
18.215	.200E-03	.230E-03			
18.400	.500E-02	.575E-02			
19.500	.500E-02	.575E-02			
21.500	.500E-02	.575E-02			
25.000	.500E-02	.575E-02			
27.300	.500E-02	.575E-02			
27.500	.230E-02	.264E-02			
30.000	.230E-02	.264E-02			

BAND 6 FILTER DATA

LAMBDA(μM)	t(LAMBDA)	R(LAMBDA)	LAMBDA(μM)	t(LAMBDA)	R(LAMBDA)
1.111	.500E-02	.862E-02	25.000	.540	.931
1.250	.500E-02	.862E-02	25.641	.460	.793
1.299	.300E-02	.517E-02	26.316	.260	.448
1.333	.250E-02	.431E-02	26.667	.110	.190
1.471	.250E-02	.431E-02	27.027	.260	.448
1.739	.250E-02	.431E-02	27.322	.340	.586
2.000	.250E-02	.431E-02	27.933	.360	.621
2.222	.250E-02	.431E-02	28.571	.300	.517
2.500	.250E-02	.431E-02	28.736	.530	.914
2.703	.250E-02	.431E-02	28.986	.470	.810
2.857	.500E-02	.862E-02	29.412	.180	.310
3.333	.500E-02	.862E-02	30.303	.130	.224
3.800	.120E-02	.207E-02	30.581	.200	.345
4.200	.100E-02	.172E-02	31.250	.100	.172
4.900	.600E-03	.103E-02	31.746	.400E-01	.690E-01
5.800	.180E-03	.310E-03	31.750	.400E-01	.690E-01
6.500	.350E-03	.603E-03	32.300	.500E-01	.862E-01
7.900	.350E-03	.603E-03	33.003	.100	.172
9.100	.430E-03	.741E-03	33.300	.500E-01	.862E-01
9.600	.480E-03	.828E-03	34.483	.140	.241
10.800	.230E-03	.397E-03	34.500	.600E-01	.103
11.300	.380E-03	.655E-03	35.700	.900E-01	.155
12.600	.700E-03	.121E-02	35.714	.200	.345
13.600	.700E-03	.121E-02	36.300	.300E-01	.517E-01
15.408	.130E-02	.224E-02	36.364	.500E-01	.862E-01
15.504	.150E-01	.259E-01	36.765	.280E-02	.483E-02
15.601	.600E-02	.103E-01	36.800	.600E-03	.103E-02
16.000	.600E-01	.103	37.037	.100E-01	.172E-01
16.129	.120	.207	37.500	.280E-01	.483E-01
16.340	.200	.345	37.736	.500E-01	.862E-01
16.393	.180	.310	38.462	.700E-01	.121
-16.667	.340	.586	40.000	.100E-01	.172E-01
16.949	.480	.828	41.667	.100E-01	.172E-01
17.241	.500	.862	41.999	.230E-01	.397E-01
17.544	.470	.810	42.499	.110E-01	.190E-01
17.699	.500	.862	42.500	.180E-02	.310E-02
18.519	.500	.862	44.000	.350E-02	.603E-02
19.048	.530	.914	44.500	.170E-02	.293E-02
19.305	.450	.776	45.005	.140E-01	.241E-01
19.608	.480	.828	45.300	.280E-02	.483E-02
20.000	.500	.862	46.800	.100E-02	.172E-02
20.325	.560	.966	47.801	.280E-01	.483E-01
20.408	.540	.931	48.500	.150E-02	.259E-02
20.830	.580	1.00	48.996	.150E-01	.259E-01
20.833	.580	1.00	49.500	.650E-03	.112E-02
22.026	.490	.845	50.000	.400E-02	.690E-02
22.624	.425	.733	51.600	.350E-03	.603E-03
23.148	.500	.862	52.500	.650E-03	.112E-02
23.810	.500	.862	60.000	.450E-03	.776E-03

BAND 6 FILTER DATA

LAMBDA(UM)	t(LAMBDA)	R(LAMBDA)	LAMBDA(UM)	t(LAMBDA)	R(LAMBDA)
61.805	.500E-03	.862E-03	137.900	.215	.371
61.996	.100E-02	.172E-02	139.900	.190	.328
63.012	.800E-02	.138E-01	140.800	.220	.379
63.800	.650E-03	.112E-02	142.900	.200	.345
63.980	.220E-01	.379E-01	143.900	.210	.362
64.000	.180E-02	.310E-02	144.900	.190	.328
65.000	.750E-02	.129E-01	147.100	.210	.362
66.000	.160E-01	.276E-01	148.100	.200	.345
66.667	.700E-01	.121	153.800	.200	.345
67.000	.280E-01	.483E-01	156.300	.210	.362
68.966	.150	.259	158.700	.200	.345
71.400	.700E-01	.121	161.300	.180	.310
71.429	.210	.362	166.700	.190	.328
76.923	.340	.586	172.400	.180	.310
80.000	.360	.621	181.800	.190	.328
83.300	.150	.259	200.000	.240	.414
83.333	.350	.603	232.600	.280	.483
90.900	.190	.328	243.900	.275	.474
90.909	.420	.724	246.900	.300	.517
95.238	.390	.672	250.000	.290	.500
100.000	.135	.233	256.100	.310	.534
111.100	.180	.310	270.300	.280	.483
111.111	.390	.672	285.700	.320	.552
111.500	.160	.276	289.900	.300	.517
112.600	.120	.207	307.700	.300	.517
113.600	.175	.302	312.500	.315	.543
114.300	.120	.207	327.900	.300	.517
114.900	.170	.293	333.300	.270	.466
116.300	.120	.207	344.800	.250	.431
117.300	.180	.310	357.100	.300	.517
117.900	.140	.241	370.400	.290	.500
118.800	.185	.319	384.600	.270	.466
119.800	.140	.241	400.000	.290	.500
120.500	.190	.328	408.200	.280	.483
122.000	.160	.276	416.700	.300	.517
122.700	.200	.345	431.000	.280	.483
123.500	.160	.276	436.700	.300	.517
125.000	.195	.336	454.500	.270	.466
125.800	.160	.276	471.700	.300	.517
126.600	.200	.345	485.400	.270	.466
128.200	.188	.324	500.000	.305	.526
129.000	.210	.362	520.200	.275	.474
129.900	.180	.310	531.900	.320	.552
131.600	.200	.345	561.800	.290	.500
132.500	.175	.302	581.400	.330	.569
133.700	.205	.353	606.100	.300	.517
135.100	.180	.310	625.000	.310	.534
135.500	.215	.371	645.200	.290	.500
137.400	.180	.310	666.700	.300	.517

BAND 6 FILTER DATA

LAMBDA(um)	t(LAMBDA)	R(LAMBDA)	LAMBDA(um)	t(LAMBDA)	R(LAMBDA)
689.700	.270	.466			
714.700	.330	.569			
769.200	.240	.414			
800.000	.330	.569			
833.300	.250	.431			
909.100	.340	.586			
952.400	.180	.310			
1000.000	.350	.603			

BAND 7 FILTER DATA

LAMBDA(μM)	t(LAMBDA)	R(LAMBDA)	LAMBDA(μM)	t(LAMBDA)	R(LAMBDA)
1.111	.130E-01	.260E-01	84.000	.250E-03	.500E-03
1.176	.800E-02	.160E-01	84.034	.250E-03	.500E-03
1.333	.400E-02	.800E-02	90.000	.250E-03	.500E-03
1.667	.300E-02	.600E-02	99.000	.900E-03	.180E-02
1.818	.250E-02	.500E-02	108.000	.250E-03	.500E-03
2.128	.250E-02	.500E-02	122.000	.250E-03	.500E-03
2.500	.300E-02	.600E-02	150.000	.200E-03	.400E-03
2.703	.400E-02	.800E-02	200.000	.200E-03	.400E-03
3.333	.400E-02	.800E-02	250.000	.200E-03	.400E-03
3.800	.120E-02	.240E-02	300.000	.200E-03	.400E-03
5.000	.400E-03	.800E-03	350.000	.200E-03	.400E-03
5.600	.300E-03	.600E-03	400.000	.200E-03	.400E-03
7.200	.250E-03	.500E-03	430.000	.200E-03	.400E-03
10.000	.250E-03	.500E-03	500.000	.150E-03	.300E-03
16.000	.250E-03	.500E-03	570.000	.100E-01	.200E-01
20.000	.350E-03	.700E-03	588.000	.130E-01	.260E-01
23.800	.500E-03	.100E-02	605.000	.105E-01	.210E-01
26.000	.100E-02	.200E-02	640.000	.380E-01	.760E-01
28.249	.250E-03	.500E-03	650.000	.420E-01	.840E-01
29.070	.200E-02	.400E-02	700.000	.800E-01	.160
30.030	.600E-02	.120E-01	740.000	.800E-01	.160
30.400	.200E-02	.400E-02	847.000	.275	.550
30.488	.100E-01	.200E-01	909.000	.200	.400
32.000	.200E-01	.400E-01	1000.000	.360	.720
32.787	.300E-01	.600E-01			
33.898	.300E-01	.600E-01			
34.843	.400E-01	.800E-01			
35.971	.200E-01	.400E-01			
37.037	.250E-03	.500E-03			
37.500	.250E-03	.500E-03			
37.807	.250E-03	.500E-03			
38.023	.200E-02	.400E-02			
38.462	.250E-01	.500E-01			
39.216	.900E-01	.180			
40.000	.150	.300			
41.667	.215	.430			
44.444	.315	.630			
46.512	.370	.740			
50.000	.425	.850			
52.632	.460	.920			
57.143	.490	.980			
62.500	.500	1.00			
66.667	.430	.860			
71.429	.300	.600			
74.074	.170	.340			
76.923	.800E-01	.160			
80.000	.200E-01	.400E-01			
81.967	.350E-02	.700E-02			
82.988	.100E-02	.200E-02			

BAND 8 FILTER DATA

LAMBDA(um)	t(LAMBDA)	R(LAMBDA)	LAMBDA(um)	t(LAMBDA)	R(LAMBDA)
1.111	.180E-01	.271E-01	111.900	.580	.872
1.176	.140E-01	.211E-01	113.000	.555	.835
1.250	.800E-02	.120E-01	114.300	.570	.857
1.333	.600E-02	.902E-02	114.900	.560	.842
1.389	.400E-02	.602E-02	115.900	.565	.850
1.538	.300E-02	.451E-02	117.900	.560	.842
1.667	.250E-02	.376E-02	123.500	.560	.842
2.000	.250E-02	.376E-02	125.000	.550	.827
2.222	.400E-02	.602E-02	125.800	.560	.842
2.500	.400E-02	.602E-02	126.900	.520	.782
2.857	.200E-01	.301E-01	128.200	.550	.827
3.333	.200E-01	.301E-01	129.900	.505	.759
3.800	.170E-02	.256E-02	130.700	.550	.827
4.500	.170E-02	.256E-02	132.500	.495	.744
5.300	.600E-03	.902E-03	133.700	.550	.827
6.000	.330E-03	.496E-03	135.100	.500	.752
7.500	.230E-03	.346E-03	136.800	.540	.812
9.700	.280E-03	.421E-03	137.900	.510	.767
11.200	.300E-03	.451E-03	141.000	.520	.782
16.000	.400E-03	.602E-03	143.000	.520	.782
18.200	.600E-03	.902E-03	145.000	.540	.812
21.500	.800E-03	.120E-02	147.000	.515	.774
23.500	.100E-02	.150E-02	149.000	.540	.812
24.300	.180E-02	.271E-02	152.000	.520	.782
38.000	.230E-02	.346E-02	154.000	.565	.850
40.500	.300E-02	.451E-02	155.000	.510	.767
42.000	.600E-02	.902E-02	157.000	.600	.902
48.500	.600E-02	.902E-02	159.000	.520	.782
50.000	.200E-03	.301E-03	161.000	.600	.902
62.000	.200E-03	.301E-03	164.000	.530	.797
64.500	.150E-03	.226E-03	166.000	.575	.865
65.000	.100E-02	.150E-02	167.000	.555	.835
66.000	.100E-01	.150E-01	169.000	.570	.857
66.500	.250E-01	.376E-01	172.000	.570	.857
67.000	.400E-01	.602E-01	174.000	.605	.910
68.000	.650E-01	.977E-01	176.000	.570	.857
70.000	.150	.226	179.000	.615	.925
76.900	.220	.331	182.000	.580	.872
80.000	.300	.451	185.000	.620	.932
89.300	.470	.707	189.000	.590	.887
92.600	.450	.677	192.000	.640	.962
95.200	.520	.782	196.000	.600	.902
100.000	.510	.767	198.000	.640	.962
103.000	.540	.812	202.000	.595	.895
105.300	.550	.827	206.000	.615	.925
107.500	.560	.842	208.000	.600	.902
109.300	.560	.842	212.000	.630	.947
109.900	.570	.857	214.000	.610	.917
111.100	.560	.842	218.000	.660	.992

BAND 8 FILTER DATA

LAMBDA(μM)	t(LAMBDA)	R(LAMBDA)	LAMBDA(μM)	t(LAMBDA)	R(LAMBDA)
222.000	.630	.947			
226.000	.665	1.00			
238.000	.590	.887			
241.000	.600	.902			
247.000	.540	.812			
250.000	.600	.902			
256.000	.520	.782			
263.000	.590	.887			
270.000	.515	.774			
278.000	.630	.947			
286.000	.450	.677			
294.000	.625	.940			
302.000	.370	.556			
310.000	.485	.729			
323.000	.340	.511			
333.000	.410	.617			
345.000	.340	.511			
357.000	.595	.895			
368.000	.355	.534			
377.000	.490	.737			
400.000	.310	.466			
417.000	.420	.632			
435.000	.300	.451			
444.000	.410	.617			
465.000	.310	.466			
513.000	.400	.602			
532.000	.335	.504			
556.000	.520	.782			
588.000	.360	.541			
617.000	.545	.820			
658.000	.340	.511			
676.000	.390	.586			
758.000	.380	.571			
781.000	.340	.511			
833.000	.460	.692			
909.000	.370	.556			
1000.000	.550	.827			

BAND 9 FILTER DATA

LAMBDA(UM)	t(LAMBDA)	R(LAMBDA)	LAMBDA(UM)	t(LAMBDA)	R(LAMBDA)
1.111	.100E-01	.377E-01	129.500	.185	.698
1.176	.200E-01	.755E-01	130.700	.150	.566
1.299	.800E-02	.302E-01	132.100	.210	.792
1.538	.300E-02	.113E-01	133.700	.170	.642
1.818	.300E-02	.113E-01	135.100	.230	.868
2.000	.250E-02	.943E-02	136.600	.175	.660
2.222	.750E-02	.283E-01	138.100	.235	.887
2.500	.300E-02	.113E-01	139.500	.180	.679
2.857	.400E-02	.151E-01	141.000	.235	.887
3.333	.800E-02	.302E-01	143.300	.170	.642
3.950	.700E-03	.264E-02	145.300	.255	.962
5.100	.350E-03	.132E-02	147.100	.180	.679
6.300	.350E-03	.132E-02	149.300	.220	.830
7.500	.330E-03	.125E-02	151.000	.180	.679
8.600	.350E-03	.132E-02	152.700	.215	.811
9.800	.350E-03	.132E-02	155.000	.185	.698
10.800	.380E-03	.143E-02	156.700	.220	.830
11.600	.450E-03	.170E-02	158.700	.180	.679
13.600	.600E-03	.226E-02	160.500	.265	1.00
16.000	.600E-03	.226E-02	164.000	.160	.604
20.000	.120E-02	.453E-02	167.000	.200	.755
22.000	.600E-03	.226E-02	168.000	.165	.623
23.300	.170E-02	.642E-02	175.000	.165	.623
23.500	.800E-03	.302E-02	176.000	.200	.755
24.200	.320E-02	.121E-01	179.000	.140	.528
24.800	.320E-02	.121E-01	182.000	.170	.642
27.800	.200E-02	.755E-02	187.000	.130	.491
31.000	.200E-02	.755E-02	189.000	.170	.642
39.683	.500E-02	.189E-01	196.000	.120	.453
44.444	.400E-02	.151E-01	202.000	.150	.566
52.632	.650E-02	.245E-01	206.000	.110	.415
60.606	.800E-02	.302E-01	209.000	.165	.623
88.496	.120E-01	.453E-01	215.000	.100	.377
100.000	.100E-01	.377E-01	220.000	.170	.642
105.300	.200E-01	.755E-01	227.000	.100	.377
107.500	.350E-01	.132	233.000	.180	.679
108.900	.200E-01	.755E-01	235.000	.800E-01	.302
111.100	.450E-01	.170	238.000	.900E-01	.340
112.000	.250E-01	.943E-01	241.000	.750E-01	.283
112.600	.450E-01	.170	247.000	.125	.472
113.900	.500E-01	.189	253.000	.600E-01	.226
114.700	.150E-01	.566E-01	260.000	.900E-01	.340
117.600	.300E-01	.113	269.000	.500E-01	.189
119.800	.900E-01	.340	276.000	.105	.396
120.500	.655E-01	.247	280.000	.450E-01	.170
122.700	.110	.415	299.000	.800E-01	.302
125.300	.110	.415	308.000	.400E-01	.151
126.600	.170	.642	319.000	.550E-01	.208
128.200	.130	.491	350.000	.250E-01	.943E-01

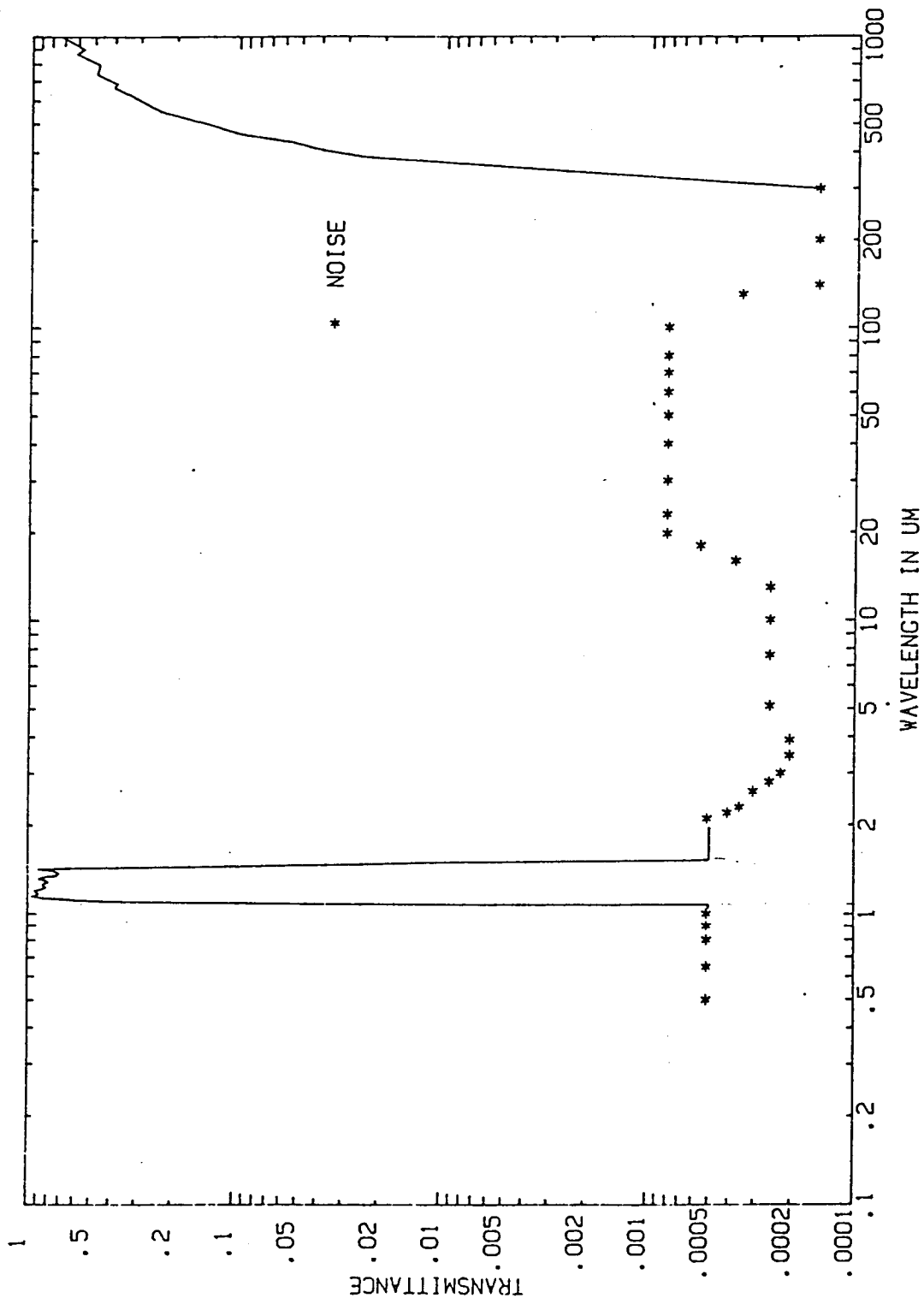
BAND 9 FILTER DATA

LAMBDA(μM)	t(LAMBDA)	R(LAMBDA)	LAMBDA(μM)	t(LAMBDA)	R(LAMBDA)
362.000	.500E-01	.189			
373.000	.180E-01	.679E-01			
385.000	.450E-01	.170			
415.000	.150E-01	.566E-01			
440.000	.450E-01	.170			
462.000	.130E-01	.491E-01			
480.000	.250E-01	.943E-01			
494.000	.250E-01	.943E-01			
525.000	.120E-01	.453E-01			
535.000	.250E-01	.943E-01			
550.000	.300E-01	.113			
588.000	.750E-02	.283E-01			
640.000	.190E-01	.717E-01			
662.000	.170E-01	.642E-01			
690.000	.450E-02	.170E-01			
710.000	.120E-01	.453E-01			
740.000	.130E-01	.491E-01			
762.000	.180E-01	.679E-01			
835.000	.600E-03	.226E-02			
863.000	.950E-02	.358E-01			
908.000	.850E-03	.321E-02			
942.000	.160E-01	.604E-01			
990.000	.100E-03	.377E-03			
1000.000	.100E-03	.377E-03			

BAND 10 FILTER DATA

LAMBDA(μM)	t(LAMBDA)	R(LAMBDA)	LAMBDA(μM)	t(LAMBDA)	R(LAMBDA)
1.111	.100E-01	.357E-01	227.273	.200	.714
1.176	.100E-01	.357E-01	231.482	.265	.946
1.250	.700E-02	.250E-01	238.095	.142	.507
1.333	.500E-02	.179E-01	243.902	.165	.589
1.538	.300E-02	.107E-01	246.914	.110	.393
1.667	.300E-02	.107E-01	250.000	.137	.489
2.000	.300E-02	.107E-01	256.410	.980E-01	.350
2.222	.500E-02	.179E-01	259.740	.140	.500
2.857	.600E-02	.214E-01	270.270	.650E-01	.232
3.333	.100E-01	.357E-01	279.330	.900E-01	.321
3.800	.200E-02	.714E-02	285.714	.500E-01	.179
4.500	.120E-02	.429E-02	294.118	.100	.357
4.900	.650E-03	.232E-02	304.878	.350E-01	.125
6.000	.400E-03	.143E-02	317.460	.750E-01	.268
7.000	.230E-03	.821E-03	333.333	.280E-01	.100
8.700	.230E-03	.821E-03	370.370	.400E-01	.143
11.000	.250E-03	.893E-03	392.157	.150E-01	.536E-01
13.000	.340E-03	.121E-02	413.223	.500E-01	.179
14.000	.450E-03	.161E-02	425.532	.150E-01	.536E-01
18.800	.800E-03	.286E-02	480.769	.100E-01	.357E-01
20.400	.110E-02	.393E-02	500.000	.420E-01	.150
22.700	.330E-02	.118E-01	531.915	.100E-01	.357E-01
24.500	.330E-02	.118E-01	574.713	.200E-01	.714E-01
28.409	.110E-02	.393E-02	617.284	.800E-02	.286E-01
32.258	.110E-02	.393E-02	657.895	.210E-01	.750E-01
36.364	.600E-03	.214E-02	714.286	.500E-03	.179E-02
42.017	.700E-03	.250E-02	800.000	.200E-01	.714E-01
48.780	.600E-03	.214E-02	869.565	.500E-02	.179E-01
60.606	.600E-03	.214E-02	1000.000	.100E-01	.357E-01
66.667	.100E-02	.357E-02			
81.301	.700E-03	.250E-02			
93.458	.600E-02	.214E-01			
105.263	.520E-02	.186E-01			
133.333	.480E-02	.171E-01			
149.254	.480E-02	.171E-01			
157.480	.500E-02	.179E-01			
158.730	.100E-01	.357E-01			
165.289	.100E-01	.357E-01			
167.224	.340E-01	.121			
172.414	.300E-01	.107			
175.439	.200E-01	.714E-01			
178.571	.500E-01	.179			
181.818	.300E-01	.107			
190.476	.100	.357			
192.308	.750E-01	.268			
200.803	.950E-01	.339			
204.082	.205	.732			
208.333	.130	.464			
222.222	.280	1.00			

BAND 1
AG 1.11 TEMPERATURE 2K



BAND 2
AG 2.11 TEMPERATURE 2K

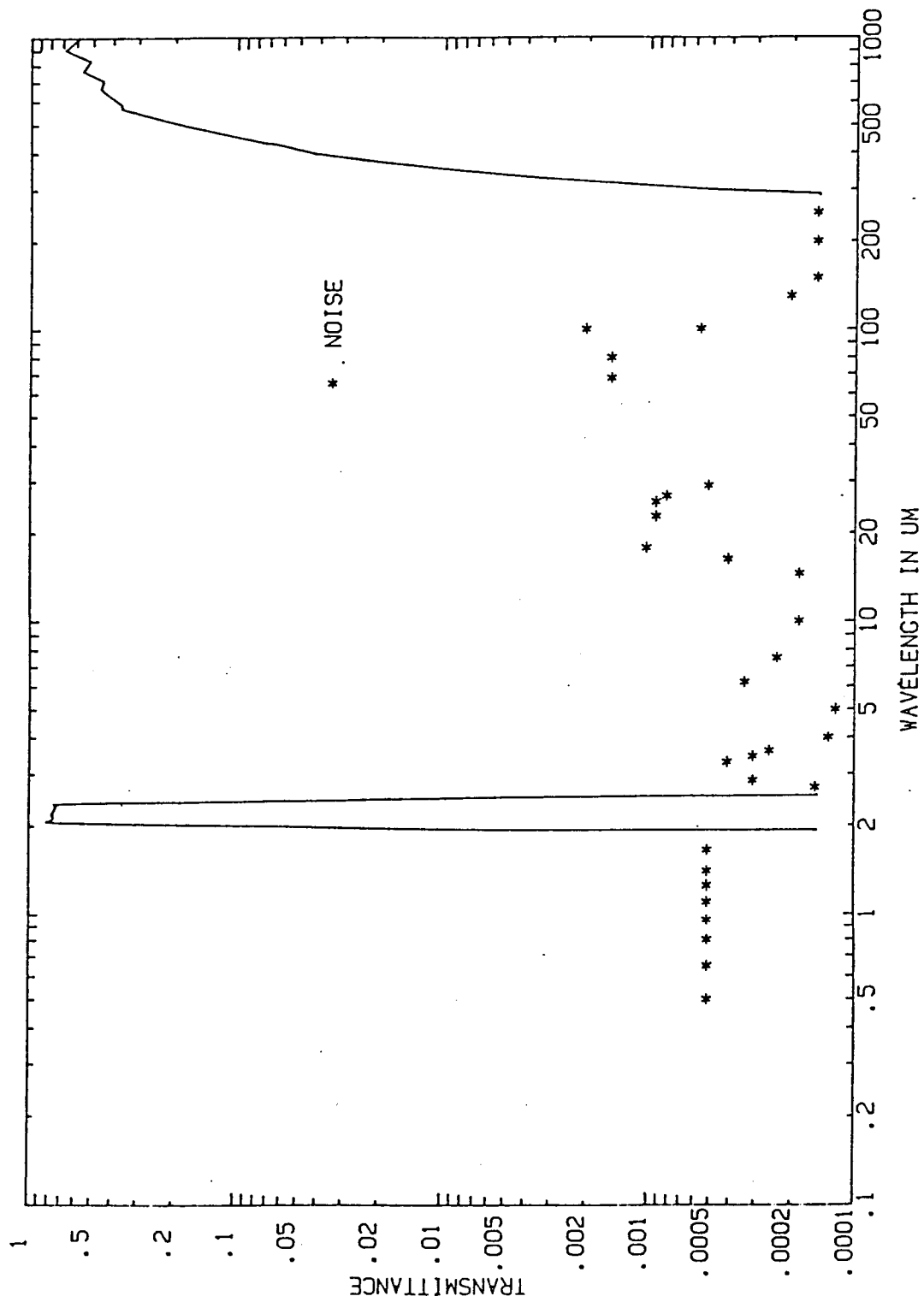


Figure A-2. Band 2, AG 2.11, Temperature 2°K, Wavelength vs. Transmittance.

BAND 3
AG 3.11
TEMPERATURE 2K

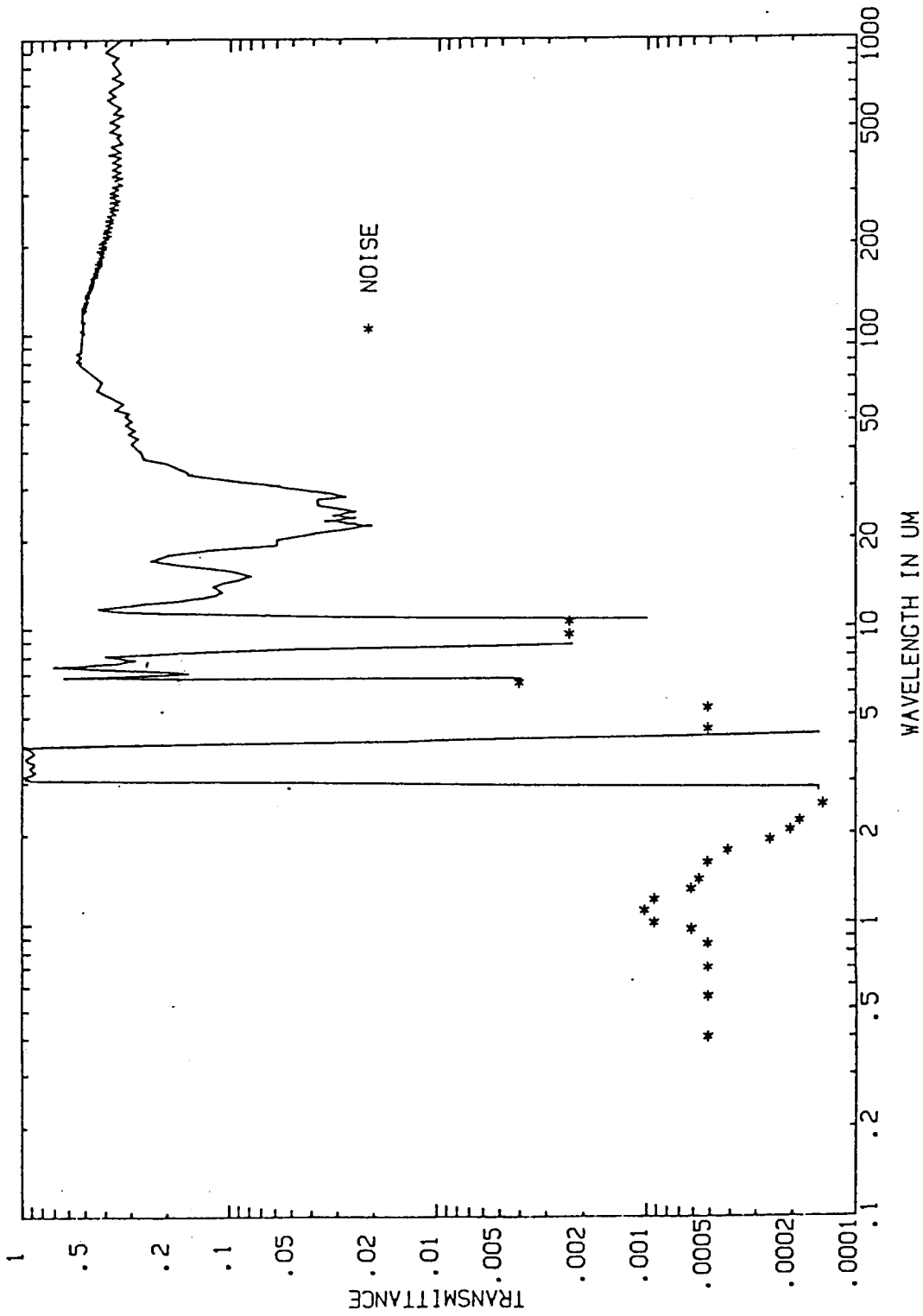


Figure A-3. Band 3, AG 3.11, Temperature 2°K, Wavelength vs. Transmittance.

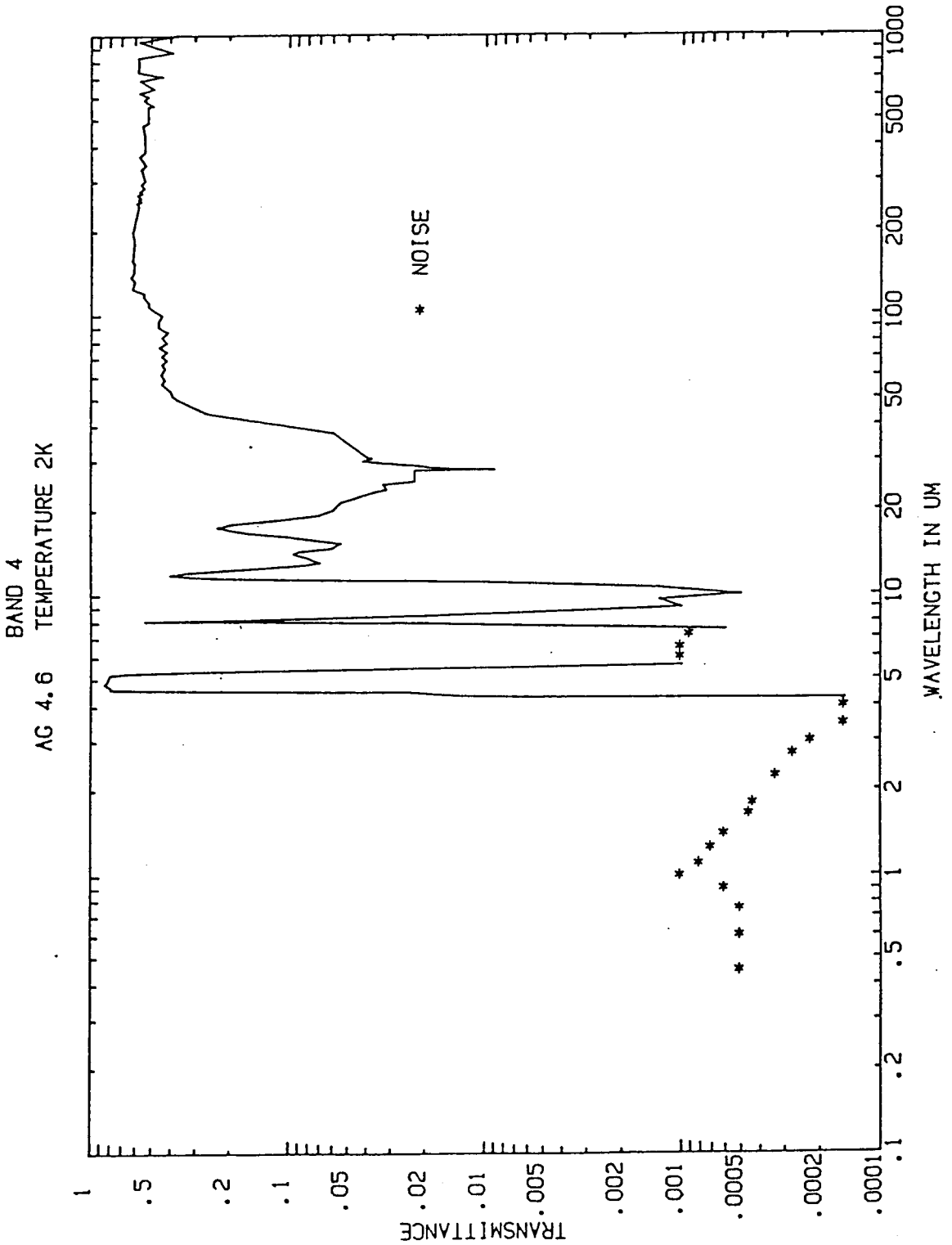


Figure A-4. Band 4, AG 4.6, Temperature 2°K, Wavelength vs. Transmittance.

BAND 5
BA 5.1 & BA 5.1A TEMPERATURE 2K

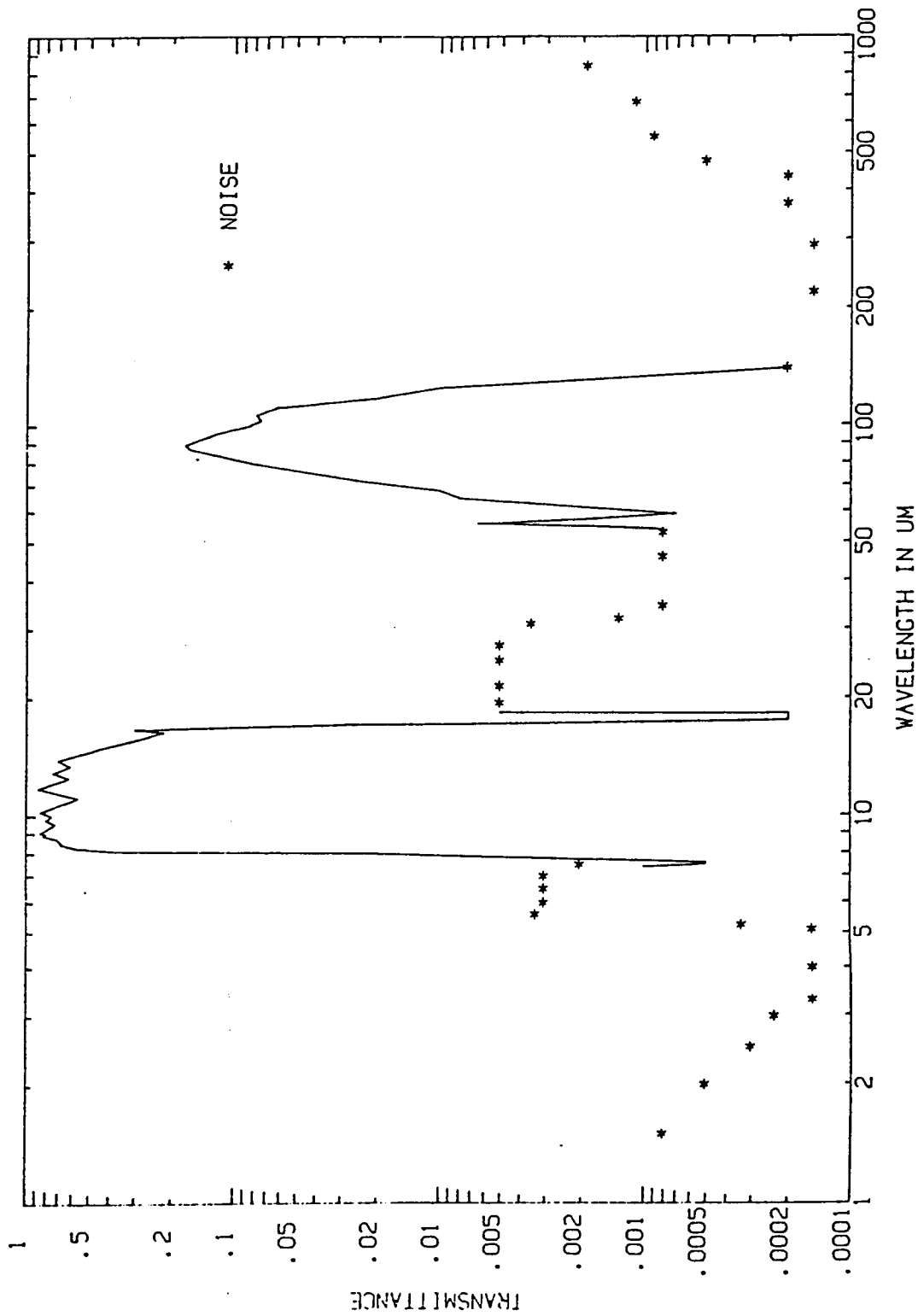


Figure A-5. Band 5, BA 5.1 and BA 5.1A, Temperature 2°K, Wavelength vs. Transmittance.

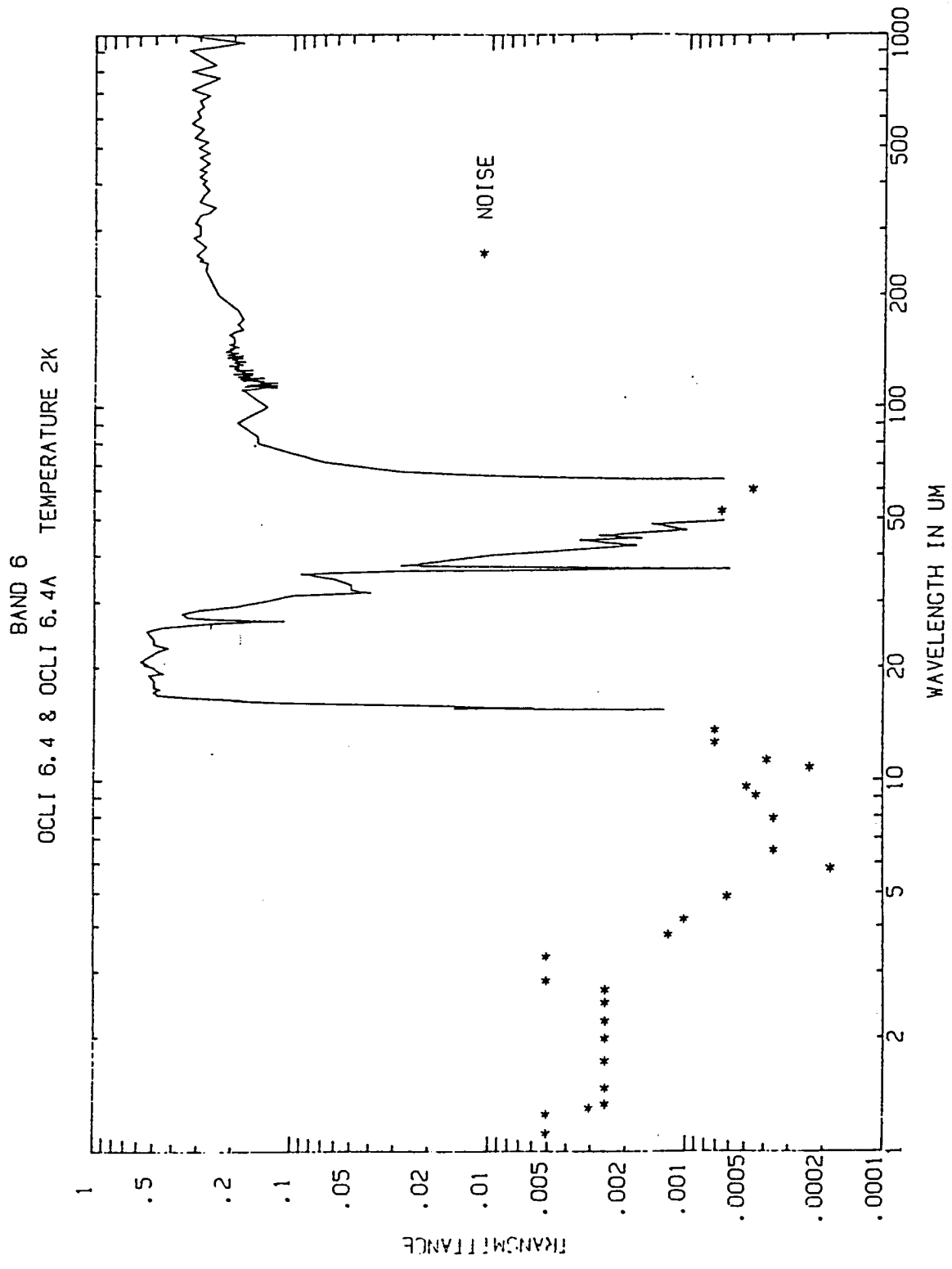


Figure A-6. Band 6, OCLI 6.4 and OCLI 6.4A, Temperature 2°K, Wavelength vs. Transmittance.

BAND 7
 OCLI 7.3 TEMPERATURE 2K

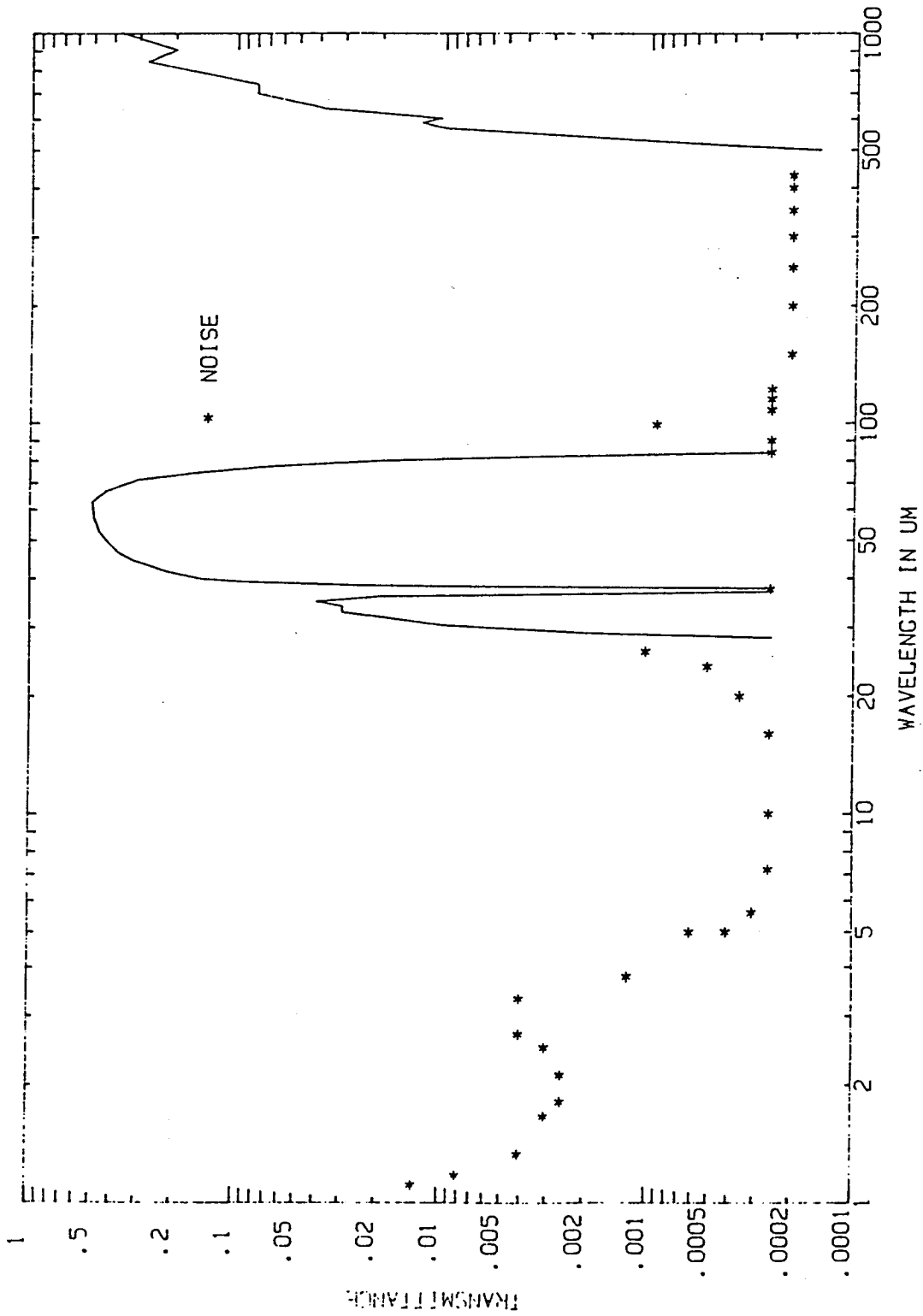


Figure A-7. Band 7, OCLI 7.3, Temperature 2°K, Wavelength vs. Transmittance.

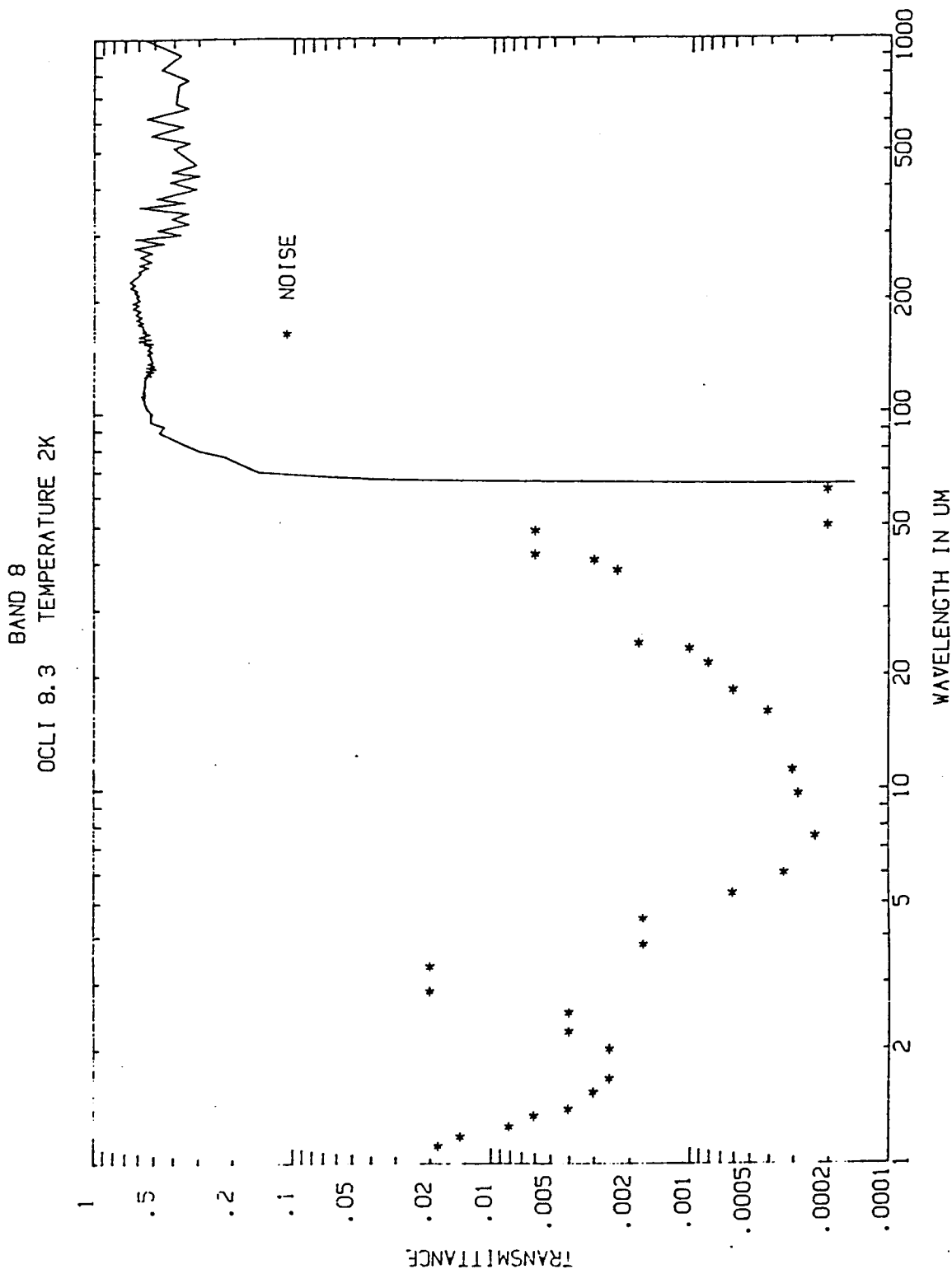


Figure A-8. Band 8, OCLI 8.3, Temperature 2°K, Wavelength vs. Transmittance.

BAND 9
PE 9.1 TEMPERATURE 2K

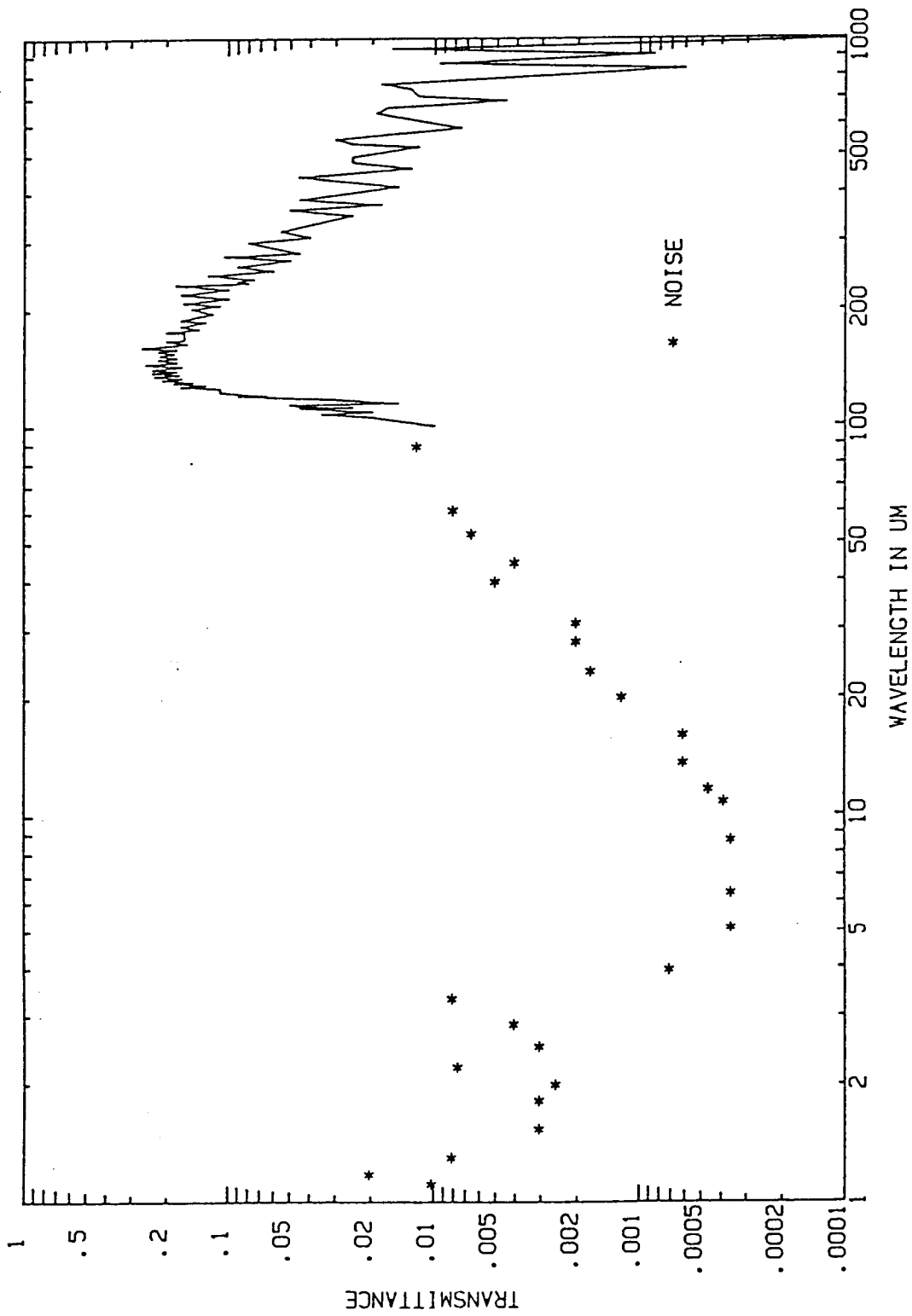


Figure A-9. Band 9, PE 9.1, Temperature 2°K, Wavelength vs. Transmittance.

BAND 10
PE 10.1 TEMPERATURE 2K

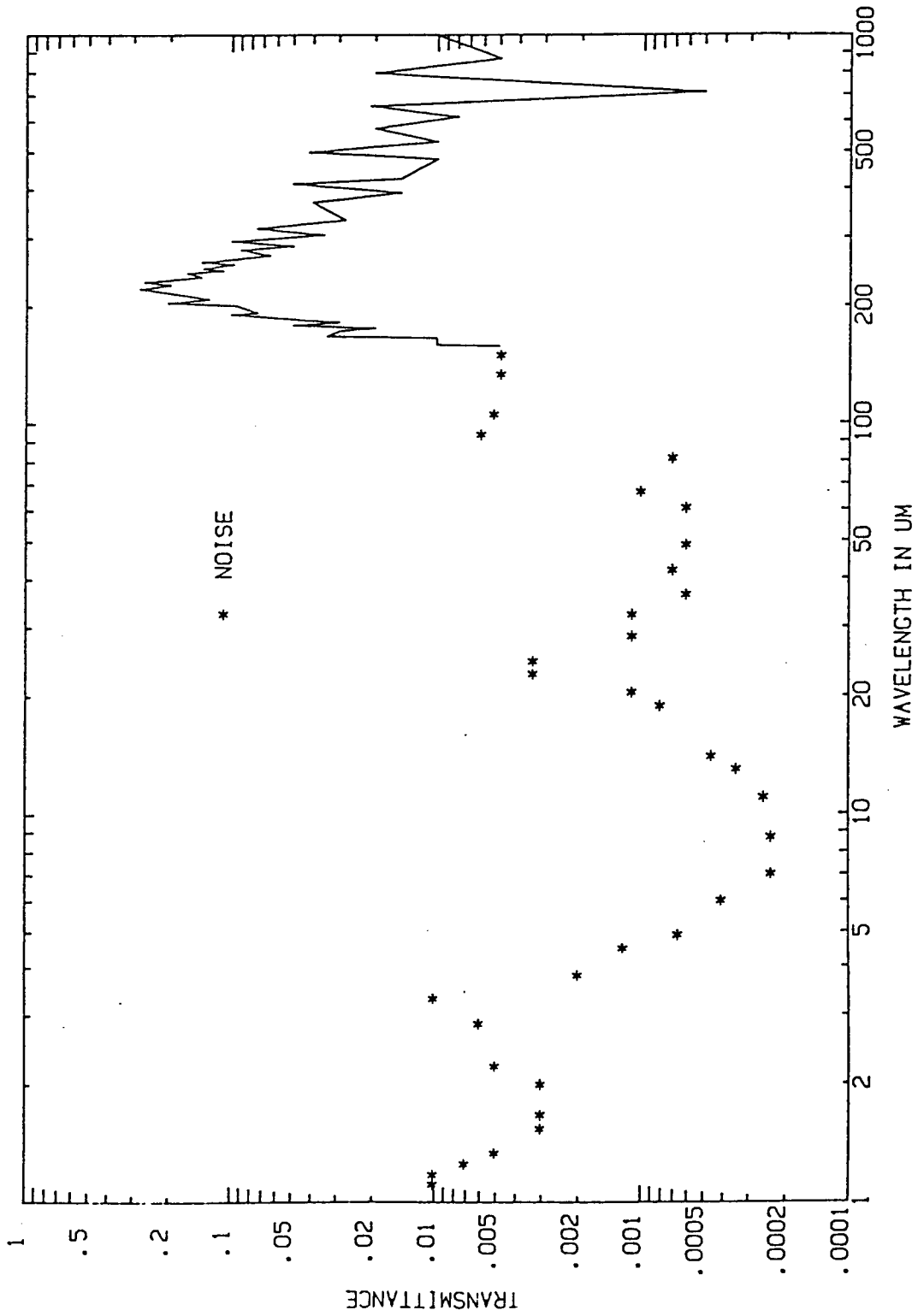


Figure A-10. Band 10, PE 10.1, Temperature 2°K, Wavelength vs. Transmittance.

APPENDIX B

Description of CMU

Electronics and Operation

The organization of the CMU is given within this Appendix in the following order:

Description of Electronics

- STD BUS
- Digital Electronics in The STD Box
- Analog Electronics
- Bolometer Battery Postamps
- Wiring

Description of CMU Operation

- Wheel Moves
- Wheel Position Requests
- Beam Sample Mirror Moves
- Beam Sample Mirror Position Requests
- Pointing Mirror Moves
- Pointing Mirror Position Requests
- LVDT Control
- Bolometer Signal Requests
- Chopper Monitors and Control
- Preamp Monitors and Control
- Bias Monitors and Control
- Temperature Monitor Requests
- Source Control

PRECEDING PAGE BLANK NOT FILMED

ELECTRONICS

The CMU consists of electronics located in three separate boxes. The STD box contains the STD BUSS and a card cage with four boards which handle the wheel position encoders and stepper motor drivers. All of the AC supplies for the system are also located in this box. A smaller analog electronics box contains the signal conditioning and amplifier boards used in the system. The third box in the system has been built as part of the outer vacuum connector plate. This box contains the batteries which supply power and bias to the bolometer circuits, and provide the first stage of gain for the bolometer signals. This box is located on the outer vacuum flange to minimize the noise on these signals.

STD BUSS

The STD BUSS consists of 9 boards in the card cage with the PRO-LOG motherboard on the back plane. All of the boards in the STD BUSS are from commercial vendors, and 3 copies of all manuals will be included in the documentation supplied. A single paragraph describing each of the boards in the system will follow to acquaint the user with the features and uses of each board in the system.

The Pro-Log 7806 Multifunction CPU card is the heart of the system. It contains the microprocessor which controls the show. Also on this card is 4 memory chips. One of the sockets contains an 8K x 8 RAM memory chip. One socket contains a 27256 EPROM which contains the assembly language program. One socket contains a 27256 EPROM which contains the Temperature lookup conversion tables. The last socket contains a 27256 EPROM which contains the lookup table to convert the LVDT sensor volts to angular degrees of the beam. Also contained on this board is the serial port which allows the processor to communicate with the IBM PC at 9600 baud.

The Pro-Log 7601 Input/Output Port Card gives the system 32 bits of input and 32 bits of output. This card reads all of the position encoder bits which are on the wheels and Beam Sample mirror in the system. The output bits are used to control switches which turn choppers, LVDT's bias', and preamps power on and off. They are also used to select which motor we will drive with the signals from the stepper motor controller boards. They are also used to set up a seek address to the wheel position boards when we are moving wheels to a new position.

There are two Applied Micro Technology ST4303 Analog to Digital converter boards in the system. They have been arbitrarily called A/D board 0 and A/D board 1. We are using 24 channels of input on board 0, so it has wires going to both of the connectors on the end of the board. Board 0 has been set to give an input range of 0 to +10 volts. It converts the input signal to a 12 bit digital count with 0 volts being count 0 and +10 volts being a count of 4095. A/D board 1 uses 16 input signals, so only one of its connectors on the top of the board is used. This board has been set up with an input range of -10 volts to +10 volts. It gives an offset binary output, so -10 volts gives a count of 0 and +10 volts gives a count of 4095.

Both of the A/D converter boards discussed above required a ± 15 voltage supply to operate which is not available on the STD BUSS backplane. So an Applied Micro Technology ST4309 DC Power Supply board is used in one of the STD BUSS slots. This board converts the +5 volts from the STD BUSS to ± 15 volts to be used by the A/D converter boards.

A RMAC (name changed to Ultra Link on later manuals) DA-16 Digital to Analog converter board is used in the system. This board is set up to output 0 to 10 volts. This board is used to obtain a voltage to use in driving the various sources in the system. The full 0 to 10 volt range is used, and divided down on the driver circuits for the sources which are limited to inputs less than 10 volts.

There are two Technology 80 Inc. Model 4302 Stepper Motor controllers used in the system. These boards allow the microprocessor to set a maximum number of steps, a speed, and a direction to step a motor. The controller will continue to step until the maximum number of steps has been reached or until a stop pulse is received. We are using the two controllers to drive 7 motors in the system. There are 4 motors which may be driven by one board and 3 motors which may be driven by the other board. Each board can only drive one motor at a time, but both boards may be driving a motor at the same time. This allows us to move both the X and the Y axis motors of the pointing mirror at the same time.

The last board in the STD BUSS system is the Pro-Log 7909A Terminator Card. This card terminates all of the address, data and control signals of the STD BUSS. This board must be placed to the left of the last board in the system. This board has a + 5 volt indicator LED and a pushbutton reset for the microprocessor. We have also added a relay to provide remote reset capability. A reset BNC is located on the back of the STD Box. A BNC cable may be run to a convenient location to have a reset switch. A reset is accomplished by shorting the two leads in the BNC. This could be accomplished with a momentary switch.

DIGITAL ELECTRONICS IN STD BOX

A card cage is located in the right front quarter of the STD box which contains the Wheel Position and Stepper Driver boards. These boards are located in this area to keep switching noise away from the analog electronics. There are four boards in the rack including two Stepper Driver boards, and two Wheel Position boards.

The Stepper driver boards occupy slots 1 and 4 of the rack. The boards are identical and may be interchanged without any problems. The boards receive phase 1 through phase 4, and a motor enable from the Stepper motor controller boards in the STD BUSS.

Each board also receives 2 bits from the Input/Output Port card in the STD BUSS to select which of the 4 sets of drivers on the board to direct the phase signals to. There are power resistors mounted in the STD box next to this card rack which limit the current to approx. 1 amp per phase to the motors.

The Wheel Position Boards occupy slots 2 and 3 of the rack. These boards are identical, and may be interchanged when troubleshooting. At the top of the schematic you will find 4 optical isolator circuits. These are used to keep the digital 5 volts separated from the other power in the system. These isolators receive inputs from bits on the Input/Output Port card in the STD BUSS. They control switches which turn choppers, bias, preamps, and LVDTs on and off. The board in ECC 2 has the isolators for the FTM chopper, bias, and preamp. The LVDT control on the board in ECC 2 is not used. The board in ECC 3 has the isolators for the AR chopper, bias, and preamp, as well as the LVDT control. The rest of the Wheel Position Boards serve a dual purpose. First, they convert the switches used in position encoders to TTL signal levels which are read by the Input/Output Port card when wheel position data is requested. The board is also used as a comparator to determine when to stop stepping during a command which caused a wheel to be moved to a new position. Names such as WOS0 (Wheel 0 Switch for bit 0) are inputs from the switches. The board in ECC 2 has Wheel 0 assigned to the Aperture wheel, Wheel 1 is the Filter Wheel. The board in ECC 3 has Wheel 0 assigned to the AR Filter wheel, and Wheel 1 is the Mode select wheel. Names such as WHEEL0S0B are TTL outputs which go to inputs on the Input/Output Port card in the STD BUSS. There are also 7 bits which come onto the boards from the Input/Output Port card in the STD BUSS. These bits are used to set up a position to move a wheel to. Bits 6 and 5 select which wheel to compare, and bits 4 through 0 set up a new address to move the wheel to. We set up a multiplexer to compare the position of the selected wheel with the desired position. When the wheel is in the correct position for 16 steps of the motor,

we send a stop stepping pulse to the Stepper motor controller card in the STD BUSS.

ANALOG ELECTRONICS

The analog electronics are located in the box with blue sides. There is a card cage with 8 slots. Seven of the slots are used with the eighth slot provided as a spare. In this section, a brief overview of the function of each board will be given. A description of the methods used to set potentiometers on the boards will also be included.

ECC 101 contains a Temperature Sensor conditioning card. This card handles all 9 silicon temperature sensors used in the system. The basic circuit used is the same for all sensors. The first stage of the circuit provides a constant 10 μ A current which goes through the sensor. The 10 μ A level is adjusted by the 10 K pot in the first stage. A good current meter may be connected from the Temperature Sensor input to ground, and the current adjusted to 10 μ A. The voltage on the output of the first stage is equivalent to the voltage given in the calibration on Silicon Diode # D36278 by Lake Shore Cryotronics, Inc.. The second stage of each circuit is a gain stage to use more of the 0 to 10 volt range of the A/D converter. The 10 K pot in the feedback of the stage should be adjusted to give a gain of 3.5 for the stage. Note that for the Large Area Source temperature sensor an additional stage with a gain of 2 is provided to give more resolution for warmer temperatures.

ECC 102 will contain a Synchronous Rectifier and Gains board. The board in this slot will process the Full Time Monitor signals. The board is interchangeable with the board in ECC 103 which handles the AR signals. There are two circuits on the board. The first circuit handles the Germanium Resistor temperature sensor located in the block where the bolometer is mounted. One stage of the circuit gives a constant 5 μ A current to the sensor. This current can be adjusted by hooking a

current meter from pin e to ground, and adjusting pot R9 to give 5 μ A. The circuit with U16, U17, U7 and U8 make up a high input impedance gain stage to read the voltage across the sensor and amplify it by a gain of 180. Note: potentiometer R10 will have to be set to null the offset with input shorted, and R11 will have to be adjusted to give a gain of 180. The rest of the board contains the amplifier and rectifier circuits. The signal coming from the battery postamp goes to a unity gain differential amplifier using U13. The signal is then passed on to a bandpass filter with a gain of 10, a Q of 10 and center frequency of 25 hertz. This signal is passed out to the BNC connector on the back of the STD Box as well as to the synchronous rectifier on the board. The signal also goes to a voltage comparator U14 which checks if the signal exceeds 10 volts. If the signal does exceed 10 volts, we switch the output to get -10 volts out of the system.

If the signal is not saturated, we rectify the signal, using the trigger from the chopper driver board. The output of the rectifier circuit goes through a 3 pole 1 hertz low-pass filter. The output of the filter goes to 4 gain stages which are in parallel with each other. Pot R4 must be used to null off any offset from the filter when capacitor C36 has been shorted. The Gain X1 output actually has a gain of approximately 2 from the output of the filter. This gain does not have to be exact. The gain of the X10 stage must be set to equal 10 times the X1 gain output. This can be accomplished by getting a signal of slightly less than 1 volt on X1 output, and adjusting R3 to get 10 times the signal on X10 output. The same procedure is followed for the X100 and X1000 gains. Note: The offset nulls must be set on the X100 and X1000 outputs before the gains are set.

ECC 103 contains the Synchronous Rectifier and Gains board for the AR monitor. It is interchangeable with the board in ECC 102. The board works exactly the same as explained above for the Full Time monitor.

ECC 104 contains the Source Driver board. This board gets its inputs from the D/A converter. A separate channel of the D/A is used for each of the 5 sources in the system. The output of the D/A converter is 0 to + 10 volts. Source 1 is the Large Area IR source, which may use 0 to 10 volts, so the optional voltage divider on the input of the circuit is not used. Op Amp U15 and transistor Q5 make up a circuit to control the drive voltage to the source to the same value as on the input from the D/A converter. Op Amp U13 monitors the voltage driving the source, and Op Amp U14 gives us a voltage proportional to the current to the source. This current is adjusted using pot P5 to give 10 volts out when 200 mA is flowing into the source. The drive circuits for Sources 2 and 3 have voltage dividers on the input stage to limit the drive voltage to the bulbs to 0 to 3.87 volts as the input from the D/A goes from 0 to 10 volts. The circuit which converts the current to a monitor voltage is also a little different. They have been set with Pots P3 and P2 to give 0 to 10 volts out for 0 to 100 mA through the bulbs. The drive circuits for sources 4 and 5 have voltage dividers on the inputs which limit the drive voltage to 0 to 1.27 volts as the input from the D/A converter goes from 0 to 10 volts. The current monitor circuits are set with Pots P1 and P4 to give 0 to 10 volts out for 0 to 50 mA of current through the bulbs.

ECC 105 contains the LVDT Conditioning Card. This board contains the circuitry for both the X and Y axis sensors. Relays control switching the primary excitation to the primary coils of the sensor. When the LVDTs are turned off, the primary coils are grounded to eliminate any noise which may be picked up by the instrument from the LVDTs. The modules U5 and U6 from Schaevitz provide zero offset with the two 10 K pots for the X and Y axis. The Op Amps U2 and U3 provide gain adjustment for the two axes. The backup board has been set to provide the same gain and zero points. This was done by moving the mirror to position 0,0 with the calibrated board, then changing to the backup board, and adjusting the zero until the system read out 0,0. Then the

mirror would be moved to position 4,4 with the calibrated board in, and the backup board would be put back in, and gain would be adjusted to get a readout of 4,4. This process was repeated a number of times, as the gain would affect the zero point somewhat.

When this process was completed, I verified at 2 degree intervals from -4 to 4 degrees. The results of that test were as follows:

Calibrated Board Readouts		Backup Board Readouts	
X	Y	X	Y
-3.99	-4.02	-4.00	-4.00
-2.00	-1.99	-2.00	-1.96
-0.01	-0.02	0.00	0.00
2.00	1.99	2.00	2.01
3.98	3.97	4.00	3.99

ECC 106 and ECC 107 contain Chopper Driver boards. These boards are identical and may be interchanged with each other. The board in ECC 106 controls the AR chopper, and the board in ECC 107 controls the FTM chopper. The following operational description applies to both of the boards. A JFET and analog switch control whether the chopper is turned on or off by disconnecting the driver U5 from the drive coil of the chopper. The feedback from the chopper goes through a gain stage U10, and also to the source of the FET which adjusts the amount of drive sent to U5 and on to the chopper drive coil. The signal coming from the gain stage U 10 goes to two circuits. The first circuit using Op Amp U11 provides a means of adjusting the phase of the

sync pulse used in the synchronous rectifier. The phase may be adjusted over a 90 degree range with Pot R19. The signal proceeds through a hysteresis gain stage U8 and is squared up. A 180 degree phase adjustment may be made using the jumper on the board to select the inverted or noninverted signal. The signal from the gain stage U10 also goes to a circuit which picks off the amplitude of the negative peak of the signal. This circuit involves chips U2, U3, U6 and U7. When the signal from the gain stage U10 goes towards a negative value, U6 and U7 essentially become voltage followers. Capacitor C3 is discharged through diode D3. When the input signal reaches the negative peak and starts back toward 0 volts, diode D3 is reverse biased, so capacitor C3 no longer follows the input voltage. The section of the circuit with U6 becomes a high gain amplifier, so the output quickly goes from the negative peak to positive saturation. This transition clocks flip flop U3, which triggers the first stage of the one-shot. Flip flop U3 will now ignore any additional pulses until it is cleared by the second one-shot. The first one-shot closes the switch from the output of Op Amp U7 to capacitor C2. Since capacitor C3 has been charged to the negative peak, this voltage is passed on to capacitor C2. When the first stage of the one-shot has timed out (approximately 12 milliseconds), the second one-shot is triggered. The second one-shot closes the switch which shorts capacitor C3 to ground. This gets the circuit ready to start tracking the output when the input gets back to 0 volts. The second one-shot also clears the flip flop to prepare for the next rising edge clock. The second one-shot times out in approximately 10 milliseconds, which will be well before the input signal reaches 0 volts on its positive to negative cycle. The voltage on capacitor C2 is used to set the gate voltage on the FET which sets the amount of drive sent to the chopper.

The chopper drive amplitude may be adjusted to change how far the blades of the chopper travel. To make this adjustment, connect a scope to the output of Op Amp U10. Adjust the scope to

approximately 10 milliseconds per division, and 1 volt per division. Adjust Pot R18 to get more or less amplitude of the signal. If the chopper is overdriven, high frequency noise will be on the 25 hertz feedback signal. If this occurs, back off the pot to avoid damaging the chopper. This happens when the chopper blades are hitting the ends, and are chattering from hitting the solid stop.

The signal used to synchronously rectify the bolometer signal is generated on the Chopper Drive boards. To adjust the phase of the rectifier, make sure the system has coldsoaked to insure that the chopper blades are cold, then adjust a source to get a mid-range signal. Then connect the scope to the output of the rectifier before the 1 Hz lowpass filter (Pin 13 of U15 on Sync Rectifier board). The signal should be a rectified sine wave, going in the positive direction. Pot R19 on the Chopper Drive board should be adjusted to make the rectified signal symmetrically positive.

BOLOMETER BATTERY POSTAMPS

We built a box as part of the outer vacuum flange which houses the batteries and boards to operate the bolometers. This was designed to place the battery supplies and a warm gain stage as close as possible to the bolometers and cold JFET's. We have used separate + and - 12 volt mercury batteries for both of the bolometer's preamps. We have also used separate 1.4 volt AA mercury batteries for bias on each of the two bolometers. These batteries are located in the top of the box attached to the top flange. Also included in this box are two circuit boards, the Battery Switching/Monitor board, and the Battery Postamp board.

The Battery Switching/Monitor board controls and monitors the preamp and bias batteries for both the AR and FTM bolometer circuits. Relays switch the power used for the circuits to the appropriate batteries when turned on, or to ground when turned off. The preamp battery monitor circuits operate when the relays

are turned on, to give a voltage which is 0.33 times the voltage from the +12.6 volt battery to the -12.6 battery. The Bias battery monitor circuits give an output voltage which is equal to the battery voltage when the bias relays are turned on.

The Battery Postamp board contains circuitry for both bolometers in the system. The description given will cover the AR circuit, with an identical circuit existing on the board for the FTM. The source resistor R29 is mounted on the board, which supplies a limit to the bias current through the cold JFET. We pick off the DC signal from the source and go to a voltage follower Op Amp U1 to reduce loading on the JFET source. This output goes to an amplifier circuit with a gain of 4. The output of this amplifier is sent to the A/D converter. Capacitor C15 AC couples the signal to allow sufficient gain to be applied to the signal. The signal goes through the amplifier stage using U5 which amplifies by 100 and filters out frequencies above 250 hertz. The signal is then passed to the Synchronous Rectifier board in the Analog Electronics box.

WIRING SCHEME USED IN DEC

The wiring lists giving the name of the signal, and connection points for each pin in each connector is given in the binder labeled DEC Wiring lists. The basic scheme used was to number connectors in the system according to where they are located and where they connect to. Each connector has a letter and a number associated with the name such as J101. The letters J and P are used to signify jack or plug respectively, thus J101 will connect to P101. Connectors 1 through 9 are located at the rear of the STD Box. Connectors 101 through 105 are located at the rear of the Analog electronics box and the cables go over to the STD Box. Connectors 201 through 204 are also located at the rear of the Analog electronics box, but the cables connecting to them go to the dewar. Connectors 301 through 309 are located on the outer room temperature vacuum flange of the dewar.

Connectors 401 through 406 are located on the flange which will mount to the Liquid nitrogen shield in the dewar. Connectors 501 through 506 are located on the flange which will mount to the Helium shield in the dewar. Connectors 601 through 609 are located on the lid of the DEC, and Connectors 701 through 717 are located on the various modules inside the DEC. The wires going from the room temperature flange to the liquid nitrogen flange, and the wires from the liquid nitrogen flange to the helium flange are all made with stainless steel wire to reduce the heat load. The reader is referred to the section on heat loading in the Critical Design Review for details of heat loading due to conduction of wires.

Description of CMU Operation

To understand in any detail the operation of the CMU requires a general understanding of the components used in the system, plus an understanding of how the assembly language software operates. The following brief summary of the various operations will help the user understand the methods used for the various operations. It will also help the user to follow the logic of the assembly language software if the need should arise. The complete listing of the software is given in the binder entitled "software listings". This description will not attempt to define what registers are used for what, but will attempt to describe the general steps involved in each process. The assembly language listing includes extensive comments to help understand the programming.

WHEEL MOVES

This section describes the process to move the system's 4 wheels. The command is received by the processor in the STD Buss, and a check is made to insure that the command was received without serial transmission errors. The command string is then checked to insure an L was received for last character in the correct position. The command is examined and the new position or number of steps to move is saved. The bits of the PIO are set to select the correct motor to send the drive steps. Next, if we are moving the wheel to a new position, we place the new position in the correct bits of the PIO to send to the Wheel Position Board to generate a stop stepping pulse when we reach the new position. If we are to move the wheel by a number of steps, we set the new address to seek to 32 so the Wheel Position Board will not generate a stop stepping pulse before the controller has stepped the desired number of steps. We determine the direction to step by examining the sign bit if moving by steps, or by deciding which direction will bring us to

the new position in the least amount of steps. If the command is to move by a number of steps we send the command to the controller to move the desired number of steps in the desired direction, at the rate selected by the motor speed flag. If the command is to move to a new position, we command the controller to move in the closest direction, by 8000 steps, at the rate selected by the flag. The 8000 steps is a maximum timeout value. The wheel will actually be stopped by the stop stepping signal from the Wheel Position board to the controller when the wheel reaches the new position. The 8000 step unit was chosen to allow the wheel to reach the correct position if the wheel is not at a defined position when we check which direction to step to reach the new position, and we have to step nearly one complete revolution to find the new position. Some safety is also provided in the 8000 steps to reach the new position.

The processor then waits until the stepping is complete, turns the motor power off, and examines what made the motor stop. If the wheel was commanded to move to a new position, and the motor was stopped because the controller had stepped the full 8000 steps, a status error is returned. If the wheel was to move a number of steps, and was stopped due to a stop stepping pulse, an error is returned. Otherwise a status = 0 is returned to the user.

WHEEL POSITION REQUESTS

This section describes the process used when a request is made for the position of one of the wheels in the system. The request is received by the processor in the STD Buss, and a check is made to insure that the command was received without any parity or framing errors. The command is examined to insure that the wheel (which data has been requested from) is a valid number. A check is also made of the L for last character in the command. The bits on the PIO are read which contain the position of the wheel requested. The data is examined to see if the wheel is in a defined geneva position. If the wheel is in a good position,

the data is returned to the PC. If the wheel is not in a good geneva position, position 0 is returned to the PC as the current position. Note: user may examine the bits by requesting the appropriate raw PIO data.

BEAM SAMPLE MIRROR MOVE

This section describes the process used to move the beam sample mirror. The command is received by the processor in the STD Buss, and a check is made to insure the command was received without parity or framing errors. The command string is then checked to insure an L was received for last character in the correct position. The command is examined and the new position or number of steps to move is saved. The bits of the PIO are set to select the Beam Sample motor to send the drive steps. Next, if we are moving the mirror to a new position, we place the new position in the correct bit of the PIO to send to the Wheel Position Board to generate a stop stepping pulse when we reach the new position. If we are to move the mirror by a number of steps, we set the new address to seek to 32 so the Wheel Position Board will not generate a stop stepping pulse before the controller has stepped the desired number of steps. We determine the direction to step by examining the sign bit if moving by steps, or by examining the new position if moving to a new position. If the command is to move by a number of steps we send the command to the controller to move the desired number of steps in the desired direction, at the rate selected by the motor speed flag. If the command is to move to a new position, we command the controller to move in the desired direction, by 5000 steps, at the rate selected by the flag. The 5000 steps is a maximum timeout value. The mirror will actually be stopped by the stop stepping signal from the Wheel Position board to the controller when the mirror reaches the new position. The 5000 step unit was chosen to allow the mirror to reach the correct position with some safety in case a few steps are missed.

The processor then waits until the stepping is complete. When the controller has stopped stepping the motor, we examine what caused the motor to stop stepping. If we are in the mode to move by steps, and a stop stepping pulse stopped the controller, we send a status error. If we were moving to a new position, and exceeded the 5000 steps, we send a status error. If we were moving to a new position, and were stopped by a stop stepping pulse, we have reached the point where the limit switch has been closed, so we step another 400 steps in the same direction to spring load the arm against the mechanical stop. Then the processor turns the motor power off, and returns a status = 0 to the PC.

BEAM SAMPLE MIRROR POSITION REQUESTS

This section will describe the process which is used when a request is made for the position of the beam sample mirror. The request is received by the processor in the STD Buss, and a check is made to insure that the command was received without any parity or framing errors. The command is examined to insure that an L for last character in the command was in the correct place. The bits on the PIO are read which contain the position of the Beam Sample mirror. The data read is formatted and sent to the PC. Note: a 3 would indicate that both limit switches are closed, a 2 indicates the mirror is fully into the beam, a 1 indicates the mirror is fully out of the beam, and a 0 indicates that neither limit switch closed.

POINTING MIRROR MOVES

This section will describe the process which is used to move the pointing mirror. The command to move the pointing mirror is received by the processor in the STD Buss, and a check is made to insure that the command was received without any parity or framing errors. The command string is then checked to insure that an L was received for the last character, and was in the correct position for the command.

There are actually three types of commands which move the pointing mirror. Absolute and Relative position moves are converted by the PC into an absolute X and Y axis position to move to, which is sent on to the STD Buss, so these are actually only two types of moves sent to the STD BUSS. This section will examine the move to a new position command first, and then the move by steps command.

When an absolute move command is received, we check if the LVDTs have been turned on. If the flag indicates that the LVDTs are off, a status error is returned to the PC and no attempt is made to move the mirror. If the flag indicates that the LVDTs are on, we read the data which gives the new position the mirror to move to. If the new position is outside a -4 to +4 degree window, we return a status error. If we have good values, then we use the new positions to look up what 12 bit A/D counts correspond to the desired positions. The bits of the PIO are set to select the X-Axis motor on one Stepper driver board, and the Y-Axis motor on the other. Then we place 32s in the Wheel Position Boards as the new seek addresses to prevent being stopped by a stop stepping pulse. Then we start through a loop which samples and compares the present position with the desired position. If we are more than 255 counts away from the desired position, we move 80 steps in the necessary direction. If we are within 255 counts of the desired position, we move 4 steps in the necessary direction. We continue this loop until the correct position is reached or until a timeout limit is exceeded. When we have reached the correct position with both motors, or have timed out, we turn off both motors, and return to the PC with a status to indicate the results.

When a command to move by steps is received, we check if the LVDTs have been turned on. If the flag indicates that the LVDTs are off, a status error is returned to the PC and no attempt is made to move the mirror. If the flag indicates that the LVDTs are on, we read the data which gives the number of steps to move the mirror. The bits of the PIO are set to select the X-Axis

motor on one Stepper driver board, and the Y-Axis motor on the other. Then we place 32s in the Wheel Position Boards as the new seek addresses to prevent being stopped by a stop stepping pulse. We determine the direction to step by examining the sign bit. The command is sent to the controller to move the desired number of steps in the desired direction, at the rate selected by the motor speed flag. The processor then monitors the LVDTs as the controllers are stepping the motors. If either LVDT gets above or below a boundary window, the stepping is stopped, the motors turned off, and a status error returned to the PC indicating a boundary problem. If the window is not exceeded, the processor waits for the motors to finish stepping, then turns the motors power off, and examines what made the motors stop. If the motors were stopped due to a stop stepping pulse, an error is returned. Otherwise a status = 0 is returned to the user.

POINTING MIRROR POSITION REQUESTS

This section describes the process used when a request is made for the position of the pointing mirror in the system. The request is received by the processor in the STD Buss, and a check is made to insure that the command was received without any parity or framing errors. The command is examined to verify that the L for the last character was received in the correct position. The control word which contains the status of the LVDTs is checked to verify that the LVDTs are currently turned on. If the LVDTs are not turned on, the output is meaningless and a status 81 is returned to indicate invalid data. If the LVDTs are turned on, the A/D channel for the X-Axis position is sampled and the output is converted to angular degrees from the X-Axis lookup table. Then the A/D channel for the Y-Axis position is sampled and the output is converted to angular degrees from the Y-Axis lookup table. The results are then passed back to the PC with a status indicating successful completion, or noting any problems encountered during the process.

LVDT CONTROL

This section describes the process used to command the LVDTs in the system. The command to turn the LVDTs on or off is received by the processor in the STD Buss, and a check is made to insure that the command was received without any parity or framing errors. The command string is then checked to insure an L was received for the last character, and was in the correct position for the command. The command is examined to determine whether to turn the LVDTs on or off. The bit which controls the LVDTs is set or reset as commanded. The control word which indicates the state of all commands is updated with the new command, and sent to the PIO board. This control word is checked by data requests, and the pointing mirror moves to make sure the LVDTs are on before returning data or moving the mirror.

BOLOMETER SIGNAL REQUEST

This section describes the process which is used when a request is made for the rectified and DC bolometer signals. The request is received by the processor in the STD Buss, and a check is made to insure that the command was received without any parity or framing errors. The command is examined to verify that the L for the last character was received in the correct position. The control word which contains the status of the choppers, preamp power, and bias is checked to verify that the necessary functions are turned on. If a request for Bolometer DC level is made, we make sure the Preamp is turned on. If a request is made for a rectified Bolometer signal, we make sure the preamp, bias, and chopper are all turned on. If the necessary functions are not turned on as described above, we return a status error to indicate what is not turned on. In this case, the output is not valid so we do not even sample the signal.

C - 3

If the request is for a Bolometer DC signal, we examine the command to determine if the request is for ARBOLDC or FTBOLDC. Then we sample the appropriate channel of the A/D converter and send the results back to the PC.

If the request is for a rectified Bolometer signal, we examine the command to determine if the request is for the ARBOL or FTBOL signal. Then we begin by sampling the A/D channel which contains the X1 Gain of the appropriate bolometer. We check to see if the signal is less than -0.5 volts to indicate system saturation. If signal is less than -0.5 volts, we send the result to the PC. If the signal is not less than -0.5 volts, we check if the signal is above 0.98 volts. If the signal is above 0.98 volts, we send it to the PC.

If the signal on X1 gain is between -0.5 volts and 0.98 volts, we go on to sample the X10 gain channel of the A/D converter. If the signal on the X10 gain is less than -0.5 volts, or greater than 0.98 volts, we send the result to the PC. If the signal on the X10 gain is between -0.5 volts and 0.98 volts, we go on to sample the X100 gain channel of the A/D converter. If the signal on the X100 gain is less than -0.5 volts, or greater than 0.98 volts, we send the result to the PC. If the signal on the X100 gain is between -0.5 volts and 0.98 volts, we sample the X1000 gain channel of the A/D converter and send the result to the PC.

When the result is sent to the PC, we send a bit to indicate which gain the data was taken from. The PC will take the data returned and the gain it is from and normalize the data to the X1 gain. This will give data from 10 volts down to 0.98 volts from X1 gain channel. Data from 0.98 volts down to approximately 0.098 volts will be from X10 gain channel. Data from approximately 0.098 volts to approximately 0.0098 volts will be from the X100 gain channel, and data less than approximately 0.0098 volts will be from the X1000 gain.

CHOPPER MONITORS AND CONTROL

This section describes the process used to monitor and command the two choppers in the system. The data request or command to turn the Choppers on or off is received by the processor in the STD Buss, and a check is made to insure that the request or command was received without any parity or framing errors. The command string is then checked to insure that an L was received for the last character, and was in the correct position for the command.

When a Chopper Monitor signal is requested, we first check the control word to see if the chopper is turned on. If the chopper is not on, a status 82 is returned. If the chopper is turned on, we sample the appropriate A/D channel. The result is returned to the PC. This monitor does not give an absolute amplitude of the chopper, but will give a good relative drive for the given chopper and board. When chopper driver boards are changed, a new value may be returned when the chopper is driving the same amount. This value should only be used in comparing the chopper under repeated conditions.

When a Chopper command is received, we examine the command to determine which chopper to command, and whether to turn the Chopper on or off. The bit which controls the Chopper is set or reset as commanded. The control word which indicates the state of all commands is updated with the new command, and sent to the PIO board. This control word is checked by data requests to insure that the choppers are on before returning data which must have choppers on to get valid outputs.

PREAMP MONITORS AND CONTROL

This section describes the process used to monitor and command the two preamps in the system. The data request or command to turn the preamps on or off is received by the processor in the STD Buss, and a check is made to insure that the request or command was received without any parity or framing

errors. The command string is then checked to insure that an L was received for the last character, and was in the correct position for the command.

When a preamp battery voltage is requested, we first check the control word to see if the preamp is turned on. If the preamp is not on, a status 84 is returned. If the preamp is turned on, we sample the appropriate A/D channel. The result is returned to the PC. This monitor gives the voltage from the -12.6 volt battery to the +12.6 battery. It will not tell which battery has dropped in voltage, but will monitor the battery pair.

When a Preamp Command is received, we examine the command to determine which preamp to command, and whether to turn the preamp on or off. The bit which controls the preamp is set or reset as commanded. The control word which indicates the state of all commands is updated with the new command, and sent to the PIO board. This control word is checked by data requests to insure preamps are on before returning data which must have preamps on to get valid outputs.

BIAS MONITORS AND CONTROL

This section describes the process used to monitor and command the system's two biases. The data request or command to turn the bias on or off is received by the processor in the STD Buss, and a check is made to insure that the request or command was received without any parity or framing errors. The command string is then checked to insure that an L was received for the last character, and was in the correct command position.

When a bias battery voltage is requested, we first check the control word to see if the bias is turned on. If the bias is not on, a status 83 is returned. If the bias is turned on, we sample the appropriate A/D channel. The result is returned to the PC. This monitor gives the voltage of the 1.5 volt bias battery.

When a Bias Command is received, we examine the command to determine which bias to command, and whether to turn the bias on or off. The bit which controls the bias is set or reset as commanded. The control word which indicates the state of all commands is updated with the new command, and sent to the PIO board. This control word is checked by data requests to insure the bias is on before returning data which must have the bias on to get valid outputs.

TEMPERATURE MONITOR REQUEST

This section describes the process used to monitor the temperature sensors in the system. The data request is received by the processor in the STD Buss, and a check is made to insure that the request was received without any parity or framing errors. The command string is then checked to insure that an L was received for the last character, and was in the correct position for the request.

The command string is examined to determine which temperature monitor has been requested. The appropriate channel of the A/D converter is sampled to read the voltage from the sensor circuit. The output of the A/D converter is used as an address to lookup tables to read the temperature in degrees Kelvin. Three temperature lookup tables are used in the system. All of the silicon diode sensors use a common lookup table, and separate tables are used for the germanium sensors located in the blocks with the bolometers. The output from the lookup tables are sent back to the PC. The bolometer temperature sensors have been calibrated from 1.4 to 6.0 K, to give greater resolution in the range where the bolometers are operational. The silicone sensors are all matched at LHe, LN², and room temperatures. We performed a calibration on the silicon sensors, and have plotted the error versus temperature for each sensor in "DEC Temperature Curves". The readings from the sensors are corrected for these

errors in the SDL primitives software on the PC. The silicon sensors have been calibrated from 1.4 to 320 K.

SOURCE CONTROL

This section describes the process used to control the various sources used in the system. The command is received by the processor in the STD Buss, and a check is made to insure that the command was received without any parity or framing errors. The command string is then checked to insure that an L was received for the last character, and was in the correct position for the request.

The command string is examined to determine which source the new set point is to be sent to. There are three types of sources used in the system: the bulbs with glass envelopes on, the bulbs with envelopes removed, and the Large Area IR source.

When a command is received to set a new level for a bulb with the envelope on, the received count is checked to make sure it is between 0 and 4095. If the new set point is between 0 and 4095, we send the new count to the appropriate channel of the D/A board which drives the desired source.

When a command is received to set a new level for a bulb which has had the envelope removed, we must use a little caution before sending the new count to the D/A. If the system is not in a adequate vacuum, and these bulbs are turned on, the filament will burn out. To determine if we are in a adequate vacuum we have decided to check if the temperature of the Integrating Sphere Module, Base Plate #1 or Base Plate #2 is from 1 to 10 K. If any one of the three monitors indicate we are in the temperature range, we go ahead and send the new count to the D/A board to set a new drive voltage for the source. We also run a check when we are looping waiting for a request from the IBM, to protect these bulbs. If a bulb with it's envelope removed is turned on, we will check the same three temperature monitors as above. If none of the monitors indicate a temperature from 1 to

20 K, we will turn off the bulbs. This is to prevent burning the bulbs out if the system warms up due to a loss of vacuum.

When a command is received to set a new temperature for the Large Area IR Source, we check to make sure the new set temperature is from 0 to 320 K. If the new temperature is outside these bounds, a status error is returned to the user, and the system remains at the last set temperature. When a valid new temperature set point is received, a flag is set indicating we have received a new temperature set point. We then go to a lookup table to get the count from the A/D converter which will correspond to the new set temperature. This count is saved as the desired A/D count. We also lookup an approximate drive count to send to the D/A for the desired temperature. This count is saved as the Approximate Drive count. Then a command received reply is sent back to the PC.

As the processor in the STD Buss is looping waiting for a request to be received from the PC, it temperature controls the Large Area IR Source. When a new temperature set point is received from the PC, the processor checks the present temperature of the source. If the present temperature is above the new temperature set point, the heater is turned off to allow the source to cool down as quickly as possible. If the present temperature is less than the new set point, we drive the source with a count = ((approximate drive count) * 4) + 200. If the obtained count is greater than 4095, we send the count of 4095. This helps to get to the desired temperature faster. If we do get a request from the PC while we are overdriving the source, we set the drive back to the approximate count while we service the request from the PC to avoid overheating the source. When we are overdriving the source and get to about 5 to 10 degrees below the desired temperature, or when we have turned the source off to cool down to the desired temperature and have finally reached the desired temperature, we start driving the source with the approximate drive voltage. When we are close to the desired temperature, we start adjusting the drive to the source about

every 8 seconds. We check to see if we are too hot or too cold, and gradually adjust the drive count accordingly. We also look at how large the error is and temporarily add or subtract 32 times the error to the drive count. This keeps the temperature close to the desired level while the drive voltage is adjusting to the desired level.

APPENDIX C
Operating Instructions

This page intentionally left blank.

OPERATING INSTRUCTIONS

The operating instructions of the DECCMU will be given in the following order:

Power up procedure

Software Organization

Definitions of Variables to request data or send commands

UZFUNCTION% defined

Position Data request

Temperature Data request

Monitor Signal Data request

Motor Move Commands

Source Set Commands

System Control Commands

System Initialize Command

Raw A/D Data request

Raw PIO Data request

Definitions of Variables in which data is returned

Position Data

Temperature Data

Monitor Signal Data

Raw A/D Data

Raw PIO Data

Definitions of returned Status Codes

PRECEDING PAGE BLANK NOT FILMED

This page intentionally left blank.

POWER UP PROCEDURE

The DECCMU should be powered on in the following order. First, the STD Box power should be turned on by means of the AC power switch located on the box's back panel. The power supplies for the STD BUS and all of the analog and digital electronics are powered by this switch. The IBM PC is powered up next. The IBM PC ~Guide to Operations~ advises powering the expansion unit first, followed by the PC itself. After the power is applied, the computer will go through a self memory test, and then boot from the hard disk. The user may then run the appropriate program on the PC to carry out the desired testing.

SOFTWARE ORGANIZATION

The software procedure named SDL primitives will be run by the user with the necessary variables defined to send a command or request data from the STD BUS. Definitions of the variables used to send commands or request data are given in this document. The procedure sets up the necessary string to send to the STD BUS as defined in Communication Format Between IBM-PC and STD BUS. The procedure waits for the reply from the STD BUS and converts the reply to a result and/or status which is placed in the appropriate variables to pass back to the user. The variables in which data and status are returned to the user are also defined in this section.

PRECEDING PAGE BLANK NOT FILMED

DEFINITIONS OF VARIABLES TO REQUEST DATA OR SEND COMMANDS

The user will select the type of command or data requested by setting the variable UZFUNCTION% to any of the following values:

UZFUNCTION% = 1	REQUEST POSITION DATA
UZFUNCTION% = 2	REQUEST TEMPERATURE DATA
UZFUNCTION% = 3	REQUEST MONITOR SIGNAL DATA
UZFUNCTION% = 4	MOTOR COMMANDS
UZFUNCTION% = 5	INFRARED SOURCE CONTROL COMMANDS
UZFUNCTION% = 6	SYSTEM CONTROL COMMANDS
UZFUNCTION% = 7	SYSTEM INITIALIZE COMMAND
UZFUNCTION% = 8	REQUEST RAW A/D DATA
UZFUNCTION% = 9	REQUEST RAW PIO INPUT DATA

POSITION DATA REQUEST

(UZFUNCTION%=1)

Variable UZPOS% must be set to 1 thru 7 to select which channel the user wants position data from.

UZPOS% = 1 X and Y axis pointing mirror position request

UZPOS% = 2 X and Y axis pointing mirror position request

Note: UZPOS% = 1 or 2 are redundant because both values are required to map from coordinate systems, so we will update both positions with either request.

UZPOS% = 3 Beam sample mirror position request

UZPOS% = 4 Absolute radiometer filter wheel position request

UZPOS% = 5 Aperture wheel position request

UZPOS% = 6 Mode selector wheel position request

UZPOS% = 7 Filter wheel position request

TEMPERATURE DATA REQUEST

(UZFUNCTION%=2)

Variable UZTEMP% must be set to 1 thru 11 to select which channel the user wants temperature data from.

- UZTEMP% = 1 Pointing mirror temperature request
- UZTEMP% = 2 Primary mirror temperature request
- UZTEMP% = 3 Beam sample mirror temperature request
- UZTEMP% = 4 Absolute radiometer detector temperature request. Range: 1.4 to 6.0 K
- UZTEMP% = 5 Absolute radiometer module temperature request
- UZTEMP% = 6 Full time monitor detector temperature request. Range: 1.4 to 6.0 K
- UZTEMP% = 7 Base plate #1 temperature request
- UZTEMP% = 8 Large Area Source temperature request
- UZTEMP% = 9 Integrating sphere module temperature request
- UZTEMP% = 10 Base plate #2 temperature request
- UZTEMP% = 11 Base plate #3 temperature request

MONITOR SIGNAL DATA REQUEST

(UZFUNCTION%=3)

Variable UZSIG% must be set to 1 thru 20 to select the channel the user wants to read data from.

- UZSIG% = 1 Absolute radiometer monitor signal request
- UZSIG% = 2 Full time monitor signal request
- UZSIG% = 3 Large Area Source drive voltage request
- UZSIG% = 4 Large Area Source drive current request
- UZSIG% = 5 Bulb with envelope on #1 drive voltage request
- UZSIG% = 6 Bulb with envelope on #1 drive current request
- UZSIG% = 7 Bulb with envelope on #2 drive voltage request
- UZSIG% = 8 Bulb with envelope on #2 drive current request
- UZSIG% = 9 Bulb with envelope removed #1 drive voltage request
- UZSIG% = 10 Bulb with envelope removed #1 drive current request

UZSIG% = 11 Bulb with envelope removed #2 drive voltage request
UZSIG% = 12 Bulb with envelope removed #2 drive current request
UZSIG% = 13 A.R. Chopper DC Monitor request
UZSIG% = 14 Absolute Radiometer Bias voltage request
UZSIG% = 15 Full Time Monitor Bias voltage request
UZSIG% = 16 Absolute Radiometer Preamp Battery voltage
UZSIG% = 17 Full Time Monitor Preamp Battery voltage
UZSIG% = 18 FTM Chopper DC Monitor request
UZSIG% = 19 AR Bolometer DC signal
UZSIG% = 20 FTM Bolometer DC signal

MOTOR MOVE COMMANDS

(UZFUNCTION%=4)

Variable UZMOT% must be set to 1 thru 8 to select type of motor move command. Note: the user must have the proper variable or variables defined as described below to tell the system where to move the motor to.

UZMOT% = 1 Pointing mirror absolute position move command. Moves the pointing mirror to the coordinate (UZNEWABSPOSX, UZNEWABSPOSY), which is referenced to the DIRBE coordinates. The user must set the two variables UZNEWABSPOSX and UZNEWABSPOSY before doing an absolute position move command. We will be able to move the mirror to any coordinate in the range -2.00 to +2.00 for X and Y referenced to the DEC coordinates.

If a coordinate lies outside the window when we map into the DEC coordinates, we will not send a command to the STD Buss, we will simply return to the user's program with a status error in variable Sdl.UZSTATUS% informing the user that the command was not executed because the coordinate was outside our window. When we are able to send the command to the STD Buss, we will wait for a reply from the STD Buss, and return to the user with Sdl.UZSTATUS% indicating the status of the operation performed by the STD Buss.

We will move the mirror to obtain the desired angle of the beam ± 0.02 degrees or better.

Note: The coordinates passed to us will be referenced to the DIRBE axis. We will allow the user to define the DIRBE axis with respect to the DEC axis by setting SDL.UZXOFFSET, SDL.UZYOFFSET, and SDL.UZANGLERAD variables.

UZMOT% = 2 Pointing mirror relative position move command. This command moves the pointing mirror relative to the last commanded position by UZNEWRELPOSX in the x-axis, and UZNEWRELPOSY in the y-axis. The maximum value of these variables will depend upon the last commanded position of the mirror. As with an absolute position move command, if the coordinate we are trying to move to lies outside the window when we map into the DEC coordinates, we will not send a command to the STD Buss, we will simply return to the users program with a status error in Sdl.UZSTATUS% informing the user that the command was not executed because the coordinate was outside our window. When we are able to send the command to the STD Buss, we will wait for a reply from the STD Buss, and return to the user with Sdl.UZSTATUS% indicating the status of the operation.

UZMOT% = 3 Beam sample move command. The user must set the variable UZBSPOS% to 1 to move the mirror into the beam, or set to 0 to move the mirror out of the beam. We will allow the user to set UZBSPOS% to + or - 1XXXX, to have the system step the motor XXXX steps. If +, we will move the mirror in the direction towards the beam. If the sign is -, we will move the mirror in the direction out of the beam. XXXX may be any integer from 0000 to 9999.

UZMOT% = 4 Absolute radiometer filter move command. The user must set the variable UZNEWPOS% to 1 thru 18 to define the position in which to move the filter wheel in the Absolute radiometer. We will also allow the user to set UZNEWPOS% to +

or - 1XXXX, to have the system move the motor XXXX steps in the direction determined by the sign. XXXX can be any integer from 0000 to 9999.

UZMOT% = 5 Aperture wheel move command.

The user must set the variable UZNEWPOS% to 1 thru 18 to define the position in which to move the aperture wheel between the two integrating spheres to. We will also allow the user to set UZNEWPOS% to + or - 1XXXX, to have the system move the motor XXXX steps in the direction determined by the sign. XXXX may be any integer from 0000 to 9999.

UZMOT% = 6 Mode selector wheel move command.

The user must set the variable UZNEWPOS% to 1 thru 18 to define the position to move the mode selector wheel to. We will also allow the user to set UZNEWPOS% to + or - 1XXXX, to have the system move the motor XXXX steps in the direction determined by the sign. XXXX may be any integer from 0000 to 9999.

UZMOT% = 7 Filter wheel move command.

The user must set the variable UZNEWPOS% to 1 thru 18. This defines the position that the filter wheel located between the integrating spheres will be moved to. We will allow the user to set UZNEWPOS% to + or - 1XXXX, to have the system move the motor XXXX steps in the direction determined by the sign. XXXX may be any integer from 0000 to 9999.

UZMOT% = 8 Pointing mirror move command to move the pointing mirror by the number of steps in the variables UZXSTEP% and UZYSTEP%.

If the variables are + we will move forward, and in reverse direction if the sign is -.

SOURCE SET COMMANDS

(UZFUNCTION%=5)

Variable UZSRC% must be set to 1 thru 5 to select which source to set with this command.

UZSRC% = 1 Large Area Source control command.

The user must set the variable UZSETSRC% to a value ranging from 0 to 320 thereby selecting the control temperature of the source. NOTE: we are only controlling by adding heat, so setting UZSETSRC% to any value below the module temperature will turn the source off. The large area source may be tested at room temperature by setting UZSETSRC%=320, and monitoring the Large Area Source drive voltage and current. The STD Buss will send a reply back to the PC indicating it has received the new temperature set point, and is moving the temperature of the source to that value. The user must monitor the temperature of the source and determine when it has sufficiently stabilized for the test being conducted.

UZSRC% = 2 Bulb with envelope on #1 control command.

The user must set the variable UZSETSRC% to some value from 0 to 4095 when executing this command. The value of UZSETSRC% will be passed to the D/A converter to set the drive voltage to the bulb. Note: a value of 0 will turn the bulb off.

UZSRC% = 3 Bulb with envelope on #2 control command.

The user must set the variable UZSETSRC% defined the same as in the preceding bulb control command.

UZSRC% = 4 Bulb with envelope removed #1 control command.

The user must set the variable UZSETSRC% the same as for the previous two commands. (Note: we will check the temperatures of the Integrating Sphere Module, Base Plate #2, or Base Plate #1.

If none of these sensors are below 10 K, we will not allow the user to turn on these bulbs.)

UZSRC% = 5 Bulb with envelope removed #2 control command. The user must set the variable UZSETSRC% the same as for the last three commands. (Also note we will test the same as above to prevent the bulbs from being burned out)

SYSTEM CONTROL COMMANDS

(UZFUNCTION%=6)

Variable UZFN% must be set to 1 thru 16 to select the type of system control command the user wishes to perform.

UZFN% = 1 Absolute radiometer bias on command. Used to turn on the AR bias.

UZFN% = 2 Full time monitor bias on command. Use to turn on the FTM Bias.

UZFN% = 3 Absolute Radiometer Chopper on command. Used to turn on the AR Chopper.

UZFN% = 4 LVDTs on command. Turns on the LVDTs which are used to sense the position of the pointing mirror.

UZFN% = 5 Full Time Monitor Chopper on command. Used to turn on the FTM chopper.

UZFN% = 6 Absolute Radiometer Preamp Power On command. Turns on the preamp battery power for the AR.

UZFN% = 7 Full Time Monitor Preamp Power On command. Turns on the preamp battery power for the FTM.

UZFN% = 8 Motor Half Speed Enable command. Puts all motor commands in a slower speed mode. This will take longer to move all mechanisms, but gives more torque if a motor is stalling.

UZFN% = 9 Absolute radiometer bias off command. Used to turn off the AR bias

UZFN% = 10 Full time monitor bias off command. Used to turn off the FTM Bias.

UZFN% = 11 Absolute Radiometer Chopper off command. Used to turn off the AR Chopper.

UZFN% = 12 LVDTs off command. Turns off the LVDTs which are used to sense position of the pointing mirror.

UZFN% = 13 Full Time Monitor Chopper off command. Used to turn off the FTM chopper.

UZFN% = 14 Absolute Radiometer Preamp Power Off command. Turns off the preamp battery power for the AR.

UZFN% = 15 Full Time Monitor Preamp Power Off command. Turns off the preamp battery power for the FTM.

UZFN% = 16 Motor Normal Speed Enable command. Puts all motors in the normal speed mode.

SYSTEM INITIALIZE COMMAND

(UZFUNCTION%=7)

There will not be any variables other than UZFUNCTION% = 7 to be defined to execute a System Initialize command.

This command will be used to initialize the system after a power up, or to reset the system following a fatal error. When a fatal error does occur, the STD Buss will wait for the next command or request for data and reply with a fatal error message to the PC. Then it will ignore all future commands before a system initialize. This will insure that the user knows all source set points and system operating modes have been reset to the off state.

When the STD Buss receives this command, it will reply with a status response indicating status ok to allow the system to continue.

RAW A/D DATA REQUEST

(UZFUNCTION%=8)

Variable UZRAWADCH% must be set to 1 thru 40 to select which channel the user wants to get raw A/D data from.

Note: Board 0 has a range of 0 to +10 volts, and board 1 has a range of -10 to +10 volts. Both are 12 bit A/D converters. Board 1 reads offset binary, so a count of 0 is output for -10 Volts and a count of 4095 is output for +10 Volts.

The channel assignments on the A/D converters are:

System Channel	A/D board number	Channel on Board	Function Description
1	0	1	Pointing Mirror Temperature
2	0	2	Primary Mirror Temperature
3	0	3	Beam Sample Mirror Temperature
4	0	4	Abs. Radiometer Bolometer Temp
5	0	5	Abs. Radiometer Module Temp
6	0	6	Full Time Mon Bolometer Temp
7	0	7	Base Plate #1 Temperature
8	0	8	Large Area IR Source Temp X1
9	0	9	Integrating Sphere Module Temp
10	0	10	Base Plate #2 Temperature
11	0	11	Base Plate #3 Temperature
12	0	12	Large Area IR Source Temp X2
13	0	13	AR Bolometer DC
14	0	14	FTM Bolometer DC
15	0	15	Large Area IR Srce Drive Volts
16	0	16	Large Area IR Srce Drive current
17	0	17	Bulb w/envelope #1 Drive Volts
18	0	18	Bulb w/envelope #1 Drive current

19	0	19	Bulb w/envelope #2 Drive Volts
20	0	20	Bulb w/envelope #2 Drive current
21	0	21	Bulb w/o envelope #1 Drive Volts
22	0	22	Bulb w/o envelope #1 Drive current
23	0	23	Bulb w/o envelope #2 Drive Volts
24	0	24	Bulb w/o envelope #2 Drive current
25	1	1	X-Axis pointing mirror LVDT
26	1	2	Y-Axis pointing mirror LVDT
27	1	3	AR rectified signal X1
28	1	4	AR rectified signal X10
29	1	5	AR rectified signal X100
30	1	6	AR rectified signal X1000
31	1	7	FTM rectified signal X1
32	1	8	FTM rectified signal X10
33	1	9	FTM rectified signal X100
34	1	10	FTM rectified signal X1000
35	1	11	AR Preamp battery voltage
36	1	12	AR Bias battery voltage
37	1	13	FTM Preamp battery voltage
38	1	14	FTM Bias battery voltage
39	1	15	AR Chopper DC monitor
40	1	16	FTM Chopper DC monitor

RAW PIO DATA REQUEST

(UZFUNCTION%=9)

Variable UZRAWPIOCH% must be set to 1 thru 9 by the user to select the channel of PIO input data which the user wants to access.

UZRAWPIOCH%	Board Channel	Bits	Function assigned
1	1	7	Beam sample mirror IN switch
2	1	6	Beam sample mirror OUT switch
3	1	5-0	Aperture Wheel Position (bit 5 = in good position) (bits 4-0 are binary count)
4	2	7-6	Spare
5	2	5-0	Filter Wheel Position (bit 5 = in good position) (bits 4-0 are binary count)
6	3	7-6	Spare
7	3	5-0	Abs. Radiometer Filter Wheel (bit 5 = in good position) (bits 4-0 are binary count)
8	4	7-6	Spare
9	4	5-0	Mode Select Wheel Position (bit 5 = in good position) (bits 4-0 are binary count)

DEFINITIONS OF DATA VARIABLES

Data will be returned to the user anytime a request for data is made, providing the data was successfully sampled. The following values of UZFUNCTION% will result in data being returned to the user:

UZFUNCTION% = 1	POSITION DATA REQUEST
UZFUNCTION% = 2	TEMPERATURE DATA REQUEST
UZFUNCTION% = 3	MONITOR SIGNAL DATA REQUEST
UZFUNCTION% = 8	RAW A/D DATA REQUEST
UZFUNCTION% = 9	RAW PIO DATA REQUEST

Note: when Sdl primitives has been called with UZFUNCTION% set to 4 thru 7, a command is being sent, and no results will be returned to the user. A status indicating the ability to carry out the command will be returned to the user from all commands or requests.

VARIABLE POSITION DATA

(UZFUNCTION%=1)

When the user has requested position data, he will find the result returned in the element of the array UZRPOS(X) defined as:

UZRPOS(1) Will contain the X-axis pointing mirror position (units will be angular degrees referenced to DIRBE's coordinate system). Note: mechanical error should be < 0.05 degrees in the Range of -2.00 thru 2.00 degrees. Status error will be returned when data requested if LVDTs not turned on.

UZRPOS(2) Will contain the Y-axis pointing mirror position (units will be angular degrees referenced to DIRBE's coordinate system). Note: mechanical error should be < 0.05 degrees in the Range -2.00 thru 2.00 degrees. A status error will be returned when data requested if LVDTs not turned on.

UZRPOS(3) Will contain the Beam sample mirror position (position will be defined as 2=mirror fully in, 1=mirror fully out, and 0=mirror not at either limit).

UZRPOS(4) Will contain the Absolute radiometer filter wheel position (position will be defined as positions 1 to 18, or 0 when wheel is not at a defined position).

UZRPOS(5) Will contain the Aperture wheel position (position will be defined as positions 1 to 18, or 0 when wheel is not at a defined position).

UZRPOS(6) Will contain the Mode selector wheel position (position will be defined as positions 1 to 18, or 0 when wheel is not at a defined position).

UZRPOS(7) Will contain the Filter wheel position (position will be defined as positions 1 to 18, or 0 when the wheel is not at a defined position).

VARIABLE TEMPERATURE DATA

(UZFUNCTION%=2)

When the user has requested temperature data, he will find the result returned in the element of the array UZRTEMP(X) defined as:

UZRTEMP(1) Will contain the Pointing mirror temperature (range 1.5 to 320 K)

UZRTEMP(2) Will contain the Primary mirror temperature (range 1.5 to 320 K)

UZRTEMP(3) Will contain the Beam sample mirror temperature (range 1.5 to 320 K)

UZRTEMP(4) Will contain the Absolute radiometer detector temperature (range 1.5 to 6.0 K)

UZRTEMP(5) Will contain the Absolute radiometer module temperature (range 1.5 to 320 K)

UZRTEMP(6) Will contain the Full time monitor detector temperature (range 1.5 to 6.0 K)

UZRTMP(7) Will contain the Base plate #1 temperature
(range 1.5 to 320 K)

UZRTMP(8) Will contain the Large area IR source
temperature (range 1.5 to 320 K)

UZRTMP(9) Will contain the Integrating sphere module
temperature (range 1.5 to 320 K)

UZRTMP(10) Will contain the Base plate #2 temperature
(range 1.5 to 320 K)

UZRTMP(11) Will contain the Base plate #3 temperature
(range 1.5 to 320 K)

VARIABLE MONITOR SIGNAL DATA WILL BE RETURNED IN
(UZFUNCTION%=3)

When the user has requested monitor signal data, he will
find the result returned in the element of the array UZRSIG(X)
defined as:

UZRSIG(1) Will contain the Absolute radiometer monitor
signal (data will be in volts) Note: This will be the rectified
1HZ bandwidth signal. We will select the highest gain channel
which is not saturated and send it to the PC. All data will be
referenced to the X1 channel Range: -0.0100 thru 10.000 volts.
Note: -10 volts will be returned when the system is saturated.
Status error will be returned if chopper, preamp, and bias are
not turned on when this data is sampled.

UZRSIG(2) Will contain the Full time monitor signal (data
will be in volts) This signal will be handled the same as the AR
monitor described above. Status error will be returned if
chopper, preamp, and bias are not turned on when this data is
sampled.

UZRSIG(3) Will contain the Large Area Source drive
voltage (data will be in volts).

UZRSIG(4) Will contain the Large Area Source drive
current (data will be in milliamps).

UZRSIG(5) Will contain the Bulb with envelope on #1 drive voltage (data will be volts).

UZRSIG(6) Will contain the Bulb with envelope on #1 drive current (data will be in milliamps).

UZRSIG(7) Will contain the Bulb with envelope on #2 drive voltage (data will be in volts).

UZRSIG(8) Will contain the Bulb with envelope on #2 drive current (data will be in milliamps).

UZRSIG(9) Will contain the Bulb with envelope removed #1 drive voltage (data will be in volts).

UZRSIG(10) Will contain the Bulb with envelope removed #1 drive current (data will be in milliamps).

UZRSIG(11) Will contain the Bulb with envelope removed #2 drive voltage (data will be in volts).

UZRSIG(12) Will contain the Bulb with envelope removed #2 drive current (data will be in milliamps).

UZRSIG(13) Will contain the A.R. Chopper DC Monitor (data will be in volts). This monitor indicates to the user the relative amount of drive going to the chopper. Status error will be returned if data is requested when chopper is not turned on.

UZRSIG(14) Will contain the Absolute Radiometer Bias battery voltage (data will be in volts). Status error will be returned if bias is not turned on.

UZRSIG(15) Will contain the Full Time Monitor Bias battery voltage (data will be in volts). Status error will be returned if bias is not turned on.

UZRSIG(16) Will contain the Absolute Radiometer Preamp Battery voltage (data will be in volts). Status error will be returned if preamp is not turned on.

UZRSIG(17) Will contain the Full Time Monitor Preamp Battery voltage (data will be in volts). Status error will be returned if preamp is not turned on.

UZRSIG(18) Will contain the Full Time Monitor Chopper DC Monitor (data will be in volts). Same as explained above in 13 for AR.

UZRSIG(19) Will contain the AR Bolometer DC level which will tell the user the relative temperature of the bolometer to correct the data (data will be in volts). Status error will be returned if preamp power is not turned on when data is sampled.

UZRSIG(20) Will contain the FTM Bolometer DC level. (data will be in volts). Status error will be returned if preamp power is not turned on when data is sampled.

VARIABLE RAW A/D DATA WILL BE RETURNED IN
(UZFUNCTION%=8)

When the user has requested raw A/D data, he will find the result returned in the element of the array UZRETRAWAD%(X). Note: the signal presented to the channel of the A/D converter will be returned to the user. There are times when the data will be meaningless. For example the output of the LVDTs when not turned on will give a voltage which may be misleading if converted to a position of the pointing mirror. Elements of the array UZRETRAWAD%(X) are defined as:

UZRETRAWAD%(X) Will contain an integer from 0 to 4095 which is the 12 bit data read from channel X of the A/D converter (data will be converted to decimal number). Note: Channels 1 to 24 are 0 to +10V range, so the voltage is $10 * (\text{Count} / 4095)$ Channels 25 - 40 are -10V to +10V range, so the voltage is found by $20 * (\text{Count} / 4095) - 10$.

UZRETRAWAD%	Signal on channel
1	Pointing Mirror Temperature
2	Primary Mirror Temperature
3	Beam Sample Mirror Temperature
4	Abs. Radiometer Bolometer Temp
5	Abs. Radiometer Module Temp

6	Full Time Mon Bolometer Temp
7	Base Plate #1 Temperature
8	Large Area IR Source Temp X1
9	Integrating Sphere Module Temp
10	Base Plate #2 Temperature
11	Base Plate #3 Temperature
12	Large Area IR Source Temp X2
13	AR Bolometer DC
14	FTM Bolometer DC
15	Large Area IR Source Drive Voltage
16	Large Area IR Source Drive current
17	Bulb w/envelope #1 Drive Voltage
18	Bulb w/envelope #1 Drive current
19	Bulb w/envelope #2 Drive Voltage
20	Bulb w/envelope #2 Drive current
21	Bulb w/o envelope #1 Drive Voltage
22	Bulb w/o envelope #1 Drive current
23	Bulb w/o envelope #2 Drive Voltage
24	Bulb w/o envelope #2 Drive current
25	X-Axis pointing mirror LVDT
26	Y-Axis pointing mirror LVDT
27	AR rectified signal X1
28	AR rectified signal X10
29	AR rectified signal X100
30	AR rectified signal X1000
31	FTM rectified signal X1
32	FTM rectified signal X10
33	FTM rectified signal X100
34	FTM rectified signal X1000
35	AR Preamp battery voltage
36	AR Bias battery voltage
37	FTM Preamp battery voltage
38	FTM Bias battery voltage
39	AR Chopper DC monitor
40	FTM Chopper DC monitor

VARIABLE RAW PIO DATA WILL BE RETURNED IN
(UZFUNCTION%=9)

When the user has requested raw PIO data, he will find the result returned in the element of the array UZRETRAWPIO%(X) defined as:

UZRETRAWPIO%(1) Will contain either a 0 or a 1 to indicate the state of the Beam Sample In switch. A 0 will indicate the switch is open, and a 1 will indicate that the switch is closed.

UZRETRAWPIO%(2) Will contain either a 0 or a 1 to indicate the state of the Beam Sample Out switch. A 0 will indicate the switch is open, and a 1 will indicate that the switch is closed.

UZRETRAWPIO%(3) Will contain an integer from 0 to 31 or 100 to 131. This number will show the encoder switch readouts for the Aperture Wheel between the integrating spheres. A number from 0 to 31 will indicate the Geneva gear is in a good position, and the 5 encoder switches will give the number. When a number from 100 to 131 is returned it will indicate that the wheel is not in a good Geneva position, and the last two numbers will show the count being returned by the 5 encoder switches.

UZRETRAWPIO%(4) Will contain an integer from 0 to 3 which is the value of the two spare bits (bits 7 and 6) of channel 2 on the PIO board. They are not meaningful now, but could be connected to something later so they are provided for flexibility.

UZRETRAWPIO%(5) Will contain an integer from 0 to 31 or 100 to 131. This number will show the encoder switch readouts for the Filter Wheel between the integrating spheres. A number from 0 to 31 will indicate the Geneva gear is in a good position, and the 5 encoder switches will give the number. When a number from 100 to 131 is returned it will indicate that the wheel is not in a good Geneva position, and the last two numbers will show the count being returned by the 5 encoder switches.

UZRETRAWPIO%(6) Will contain an integer from 0 to 3 which is the value of the two spare bits (bits 7 and 6) of channel 3 on

the PIO board. They are not meaningful now, but could be connected to something later, they have been included for system flexibility.

UZRETRAWPIO%(7) Will contain an integer from 0 to 31 or 100 to 131. This number will show the encoder switch readouts for the Absolute Radiometer Filter Wheel. A number from 0 to 31 will indicate the Geneva gear is in a good position, and the 5 encoder switches will give the number. When a number from 100 to 131 is returned it will indicate that the wheel is not in a good Geneva position, and the last two numbers will show the count being returned by the 5 encoder switches.

UZRETRAWPIO%(8) Will contain an integer from 0 to 3 which is the value of the two spare bits (bits 7 and 6) of channel 4 on the PIO board. They are not meaningful now, but could be connected to something later; they have been included for system flexibility.

UZRETRAWPIO%(9) Will contain an integer from 0 to 31 or 100 to 131. This number will show the encoder switch readouts for the Mode Select Wheel. A number from 0 to 31 will indicate the Geneva gear is in a properly aligned, and the 5 encoder switches will give the number. When a number from 100 to 131 is returned it will indicate that the wheel is not in a good Geneva position, and the last two numbers will show the count being returned by the 5 encoder switches.

DEFINITION OF STATUS CODES RETURNED

The variable Sdl.UZSTATUS% will be defined during every command or request for data. The user should always check this variable when the PC returns to his next program line following a Sdl primitives (SDL). When there have been no problems in executing a command, or obtaining data, Sdl.UZSTATUS% will be returned as 0. If there have been any problems, Sdl.UZSTATUS% will contain a number which will be defined to inform the user what type of problem was encountered. The user must then decide

what actions he wants to take to correct the problem. There are two groups of status codes which may be returned to the user. The first group "PC STATUS CODES", are errors which have been detected in the Sdl primitives software on the PC. The second group "ERROR CODES RETURNED BY STD BUS" are errors which have been detected by the processor in the STD BUS.

PC STATUS CODES

- 0 No errors detected or received from STD Buss.
- 1 Com 1 error has occurred.
- 2 No "S" start character received from STD Buss.
- 3 No "L" last character was received from STD Buss.
- 4 String received from STD Buss was not the correct length as defined in reply format.
- 5 Character received to indicate which type of data is being returned from STD Buss was undefined (not A thru H).
- 6 Channel number received from STD Buss was undefined for the type of data being returned.
- 7 Data defined to always be 0 was not returned as 0.
- 8 Data received from STD Buss was undefined.
- 9 Trying to move Pointing mirror outside of window set up in Sdl primitives.

ERROR CODES RETURNED BY STD BUS

- 65 STD Buss received an undefined character in the position to tell what type of command was being sent (Not A thru I).
- 66 STD Buss received an undefined channel number for the type of command or data request.
- 67 STD Buss received too many characters before the "L" for last character in the command string.

- 68 STD Buss received invalid data in the previous command.
- 69 STD Buss had an error in trying to send to the PC.
- 70 STD Buss had an error in selecting a memory block for lookup table.
- 71 STD Buss received a parity, framing or overrun error.
- 72 STD Buss received RTS = 0 before receiving a "L" for last character in command or data request.
- 73 STD Buss had a error in selecting which channel of gain to send to the PC.
- 74 STD Buss has not been initialized since last power-up.
Note: this means everything has been turned off.
- 75 STD Buss received some non-zero characters in bits which are defined to be always zero.
- 76 STD Buss detected a bad channel in WHLCMD section.
- 77 STD Buss did not receive all 0's in bits 14 - 5 in wheel move command data.
- 78 STD Buss received an undefined position at which to move a wheel.
- 79 STD Buss had an error in trying to move a wheel. This error may be caused by the following: In trying to move a wheel or Beam sample mirror to a new position, we did not find the desired new position within 8000 steps, so we have stopped the motor and turned it off. When we are trying to move a wheel, Beam sample mirror, or Pointing mirror by steps, we can get this error if we are stopped by a trigger and have not moved the desired number of steps yet.
- 80 A flag that is used in the STD Buss had a undefined value.
- 81 LVDT was not turned on when a command or request for data was received by STD Buss which required use of LVDTs.
- 82 Chopper was not turned on as required to get requested data.
- 83 Bias was not turned on, and it is needed for requested data.

84 Preamp power was not turned on so data would be misleading.

85 We have checked the Integrating Sphere module, Base plate #2, and Base plate #3 thermal sensors, and have not found any to be below 10 degrees kelvin, so we will not allow the bulbs without envelopes to be turned on since we may not be in a adequate vacuum, and bulbs may be damaged.

86 We have had a bad temperature control status in Large Area Source temperature control loop. Therefore we have turned the source off to prevent overheating. User will have to reset the source to the desired temperature.

87 We had an error from D/A board when trying to set the source to a new value. We have probably not been able to set the source to the new value.

88 We have had an error in trying to send a new voltage to drive the Large Area Source. We have tried to turn the source off to prevent problems of overheating. We are returning this reply to the command or data requested. We did not carry out the command or sample data because we could not return results of the operation.

89 The Program Counter on the STD Buss was outside the program area. We have turned off the Large Area Source, and we are waiting for an initialize command to be sent.

90 We had an error in moving the pointing mirror. We have timed out because we were not able to reach the new desired position in the number of steps we should have been able to reach any position with.

91 We have stopped moving the pointing mirror by steps because we have reached the limit of ± 4 degrees. Note: we have stopped both motors.

92 We had an error in checking the present position to make sure we are not exceeding the limits when moving pointing mirror by steps. We have therefore stopped and turned off both motors.

- 128 Undefined channel number error by A/D converter board 0.
- 129 Undefined channel number error by A/D converter board 1.
- 130 Undefined A/D converter board number.
- 131 A/D board 0 took too long to sample channel.
- 132 A/D board 1 took too long to sample channel.
- 133 D/A board was initializing when we tried to access.
- 134 D/A board busy and we have timed out waiting for it.
- 135 D/A received more than 12 bits.
- 136 Channel sent to D/A board was out of range.
- 137 Channel sent to PIO board was out of range.

APPENDIX D
Source Stability Report

NOTE
PRINT APPENDIX D
single sided
do not duplex this
appendix

BLACKBODY SOURCE EVALUATION
UTILIZING A COMPARATOR RADIOMETER

by

Hasan Niaz

A thesis submitted in partial fulfillment
of the requirements for the degree

of

MASTER OF SCIENCE

in

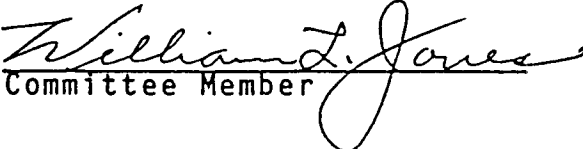
Engineering

(Electrical)

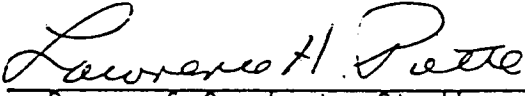
Approved:


Major Professor


Committee Member


Committee Member


Committee Member


Dean of Graduate Studies

UTAH STATE UNIVERSITY
Logan, Utah

1984

APPENDIX D

ACKNOWLEDGMENTS

I wish to express my profound gratitude to my major professor, Dr. Clair L. Wyatt for the paternal and constructive guidance he extended during his supervision of my work on this research project. I am deeply indebted to my committee members, Dr. Kay D. Baker, Dr. William L. Jones, and Dr. Dyke Stiles, whose invaluable suggestions and instructions helped me a lot. Special gratitude is extended to Dr. Doran J. Baker, Head of the Electrical Engineering Department, for his cooperation and help. I would like to earnestly thank the staff of the Space Dynamics Laboratories who were helpful in one way or another and especially Mindy Vance, for her patient and skillful typing. My special thanks go to my parents and uncle (Mama) for their support and love during my studies.

Hasan Niaz

TABLE OF CONTENTS

	Page
ACKNOWLEDGMENTS	ii
LIST OF TABLES	iv
LIST OF FIGURES	v
ABSTRACT	vi
Chapter	
I. INTRODUCTION AND OBJECTIVES	1
II. THEORETICAL ANALYSIS	4
THE EFFECTIVE FLUX	4
NOISE EQUIVALENT DIFFERENTIAL TEMPERATURE	6
CONCLUSIONS	7
III. RESULTS	8
COMPARATOR RADIOMETER SYSTEM EVALUATION	8
Comparator Responsivity	8
Comparator Stability	9
CIRRIS SOURCE EVALUATION	11
Control Circuit Stability	13
Conclusions	14
REFERENCES	16
APPENDICES	17
APPENDIX A. SPECIFICATIONS OF INFRARED DETECTOR	18
APPENDIX B. DETECTION SYSTEM DESIGN	20
APPENDIX C. SPECIFICATIONS OF LABORATORY STANDARD BLACKBODIES	26
APPENDIX D. SPECIFICATIONS OF HYSTERESIS MOTOR AND ASSEMBLY	30
APPENDIX E. SPECIFICATIONS OF LOW-NOISE OPERATIONAL AMPLIFIER	31

LIST OF TABLES

Table	Page
1. Data for Product Integral Solution Where $\delta\lambda = 0.25 \mu\text{m}$	5
2. Comparator Radiometer System Long-Term Drift Measured Using Two Identical Standard Sources	10
3. "Grain of Wheat" Bulb Short-Term Repeatability Data (Source Voltage 0.86 V, Source Current 20.3 mA)	12
4. "Grain of Wheat" Bulb Long-Term Stability Data (Source Voltage 0.86 V, Source Current 20.3 mA)	12
5. "Grain of Wheat" Bulb Temperature Change as a Function of Control Circuit Temperature ($V = 0.113$, $i = 23.4 \text{ mA}$)	13
6. Temperature Change as a Function of Primary Power Source ($V = 1.13\text{V}$, $i = 23.4 \text{ mA}$, $T = 75 \text{ F}$)	14

LIST OF FIGURES

Figure	Page
1. Functional Block Diagram of Comparator Radiometer	34
2. Optical Layout	35
3. Waveform at the Output of Detector	36
4. Chopper Mirror	37
5. Optics Box	38
6. Circuit Description of U-Type Photo Device	39
7. Circuit Diagram of Pre-Amplifier	40
8. Block Diagram of Phase-Lock Amplifier	41

ABSTRACT

Blackbody Source Evaluation
Utilizing A Comparator Radiometer

by

Hasan Niaz, Master of Science

Utah State University, 1984

Major Professor: Dr. Clair L. Wyatt
Department: Electrical Engineering

An infrared source is evaluated for use on the Shuttle-borne CIRRIS interferometer spectrometer as an internal reference calibration source. A comparator radiometer system has been designed, fabricated, and tested that utilizes an Infrared Industries model 463 laboratory blackbody as a standard for comparison, lead sulfide detector, optics and reflective chopper to merge the source flux, and a phase-lock amplifier to measure the source difference. The stability of the standard blackbody is observed by comparison with an identical unit. The worst case drift is 0.66 degree/hr. The comparator sensitivity is 5.3 mV/K providing capability to measure short-term source repeatability of the order of 0.07 degree. A Chicago miniature lamp model CM8-680 was tested as a candidate CIRRIS internal reference source and found to

exhibit a short-term repeatability of ± 0.1 degree; and the long-term drift of ± 0.48 degree/hour. The effects of fluctuation in mainline voltage and temperature effects are found to be negligible.

(42 pages)

CHAPTER I
INTRODUCTION AND OBJECTIVES

The objective of this research is to design, develop and fabricate a comparator radiometer system through which the performance of various internal reference sources for CIRRIS (Cryogenic Infrared Radiometer Interferometer Spectrometer) can be evaluated. These internal reference sources (blackbody simulators) are utilized for in-flight calibration of the shuttle-borne CIRRIS sensors. CIRRIS is a sophisticated system of sensors that obtain radiometric and interferometric measurements of the earth limb. It is scheduled to be part of a future payload for the Space Shuttle.

Both the absolute and relative spectral response functions of the CIRRIS interferometer are dependent upon critical mirror alignment. Thus, the internal reference source provides a means to correct for changes in the interferometer responsivity due to the mirror alignment.

However, the use of an internal reference source is only of value provided that its precision and accuracy are known. An in-flight calibration that indicates a change in response to the internal reference source, can be used to correct for mirror alignment responsivity changes, provided that the observed changes exceed the uncertainties of the reference source. Thus, the source uncertainties must be determined by measurement.

The comparator radiometer system includes a laboratory standard source, whose characteristics are well known. Then, the test source can be compared with the laboratory standard as illustrated in the system block diagram of Fig. 1.

The working principle of the radiometer comparator is that the infrared radiation from the reference and test sources is received by a single infrared detector alternatively. The radiation from these sources is directed to the detector using a rotating reflective chopper. A set of lenses is used, in a relay mode, to focus the radiating sources on the detector (see Fig. 2). The detector output consists of a square wave (see Fig. 3); the peak to peak value $\Delta V = V_2 - V_1$ is related to the source radiation (or temperature) difference. The phase-lock amplifier [1] is used to provide a sensitive measure of the small ΔV .

The most general parameter for source characterization is the effective temperature. The effective temperature is defined as the temperature of an ideal blackbody that would produce the same response in the comparator radiometer. Thus, the comparator radiometer system must be calibrated so that the differential voltage can be used to deduce a differential temperature.

The noise equivalent differential temperature (NEDT) is defined as a temperature difference that produces a change in the average value of the phase-lock output equal

to the rms noise. The phase-lock amplifier is well suited to this task since the time constant can be adjusted for long integration times and the mean value of the noise is always zero.

It is not necessary to know the absolute temperature of the CIRRIIS blackbody simulator; however, it is vital to know the repeatability and stability of the source. The design goal of the comparator radiometer is that it have the capability to measure differential temperatures of ± 1 degree, or less, at an effective temperature of 600 C.

This thesis presents the design and evaluation of a comparator radiometer system and the characterization of a candidate blackbody simulator source for CIRRIIS.

CHAPTER II
THEORETICAL ANALYSIS

The purpose of this chapter is to calculate the effective flux incident upon the detector from the 600 C source and, based upon the detector parameters of responsivity and detectivity, find the theoretical NEDT.

THE EFFECTIVE FLUX

The effective flux, incident upon the detector, is given as the product-integral of the source sterance [radiance], the detector relative response function, and certain geometrical and loss parameters [2 p. 44]

$$\phi_d = \frac{\tau T}{\beta \gamma} \int_{\lambda_1}^{\lambda_2} L(\lambda)R(\lambda)d\lambda = 4.75 \times 10^{-5} \text{ W} \quad (1)$$

where the throughput T is given by [2 p. 25]

$$T = \frac{A_d \pi}{4F^2} = \frac{0.01 \times \pi}{4 \times 1.81^2} = 2.40 \times 10^{-3} \text{ cm}^2 \text{ sr} \quad (2)$$

for a 1 mm square detector and an $F/1.81$ relay lens. The term γ takes into account the increase in noise due to coherent phase detection [3, pp. 240-242] and is $\sqrt{2}$. The optical efficiency τ is given approximately by

$$\tau = (0.95)^3 = 0.857 \quad (3)$$

for 2 lenses and one reflective surface. The chopping factor β is approximated by the factor 3. The integral is approximated in terms of a summation

$$\int_{\lambda_1}^{\lambda_2} L(\lambda)R(\lambda)d\lambda = \delta \lambda \sum_{i=1}^n L_i(\lambda)R_i(\lambda) = 9.79 \times 10^{-2} \text{ W} \quad (4)$$

Where the data for the detector relative response $R(\lambda)$ is taken from typical PbS detector response curve (Appendix A) and $L(\lambda)$ is calculated from Planck's equation [4, p. 29].

$$L(\lambda) = [C_1/\lambda^5] \times [\exp(C_2/\lambda T) - 1]^{-1} \quad (5)$$

where $C_1 = 11910.66$

$C_2 = 14388.3$

$T = 600 \text{ C (873 K)}$

The data for the solution of Eqs. (4) and (5) are given in Table 1; in addition, the equivalent ideal bandwidth of the PbS detector is given by [2 p. 124]

$$\Delta\lambda = \delta\lambda \sum_{i=1}^n R_i(\lambda) = 1.39 \mu\text{m} \quad (6)$$

where the summation is given in Table 1.

INDEX	WAVE-LENGTH (μm)	$L(\lambda)$	$R(\lambda)$	$L(\lambda)Rd(\lambda)$
1	1.00	8.28×10^{-4}	0.70	5.80×10^{-4}
2	1.25	7.33×10^{-3}	0.75	5.50×10^{-3}
3	1.50	2.65×10^{-2}	0.80	2.12×10^{-2}
4	1.75	5.90×10^{-2}	1.00	5.90×10^{-2}
5	2.00	9.82×10^{-2}	0.90	8.84×10^{-2}
6	2.25	1.36×10^{-1}	0.70	9.53×10^{-2}
7	2.50	1.67×10^{-1}	0.50	8.37×10^{-2}
8	2.75	1.89×10^{-1}	0.20	3.79×10^{-2}
SUM			5.55	0.392

Table 1. Data for Product Integral Solution
Where $\delta\lambda = 0.25 \mu\text{m}$

The detector absolute responsivity R is given in the specifications (Appendix A) as 5×10^3 V/W, thus the output signal voltage V_S (including the preamplifier gain $G=11$) is given by

$$V_S = \phi_d R G = 4.75 \times 10^{-5} \times 5 \times 10^3 \times 11 = 2.61 \text{ V} \quad (7)$$

the noise equivalent power NEP is obtained as

$$\text{NEP} = (A_d \Delta f)^{1/2} / D^* = 7.28 \times 10^{-12} \text{ W} \quad (8)$$

where $D^* = 1 \times 10^{10}$ ($\text{cmHz}^{1/2}/\text{W}$) and where the electrical noise bandwidth Δf is set at 1.96 Hz for a (300 ms time constant). Thus, the signal to noise ratio is expected to be

$$\text{SNR} = 4.75 \times 10^{-5} / 7.28 \times 10^{-12} = 6.52 \times 10^6 \quad (9)$$

and the noise voltage V_n is

$$V_n = V_S / \text{SNR} = 2.61 / 6.52 \times 10^6 = 4 \times 10^{-7} \text{ V}_{\text{rms}} \quad (10)$$

NOISE EQUIVALENT DIFFERENTIAL TEMPERATURE

The derivative of Planck's equation (Eq. 5) with respect to temperature yields

$$\frac{dL(\lambda)}{dT} = \frac{C_1 C_2}{\lambda^6 T^2} \times \frac{1}{\exp(C_2/\lambda T)} \quad (11)$$

and the incremental change in total flux with respect to temperature is

$$\frac{\Delta L}{\Delta T} = \Delta \lambda \frac{dL(\lambda)}{dT} \quad (12)$$

This must be solved in terms of the effective flux ϕ_d incident upon the detector. Multiplying both sides of Eq. (12) by the geometric and loss factors of Eq. (1) provides

$$\frac{\Delta\phi_d}{\Delta T} = \frac{\tau T \Delta\lambda}{\beta\sqrt{2}} \times \frac{C_1 C_2}{\lambda^6 T^2} \times \frac{1}{\exp(C_2/\lambda T)} = 7.76 \times 10^{-7} \text{ W/K} \quad (13)$$

where $\Delta\lambda = 1.39 \text{ } \mu\text{m}$ (from above) and $\lambda = 2.5 \text{ } \mu\text{m}$ (Table 1).

Thus, ΔT becomes the NEDT, in Eq. (13) when NEP is substituted for $\Delta\phi_d$, and

$$\text{NEDT} = \text{NEP}/7.76 \times 10^{-7} = 1 \times 10^{-5} \text{ degree} \quad (14)$$

CONCLUSIONS

The solution to Eq. (14) indicates that the Pbs detector is capable of detecting 1×10^{-5} degree change in a 600 C temperature source. Thus, the system will be limited primarily by the standard reference source stability. The system, detailed in Appendix B, is theoretically capable of evaluating various 600 C sources for use in the CIRRIIS sensor.

CHAPTER III

RESULTS

This chapter gives the measured performance of the comparator radiometer system and establishes the limits of stability and repeatability for which it can be used to evaluate candidate sources for CIRRIIS. This chapter also gives the results of testing of the Chicago Miniature Lamp Works, No. CM-680 ("Grain of Wheat" bulb) as a candidate source for CIRRIIS.

COMPARATOR RADIOMETER SYSTEM EVALUATION

The ability of the comparator radiometer system to evaluate a candidate source depends upon the stability of the standard reference source. There exist three identical blackbody standards at USU at the present time. They are Infrared Industries No. 463; specified at ± 0.5 degree long term stability, ± 0.1 degree setability.

An estimate of the source uncertainty can be obtained by comparing the unit to be used as the standard reference source with another identical unit. The sources were turned on and permitted to stabilize over a period of several hours for each of the tests to be described below.

Comparator Responsivity

The responsivity, in units of differential volts per degree difference was measured by first nulling the sources, as described above, and then by incrementing one

source by 10 degrees and noting the resultant difference voltage. The observed change of 53 mV, resulting from a 10 degree change yields a differential responsivity

$$\Delta R \approx 5.3 \text{ mV/K} \quad (15)$$

With one channel blocked, the response of the comparator radiometer system to a 600 C blackbody source is measured at 3.0 volts; this includes a preamplifier gain of 11. Thus, the detector responsivity is

$$R_d = V/(G \times \phi_{\text{eff}}) = 5.74 \times 10^3 \quad (16)$$

which agrees with the specifications given in Appendix A.

The NEDT can be calculated using Eqs. (10) and (15)

$$\text{NEDT} = V_n/\Delta R = 4 \times 10^{-7}/5 \times 10^{-3} = 8 \times 10^{-5} \text{ K}$$

based upon detector specified noise only.

Comparator Stability

The comparator stability was measured using two standard sources nulled after sufficient warm-up time as described above. The test was continued for about 12 hours, and results are tabulated in Table 2.

The data in Table 2 are interpreted as follows:

- (1) The worse case drift-rate observed is approximately 0.66 degree/hour.
- (2) The average drift observed is 0.14 degree/hour.

The performance of the comparator radiometer is limited by standard source drift as postulated above. However, the measured drift, even in the worse case of 0.66 degree/hr is sufficiently small to permit evaluation of the

TIME (hr)	TOTAL DRIFT (mV)	DRIFT (mV/hr)	Drift (ΔT /hr)
0.00	0.0	--	--
1.03	3.6	3.50	0.66
2.00	1.6	2.06	0.39
3.17	1.6	0.00	0.00
4.42	1.2	0.32	0.06
5.42	1.2	0.00	0.00
6.42	0.8	0.40	0.08
7.42	1.0	0.20	0.04
9.45	1.0	0.00	0.00
10.92	1.0	0.00	0.00
0.00*	0.0	--	--
1.23	1.2	0.98	0.18

* Reverse blackbody sources

Table 2. Comparator Radiometer System Long-Term Drift Measured Using Two Identical Standard Sources

candidate CIRRIS sources. This is true because the CIRRIS flight source will be operated with a very low duty cycle; that is, it will be activated for short periods (less than 6 minutes) and then deactivated for many hours at a time. Thus, the short-term repeatability evaluation of candidate CIRRIS sources can be obtained to an accuracy uncertainty of the order of 0.07 degree (over 1/10 hour). The long-term drift of CIRRIS sources is of less interest; however, as indicated above, the worse case long-term drift is of the order of 1 degree/hour which agrees with the blackbody stability specification as given in Appendix C.

CIRRIS SOURCE EVALUATION

Considerable time was used in attempts to test an Infrared Laboratories nichrome film source. The source was operated, failed, shipped to the vendor and repaired, and returned repeatedly, never getting sustained or repeatable performance. Therefore, it was determined to evaluate and use the comparator radiometer system by testing a Chicago Miniature Lamp Works No. CM-680 ("Grain of Wheat" bulb) as a possible source for CIRRIS. The Chicago Miniature Lamp Works envelope was cut off to allow the filament to radiate without the spectral limit of the glass. In addition, the CIRRIS control circuit (unmodified) could be used to keep lamp operation at an effective temperature of 600 C.

Preliminary tests showed that the exposed filament degraded and became "open circuit" within several minutes if operated at 600 C in an ambient atmosphere, as was also true of the Infrared Laboratories nichrome film source. Therefore, the bulb was subsequently tested under hard vacuum conditions.

The data from the short-term repeatability evaluation for the "Grain of Wheat" bulb is given in Table 3. The data in Table 3 are interpreted as follows:

- (1) The worse case temperature difference observed for 60 seconds cycle time is 0.1 degree (or 6 degree/hour). This is considerably greater than the drift observed in the comparator radiometer system.

(2) The short-term repeatability mean uncertainty is 0.03 degrees.

The data for long-term stability evaluation is given in Table 4. The data in Table 4 are interpreted as follows:

TEST NO.	OFF TIME (SEC)	OUTPUT VOLTAGE CHANGE (MV)	SOURCE TEMP DIFFERENCE (C)
1	30	0.00	0.0
2	30	0.00	0.0
3	30	0.00	0.0
4	60	0.05	0.1
5	60	0.00	0.0
6	60	0.05	0.1
7	300	0.00	0.0
8	300	0.05	0.1
9	300	0.00	0.0

Note: Output voltage resolution ± 0.01 Volts

Table 3. "Grain of Wheat" Bulb Short-Term Repeatability Data (Source Voltage 0.86 V, Source Current 20.3 mA)

INDEX	LENGTH OF TEST (hr)	HEAT-SINK TEMP (K)	TOTAL ΔV (mV)	DRIFT (mV/hr)	DRIFT (ΔT /hr)
1	1.25	295	3.00	2.40	0.48
2	1.50	295	2.80	1.86	0.36
3	1.50	295	5.80	3.86	0.77
4	2.00	10	1.85	0.92	0.18
5	1.00	295	1.80	1.80	0.36

Table 4. "Grain of Wheat" Bulb Long-Term Stability Data (Source Voltage 0.86 V, Source Current 20.3 mA)

(1) the maximum drift observed is 0.48 degree/hr.

(2) the mean of the drift is 0.43 degree/hr.

The short-term repeatability performance of the "Grain of Wheat" bulb is much better than the performance goal of ± 1 degree which warrants further investigation of the bulb as a possible source for CIRRIIS.

Control Circuit Stability

The source stability is also dependent upon the control circuit stability. The change in source temperature was measured as a function of control circuit temperature and primary supply voltage, the data are given in Tables 5 and 6, and are interpreted as follows: the effect of the temperature, over the range of -17.8 C to 23.9 C, and variations in primary voltage of ± 10 percent are in the worse case less than 0.1 degree and are negligible.

TEST NO.	TEMP (C)	OUTPUT VOLTAGE CHANGE	SOURCE TEMP CHANGE (K)
1	23.9	0.00	--
2	04.4	0.40	0.076
3	17.8	0.00	--
4	23.9	0.05	0.009

Table 5. "Grain of Wheat" Bulb Temperature Change as a Function of Control Circuit Temperature ($V = 0.113$, $i = 23.4$ mA)

Conclusions

A comparator radiometer system has been designed, fabricated, tested, and applied to the interferometer calibration on CIRRIIS.

TEST NO.	PRIMARY SUPPLY (V rms)	OUTPUT VOLTAGE CHANGE (MV)	SOURCE TEMPERATURE CHANGE (K)
1	110	0.00	0.000
2	099	0.01	0.002
3	120	0.01	0.002
4	118	0.10	0.020

Table 6. Temperature Change as a Function of Primary Power Source (V = 1.13V, i = 23.4 mA, T = 75 F)

The theoretical NEDT is 1×10^{-5} degree; this calculation is based upon the use of a 600 C blackbody, specified PbS detectivity and responsivity, and the comparator optical throughput and losses.

The comparator radiometer responsivity is 5.3 mV/K (when the source is 600 C); this is measured using two standard reference blackbodies offset by 10 degrees and noting the resultant difference voltage.

A measure of the drift in the standard reference source was obtained by comparing two identical reference sources. The worse case drift rate observed during the first hour of a 12-hour test was about 1.0 degree/hr while the average drift observed is 0.14 degrees/hr. Thus, the

system NEDT is limited by the standard source and depends upon the duration of the test; and the uncertainty in the comparator system does not preclude short-term stability measurements of prospective CIRRIS sources to an uncertainty less than 1 degree.

Preliminary tests were accomplished on a "Grain of Wheat" bulb, Chicago Miniature Lamp Works, No. CM-680 as a possible candidate source. Short-term repeatability measurements on the bulb indicate that the temperature uncertainty is in the order of 0.1 degree. The long-term repeatability of the bulb is in the order of 0.48 degree/hr.

The control circuit that supplies power to the bulb was tested, in terms of bulb temperature change, with respect to primary power and environmental temperature and the bulb temperature change with these parameters is negligible.

The Chicago Miniature Lamp Works, No. CM-680 performance is considerably better than the ± 1 degree design goal and warrants further consideration as a possible internal reference source for CIRRIS.

REFERENCES

1. R.H. Dicke, "The measurement of thermal radiation at microwave frequencies, The Review of Scientific Instruments, 17, pp. 260-275, July, 1946.
2. C.L. Wyatt, "Radiometric Calibration: Theory and Methods", New York, Academic Press, 1978.
3. R.A. Smith, F.E. Jones, and R.P. Chasman, "The Detection and Measurement of Infra-red Radiation", London, Oxford Press, 1960.
4. P.W. Kruse, L.D. McGlauchlin, R.B. McQuistan, "Elements of Infrared Technology: Generation, Transmission, and Detection", New York, John Wiley & Sons, Inc., 1962.
5. E.J. Kelley, D.H. Lyons, and W.L. Root, "The Sensitivity of Radiometric Measurements", J. Soc. Indust. Appl. Math., 11, pp. 235.257.

APPENDICES

APPENDIX A. SPECIFICATIONS OF INFRARED DETECTOR**Mullard**

LEAD SULPHIDE INFRARED DETECTORS (chemically deposited types)

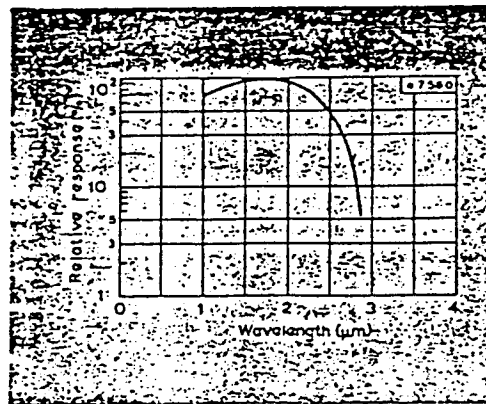
Mullard lead-sulphide infrared detectors made by chemically depositing the active material onto quartz substrates are capable of operation up to 333°K. They are available either in a TO-5 envelope with an end-viewing window or in a flat-pack design.

Material	Lead sulphide (chemically deposited)
Operating temperature	293°K
Spectral response range	
Without filter	Visible to 2.8 μ m
With germanium filter	1.5 to 2.8 μ m

Type number	Element dimensions (mm)	Encapsulation
119CPY } 119-1CPY*	1 × 1	Flat plate
120CPY } 139CPY } 139-1CPY*	6 × 1	Flat plate
	1 × 1	TO-5

*With germanium filter fitted to detector

In addition to the standard types listed above, single-element detectors can be supplied having sensitive areas ranging from 0.5 × 0.5mm to 2 × 2cm. Linear arrays can also be supplied.



Relative spectral response

Peak spectral response	2.0 μm
Operating temperature	293 °K
Resistance	
1 × 1mm element	≥ 200kΩ
6 × 1mm element	≥ 33kΩ
Time-constant (typical)	
1 × 1mm element	250 μs
6 × 1mm element	250 μs
Detectivity	
D* (500 °K, 800, 1)	≥ 1 × 10 ⁸ cm Hz ^{1/2} W ⁻¹
D* (2 μm, 800, 1)	≥ 1 × 10 ¹⁰ cm Hz ^{1/2} W ⁻¹
Responsivity	
(500 °K, 800, 1)	
1 × 1mm element	5 × 10 ³ VW ⁻¹
6 × 1mm element	1 × 10 ³ VW ⁻¹

APPENDIX B. DETECTION SYSTEM DESIGN

This chapter gives the design of the radiometer comparator. The laboratory standard blackbody and the phase-lock amplifier are considered part of the system. As illustrated in the block diagram (see Fig. 1) the radiometer comparator consists of a laboratory standard source, beam-merging optics, a PbS detector, and preamplifier. Each of the blocks is treated individually.

Laboratory Standard Blackbody

The blackbody simulator (Infrared Laboratory Model No. 463), selected as a standard radiation source, provides infrared radiation of known flux and spectral distribution. A specification sheet of the blackbody is given in Appendix C. Its radiation source consists of a stainless steel cylinder. The cylinder contains a 20 degree recessed conical cavity. The emissivity of this cavity is nearly unity because of its geometrical form and due to production of uniform layer of oxidation on its surface.

The stainless steel cylinder is heated by means of a resistance heating element. Power is supplied by its temperature controller, Model No. 101B. A platinum resistance thermometer is used to sense the temperature for the controller. The platinum thermometer is placed between the steel cylinder and the resistance heater.

In this research, two identical laboratory standard blackbodies are used. Though they have the same construction and specifications, their respective calibration curves are slightly different. These calibration curves are also given in Appendix C. These standard blackbodies are used to evaluate the performance of the radiometer comparator and the test source.

Optics

A set of single convex lenses is selected for imaging the detector on the radiation source. They are shown in Fig. 2. Each has a diameter of 19 mm and the focal length is 23 mm. In addition, a chopping mirror is used, as shown in Fig. 4. It serves two purposes: First, it reflects the infrared radiation by 90 degrees from the initial direction of propagation (see Fig. 2). Second, its rotary chopping action allows the radiation to fall upon the detector sequentially from the test source and the reference source.

In the theoretical analysis of Chapter II, the optical efficiency is assumed to be 0.95 for each lens and the mirror. The factor 3 is used for the chopping losses.

Optics Box

The optics box, as shown in Fig. 5 has three baffled lens cells mounted on three of its sides. The single convex lenses are fitted in these lens cells which are attached to the walls of the optics box. The baffles

in the lens cells are designed to reject off-axis radiation. The length of each lens cell is approximately equal to the focal length of the lens used therein. In addition, an iris is placed in each source-cell to provide for rough adjustment of the beam null. Fine scale nulling is accomplished on the phase-lock amplifier.

The chopper mirror is positioned at the intersection of two radiation paths as shown in Fig. 2. This mirror is rotated by a hysteresis synchronous ac gear-motor at a speed of about 108 rpm. This gives a chopping frequency of about 3.6 Hz, since the chopping mirror has two blades. The motor is operated at 115 V ac and 60 Hz and rotates it at 3600 rpm, the speed reduction gear assembly has a reduction ratio of 33.28:1.

The major advantage of this motor is that it can be operated directly from the main power line. It also fulfills the other requirements of space, torque, etc. The specification sheet of this motor is given in Appendix E.

An aluminum reticle of the identical shape of the chopping mirror is attached to the motor shaft. An optical pick-up device, part No. OS-561-A, is used to generate a coherent reference signal. The electrical schematic of the photo-device is presented in Fig. 6. The purpose of this reference signal is to permit phase-lock detection of the difference signal.

The infrared detector is mounted on the exit cell preamplifier. The detector and preamplifier are mounted

on a printed circuit board such that the detector is at the focal point of the lens. This circuit board is shielded from light and electric fields by a cylindrical cover. The optical section is anodized black to reduce the optical scattering.

Infrared Detector

The detector area is 1 mm^2 . The relative spectral response curve and other specifications are given in Appendix A. The optics functions as a relay system to image the detector on the source. The detector is selected on the basis of its detectivity, spectral response, and operating conditions to provide adequate NEDT. There are two detector types which are possible for this design. One is a lead-sulphide PbS, whose resistance, detectivity D^* , and responsivity R are respectively $200 \text{ K}\Omega$, $1 \times 10^{10} \text{ Cm Hz}^{1/2} \text{ W}^{-1}$ @ $2 \text{ }\mu\text{m}$ and $5 \times 10^3 \text{ V/W}$. The other one is lead-selenide PbSe, whose dark resistance, detectivity and responsivity are respectively $1 \times 10^7 \text{ ohms/mm}^2$, $1 \times 10^9 \text{ Cm Hz}^{1/2} \text{ W}^{-1}$ (for elements $< 3 \text{ mm} \times 3 \text{ mm}$) and 2×10^3 to $1.5 \times 10^4 \text{ V/W}$ @ 295 K . The PbSe detector exhibits much higher D^* than the PbS detector, and is the primary reason for selecting PbS.

Low-Noise Preamplifier

A single stage amplifier is used for radiation measurement (Fig. 7). The operational amplifier, Model No. OPA 101 has low noise, high gain-bandwidth product, and

high input impedance characteristics. The main advantage of this operational amplifier is the low-noise characteristic. The specification sheet is given in Appendix E.

The values of the circuit components are calculated as follows: The dark detector resistance R_d is measured at 186.4 k Ω . The detector load resistor R_1 is chosen as a matched load of 180 k Ω .

The detector bias is obtained from the +5 V supply but is decoupled with a low-pass filter. The values of R and C for a break-frequency of 10 Hz is as follows

$$C = 1/[2\pi fR] = 0.795 \mu\text{F} \approx 1.0 \mu\text{F}$$

The value of the coupling capacitor (used to block the dc bias) is determined as follows:

$$R_{eq} = R_3 + R_d R_1 / (R_d + R_1) = 190 \text{ K}\Omega$$

$$C_1 = 1/(2\pi f R_{eq}) = 0.47 \mu\text{F}$$

where the frequency 1.8 Hz is used, which is 1/2 the chopping frequency of 3.8 Hz. A value of 1.0 μF is used.

R_4 is selected as 47 Ω to protect and isolate the output stage of the operational amplifier. In addition, 1 μF capacitors are used at the operational amplifier power supply terminals to decouple the dc power supplies.

The closed loop voltage gain of this amplifier in the noninverting mode is

$$G_V = 1 + R_4/R_5 = 11$$

A 100 k Ω pot (R_7) and a 47 K pot (R_8) are used to

adjust offset voltage and to improve resolution and limit range respectively.

Phase Detector (Phase-Lock Amplifier)

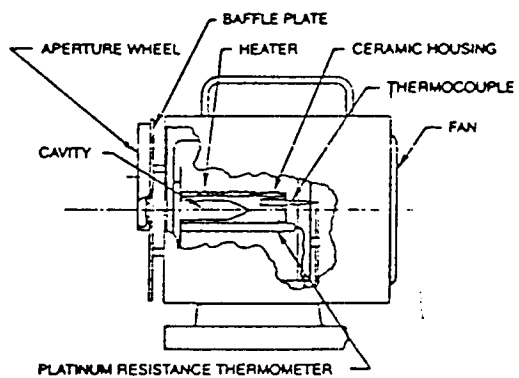
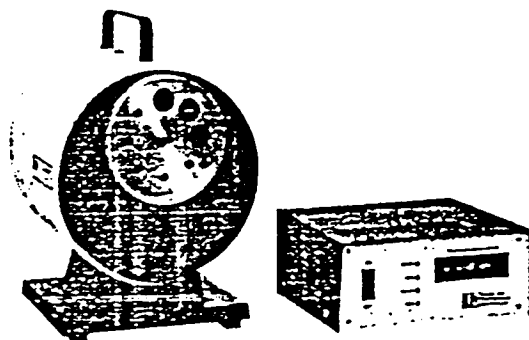
The phase-lock amplifier used here as a difference detector comprises three distinct sections, the signal channel, reference channel and phase sensitive detector along with its output circuitry. The block diagram is shown in Fig. 8. The signal being measured, combined with any noise, is amplified in the signal channel which has a variable bandwidth capable of reducing the noise before submitting the signal to the detector. The reference channel has the function of correlating the phase detector with the phase of the signal. The system has the capability of shifting the phase of the reference signal by a full 360 degrees. The detector produces the sum and difference frequencies of the signal and the reference. The difference is zero frequency, or simply dc, with an amplitude proportional to the signal. All uncorrelated noise has an average value of zero and can be arbitrarily reduced by a low-pass filter [5].

APPENDIX C. SPECIFICATIONS OF LABORATORY STANDARD
BLACKBODIES

IRI MODEL 463 BLACKBODY

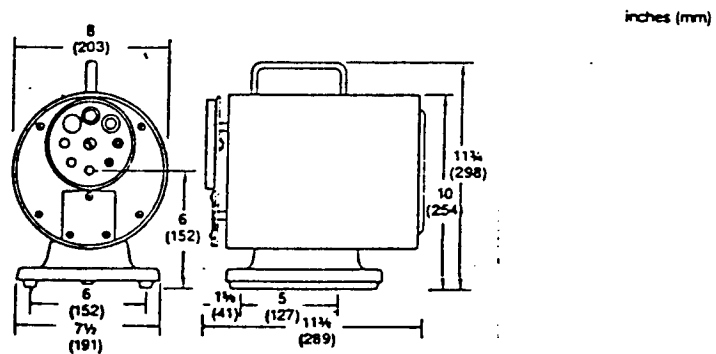
IRI MODEL 101B AND 101BR CONTROLLER

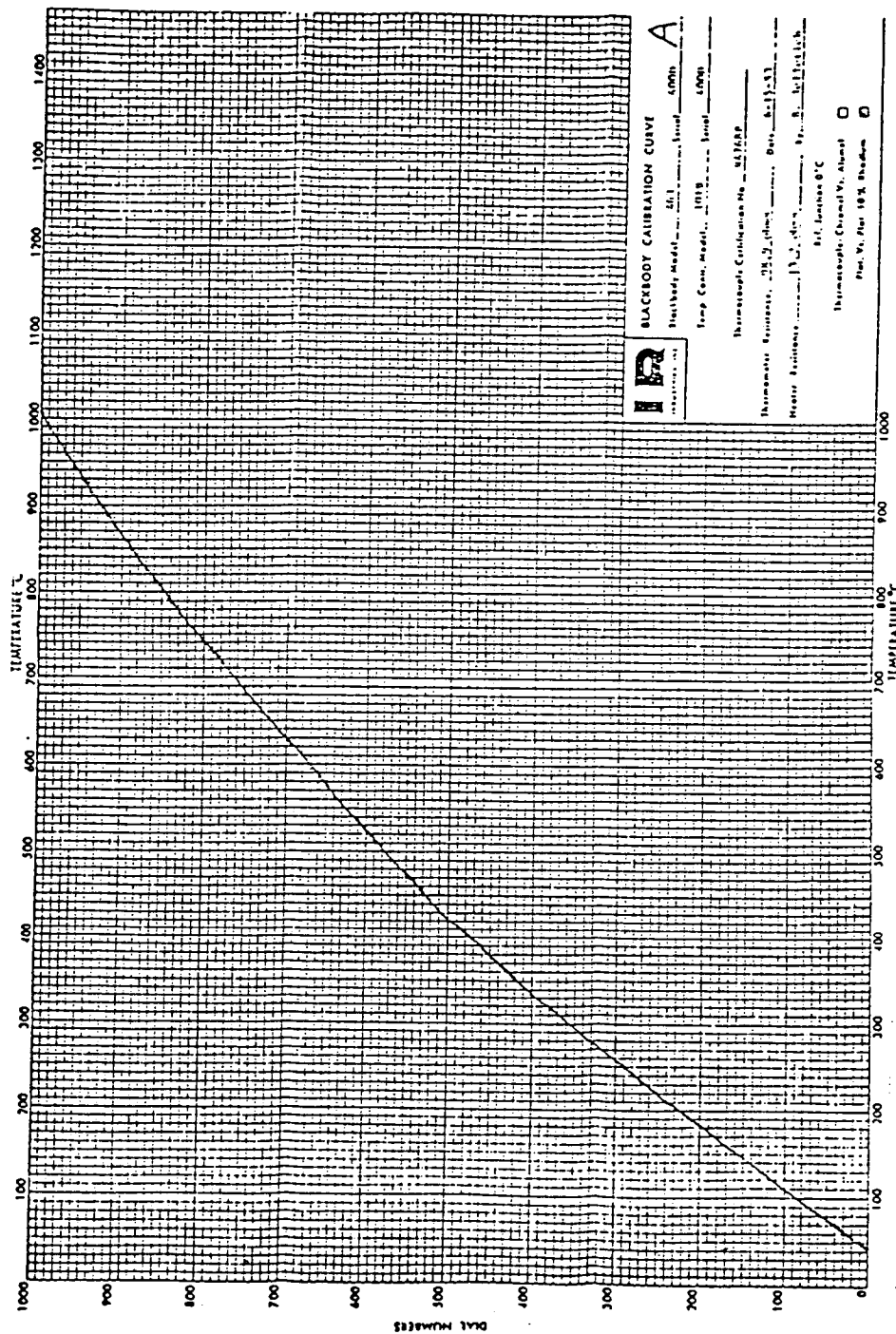
Control Range	50° C to 1000° C
Control Stability	± 0.5° C over any 5-hour period
Control Setability	Within ± 1° C, COARSE; within ± 0.1° C, FINE
Type of Control	Electronic Proportional Control
Sensing Element	Platinum Resistance Thermometer
Thermocouple	Platinum/Platinum 10% Rhodium
Cavity Type	Recessed 20° Cone
Cavity Opening	1 inch
Cavity Emissivity	99% ± 1%
Apertures	0.600, 0.400, 0.200, 0.100, 0.050, 0.0250, 0.0125
Power Requirement	105-125 Volts, 50-60 Hz, 1 0, 7.5 amp. max.
Warm-up Time	Less than 60 minutes from ambient to 1000° C
Housing Temperature	Less than 10° C above ambient at 1000° C
Aperture Temperature	Less than 10° C above ambient at 1000° C



ORIGINAL PAGE IS
OF POOR QUALITY

IR-460 SERIES BLACKBODY RADIATION SOURCE





ORIGINAL PAGE IS
OF POOR QUALITY

APPENDIX D. SPECIFICATIONS OF HYSTERESIS MOTOR AND ASSEMBLY

B-1732

TRW GLOBE

Standard Part Numbers and Data

Gearmotor Performance and Data

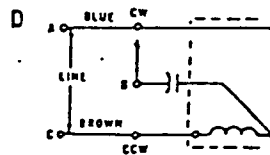
SPEED REDUC. RATIO*	TORQUE max. cont. limit (oz. in.)	TORQUE MULTIPLIER	OUTPUT SPEED					MIN. MOTOR SPEED @ RATED LOAD			DIM. "L" max.
			with hysteresis synchronous drive motors					with induction drive motors			
			24,000 rpm input	12,000 rpm input	8,000 rpm input	3,600 rpm input	1,200 rpm input	21,000 rpm input	10,000 rpm input	6,000 rpm input	
3.82:1	1.0	3.1	6282.272	3141.136	2104.561	942.408	314.113	5497	2617	1571	2.31
5.77:1	1.5	4.6	4159.445	2079.722	1393.413	623.916	207.972	3639	1733	1040	2.31
14.58:1	3.0	10.5	1646.090	823.045	551.440	246.913	82.304	1440	686	411	2.55
22.03:1	4.5	15.8	1089.423	544.711	364.956	163.413	54.471	953	454	272	2.55
33.28:1	7.0	24	721.153	360.576	241.585	108.173	36.057	631	300	180	2.55
55.66:1	10.0	34	431.189	215.594	144.447	64.678	21.559	377	179	108	2.72
84.11:1	14.0	51	285.340	142.670	95.588	42.801	14.267	250	118	71	2.72
127.10:1	21.0	77	188.827	94.413	63.256	28.324	9.441	165	78	47	2.72
192:1	30.0	117	125.000	62.500	41.875	18.750	6.250	109	52	31	2.72
321:1	45.0	166	74.766	37.383	25.046	11.214	3.738	65	31	18	2.89
485:1	70.0	250	49.484	24.742	16.577	7.422	2.474	43	21	12	2.89
733:1	100.0	382	32.742	16.371	10.968	4.911	1.637	28	14	8.1	2.89
1108:1	150.0	580	21.661	10.830	7.256	3.249	1.083	19	9.0	5.4	2.89
1853:1	200.0	817	12.951	6.475	4.338	1.942	0.647	11	5.4	3.2	3.06
2799:1	300.0	1,230	8.574	4.287	2.872	1.286	0.428	7.5	3.6	2.1	3.06
4230:1	300.0	1,860	5.673	2.836	1.900	0.851	0.283	4.9	2.4	1.4	3.06
6391:1	300.0	2,710	3.755	1.877	1.257	0.563	0.187	3.3	1.5	.93	3.06
10,689:1	300.0	3,950	2.245	1.122	0.751	0.336	0.112	1.9	.93	.56	3.22
16,150:1	300.0	6,000	1.486	0.743	0.498	0.223	0.074	1.3	.62	.37	3.22
24,403:1	300.0	9,000	0.983	0.491	0.329	0.147	0.049	.86	.41	.24	3.22
36,873:1	300.0	13,600	0.650	0.325	0.217	0.097	0.032	.57	.27	.16	3.22

Basic Motor Performance

Hysteresis Synchronous

VOLT-AGE	FRE-QUENCY (Hz.)	P P O H M A T I C L A S S E S E	SCHE- M A T I C	LEAD COLOR			PHASING CAPACITOR (mfd.) (wvac)	MOTOR SYNC. SPEED (rpm)	NORMAL MIN. RATED PULL UP TORQUE (oz. in.)	MIN. TORQUE (oz. in.)	MAX. POWER (watts)		STANDARD GEARMOTOR PART NUMBER PREFIX*
				B	C	VAR.					NO LOAD	NORMAL RATED LOAD	
27	400	2 1 A	A	BLK	1.25	100	24,000	.16	.16	11	11	59A1002	
27	400	2 3 B	B	BLK	Not req'd		24,000	.13	.13	11	11	59A1004	
27	400	4 1 A	A	GRN	1.5	100	12,000	.16	.16	12	12	59A1006	
27	400	4 3 B	B	GRN	Not req'd		12,000	.20	.20	11	11	59A1008	
115	400	2 1 A	A	BLK	0.068	300	24,000	.16	.16	11	11	59A1012	
115	400	2 3 B	B	BLK	Not req'd		24,000	.13	.13	11	11	59A1014	
115	400	4 1 A	A	GRN	0.068	300	12,000	.16	.16	12	12	59A1016	
115	400	4 3 B	B	GRN	Not req'd		12,000	.20	.20	11	11	59A1018	
115	400	6 1 C	C	BLK GRN	0.22	300	8,000	.10	.10	15	15	59A109	
200	400	2 3 B	B	BLK	Not req'd		24,000	.13	.13	11	11	59A1022	
200	400	4 3 B	B	GRN	Not req'd		12,000	.20	.20	11	11	59A1024	
115	60	2 1 D	D	BRN	2.00	200	3,600	.07	.07	8	8	59A113	
115	60	6 1 D	D	BLK	2.50	200	1,200	.05	.05	9	9	59A112	


Schematic Wiring

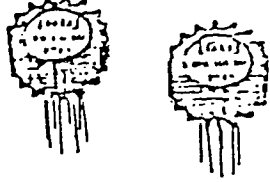


SINGLE PHASE ONLY. CAPAC. TOP A AND B FOR CW ROTATION VIEWED FROM SHAFT END. B TO C FOR CCW ROTATION

APPENDIX E. SPECIFICATIONS OF LOW-NOISE OPERATIONAL
AMPLIFIER

BURR-BROWN®





**OPA101
OPA102**

**Low Noise - Wideband
PRECISION JFET INPUT OPERATIONAL
AMPLIFIER**

FEATURES

- GUARANTEED NOISE SPECTRAL DENSITY - 100% Tested
- LOW VOLTAGE NOISE - $8\text{nV}/\sqrt{\text{Hz}}$ max at 10kHz
- LOW VOLTAGE DRIFT - $5\mu\text{V}/^\circ\text{C}$ max (B grade)
- LOW OFFSET VOLTAGE - $250\mu\text{V}$ max (B grade)
- LOW BIAS CURRENTS - 10pA max at 25°C Ambient (B Grade)
- HIGH SPEED - $10\text{V}/\mu\text{sec}$ min (OPA102)
- GAIN BANDWIDTH PRODUCT - 40MHz (OPA102)

APPLICATIONS

- LOW NOISE SIGNAL CONDITIONING
- LIGHT MEASUREMENTS
- RADIATION MEASUREMENTS
- PIN DIODE APPLICATIONS
- DENSITOMETERS
- PHOTODIODE/PHOTOMULTIPLIER CIRCUITS
- LOW NOISE DATA ACQUISITION

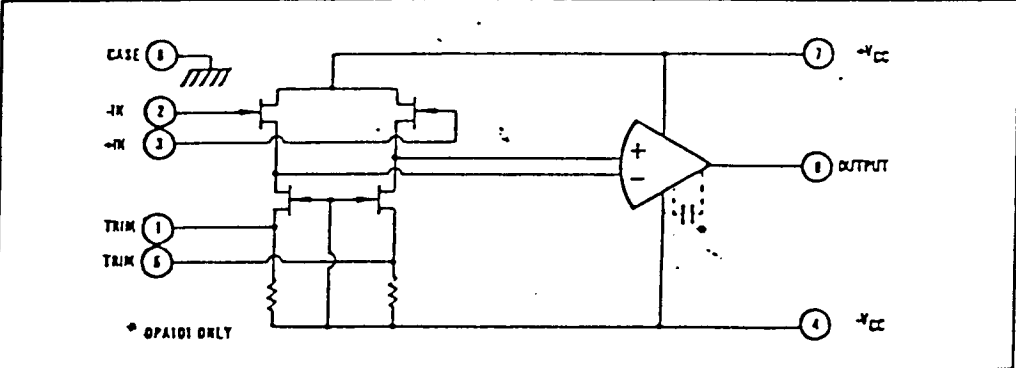
DESCRIPTION

The OPA101 and OPA102 are the first FET operational amplifiers available with noise characteristics (voltage spectral density) guaranteed and 100% tested.

The amplifiers have a complementary set of specifications permitting low errors in signal conditioning applications: low noise, low bias current, high open-loop gain, high common-mode rejection, low offset voltage, low offset voltage drift, etc.

In addition, the amplifiers have moderately high speed. The OPA101 is compensated for unity gain stability and has a slew rate of $5\text{V}/\mu\text{sec}$, min. The OPA102 is compensated for gains of $3\text{V}/\text{V}$ and above and has a slew rate of $10\text{V}/\mu\text{sec}$, min.

Each unit is laser-trimmed for low offset voltage and low offset voltage drift versus temperature. Bias currents are specified with the units fully warmed up at $+25^\circ\text{C}$ ambient temperature.



* OPA101 ONLY

International Airport Industrial Park - P.O. Box 11400 - Tucson, Arizona 85734 - Tel. (602) 746-1111 - Tlx: 910 952-1111 - Cable BBRCDRP - Telex 66-6491

ORIGINAL PAGE IS
OF POOR QUALITY

SPECIFICATIONS

ELECTRICAL

Specifications at $T_A = +25^\circ\text{C}$ and $\pm V_{CC} = \pm 15\text{VDC}$ unless otherwise noted

MODEL	PARAMETER	CONDITION	OPA101/102AM			OPA101/102BM			UNITS
			MIN	TYP	MAX	MIN	TYP	MAX	
INPUT NOISE									
Voltage Noise Density		$f_b = 1\text{Hz}^{(1)}$		100	200		80	100	$\text{nV}/\sqrt{\text{Hz}}$
		$f_b = 10\text{Hz}$		32	60		25	30	$\text{nV}/\sqrt{\text{Hz}}$
		$f_b = 100\text{Hz}$		14	30		11	15	$\text{nV}/\sqrt{\text{Hz}}$
		$f_b = 1\text{kHz}$		9	15		8	12	$\text{nV}/\sqrt{\text{Hz}}$
		$f_b = 10\text{kHz}$		7	8		8	8	$\text{nV}/\sqrt{\text{Hz}}$
		$f_b = 100\text{kHz}$		6.5	8		6.5	8	$\text{nV}/\sqrt{\text{Hz}}$
f_c : 1/f Corner Frequency			125			100		Hz	
Voltage Noise		$f_b = 0.1\text{Hz}$ to $10\text{Hz}^{(1)}$		1.3	2.6		1.0	1.3	μV , p-p
		$f_b = 10\text{Hz}$ to 10kHz		1.0	1.2		0.8	1.0	μV , rms
		$f_b = 10\text{Hz}$ to 100kHz		2.1	2.6		2.1	2.6	μV , rms
Current Noise Density		$f_b = 0.1\text{Hz}$ thru 10kHz		2.0			1.4		$\text{fA}/\sqrt{\text{Hz}}$
		Current Noise		38			26		fA , p-p
		$f_b = 10\text{Hz}$ to 10kHz		200			140		fA , rms
DYNAMIC RESPONSE									
Bandwidth, Unity Gain	Small Signal	OPA101		10					MHz
		OPA102		Note 2					
Gain-Bandwidth Product	$A_{CL} = 100$	OPA101		20					MHz
		OPA102		40					MHz
Full Power Bandwidth	$V_o = 20\text{V}$, p-p; $R_L = 1\text{k}\Omega$	OPA101	80	100					kHz
		OPA102	160	210					kHz
Slew Rate	$V_o = \pm 10\text{V}$; $R_L = 1\text{k}\Omega$	OPA101		5					$\text{V}/\mu\text{s}$
		OPA102		10					$\text{V}/\mu\text{s}$
Settling Time (OPA101)	$V_o = \pm 5\text{V}$; $A_{CL} = -1$; $R_L = 1\text{k}\Omega$	$e = 1\%$		2					μs
		$e = 0.1\%$		2.5					μs
		$e = 0.01\%$		10					μs
Settling Time (OPA102)	$V_o = \pm 5\text{V}$; $A_{CL} = -3$; $R_L = 1\text{k}\Omega$	$e = 1\%$		1					μs
		$e = 0.1\%$		1.5					μs
		$e = 0.01\%$		8					μs
Small-Signal Overshoot	$R_L = 1\text{k}\Omega$; $C_L = 100\text{pF}$	OPA101		15					%
		OPA102		20					%
Rise Time	10% to 90%, Small Signal	OPA101		40					ns
		OPA102		30					ns
Phase Margin	$R_L = 1\text{k}\Omega$	OPA101		60					Degrees
		OPA102		45					Degrees
Overload Recovery ⁽²⁾	$A_{CL} = -1$, 50% overdrive	OPA101		1					μs
		OPA102		0.8					μs
OPEN-LOOP GAIN, DC									
Full Load	$V_o = \pm 10\text{V}$; $R_L = 1\text{k}\Omega$		94	105					dB
No Load	$V_o = \pm 10\text{V}$; $R_L \geq 10\text{k}\Omega$		96	106					dB
RATED OUTPUT									
Voltage	$I_b = \pm 12\text{mA}$		± 12	± 13					V
Current	$V_o = \pm 12\text{V}$		± 12	± 30					mA
Output Resistance	Open-Loop, $f = \text{DC}$			500					Ω
Short-Circuit Current				± 45					mA
Capacitive Load Range	Phase Margin $\geq 25^\circ$	OPA101		500					pF
		OPA102		300					pF
INPUT OFFSET VOLTAGE									
Initial Offset	$T_A = +25^\circ\text{C}$		± 100	± 500		± 50	± 250		μV
vs Temperature	$-25^\circ\text{C} \leq T_A \leq +85^\circ\text{C}$		± 6	± 10		± 3	± 5		$\mu\text{V}/^\circ\text{C}$
vs Supply Voltage	$\pm 5\text{VDC} \leq V_{CC} \leq \pm 20\text{VDC}$		± 10	± 50					$\mu\text{V}/\text{V}$
vs Time			± 10						$\mu\text{V}/\text{mo.}$
Adjustment Range	Circuit in "Connection Diagram"		± 1						mV
INPUT BIAS CURRENT									
Initial Bias	$T_A = +25^\circ\text{C}$		-12	-15		-5	-10		pA
vs Temperature			Note 4						
vs Supply Voltage			Note 5						

ELECTRICAL (CONT)

MODEL	PARAMETER	CONDITION	OPA101/102AM			OPA101/102PM			UNITS
			MIN	TYP	MAX	MIN	TYP	MAX	
INPUT DIFFERENCE CURRENT									
Initial Difference vs Temperature vs Supply Voltage		$T_A = +25^\circ\text{C}$		± 3 Note 4	± 6		± 1.5	± 4	pA
INPUT IMPEDANCE									
Differential Resistance				10^{12}					Ω
Capacitance				1					pF
Common-mode Resistance				10^{12}					Ω
Capacitance				3					pF
INPUT VOLTAGE RANGE									
Common-mode Voltage Range		Linear Operation		$\pm 1 V_{CC} - 3$					V
Common-mode Rejection		$I_b = \text{DC}, V_{CM} = \pm 10\text{V}$	80	105					dB
POWER SUPPLY									
Rated Voltage				± 15					VDC
Voltage Range		Derated Performance	± 5	5.8	± 20				VDC
Current, Quiescent				5.8	8				mA
TEMPERATURE RANGE									
Specification			-25		+65				$^\circ\text{C}$
Operating		Derated Performance	-55		+125				$^\circ\text{C}$
Storage			-65		+150				$^\circ\text{C}$

NOTES: *Specifications same as for OPA101/102AM.

- Parameter is untested and is not guaranteed. This specification is established to a 90% confidence level.
- Minimum stable gain for the OPA102 is 3V/V.

- Time required for output to return from saturation to linear operation following the removal of an input overdrive signal
- Doubles approximately every 8.5 $^\circ\text{C}$.
- See Typical Performance Curves.

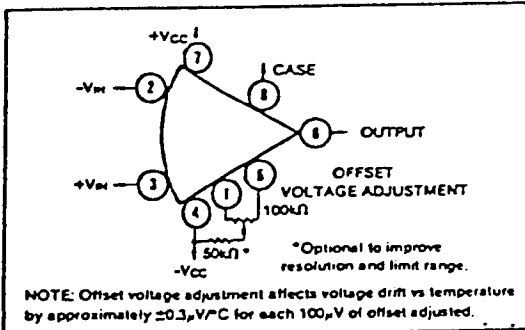
ABSOLUTE MAXIMUM RATINGS

Supply	$\pm 20\text{VDC}$
Internal Power Dissipation(1)	750mW
Differential Input Voltage(2)	$\pm 20\text{VDC}$
Input Voltage, Either Input(2)	$\pm 20\text{VDC}$
Storage Temperature Range	-65°C to $+50^\circ\text{C}$
Operating Temperature Range	-65°C to $+125^\circ\text{C}$
Lead Temperature (soldering, 10 seconds)	$+300^\circ\text{C}$
Output Short-Circuit Duration(3)	80 seconds
Junction Temperature	$+175^\circ\text{C}$

NOTES:

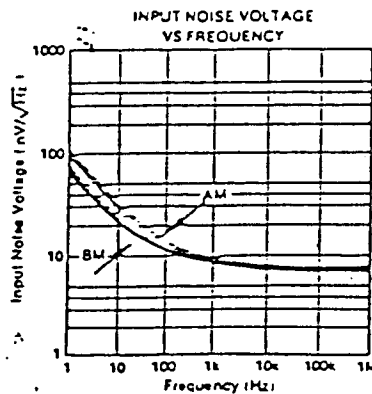
- Package must be derated according to the details in the Application Information section.
- For supply voltages less than $\pm 20\text{VDC}$, the absolute maximum input is equal to the supply voltage.
- Short-circuit may be to ground only. See discussion of Thermal Model in the Application Information section.

CONNECTION DIAGRAM

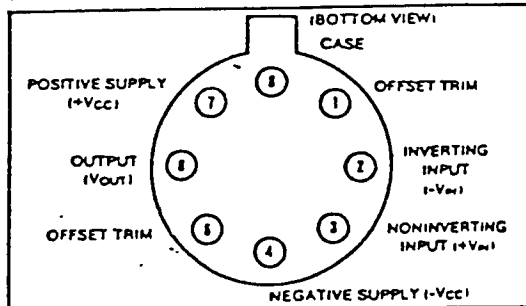


TYPICAL PERFORMANCE CURVE

$T_A = +25^\circ\text{C}, \pm V_{CC} = \pm 15\text{VDC}$, unless otherwise noted. Performance



PIN CONFIGURATION



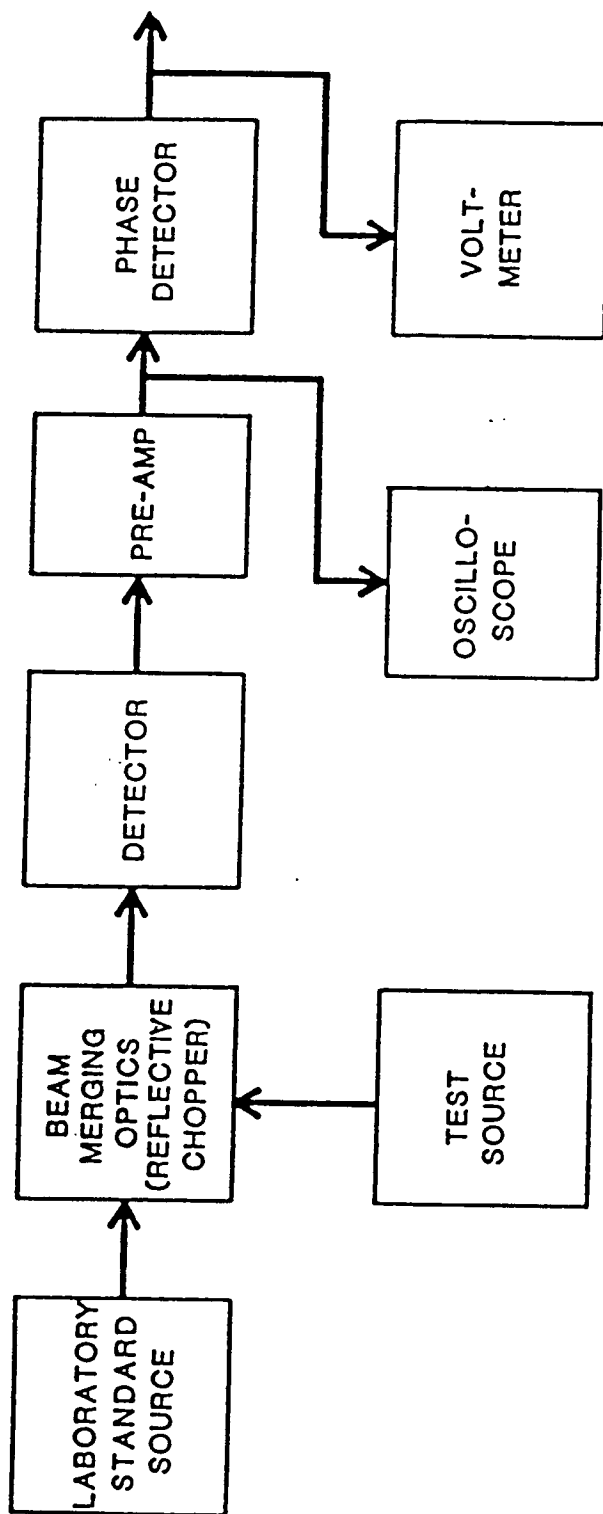


Figure 1.: Functional Block Diagram of Comparator Radiometer

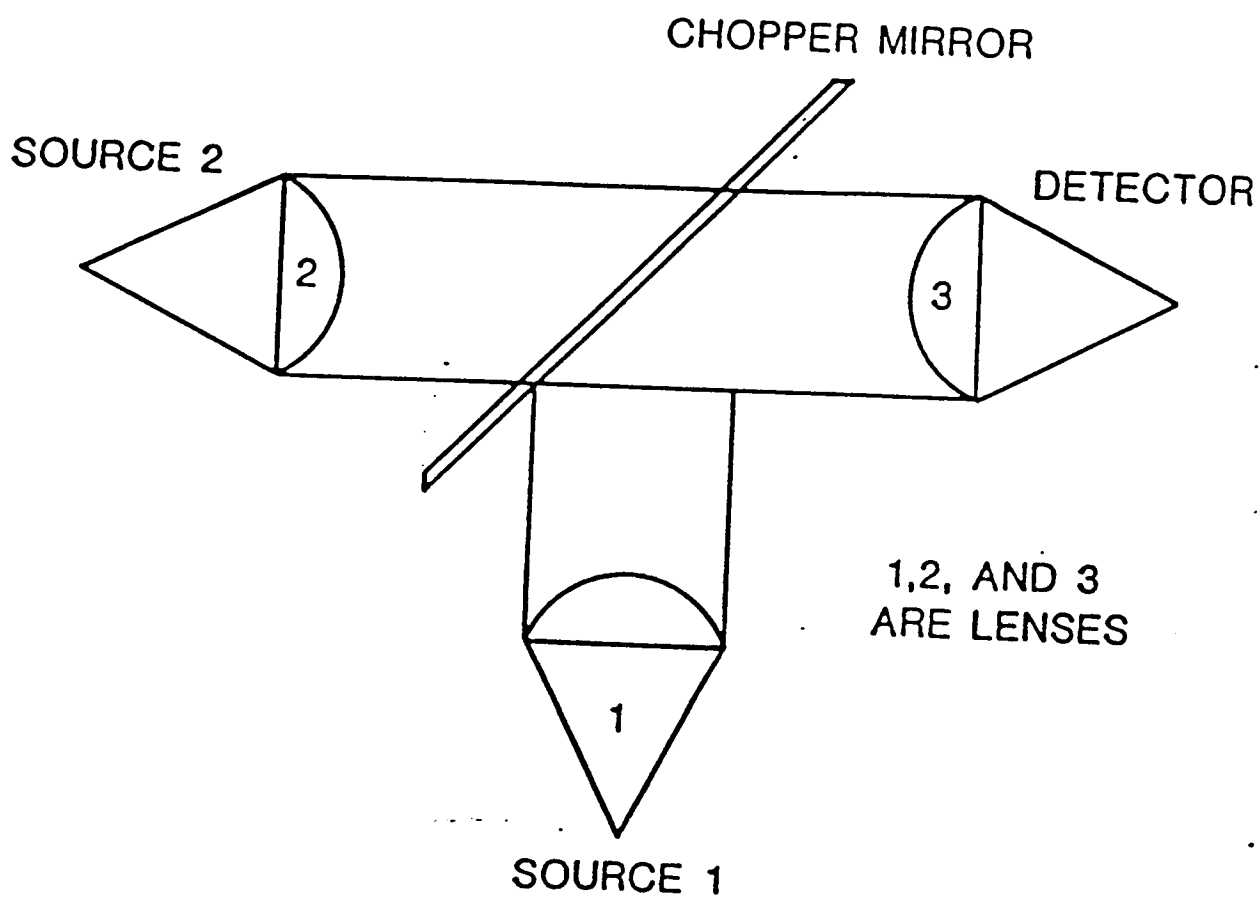


Figure 2. Optical Layout

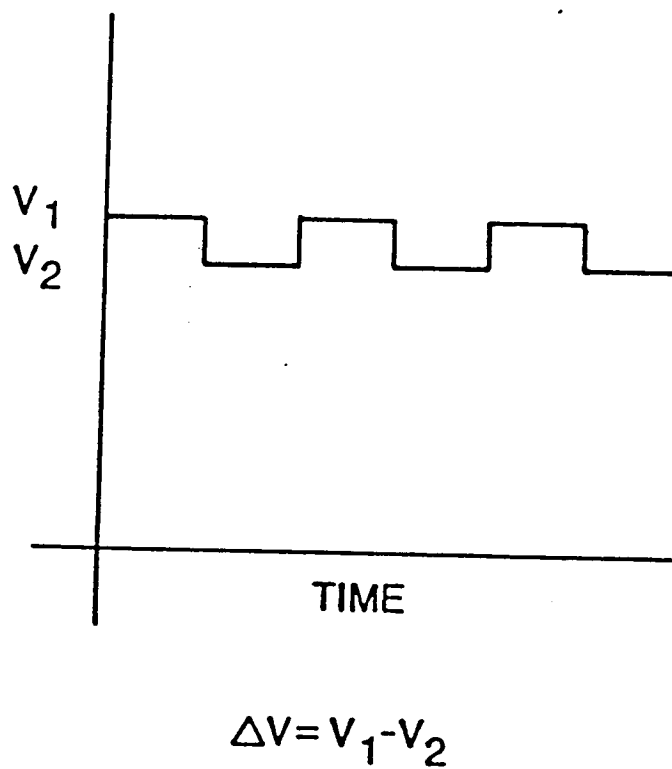


Figure 3. Waveform at the Output of Detector

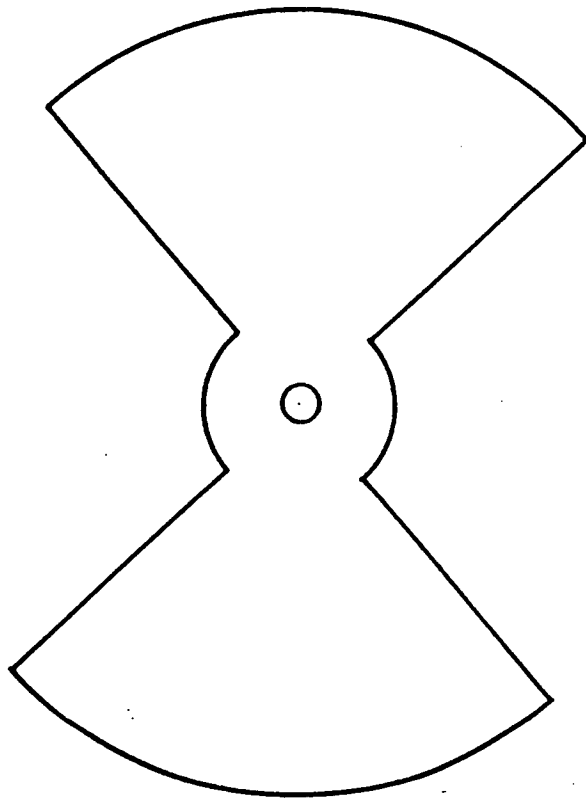


Figure 4. Chopper Mirror

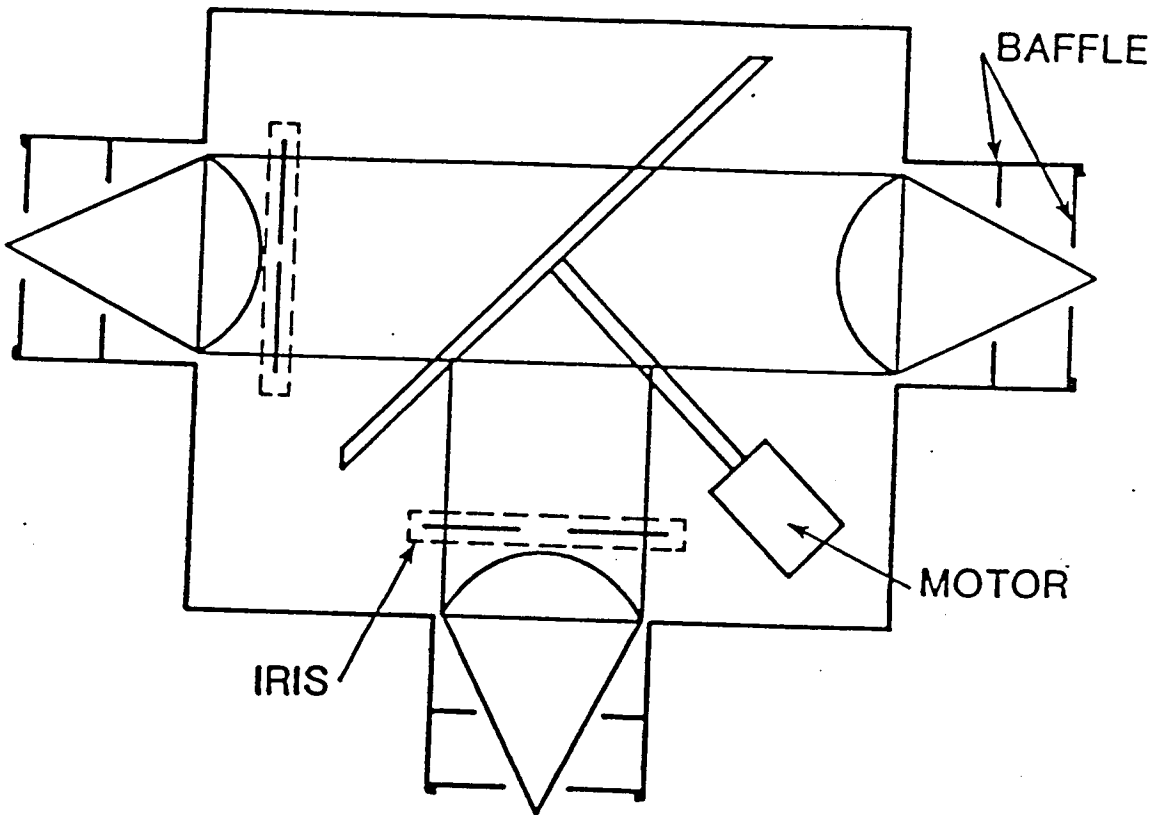
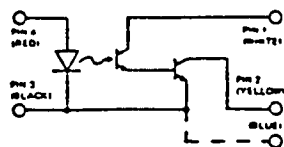
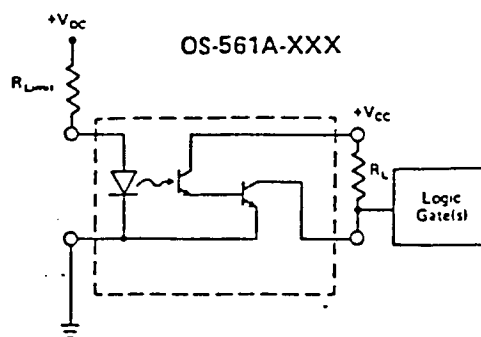


Figure 5. Optics Box



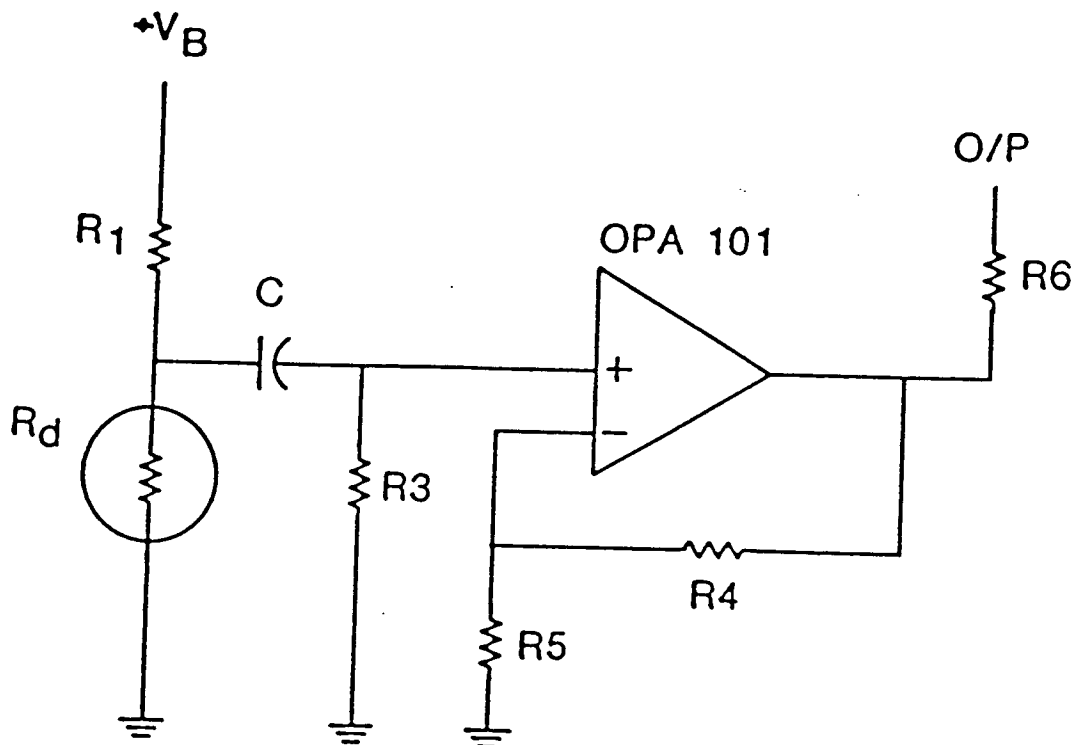
OS-561A-XXX

**Notes:**

1. Derate 1.2%/°C above 25°C ambient.
2. Switching speeds are based on pulsing the LED at 100 HZ with 25% duty cycle, $V_{CC} = 5V$. For OS-521 and OS-581, $R_L = 100$ ohms and the LED current is adjusted for an output of 4.0 mA. For OS-561A and OS-591S, $R_L = 1$ K ohms and the LED current is adjusted for an output current of 4.8 mA. ($V_{CE} (sat.) = .2V$ typical).
3. Rise time is defined as the time necessary for the collector current to rise from 10% to 90% of the peak value. Fall time is just the opposite decreasing from 90% to 10% of peak value.
4. Frequency is based on continuously pulsing the LED.

HEI inc.

Figure 6. Circuit Description of U-Type Photo Device



R_d = Resistance of Detector = 186 K Ω

R_1 = 180 K Ω

R_3 = 100 K Ω

R_4 = 10 K Ω

R_5 = 1 K Ω

R_6 = 47 Ω

Figure 7. Circuit Diagram of Pre-Amplifier

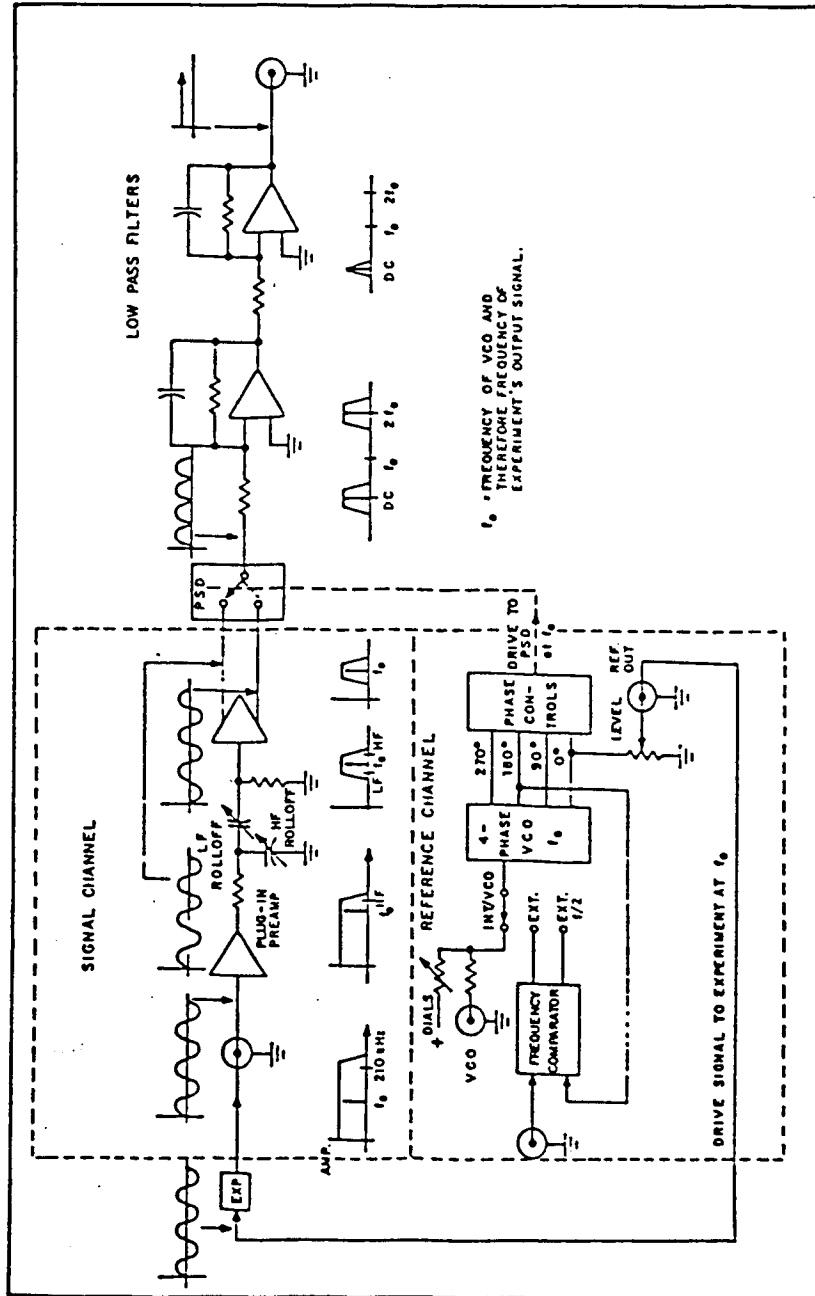


Figure 8. Block Diagram of Phase-Lock Amplifier

VITA

Hasan Niaz

Candidate for the Degree of
Master of Science

Thesis: Blackbody Source Evaluation Utilizing a Comparator Radiometer

Major Field: Electrical Engineering

Biographical Information:

Personal Data: [REDACTED]
[REDACTED] Son of S. Niaz Ahmad and Mobina [REDACTED];
single.

Education: Received the Bachelor of Science degree from Habib College of Tech (University of Sind), Pakistan, with major in Industrial Technology in 1977; 1982 completed the requirements for the Bachelor of Science degree at NED University of Engineering and Technology, Karachi, Pakistan, with a major in Electrical Engineering; 1984 completed the requirements for the Master of Science degree at Utah State University, Logan, Utah, with a major in Electrical Engineering.

Professional Experience: 3/82-8/82, Technical Executive State Petroleum Refining and Petrochemical Corp. (PETROMAN), Karachi, Pakistan; 8/82-12/82, Lecturer in Electrical Engineering Department NED University of Engineering and Technology, Karachi, Pakistan; 1/83-6/83, teaching assistant at Utah State University, Dept. of Electrical Engineering; 8/83-6/84, Research Assistant, Space Dynamics Laboratories, Utah State University, Logan, Utah.

APPENDIX E
Absolute Radiometer
Calibration Report

This page intentionally left blank.

Introduction

This appendix is a complete stand-alone calibration report. The intent is to provide the users with all of the raw data that entered into the data analysis so that they can duplicate the analysis we provide, or make their own analysis if preferred.

The Absolute Radiometer (AR) calibration proceeded as follows:

A preliminary calibration test was conducted on the USU Extended-area source on 25 March 1985. The results of this test verified that bolometer detector response and noise are of the correct order of magnitude.

The first calibration test was conducted on the USU Cold Collimator on 3 May 1985. In this test a small cold pin-hole (0.007 inch diameter) was mounted in the AR aperture to prevent overloading from the collimator background (10°K to 20°K) (See Figures H-5, H-6, and H-7). The noise was measured and found to be excessive. The field-of-view was mapped and appeared to be greatly influenced by the cold pin-hole. An attempt was made to measure the bolometer linearity using the precision aperture method.

The AR was again calibrated on the USU Cold Collimator on 10 May 1985. This time the AR aperture was wide open and the response was reduced by using a very low detector bias. The phase of the chopped signal varied as the image of a point source (used to map the field-of-view) was moved normal to the chopper blades. The phase was adjusted with the source centered and the field-of-view was mapped a second time.

The AR was calibrated on the USU Extended-area Source on 16 May 1985. A cold pin-hole (0.3579-inch diameter) was mounted in the AR aperture to reduce its sensitivity. The chopper phase was optimized for the extended-area source and good data were obtained as a function of source temperature.

The AR was calibrated on the USU Cold Collimator one more time on 21 May 1985. The 0.3579-inch cold pin-hole was mounted

in the AR aperture to reduce its sensitivity. Additional field-of-view data were obtained and the AR response as a function of source temperature obtained.

Appendix H gives some details of the special test Dewar, the USU Cold Collimator, the location of the cold pinholes, and the necessary interface fixtures.

The design and calibration of the AR are based upon the following assumptions:

- 1.) The sterance [radiance] of the DEC beam is uniform
- 2.) The calibration should be independent of the DEC geometry

DEC geometrical independence is achieved in the diffuse source mode, by making the AR collector both the limiting aperture and field stop in the system. In this mode, the calibration is related to the DEC in terms of the beam sterance [radiance] $W\text{ cm}^{-2}\text{ sr}^{-1}$. For these conditions to occur the DEC beam must overfill both the AR collector (9-inches vs. 4-inches) and the field-of-view (2.55° vs. 1.08°).

The full angle divergence of the DEC beam is given by

$$\theta_{\text{DEC}} = \tan^{-1} \left(\frac{0.75}{16.831} \right) = 2.55^\circ$$

where 0.75 inches is the mode select wheel aperture diameter for the DSM, and 16.831 inches is the collimator mirror focal length.

The full angle divergence of the AR field-of-view is given by

$$\theta_{\text{AR}} = \tan^{-1} \left(\frac{6}{25.4 \times 12.5} \right) = 1.08^\circ$$

where 6 mm is the diameter of the AR bolometer entrance aperture (cone mouth) and the AR main mirror (spherical collector) focal length (in mm) is 25.4 x 12.5 (See Figure 23 in main text).

For the diffuse source mode, the AR essentially measures the average DEC beam sterance [radiance] over the central 4 inches of the beam. The DEC beam power incident upon a DIRBE detector is given by the product of the beam sterance and the DIRBE detector throughput -- provided the DEC beam is uniform.

Corrections for a nonuniform DEC beam are obtained by taking ratios of averages calculated over that portion of the beam sampled by the AR to that portion sampled by DIRBE.

In the point source mode, the AR collector is still the limiting aperture stop in the system, but is not being overfilled by the DEC field-of-view. Therefore, in this case, the calibration of the AR is related to the DEC in terms of areance [irradiance] $W\text{ cm}^{-2}$.

The full angle divergence of DEC in the point source mode is given by

$$\theta_{PS} = \tan^{-1} \left(\frac{0.017}{16.831} \right) = 0.0579^\circ$$

as compared to the AR field-of-view of 1.08° .

For the point source mode, the AR essentially measures the average DEC beam areance [irradiance] over the central 4-inches of the beam. The beam power incident upon a DIRBE detector is given by the product of the beam areance and the DIRBE aperture area, provided the DEC beam is uniform. Corrections for a nonuniform DEC beam proceed along the same lines as given above.

Thus, the primary outcome of the AR calibration is a set of equations, one equation for the beam sterance [radiance] to be used in the diffuse source mode, and one equation for the beam areance [irradiance] to be used in the point source mode. In addition, the calibration uncertainties are provided.

Gain Normalized Response

A block diagram of the electronics system is given in Figure E-1. A battery powered preamplifier, mounted on the test dewar has a gain of 100. This preamplifier serves to boost the low level bolometer signal above the noise generated by the long cable that runs to the CMU. The bandpass amplifier has a gain of 10 and an electrical noise bandwidth of 1 Hz, the coherent rectifier has a peak to average signal conversion of about 1/3, and the dc preamplifier has a gain of 2 for the low gain output.

The signal conditioning electronics contain 4 linear outputs that have an approximate gain difference of 10 in order to extend the system dynamic range. Each channel is converted with a 12-bit analog to digital converter (A/D) over the range of ± 10 V. The control and monitor unit (CMU) automatically refers the detector output to the low gain output. The output voltage reported by the CMU is given by

$$V = [(S_i - 2047.5)/2047.5] \times A_i \quad (E-1)$$

where S_i = the i th A/D output (0 to 4095)

$$A_1 = 10$$

$$A_2 = 1.01704$$

$$A_3 = 0.10304$$

$$A_4 = 0.0099095$$

The reported output voltage ranges from the noise level to a maximum of 10 V. Thus, the bolometer signals experience a minimum gain of

$$G_{min} = 100 \times 10 \times 2/3 = 667$$

Detector Response vs. Detector Temperature

During the extended-area source test of 16 May 1985, we measured the steady source response as the bolometer warmed. These data consist of the bolometer dc vs. the bolometer output in response to the extended-area source.

The bolometer dc was obtained as the difference between the bolometer FET output with and without bias. Using the CMU nomenclature, the bolometer dc is given by

$$V_{dc} = \text{ARBODC} \Big|_{\text{bias on}} - \text{ARBODC} \Big|_{\text{bias off}}$$

where ARBODC is the AR Bolometer DC.

The data are illustrated in Figure E-2, where the data points are plotted with least-squares best fit superimposed. The computer report is given in Table E-1, where it is given that the rms error is 0.17 percent for equally weighted points.

The data given in Table E-1 and illustrated in Figure E-2 are modeled as

$$\text{Output (V)} = -0.1175 + 2.569 \times V_{dc} \quad (\text{E-2})$$

It is necessary to establish a "norm" operating condition to which all measurements can be corrected when the bolometer dc (which is directly related to bolometer operating temperature) differs from the norm. We have arbitrarily chosen a bolometer norm of

$$V_{dc} = 0.30 \text{ volts ("norm")}$$

for which the solution of Eq. (E-2) yields

$$\text{Output (V)} = 0.6532$$

Thus, the CMU output voltage, corrected for bolometer V_{dc} is given by

$$V_e = V \times 0.6532 / [-0.1175 + 2.569 \times V_{dc}] \quad (\text{E-3})$$

where V is the output reported by the CMU.

(NOTE: As indicated below, a bolometer $V_{dc} = 0.30$ corresponds to a bolometer operating temperature of 1.557°K .)

All data obtained and utilized in the calibration of the AR were gain normalized using Eq. (E-1) (automatically by the CMU software) and by Eq. (E-3) to correct for temperature variations.

Bolometer Temperature vs. Bolometer DC

There is a temperature sensor mounted near but not on the bolometer. It is of interest to know if the bolometer V_{dc} and the bolometer temperature are highly correlated. Figure E-3 gives the data set of bolometer V_{dc} vs. bolometer temperature with a least squares best fit superimposed. Table E-2 gives the computer report for which the bolometer temperature T_{bol} is given as

$$T_{bol} = 2.535 - 4.835 \times V_{dc} + 5.252 \times V_{dc}^2 \quad (E-4)$$

where V_{dc} is defined above, and where the rms error (best fit) is given as 0.24% for equally weighted points, thus the bolometer V_{dc} is highly correlated with its measured temperature.

The data plotted in Figure E-3 were obtained as the AR was allowed to warm up over a range of 1.547° to 2.008°K. Normal operating temperature for the bolometer was 1.547° ($V_{dc} = 0.305$). Thus, corrections for bolometer V_{dc} were very small. It is important to use this correction, Eq. (E-3), since the operating temperature in the DIRBE configuration might be significantly different from the "norm" selected here.

Field-of-View Calibration

The field-of-view was measured under several conditions as noted in the introduction above. The data include two attempts to map the field-of-view as a 25 x 25 matrix, and some single scans which are given as a cross-section.

The first field-of-view map was obtained with a 0.007-inch diameter cold pin-hole mounted in the AR entrance aperture to reduce the background loading of the collimator which was operating at a temperature of 10° to 20°K. The results are illustrated in Figures E-4 and E-5 and give an indication that the cold pin-hole is causing a diffraction effect.

The second field-of-view map was obtained with a full aperture and reduced bias. The results are illustrated in Figures E-6 and E-7. The measured solid angle field-of-view is 2.105×10^{-4} steradians; the linear half-angle for a circularly symmetrical field-of-view is therefore 0.469°. This field-of-view is very nonuniform compared with systems that do not use a Winston cone as the field stop. However, the numerical values are relatively close to the design values of 2.4×10^{-4} sr and 0.5° as given in the introduction.

We have no explanation for the hole in the center of the field-of-view. However, considering the AR blur diameter (2×10^{-4} rad or 0.1 mm dia) and the field stop size (6 mm dia) the field-of-view should be nearly ideal (flat topped and steep transition zone). The Winston cone is likely the source of the observed nonuniform response.

The final attempt to measure the field-of-view was made on 21 May 1985 with the 0.3579 inch diameter cold pin-hole mounted in the AR aperture. In this case a cross-section plot was made as illustrated in Figure E-8. Again the Winston cone and/or the pin-hole has a marked effect on the field-of-view.

The most valid measurement of the field-of-view is that given in Figures E-6, E-7, for which the solid angle is

$$2.105 \times 10^{-4} \text{ sr and } \theta = 0.469 \text{ (half angle),}$$

since these data were obtained with the full aperture--the normal operating mode for the AR. Consequently, we include below the analysis and complete data set used to derive these plots and values.

Field-Of-View Analysis and Complete Data Set

The field-of-view was measured by scanning in the x-axis direction and incrementing in the y-axis direction. Thus, the printouts included as Table E-3, give the data points beginning with $y = -0.025^\circ$ for 25 points in x, ranging from $x = -.0317^\circ$ to $x = 1.694^\circ$. Then the y-axis is incremented again followed by another set of 25 points in the x-axis direction, etc. The third column gives an average x-angle for the entire set of 25 y-axis increments; these are the values used in the graphics for the x- and y-coordinates for each point in the matrix. The column labeled "VOLTAGE" is the raw data obtained from the AR as digitized by the Tektronic data acquisition system used in this test. The "REL OUT" column is the linearized and normalized relative response which is plotted against the x- and y-coordinates. The last page of the computer printout gives the effective solid angle field-of-view Ω_{EFF} , which is obtained by the following

$$\Omega_{EFF} = \delta\Omega \sum_{i=1}^{625} R_i = 2.105 \times 10^{-4} \text{ sr}$$

where

$$\delta\Omega = \sin \delta x \sin \delta y$$

is the incremental solid angle (which is uniform over the matrix), and R_i is the relative response (the last column in Table E-3).

The solid angle Ω_{EFF} is also given in terms of the ideal-equivalent area half-angle θ in degrees by

$$\Omega_{EFF} = \pi \sin^2 \theta$$

solving for θ , we have

$$\theta = \sin^{-1} \sqrt{\Omega_{EFF} / \pi} = 0.469^\circ$$

Linearity Calibration

An attempt was made to evaluate the AR linearity with the USU Cold Collimator during the 3 May calibration. Two data sets were obtained for the collimator apertures using 2 temperature settings to increase the total dynamic range. The values of the temperatures utilized in this test do not enter into the data analysis as given below.

The 0.007-inch aperture was used on the AR during this test. The linearity was measured using the cold collimator precision aperture set. It is important that the image of the collimator aperture not overfill the AR field-of-view.

The largest aperture used in the linearity test has a diameter of 0.4° . Examination of Figures E-4 and E-5 (the field-of-view obtained with the 0.007 inch aperture) shows that the response is down to about 0.707 (1st contour) for a full-angle of about 0.5° . Thus, some "apparent" nonlinearity might be evident for the larger apertures in this data.

We experienced a noise problem in this test, resulting from inadequate magnetic shielding of the chopper, that corrupted the low-level data.

One reason for obtaining two linearity data sets (in addition to extending the dynamic range) is to examine the dependence of nonlinearities upon both aperture size and signal level. The data illustrated in Figure E-9 clearly show that the nonlinearity is a function of absolute output signal, but not of aperture area. Thus, we can conclude that there exists real nonlinearity in the AR response that is not caused by field-of-view nonuniformity. The nonlinearities exist only for absolute output voltages greater than about 1.0 to 2.0 volts (this corresponds to bolometer-preamplifier outputs of $1/667 = 0.0015$ volts). The cause of this nonlinearity is not known.

Extended-area Calibration

The extended-area calibration of the DEC Absolute Radiometer was accomplished utilizing the USU low temperature extended-area source. This source consists of a temperature controlled, blackened, honeycombed surface as illustrated in Appendix H.

The extended-source calibration consisted of measuring the AR response during a series of tests in which the source temperature was varied from very low levels to sensor saturation. Data were obtained using the DEC CMU in order to include that unit in the calibration. The data accumulated were later sorted and corrected for bolometer dc as noted.

AR filters 9 and 10 were not available at the time the AR extended-area calibrations were accomplished; consequently, filter position #9 contained an opaque blank, and position #10 was left open. The AR filters are identical to the 10 DIRBE filters. Filter data are given in Appendix A in the form of tabulations and graphic representations. The filter data includes spectral transmittance for out-of-band wavelengths.

Data were not obtained for bands 1 - 4 since the USU extended-area source could not provide sufficient output in that wavelength region to induce response from the AR.

A data analysis was performed subsequent to the tests and is reported below for the AR response using filters 5 - 8 and 10 (open). That data for filter positions 5 through 8 and 10 are given in Tables E-4 through E-8.

The Effective Sterance [Radiance]

The effective band sterance [radiance] (L_{BAND}) for a calibration test is calculated using the source temperature and the filter curves as follows:

$$L_{\text{BAND}} = \tau_p(\lambda) k \Sigma L(\lambda)_{\pm} \delta \lambda_{\pm} R(\lambda)_{\pm} \quad \text{W cm}^{-2} \text{ sr}^{-1} \quad (\text{E-5})$$

where

$$k = (0.3579/4)^2 = 8.01 \times 10^{-3} \quad (\text{E-6})$$

which is the ratio of the precision 0.3579-inch cold pinhole area to the full 4-inch AR aperture area. This is the correction factor for the cold aperture used to reduce the AR sensitivity. And where

$\tau_p(\lambda)$ is the peak filter transmittance,

$L(\lambda)$ is the sterance [radiance] obtained using Planck's equation,

$\delta\lambda_i$ is the incremental bandwidth,

$R(\lambda)$ is the filter relative transmittance,

i is the summing index,

and where the summation is carried out over the nominal bandpass as defined by $R(\lambda)$ values greater than 0.01 (see Appendix A).

The "band" sterance [radiance] is given in the 4th column of Tables E-4 through E-7 for Bands 5 through 8. The total sterance [radiance] was calculated using Eq. (E-5) for all of the filter transmittance values out to 1000 μm . The "total" sterance [radiance] is given in the 5th column of Tables E-4 through E-7 for Bands 5 through 8. In each case, the sterance [radiance] is given for a range of temperatures from 12 to 101.9°K.

The effective sterance [radiance] for the open position is calculated using the Stefan-Boltzmann law as follows:

$$L_{\text{TOTAL}} = k \times \sigma T^4 / \pi \quad \text{W cm}^{-2} \text{ sr}^{-1} \quad (\text{E-7})$$

and is given in the 4th column of Table E-8 (band 10 open) over the same range of source temperatures.

AR Voltage Response

The output voltage for each gain range was obtained using Equation (E-1) and corrected for bolometer temperature using Equation (E-3). Tabulations of source temperature, output voltage, output voltage (corrected) and flux are also given in Tables E-4 through E-8. The corrected voltages vs. total sterance [radiance] are plotted in Figures E-10 through E-14. Figure E-14 and Table E-9 provide the results of a best bit analysis of the open position extended-area source calibration.

The response is modeled as a 2nd degree equation which exhibits a full-scale nonlinearity of 39% and an rms error of 7.22%. The following sections discuss the validity of this extended-area calibration in terms of data consistency and radiometric analysis. Then the sterance [radiance] calibration equation is formulated from the best fit analysis given in Figure E-14 and reported in Table E-9.

It is to be noted that with the exception of band 10, all of the data show strong evidence of long wavelength leakage. The response is excessive for lower source temperature, which represents the case where most of the blackbody energy is shifted into the long wavelength leak region.

The curves tend to approach an asymptote at higher temperatures where more of the energy from the blackbody is shifted into the bandpass region.

It is also noteworthy that a comparison of the absolute output voltage for the highest temperature shows that all of the filters are passing most of the source energy, again illustrating the magnitude of the filter leaks.

The only data that merit detailed analysis are those obtained in the open position where the data are not corrupted by filter leaks. These are given in Table E-8, E-9, and Figure E-14.

Data Consistency

Two major questions must be addressed concerning the validity of the open position extended-area source absolute calibration: (1) Is the detector non-linear? and (2) How well does the extended-area source approximate an ideal blackbody at the indicated temperature? The answer to both of these questions is best given in terms of the "open" filter position for which the total flux is given by the T^4 law.

Figure E-14 is a plot of the measured data points vs. the total flux for filter position 10 (open) with a second degree least-squares best-fit superimposed. The computer report for

this data is given in Table E-9 which gives the full-scale nonlinearity as 39.20% and the rms error for equally weighted points as 7.22%.

A final check of nonlinearity in the AR can be made by looking at the data obtained in the 25 July 1985 cold test and the 2 September 1985 cold test, both of which are given in the body of the main report in Tables 17 and 20 respectively.

The data given in Table 17 shows an aperture position #14 (10.0 volt output) nonlinearity of 48.9%; while the data given in Table 20 shows an aperture position #14 (10.0 volt output) nonlinearity of 37.15%. In both cases this should be the sum of the integrating sphere aperture nonlinearity and that of the AR. Assuming that 11% of the observed nonlinearity is attributed to the aperture set, the AR nonlinearity should be at most between 35 and 48%, which agrees relatively well with the 39.2% reported here.

The question about the performance of the extended-source blackbody that is considered here is this: "Is the radiant temperature the same as the indicated temperature (from which the flux is calculated using Eq. (E-5))?" The best that can be done to answer this question is:

1.) This blackbody has been used numerous times to calibrate circular variable filter (CVF) spectrometers over a wavelength range of 5 - 25 μm . The results are in good agreement with other calibrations using the cold collimator and commercial cavity blackbody sources on the same sensors.

2.) The possibility of temperature gradients existing between the temperature-sensor and the radiating surface can be considered as follows: At low temperatures (of the order of 10°K) very little radiant thermal coupling exists between the source and the sensor (the AR in this case), which is operating below 10°K. One would expect the measured temperature to agree well with the radiant temperature of the surface when there exists little or no thermal coupling.

The worst case would occur when the source is near 300°K and thermal energy radiated into the sensor is of the order of watts. In this case a temperature gradient is much more likely to exist in the source. However, in numerous tests on CVF spectrometers the data fits the measured transfer function (from the linearity test) over the entire range of temperatures.

Although the maximum temperature used in this test was 100°K, the data plotted in Figure E-14 exhibits linear response up to 1 to 2 volts, as does the linearity test data of Figure E-9. The computer report that accompanies Figure E-14 is given in Table E-9. It shows a full-scale nonlinearity (10V) of 39.2%. See also the discussion of beam linearity (main body of this report) and calibration uncertainties (later in this appendix).

Another measure of internal consistency of the extended-source data plotted in Figure E-14 is the rms error of the best-fit. The data points appear well clustered on the best-fit equation and this is confirmed by an rms error of only 7.22%.

The coefficients given in Table E-9 constitute the "Sterance [radiance] Calibration Equation" as given below.

Radiometric Analysis

Confidence in the performance of the extended-area source calibration can be further increased by a radiometric analysis wherein the predicted response is compared with the measured response for the open filter position.

The detector data (see Appendix G) gives the calculated detector responsivity for unit #906 as 2.93×10^6 Volts/Watt at 1.5°K. This number can be verified as follows: Table E-9 gives the inverse sterance [radiance] responsivity as

$$C = 9.281 \times 10^{-8} \text{ (W cm}^{-2} \text{ sr}^{-1})/\text{V.}$$

The detector responsivity (V/W) is given as

$$R_{\text{DET}} = \frac{1}{C \times A \Omega \times G \times \tau_d} = 1.96 \times 10^6 \text{ V/W}$$

where the gain $G = 667$. The measured throughput of the AR is

$$A\Omega = \pi(2 \times 2.54)^2 \times \pi \sin^2 0.469 = 1.71 \times 10^{-2} \text{ cm}^2\text{-sr}$$

for a 4-inch aperture and a 0.469° half-angle field-of-view. The optical efficiency $\tau_d = 0.49$, which consists of an effective detector absorptance of 0.7 and cone transmittance of 0.7 (Reference Infrared Laboratories, Inc. private communication).

The agreement, $2.93 \times 10^6 \text{ V/W}$ specified vs. $1.96 \times 10^6 \text{ V/W}$ is not bad considering the detector specifications are based upon design rather than measurement.

Sterance [radiance] Calibration

The coefficients given in Table E-9 constitute the "Sterance [Radiance] Calibration Equation" as

$$L = 9.281 \times 10^{-9} \times V_c + 5.984 \times 10^{-9} \times V_c^2 \text{ W cm}^{-2} \text{ sr}^{-1} \quad (\text{E-9})$$

which gives the average sterance [radiance] of the DEC beam for the open filter wheel position and for the diffuse source mode. This calibration applies at all wavelengths of interest since the bolometer exhibits uniform response.

Band Sterance [Radiance] Calibration

We were originally led to believe that the bandpass filters were adequately blocked. It seemed important that the AR exhibit the same spectral response as the DIRBE. This arises from the fact that the integrating spheres exhibit spectral dependencies that may change with time because of the buildup of contaminants on the reflective surface of the spheres. Insignificant absorption spectra may become important because of the many reflections that occur before a ray finally exits from the spheres.

The measurement of the DEC (output) beam power by the AR creates no problem when the AR spectral response matches that of

the DIRBE and that was the assumption under which the system was designed. We later learned from GSFC personnel that DIRBE achieves long wavelength blocking by the use of detectors that exhibit appropriate long wavelength cutoff. The AR utilizes a bolometer (as recommended by GSFC) that has uniform response to beyond 1000 μm for all bands. We also learned that the filters are not blocked. In fact, some of the filters exhibit total integrated transmittance in the leak regions that approaches that of no filter (open position). Consequently, a very great mismatch exists between the DIRBE and AR spectral response.

In principle, it is possible to determine the band power (as defined by DIRBE) by calculating band power and total power, as is given in Tables E-4 through E-7. This requires an accurate knowledge of the filter transmittance throughout the leak regions. At this point, GSFC personnel entered into a measurement program producing the response data tabulated in Appendix A and which was used to calculate the total flux given in Tables E-4 through E-7.

Figures E-10 through E-13 are plots of the data points for filter positions 5 through 8 respectively. The construction line is plotted at 45-degrees to provide a visualization of linear response. The data points correspond to total sterance [radiance] calculated over the range of 0.5 to 1000 μm and are obtained using Eq. E-5. In each case the data seems to be asymptotic to a linear line for high temperature points where the flux is mostly in the passband. For low temperature data most of the energy is in the long wavelength leak regions and without exception the response is too large. This can be explained on the basis that the filter leak-transmittance is greater in the DEC operating at 1.5°K than when it was measured by GSFC at approximately 10°K. It is apparent that the filters in the AR cannot be used to measure the band power as defined by the DIRBE bands.

The integration utilized in Eq. (E-5) is based upon the $R(\lambda)$ values. The peak transmittance was unity in the calculations

given in the tables, but can be derived from the data as follows: The inverse slope of the asymptotes corresponds to the inverse responsivity given by the linear term in Eq. (E-9). In each case, the ratio of the inverse responsivity of the open position to that of a particular filtered band corresponds roughly to the peak filter transmittance of that band (see Appendix A): for band 6 it is 0.368, band 7 it is 0.418, and for band 8 it is 0.460.

Noise Equivalent Sterance [radiance]

The noise equivalent sterance [radiance] (1 Hz bandwidth) is obtained by substituting the measured rms noise voltage into Eq. (E-9). Figures E-15 and E-16 illustrate the noise voltage measured using the Tektronic data acquisition system connected directly to the high gain channel output. The numerical data in these figures must be referenced to the low-gain channel using the coefficient A_4 of Eq. (E-1). Figure E-15 gives the short-term noise as

$$0.137 \times 0.0099095 = 1.36 \times 10^{-3} \text{ Vrms} \quad (\text{E-10})$$

and Figure E-16 gives the long-term noise as

$$0.293 \times 0.0099095 = 2.90 \times 10^{-3} \text{ Vrms} \quad (\text{E-11})$$

for the AR.

The actual detector noise is given by the above values divided by the low-gain factor of 2000 (the coherent rectifier passes incoherent noise unchanged - thus, the factor of 3 does not apply here).

The measured noise, referred to the detector-preamplifier output is

$$1.36 \times 10^{-3} / 2 \times 10^3 = 6.8 \times 10^{-7} \text{ V(rms)} \quad \text{short term,}$$

and

$$2.90 \times 10^{-3} / 2 \times 10^3 = 1.45 \times 10^{-6} \text{ V(rms) long term.}$$

Substitution of the low gain values from Eq. (E-10) into Eq. (E-9) yields the noise equivalent sterance [radiance] [NES] as follows:

$$\text{NES} = 1.26 \times 10^{-10} \text{ W cm}^{-2} \text{ sr}^{-1} \quad (\text{E-12})$$

for the short-term, and using Eq. (E-11)

$$\text{NES} = 2.69 \times 10^{-10} \text{ W cm}^{-2} \text{ sr}^{-1} \quad (\text{E-13})$$

for the long term.

Point Source Calibration

The USU 8-inch cold collimator was used to measure the AR field-of-view and linearity as given above. In addition, on 21 May 1985, we attempted to obtain an absolute areance [irradiance] calibration. We accomplished this by varying the source temperature over the range of 326.2° to 1254.3°K in 20 steps; the output was recorded for filter positions 1 through 10 as before.

The cold collimator utilizes external blackbody simulators. The vacuum IR window is CdTe (cadmium telluride) which exhibits uniform transmittance of about 0.6 from 1 μm to beyond 27 μm . The lowest temperature used in the point source calibration is 326°K for which 90% of the energy falls below 27 μm . Thus, the window should have little effect upon the spectral properties of the source for bands 1 through 5, provided they have no long wavelength leakage. The window will essentially block the source for bands 7 and 8.

The USU cold collimator normally operates in the temperature range of 10° to 30°K. For this reason a cold pinhole was placed in the AR aperture to reduce its sensitivity to the relatively warm background environment of the collimator.

The test was not very successful; the data for band #8, for example, exhibited a continuous decrease in output as a function of time throughout the test. This is explained on the basis of (1) continual cooling of the collimator from about 25°K to about 10°K during the period of the test, and (2) the signal from the relatively high temperature source was essentially zero in that long-wave band.

The data in the short wavelength bands were also corrupted by the collimator background, although to a lesser extent.

All of the data obtained in the point-source calibration are given in Tables E-10 through E-19 for Bands 1 through 10. Band 9 is a closed position and shows how the AR dark noise varied with time and is consistent with other noise evaluations. Band 10 is the open position. The band and total sterance [radiance] were calculated as in the Extended-area Calibration section (above).

The graphic plots, given in Figure E-17 through E-26, are all based upon voltage vs. total areance [irradiance]; the collimator geometrical coefficients to convert from sterance [radiance] to areance [irradiance] were used.

The areance [irradiance] is given in terms of the source sterance [radiance] L_{bb} as follows

$$E = SL_{bb} A_s/f^2$$

where

$S = 0.6$ (window loss factor)

$A_s =$ Source aperture (6.30×10^{-4} cm²)

$f =$ Collimator focal length (63.5 cm)

These calibrations were achieved using 3 each IRI model 430 blackbody simulators which can operate over a range of 50°C to 1000°C. Initially, blackbody A was set at 326.2°K, blackbody B was set at 561.7°K, and blackbody C was set to 952.6°K. The blackbodies were allowed to stabilize and readings were taken for all three. Note that the graphic data shows three distinct sets of data. The first set is the response to Blackbody A, the second to blackbody B, and the third to blackbody C. The first data point (to the left) in each of these subsets were taken at about the same time (within several minutes of each other).

The blackbodies were then set to 376.4°K, 619.2°K, and 1011.2°K respectively, and a stabilization period of 30 to 40 minutes allowed. Following the stabilization period another set of 3 data points were taken. These 3 points are the second to left points in the three subsets. This procedure was continued until about 7 readings had been taken on each of the 3 blackbodies.

Note that as time passed, the apparent response to each of the blackbodies decreased; what we are seeing is a combination of AR response to the small-omega hot blackbody and the large-omega relatively warm collimator. With time, the collimator was cooling.

In the case of band 2 (see Figure E-18), the collimator background signal was less overwhelming and we see a general increase with blackbody temperature. The minor discontinuities are related to the collimator cooling and the time delays using 3 blackbodies.

In the case of band 8 (see Figure E-24), the collimator dominated and we see very little difference in the readings for all 3 blackbodies taken at the same time; but a general decrease in the signal with time as the collimator cooled from about 25°K to about 10°K.

It is doubtful that this data is useful for anything except perhaps some laughs and tears. It certainly illustrates some limitations to calibrating wide-band bolometer detectors with filters that have long wavelength leaks to and beyond 1000 μm .

An areance [irradiance] calibration equation can be derived however, from the extended-area source calibration and the measured field-of-view. This is often a preferred method to obtain an areance [irradiance] calibration since the absolute response to a collimator is more subject to errors than the extended-area absolute response. These errors arise from factors such as phase of the chopped signal being a function of position within the field-of-view (as discussed above). It is also difficult to determine the exact transmittance of the collimator window, reflectance of mirrors, focal length and aperture area, all terms that enter into an absolute point source calibration.

The areance [irradiance] calibration equation for the AR is given as the product of the measured field-of-view in units of steradians and the sterance [radiance] equation (Eq. E-9). Thus,

$$E = 1.95 \times 10^{-11}V + 1.26 \times 10^{-12} V^2 \quad \text{W/cm}^2 \quad (\text{E-14})$$

Equation (E-14) gives the beam areance [irradiance] for the DEC beam for the open filter wheel position and for the point source mode.

Beam Uniformity and Spectral Band Corrections

Corrections must be made for the beam nonuniformity and for the DIRBE spectral band. The corrections for beam nonuniformity are accomplished by finding a factor F_{BEAM} which is used to correct the beam power as calculated from an AR calibration. the beam flux is given as a fraction F_{BEAM} of the total flux measured by the AR, where

$$F_{\text{BEAM}} = \frac{\frac{1}{N} \sum_{i=1}^N \Phi_i \text{ (DIRBE beam)}}{\frac{1}{M} \sum_{i=1}^M \Phi_i \text{ (BSM beam)}} \quad (\text{E-15})$$

where the numerator is the average relative beam intensity over that portion of the beam sampled by DIRBE and N is the number of sample points in that set; where the denominator is the average of the relative beam intensity sampled by the beam sample mirror (BSM) (the central 4 inches), and where Φ is taken from the beam uniformity measurement data, Appendix J.

The best that can be done to determine the DIRBE data subset is to assume a concentric 19 cm diameter region in the center of the DEC beam. A similar argument applies to the beam sample mirror subset, namely, assume a concentric 4-inch diameter (10.16 cm) region centered on the DEC beam. The exact locations depend upon the machine tolerance buildup and are not known. Perhaps they can be measured at NASA.

The corrections for a specific DEC band are also made by calculating a correction factor F_{BAND} which is used to correct the beam power as calculated from an AR calibration. The band flux is given as a fraction F_{BAND} of the total flux measured by the AR, in the open filter position where

$$F_{\text{BAND}} = \frac{\int \frac{L(\lambda) R(\lambda) d\lambda}{\text{DIRBE spectral band}}}{\sigma T^4 / \pi} \quad (\text{E-16})$$

where the integration is carried out over the DIRBE spectral bandpass function $R(\lambda)$, and the denominator gives the total sterance [radiance] for the open position. We do not believe the filters installed in the DEC are useful in this calibration for 2 reasons: 1) Their response function in the leak region is not presently known. 2) Even if the response function in the leak region was known to a high degree of accuracy, the leak is so enormous that the response with the filter in place is generally within an order of magnitude of the open response (see Extended-area Source data). The only clear-cut solution to this problem is based upon the original premise that the DEC AR spectral response be matched to the DIRBE response.

The band corrections detailed above also require a knowledge of the spectral characteristics of the source and the integrating spheres. This should be straight-forward for the large-area source. This source should be an excellent blackbody simulator. However, the spectral properties of the lamps and the spheres poses more of a problem inasmuch as they have not been characterized in the spectral domain.

Calibration Uncertainties

The best that can be done is to estimate the calibration uncertainties. A certain amount of subjectivity is always associated with such estimates. The estimates can be more objective when they are based upon statistical analysis of reasonably large data sets obtained in experiments designed to measure various parameters in an independent fashion.

The sterance [radiance] calibration for total flux utilizing an extended-area source blackbody simulator (see Equation (E-9)) is the most direct and simple of calibrations: The flux is given in terms of the sterance [radiance] in units of watts per square centimeter per steradian using the Stefan-Boltzmann law. In this case the only parameters that enter into the uncertainty are the source temperature and emissivity. An exception occurs in our case in that a precision aperture was used to reduce the AR throughput.

Obtaining a relatively large data set of sensor output as a function of source temperature over the entire dynamic range of the sensor provides information on the sensor linearity and spectral purity, and by using a best-fit technique provides a measure of the sensor precision over the dynamic range for which data were obtained.

The usual approach to determine the sensor precision is to obtain a statistical sample of data for a given test and then determine the mean and standard deviation. In the case of the extended-area source calibration for the sterance [radiance], the calibration coefficients are obtained by a process of best-fit in which the mean square error is minimized. The square root of the mean square error, or standard deviation, is interpreted as giving the repeatability uncertainty over the entire dynamic range for a single measurement. Accordingly, the repeatability uncertainty (precision) in the extended-area source is (see Table E-9)

$$\sigma_p(L) = \pm 7.22\%$$

(Sterance [radiance] repeatability uncertainty)

for signals large compared to system noise.

By a spectral purity test we mean a test that essentially determines if the same responsivity is obtained when the source temperature is changed in a series of measurements. When the responsivity appears to increase at lower temperatures it may be because of a long wavelength filter leak; the blackbody is shifting most of its energy into the long wavelength leak region of the filter at lower temperatures. This is precisely what happened on bands 5 through 8, (see Figures E-10 through E-13). In the case of the open calibration, Figure 14, there is no evidence of spectral impurities.

The usual approach to measuring linearity is to change the flux using constant temperature so the data are not corrupted by possible spectral impurities. This was accomplished using the precision apertures in the integrating sphere and in the USU cold collimator: these data were relatively consistent in indicating a full-scale (10 V) nonlinearity of about 40%, as indicated above. The nonlinearity obtained in the extended-source calibration is then examined to see if it is consistent with that measured using the precision apertures. Such consistency strongly suggests that the nonlinearity observed in the extended-area source calibration is real and is not caused by spectral purity or other problems.

The source uncertainty is based primarily upon the temperature uncertainty. This is where we are forced to make some subjective evaluations. They are based upon experience with a system over a number of years and tests in which one feels that consistent results have been achieved.

Our experience is that the honeycomb blackbody simulator has an emissivity approaching unity at wavelengths up to 25 μm . Since the honeycombs are large compared with 1000 μm wavelength we expect the emissivity to be near unity uniformly up to 1000 μm or more.

Our experience with the temperature measurement is that even though we can read the temperature to $\pm 0.1^\circ\text{K}$, we think that we cannot know the temperature any better than $\pm 1.0^\circ$ including

possible gradients between the measured and radiation temperatures; thus, the sterance [radiance] uncertainty is based upon the spread in total flux (Stefan-Boltzman law) for a spread in temperature of $\pm 1.0^\circ$. But, the question arises in a test like that of Table E-8, "What temperature do you use to calculate the uncertainty?" The best case is the highest temperature which for 100°K yields $\pm 4\%$; the worst case is the lowest temperature which for 10°K yields $\pm 46\%$. We prefer to use the average temperature in the data set which is 55°K and for which the source uncertainty is

$$\sigma(s) = \pm 7.43\% \quad (\text{Source uncertainty}).$$

The coefficient k in Equation (E-6) relates to the precision aperture that was used to reduce the AR sensitivity. The uncertainties associated with the factor k must also be considered. The manufacturing tolerances will suffice for such an analysis. The entrance aperture diameter is 4 inches ± 0.010 inches, while the precision aperture diameter is 0.3579 inches ± 0.0003 inches. The worst case uncertainty in the parameter k is given by

$$\Delta k = \left(\frac{0.3579 \pm 0.0003}{4.00 \pm 0.010} \right) \times 100 \approx \pm 1\%$$

and is negligible compared to other factors given here.

The accuracy (absolute uncertainty) is given by the square root of the sum of the squares of $\sigma(e)$, Δk , and $\sigma(s)$, or

$$\sigma_a(L) = \sqrt{7.22^2 + 1.0 + 7.43^2} = \pm 10.36\%$$

(Sterance [radiance] accuracy uncertainty)

The above figures of precision and repeatability apply only to the measurement of sterance [radiance] with the filter wheel in the open position. the calibration equation yields the average sterance [radiance] over the AR spatial response region.

The areance [irradiance] calibration for total flux utilizing an extended-area source blackbody simulator is derived from the sterance [radiance] equation and the measured solid-angle field-of-view, (see Equation (E-14)). Consequently the uncertainty in the areance [irradiance] calibration must include the uncertainty in the measured field-of-view.

As indicated above, the uncertainty of a direct areance [irradiance] calibration is extremely difficult to estimate because it includes the uncertainties associated with the variation in the phase of the signal with respect to chopper position, the transmittance of the IR window in the collimator, the reflectance of the mirrors, and the uncertainties in the aperture sizes and collimator focal lengths.

The uncertainty of the field-of-view calibration should be, to a first order estimate, $1/N$ where N is the number of data points obtained in mapping the field-of-view, or $1/625$. A more conservative approach is to use $1/N'$, where N' is the number of data points in the inner core--numbers that contribute most significantly to the value of the solid angle field-of-view. In this case the uncertainty estimate is about $1/100$.

The method we prefer to estimate the uncertainty of the field-of-view for point source measurements, is to examine the nonuniformity within the inner core of the field-of-view. The inner core can be defined as the inner 80% of the nominal field-of-view design. The nonuniformity was calculated, in this case by finding the mean and standard deviation of all response points greater than 3.00 volts. The peak response was 4.985. The following is observed (See Field-of-View discussion earlier in this appendix):

Range of points included = 3.00 to 4.985 volts

Number of points in the data set . . = 111

Mean response = 3.924

Standard Deviation = 0.450

Percent error = 11.46%

Thus, the repeatability uncertainty for the field-of-view is

$$\sigma(\text{fov}) = 11.46\% \quad (\text{Field-of-view uncertainty})$$

The overall repeatability uncertainty for areance [irradiance] measurements is given by the square root of the sum of the squares of $\sigma(e)$ and $\sigma(\text{fov})$, and is

$$\sigma_P(E) = \sqrt{11.46^2 + 7.22^2} = 13.54\%$$

(Areance [irradiance] repeatability uncertainty)

The areance [irradiance] accuracy uncertainty is obtained as the square root of the sum of the squares of the repeatability $\sigma_P(E)$ and the extended-area source uncertainty $\sigma(s)$

$$\sigma_A(E) = \sqrt{13.54^2 + 7.43^2} = 15.45\%$$

(Areance [irradiance] accuracy uncertainty)

The uncertainty in the DIRBE-DEC beam is another matter. The uncertainty of the beam uniformity correction needs to be estimated as does the correction for the DIRBE spectral response.

A first order estimate of the beam correction uncertainty is given by $1/N$ where N is the number of sample points used in the measurement. That is valid only if each point adds equally to the sum obtained in finding the beam averages. A more conservative estimate is $1/N'$ where N' is the number of points that exhibit values close to the peak values in the beam since the sum depends primarily on the larger values.

An estimate of the band correction uncertainty is very difficult to make: The spectral characteristics of the large area source are probably not far from ideal--but how far? The spectral reflectance of the sphere is totally unknown, and the sphere geometrical factors are not very well known. It is our opinion that so long as the spectral response of the AR does not match the spectral response of DIRBE, no meaningful absolute calibrations of the DIRBE bands can be made. Good Luck.

TABLE E-1
 Computer Report Corresponding to the Best-Fit
 Analysis of Figure E-2

MODEL DEC-AR, 1 CHANNEL Absolute Radiometer
 SOURCE USU Extended-Area DATE: 16 May 1985

LINEARITY DATA SET (VOLTAGES ADJUSTED TO CH-LO)

BOL DC	OUTPUT(V)	BOL DC	OUTPUT(V)
0.306	6.680E-001	0.306	6.680E-001
0.286	6.170E-001	0.267	5.700E-001
0.234	4.830E-001	0.234	4.830E-001
0.225	4.590E-001	0.215	4.350E-001
0.205	4.110E-001	0.190	3.697E-001
0.181	3.470E-001	0.170	3.190E-001
0.158	2.880E-001	0.148	2.630E-001
0.138	2.370E-001		

FULL SCALE VOLTAGE REFERRED TO CH HI IS 10 VOLTS

TRANSFER FUNCTION*

TERM NO.	TERM
1	-1.175E-001
2	2.569E+000

QUALITY OF FIT AND NONLINEARITY*

STANDARD DEVIATION (PERCENT)	FULL-SCALE NONLINEARITY (PERCENT)
0.17	0.00

* INTERCEPT TERM INCLUDED

TABLE E-2

Computer Report Corresponding to the Best-Fit
Analysis of Figure E-3

MODEL DEC-AR, 1 CHANNEL Absolute Radiometer
SOURCE USU Extended area DATE: 16 May 1985

LINEARITY DATA SET (VOLTAGES ADJUSTED TO CH-LO)

BOL DC	BOL TEMP K	BOL DC	BOL TEMP K
0.306	1.547E+000	0.306	1.548E+000
0.286	1.580E+000	0.267	1.614E+000
0.234	1.696E+000	0.234	1.696E+000
0.225	1.719E+000	0.215	1.740E+000
0.205	1.763E+000	0.190	1.798E+000
0.181	1.826E+000	0.170	1.864E+000
0.158	1.903E+000	0.148	1.936E+000
0.138	1.969E+000	0.127	2.008E+000

FULL SCALE VOLTAGE REFERRED TO CH HI IS 10 VOLTS

TRANSFER FUNCTION*

TERM NO.	TERM
1	2.535E+000
2	-4.835E+000
3	5.252E+000

QUALITY OF FIT AND NONLINEARITY*

STANDARD DEVIATION (PERCENT)	FULL-SCALE NONLINEARITY (PERCENT)
0.24	109.56

* INTERCEPT TERM INCLUDED

TABLE E-3

Near Field-of-View Analysis

NEAR FIELD OF VIEW ANALYSIS

MODEL DEC--AR, 1 CHANNEL RADIOMETER
 SOURCE COLD COLLIMATOR DATE: 10 MAY 1985

NEAR FIELD DATA SET

ANGLE Y	ANGLE X	ANGLE X'	VOLTAGE	REL OUT
-0.025	-0.317	-0.330	0.049	9.794E-003
	-0.239	-0.246	0.049	9.794E-003
	-0.156	-0.163	0.049	9.794E-003
	-0.078	-0.079	0.044	8.815E-003
	0.005	0.005	0.044	8.815E-003
	0.088	0.088	0.049	9.794E-003
	0.171	0.172	0.049	9.794E-003
	0.254	0.255	0.054	1.077E-002
	0.332	0.339	0.068	1.371E-002
	0.425	0.422	0.093	1.861E-002
	0.508	0.506	0.117	2.351E-002
	0.596	0.589	0.137	2.742E-002
	0.679	0.673	0.146	2.938E-002
	0.762	0.757	0.137	2.742E-002
	0.850	0.840	0.127	2.547E-002
	0.938	0.924	0.098	1.959E-002
	1.016	1.007	0.078	1.567E-002
	1.104	1.091	0.059	1.175E-002
	1.191	1.174	0.049	9.794E-003
	1.270	1.258	0.049	9.794E-003
	1.357	1.342	0.049	9.794E-003
	1.440	1.425	0.049	9.794E-003
	1.523	1.509	0.044	8.815E-003
	1.602	1.592	0.044	8.815E-003
	1.694	1.676	0.044	8.815E-003
0.045	-0.337	-0.330	0.049	9.794E-003
	-0.259	-0.246	0.049	9.794E-003
	-0.181	-0.163	0.044	8.815E-003
	-0.098	-0.079	0.044	8.815E-003
	-0.020	0.005	0.049	9.794E-003
	0.063	0.088	0.049	9.794E-003
	0.146	0.172	0.049	9.794E-003
	0.229	0.255	0.054	1.077E-002
	0.313	0.339	0.068	1.371E-002
	0.400	0.422	0.093	1.861E-002
	0.479	0.506	0.127	2.547E-002
	0.566	0.589	0.156	3.134E-002
	0.645	0.673	0.166	3.330E-002
	0.732	0.757	0.166	3.330E-002
	0.820	0.840	0.156	3.134E-002
	0.903	0.924	0.132	2.644E-002
	0.991	1.007	0.098	1.959E-002
	1.074	1.091	0.073	1.469E-002

TABLE E-3 (Cont.)
Near Field-of-View Analysis

NEAR FIELD OF VIEW ANALYSIS

MODEL DEC--AR, 1 CHANNEL RADIOMETER
SOURCE COLD COLLIMATOR DATE: 10 MAY 1985

NEAR FIELD DATA SET

ANGLE Y	ANGLE X	ANGLE X'	VOLTAGE	REL OUT
	1.162	1.174	0.059	1.175E-002
	1.245	1.258	0.049	9.794E-003
	1.328	1.342	0.049	9.794E-003
	1.411	1.425	0.049	9.794E-003
	1.499	1.509	0.049	9.794E-003
	1.577	1.592	0.049	9.794E-003
	1.660	1.676	0.044	8.815E-003
0.115	-0.313	-0.330	0.049	9.794E-003
	-0.234	-0.246	0.044	8.815E-003
	-0.151	-0.163	0.049	9.794E-003
	-0.068	-0.079	0.049	9.794E-003
	0.015	0.005	0.049	9.794E-003
	0.093	0.088	0.054	1.077E-002
	0.176	0.172	0.059	1.175E-002
	0.259	0.255	0.088	1.763E-002
	0.342	0.339	0.132	2.644E-002
	0.425	0.422	0.195	3.918E-002
	0.508	0.506	0.444	8.913E-002
	0.596	0.589	0.806	1.616E-001
	0.674	0.673	1.021	2.047E-001
	0.762	0.757	0.972	1.949E-001
	0.845	0.840	0.674	1.352E-001
	0.933	0.924	0.293	5.877E-002
	1.016	1.007	0.156	3.134E-002
	1.104	1.091	0.112	2.253E-002
	1.187	1.174	0.073	1.469E-002
	1.270	1.258	0.054	1.077E-002
	1.357	1.342	0.049	9.794E-003
	1.440	1.425	0.049	9.794E-003
	1.523	1.509	0.044	8.815E-003
	1.602	1.592	0.049	9.794E-003
	1.694	1.676	0.044	8.815E-003
0.185	-0.356	-0.330	0.049	9.794E-003
	-0.273	-0.246	0.044	8.815E-003
	-0.195	-0.163	0.049	9.794E-003
	-0.112	-0.079	0.049	9.794E-003
	-0.029	0.005	0.049	9.794E-003
	0.049	0.088	0.054	1.077E-002
	0.132	0.172	0.063	1.273E-002
	0.210	0.255	0.093	1.861E-002
	0.298	0.339	0.146	2.938E-002
	0.381	0.422	0.273	5.485E-002
	0.469	0.506	0.840	1.685E-001

TABLE E-3 (Cont.)
Near Field-of-View Analysis

N E A R F I E L D O F V I E W A N A L Y S I S

MODEL DEC--AR, 1 CHANNEL RADIOMETER
SOURCE COLD COLLIMATOR DATE: 10 MAY 1985

NEAR FIELD DATA SET

ANGLE Y	ANGLE X	ANGLE X'	VOLTAGE	REL OUT
	0.552	0.589	1.436	2.880E-001
	0.635	0.673	1.851	3.712E-001
	0.718	0.757	1.904	3.820E-001
	0.801	0.840	1.670	3.350E-001
	0.889	0.924	1.133	2.272E-001
	0.972	1.007	0.479	9.598E-002
	1.064	1.091	0.176	3.526E-002
	1.143	1.174	0.117	2.351E-002
	1.230	1.258	0.073	1.469E-002
	1.313	1.342	0.054	1.077E-002
	1.406	1.425	0.049	9.794E-003
	1.484	1.509	0.044	8.815E-003
	1.567	1.592	0.049	9.794E-003
	1.650	1.676	0.044	8.815E-003
0.255	-0.313	-0.330	0.049	9.794E-003
	-0.234	-0.246	0.049	9.794E-003
	-0.151	-0.163	0.049	9.794E-003
	-0.073	-0.079	0.054	1.077E-002
	0.010	0.005	0.054	1.077E-002
	0.088	0.088	0.073	1.469E-002
	0.171	0.172	0.127	2.547E-002
	0.254	0.255	0.229	4.603E-002
	0.342	0.339	1.045	2.096E-001
	0.420	0.422	2.183	4.378E-001
	0.508	0.506	2.974	5.965E-001
	0.596	0.589	3.477	6.974E-001
	0.674	0.673	3.574	7.169E-001
	0.762	0.757	3.491	7.003E-001
	0.840	0.840	3.174	6.366E-001
	0.933	0.924	2.520	5.054E-001
	1.016	1.007	1.582	3.173E-001
	1.104	1.091	0.532	1.068E-001
	1.187	1.174	0.156	3.134E-002
	1.270	1.258	0.098	1.959E-002
	1.357	1.342	0.059	1.175E-002
	1.440	1.425	0.049	9.794E-003
	1.523	1.509	0.049	9.794E-003
	1.602	1.592	0.049	9.794E-003
	1.694	1.676	0.044	8.815E-003
0.325	-0.317	-0.330	0.049	9.794E-003
	-0.234	-0.246	0.054	1.077E-002
	-0.156	-0.163	0.054	1.077E-002
	-0.068	-0.079	0.054	1.077E-002

TABLE E-3 (Cont.)
Near Field-of-View Analysis

NEAR FIELD OF VIEW ANALYSIS

MODEL DEC--AR, 1 CHANNEL RADIOMETER
SOURCE COLD COLLIMATOR DATE: 10 MAY 1985

NEAR FIELD DATA SET

ANGLE Y	ANGLE X	ANGLE X'	VOLTAGE	REL OUT
	0.010	0.005	0.068	1.371E-002
	0.088	0.088	0.107	2.155E-002
	0.171	0.172	0.186	3.722E-002
	0.254	0.255	0.977	1.959E-001
	0.337	0.339	2.393	4.799E-001
	0.420	0.422	3.486	6.993E-001
	0.508	0.506	3.916	7.855E-001
	0.586	0.589	3.916	7.855E-001
	0.674	0.673	3.984	7.992E-001
	0.752	0.757	3.936	7.894E-001
	0.850	0.840	3.818	7.659E-001
	0.928	0.924	3.628	7.277E-001
	1.016	1.007	2.925	5.867E-001
	1.104	1.091	1.729	3.467E-001
	1.187	1.174	0.459	9.207E-002
	1.270	1.258	0.146	2.938E-002
	1.357	1.342	0.078	1.567E-002
	1.440	1.425	0.054	1.077E-002
	1.519	1.509	0.049	9.794E-003
	1.606	1.592	0.049	9.794E-003
	1.689	1.676	0.044	8.815E-003
0.395	-0.313	-0.330	0.054	1.077E-002
	-0.225	-0.246	0.054	1.077E-002
	-0.142	-0.163	0.059	1.175E-002
	-0.068	-0.079	0.059	1.175E-002
	0.015	0.005	0.088	1.763E-002
	0.098	0.088	0.146	2.938E-002
	0.176	0.172	0.483	9.696E-002
	0.264	0.255	1.963	3.937E-001
	0.342	0.339	3.442	6.905E-001
	0.430	0.422	3.965	7.953E-001
	0.513	0.506	4.023	8.071E-001
	0.596	0.589	4.121	8.266E-001
	0.679	0.673	4.268	8.560E-001
	0.771	0.757	4.307	8.639E-001
	0.850	0.840	4.063	8.149E-001
	0.938	0.924	3.853	7.728E-001
	1.025	1.007	3.535	7.091E-001
	1.108	1.091	2.461	4.936E-001
	1.191	1.174	0.981	1.969E-001
	1.279	1.258	0.176	3.526E-002
	1.362	1.342	0.093	1.861E-002
	1.445	1.425	0.059	1.175E-002

TABLE E-3 (Cont.)
Near Field-of-View Analysis

NEAR FIELD OF VIEW ANALYSIS

MODEL DEC--AR, 1 CHANNEL RADIOMETER
SOURCE COLD COLLIMATOR DATE: 10 MAY 1985

NEAR FIELD DATA SET

ANGLE Y	ANGLE X	ANGLE X'	VOLTAGE	REL OUT
	1.533	1.509	0.049	9.794E-003
	1.611	1.592	0.044	8.815E-003
	1.699	1.676	0.049	9.794E-003
0.465	-0.342	-0.330	0.054	1.077E-002
	-0.264	-0.246	0.054	1.077E-002
	-0.186	-0.163	0.054	1.077E-002
	-0.107	-0.079	0.059	1.175E-002
	-0.024	0.005	0.078	1.567E-002
	0.059	0.088	0.137	2.742E-002
	0.142	0.172	0.391	7.835E-002
	0.225	0.255	1.899	3.810E-001
	0.303	0.339	3.379	6.778E-001
	0.391	0.422	4.014	8.051E-001
	0.474	0.506	4.111	8.247E-001
	0.562	0.589	4.292	8.609E-001
	0.640	0.673	4.668	9.363E-001
	0.732	0.757	4.619	9.265E-001
	0.811	0.840	4.482	8.991E-001
	0.898	0.924	4.131	8.286E-001
	0.986	1.007	3.857	7.738E-001
	1.064	1.091	3.462	6.944E-001
	1.152	1.174	2.231	4.476E-001
	1.235	1.258	0.674	1.352E-001
	1.323	1.342	0.156	3.134E-002
	1.406	1.425	0.078	1.567E-002
	1.494	1.509	0.049	9.794E-003
	1.572	1.592	0.049	9.794E-003
	1.660	1.676	0.049	9.794E-003
0.535	-0.313	-0.330	0.054	1.077E-002
	-0.234	-0.246	0.059	1.175E-002
	-0.146	-0.163	0.059	1.175E-002
	-0.073	-0.079	0.068	1.371E-002
	0.010	0.005	0.122	2.449E-002
	0.093	0.088	0.234	4.701E-002
	0.176	0.172	1.460	2.929E-001
	0.259	0.255	3.076	6.170E-001
	0.342	0.339	3.906	7.835E-001
	0.425	0.422	4.058	8.139E-001
	0.508	0.506	4.619	9.265E-001
	0.591	0.589	4.985	1.000E+000
	0.674	0.673	4.805	9.638E-001
	0.762	0.757	4.639	9.305E-001
	0.840	0.840	4.468	8.962E-001

TABLE E-3 (Cont.)
Near Field-of-View Analysis

NEAR FIELD OF VIEW ANALYSIS

MODEL DEC--AR, 1 CHANNEL RADIOMETER
SOURCE COLD COLLIMATOR DATE: 10 MAY 1985

NEAR FIELD DATA SET

ANGLE Y	ANGLE X	ANGLE X'	VOLTAGE	REL OUT
	0.933	0.924	4.272	8.570E-001
	1.016	1.007	3.896	7.816E-001
	1.104	1.091	3.574	7.169E-001
	1.187	1.174	2.334	4.682E-001
	1.270	1.258	0.654	1.312E-001
	1.357	1.342	0.156	3.134E-002
	1.440	1.425	0.073	1.469E-002
	1.523	1.509	0.049	9.794E-003
	1.602	1.592	0.049	9.794E-003
	1.694	1.676	0.049	9.794E-003
0.605	-0.356	-0.330	0.054	1.077E-002
	-0.283	-0.246	0.054	1.077E-002
	-0.195	-0.163	0.059	1.175E-002
	-0.122	-0.079	0.063	1.273E-002
	-0.034	0.005	0.098	1.959E-002
	0.044	0.088	0.176	3.526E-002
	0.127	0.172	0.840	1.685E-001
	0.210	0.255	2.588	5.191E-001
	0.288	0.339	3.706	7.434E-001
	0.376	0.422	3.926	7.875E-001
	0.469	0.506	4.346	8.717E-001
	0.547	0.589	4.922	9.873E-001
	0.625	0.673	4.937	9.902E-001
	0.713	0.757	4.404	8.834E-001
	0.796	0.840	3.472	6.964E-001
	0.879	0.924	4.326	8.678E-001
	0.967	1.007	4.209	8.443E-001
	1.055	1.091	3.916	7.855E-001
	1.143	1.174	3.418	6.856E-001
	1.221	1.258	1.895	3.800E-001
	1.309	1.342	0.342	6.856E-002
	1.392	1.425	0.127	2.547E-002
	1.479	1.509	0.059	1.175E-002
	1.558	1.592	0.054	1.077E-002
	1.646	1.676	0.049	9.794E-003
0.675	-0.356	-0.330	0.054	1.077E-002
	-0.273	-0.246	0.054	1.077E-002
	-0.186	-0.163	0.059	1.175E-002
	-0.112	-0.079	0.068	1.371E-002
	-0.029	0.005	0.107	2.155E-002
	0.049	0.088	0.195	3.918E-002
	0.137	0.172	1.123	2.253E-001
	0.215	0.255	2.856	5.730E-001

TABLE E-3 (Cont.)
Near Field-of-View Analysis

NEAR FIELD OF VIEW ANALYSIS

MODEL DEC--AR, 1 CHANNEL RADIOMETER
SOURCE COLD COLLIMATOR DATE: 10 MAY 1985

NEAR FIELD DATA SET

ANGLE Y	ANGLE X	ANGLE X'	VOLTAGE	REL OUT
	0.298	0.339	3.828	7.679E-001
	0.386	0.422	3.916	7.855E-001
	0.469	0.506	4.360	8.746E-001
	0.552	0.589	4.795	9.618E-001
	0.635	0.673	4.824	9.677E-001
	0.723	0.757	3.232	6.484E-001
	0.801	0.840	3.076	6.170E-001
	0.894	0.924	4.194	8.413E-001
	0.977	1.007	4.238	8.501E-001
	1.064	1.091	3.975	7.973E-001
	1.147	1.174	3.486	6.993E-001
	1.230	1.258	1.899	3.810E-001
	1.318	1.342	0.342	6.856E-002
	1.406	1.425	0.127	2.547E-002
	1.489	1.509	0.059	1.175E-002
	1.567	1.592	0.054	1.077E-002
	1.650	1.676	0.049	9.794E-003
0.745	-0.337	-0.330	0.054	1.077E-002
	-0.254	-0.246	0.059	1.175E-002
	-0.171	-0.163	0.059	1.175E-002
	-0.088	-0.079	0.068	1.371E-002
	-0.015	0.005	0.127	2.547E-002
	0.073	0.088	0.234	4.701E-002
	0.156	0.172	1.465	2.938E-001
	0.239	0.255	3.242	6.503E-001
	0.322	0.339	3.877	7.777E-001
	0.405	0.422	3.950	7.924E-001
	0.493	0.506	4.326	8.678E-001
	0.571	0.589	4.585	9.197E-001
	0.659	0.673	4.155	8.335E-001
	0.742	0.757	3.154	6.327E-001
	0.830	0.840	3.643	7.307E-001
	0.908	0.924	4.307	8.639E-001
	1.001	1.007	4.136	8.296E-001
	1.094	1.091	3.926	7.875E-001
	1.172	1.174	3.101	6.219E-001
	1.255	1.258	1.377	2.762E-001
	1.338	1.342	0.220	4.407E-002
	1.426	1.425	0.103	2.057E-002
	1.504	1.509	0.054	1.077E-002
	1.592	1.592	0.054	1.077E-002
	1.675	1.676	0.049	9.794E-003
0.815	-0.342	-0.330	0.054	1.077E-002

TABLE E-3 (Cont.)
Near Field-of-View Analysis

N E A R F I E L D O F V I E W A N A L Y S I S

MODEL DEC--AR, 1 CHANNEL RADIDMETER
SOURCE COLD COLLIMATOR DATE: 10 MAY 1985

NEAR FIELD DATA SET

ANGLE Y	ANGLE X	ANGLE X'	VOLTAGE	REL OUT
	-0.264	-0.246	0.059	1.175E-002
	-0.181	-0.163	0.059	1.175E-002
	-0.103	-0.079	0.068	1.371E-002
	-0.020	0.005	0.112	2.253E-002
	0.063	0.088	0.195	3.918E-002
	0.146	0.172	0.957	1.920E-001
	0.229	0.255	2.783	5.583E-001
	0.313	0.339	3.882	7.786E-001
	0.400	0.422	3.936	7.894E-001
	0.479	0.506	4.053	8.129E-001
	0.566	0.589	4.316	8.658E-001
	0.645	0.673	4.277	8.580E-001
	0.732	0.757	4.097	8.217E-001
	0.815	0.840	4.141	8.306E-001
	0.903	0.924	4.170	8.364E-001
	0.986	1.007	4.019	8.061E-001
	1.074	1.091	3.877	7.777E-001
	1.162	1.174	2.969	5.955E-001
	1.240	1.258	1.240	2.488E-001
	1.328	1.342	0.210	4.212E-002
	1.416	1.425	0.103	2.057E-002
	1.499	1.509	0.054	1.077E-002
	1.582	1.592	0.049	9.794E-003
	1.665	1.676	0.049	9.794E-003
0.885	-0.332	-0.330	0.059	1.175E-002
	-0.254	-0.246	0.054	1.077E-002
	-0.166	-0.163	0.059	1.175E-002
	-0.088	-0.079	0.068	1.371E-002
	-0.010	0.005	0.107	2.155E-002
	0.068	0.088	0.186	3.722E-002
	0.156	0.172	0.801	1.606E-001
	0.234	0.255	2.534	5.083E-001
	0.317	0.339	3.809	7.640E-001
	0.400	0.422	3.945	7.914E-001
	0.488	0.506	3.945	7.914E-001
	0.576	0.589	4.111	8.247E-001
	0.654	0.673	4.180	8.384E-001
	0.742	0.757	4.141	8.306E-001
	0.825	0.840	4.121	8.266E-001
	0.908	0.924	4.004	8.031E-001
	0.996	1.007	3.945	7.914E-001
	1.084	1.091	3.687	7.395E-001
	1.162	1.174	2.456	4.927E-001

TABLE E-3 (Cont.)
Near Field-of-View Analysis

NEAR FIELD OF VIEW ANALYSIS

MODEL DEC--AR, 1 CHANNEL RADIOMETER
SOURCE COLD COLLIMATOR DATE: 10 MAY 1985

NEAR FIELD DATA SET

ANGLE Y	ANGLE X	ANGLE X'	VOLTAGE	REL OUT
	1.250	1.258	0.762	1.528E-001
	1.338	1.342	0.176	3.526E-002
	1.421	1.425	0.088	1.763E-002
	1.504	1.509	0.054	1.077E-002
	1.592	1.592	0.049	9.794E-003
	1.670	1.676	0.049	9.794E-003
0.955	-0.337	-0.330	0.054	1.077E-002
	-0.254	-0.246	0.054	1.077E-002
	-0.176	-0.163	0.054	1.077E-002
	-0.088	-0.079	0.059	1.175E-002
	-0.015	0.005	0.068	1.371E-002
	0.068	0.088	0.117	2.351E-002
	0.156	0.172	0.195	3.918E-002
	0.234	0.255	0.625	1.254E-001
	0.313	0.339	2.012	4.035E-001
	0.400	0.422	3.154	6.327E-001
	0.479	0.506	3.721	7.463E-001
	0.566	0.589	3.779	7.581E-001
	0.654	0.673	3.789	7.600E-001
	0.732	0.757	3.755	7.532E-001
	0.820	0.840	3.730	7.483E-001
	0.903	0.924	3.701	7.424E-001
	0.991	1.007	3.203	6.425E-001
	1.074	1.091	2.178	4.368E-001
	1.162	1.174	0.815	1.636E-001
	1.250	1.258	0.205	4.114E-002
	1.328	1.342	0.107	2.155E-002
	1.416	1.425	0.059	1.175E-002
	1.499	1.509	0.049	9.794E-003
	1.582	1.592	0.049	9.794E-003
	1.665	1.676	0.049	9.794E-003
1.025	-0.313	-0.330	0.054	1.077E-002
	-0.229	-0.246	0.049	9.794E-003
	-0.146	-0.163	0.054	1.077E-002
	-0.073	-0.079	0.059	1.175E-002
	0.010	0.005	0.068	1.371E-002
	0.093	0.088	0.098	1.959E-002
	0.171	0.172	0.166	3.330E-002
	0.259	0.255	0.264	5.289E-002
	0.342	0.339	1.064	2.135E-001
	0.425	0.422	2.095	4.202E-001
	0.508	0.506	2.900	5.818E-001
	0.596	0.589	3.364	6.748E-001

TABLE E-3 (Cont.)
Near Field-of-View Analysis

N E A R F I E L D O F V I E W A N A L Y S I S

MODEL DEC--AR, 1 CHANNEL RADIOMETER
SOURCE COLD COLLIMATOR DATE: 10 MAY 1985

NEAR FIELD DATA SET

ANGLE Y	ANGLE X	ANGLE X'	VOLTAGE	REL OUT
	0.674	0.673	3.506	7.032E-001
	0.762	0.757	3.452	6.925E-001
	0.850	0.840	3.115	6.249E-001
	0.928	0.924	2.529	5.073E-001
	1.016	1.007	1.641	3.291E-001
	1.104	1.091	0.586	1.175E-001
	1.191	1.174	0.195	3.918E-002
	1.270	1.258	0.112	2.253E-002
	1.357	1.342	0.068	1.371E-002
	1.440	1.425	0.054	1.077E-002
	1.523	1.509	0.049	9.794E-003
	1.606	1.592	0.049	9.794E-003
	1.694	1.676	0.049	9.794E-003
1.095	-0.313	-0.330	0.054	1.077E-002
	-0.229	-0.246	0.049	9.794E-003
	-0.146	-0.163	0.054	1.077E-002
	-0.073	-0.079	0.059	1.175E-002
	0.010	0.005	0.068	1.371E-002
	0.093	0.088	0.098	1.959E-002
	0.171	0.172	0.166	3.330E-002
	0.259	0.255	0.264	5.289E-002
	0.342	0.339	1.064	2.135E-001
	0.425	0.422	2.095	4.202E-001
	0.508	0.506	2.900	5.818E-001
	0.596	0.589	3.364	6.748E-001
	0.674	0.673	3.506	7.032E-001
	0.762	0.757	3.452	6.925E-001
	0.850	0.840	3.115	6.249E-001
	0.928	0.924	2.529	5.073E-001
	1.016	1.007	1.641	3.291E-001
	1.104	1.091	0.586	1.175E-001
	1.191	1.174	0.195	3.918E-002
	1.270	1.258	0.112	2.253E-002
	1.357	1.342	0.068	1.371E-002
	1.440	1.425	0.054	1.077E-002
	1.523	1.509	0.049	9.794E-003
	1.606	1.592	0.049	9.794E-003
	1.694	1.676	0.049	9.794E-003
1.165	-0.303	-0.330	0.049	9.794E-003
	-0.225	-0.246	0.054	1.077E-002
	-0.142	-0.163	0.054	1.077E-002
	-0.063	-0.079	0.054	1.077E-002
	0.020	0.005	0.059	1.175E-002

TABLE E-3 (Cont.)
Near Field-of-View Analysis

N E A R F I E L D O F V I E W A N A L Y S I S

MODEL DEC--AR, 1 CHANNEL RADIOMETER
SOURCE COLD COLLIMATOR DATE: 10 MAY 1985

NEAR FIELD DATA SET

ANGLE Y	ANGLE X	ANGLE X'	VOLTAGE	REL OUT
	0.103	0.088	0.068	1.371E-002
	0.181	0.172	0.112	2.253E-002
	0.264	0.255	0.176	3.526E-002
	0.347	0.339	0.283	5.681E-002
	0.435	0.422	0.889	1.783E-001
	0.518	0.506	1.660	3.330E-001
	0.601	0.589	2.153	4.319E-001
	0.684	0.673	2.388	4.789E-001
	0.767	0.757	2.285	4.584E-001
	0.854	0.840	1.860	3.732E-001
	0.938	0.924	1.226	2.458E-001
	1.025	1.007	0.483	9.696E-002
	1.104	1.091	0.200	4.016E-002
	1.196	1.174	0.132	2.644E-002
	1.274	1.258	0.078	1.567E-002
	1.362	1.342	0.059	1.175E-002
	1.445	1.425	0.054	1.077E-002
	1.533	1.509	0.049	9.794E-003
	1.616	1.592	0.049	9.794E-003
	1.704	1.676	0.049	9.794E-003
1.235	-0.337	-0.330	0.049	9.794E-003
	-0.264	-0.246	0.049	9.794E-003
	-0.181	-0.163	0.049	9.794E-003
	-0.103	-0.079	0.054	1.077E-002
	-0.020	0.005	0.054	1.077E-002
	0.059	0.088	0.059	1.175E-002
	0.146	0.172	0.063	1.273E-002
	0.220	0.255	0.088	1.763E-002
	0.308	0.339	0.132	2.644E-002
	0.391	0.422	0.181	3.624E-002
	0.479	0.506	0.254	5.093E-002
	0.562	0.589	0.479	9.598E-002
	0.645	0.673	0.723	1.450E-001
	0.728	0.757	0.771	1.548E-001
	0.811	0.840	0.581	1.166E-001
	0.898	0.924	0.322	6.464E-002
	0.981	1.007	0.205	4.114E-002
	1.069	1.091	0.156	3.134E-002
	1.152	1.174	0.098	1.959E-002
	1.240	1.258	0.063	1.273E-002
	1.323	1.342	0.054	1.077E-002
	1.406	1.425	0.054	1.077E-002
	1.494	1.509	0.049	9.794E-003

TABLE E-3 (Cont.)
Near Field-of-View Analysis

NEAR FIELD OF VIEW ANALYSIS

MODEL DEC--AR, 1 CHANNEL RADIOMETER
SOURCE COLD COLLIMATOR DATE: 10 MAY 1985

NEAR FIELD DATA SET

ANGLE Y	ANGLE X	ANGLE X'	VOLTAGE	REL OUT
	1.577	1.592	0.049	9.794E-003
	1.660	1.676	0.049	9.794E-003
1.305	-0.332	-0.330	0.049	9.794E-003
	-0.254	-0.246	0.049	9.794E-003
	-0.166	-0.163	0.049	9.794E-003
	-0.088	-0.079	0.054	1.077E-002
	-0.010	0.005	0.054	1.077E-002
	0.068	0.088	0.054	1.077E-002
	0.156	0.172	0.059	1.175E-002
	0.234	0.255	0.063	1.273E-002
	0.317	0.339	0.088	1.763E-002
	0.400	0.422	0.127	2.547E-002
	0.483	0.506	0.161	3.232E-002
	0.571	0.589	0.186	3.722E-002
	0.654	0.673	0.205	4.114E-002
	0.737	0.757	0.205	4.114E-002
	0.820	0.840	0.195	3.918E-002
	0.908	0.924	0.166	3.330E-002
	0.996	1.007	0.127	2.547E-002
	1.084	1.091	0.093	1.861E-002
	1.162	1.174	0.068	1.371E-002
	1.250	1.258	0.059	1.175E-002
	1.338	1.342	0.054	1.077E-002
	1.416	1.425	0.054	1.077E-002
	1.504	1.509	0.049	9.794E-003
	1.582	1.592	0.049	9.794E-003
	1.675	1.676	0.049	9.794E-003
1.375	-0.313	-0.330	0.049	9.794E-003
	-0.234	-0.246	0.049	9.794E-003
	-0.146	-0.163	0.049	9.794E-003
	-0.068	-0.079	0.049	9.794E-003
	0.010	0.005	0.054	1.077E-002
	0.093	0.088	0.054	1.077E-002
	0.176	0.172	0.054	1.077E-002
	0.254	0.255	0.059	1.175E-002
	0.342	0.339	0.059	1.175E-002
	0.425	0.422	0.078	1.567E-002
	0.503	0.506	0.098	1.959E-002
	0.596	0.589	0.107	2.155E-002
	0.674	0.673	0.117	2.351E-002
	0.762	0.757	0.117	2.351E-002
	0.840	0.840	0.107	2.155E-002
	0.928	0.924	0.088	1.763E-002

TABLE E-3 (Cont.)
Near Field-of-View Analysis

N E A R F I E L D O F V I E W A N A L Y S I S

MODEL DEC--AR, 1 CHANNEL RADIOMETER
SOURCE COLD COLLIMATOR DATE: 10 MAY 1985

NEAR FIELD DATA SET

ANGLE Y	ANGLE X	ANGLE X'	VOLTAGE	REL OUT
	1.016	1.007	0.068	1.371E-002
	1.104	1.091	0.059	1.175E-002
	1.187	1.174	0.054	1.077E-002
	1.270	1.258	0.054	1.077E-002
	1.357	1.342	0.054	1.077E-002
	1.436	1.425	0.049	9.794E-003
	1.523	1.509	0.049	9.794E-003
	1.606	1.592	0.049	9.794E-003
	1.694	1.676	0.049	9.794E-003
1.445	-0.332	-0.330	0.049	9.794E-003
	-0.254	-0.246	0.049	9.794E-003
	-0.176	-0.163	0.049	9.794E-003
	-0.088	-0.079	0.049	9.794E-003
	-0.010	0.005	0.049	9.794E-003
	0.068	0.088	0.049	9.794E-003
	0.156	0.172	0.054	1.077E-002
	0.229	0.255	0.054	1.077E-002
	0.322	0.339	0.054	1.077E-002
	0.396	0.422	0.059	1.175E-002
	0.483	0.506	0.059	1.175E-002
	0.566	0.589	0.063	1.273E-002
	0.654	0.673	0.068	1.371E-002
	0.732	0.757	0.068	1.371E-002
	0.820	0.840	0.068	1.371E-002
	0.908	0.924	0.063	1.273E-002
	0.991	1.007	0.059	1.175E-002
	1.074	1.091	0.059	1.175E-002
	1.162	1.174	0.054	1.077E-002
	1.250	1.258	0.054	1.077E-002
	1.328	1.342	0.054	1.077E-002
	1.416	1.425	0.049	9.794E-003
	1.499	1.509	0.049	9.794E-003
	1.582	1.592	0.049	9.794E-003
	1.670	1.676	0.044	8.815E-003
1.515	-0.342	-0.330	0.049	9.794E-003
	-0.269	-0.246	0.049	9.794E-003
	-0.186	-0.163	0.049	9.794E-003
	-0.107	-0.079	0.049	9.794E-003
	-0.024	0.005	0.049	9.794E-003
	0.054	0.088	0.049	9.794E-003
	0.137	0.172	0.049	9.794E-003
	0.215	0.255	0.054	1.077E-002
	0.303	0.339	0.054	1.077E-002

TABLE E-3 (Cont.)
Near Field-of-View Analysis

N E A R F I E L D O F V I E W A N A L Y S I S

MODEL DEC--AR, 1 CHANNEL RADIMETER
SOURCE COLD COLLIMATOR DATE: 10 MAY 1985

NEAR FIELD DATA SET

ANGLE Y	ANGLE X	ANGLE X'	VOLTAGE	REL OUT
	0.386	0.422	0.054	1.077E-002
	0.469	0.506	0.059	1.175E-002
	0.552	0.589	0.059	1.175E-002
	0.635	0.673	0.059	1.175E-002
	0.723	0.757	0.059	1.175E-002
	0.801	0.840	0.059	1.175E-002
	0.894	0.924	0.059	1.175E-002
	0.972	1.007	0.054	1.077E-002
	1.064	1.091	0.054	1.077E-002
	1.147	1.174	0.054	1.077E-002
	1.230	1.258	0.054	1.077E-002
	1.318	1.342	0.049	9.794E-003
	1.406	1.425	0.049	9.794E-003
	1.489	1.509	0.049	9.794E-003
	1.567	1.592	0.049	9.794E-003
	1.655	1.676	0.049	9.794E-003
1.585	-0.322	-0.330	0.044	8.815E-003
	-0.244	-0.246	0.049	9.794E-003
	-0.156	-0.163	0.044	8.815E-003
	-0.078	-0.079	0.049	9.794E-003
	0.005	0.005	0.049	9.794E-003
	0.088	0.088	0.049	9.794E-003
	0.166	0.172	0.054	1.077E-002
	0.244	0.255	0.054	1.077E-002
	0.332	0.339	0.054	1.077E-002
	0.420	0.422	0.054	1.077E-002
	0.498	0.506	0.054	1.077E-002
	0.586	0.589	0.054	1.077E-002
	0.664	0.673	0.054	1.077E-002
	0.752	0.757	0.059	1.175E-002
	0.835	0.840	0.059	1.175E-002
	0.928	0.924	0.054	1.077E-002
	1.006	1.007	0.054	1.077E-002
	1.094	1.091	0.054	1.077E-002
	1.182	1.174	0.054	1.077E-002
	1.265	1.258	0.054	1.077E-002
	1.348	1.342	0.049	9.794E-003
	1.436	1.425	0.049	9.794E-003
	1.519	1.509	0.049	9.794E-003
	1.602	1.592	0.049	9.794E-003
	1.689	1.676	0.049	9.794E-003
1.655	-0.356	-0.330	0.049	9.794E-003
	-0.273	-0.246	0.044	8.815E-003

TABLE E-3 (Cont.)
Near Field-of-View Analysis

N E A R F I E L D O F V I E W A N A L Y S I S

MODEL DEC--AR, 1 CHANNEL RADIOMETER
SOURCE COLD COLLIMATOR DATE: 10 MAY 1985

NEAR FIELD DATA SET

ANGLE Y	ANGLE X	ANGLE X'	VOLTAGE	REL OUT
	-0.195	-0.163	0.049	9.794E-003
	-0.112	-0.079	0.049	9.794E-003
	-0.034	0.005	0.049	9.794E-003
	0.049	0.088	0.049	9.794E-003
	0.132	0.172	0.049	9.794E-003
	0.210	0.255	0.049	9.794E-003
	0.303	0.339	0.054	1.077E-002
	0.381	0.422	0.054	1.077E-002
	0.469	0.506	0.054	1.077E-002
	0.547	0.589	0.054	1.077E-002
	0.635	0.673	0.054	1.077E-002
	0.718	0.757	0.054	1.077E-002
	0.801	0.840	0.054	1.077E-002
	0.889	0.924	0.054	1.077E-002
	0.967	1.007	0.054	1.077E-002
	1.060	1.091	0.054	1.077E-002
	1.143	1.174	0.054	1.077E-002
	1.230	1.258	0.054	1.077E-002
	1.313	1.342	0.049	9.794E-003
	1.406	1.425	0.049	9.794E-003
	1.484	1.509	0.049	9.794E-003
	1.567	1.592	0.049	9.794E-003
	1.650	1.676	0.049	9.794E-003

OMEGA(EFF) = 2.105E-004 SR
THETA (CIR) = 0.469 DEG
THETA (SQU) = 0.416 DEG

TABLE E-4

DEC AR Extended-Area Source Calibration for Band 5
 (See also graphic data plot included as Figure E-10)

DEC-AR EXTENDED-AREA SOURCE CALIBRATION
 DATE 16 MAY 1985
 BAND 5

Source Temp (K)	Output (V)	Output (V)	Band Radiance (W/CM ² SR)	Total Radiance (W/CM ² SR)
12.0	8.373E-03	7.349E-03	6.053E-34	3.486E-13
17.2	8.118E-03	7.285E-03	7.648E-26	9.414E-12
21.2	8.456E-03	7.654E-03	2.875E-22	4.710E-11
24.1	8.684E-03	7.907E-03	2.237E-20	1.109E-10
26.8	9.470E-03	8.597E-03	5.964E-19	2.105E-10
28.8	1.181E-02	1.078E-02	4.765E-18	3.145E-10
31.8	1.385E-02	1.241E-02	6.966E-17	5.252E-10
33.3	1.495E-02	1.356E-02	2.269E-16	6.569E-10
34.6	1.595E-02	1.447E-02	5.864E-16	7.859E-10
37.7	1.893E-02	1.667E-02	4.455E-15	1.150E-09
40.8	2.371E-02	2.130E-02	2.563E-14	1.594E-09
43.9	2.877E-02	2.601E-02	1.178E-13	2.116E-09
47.6	3.646E-02	3.288E-02	5.733E-13	2.841E-09
51.6	4.587E-02	4.143E-02	2.510E-12	3.743E-09
55.6	5.711E-02	5.188E-02	9.041E-12	4.763E-09
62.6	7.821E-02	6.916E-02	5.921E-11	6.846E-09
65.5	8.672E-02	7.861E-02	1.158E-10	7.834E-09
69.0	9.952E-02	9.043E-02	2.427E-10	9.154E-09
72.4	.106	9.556E-02	4.680E-10	1.061E-08
74.5	.114	.103	6.832E-10	1.161E-08
76.5	.122	.111	9.623E-10	1.267E-08
78.2	.130	.118	1.272E-09	1.366E-08
80.7	.142	.129	1.879E-09	1.529E-08
82.7	.154	.140	2.529E-09	1.679E-08
84.9	.167	.153	3.454E-09	1.867E-08
89.2	.203	.186	6.105E-09	2.327E-08
93.1	.237	.221	9.820E-09	2.885E-08
97.6	.286	.273	1.629E-08	3.756E-08
101.9	.347	.339	2.543E-08	4.897E-08

TABLE E-5

DEC AR Extended-Area Source Calibration for Band 6
(See also graphic data plot included as Figure E-11)

Source Temp (K)	Output (V)	Output (V)	Band Radiance (W/CM ² SR)	Total Radiance (W/CM ² SR)
11.4	9.235E-03	8.074E-03	4.927E-19	1.089E-10
17.5	1.639E-02	1.474E-02	2.093E-15	5.748E-10
20.8	2.200E-02	1.992E-02	3.276E-14	1.108E-09
24.4	3.090E-02	2.815E-02	3.296E-13	2.024E-09
26.6	3.852E-02	3.493E-02	1.062E-12	2.796E-09
29.0	4.741E-02	4.329E-02	3.258E-12	3.847E-09
31.7	6.048E-02	5.396E-02	9.862E-12	5.314E-09
33.4	6.789E-02	6.161E-02	1.848E-11	6.401E-09
34.4	7.355E-02	6.672E-02	2.617E-11	7.102E-09
37.8	9.405E-02	8.331E-02	7.690E-11	9.837E-09
40.7	.106	9.528E-02	1.729E-10	1.262E-08
44.0	.128	.116	3.933E-10	1.633E-08
47.5	.157	.141	8.526E-10	2.098E-08
51.6	.194	.175	1.898E-09	2.753E-08
55.6	.235	.213	3.782E-09	3.534E-08
62.7	.335	.301	1.076E-08	5.407E-08
65.4	.379	.343	1.524E-08	6.339E-08
69.1	.451	.412	2.368E-08	7.874E-08
72.4	.539	.483	3.397E-08	9.545E-08
74.5	.590	.537	4.215E-08	1.078E-07
76.5	.650	.592	5.129E-08	1.211E-07
78.2	.701	.641	6.019E-08	1.335E-07
80.7	.801	.728	7.536E-08	1.539E-07
82.7	.887	.811	8.946E-08	1.723E-07
84.9	.988	.903	1.072E-07	1.948E-07
93.1	1.43	1.33	1.968E-07	3.030E-07
97.6	1.68	1.62	2.645E-07	3.811E-07
101.8	1.98	1.94	3.414E-07	4.680E-07

TABLE E-6

DEC AR Extended-Area Source Calibration for Band 7

(See also graphic data plot included as Figure E-12)

Source Temp (K)	Output (V)	Output (V)	Band Radiance (W/CM ² SR)	Total Radiance (W/CM ² SR)
10.9	5.952E-03	5.174E-03	3.764E-15	6.804E-12
17.9	7.037E-03	6.333E-03	6.642E-12	2.376E-11
20.5	7.061E-03	6.378E-03	3.119E-11	5.267E-11
24.7	8.545E-03	7.685E-03	1.997E-10	2.288E-10
26.3	9.285E-03	8.466E-03	3.506E-10	3.828E-10
26.3	9.299E-03	8.427E-03	3.506E-10	3.828E-10
29.2	1.382E-02	1.262E-02	8.410E-10	8.792E-10
31.6	1.702E-02	1.514E-02	1.551E-09	1.595E-09
33.6	2.337E-02	2.124E-02	2.430E-09	2.478E-09
34.3	2.638E-02	2.388E-02	2.811E-09	2.860E-09
37.8	4.210E-02	3.739E-02	5.406E-09	5.464E-09
40.6	6.078E-02	5.419E-02	8.466E-09	8.530E-09
44.1	9.269E-02	8.405E-02	1.378E-08	1.385E-08
47.4	.126	.113	2.052E-08	2.060E-08
51.8	.188	.171	3.245E-08	3.255E-08
55.5	.259	.234	4.531E-08	4.542E-08
62.3	.438	.395	7.610E-08	7.622E-08
65.3	.510	.462	9.270E-08	9.283E-08
69.2	.631	.576	1.170E-07	1.172E-07
72.3	.758	.675	1.386E-07	1.388E-07
74.6	.826	.755	1.558E-07	1.560E-07
76.4	.905	.821	1.701E-07	1.702E-07
78.3	.969	.888	1.857E-07	1.859E-07
80.7	1.08	.976	2.065E-07	2.067E-07
82.7	1.16	1.07	2.247E-07	2.249E-07
84.9	1.26	1.15	2.455E-07	2.457E-07
89.2	1.46	1.35	2.886E-07	2.888E-07
93.1	1.65	1.53	3.304E-07	3.307E-07
97.6	1.79	1.74	3.817E-07	3.819E-07
101.8	1.98	1.93	4.323E-07	4.326E-07

TABLE E-7

DEC AR Extended-Area Source Calibration for Band 8
 (See also graphic data plot included as Figure E-13)

Source Temp (K)	Output (V)	Output (V)	Band Radiance (W/CM ² SR)	Total Radiance (W/CM ² SR)
10.4	4.940E-03	4.269E-03	1.208E-10	1.235E-10
18.4	1.419E-02	1.279E-02	1.292E-09	1.298E-09
20.2	1.811E-02	1.632E-02	1.877E-09	1.883E-09
25.0	3.440E-02	3.134E-02	4.263E-09	4.271E-09
25.9	3.903E-02	3.564E-02	4.860E-09	4.869E-09
29.3	5.857E-02	5.349E-02	7.574E-09	7.585E-09
31.4	7.502E-02	6.647E-02	9.622E-09	9.634E-09
33.6	8.856E-02	8.060E-02	1.207E-08	1.209E-08
34.3	9.505E-02	8.585E-02	1.292E-08	1.293E-08
37.9	.121	.108	1.775E-08	1.778E-08
40.5	.147	.131	2.173E-08	2.177E-08
44.2	.181	.165	2.807E-08	2.812E-08
47.3	.223	.200	3.393E-08	3.401E-08
51.9	.275	.250	4.350E-08	4.363E-08
55.4	.328	.296	5.139E-08	5.159E-08
62.8	.435	.394	6.961E-08	6.999E-08
65.2	.478	.431	7.590E-08	7.637E-08
69.2	.530	.484	8.676E-08	8.741E-08
72.3	.604	.536	9.547E-08	9.627E-08
74.7	.621	.567	1.024E-07	1.033E-07
76.4	.664	.600	1.073E-07	1.084E-07
78.3	.683	.626	1.130E-07	1.141E-07
80.7	.739	.666	1.202E-07	1.215E-07
82.8	.764	.702	1.265E-07	1.281E-07
84.9	.813	.738	1.330E-07	1.347E-07
89.2	.880	.817	1.465E-07	1.486E-07
92.5	.959	.880	1.570E-07	1.595E-07
97.7	.987	.955	1.739E-07	1.770E-07
101.7	1.06	1.02	1.871E-07	1.908E-07

TABLE E-8

DEC AR Extended-Area Source Calibration for Band 10
 (See also graphic data plot included as Figure E-14 and computer
 analysis in Table E-9)

Source Temp (K)	Output (V)	Output (V)	Total Radiance (W/CM ² SR)
9.1	8.112E-04	6.950E-04	9.887E-11
19.3	2.562E-02	2.311E-02	2.000E-09
25.4	7.778E-02	7.095E-02	6.001E-09
29.7	.135	.123	1.122E-08
31.2	.168	.148	1.366E-08
33.8	.224	.204	1.882E-08
38.4	.367	.329	3.135E-08
40.2	.452	.401	3.765E-08
44.3	.638	.582	5.553E-08
47.2	.828	.739	7.156E-08
51.9	1.15	1.05	1.046E-07
55.3	1.48	1.33	1.348E-07
62.9	2.32	2.13	2.257E-07
65.1	2.66	2.40	2.590E-07
69.4	3.25	3.00	3.345E-07
72.1	3.83	3.41	3.896E-07
74.7	4.11	3.83	4.489E-07
76.4	4.51	4.12	4.912E-07
78.3	4.78	4.49	5.419E-07
80.6	5.35	4.88	6.085E-07
82.8	5.68	5.37	6.777E-07
84.8	6.29	5.82	7.456E-07
89.3	7.15	6.87	9.169E-07
90.4	7.57	7.13	9.629E-07
91.6	7.92	7.46	1.015E-06
92.5	8.28	7.79	1.056E-06
97.7	8.93	9.04	1.314E-06
99.7	9.50	9.48	1.425E-06
101.1	9.90	9.93	1.506E-06

TABLE E-9

Linearity Analysis of DEC AR Band 10 (open)

(See also graphic plot included as Figure E-14 and data points listed in Table E-8)

MODEL DEC-AR , 1 CHANNEL ABSOLUTE RADIMETER
SOURCE USU EXTENDED-AREA DATE: 16 MAY 1985

LINEARITY DATA SET (VOLTAGES ADJUSTED TO CH-HI)

SIGNAL (V)	AREA (SQ-CM)	SIGNAL (V)	AREA (SQ-CM)
0.001	9.887E-011	0.023	2.000E-009
0.071	6.001E-009	0.123	1.122E-008
0.148	1.366E-008	0.204	1.882E-008
0.329	3.135E-008	0.401	3.765E-008
0.582	5.553E-008	0.739	7.156E-008
1.050	1.046E-007	1.334	1.348E-007
2.128	2.257E-007	2.404	2.590E-007
2.999	3.345E-007	3.406	3.896E-007
3.827	4.489E-007	4.119	4.912E-007
4.494	5.419E-007	4.884	6.085E-007
5.371	6.777E-007	5.821	7.456E-007
6.872	9.169E-007	7.126	9.629E-007
7.456	1.015E-006	7.786	1.056E-006
9.042	1.314E-006	9.482	1.425E-006
9.932	1.506E-006		

FULL SCALE VOLTAGE REFERRED TO CH HI IS 10 VOLTS

CHANNEL GAINS

CHANNEL	GAIN
MAIN	1.000

TRANSFER FUNCTION* (NO INTERCEPT TERM)

TERM NO.	TERM
1	9.281E-008
2	5.984E-009

QUALITY OF FIT AND NONLINEARITY*

STANDARD DEVIATION (PERCENT)	FULL-SCALE NONLINEARITY (PERCENT)
7.22	39.20

* REFERRED TO THE HIGH-GAIN CHANNEL

TABLE E-10

Point Source Calibration Data for Band 1
 (See also graphic plot included as Figure E-17)

BAND 1

T1	Vcorr	Eband	Ettotal
326.2	4.473175E-03	1.052021E-20	6.961855E-15
376.4	5.022836E-03	3.723228E-19	1.101383E-14
421.9	-2.877075E-04	5.655571E-18	1.601348E-14
462.3	4.340067E-03	4.440238E-17	2.178968E-14
517.0	5.729794E-04	4.621863E-16	3.237447E-14
561.7	4.452967E-03	2.299548E-15	4.499584E-14
619.2	6.384991E-06	1.315034E-14	7.369712E-14
666.8	4.488006E-03	4.485523E-14	1.241870E-13
718.6	1.709647E-03	1.428328E-13	2.474347E-13
761.5	7.691925E-03	3.323398E-13	4.621902E-13
814.8	1.200189E-02	8.420661E-13	1.009398E-12
862.4	2.650711E-02	1.758543E-12	1.965645E-12
915.1	5.179089E-02	3.644612E-12	3.903300E-12
952.6	3.454925E-02	5.837103E-12	6.137659E-12
1014.0	.174893	1.173285E-11	1.211179E-11
1056.9	.243228	1.823661E-11	1.867790E-11
1105.5	.324009	2.897168E-11	2.939147E-11
1156.2	.515138	4.479447E-11	4.540536E-11
1207.8	.784839	6.750681E-11	6.822039E-11
1254.3	1.07701	9.497962E-11	9.579461E-11

TABLE E-11

Point Source Calibration Data for Band 2
(See also graphic plot included as Figure E-18)

BAND 2

T1	Vcorr	Eband	Etotal
326.2	5.048018E-03	1.752968E-16	8.788801E-15
376.4	4.648077E-03	2.285687E-15	1.564937E-14
421.9	3.388196E-04	1.394955E-14	3.302822E-14
462.3	5.106771E-03	5.183325E-14	7.731875E-14
517.0	5.234351E-03	2.221489E-13	2.586363E-13
561.7	1.755871E-02	5.930146E-13	6.407518E-13
619.2	4.386264E-02	1.707201E-12	1.772766E-12
666.8	9.639310E-02	3.575111E-12	3.658554E-12
718.6	.156410	7.159612E-12	7.265965E-12
761.5	.243259	1.185706E-11	1.198528E-11
814.8	.405244	2.062582E-11	2.078506E-11
862.4	.599735	3.193742E-11	3.212821E-11
915.1	8.913359E-02	4.917661E-11	4.940694E-11
952.6	1.48214	6.496377E-11	6.522547E-11
1013.6	2.06528	9.783207E-11	9.815129E-11
1057.8	2.42642	1.278433E-10	1.282099E-10
1105.5	2.97651	1.666488E-10	1.670729E-10
1156.2	3.43905	2.157324E-10	2.162260E-10
1207.8	4.29054	2.744857E-10	2.750605E-10
1254.3	4.87262	3.353914E-10	3.360501E-10

TABLE E-12

Point Source Calibration Data for Band 3
(See also graphic plot included as Figure E-19)

BAND 3

T1	Vcorr	Eband	Etotal
326.2	.294100	6.423328E-14	2.111710E-12
376.4	.284871	3.199117E-13	3.796705E-12
421.9	.289565	9.943404E-13	6.198296E-12
462.3	.320157	2.268385E-12	9.350958E-12
517.0	.433431	5.671424E-12	1.579352E-11
561.7	.578428	1.053793E-11	2.353865E-11
619.2	1.19219	2.056343E-11	3.773899E-11
666.8	1.48820	3.284543E-11	5.383689E-11
718.6	1.77194	5.104466E-11	7.651609E-11
761.5	1.97492	7.036070E-11	9.977253E-11
814.8	2.44341	1.001462E-10	1.347111E-10
863.4	2.90780	1.331776E-10	1.726627E-10
915.1	3.36086	1.746549E-10	2.195792E-10
952.6	5.22654	2.088774E-10	2.578663E-10
1013.0	6.02889	2.713047E-10	3.270296E-10
1058.7	6.05670	3.244599E-10	3.854223E-10
1105.5	6.57086	3.840694E-10	4.505096E-10
1156.2	6.91241	4.543963E-10	5.268912E-10
1206.9	7.70499	5.305034E-10	6.091693E-10
1254.3	7.96373	6.066858E-10	6.912195E-10

TABLE E-13

Point Source Calibration Data for Band 4

(See also graphic plot included as Figure E-20)

BAND 4

T1	Vcorr	Eband	Ettotal
326.2	.260919	2.985009E-13	1.733209E-12
376.4	.249448	9.760877E-13	3.156188E-12
421.9	.249252	2.243970E-12	5.231564E-12
462.3	.274023	4.101738E-12	7.900730E-12
517.0	.376072	8.001200E-12	1.302336E-11
561.7	.499463	1.255837E-11	1.867304E-11
619.2	1.03733	2.041637E-11	2.804179E-11
666.8	1.22018	2.869477E-11	3.764854E-11
718.6	1.39566	3.954447E-11	5.001307E-11
761.5	1.50441	4.995937E-11	6.173100E-11
814.8	1.75359	6.464210E-11	7.808739E-11
863.4	2.00053	7.963723E-11	9.465671E-11
915.1	2.20337	9.717480E-11	1.139154E-10
952.6	3.69804	1.108592E-10	1.288765E-10
1012.4	4.06531	1.342450E-10	1.543457E-10
1058.7	4.08495	1.535816E-10	1.753347E-10
1104.6	4.26419	1.737319E-10	1.971569E-10
1157.1	4.34251	1.978901E-10	2.232692E-10
1206.9	4.76617	2.218188E-10	2.490940E-10
1254.3	4.80420	2.454402E-10	2.745605E-10

TABLE E-14

Point Source Calibration Data for Band 5
(See also graphic plot included as Figure E-21)

BAND 5

T1	Vcorr	Eband	Etotal
326.2	.186654	5.744429E-12	5.768871E-12
376.4	.281198	9.988174E-12	1.002080E-11
421.9	.341126	1.487189E-11	1.491374E-11
462.3	.422179	1.996161E-11	2.001353E-11
517.0	.541521	2.785228E-11	2.792126E-11
561.7	.674091	3.504560E-11	3.513204E-11
619.2	1.14785	4.513797E-11	4.525235E-11
667.8	1.23096	5.429735E-11	5.444094E-11
717.6	1.29673	6.419095E-11	6.437062E-11
761.5	1.31686	7.328085E-11	7.349817E-11
814.8	1.48047	8.471749E-11	8.498887E-11
863.4	1.57642	9.547758E-11	9.580715E-11
915.1	1.65680	1.072244E-10	1.076262E-10
952.6	2.77143	1.159155E-10	1.163770E-10
1011.8	2.69865	1.298917E-10	1.304610E-10
1058.7	2.61396	1.411606E-10	1.418278E-10
1104.6	2.65045	1.523375E-10	1.531119E-10
1157.1	2.61069	1.652814E-10	1.661928E-10
1206.9	2.86693	1.777000E-10	1.787563E-10
1254.3	2.73098	1.896335E-10	1.908415E-10

TABLE E-15

Point Source Calibration Data for Band 6
(See also graphic plot included as Figure E-22)

BAND 6

T1	Vcorr	Eband	Ettotal
326.2	.120230	3.015545E-12	3.089638E-12
376.4	.118542	4.198061E-12	4.291892E-12
421.9	.109300	5.352934E-12	5.470442E-12
462.3	.107547	6.429007E-12	6.575431E-12
517.0	.114726	7.944600E-12	8.149372E-12
561.7	.125290	9.222430E-12	9.499435E-12
619.2	.218911	1.090648E-11	1.132367E-11
667.8	.210890	1.235802E-11	1.294961E-11
717.6	.200219	1.386681E-11	1.470586E-11
761.5	.192457	1.521172E-11	1.633937E-11
814.8	.200874	1.686016E-11	1.844428E-11
863.4	.207517	1.837573E-11	2.049444E-11
915.1	.216065	1.999898E-11	2.282938E-11
952.6	.392968	2.118250E-11	2.463260E-11
1011.2	.358358	2.304081E-11	2.765396E-11
1060.6	.329424	2.461464E-11	3.041191E-11
1103.7	.321495	2.599248E-11	3.298994E-11
1157.1	.315498	2.770496E-11	3.642390E-11
1206.9	.347220	2.930669E-11	3.988319E-11
1254.3	.322713	3.083497E-11	4.342206E-11

TABLE E-16

Point Source Calibration Data for Band 7
 (See also graphic plot included as Figure E-23)

BAND 7

T1	Vcorr	Eband	Ettotal
326.2	8.368992E-02	4.472588E-13	4.534453E-13
376.4	5.649894E-02	5.526138E-13	5.661177E-13
421.9	3.383810E-02	6.494609E-13	6.755821E-13
462.3	2.012279E-02	7.362288E-13	7.817061E-13
517.0	1.621480E-02	8.545670E-13	9.462208E-13
561.7	1.190499E-02	9.518269E-13	1.107024E-12
619.2	6.146610E-02	1.077491E-12	1.364814E-12
667.8	4.398046E-02	1.184082E-12	1.643552E-12
717.6	2.714240E-02	1.293587E-12	2.004970E-12
761.5	1.826636E-02	1.390313E-12	2.402325E-12
814.8	1.383090E-02	1.507949E-12	3.005140E-12
864.4	8.569568E-03	1.617584E-12	3.706877E-12
915.1	7.530441E-03	1.729787E-12	4.588885E-12
952.6	8.962079E-02	1.812854E-12	5.363385E-12
1010.6	5.107891E-02	1.941439E-12	6.793756E-12
1060.6	3.237298E-02	2.052380E-12	8.281820E-12
1103.7	2.055922E-02	2.148070E-12	9.776725E-12
1157.1	1.584895E-02	2.266694E-12	1.193069E-11
1206.0	1.263691E-02	2.375378E-12	1.422515E-11
1254.3	4.637355E-03	2.482776E-12	1.682239E-11

TABLE E-17
 Point Source Calibration Data for Band 8
 (See also graphic plot included as Figure E-24)

BAND 8

T1	Vcorr	Eband	Etotal
326.2	.102049	9.611568E-14	1.129051E-13
376.4	8.624898E-02	1.143900E-13	1.445918E-13
421.9	6.156697E-02	1.310097E-13	1.858061E-13
462.3	4.650380E-02	1.457985E-13	2.414775E-13
517.0	3.571622E-02	1.658567E-13	3.667704E-13
561.7	2.865071E-02	1.822703E-13	5.355031E-13
619.2	8.953609E-02	2.034063E-13	8.824252E-13
667.8	7.545017E-02	2.212858E-13	1.328940E-12
717.6	5.384098E-02	2.396181E-13	1.972196E-12
761.5	4.247406E-02	2.557861E-13	2.725547E-12
813.8	3.216887E-02	2.750555E-13	3.887599E-12
864.4	2.626207E-02	2.937052E-13	5.321637E-12
915.1	2.200579E-02	3.123972E-13	7.098731E-12
952.6	.107566	3.262256E-13	8.651111E-12
1010.0	7.813292E-02	3.473965E-13	1.144976E-11
1060.6	6.363753E-02	3.660631E-13	1.436970E-11
1103.7	4.756284E-02	3.819652E-13	1.721283E-11
1157.1	3.821370E-02	4.016701E-13	2.121529E-11
1206.0	3.416810E-02	4.197167E-13	2.537029E-11
1254.3	3.347799E-02	4.375438E-13	2.995694E-11

TABLE E-18

Point Source Calibration Data for Band 9 (Opaque)

(See also graphic plot included as Figure E-25. These data are included to show how the AR dark noise varied with time)

BAND 9

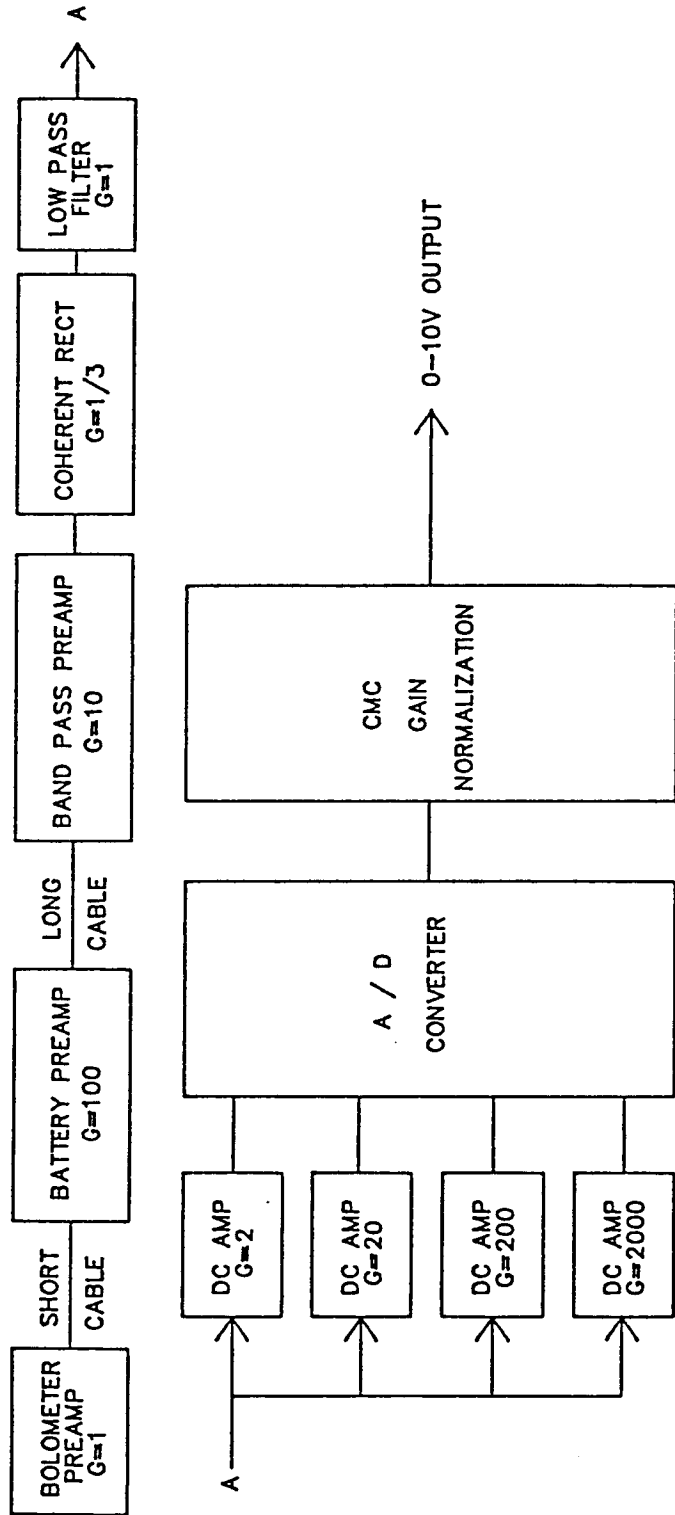
T1	Vcorr	Eband	Ettotal
326.2	1.396005E-03	2.215426E-14	8.220079E-14
376.4	1.379369E-03	2.610831E-14	1.178332E-13
421.9	1.554534E-03	2.969779E-14	1.655665E-13
462.3	1.367367E-03	3.288811E-14	2.291761E-13
517.0	1.858217E-03	3.721114E-14	3.682019E-13
561.7	1.774918E-03	4.074608E-14	5.510952E-13
619.2	1.352739E-03	4.529546E-14	9.228655E-13
668.8	1.352768E-03	4.922133E-14	1.413387E-12
717.6	1.516842E-03	5.308497E-14	2.097966E-12
761.5	1.874389E-03	5.656141E-14	2.925878E-12
813.8	1.823694E-03	6.070382E-14	4.229597E-12
864.4	2.088732E-03	6.471223E-14	5.880904E-12
916.1	2.295512E-03	6.880833E-14	8.034132E-12
952.6	1.592084E-03	7.170045E-14	9.878485E-12
1009.4	1.513525E-03	7.620147E-14	1.335637E-11
1060.6	1.194460E-03	8.025910E-14	1.720751E-11
1103.7	2.394625E-03	8.367503E-14	2.104252E-11
1157.1	1.559116E-03	8.790755E-14	2.663374E-11
1206.0	1.773110E-03	9.178362E-14	3.265705E-11
1253.4	1.830136E-03	9.554096E-14	3.940609E-11

TABLE E-19

Point Source Calibration Data for Band 10 (Open)
 See also graphic plot included as Figure E-26)

BAND 10

T1	Vcorr	Lband
326.2	1.00927	1.530553E-11
376.4	1.24332	2.713382E-11
421.9	1.49059	4.283024E-11
463.5	1.84670	6.238948E-11
517.0	2.56716	9.657720E-11
561.7	3.09570	1.345644E-10
619.2	5.40491	1.987176E-10
619.2	5.40491	1.987176E-10
668.8	6.33428	2.704565E-10
717.6	7.51771	3.584612E-10
761.5	7.68434	4.545609E-10
813.8	9.59891	5.929024E-10
864.4	10.3161	7.546950E-10
1205.1	-1.082453E-02	2.851050E-09
1253.4	-9.868621E-04	3.336347E-09



VOLTAGE GAIN CONFIGURATION OF AR ELECTRONICS

1000/7

Figure E-1. Block diagram of voltage gain configuration of AR electronics.

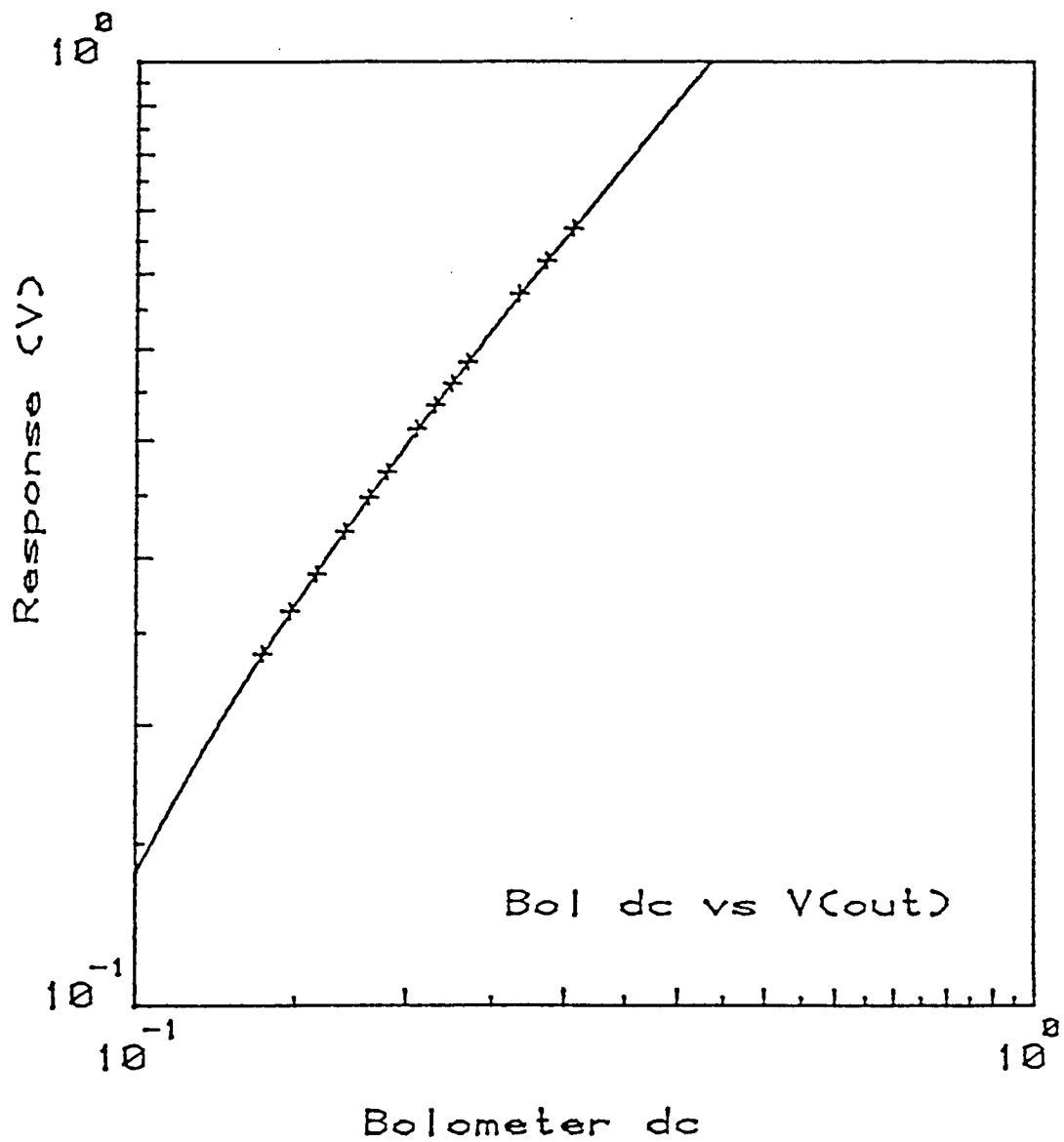


Figure E-2. Bolometer dc vs. bolometer response data points with a least squares, best-fit superimposed (See computer report contained in Table E-1).

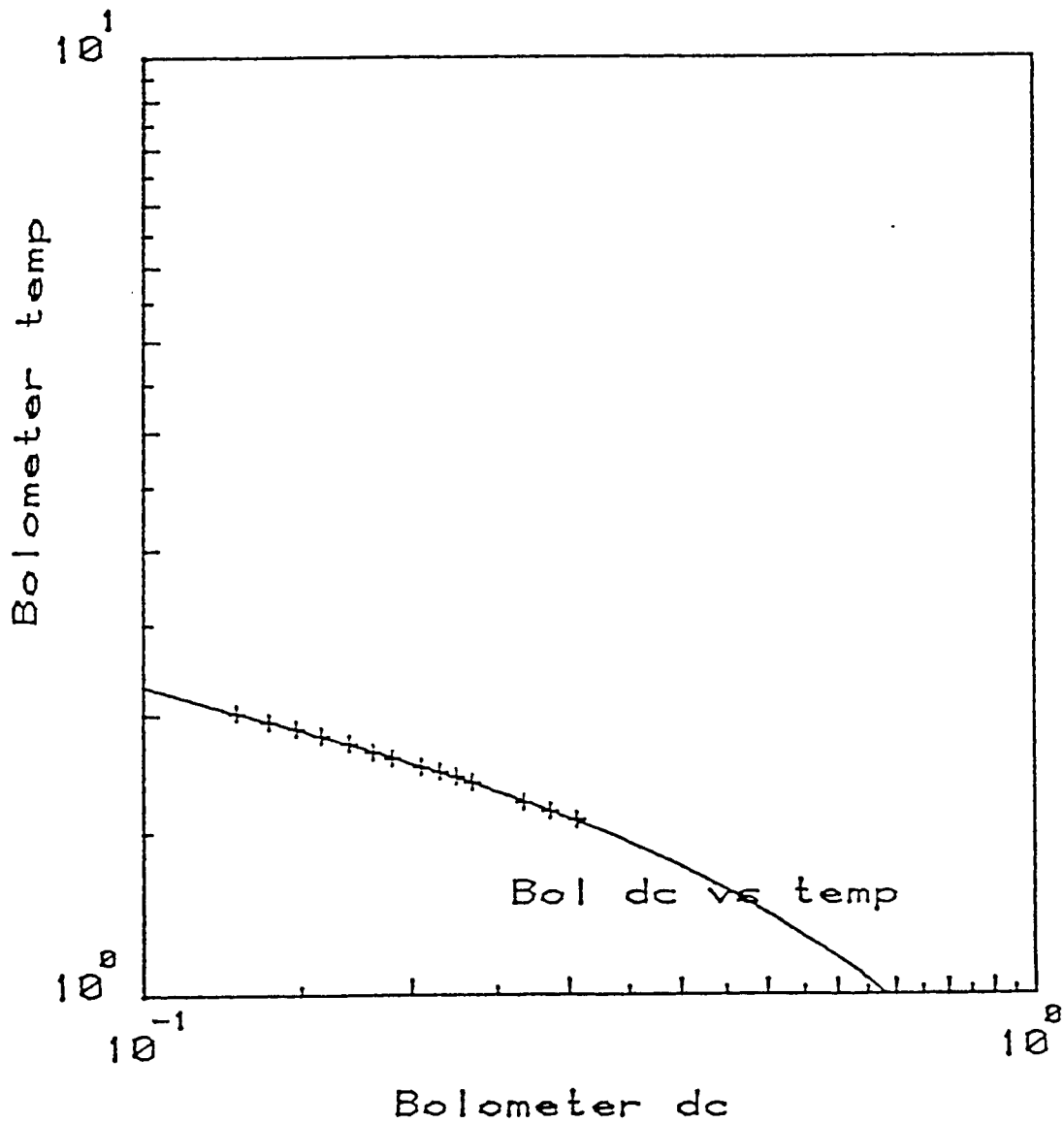


Figure E-3. Bolometer dc vs. bolometer temperature data points with a least squares, best-fit superimposed (See computer report contained in Table E-2).

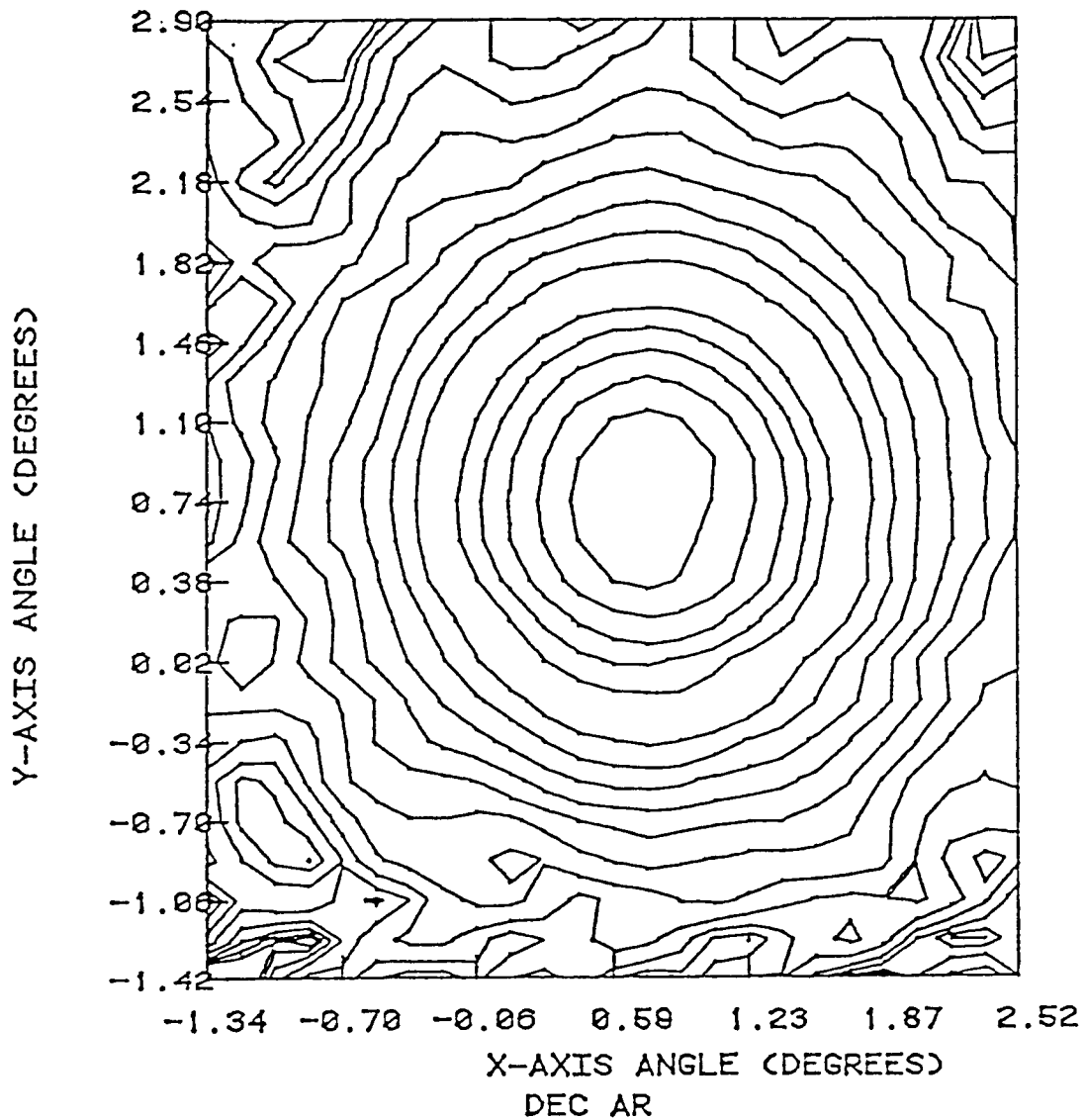
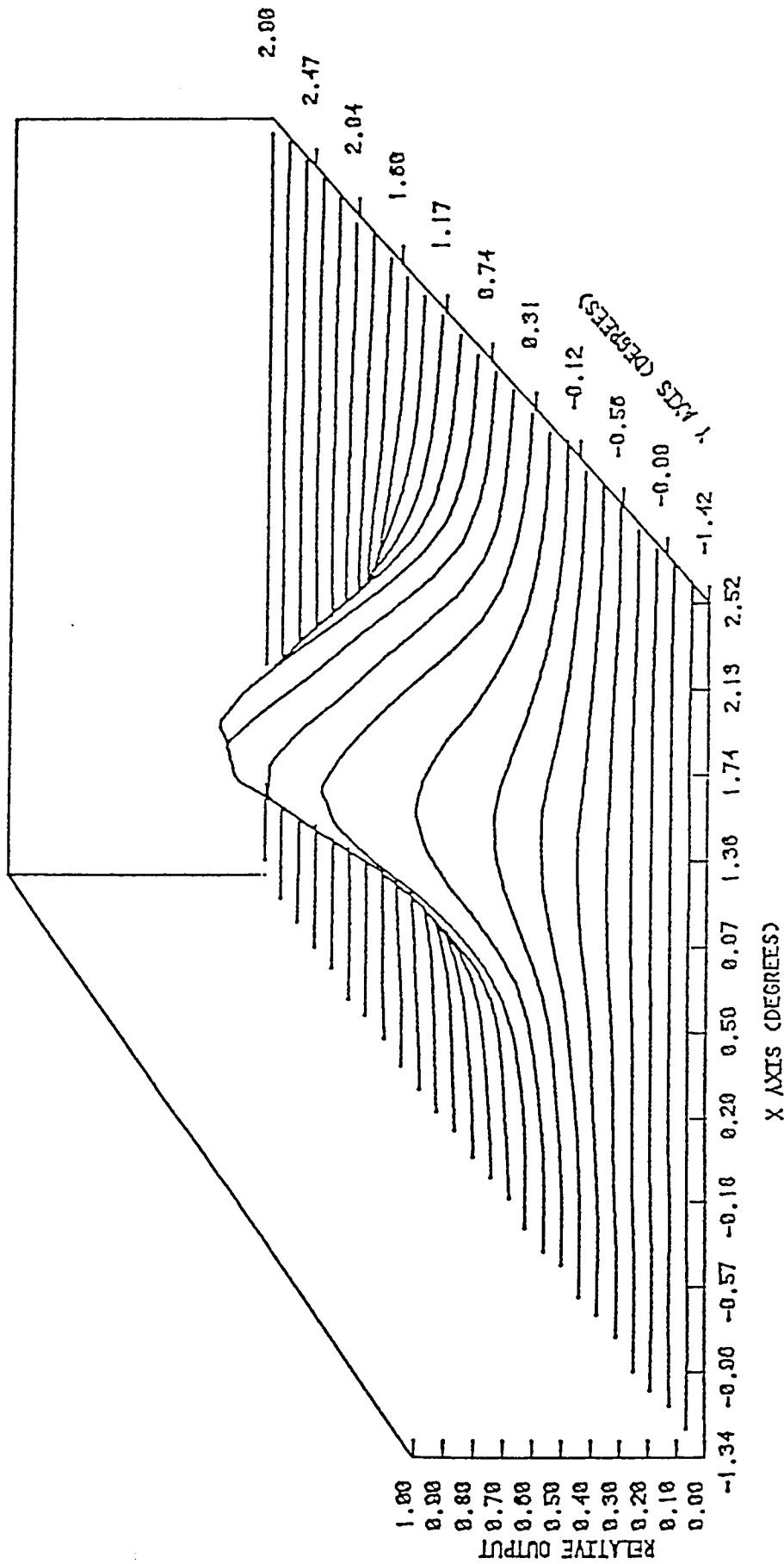


Figure E-4. Contour analysis of the AR field-of-view obtained with the 0.007-inch diameter cold pinhole mounted in the entrance aperture.



DEC AR

Figure E-5. A three dimensional representation of the AR field-of-view obtained with a 0.007-inch diameter cold pinhole mounted in the entrance aperture.

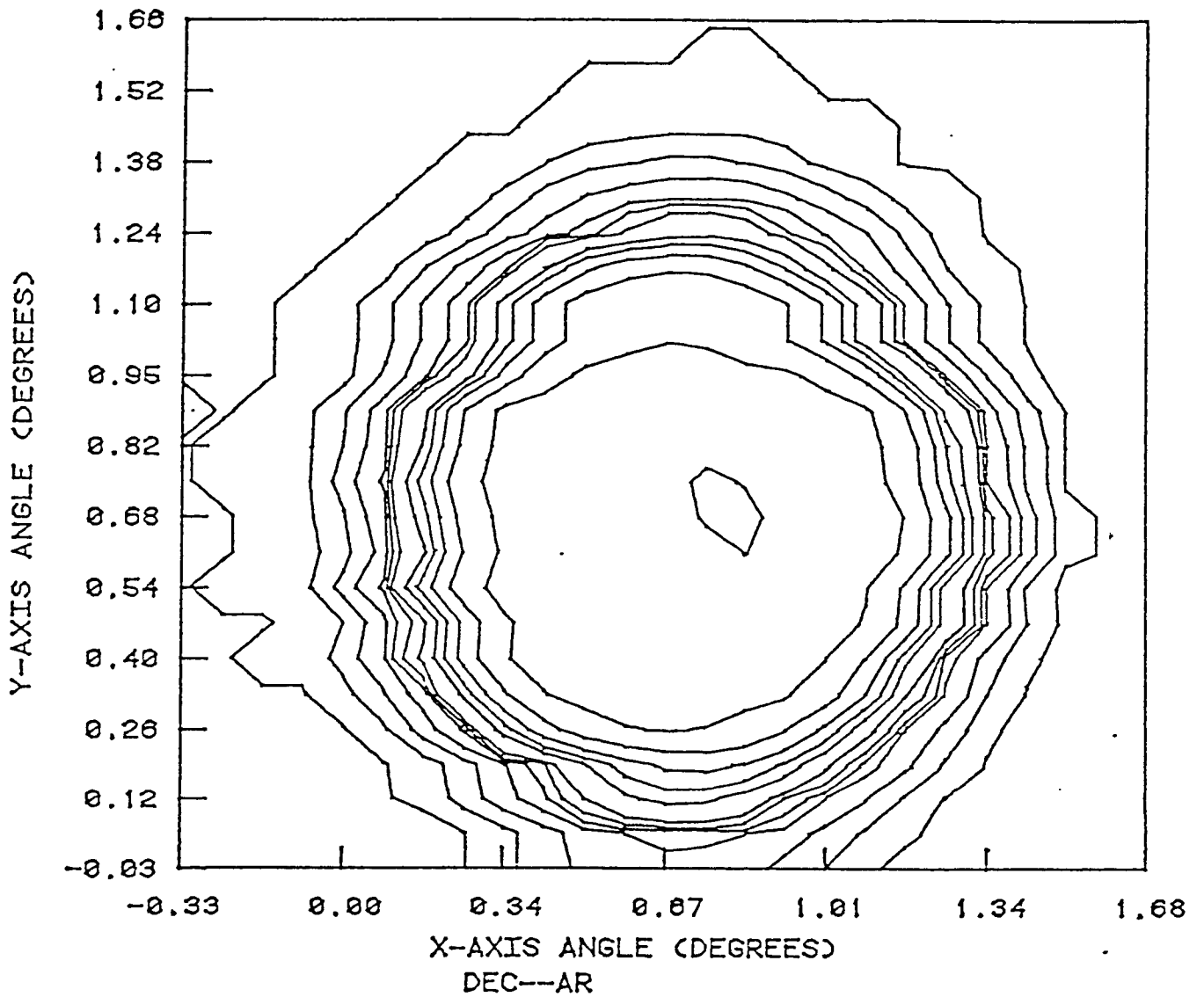


Figure E-6. Contour analysis of the AR field-of-view obtained with full entrance aperture.

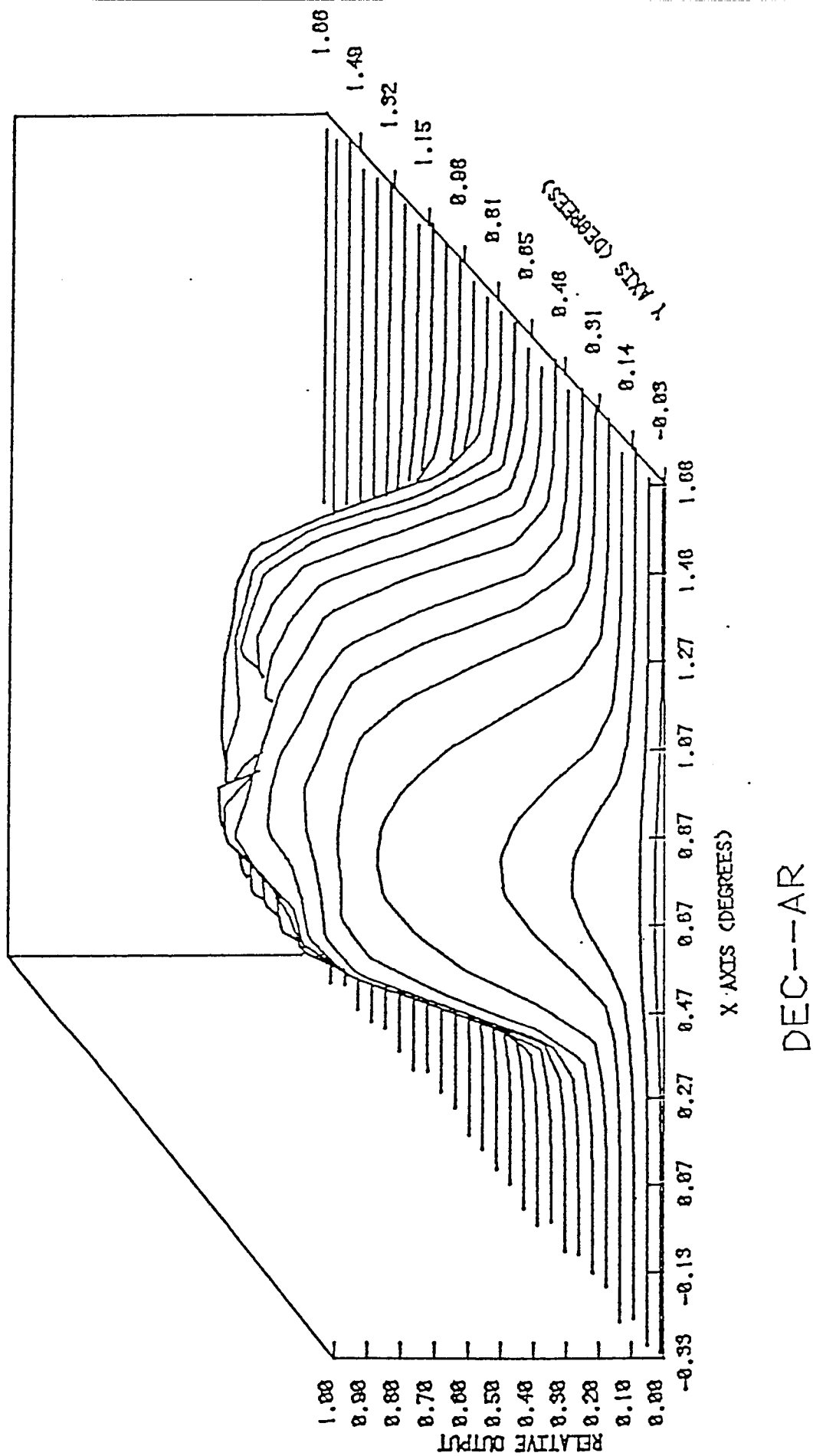


Figure E-7. Three dimensional representation of the AR field-of-view obtained with full entrance aperture.

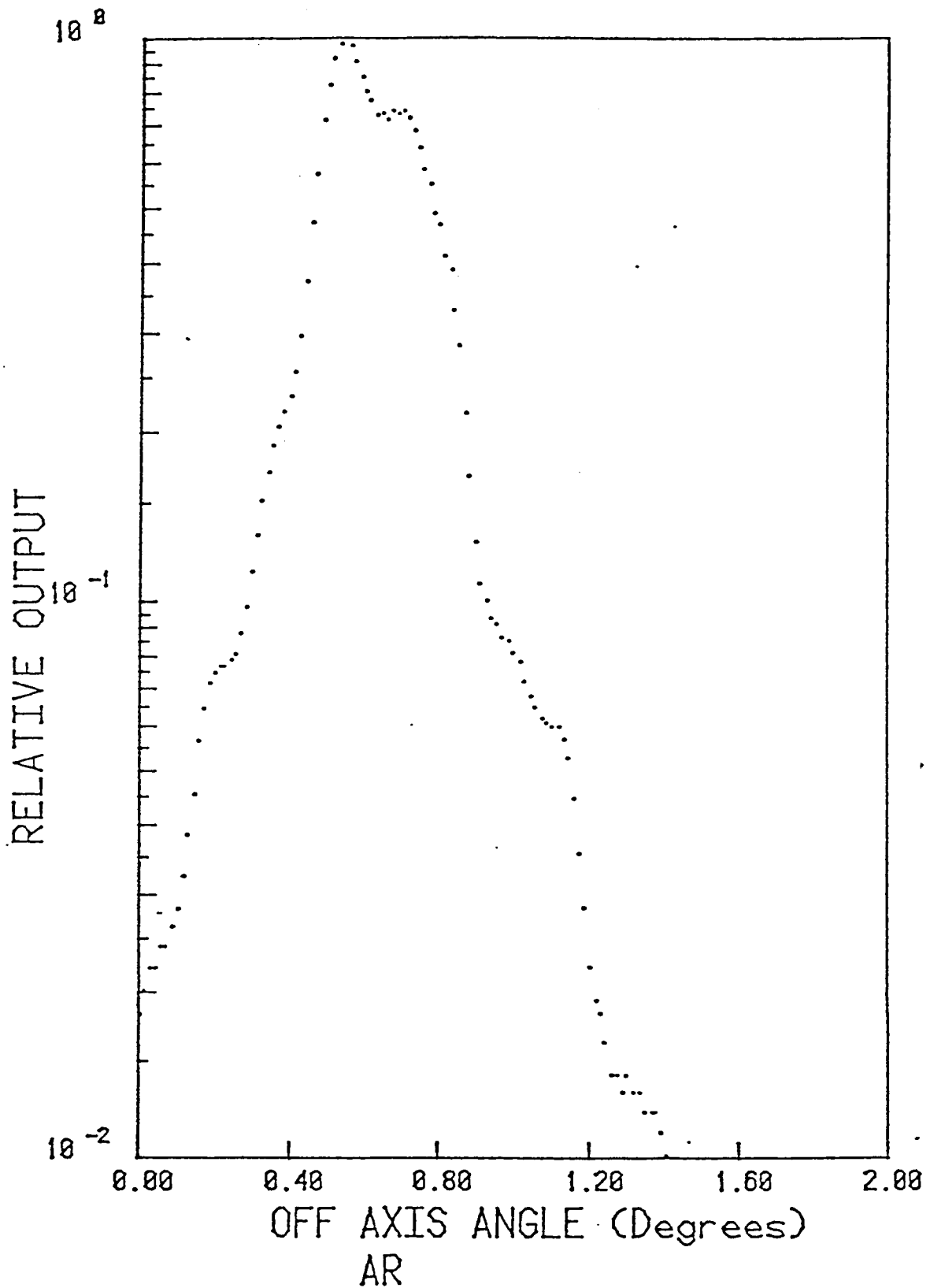


Figure E-8. The field-of-view as a cross-section is obtained with a 0.3579-inch diameter cold pinhole mounted in the entrance aperture.

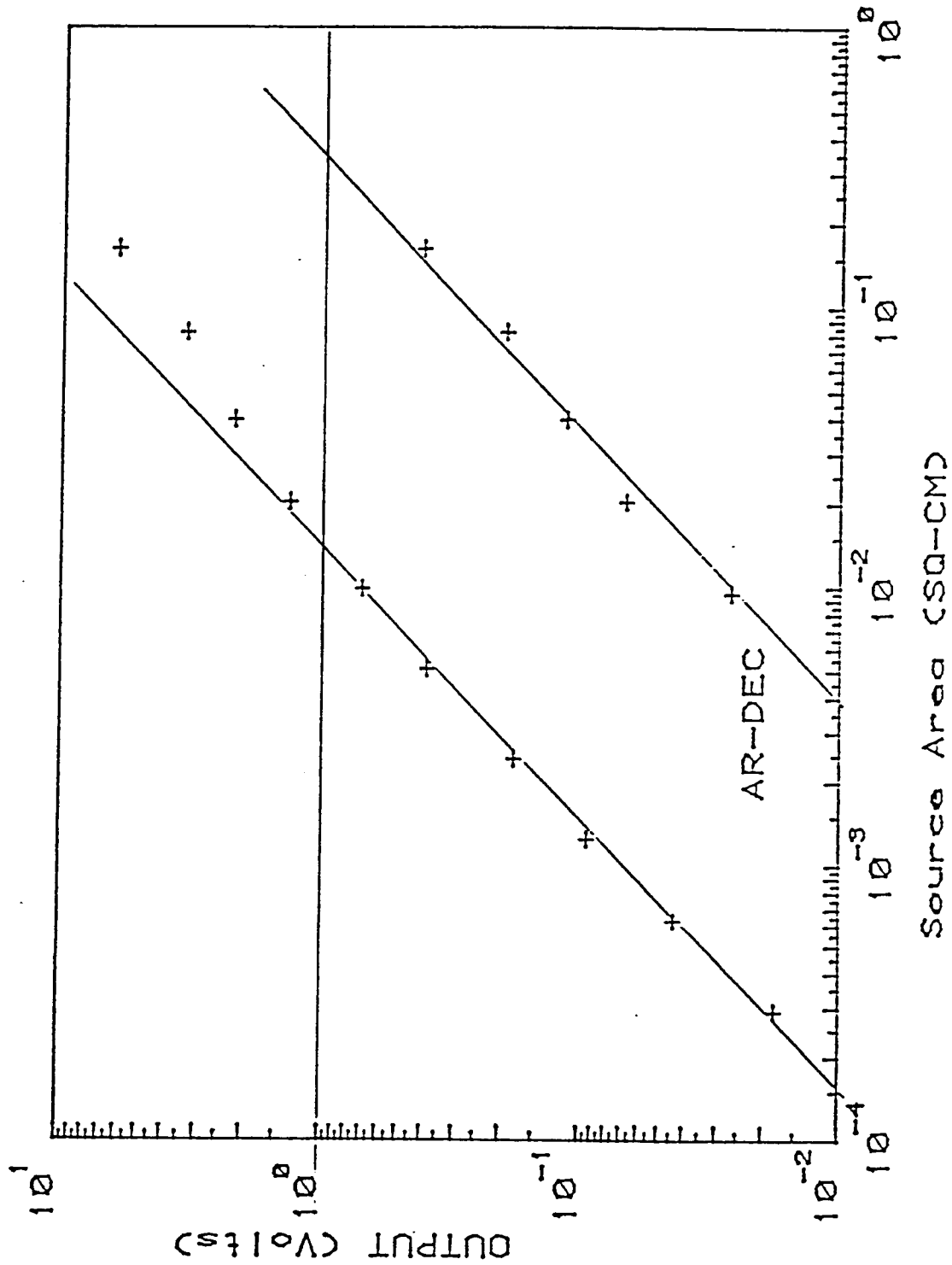


Figure E-9. Two linearity data sets obtained with the USU Cold Collimator. Note that the nonlinearity is a function of absolute signal, but not of aperture area.

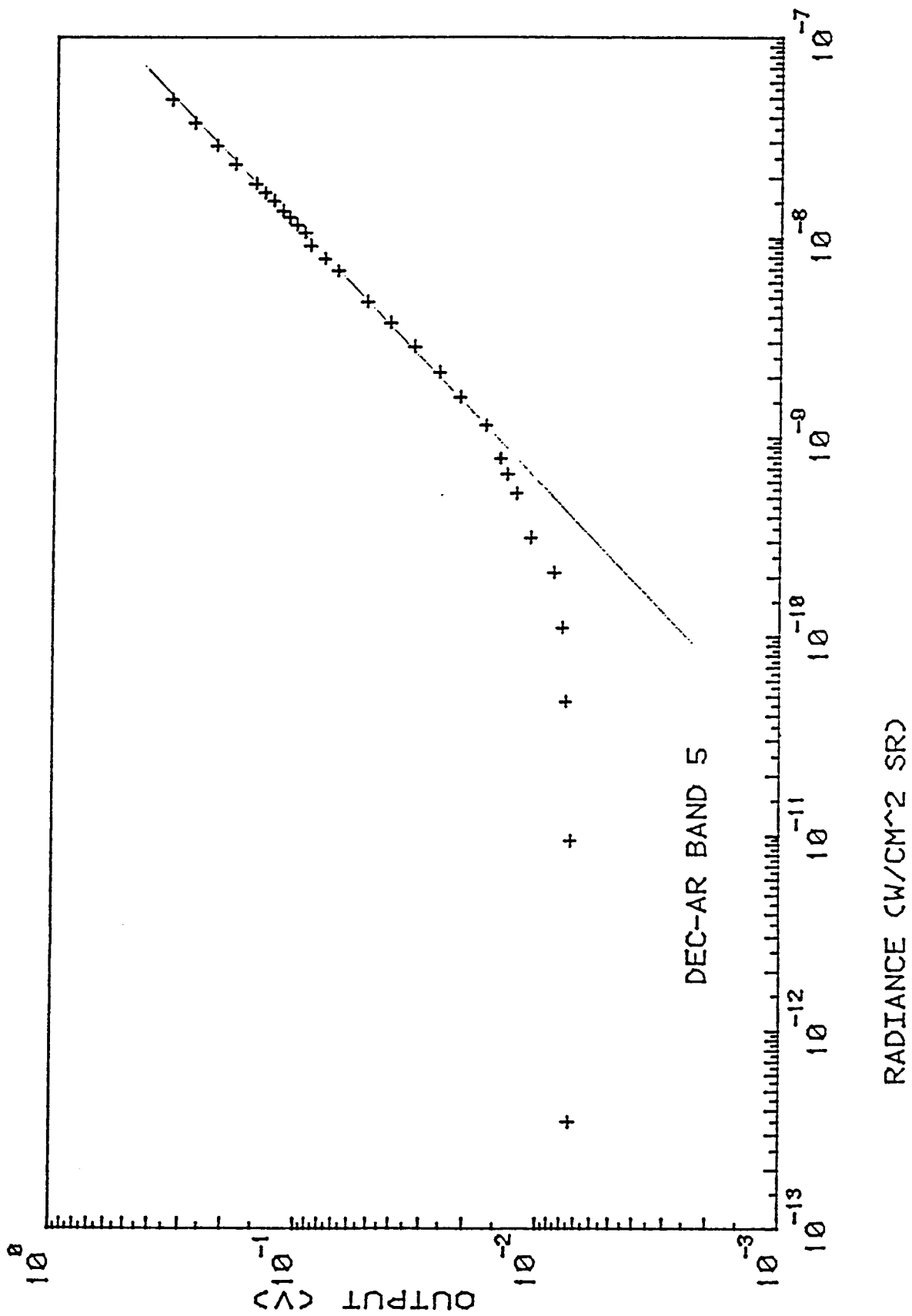


Figure E-10. A plot of extended-area calibration for Band 5 (See data points listed in Table E-4).

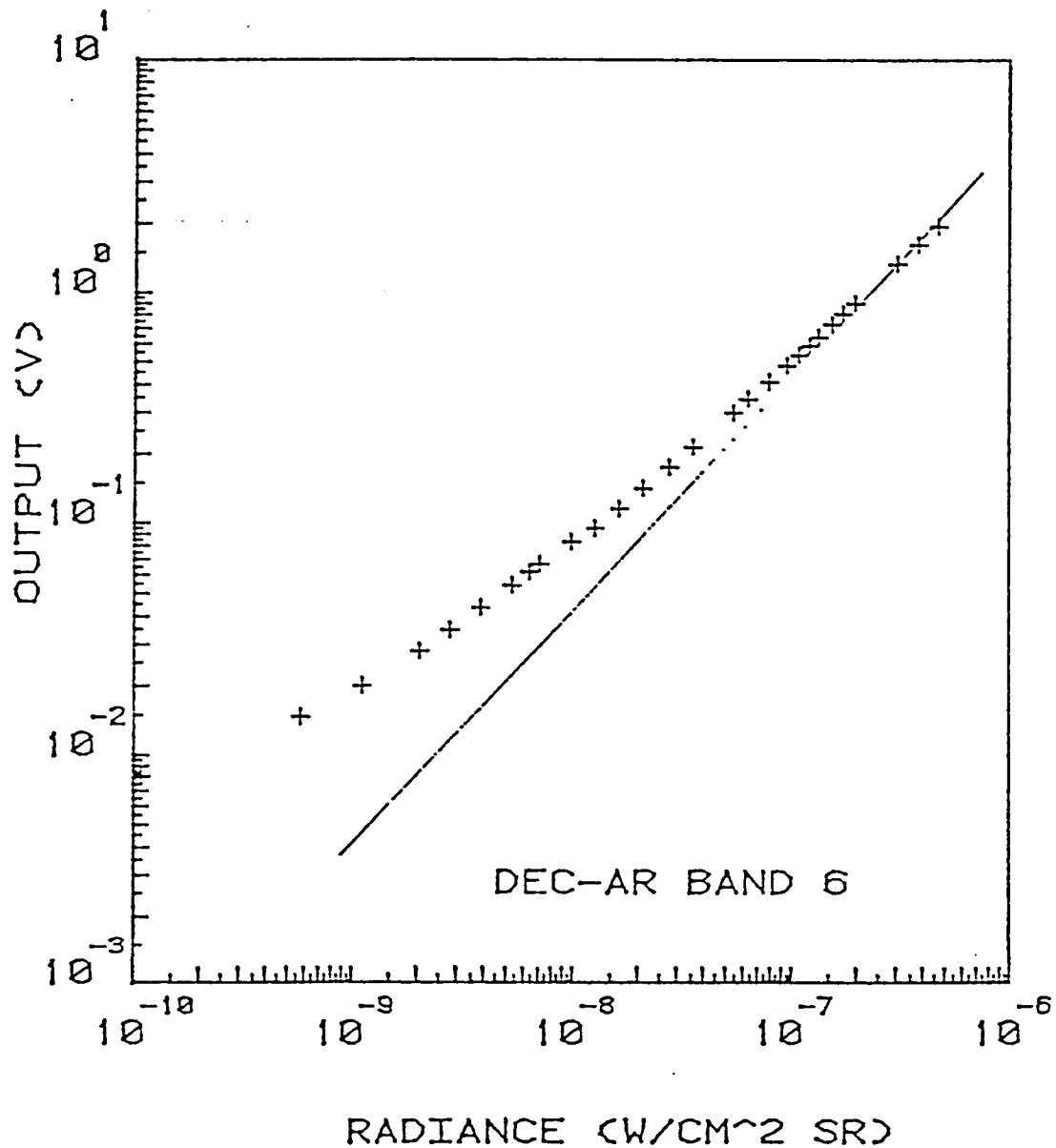


Figure E-11. The absolute calibration data total sterance [radiance] vs output voltage for Band 6 (See data points listed in Table E-5).

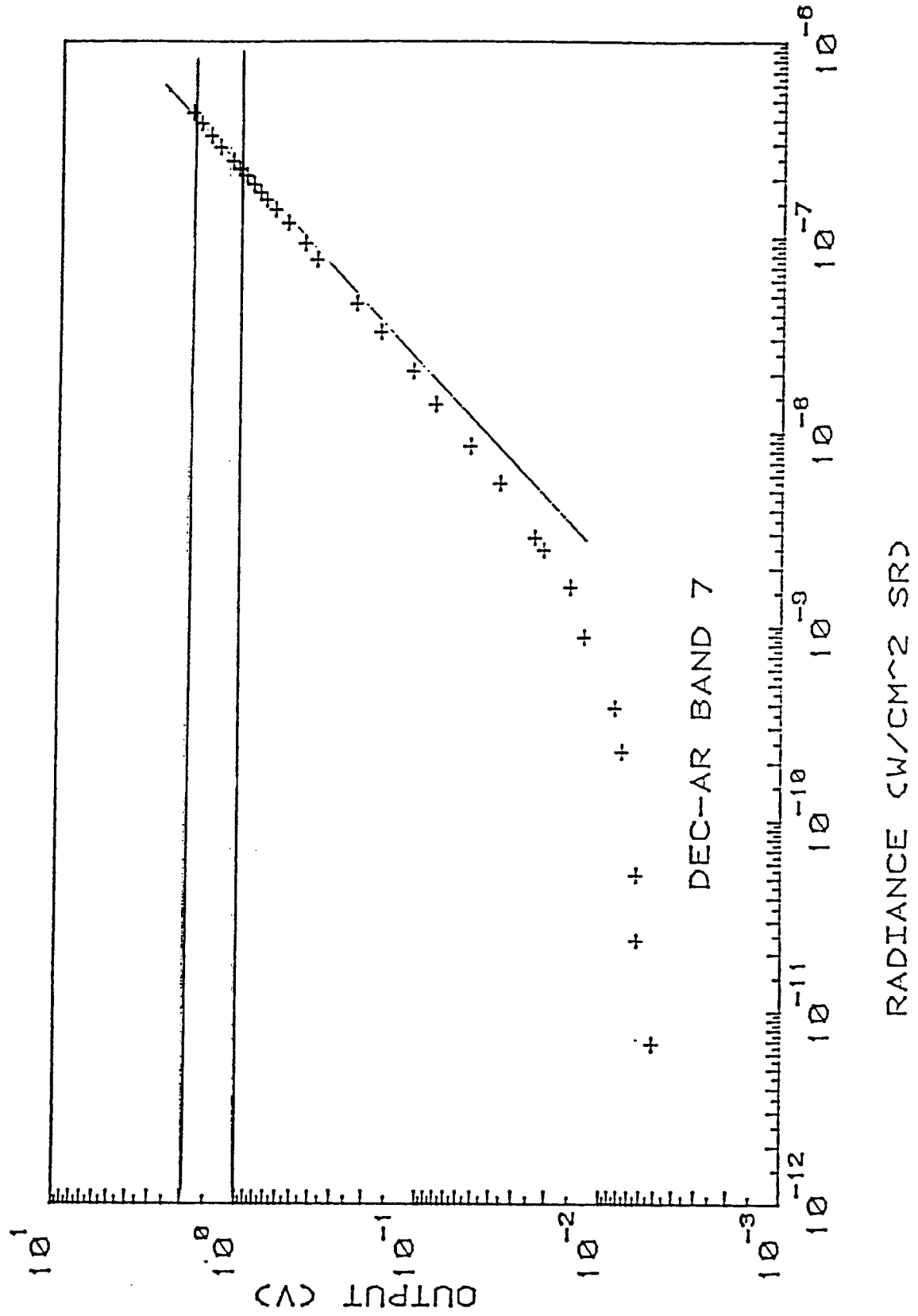


Figure E-12. The absolute calibration data total sterance [radiance] vs. output voltage data points for Band 7 (See data points listed in Table E-6).

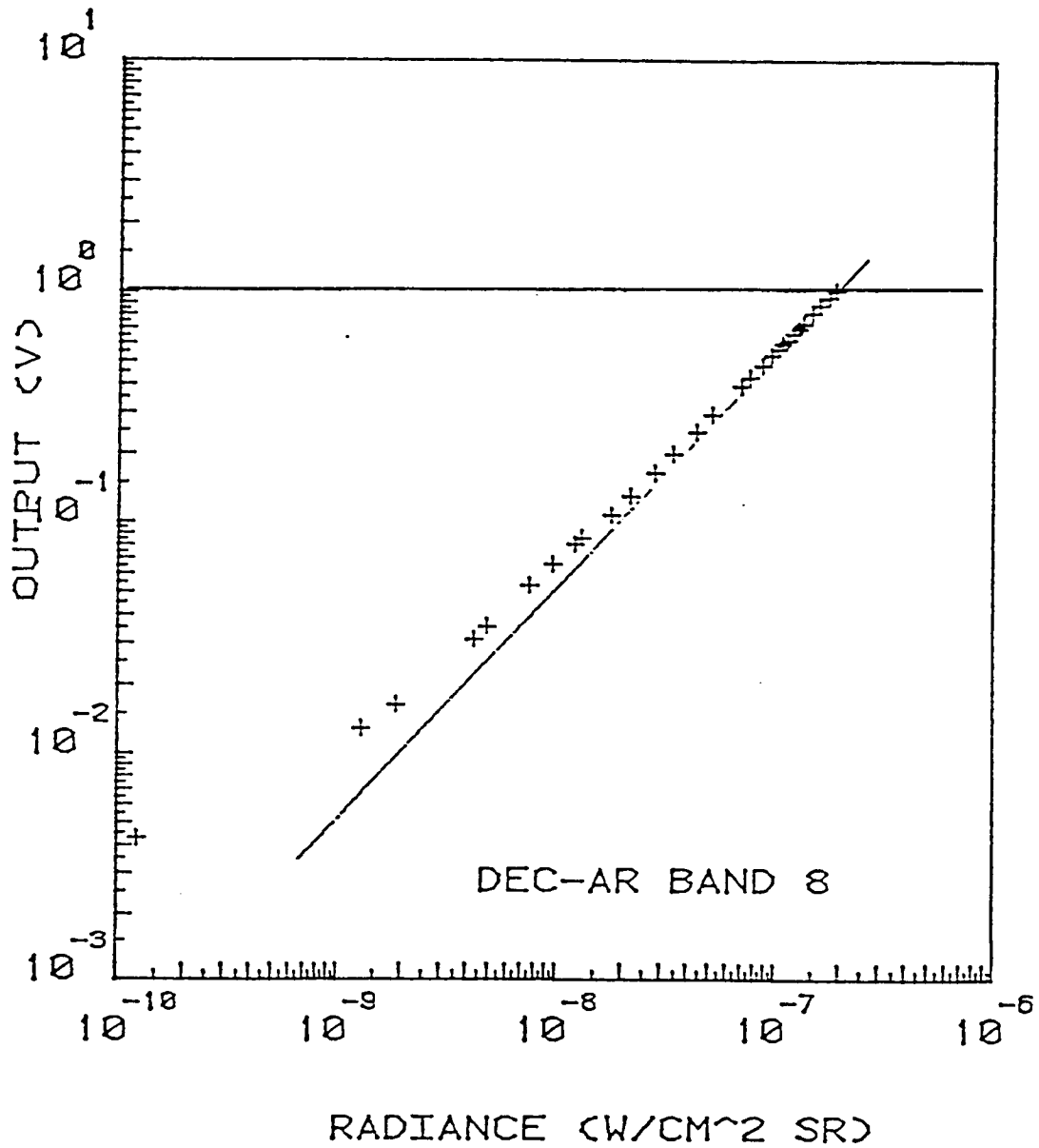


Figure E-13. The absolute calibration data total sterance [radiance] vs. output voltage data points for Band 8 (See data points listed in Table E-7).

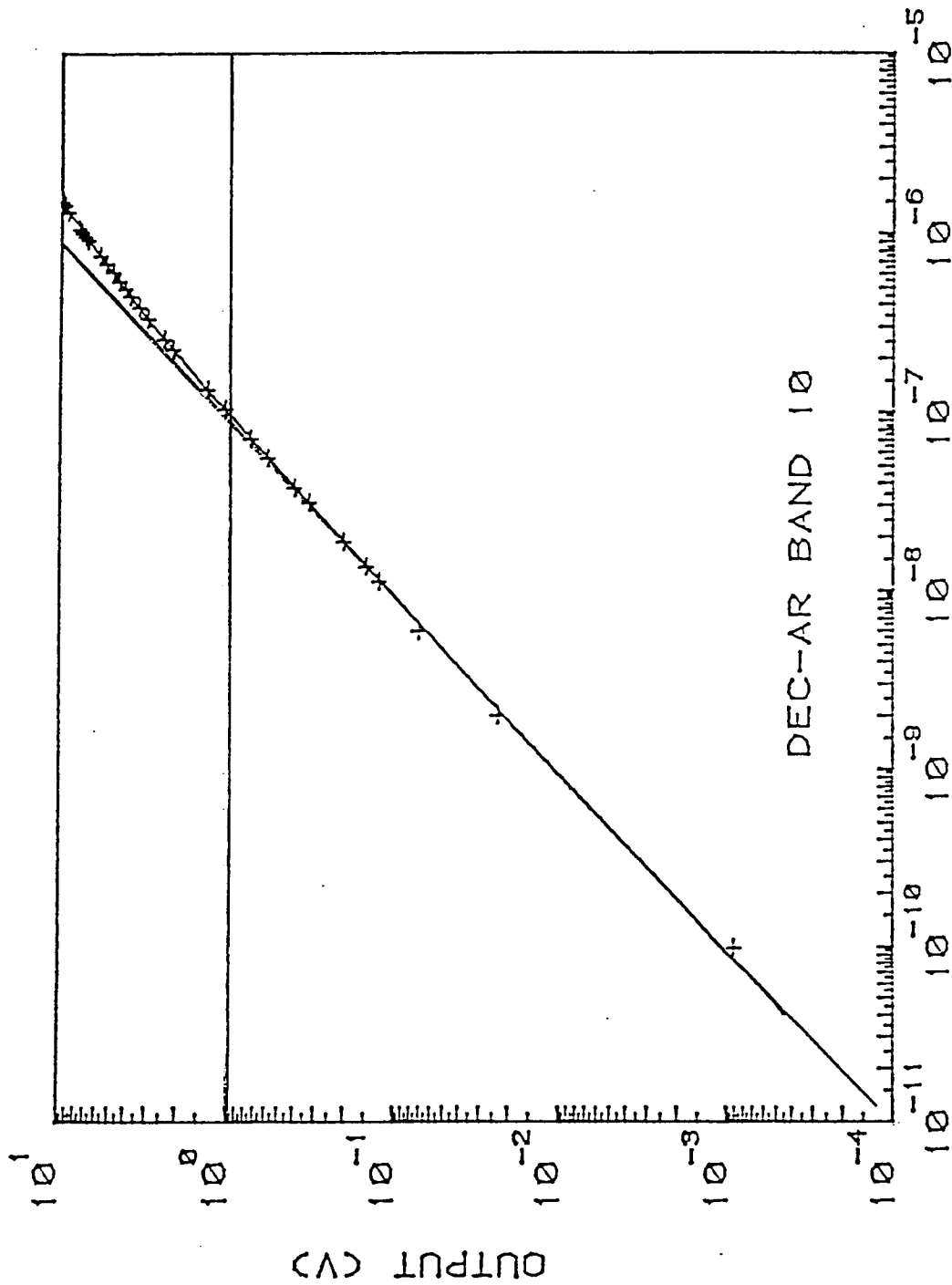


Figure E-14. The absolute calibration data sterance [radiance] vs. output voltage data points for the "open" position (Band 10) with a least squares best-fit superimposed. The data exhibit 39.2% full-scale nonlinearity and an rms error of 7.22% (See data points listed in Table E-8 and computer analysis in Table E-9).

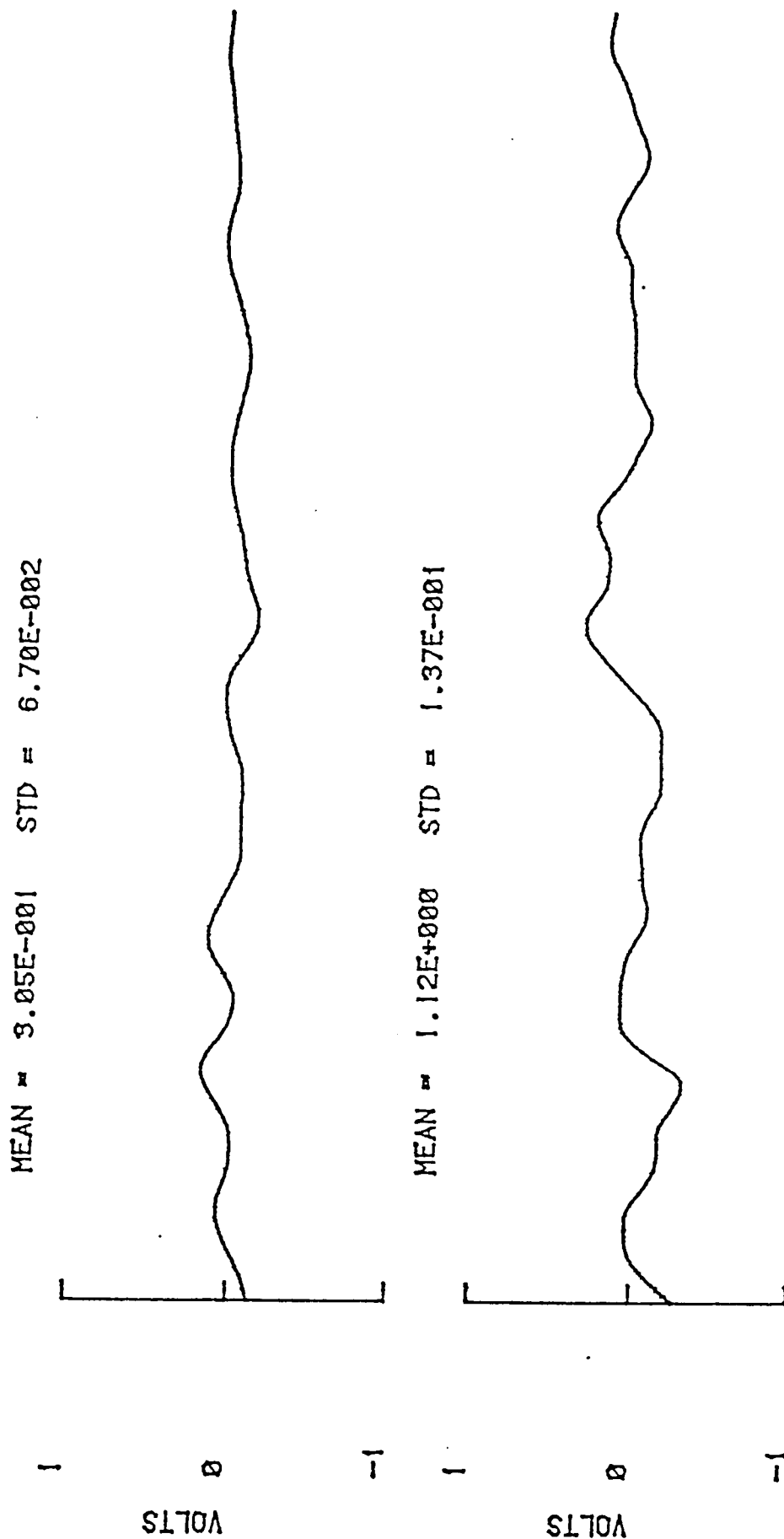
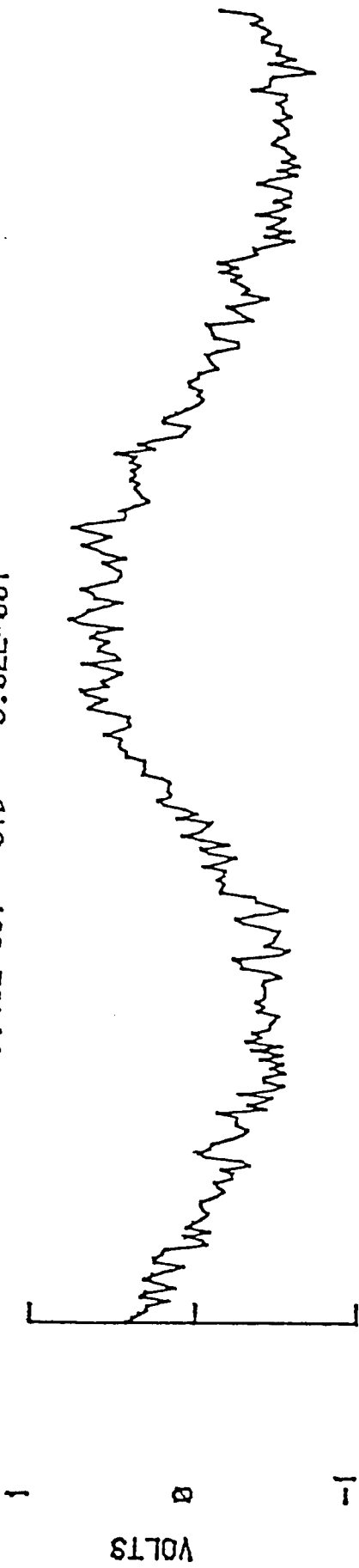


Figure E-15. Ten second dark noise scan. Top curve FTM, bottom curve AR. Note: Short term rms noise = STD (standard deviation).

MEAN = 7.45E-001 STD = 3.92E-001



MEAN = 1.92E+000 STD = 2.93E-001



Figure E-16. One hundred-fifty second dark noise scan. Top curve FTM, bottom curve AR. Note: Long term rms noise = STD (standard deviation).

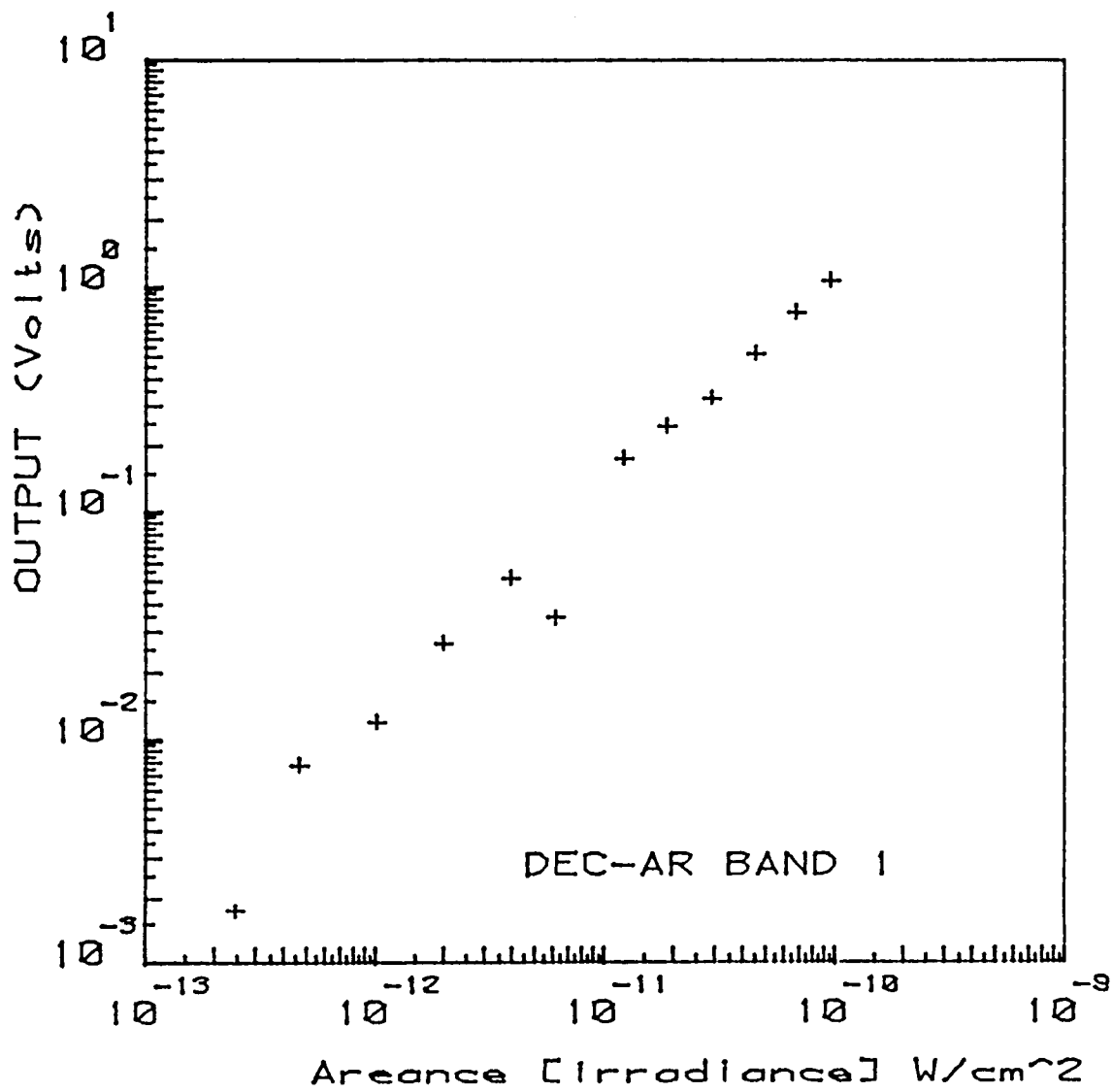


Figure E-17. Graphic plot of point source calibration for Band 1 (See data points listed in Table E-10).

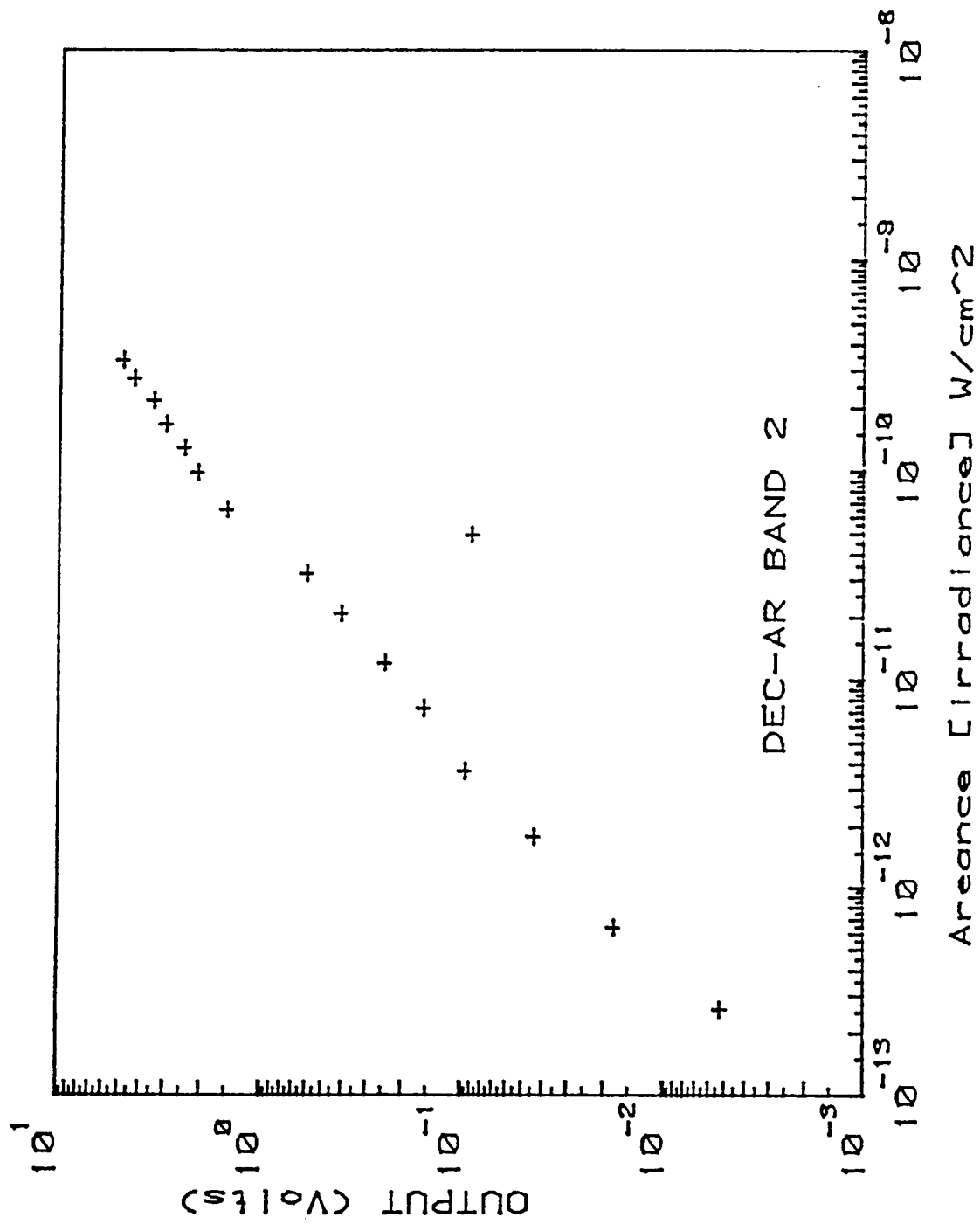


Figure E-18. Graphic plot of point source calibration for Band 2 (See data points listed in Table E-11).

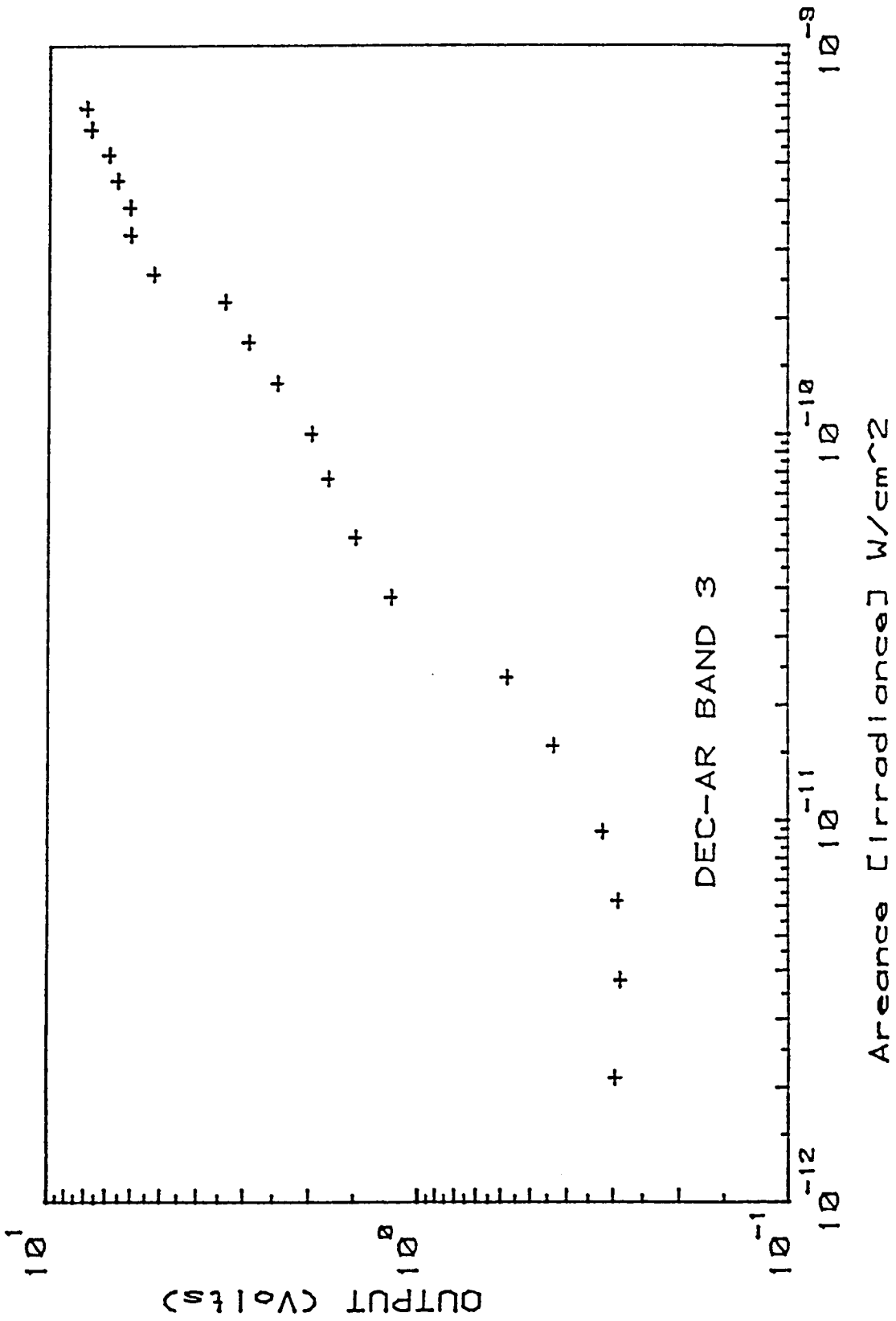


Figure E-19. Graphic plot of point source calibration for Band 3 (See data points listed in Table E-12).

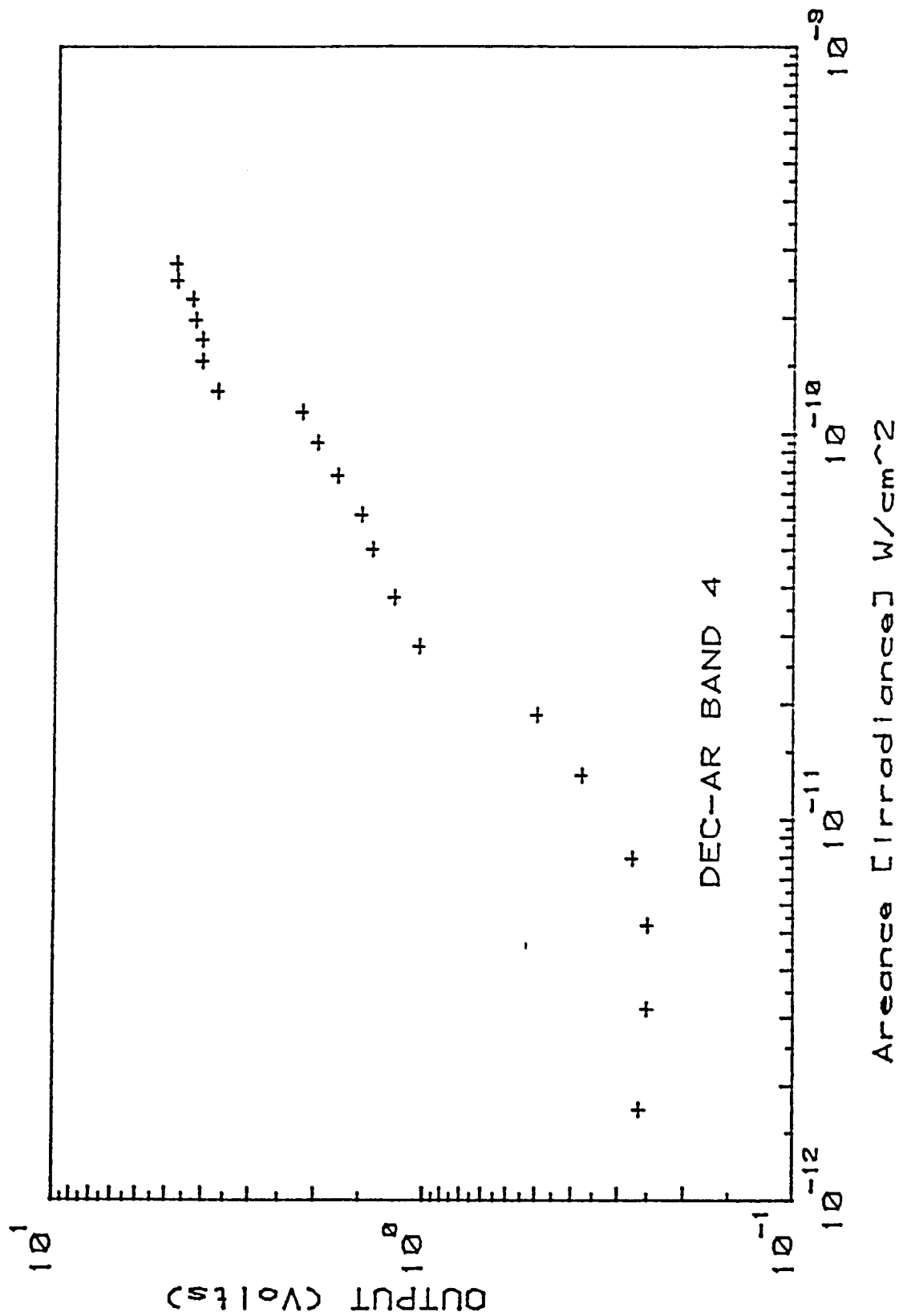


Figure E-20. Graphic plot of point source calibration for Band 4 (see data points listed in Table E-13).

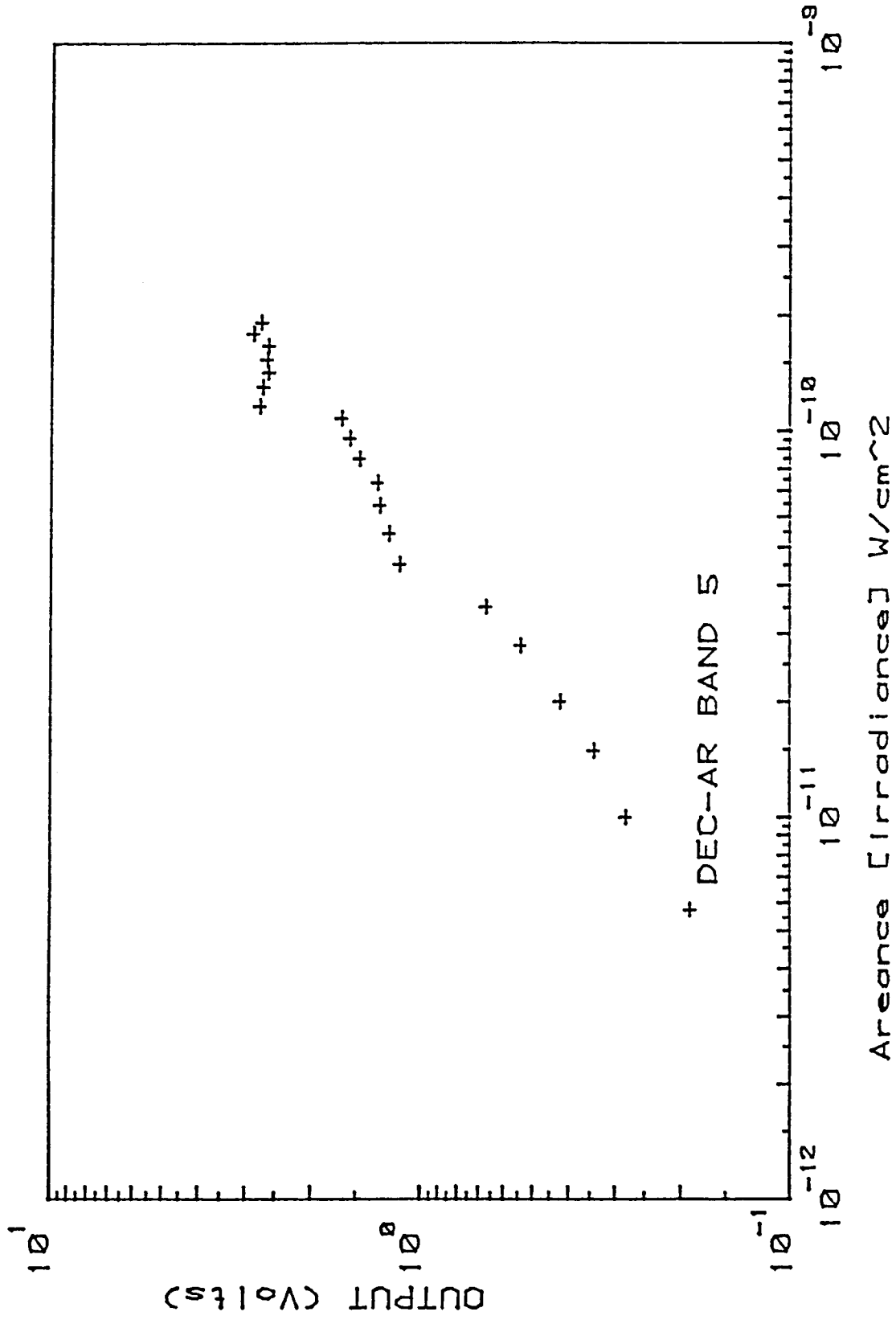


Figure E-21. Graphic plot of point source calibration for Band 5 (See data points listed in Table E-14).

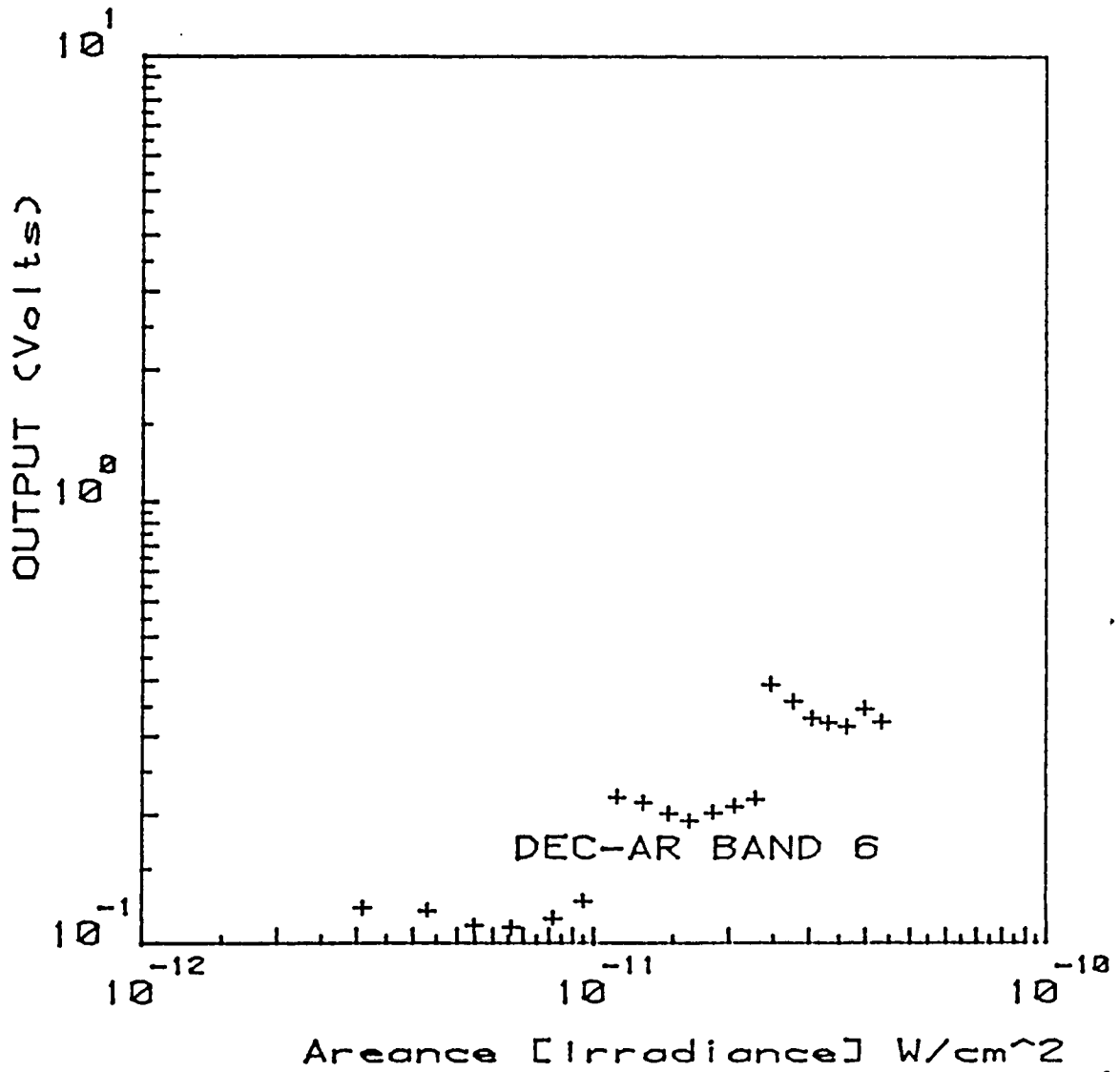


Figure E-22. Graphic plot of point source calibration for Band 6 (See data points listed in Table E-15).

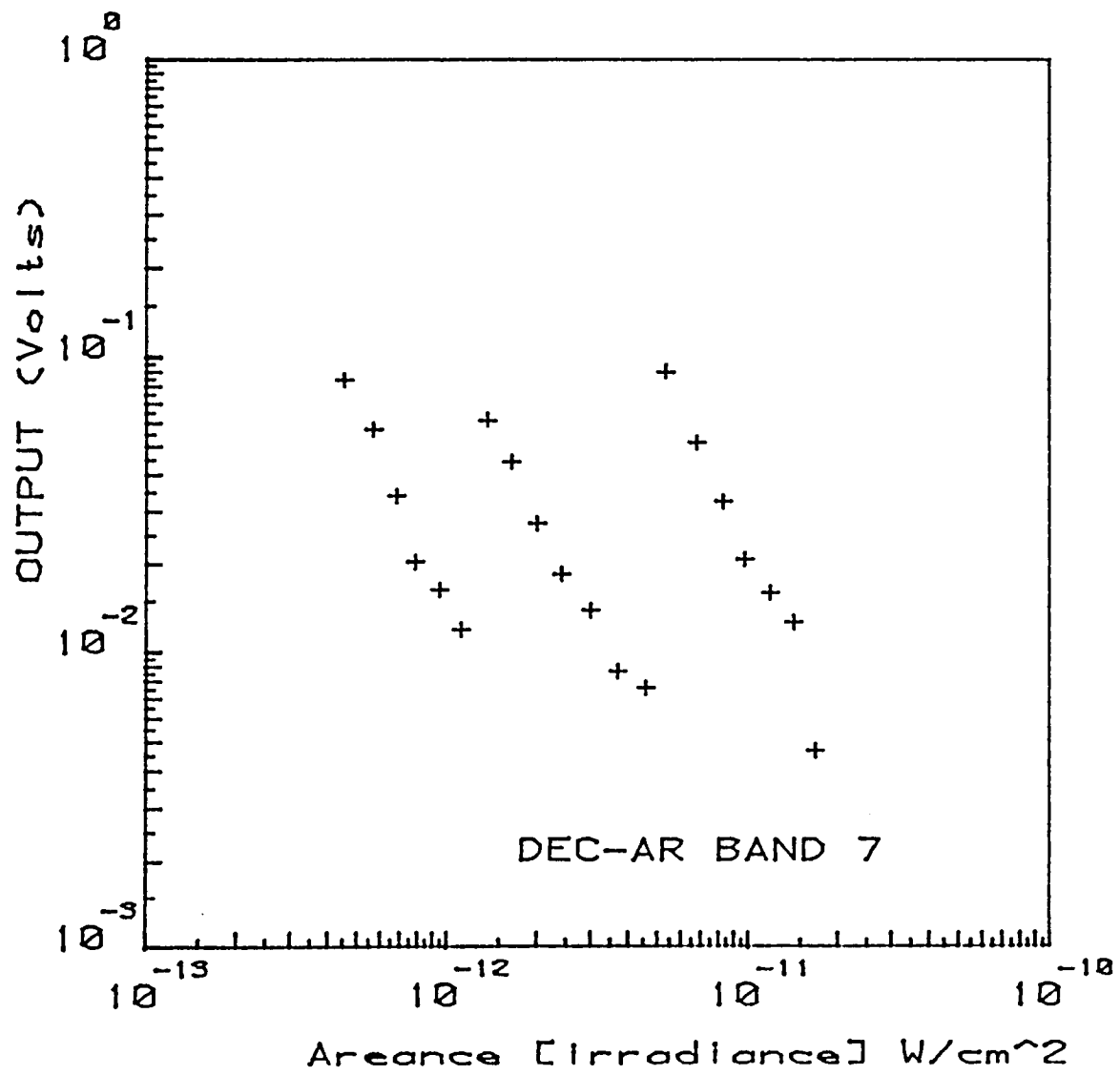


Figure E-23. Graphic plot of point source calibration for Band 7 (See data points listed in Table E-16).

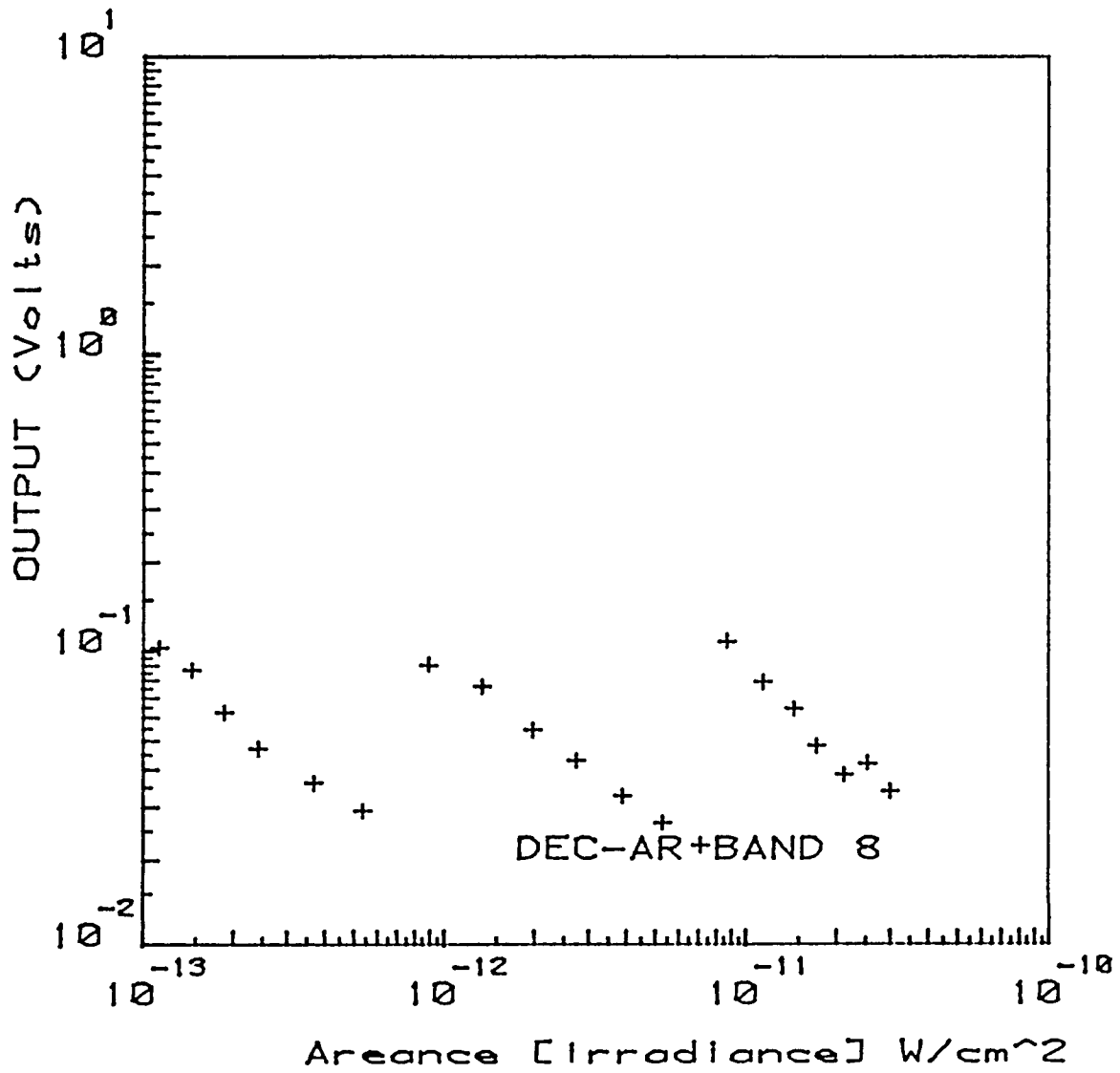


Figure E-24. Graphic plot of point source calibration for Band 8 (See data points listed in Table E-17).

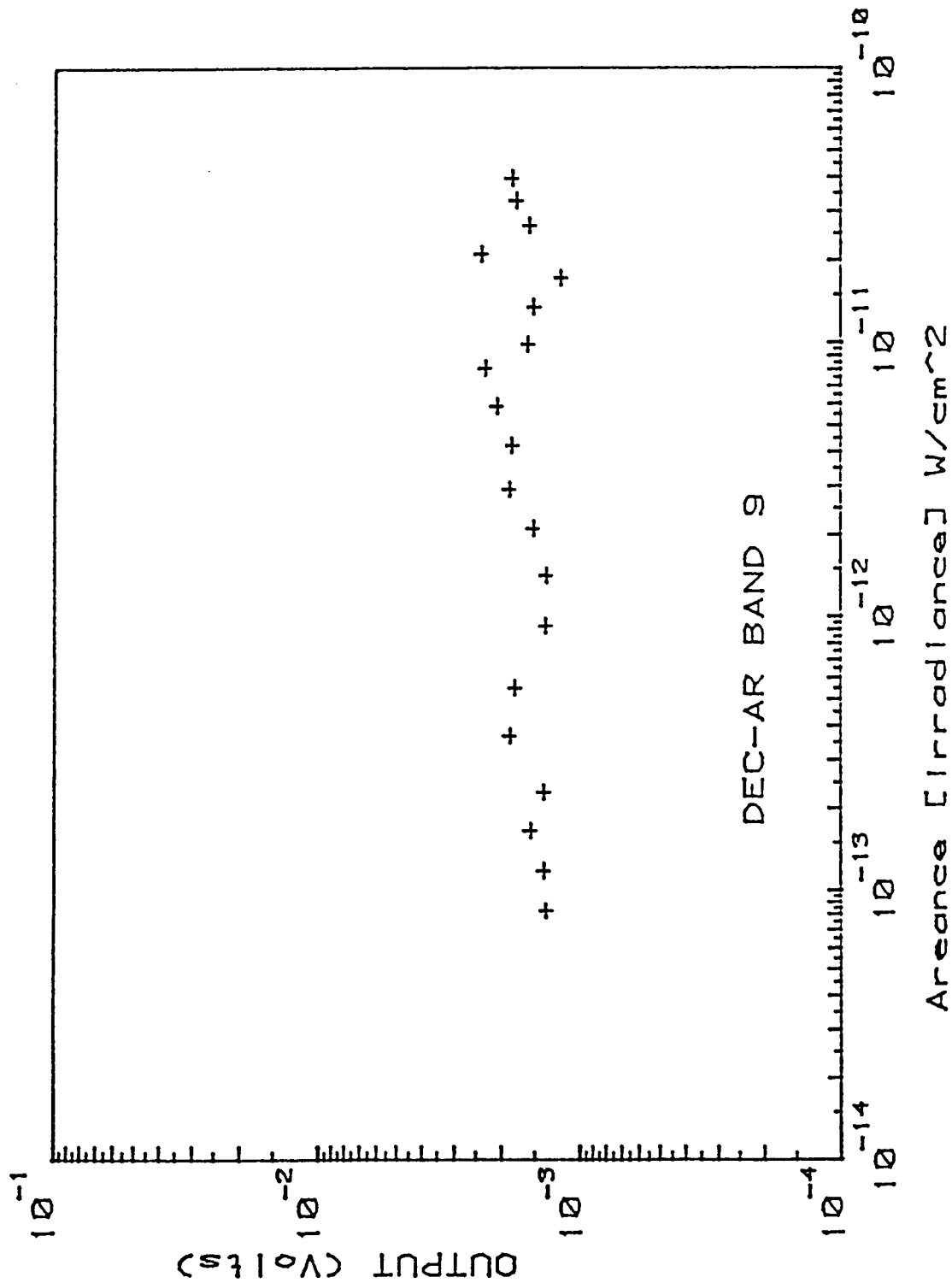


Figure E-25. Graphic plot of point source calibration for Band 9 (See data points listed in Table E-18).

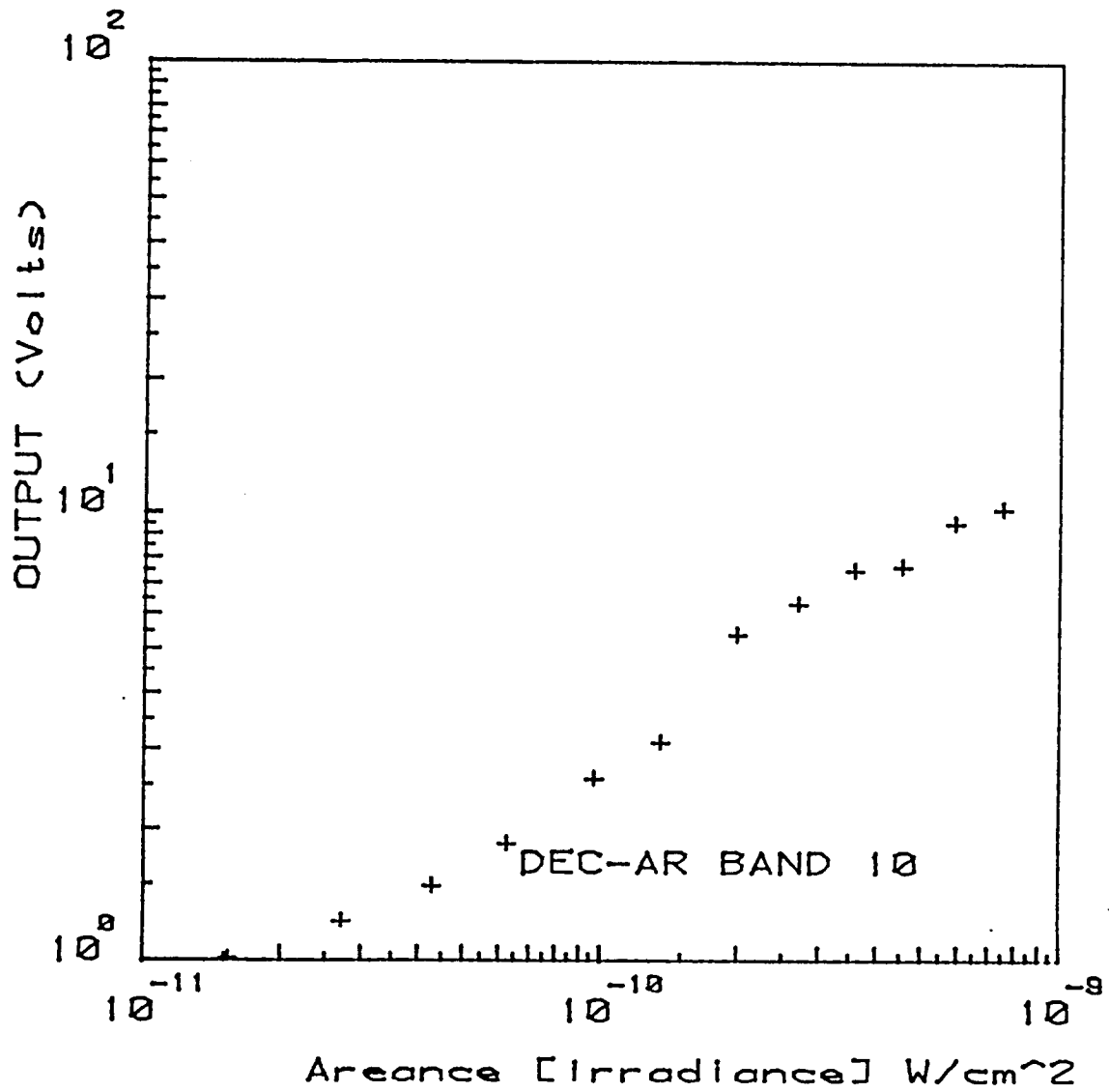


Figure E-26. Graphic plot of point source calibration for Band 10 (See data points listed in Table E-19).

APPENDIX F
Cold Test Data

This page intentionally left blank.

Introduction

This appendix describes the functional test conducted on the DEC instrument in Logan, Utah. The test was started Aug. 30, 1985 and was completed Sept. 2, 1985. The data contained herein are taken from the files listed below. These files were delivered to GSFC by USU in September 1985.

<u>Sections</u>	<u>Data from File No.</u>
100-800	08310800.CLD
902-959	08310959.CLD
960-1020	08311101.CLD
1100-1210	09011210.CLD
1211-1405	09021405.CLD

The tests documented here were set up to collect standard data sets which are called state vectors. A state vector consists of date and time, and 72 data values. There are 9 samples of rectified AR bolometer data and 9 samples of FTM bolometer data in each state vector. Integration time of the electronics is 1 second, and the 9 samples are taken at approximately 1 second time intervals. The data in this appendix contain the average of 9 samples of AR and FTM bolometer rectified signals.

There are also 9 samples each of AR bolometer DC voltage and FTM bolometer DC voltage, and 2 samples each of AR and FTM bolometer temperature sensors. Only 1 value for each of these signals are used in this appendix.

The remainder of the signals in this appendix are single data values from the state vector. There are data values in the state vector for the current flowing through each of the 5 IR sources in DEC. We felt it was not necessary to include these data in Appendix F.

There are 3 procedures which will be mentioned throughout this test description - they are defined here. They are called `Single_statevector`, `Statevector_pair` and `Bolometer_baseline`.

`Single_statevector` will refer to the process of requesting a

APPENDIX F, Page F-3

data set from the system, and saving the data in a disk file.

Statevector_pair will be the collection of two sets of data, where one set is taken with bias' turned on, and one set is taken with bias' turned off.

Bolometer_baseline will refer to a process of turning on both preamps and bias', moving all wheels in the system to the open position, and collecting a Statevector_pair. Then the Beam sample mirror is moved out of the beam, and the Mode select wheel is moved to the opaque position and a Single_statevector is collected. Next the Beam sample mirror is moved back into the beam and another Single_statevector is collected. Then the Mode select wheel is moved to the open position and a Single_statevector is collected. Finally, all wheels are moved back to the opaque position and a Statevector_pair is collected.

The following description explains each section of the functional test to help with interpretation of the results presented later in this appendix.

SECTION	DESCRIPTION
OPTICAL ZERO POINT	
100	REFERENCE POINT WITHOUT CHOPPERS 1) Bolometer_baseline before choppers are turned on.
101	LOOK FOR BACKGROUND NOT THROUGH SYSTEM 1) Turn on both choppers 2) Move all wheels to opaque positions 3) Statevector_pair 4) Move Beam sample mirror out of beam 5) 2 Statevector_pairs 6) Move all wheels to open position 7) 2 Statevector_pairs 8) Beam sample mirror into beam 9) 2 Statevector_pairs

SECTION	DESCRIPTION
102	REFERENCE WITH CHOPPERS ON 1) Bolometer_baseline
103	TEMPERATURE STABILITY 1) Move all wheels to open position 2) 5 Single_statevectors to check temperature stability
VERIFY WHEELS OPERATE ALL POSITIONS BOTH DIRECTIONS	
200	REFERENCE POINT 1) Bolometer_baseline
201	MOVE ALL WHEELS FORWARD TOGETHER 1 REVOLUTION 1) Move all wheels to position 1 2) Single_statevector 3) Increment position of all wheels 4) Single_statevector 5) continue steps 3 and 4 until position 18 is reached
202	MOVE ALL WHEELS REVERSE TOGETHER 1 REVOLUTION 1) Move all wheels to position 18 2) Single_statevector 3) Decrement position of all wheels 4) Single_statevector 5) continue steps 3 and 4 until position 1 is reached
203	MOVE ALL WHEELS FORWARD TOGETHER 1 REVOLUTION Repeat of 201
204	MOVE ALL WHEELS REVERSE TOGETHER 1 REVOLUTION Repeat of 202

SECTION	DESCRIPTION
205	MOVE ALL WHEELS FORWARD TOGETHER 1 REVOLUTION Repeat of 201
211	RUN APERTURE WHEEL WHILE OTHER WHEELS ARE IN OPEN POSITION 1) Turn on Source 2 to half power 2) Move all wheels to open position 3) 2 Single_statevectors 4) Move Aperture wheel to position 1 5) Single_statevector 6) Repeat steps 4 and 5 for positions 2 - 8 7) Increment Aperture wheel position 8) Repeat step 7 for positions 10 - 18 9) Move all wheels to open position 10) Turn Source 2 off 11) 5 Single_statevectors to show how fast system stabilizes
212	RUN FILTER WHEEL WHILE OTHER WHEELS ARE IN OPEN POSITION 1) Turn on Source 2 to half power 2) Move all wheels to open position 3) 2 Single_statevectors 4) Move Filter wheel to position 1 5) Single_statevector 6) Repeat steps 4 and 5 for position 2 7) Increment Filter wheel position 8) Repeat step 7 for positions 4 - 18 9) Move all wheels to open position 10) Turn Source 2 off 11) 5 Single_statevectors to show how fast system stabilizes

SECTION	DESCRIPTION
213	<p>RUN MODE SELECT WHEEL WHILE OTHER WHEELS ARE IN OPEN POSITION</p> <p>Repeat section 212 except Step 4) Move Mode select wheel instead of Filter wheel, and Step 7) Increment Mode select wheel instead of Filter wheel.</p>
214	<p>RUN AR FILTER WHEEL WHILE OTHER WHEELS ARE IN OPEN POSITION</p> <p>Repeat section 212 except Step 4) Move AR Filter wheel instead of Filter wheel, and Step 7) Increment AR Filter wheel instead of Filter wheel.</p>

POINTING MIRROR OPERATION AND TEMPERATURE EFFECTS

300	<p>REFERENCE POINT</p> <p>1) Bolometer_baseline</p>
301	<p>1ST MAPPING OF POINTING MIRROR</p> <p>1) Move all wheels to open position</p> <p>2) Move Pointing mirror to position (-4,-4)</p> <p>3) Single_statevector</p> <p>4) Increment X-Axis position by 1 degree</p> <p>5) Single_statevector</p> <p>6) Repeat steps 4 and 5 until data is taken with X-Axis at 4 degrees</p> <p>7) Increment Y-Axis by 1 degree</p> <p>8) Move X-Axis back to -4 degrees</p> <p>9) Repeat steps 3 - 8 until data is taken with Y-Axis at 4 degrees</p> <p>10) Turn on Source 2 to half power</p> <p>11) 5 Single_statevectors while source is stabilizing</p>

SECTION	DESCRIPTION
302	2ND MAPPING OF POINTING MIRROR
	1) Repeat all 11 steps in section 301
	2) Turn off Source 2
	3) 5 Single_statevectors while source is cooling down
	4) Move Pointing mirror to position (0,0)

POINTING MIRROR MOVE BY STEPS

400	TURN BULB ON TO SEE IF THERE ARE ANY EFFECTS
	1) Turn on Source 2 to half power
	2) Bolometer_baseline
401	STEP ACROSS DIAGONAL FROM (-4,-4)
	1) Move all wheels to open position
	2) Move Pointing mirror to position (-4,-4)
	3) Single_statevector
	4) Move Pointing mirror 900 steps X and Y Axes
	5) Single_statevector
	6) Repeat steps 4 and 5 another 8 times
402	STEP ACROSS DIAGONAL FROM (-4,4)
	1) Move Pointing mirror to position (-4,4)
	2) Single_statevector
	3) Move Pointing mirror 900 steps X Axis, and -900 steps Y Axes
	4) Single_statevector
	5) Repeat steps 4 and 5 another 8 times
	6) Turn Source off
	7) 5 Single_statevectors
	8) Move Pointing mirror to (0,0)

SECTION DESCRIPTION

**BEAM SAMPLE MIRROR OPERATION
AND TEMPERATURE EFFECTS**

- 500 REFERENCE POINT
 1) Turn Source 2 on to half power
 2) Bolometer_baseline
 3) Move all wheels to open position
 4) Single_statevector
- 501 1ST OUT/IN CYCLE OF BEAM SAMPLE MIRROR
 1) Move Beam sample mirror out of beam
 2) Single_statevector
 3) Move Beam sample mirror into beam
 4) Single_statevector
- 502 2ND OUT/IN CYCLE OF BEAM SAMPLE MIRROR
 Repeat of 501
- 503 3RD OUT/IN CYCLE OF BEAM SAMPLE MIRROR
 Repeat of 501
- 504 4TH OUT/IN CYCLE OF BEAM SAMPLE MIRROR
 Repeat of 501
- 505 5TH OUT/IN CYCLE OF BEAM SAMPLE MIRROR
 Repeat of 501
- 506 6TH OUT/IN CYCLE OF BEAM SAMPLE MIRROR
 Repeat of 501
- 507 7TH OUT/IN CYCLE OF BEAM SAMPLE MIRROR
 Repeat of 501

SECTION	DESCRIPTION
508	8TH OUT/IN CYCLE OF BEAM SAMPLE MIRROR Repeat of 501
509	9TH OUT/IN CYCLE OF BEAM SAMPLE MIRROR Repeat of 501
510	10TH OUT/IN CYCLE OF BEAM SAMPLE MIRROR Repeat of 501
511	TURN OFF SOURCE AND STABILIZE 1) Turn off Source 2 2) 5 Single_statevectors

AR AND FTM CHOPPERS OPERATION AND TEMPERATURE EFFECTS

600	REFERENCE POINT 1) Turn on Source 2 to half power 2) Bolometer_baseline 3) Move all wheels to open position 4) Single_statevector
601	1ST ON/OFF CYCLE OF CHOPPERS 1) Turn on both choppers 2) 2 Single_statevectors 3) Turn off both choppers 4) 2 Single_statevectors

SECTION	DESCRIPTION
602	2ND ON/OFF CYCLE OF CHOPPERS 1) Turn on both choppers 2) 2 Single_statevectors 3) Turn off both choppers 4) 2 Single_statevectors
603	3RD ON/OFF CYCLE OF CHOPPERS 1) Turn on both choppers 2) 2 Single_statevectors 3) Turn off both choppers 4) 2 Single_statevectors 5) Turn off Source 2 6) 5 Single_statevectors

**ALLOW SYSTEM TO
THERMALLY STABILIZE**

700	REFERENCE POINT BEFORE COLD SOAK 1) Bolometer_baseline 2) Move all wheels to open position
701	COLD SOAK WHILE MONITORING TEMPERATURES 1) Statevector_pair every 5 minutes for 1 hour

**GET ANOTHER ZERO REFERENCE
BEFORE SOURCE TESTS**

800	REFERENCE POINT 1) Bolometer_baseline
-----	------------------------------------------

SECTIONDESCRIPTIONTEST LAMPS IN DEC

- 902 STARTING POINT AND SETUP MODE SELECT WHEEL
- 1) Turn all sources off
 - 2) Move Beam sample mirror into beam
 - 3) Move all wheels to opaque position
 - 4) Statevector_pair
 - 5) Move Filter wheel to open position
 - 6) Move Mode select wheel to open position
 - 7) Single_statevector
 - 8) Move AR Filter wheel to open position
 - 9) Single_statevector
 - 10) Move Aperture wheel to 0.067" diam. aperture
 - 11) Single_statevector
 - 12) Move Aperture wheel to open position
 - 13) Single_statevector
- 903 SOURCE 2 TURNED OFF SCAN APERTURES
- 1) Move Aperture wheel to position 2 (0.00838 " diam.)
 - 2) Single_statevector
 - 3) Increment Aperture wheel position
 - 4) Single_statevector
 - 5) Repeat steps 4 and 5 until Aperture wheel is in position 4. Note: this should have continued until position 16. The test was modified to get the software working in a fast test, and this line of code was overlooked in changing back to long test.
 - 6) Move Aperture wheel to opaque position
 - 7) Move Filter wheel to opaque position
 - 8) Single_statevector
 - 9) Move all wheels to opaque position
 - 10) Statevector_pair
 - 11) Move all wheels to open position

SECTION DESCRIPTION

904 SOURCE 2 TURNED ON LOW LEVEL GENERAL BULB STUDY

- 1) Turn on Source 2 to count 511
- 2) Move Beam sample mirror into beam
- 3) Move all wheels to opaque position
- 4) Statevector_pair
- 5) Move Filter wheel to open position
- 6) Move Mode select wheel to open position
- 7) Single_statevector
- 8) Move AR Filter wheel to open position
- 9) Single_statevector
- 10) Move Aperture wheel to position 8 (0.067" diam.)
- 11) Single_statevector
- 12) Move Aperture wheel to open position
- 13) Single_statevector

905 INCREASE INTENSITY OF SOURCE 2 GENERAL BULB STUDY

Repeat of section 904 except step 1) set count to 768

906 INCREASE INTENSITY OF SOURCE 2 GENERAL BULB STUDY

Repeat of section 904 except step 1) set count to 1022

907 INCREASE INTENSITY OF SOURCE 2 GENERAL BULB STUDY

Repeat of section 904 except step 1) set count to 1533

908 INCREASE INTENSITY OF SOURCE 2 GENERAL BULB STUDY

Repeat of section 904 except step 1) set count to 2044

909 SCAN APERTURES WITH SOURCE 2 AT HALF POWER SETTING

Repeat of section 903

SECTION	DESCRIPTION
910	SPECTRAL CONTENT STUDY WITH SOURCE 2 AT HALF POWER
	1) Move Filter wheel to position 2 (Band 1)
	2) Move AR Filter wheel to position 2 (Band 1)
	3) Single_statevector
	4) Increment position of AR Filter wheel
	5) Single_statevector
	6) Repeat steps 4 and 5 until data is taken with AR Filter wheel at position 3. Note: this was supposed to be set up to scan all filter positions in AR Filter wheel, so we would continue until we reached position 9. This line of code was modified for a fast test to check the software, and it did not get changed back before test was ran.
	7) Move AR Filter wheel to open position
	8) Single_statevector
	9) Increment position of Filter wheel
	10) Repeat steps 2 - 9 until data is taken with Filter wheel at position 5. Note: this was supposed to be set up to scan all filter positions in Filter wheel, so we would continue until we reached position 12. This line of code was also modified and did not get changed back before test was ran.
	11) Move Filter wheel to open position
	12) Move AR Filter wheel to open position
	13) Single_statevector
	14) Move Aperture wheel to opaque position
	15) Move Filter wheel to opaque position
	16) Single_statevector
	17) Move all wheels to opaque position
	18) Statevector_pair
	19) Move all wheels to open position
	20) Single_statevector

SECTION	DESCRIPTION
911	<p>POLARIZATION STUDY WITH SOURCE 2 AT HALF POWER</p> <ol style="list-style-type: none"> 1) Move AR Filter wheel to pos. 12 (0 deg. polarizer) 2) Move Filter wheel to position 2 (Band 1) 3) Move Mode select wheel to open position 4) Single_statevector 5) Move Mode select wheel to pos. 4 (0 deg. polarizer) 6) Single_statevector 7) Increment position of Mode select wheel to step through the other polarizers 8) Single_statevector 9) Repeat steps 7 - 8 until data is taken with Mode select wheel in at position 7 10) Increment position of Filter wheel 11) Repeat steps 2 - 10 until data is taken with Filter wheel in position 4 12) Move Mode select wheel to open position 13) Move Filter wheel to open position 14) Move AR Filter wheel to open position 15) Single_statevector 16) Move Aperture wheel to opaque position 17) Move Filter wheel to opaque position 18) Single_statevector 19) Move all wheels to opaque position 20) Statevector_pair 21) Move all wheels to open position
912	<p>INCREASE INTENSITY OF SOURCE 2 GENERAL BULB STUDY</p> <p>Repeat of section 904 except step 1) set count to 2555</p>
913	<p>INCREASE INTENSITY OF SOURCE 2 GENERAL BULB STUDY</p> <p>Repeat of section 904 except step 1) set count to 3066</p>
914	<p>INCREASE INTENSITY OF SOURCE 2 GENERAL BULB STUDY</p> <p>Repeat of section 904 except step 1) set count to 3577</p>

SECTION	DESCRIPTION
915	INCREASE INTENSITY OF SOURCE 2 GENERAL BULB STUDY Repeat of section 904 except step 1) set count to 4088
916	SCAN APERTURES WITH SOURCE 2 AT FULL POWER Repeat of section 903
917	SPECTRAL CONTENT STUDY WITH SOURCE 2 AT FULL POWER Repeat of section 910
918	POLARIZATION STUDY WITH SOURCE 2 AT FULL POWER Repeat of section 911
919	REPEAT OF SOURCE 2 AT HALF POWER GENERAL BULB STUDY Repeat of section 904 except step 1) set count to 2044
920	REPEAT OF STARTING POINT AND SET UP MODE SELECT WHEEL Repeat of section 902 except add the following steps. to the end of section 902 14) Turn all sources off 15) 5 Single_statevectors to check for stability
922	STARTING POINT AND SETUP MODE SELECT WHEEL Repeat Section 902 except step 6) Move Mode select wheel to position 17 (0.134" diam.). This will give us a set of data with less power in beam so if the earlier set saturates during any part of the test
923	REPEAT OF BULB TEST FOR SOURCE 3 TURNED ON LOW LEVEL GENERAL BULB STUDY Repeat of Section 904 except step 1) Turn on Source 3 in place of Source 2

SECTION	DESCRIPTION
924	INCREASE INTENSITY OF SOURCE 3 GENERAL BULB STUDY Repeat of section 905 except step 1) Turn on Source 3 in place of Source 2
925	INCREASE INTENSITY OF SOURCE 3 GENERAL BULB STUDY Repeat of section 906 except step 1) Turn on Source 3 in place of Source 2
926	INCREASE INTENSITY OF SOURCE 3 GENERAL BULB STUDY Repeat of section 907 except step 1) Turn on Source 3 in place of Source 2
927	INCREASE INTENSITY OF SOURCE 3 GENERAL BULB STUDY Repeat of section 908 except step 1) Turn on Source 3 in place of Source 2
928	INCREASE INTENSITY OF SOURCE 3 GENERAL BULB STUDY Repeat of section 912 except step 1) Turn on Source 3 in place of Source 2
929	INCREASE INTENSITY OF SOURCE 3 GENERAL BULB STUDY Repeat of section 913 except step 1) Turn on Source 3 in place of Source 2
930	INCREASE INTENSITY OF SOURCE 3 GENERAL BULB STUDY Repeat of section 914 except step 1) Turn on Source 3 in place of Source 2
931	INCREASE INTENSITY OF SOURCE 3 GENERAL BULB STUDY Repeat of section 915 except step 1) Turn on Source 3 in place of Source 2

SECTION	DESCRIPTION
932	REPEAT OF SOURCE 3 AT HALF POWER GENERAL BULB STUDY Repeat of section 919 except step 1) Turn on Source 3 in place of Source 2
933	REPEAT OF STARTING POINT AND SET UP MODE SELECT WHEEL Repeat of section 920
935	STARTING POINT AND SETUP MODE SELECT WHEEL Repeat Section 902 except step 6) Move Mode select wheel to position 2 (Point source mode). This will give us a set of data in the Point source mode to check beam power.
936	REPEAT OF BULB TEST FOR SOURCE 2 + SOURCE 3 TURNED ON LOW LEVEL GENERAL BULB STUDY Repeat of Section 904 except step 1) Turn on Source 2 and Source 3 in place of Source 2
937	INCREASE INTENSITY OF SOURCE 2 + SOURCE 3 GENERAL BULB STUDY Repeat of section 905 except step 1) Turn on Source 2 and Source 3 in place of Source 2
938	INCREASE INTENSITY OF SOURCE 2 + SOURCE 3 GENERAL BULB STUDY Repeat of section 906 except step 1) Turn on Source 2 and Source 3 in place of Source 2
939	INCREASE INTENSITY OF SOURCE 2 + SOURCE 3 GENERAL BULB STUDY Repeat of section 907 except step 1) Turn on Source 2 and Source 3 in place of Source 2

SECTION	DESCRIPTION
940	INCREASE INTENSITY OF SOURCE 2 + SOURCE 3 GENERAL BULB STUDY Repeat of section 908 except step 1) Turn on Source 2 and Source 3 in place of Source 2
941	INCREASE INTENSITY OF SOURCE 2 + SOURCE 3 GENERAL BULB STUDY Repeat of section 912 except step 1) Turn on Source 2 and Source 3 in place of Source 2
942	INCREASE INTENSITY OF SOURCE 2 + SOURCE 3 GENERAL BULB STUDY Repeat of section 913 except step 1) Turn on Source 2 and Source 3 in place of Source 2
943	INCREASE INTENSITY OF SOURCE 2 + SOURCE 3 GENERAL BULB STUDY Repeat of section 914 except step 1) Turn on Source 2 and Source 3 in place of Source 2
944	INCREASE INTENSITY OF SOURCE 2 + SOURCE 3 GENERAL BULB STUDY Repeat of section 915 except step 1) Turn on Source 2 and Source 3 in place of Source 2
945	REPEAT OF SOURCE 2 + SOURCE 3 AT HALF POWER GENERAL BULB STUDY Repeat of section 919 except step 1) Turn on Source 2 and Source 3 in place of Source 2
946	REPEAT OF STARTING POINT AND SETUP MODE SELECT WHEEL Repeat of section 920

SECTION	DESCRIPTION
948	STARTING POINT AND SETUP MODE SELECT WHEEL Repeat Section 902 except step 6) Move Mode select wheel to position 3 (Open).
949	SCAN APERTURES WITH SOURCE 4 TURNED OFF Repeat of section 903
950	REPEAT OF BULB TEST FOR SOURCE 4 TURNED ON LOW LEVEL GENERAL BULB STUDY Repeat of Section 904 except step 1) Turn on Source 4 in place of Source 2
951	INCREASE INTENSITY OF SOURCE 4 GENERAL BULB STUDY Repeat of section 905 except step 1) Turn on Source 4 in place of Source 2
952	INCREASE INTENSITY OF SOURCE 4 GENERAL BULB STUDY Repeat of section 906 except step 1) Turn on Source 4 in place of Source 2
953	INCREASE INTENSITY OF SOURCE 4 GENERAL BULB STUDY Repeat of section 907 except step 1) Turn on Source 4 in place of Source 2
954	INCREASE INTENSITY OF SOURCE 4 GENERAL BULB STUDY Repeat of section 908 (except step 1) Turn on Source 4 in place of Source 2
955	SCAN APERTURES WITH SOURCE 4 AT HALF POWER SETTING Repeat of section 903
956	SPECTRAL CONTENT STUDY WITH SOURCE 4 AT HALF POWER Repeat of section 910

SECTION	DESCRIPTION
957	POLARIZATION STUDY WITH SOURCE 4 AT HALF POWER Repeat of section 911
958	INCREASE INTENSITY OF SOURCE 4 GENERAL BULB STUDY Repeat of section 912
959	INCREASE INTENSITY OF SOURCE 4 GENERAL BULB STUDY Repeat of section 913
960	INCREASE INTENSITY OF SOURCE 4 GENERAL BULB STUDY Repeat of section 914
961	INCREASE INTENSITY OF SOURCE 4 GENERAL BULB STUDY Repeat of section 915
962	SCAN APERTURES WITH SOURCE 4 AT FULL POWER Repeat of section 903
963	SPECTRAL CONTENT STUDY WITH SOURCE 4 AT FULL POWER Repeat of section 910
964	POLARIZATION STUDY WITH SOURCE 4 AT FULL POWER Repeat of section 911
965	REPEAT OF SOURCE 4 AT HALF POWER GENERAL BULB STUDY Repeat of section 919
966	REPEAT OF STARTING POINT AND SETUP MODE SELECT WHEEL Repeat of section 920

SECTION	DESCRIPTION
968	STARTING POINT AND SETUP MODE SELECT WHEEL Repeat Section 902 except step 6) Move Mode select wheel to position 17 (0.134" diam.). This will give us a set of data with less power in beam in case the earlier set saturates during any part of the test
969	REPEAT OF BULB TEST FOR SOURCE 5 TURNED ON LOW LEVEL GENERAL BULB STUDY Repeat of Section 904 except step 1) Turn on Source 5 in place of Source 2
970	INCREASE INTENSITY OF SOURCE 5 GENERAL BULB STUDY Repeat of section 905 except step 1) Turn on Source 5 in place of Source 2
971	INCREASE INTENSITY OF SOURCE 5 GENERAL BULB STUDY Repeat of section 906 except step 1) Turn on Source 5 in place of Source 2
972	INCREASE INTENSITY OF SOURCE 5 GENERAL BULB STUDY Repeat of section 907 except step 1) Turn on Source 5 in place of Source 2
973	INCREASE INTENSITY OF SOURCE 5 GENERAL BULB STUDY Repeat of section 908 except step 1) Turn on Source 5 in place of Source 2
974	INCREASE INTENSITY OF SOURCE 5 GENERAL BULB STUDY Repeat of section 912 except step 1) Turn on Source 5 in place of Source 2
975	INCREASE INTENSITY OF SOURCE 5 GENERAL BULB STUDY Repeat of section 913 except step 1) Turn on Source 5 in place of Source 2

SECTION	DESCRIPTION
976	INCREASE INTENSITY OF SOURCE 5 GENERAL BULB STUDY Repeat of section 914 except step 1) Turn on Source 5 in place of Source 2
977	INCREASE INTENSITY OF SOURCE 5 GENERAL BULB STUDY Repeat of section 915 except step 1) Turn on Source 5 in place of Source 2
978	REPEAT OF SOURCE 5 AT HALF POWER GENERAL BULB STUDY Repeat of section 919 except step 1) Turn on Source 5 in place of Source 2
979	REPEAT OF STARTING POINT AND SETUP MODE SELECT WHEEL Repeat of section 920

CYCLE LAMPS ON FULL POWER
TO OFF FOR RELIABILITY

- 1000 BASELINE AND SET UP FOR TEST
- 1) Bolometer_baseline
 - 2) Move all wheels to open position
 - 3) Move Mode select wheel to position 2 (Point Source Mode)
- 1001 CYCLE SOURCE 2 AND SOURCE 3
- 1) Turn Source 2 and Source 3 on to full power
 - 2) 2 Single_statevectors
 - 3) Turn Source 2 and Source 3 off
 - 4) 5 Single_statevectors as system stabilizes

C-5

SECTION	DESCRIPTION
1002	CYCLE SOURCE 2 AND SOURCE 3 Repeat of Section 1001
1003	CYCLE SOURCE 2 AND SOURCE 3 Repeat of Section 1001
1004	CYCLE SOURCE 2 AND SOURCE 3 Repeat of Section 1001
1005	CYCLE SOURCE 2 AND SOURCE 3 Repeat of Section 1001
1006	CYCLE SOURCE 2 AND SOURCE 3 Repeat of Section 1001
1007	CYCLE SOURCE 2 AND SOURCE 3 Repeat of Section 1001
1008	CYCLE SOURCE 2 AND SOURCE 3 Repeat of Section 1001
1009	CYCLE SOURCE 2 AND SOURCE 3 Repeat of Section 1001
1010	CYCLE SOURCE 2 AND SOURCE 3 Repeat of Section 1001
1011	CYCLE SOURCE 4 AND SOURCE 5 1) Turn Source 4 and Source 5 on to full power 2) 2 Single_statevectors 3) Turn Source 4 and Source 5 off 4) 5 Single_statevectors as system stabilizes

<u>SECTION</u>	<u>DESCRIPTION</u>
1012	CYCLE SOURCE 4 AND SOURCE 5 Repeat of Section 1011
1013	CYCLE SOURCE 4 AND SOURCE 5 Repeat of Section 1011
1014	CYCLE SOURCE 4 AND SOURCE 5 Repeat of Section 1011
1015	CYCLE SOURCE 4 AND SOURCE 5 Repeat of Section 1011
1016	CYCLE SOURCE 4 AND SOURCE 5 Repeat of Section 1011
1017	CYCLE SOURCE 4 AND SOURCE 5 Repeat of Section 1011
1018	CYCLE SOURCE 4 AND SOURCE 5 Repeat of Section 1011
1019	CYCLE SOURCE 4 AND SOURCE 5 Repeat of Section 1011
1020	CYCLE SOURCE 4 AND SOURCE 5 Repeat of Section 1011

SECTION DESCRIPTION

**SYSTEM COLD SOAK FOLLOWING
BULB TESTS
TO ALLOW SYSTEM TO STABILIZE**

- 1100 REFERENCE POINT
- 1) Bolometer_baseline
 - 2) Move all wheels to open position
- 1101 EVERYTHING OFF EXCEPT PREAMPS FOR 1 HOUR THEN GET
REFERENCE POINT
- 1) Turn everything off except preamps
 - 2) Wait for 1 hour to pass
 - 3) Bolometer_baseline
 - 4) Move all wheels to opaque position
 - 5) Statevector_pair
 - 6) Move Beam sample mirror out of beam
 - 7) 2 Statevector_pairs
 - 8) Move all wheels to open positions
 - 9) 2 Statevector_pairs
 - 10) Move Beam sample mirror into beam
 - 11) 2 Statevector_pairs
 - 12) Bolometer_baseline
 - 13) Move all wheels to opaque positions
 - 14) 5 Single_statevectors

LARGE AREA SOURCE TESTS

- 1200 REFERENCE STARTING POINT
- 1) Bolometer_baseline

SECTION	DESCRIPTION
1201	<p>SET NEW TEMPERATURE AND WAIT FOR SOURCE TO REACH NEW TEMPERATURE</p> <ol style="list-style-type: none"> 1) Set Source 1 to 10 degrees kelvin 2) Move all wheels to open position 3) Move Beam sample mirror into beam 4) Continue to take Single_statevectors until the temperature of the source reaches the desired temperature + or - 1 degree for 5 consecutive samples, or until 1 Hour has expired since the new temperature was set. 5) Bolometer_baseline
1202	<p>SPECTRAL TEST ON LARGE AREA SOURCE IN DIFFUSE SOURCE MODE</p> <ol style="list-style-type: none"> 1) Move Mode select wheel to position 3 (Diffuse Source) 2) Move Aperture wheel, AR Filter, and Filter wheels to open position 3) Single_statevector 4) Move Filter wheel to position 2 (Band 1) 5) Single_statevector 6) Move AR Filter wheel to position 2 (Band 1) 7) Single_statevector 8) Increment position of AR Filter wheel 9) Single_statevector 10) Repeat steps 8 and 9 until data has been taken with AR Filter wheel in position 9 11) Open AR Filter Wheel 12) Increment Filter wheel position 13) Repeat steps 5 - 12 until data has been taken with Filter wheel in position 11 14) Move Filter wheel and AR Filter wheel to open positions 15) Single_statevector

SECTION	DESCRIPTION
	16) Move Aperture and Filter wheels to opaque positions
	17) Single_statevector
	18) Move all wheels to opaque position
	19) Statevector_pair
1203	INCREASE SOURCE 1 SET TEMPERATURE Repeat Section 1201 except step 1) set Source 1 to 20 degrees kelvin
1204	REPEAT SPECTRAL TEST FOR NEW TEMPERATURE Repeat Section 1202
1205	INCREASE SOURCE 1 SET TEMPERATURE Repeat Section 1201 except step 1) set Source 1 to 50 degrees kelvin
1206	REPEAT SPECTRAL TEST FOR NEW TEMPERATURE Repeat Section 1202
1207	INCREASE SOURCE 1 SET TEMPERATURE Repeat Section 1201 except step 1) set Source 1 to 100 degrees kelvin
1208	REPEAT SPECTRAL TEST FOR NEW TEMPERATURE Repeat Section 1202
1209	INCREASE SOURCE 1 SET TEMPERATURE Repeat Section 1201 except step 1) set Source 1 to 200 degrees Kelvin
1210	REPEAT SPECTRAL TEST FOR NEW TEMPERATURE Repeat Section 1202

SECTION	DESCRIPTION
1211	INCREASE SOURCE 1 SET TEMPERATURE Repeat Section 1201 (except step 1) set Source 1 to 270 degrees Kelvin
1212	REPEAT SPECTRAL TEST FOR NEW TEMPERATURE Repeat Section 1202
1213	INCREASE SOURCE 1 SET TEMPERATURE Repeat Section 1201 (except step 1) set Source 1 to 300 degrees Kelvin
1214	REPEAT SPECTRAL TEST FOR NEW TEMPERATURE Repeat Section 1202

**MONITOR TEMPERATURES
WHILE LARGE AREA SOURCE
COOLS DOWN**

1300	SAMPLE DATA EVERY 2 MINUTES FOR 4 HOURS 1) Bolometer_baseline 2) Move all wheels to open position 3) Take Single_statevector every 2 minutes 4) Repeat step 3) for 4 hours
------	----------------------------------------------------------------------------------------------------------------------------------------------------------------------------------------

**TRUE COLD SOAK - EVERYTHING
OFF FOR 1 HOUR EXCEPT PREAMPS**

1400	REFERENCE 1) Bolometer_baseline 2) Move all wheels to opaque position 3) Turn everything off except preamps
------	----------------------------------------------------------------------------------------------------------------------

SECTION	DESCRIPTION
1401	<p>WAIT 1 HOUR THEN REPEAT OPTICAL ZERO POINT</p> <ol style="list-style-type: none"> 1) Wait until 1 hour has passed 2) Bolometer_baseline 3) Repeat Section 101 4) Repeat Section 102 5) Repeat Section 103 except step 1) Move all wheels to opaque instead of open position
1402	<p>SOURCE 2 ON HALF POWER, OPEN ALL WHEELS AND RUN APERTURE WHEEL THROUGH ALL POSITIONS</p> <ol style="list-style-type: none"> 1) Turn on Source 2 to half power 2) Move all wheels to open position 3) 2 Single_statevectors 4) Move Aperture wheel to position 1 5) Single_statevector 6) Increment position of Aperture wheel 7) Single_statevector 8) Repeat steps 6 and 7 for positions 2 - 18 9) Move all wheels to open position 10) Turn Source 2 off 11) 5 Single_statevectors to show how fast system stabilizes
1403	<p>SOURCE 2 ON HALF POWER, OPEN ALL WHEELS AND RUN FILTER WHEEL THROUGH ALL POSITIONS</p> <p>Repeat Section 1402 except Step 4) Move Filter wheel instead of Aperture wheel, and Step 6) Increment position of Filter wheel instead of Aperture wheel</p>
1404	<p>SOURCE 2 ON HALF POWER, OPEN ALL WHEELS AND RUN MODE SELECT WHEEL THROUGH ALL POSITIONS</p> <p>Repeat Section 1402 except Step 4) Move Mode select wheel instead of Aperture wheel, and Step 6) Increment position of Mode select wheel instead of Aperture wheel</p>

SECTION	DESCRIPTION
1405	SOURCE 2 ON HALF POWER, OPEN ALL WHEELS AND RUN AR FILTER WHEEL THROUGH ALL POSITIONS Repeat Section 1402 except Step 4) Move AR Filter wheel instead of Aperture wheel, and Step 6) Increment position of AR Filter wheel instead of Aperture wheel

A complete and exhaustive analysis of the data contained in this Appendix is not provided here. The details of the test were prescribed by NASA personnel and we have assumed that they would do most of the analysis in accordance with their measurement goals. However, temperature variations with motor usage, and light leak problems are addressed here in order to verify system performance in those areas and to illustrate the use of Appendix F.

Tests 201 through 205 (See pages F-5, F-6, and F-36 through F-37) moved all the wheels in the DEC system. The graphic data on page F-36 and F-37 shows appropriate outputs. The first and last columns provide scale calibrations and can be used with a straight-edge to read an intermediate data point. The traces show all 4 wheels moving through all their positions (these graphs resolve 19 positions, position zero indicates a nonvalid position and is the lowest graphic value; positions 1 through 18 correspond to wheel positions.

The traces also show the base plate #3 temperature (p.F-37). This graph covers a range of 0°K to 5°K with a 0.5° resolution. During test 200 (reference point), a 2° reading is indicated, and shows no change throughout the above referenced wheel tests.

Test 211 (Page F-38 and F-39) shows that when the bulb w/envelope is driven to 2.0 volts that the integrating sphere temperature does not change, but the large area source (LAS) warms up and goes off scale (greater than 10°K). This is interesting because it seems that the LAS is absorbing radiant

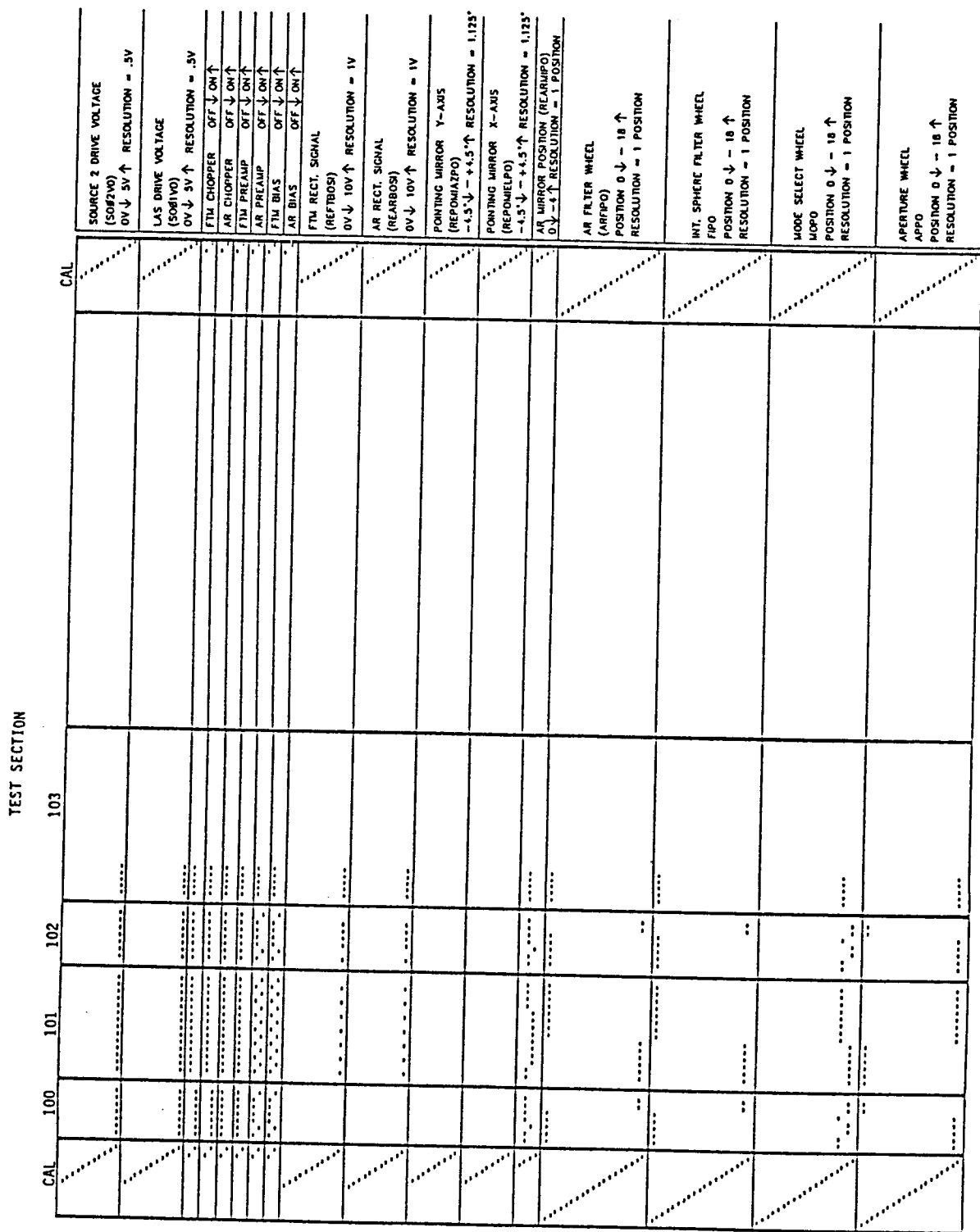
energy from the bulb.

Test 301 shows the LAS cooling some time later from the above bulb test. This test also shows the movement of the pointing mirror (PM) in both x and y axes. The PM temperature indicates temperatures fluctuating between 4 and 5°K.

Tests 500 through 511 move the beam sample mirror (BSM). in response to these movements the BSM temperature immediately rises from 2.5°K to about 6°K and levels off at about 10°K. Tests 600 through 602 show the BSM cooling down.

This page intentionally left blank.

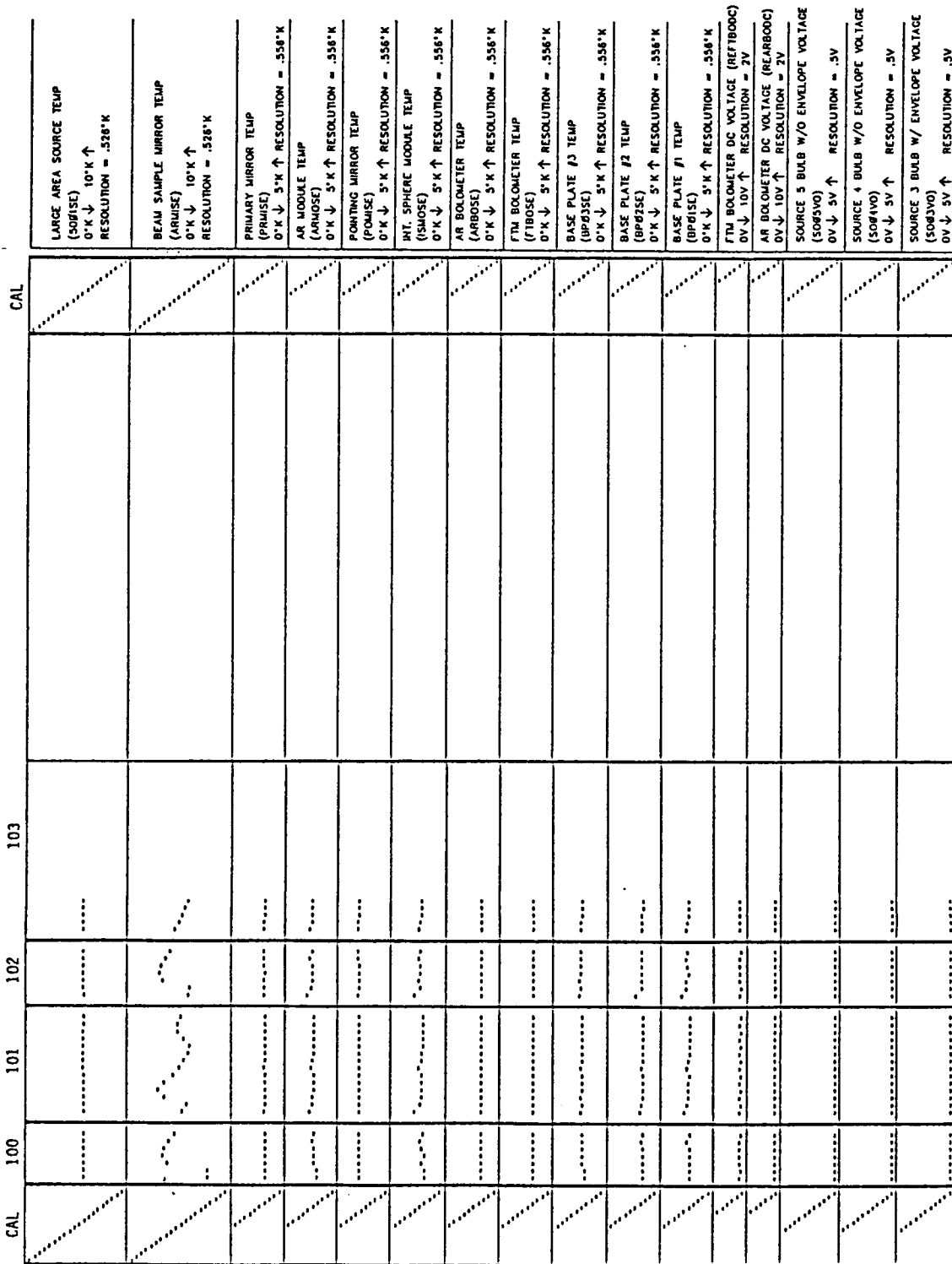
ORIGINAL PAGE IS
OF POOR QUALITY



STARTING SECTION 100

ORIGINAL PAGE IS
OF POOR QUALITY

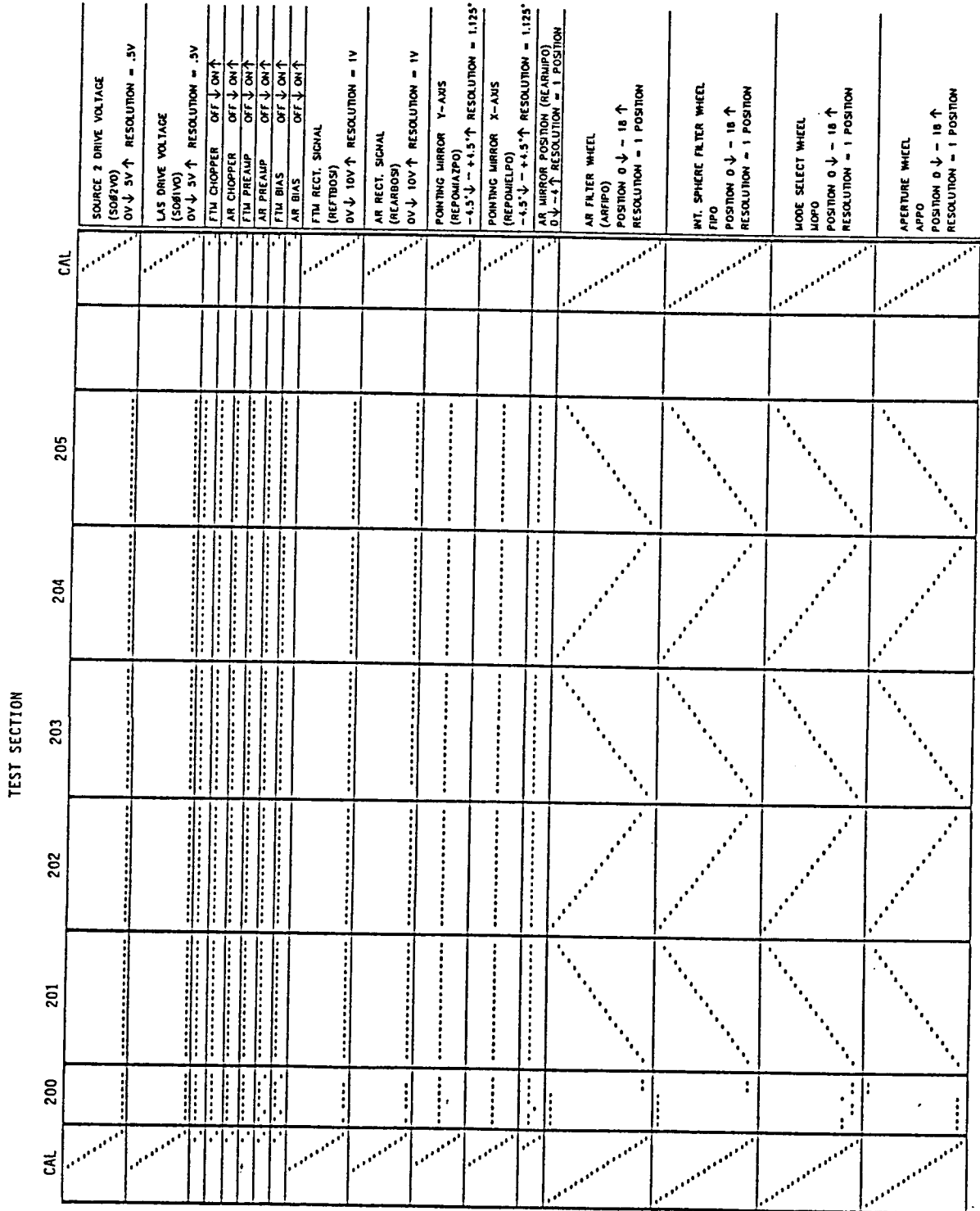
TEST SECTION



TIME →

PART 2 - STARTING SECTION 100

ORIGINAL PAGE IS
OF POOR QUALITY



TEST SECTION

TIME →

STARTING SECTION 200

SOURCE 2 DRIVE VOLTAGE (S02FV0)
0V ↓ 5V ↑ RESOLUTION = .5V

LAS DRIVE VOLTAGE (S04V0)
0V ↓ 5V ↑ RESOLUTION = .5V

FTM CHOPPER OFF ↓ ON ↑

AR CHOPPER OFF ↓ ON ↑

FTM PREAMP OFF ↓ ON ↑

AR PREAMP OFF ↓ ON ↑

FTM BIAS OFF ↓ ON ↑

AR BIAS OFF ↓ ON ↑

FTM RECT. SIGNAL (REFTB05)
0V ↓ 10V ↑ RESOLUTION = 1V

AR RECT. SIGNAL (REARB05)
0V ↓ 10V ↑ RESOLUTION = 1V

POINTING MIRROR Y-AMS (REP0HA1P0)
-4.5 ↓ - +4.5 ↑ RESOLUTION = 1.125°

POINTING MIRROR X-AMS (REP0HE1P0)
-4.5 ↓ - +4.5 ↑ RESOLUTION = 1.125°

AR MIRROR POSITION (REARMP0)
0 ↓ -4 ↑ RESOLUTION = 1 POSITION

AR FILTER WHEEL (ARFIPO)
POSITION 0 ↓ - 18 ↑
RESOLUTION = 1 POSITION

INT. SPHERE FILTER WHEEL (FIPO)
POSITION 0 ↓ - 18 ↑
RESOLUTION = 1 POSITION

MODE SELECT WHEEL (MOFO)
POSITION 0 ↓ - 18 ↑
RESOLUTION = 1 POSITION

APERTURE WHEEL (APPO)
POSITION 0 ↓ - 18 ↑
RESOLUTION = 1 POSITION

ORIGINAL PAGE IS
OF POOR QUALITY

TEST SECTION	TEST SECTION							CAL
	200	201	202	203	204	205	CAL	
LARGE AREA SOURCE TEMP (S081SE) 0°K ↓ 10°K ↑ RESOLUTION = .528°K								
BEAM SAMPLE MIRROR TEMP (A81SE) 0°K ↓ 10°K ↑ RESOLUTION = .528°K								
PRIMARY MIRROR TEMP (P81SE) 0°K ↓ 5°K ↑ RESOLUTION = .558°K								
AR MODULE TEMP (A80SE) 0°K ↓ 5°K ↑ RESOLUTION = .558°K								
PURIFIED MIRROR TEMP (P04SE) 0°K ↓ 5°K ↑ RESOLUTION = .558°K								
WT. SPHERE MODULE TEMP (S80SE) 0°K ↓ 5°K ↑ RESOLUTION = .558°K								
AR BOLONETER TEMP (A80SE) 0°K ↓ 5°K ↑ RESOLUTION = .558°K								
FTM BOLONETER TEMP (F70SE) 0°K ↓ 5°K ↑ RESOLUTION = .558°K								
BASE PLATE #3 TEMP (B80SE) 0°K ↓ 5°K ↑ RESOLUTION = .558°K								
BASE PLATE #2 TEMP (B80SE) 0°K ↓ 5°K ↑ RESOLUTION = .558°K								
BASE PLATE #1 TEMP (B80SE) 0°K ↓ 5°K ↑ RESOLUTION = .558°K								
FTM BOLONETER DC VOLTAGE (REF1000C) 0V ↓ 10V ↑ RESOLUTION = 2V								
AR BOLONETER DC VOLTAGE (REAR000C) 0V ↓ 10V ↑ RESOLUTION = 2V								
SOURCE 5 BULB W/O ENVELOPE VOLTAGE (S085V0) 0V ↓ 5V ↑ RESOLUTION = .5V								
SOURCE 4 BULB W/O ENVELOPE VOLTAGE (S084V0) 0V ↓ 5V ↑ RESOLUTION = .5V								
SOURCE 3 BULB W/ ENVELOPE VOLTAGE (S083V0) 0V ↓ 5V ↑ RESOLUTION = .5V								

TIME →

PART 2 - STARTING SECTION 200

TEST SECTION

	211	212	213	214	CAL
SOURCE 2 DRIVE VOLTAGE (SDR2VD) 0V ↓ 5V ↑ RESOLUTION = .5V
LAS DRIVE VOLTAGE (SDR1VD) 0V ↓ 5V ↑ RESOLUTION = .5V
FTM CHOPPER OFF ↓ ON ↑
AR CHOPPER OFF ↓ ON ↑
FTM PREAMP OFF ↓ ON ↑
AR PREAMP OFF ↓ ON ↑
FTM BIAS OFF ↓ ON ↑
AR BIAS OFF ↓ ON ↑
FTM RECT. SIGNAL (REF7BOS) 0V ↓ 10V ↑ RESOLUTION = 1V
AR RECT. SIGNAL (REARBOS) 0V ↓ 10V ↑ RESOLUTION = 1V
PONTING MIRROR Y-AXIS (REPOHAZPO) -4.5 ↓ - +4.5 ↑ RESOLUTION = 1.125°
PONTING MIRROR X-AXIS (REQUELPO) -4.5 ↓ - +4.5 ↑ RESOLUTION = 1.125°
AR MIRROR POSITION (REARMP) 0 ↓ -4 ↑ RESOLUTION = 1 POSITION
AR FLIER WHEEL (ARFIPO) POSITION 0 ↓ - 18 ↑ RESOLUTION = 1 POSITION
INT. SPHERE FILTER WHEEL FIPO POSITION 0 ↓ - 18 ↑ RESOLUTION = 1 POSITION
MODE SELECT WHEEL MOPO POSITION 0 ↓ - 18 ↑ RESOLUTION = 1 POSITION
APERTURE WHEEL APPO POSITION 0 ↓ - 18 ↑ RESOLUTION = 1 POSITION

TIME →

STARTING SECTION 211

ORIGINAL PAGE IS
OF POOR QUALITY

TEST SECTION

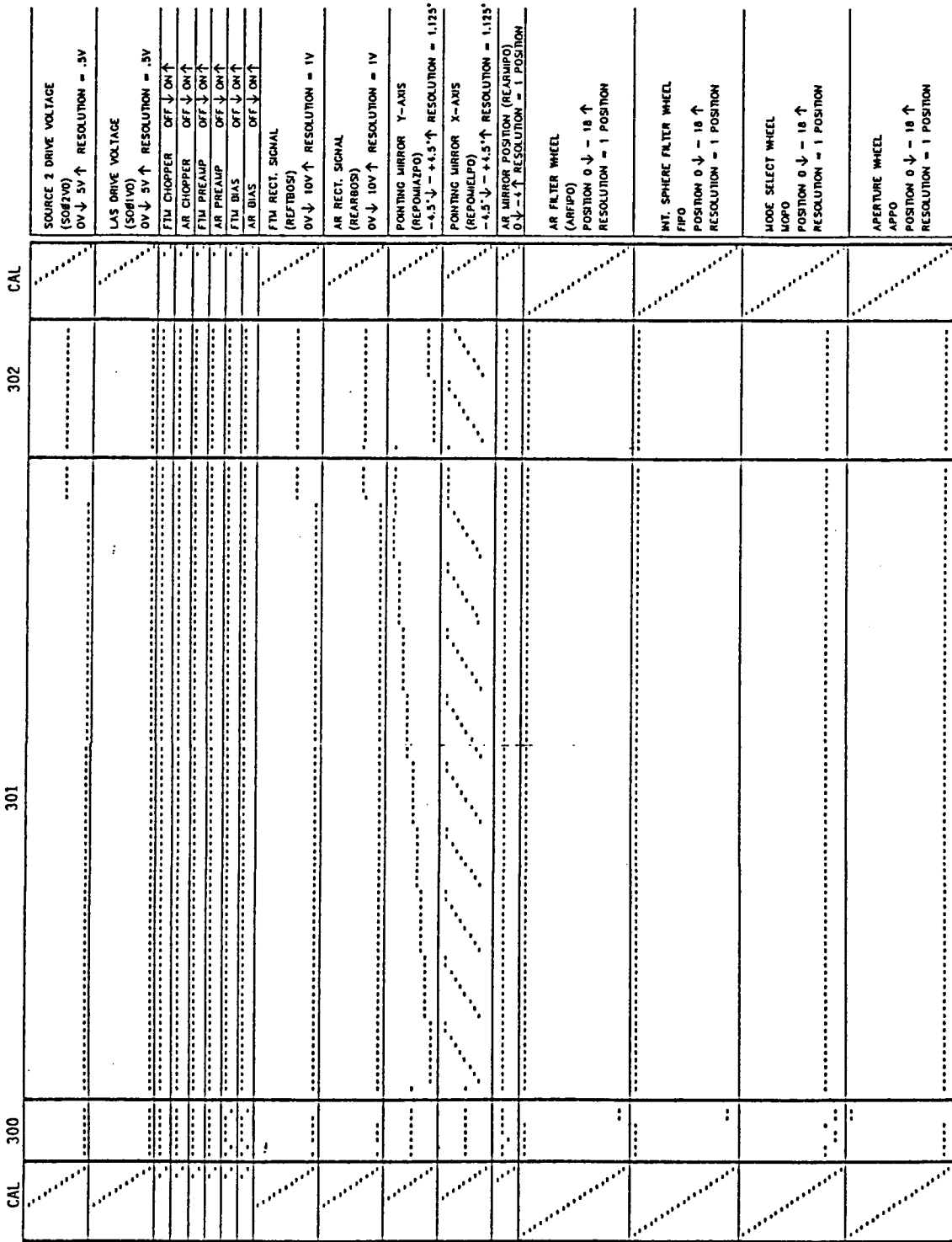
	CAL	211	212	213	214	CAL
LARGE AREA SOURCE TEMP (S0B1SE) 0°K ↓ 10°K ↑ RESOLUTION = .528°K						
BEAM SAMPLE MIRROR TEMP (ARMISE) 0°K ↓ 10°K ↑ RESOLUTION = .526°K						
PRIMARY MIRROR TEMP (PRMISE) 0°K ↓ 5°K ↑ RESOLUTION = .558°K						
AR MODULE TEMP (ARMOSE) 0°K ↓ 5°K ↑ RESOLUTION = .558°K						
POINTING MIRROR TEMP (POMISE) 0°K ↓ 5°K ↑ RESOLUTION = .558°K						
INT. SPHERE MODULE TEMP (ISMOSE) 0°K ↓ 5°K ↑ RESOLUTION = .556°K						
AR BOLOMETER TEMP (ARBOSE) 0°K ↓ 5°K ↑ RESOLUTION = .556°K						
FTM BOLOMETER TEMP (FTBOSE) 0°K ↓ 5°K ↑ RESOLUTION = .558°K						
BASE PLATE #3 TEMP (BP#3SE) 0°K ↓ 5°K ↑ RESOLUTION = .558°K						
BASE PLATE #2 TEMP (BP#2SE) 0°K ↓ 5°K ↑ RESOLUTION = .558°K						
BASE PLATE #1 TEMP (BP#1SE) 0°K ↓ 5°K ↑ RESOLUTION = .558°K						
FTM BOLOMETER DC VOLTAGE (REF1B00C) 0V ↓ 10V ↑ RESOLUTION = 2V						
AR BOLOMETER DC VOLTAGE (REARB00C) 0V ↓ 10V ↑ RESOLUTION = 2V						
SOURCE 5 BULB W/O ENVELOPE VOLTAGE (S0M5V0) 0V ↓ 5V ↑ RESOLUTION = .5V						
SOURCE 4 BULB W/O ENVELOPE VOLTAGE (S0B4V0) 0V ↓ 5V ↑ RESOLUTION = .5V						
SOURCE 3 BULB W/ ENVELOPE VOLTAGE (S0B3V0) 0V ↓ 5V ↑ RESOLUTION = .5V						

TIME →

PART 2 - STARTING SECTION 211

ORIGINAL PAGE IS
OF POOR QUALITY

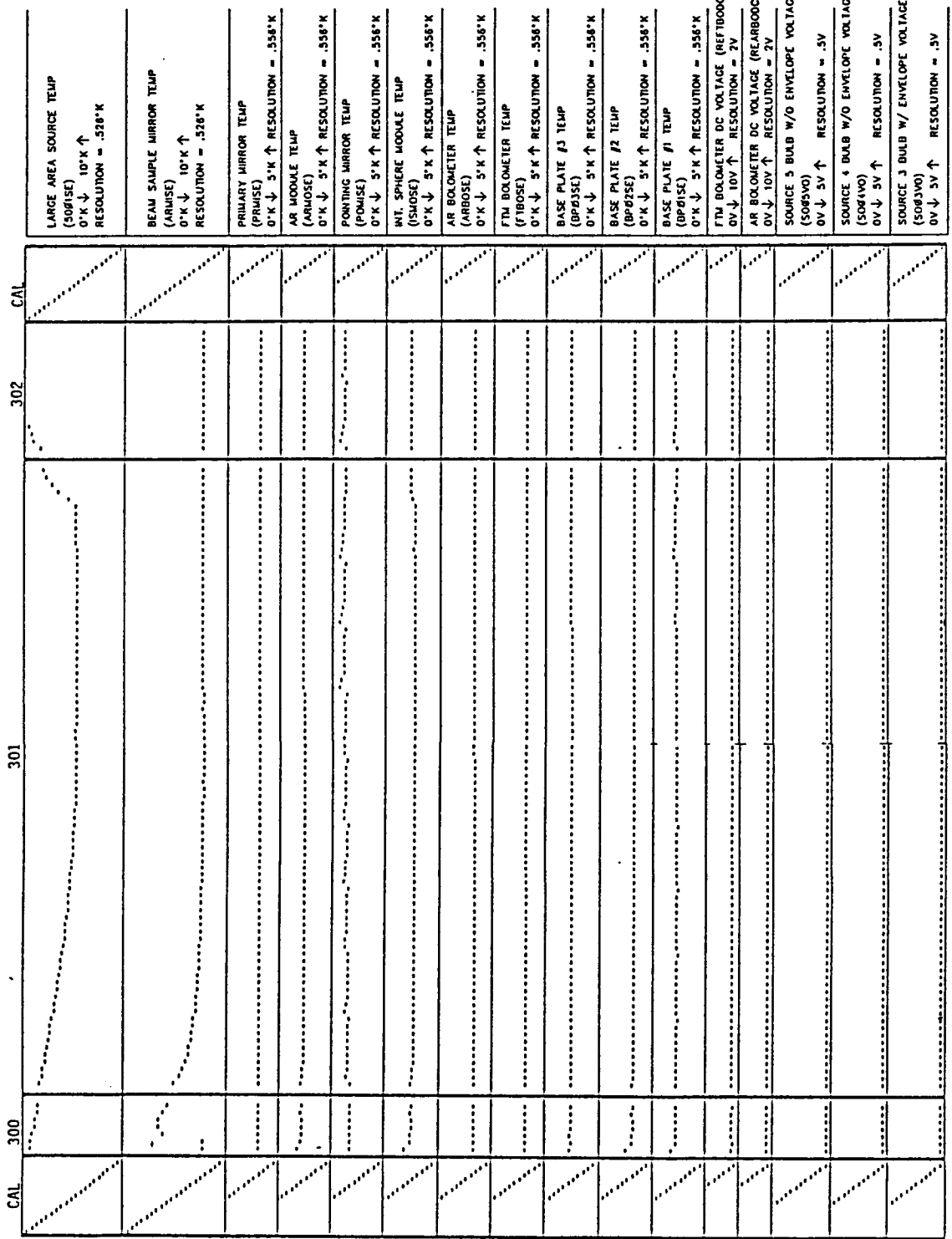
TEST SECTION



TIME →

STARTING SECTION 300

TEST SECTION



LARGE AREA SOURCE TEMP (50P15E) 0°K ↓ 10°K ↑ RESOLUTION = .528°K
BEAM SAMPLE MIRROR TEMP (ARH5E) 0°K ↓ 10°K ↑ RESOLUTION = .528°K
PRIMARY MIRROR TEMP (PRH5E) 0°K ↓ 5°K ↑ RESOLUTION = .556°K
AR MODULE TEMP (ARH05E) 0°K ↓ 5°K ↑ RESOLUTION = .556°K
POINTING MIRROR TEMP (POM5E) 0°K ↓ 5°K ↑ RESOLUTION = .556°K
WT. SPHERE MODULE TEMP (5SH05E) 0°K ↓ 5°K ↑ RESOLUTION = .556°K
AR BOLOMETER TEMP (ARH05E) 0°K ↓ 5°K ↑ RESOLUTION = .556°K
FTM BOLOMETER TEMP (F1B05E) 0°K ↓ 5°K ↑ RESOLUTION = .556°K
BASE PLATE #3 TEMP (BP#35E) 0°K ↓ 5°K ↑ RESOLUTION = .556°K
BASE PLATE #2 TEMP (BP#25E) 0°K ↓ 5°K ↑ RESOLUTION = .556°K
BASE PLATE #1 TEMP (BP#15E) 0°K ↓ 5°K ↑ RESOLUTION = .556°K
FTM BOLOMETER DC VOLTAGE (REF1000C) 0V ↓ 10V ↑ RESOLUTION = 2V
AR BOLOMETER DC VOLTAGE (REAR000C) 0V ↓ 10V ↑ RESOLUTION = 2V
SOURCE 5 BULB W/O ENVELOPE VOLTAGE (S065V0) 0V ↓ 5V ↑ RESOLUTION = .5V
SOURCE 4 BULB W/O ENVELOPE VOLTAGE (S04V0) 0V ↓ 5V ↑ RESOLUTION = .5V
SOURCE 3 BULB W/ ENVELOPE VOLTAGE (S063V0) 0V ↓ 5V ↑ RESOLUTION = .5V

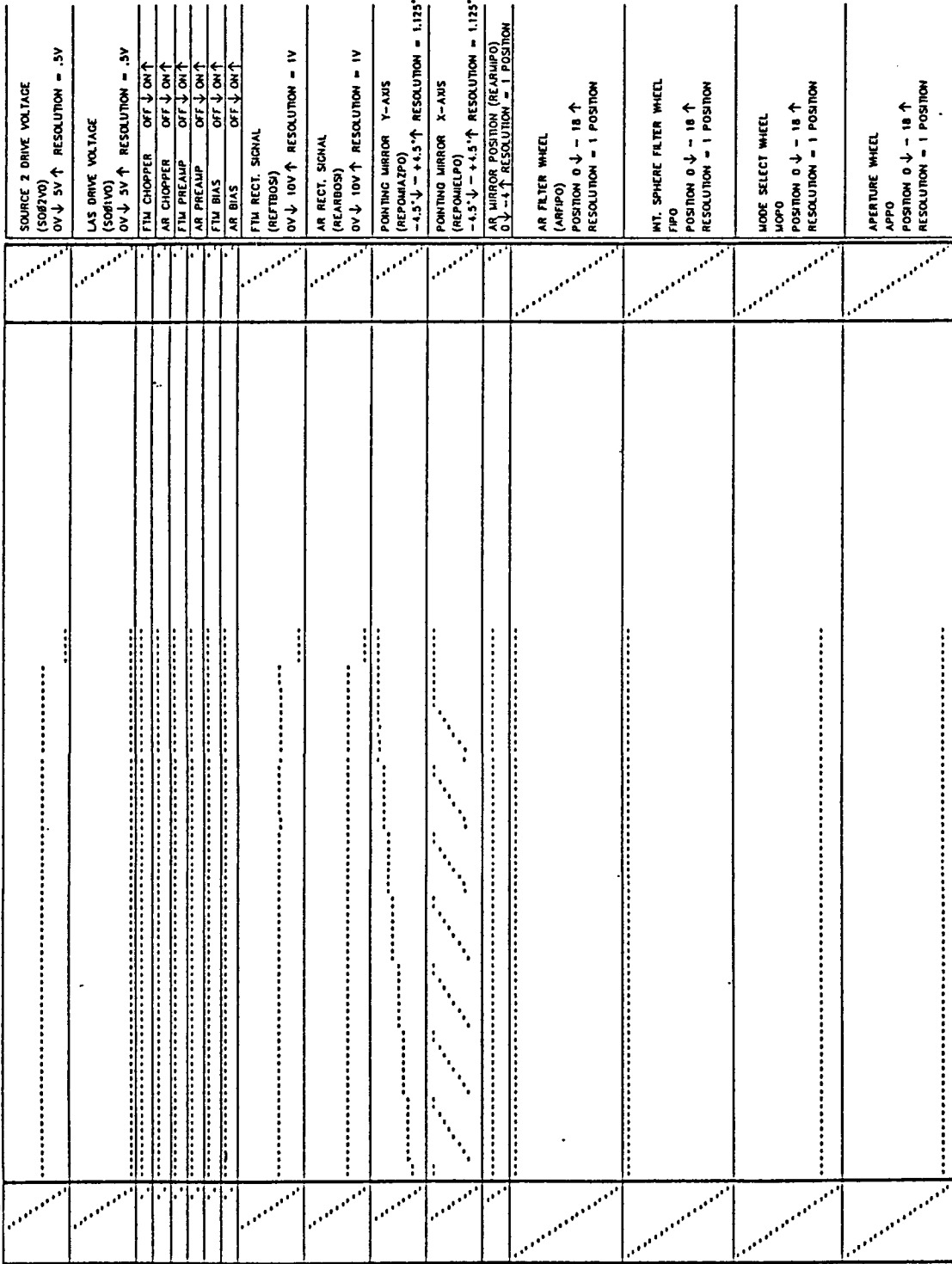
PART 2 - STARTING SECTION 300

TEST SECTION

302

CAL

CAL



TIME →

SOURCE 2 DRIVE VOLTAGE
(S082V0) 0V ↓ 5V ↑ RESOLUTION = .5V

LAS DRIVE VOLTAGE
(S081V0) 0V ↓ 5V ↑ RESOLUTION = .5V

FTM CHOPPER OFF ↓ ON ↑

AR CHOPPER OFF ↓ ON ↑

FTM PREAMP OFF ↓ ON ↑

AR PREAMP OFF ↓ ON ↑

FTM BIAS OFF ↓ ON ↑

AR BIAS OFF ↓ ON ↑

FTM RECT. SIGNAL
(REFTBOS) 0V ↓ 10V ↑ RESOLUTION = 1V

AR RECT. SIGNAL
(REARBOS) 0V ↓ 10V ↑ RESOLUTION = 1V

PONTING MIRROR Y-AXIS
(REPMIAZPO) -4.5° ↓ -4.5° ↑ RESOLUTION = 1.125°

PONTING MIRROR X-AXIS
(REPMIEIPO) -4.5° ↓ -4.5° ↑ RESOLUTION = 1.125°

AR MIRROR POSITION (REARMIPO)
0 ↓ -1 ↑ RESOLUTION = 1 POSITION

AR FILTER WHEEL
(ARFIPO) POSITION 0 ↓ - 18 ↑
RESOLUTION = 1 POSITION

INT. SPHERE FILTER WHEEL
FIPO POSITION 0 ↓ - 18 ↑
RESOLUTION = 1 POSITION

MODE SELECT WHEEL
MOPPO POSITION 0 ↓ - 18 ↑
RESOLUTION = 1 POSITION

APERTURE WHEEL
APPO POSITION 0 ↓ - 18 ↑
RESOLUTION = 1 POSITION

STARTING SECTION 302

TEST SECTION

302

CAL		CAL		LARGE AREA SOURCE TEMP (50P15E) 0°K ↓ 10°K ↑ RESOLUTION = .528°K
				BEAM SAMPLE MIRROR TEMP (AR15E) 0°K ↓ 10°K ↑ RESOLUTION = .528°K
				PRIMARY MIRROR TEMP (PR15E) 0°K ↓ 5°K ↑ RESOLUTION = .558°K
				AR MIRROR TEMP (AR15E) 0°K ↓ 5°K ↑ RESOLUTION = .558°K
				POINTING MIRROR TEMP (PM15E) 0°K ↓ 5°K ↑ RESOLUTION = .558°K
				INT. SPHERE MODULE TEMP (ISM15E) 0°K ↓ 5°K ↑ RESOLUTION = .558°K
				AR BOLOMETER TEMP (AR15E) 0°K ↓ 5°K ↑ RESOLUTION = .558°K
				FTM BOLOMETER TEMP (FT15E) 0°K ↓ 5°K ↑ RESOLUTION = .558°K
				BASE PLATE J3 TEMP (BP315E) 0°K ↓ 5°K ↑ RESOLUTION = .558°K
				BASE PLATE J2 TEMP (BP215E) 0°K ↓ 5°K ↑ RESOLUTION = .558°K
				BASE PLATE J1 TEMP (BP115E) 0°K ↓ 5°K ↑ RESOLUTION = .558°K
				FTM BOLOMETER DC VOLTAGE (REF1500C) 0V ↓ 10V ↑ RESOLUTION = 2V
				AR BOLOMETER DC VOLTAGE (REAR1500C) 0V ↓ 10V ↑ RESOLUTION = 2V
				SOURCE 5 BULB W/O ENVELOPE VOLTAGE (S0515V0) 0V ↓ 5V ↑ RESOLUTION = .5V
				SOURCE 4 BULB W/O ENVELOPE VOLTAGE (S0415V0) 0V ↓ 5V ↑ RESOLUTION = .5V
				SOURCE 3 BULB W/ ENVELOPE VOLTAGE (S0315V0) 0V ↓ 5V ↑ RESOLUTION = .5V

TIME →

PART 2 - STARTING SECTION 302

ORIGINAL PAGE IS
OF POOR QUALITY

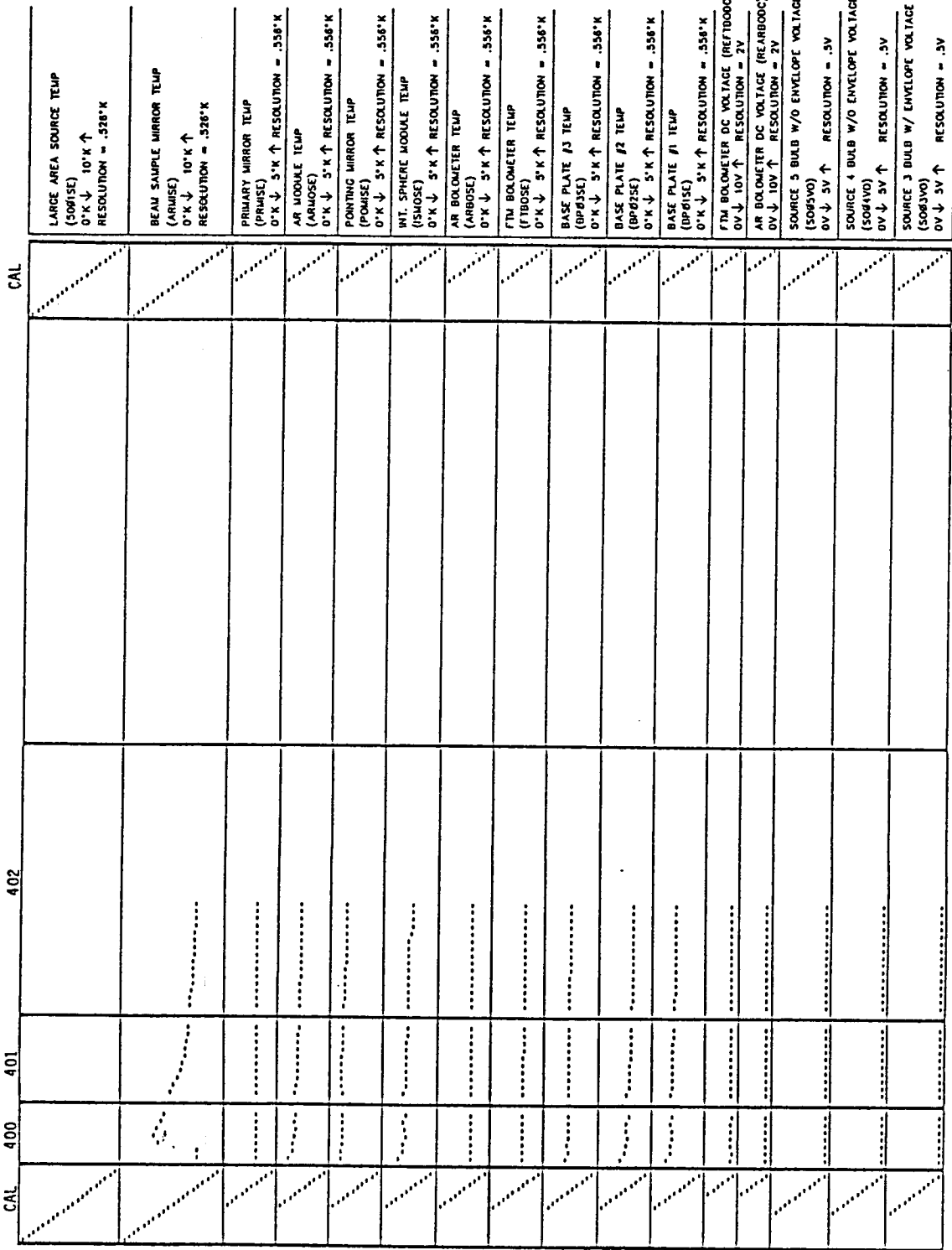
TEST SECTION

400	401	402	CAL	
CAL				SOURCE 2 DRIVE VOLTAGE (SOB2V0) OV ↓ 5V ↑ RESOLUTION = .5V
				LAS DRIVE VOLTAGE (SOB1V0) OV ↓ 5V ↑ RESOLUTION = .5V
				FTM CHOPPER OFF ↓ ON ↑
				AR CHOPPER OFF ↓ ON ↑
				FTM PREAMP OFF ↓ ON ↑
				AR PREAMP OFF ↓ ON ↑
				FTM BIAS OFF ↓ ON ↑
				AR BIAS OFF ↓ ON ↑
				FTM RECT. SIGNAL (REFTR0S) OV ↓ 10V ↑ RESOLUTION = 1V
				AR RECT. SIGNAL (REAR0S) OV ↓ 10V ↑ RESOLUTION = 1V
				POINTING MIRROR Y-AXIS (REPOHAYPO) -4.5° ↓ - +4.5° ↑ RESOLUTION = 1.125°
				POINTING MIRROR X-AXIS (REPOHELPO) -4.5° ↓ - +4.5° ↑ RESOLUTION = 1.125°
				AR MIRROR POSITION (REARJPO) 0 ↓ - 1 ↑ RESOLUTION = 1 POSITION
				AR FILTER WHEEL (ARFJPO) POSITION 0 ↓ - 18 ↑ RESOLUTION = 1 POSITION
				INT. SPHERE FILTER WHEEL FIPO POSITION 0 ↓ - 18 ↑ RESOLUTION = 1 POSITION
				MODE SELECT WHEEL MOP0 POSITION 0 ↓ - 18 ↑ RESOLUTION = 1 POSITION
				APERTURE WHEEL APPO POSITION 0 ↓ - 18 ↑ RESOLUTION = 1 POSITION

TIME →

STARTING SECTION 400

TEST SECTION



PART 2 - STARTING SECTION 400

TIME →

LARGE AREA SOURCE TEMP (S0R1SE) 0°K ↓ 10°K ↑ RESOLUTION = .528°K
BEAM SAMPLE MIRROR TEMP (AR1MSE) 0°K ↓ 10°K ↑ RESOLUTION = .528°K
PRIMARY MIRROR TEMP (PR1MSE) 0°K ↓ 5°K ↑ RESOLUTION = .558°K
AR MODULE TEMP (AR1MOSE) 0°K ↓ 5°K ↑ RESOLUTION = .558°K
PONTING MIRROR TEMP (PO1MSE) 0°K ↓ 5°K ↑ RESOLUTION = .558°K
INT. SPHERE MODULE TEMP (IS1MOSE) 0°K ↓ 5°K ↑ RESOLUTION = .558°K
AR BOLOMETER TEMP (AR1BOSE) 0°K ↓ 5°K ↑ RESOLUTION = .558°K
FTM BOLOMETER TEMP (FT1BOSE) 0°K ↓ 5°K ↑ RESOLUTION = .558°K
BASE PLATE #3 TEMP (BP#3SE) 0°K ↓ 5°K ↑ RESOLUTION = .558°K
BASE PLATE #2 TEMP (BP#2SE) 0°K ↓ 5°K ↑ RESOLUTION = .558°K
BASE PLATE #1 TEMP (BP#1SE) 0°K ↓ 5°K ↑ RESOLUTION = .558°K
FTM BOLOMETER DC VOLTAGE (REF7D00C) 0V ↓ 10V ↑ RESOLUTION = 2V
AR BOLOMETER DC VOLTAGE (REAR800C) 0V ↓ 10V ↑ RESOLUTION = 2V
SOURCE 5 BULB W/O ENVELOPE VOLTAGE (S0R5V0) 0V ↓ 5V ↑ RESOLUTION = .5V
SOURCE 4 BULB W/O ENVELOPE VOLTAGE (S0R4V0) 0V ↓ 5V ↑ RESOLUTION = .5V
SOURCE 3 BULB W/ ENVELOPE VOLTAGE (S0R3V0) 0V ↓ 5V ↑ RESOLUTION = .5V

TEST SECTION		TIME →										
		500	505	510	511	CAL						
STARTING SECTION 500	SOURCE 2 DRIVE VOLTAGE (SOP2V0) OV ↓ 5V ↑ RESOLUTION = .5V	
	LAS DRIVE VOLTAGE (SOL1V0) OV ↓ 5V ↑ RESOLUTION = .5V	
	FTM CHOPPER OFF ↓ ON ↑	
	AR CHOPPER OFF ↓ ON ↑	
	FTM PREAMP OFF ↓ ON ↑	
	AR PREAMP OFF ↓ ON ↑	
	FTM BIAS OFF ↓ ON ↑	
	AR BIAS OFF ↓ ON ↑	
	FTM RECT. SIGNAL (REF2B0S) OV ↓ 10V ↑ RESOLUTION = 1V
	AR RECT. SIGNAL (REAR2B0S) OV ↓ 10V ↑ RESOLUTION = 1V
	PONTING MIRROR Y-AXIS (REP0MAY2P0) -4.5 ↓ - +4.5 ↑ RESOLUTION = 1.125°
	PONTING MIRROR X-AXIS (REP0MEX2P0) -4.5 ↓ - +4.5 ↑ RESOLUTION = 1.125°
	AR MIRROR POSITION (REARMI2P0) 0 ↓ - ↑ RESOLUTION = 1 POSITION
	AR FILTER WHEEL (ARFI2P0) POSITION 0 ↓ - 18 ↑ RESOLUTION = 1 POSITION
MT. SPHERE FILTER WHEEL (MSPFI2P0) POSITION 0 ↓ - 18 ↑ RESOLUTION = 1 POSITION	
MODE SELECT WHEEL (MOS2P0) POSITION 0 ↓ - 18 ↑ RESOLUTION = 1 POSITION	
APERTURE WHEEL (AP2P0) POSITION 0 ↓ - 18 ↑ RESOLUTION = 1 POSITION	

STARTING SECTION 500

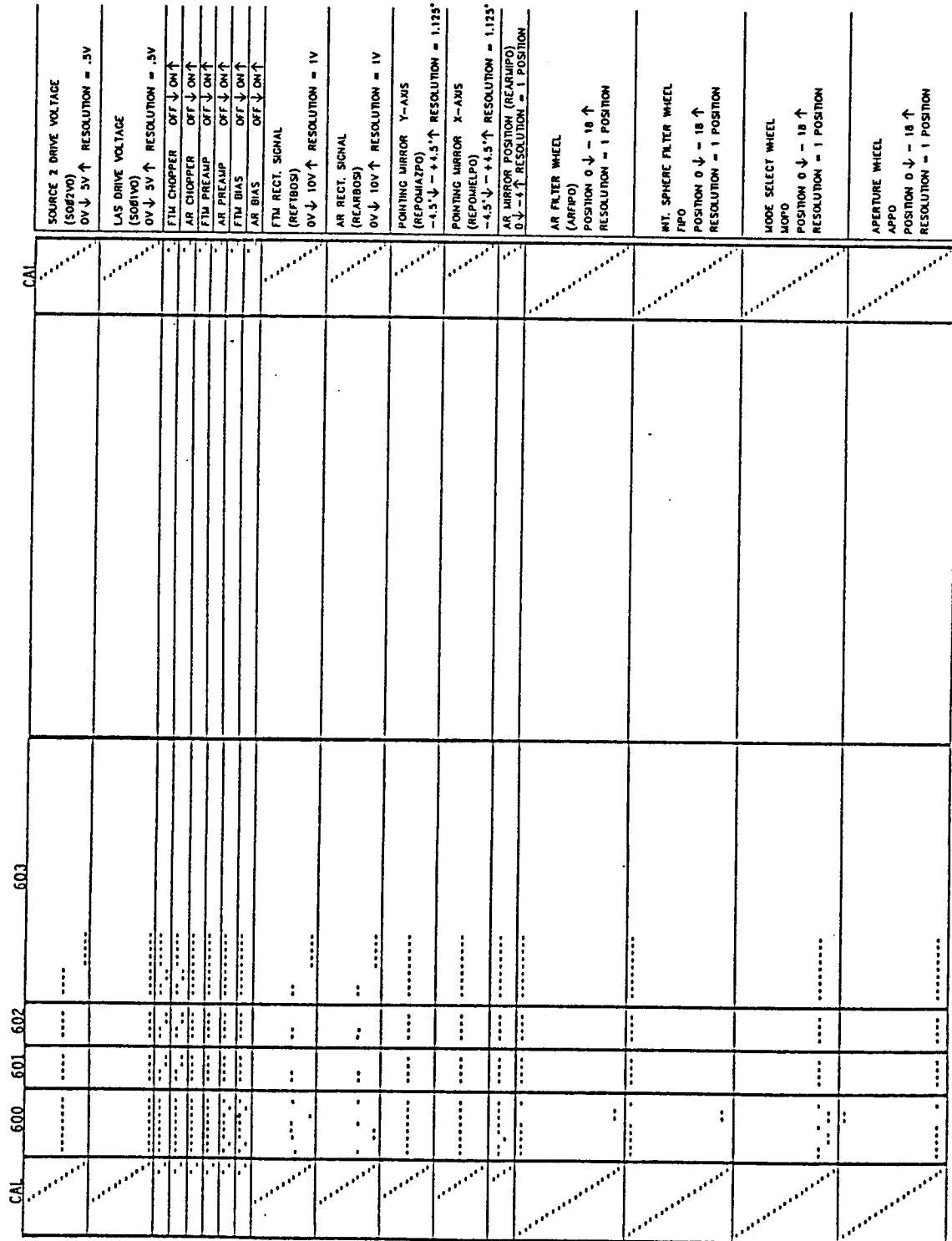
PART 2 - STARTING SECTION 500

TEST SECTION	500										505										510										511									
	CAL																																							
LARGE AREA SOURCE TEMP (S07ISE) 0°K ↓ 10°K ↑ RESOLUTION = .528°K	CAL																																							
BEAM SAMPLE MIRROR TEMP (ARHISE) 0°K ↓ 10°K ↑ RESOLUTION = .528°K	CAL																																							
PRIMARY MIRROR TEMP (PRHISE) 0°K ↓ 5°K ↑ RESOLUTION = .558°K	CAL																																							
AR MODULE TEMP (ARHISE) 0°K ↓ 5°K ↑ RESOLUTION = .558°K	CAL																																							
PONTING MIRROR TEMP (POMISE) 0°K ↓ 5°K ↑ RESOLUTION = .558°K	CAL																																							
INT. SPHERE MODULE TEMP (SMOSE) 0°K ↓ 5°K ↑ RESOLUTION = .558°K	CAL																																							
AR BOLOMETER TEMP (ARBHISE) 0°K ↓ 5°K ↑ RESOLUTION = .558°K	CAL																																							
F7M BOLOMETER TEMP (F7BHOSE) 0°K ↓ 5°K ↑ RESOLUTION = .558°K	CAL																																							
BASE PLATE J3 TEMP (BP#3ISE) 0°K ↓ 5°K ↑ RESOLUTION = .558°K	CAL																																							
BASE PLATE J2 TEMP (BP#2ISE) 0°K ↓ 5°K ↑ RESOLUTION = .558°K	CAL																																							
BASE PLATE J1 TEMP (BP#1ISE) 0°K ↓ 5°K ↑ RESOLUTION = .558°K	CAL																																							
F7M BOLOMETER DC VOLTAGE (REF7B00C) 0V ↓ 10V ↑ RESOLUTION = 2V	CAL																																							
AR BOLOMETER DC VOLTAGE (REARB00C) 0V ↓ 10V ↑ RESOLUTION = 2V	CAL																																							
SOURCE 5 BULB W/O ENVELOPE VOLTAGE (S06SV0) 0V ↓ 5V ↑ RESOLUTION = .5V	CAL																																							
SOURCE 4 BULB W/O ENVELOPE VOLTAGE (S06AV0) 0V ↓ 5V ↑ RESOLUTION = .5V	CAL																																							
SOURCE 3 BULB W/ ENVELOPE VOLTAGE (S06JV0) 0V ↓ 5V ↑ RESOLUTION = .5V	CAL																																							

TIME →

ORIGINAL PAGE IS
OF POOR QUALITY

TEST SECTION



TIME →

SOURCE 2 DRIVE VOLTAGE (SOB2V0)
0V ↓ 5V ↑ RESOLUTION = .5V

LAS DRIVE VOLTAGE (SOB1V0)
0V ↓ 5V ↑ RESOLUTION = .5V

FTM CHOPPER OFF ↓ ON ↑

AR CHOPPER OFF ↓ ON ↑

FTM PREAMP OFF ↓ ON ↑

AR PREAMP OFF ↓ ON ↑

FTM BIAS OFF ↓ ON ↑

AR BIAS OFF ↓ ON ↑

FTM RECT. SIGNAL (REF1B0S)
0V ↓ 10V ↑ RESOLUTION = 1V

AR RECT. SIGNAL (REF2B0S)
0V ↓ 10V ↑ RESOLUTION = 1V

POINTING MIRROR Y-AXIS (REPOMIAZPO)
-1.5° ↓ - +4.5° ↑ RESOLUTION = 1.125°

POINTING MIRROR X-AXIS (REPOMIELPO)
-4.5° ↓ - +4.5° ↑ RESOLUTION = 1.125°

AR MIRROR POSITION (REARMIPO)
0 ↓ -4 ↑ RESOLUTION = 1 POSITION

AR FILTER WHEEL (ARFIPO)
POSITION 0 ↓ - 18 ↑ RESOLUTION = 1 POSITION

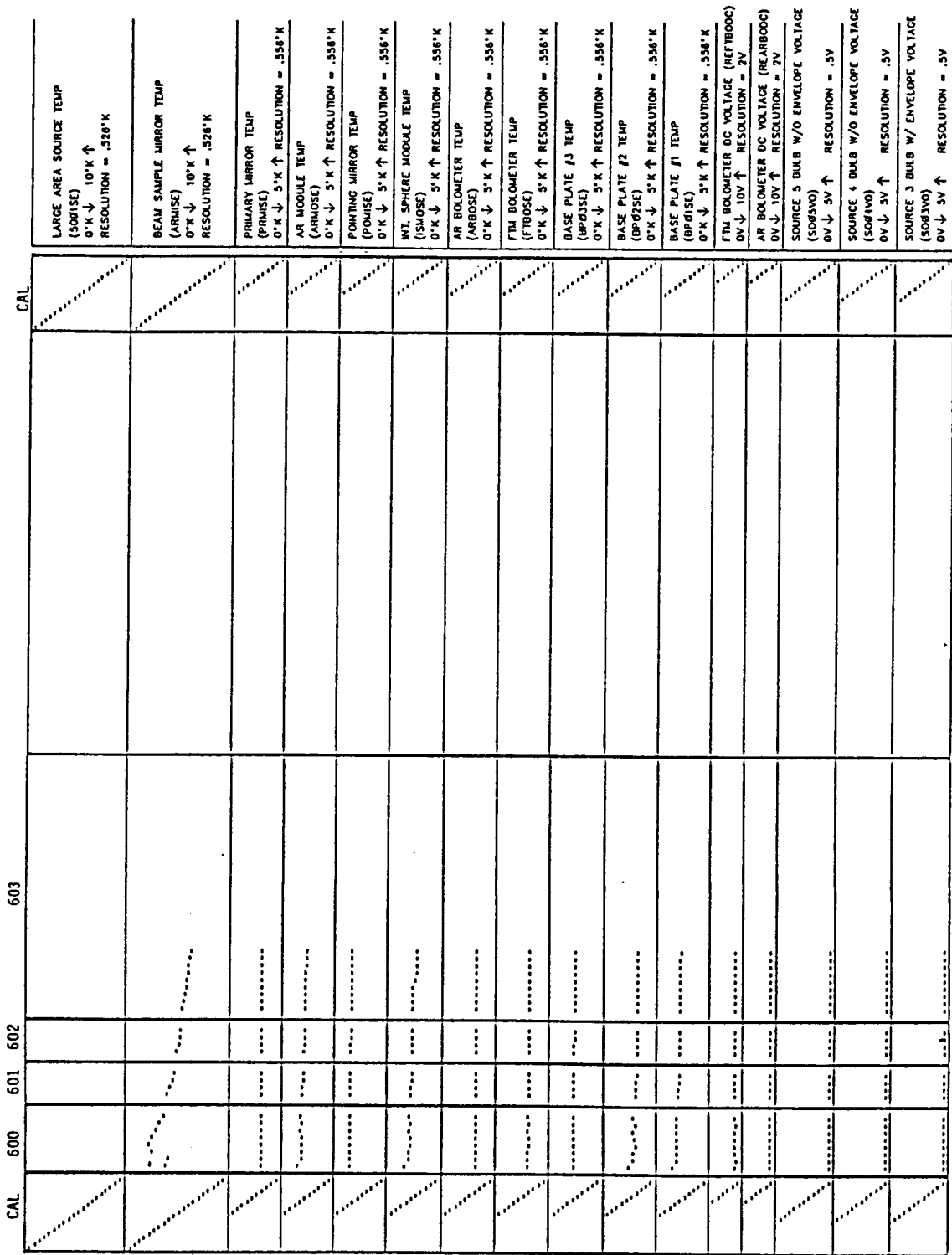
INT. SPHERE FILTER WHEEL (FIPO)
POSITION 0 ↓ - 18 ↑ RESOLUTION = 1 POSITION

MODE SELECT WHEEL (MOPD)
POSITION 0 ↓ - 18 ↑ RESOLUTION = 1 POSITION

APERTURE WHEEL (APPO)
POSITION 0 ↓ - 18 ↑ RESOLUTION = 1 POSITION

STARTING SECTION 600

TEST SECTION



PART 2 - STARTING SECTION 600

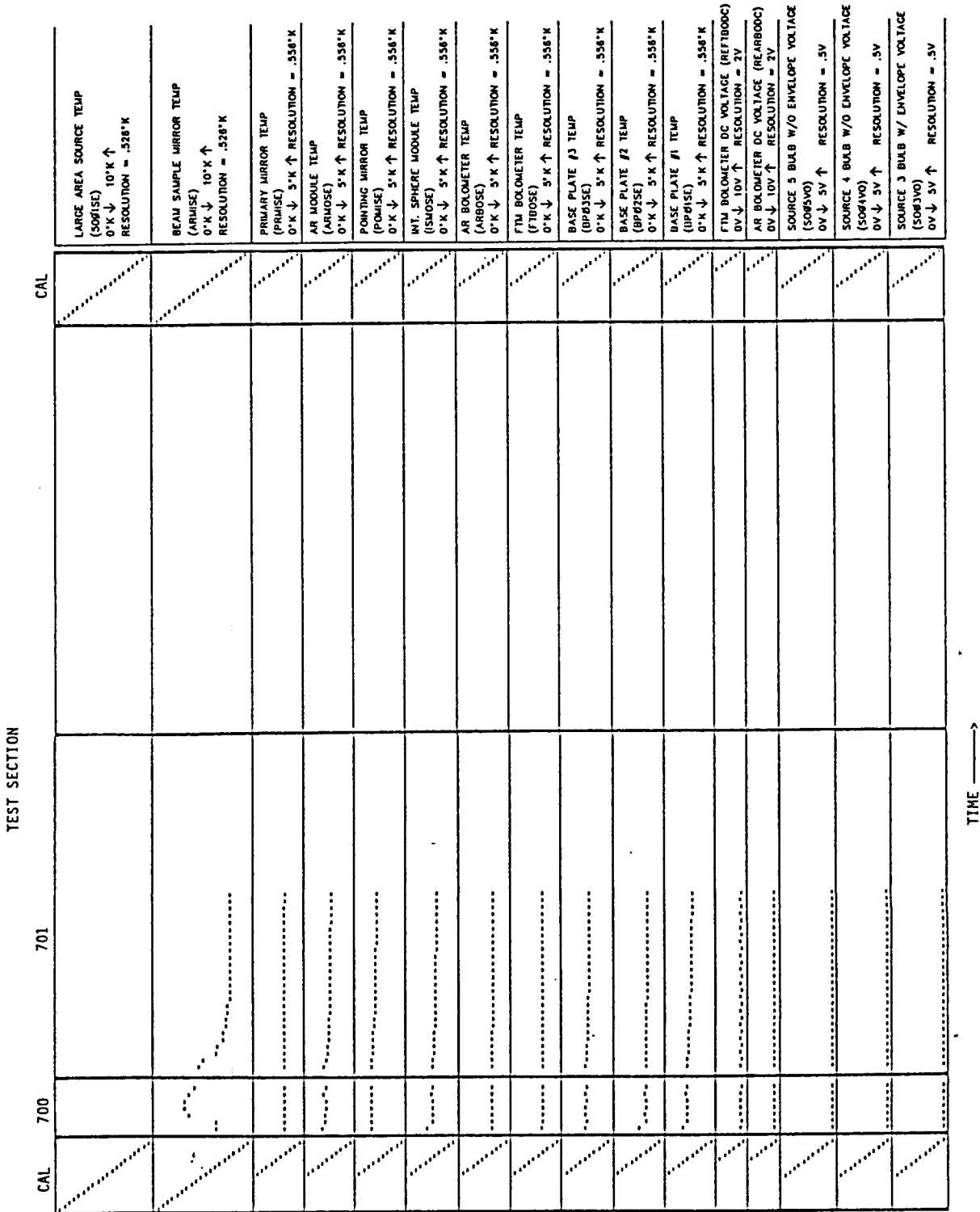
TIME →

TEST SECTION		701		700		CAL
SOURCE 2 DRIVE VOLTAGE (SOB2V0) 0V ↓ 5V ↑ RESOLUTION = .5V						
LAS DRIVE VOLTAGE (SOB1V0) 0V ↓ 5V ↑ RESOLUTION = .5V						
FTM CHOPPER OFF ↓ ON ↑						
AR CHOPPER OFF ↓ ON ↑						
FTM PREAMP OFF ↓ ON ↑						
AR PREAMP OFF ↓ ON ↑						
FTM BIAS OFF ↓ ON ↑						
AR BIAS OFF ↓ ON ↑						
FTM RECT. SIGNAL (REFTBOS) 0V ↓ 10V ↑ RESOLUTION = 1V						
AR RECT. SIGNAL (REARBOS) 0V ↓ 10V ↑ RESOLUTION = 1V						
POINTING MIRROR Y-AXIS (REPOHATPO) -4.5 ↓ - +4.5 ↑ RESOLUTION = 1.125°						
POINTING MIRROR X-AXIS (REPOHELPO) -4.5 ↓ - +4.5 ↑ RESOLUTION = 1.125°						
AR MIRROR POSITION (REARMPO) 0 ↓ -1 ↑ RESOLUTION = 1 POSITION						
AR FILTER WHEEL (ARFIPO) POSITION 0 ↓ - 18 ↑ RESOLUTION = 1 POSITION						
INT. SPHERE FILTER WHEEL (FIPO) POSITION 0 ↓ - 18 ↑ RESOLUTION = 1 POSITION						
MODE SELECT WHEEL (MOPO) POSITION 0 ↓ - 18 ↑ RESOLUTION = 1 POSITION						
APERTURE WHEEL (APPO) POSITION 0 ↓ - 18 ↑ RESOLUTION = 1 POSITION						

TIME →

STARTING SECTION 700

ORIGINAL PAGE IS
OF POOR QUALITY



PART 2 - STARTING SECTION 700

TEST SECTION

800

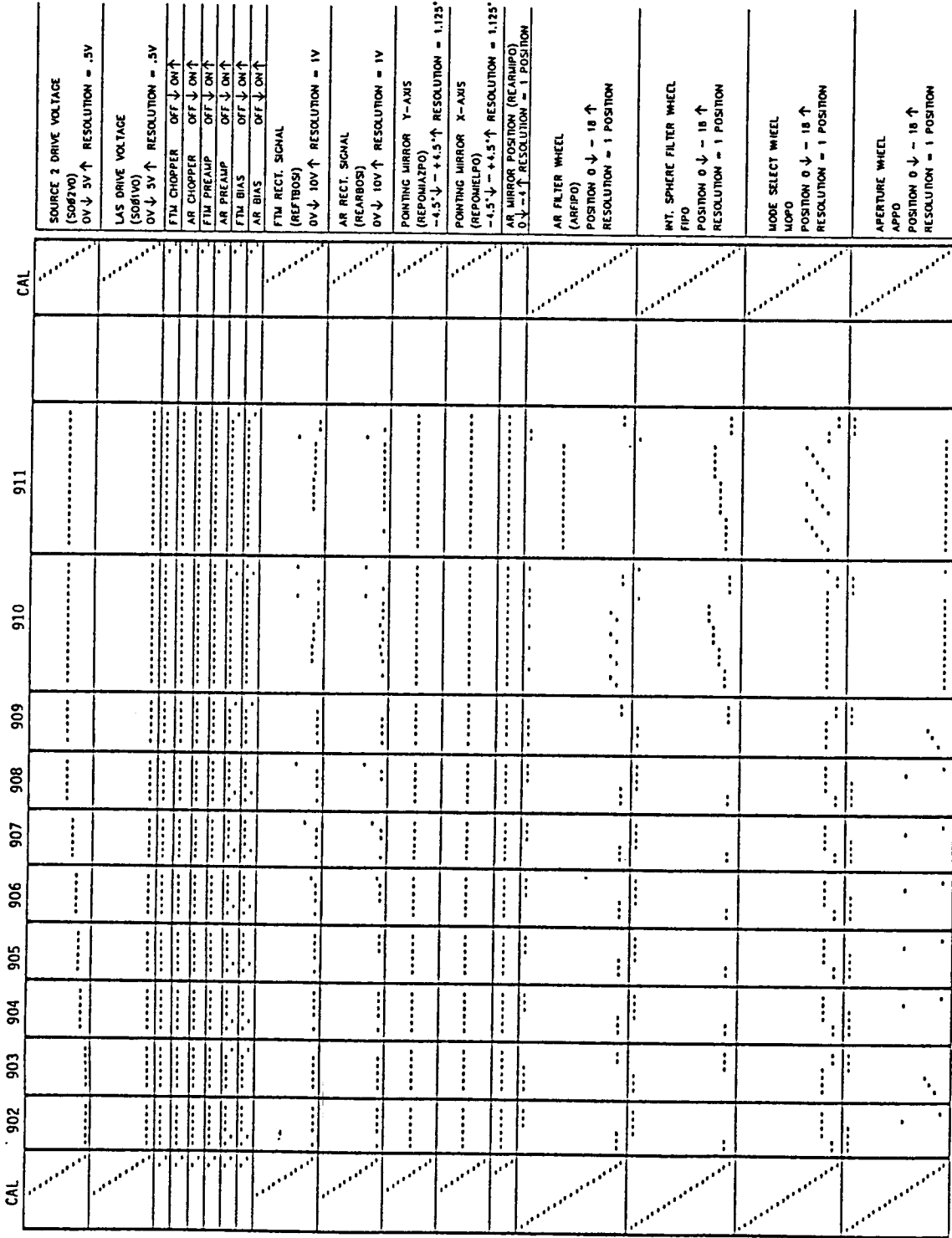
CAL

<p>SOURCE 2 DRIVE VOLTAGE (S0472V0) 0V ↓ 3V ↑ RESOLUTION = .5V</p>	<p>LAS DRIVE VOLTAGE (S081V0) 0V ↓ 5V ↑ RESOLUTION = .3V</p>	<p>FTM CHOPPER OFF ↓ ON ↑</p>	<p>AR CHOPPER OFF ↓ ON ↑</p>	<p>FTM PREAMP OFF ↓ ON ↑</p>	<p>AR PREAMP OFF ↓ ON ↑</p>	<p>FTM BIAS OFF ↓ ON ↑</p>	<p>AR BIAS OFF ↓ ON ↑</p>	<p>FTM RECT. SIGNAL (REFTBOS) 0V ↓ 10V ↑ RESOLUTION = 1V</p>	<p>AR RECT. SIGNAL (REARBOS) 0V ↓ 10V ↑ RESOLUTION = 1V</p>	<p>PONTING MIRROR Y-AXIS (REPOHAZPO) -4.5 ↓ - +4.5 ↑ RESOLUTION = 1.125°</p>	<p>PONTING MIRROR X-AXIS (REPOHELPO) -4.5 ↓ - +4.5 ↑ RESOLUTION = 1.125°</p>	<p>AR MIRROR POSITION (REARMIPO) 0 ↓ -4 ↑ RESOLUTION = 1 POSITION</p>	<p>AR FILTER WHEEL (ARFIPO) POSITION 0 ↓ - 18 ↑ RESOLUTION = 1 POSITION</p>	<p>INT. SPHERE FILTER WHEEL FIPO POSITION 0 ↓ - 18 ↑ RESOLUTION = 1 POSITION</p>	<p>MODE SELECT WHEEL MOPO POSITION 0 ↓ - 18 ↑ RESOLUTION = 1 POSITION</p>	<p>APERTURE WHEEL APPO POSITION 0 ↓ - 18 ↑ RESOLUTION = 1 POSITION</p>
CAL																

STARTING SECTION 800

TIME →

TEST SECTION



TIME →

SOURCE 2 DRIVE VOLTAGE (SOE2V0) 0V ↓ 5V ↑ RESOLUTION = .5V

LAS DRIVE VOLTAGE (SOE1V0) 0V ↓ 5V ↑ RESOLUTION = .5V

FTM CHOPPER OFF ↓ ON ↑

AR CHOPPER OFF ↓ ON ↑

FTM PREAMP OFF ↓ ON ↑

AR PREAMP OFF ↓ ON ↑

FTM BIAS OFF ↓ ON ↑

AR BIAS OFF ↓ ON ↑

FTM RECT. SIGNAL (REF1B05) 0V ↓ 10V ↑ RESOLUTION = 1V

AR RECT. SIGNAL (REARB05) 0V ↓ 10V ↑ RESOLUTION = 1V

POINTING MIRROR Y-AXIS (REP01A12P0) -4.5 ↓ - +4.5 ↑ RESOLUTION = 1.125°

POINTING MIRROR X-AXIS (REP01E1P0) -4.5 ↓ - +4.5 ↑ RESOLUTION = 1.125°

AR MIRROR POSITION (REAR1P0) 0 ↓ -1 ↑ RESOLUTION = 1 POSITION

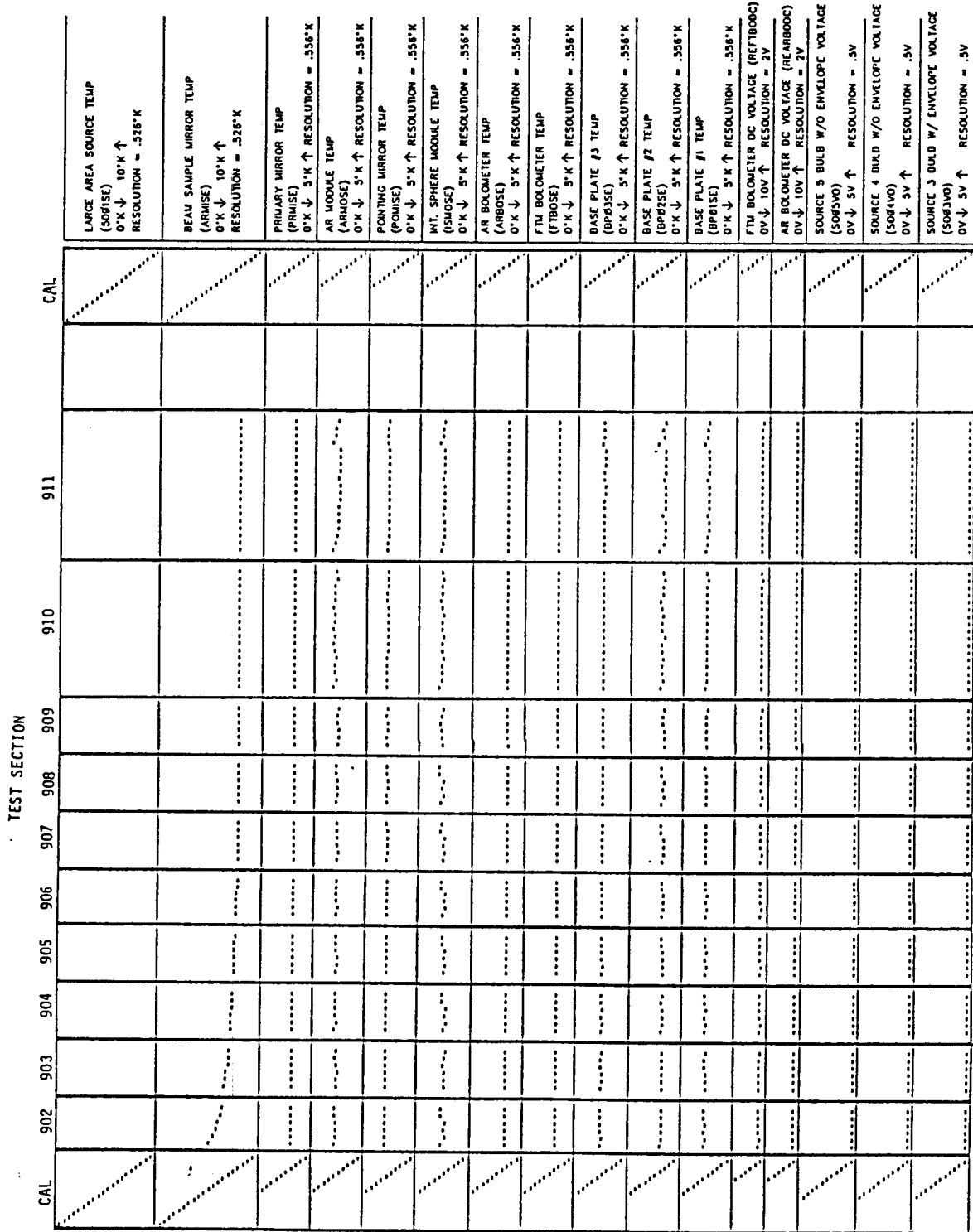
AR FILTER WHEEL (ARFIPO) POSITION 0 ↓ - 18 ↑ RESOLUTION = 1 POSITION

INT. SPHERE FILTER WHEEL FIPO POSITION 0 ↓ - 18 ↑ RESOLUTION = 1 POSITION

MODE SELECT WHEEL M0P0 POSITION 0 ↓ - 18 ↑ RESOLUTION = 1 POSITION

APERTURE WHEEL APPO POSITION 0 ↓ - 18 ↑ RESOLUTION = 1 POSITION

STARTING SECTION 902



PART 2 - STARTING SECTION 902

TIME →

TEST SECTION

CAL	912	913	914	915	916	917	918	919	920	922	CAL
SOURCE 2 DRIVE VOLTAGE (SOM2VO) OV ↓ 5V ↑ RESOLUTION = .5V											
LAS DRIVE VOLTAGE (SOM1VO) OV ↓ 5V ↑ RESOLUTION = .5V											
FTM CHOPPER OFF ↓ ON ↑											
AR CHOPPER OFF ↓ ON ↑											
FTM PREAMP OFF ↓ ON ↑											
AR PREAMP OFF ↓ ON ↑											
FTM BIAS OFF ↓ ON ↑											
AR BIAS OFF ↓ ON ↑											
FTM RECT. SIGNAL (REFTBOS) OV ↓ 10V ↑ RESOLUTION = 1V											
AR RECT. SIGNAL (REARBOS) OV ↓ 10V ↑ RESOLUTION = 1V											
POINTING MIRROR Y-AXIS (REPOMIAZPO) -4.5° ↓ - +4.5° ↑ RESOLUTION = 1.125°											
POINTING MIRROR X-AXIS (REPOMIEPO) -4.5° ↓ - +4.5° ↑ RESOLUTION = 1.125°											
AR MIRROR POSITION (REARIBOS) 0 ↓ - 18 ↑ RESOLUTION = 1 POSITION											
AR FILTER WHEEL (ARFPO) POSITION 0 ↓ - 18 ↑ RESOLUTION = 1 POSITION											
INT. SPHERE FILTER WHEEL (FPO) POSITION 0 ↓ - 18 ↑ RESOLUTION = 1 POSITION											
MODE SELECT WHEEL (MOP) POSITION 0 ↓ - 18 ↑ RESOLUTION = 1 POSITION											
APERTURE WHEEL (APPO) POSITION 0 ↓ - 18 ↑ RESOLUTION = 1 POSITION											

TIME →

STARTING SECTION 912

ORIGINAL PAGE IS
OF POOR QUALITY

TEST SECTION		912	913	914	915	916	917	918	919	920	922	CAL
LARGE AREA SOURCE TEMP (5001SE) 0°K ↓ 10°K ↑ RESOLUTION = .528°K												
BEAM SAMPLE MIRROR TEMP (ARMISE) 0°K ↓ 10°K ↑ RESOLUTION = .528°K												
PRIMARY MIRROR TEMP (PRMISE) 0°K ↓ 5°K ↑ RESOLUTION = .556°K												
AR MODULE TEMP (ARMOSE) 0°K ↓ 5°K ↑ RESOLUTION = .556°K												
POINTING MIRROR TEMP (PMOISE) 0°K ↓ 5°K ↑ RESOLUTION = .556°K												
WT. SPHERE MODULE TEMP (SMOSE) 0°K ↓ 5°K ↑ RESOLUTION = .556°K												
AR BOLOMETER TEMP (ARBOSE) 0°K ↓ 5°K ↑ RESOLUTION = .556°K												
FTM BOLOMETER TEMP (FTBOSE) 0°K ↓ 5°K ↑ RESOLUTION = .556°K												
BASE PLATE #3 TEMP (BPJ3SE) 0°K ↓ 5°K ↑ RESOLUTION = .556°K												
BASE PLATE #2 TEMP (BPJ2SE) 0°K ↓ 5°K ↑ RESOLUTION = .556°K												
BASE PLATE #1 TEMP (BPJ1SE) 0°K ↓ 5°K ↑ RESOLUTION = .556°K												
FTM BOLOMETER DC VOLTAGE (REF1800C) 0V ↓ 10V ↑ RESOLUTION = 2V												
AR BOLOMETER DC VOLTAGE (REAR00C) 0V ↓ 10V ↑ RESOLUTION = 2V												
SOURCE 5 BULB W/O ENVELOPE VOLTAGE (S085V0) 0V ↓ 5V ↑ RESOLUTION = .5V												
SOURCE 4 BULB W/O ENVELOPE VOLTAGE (S084V0) 0V ↓ 5V ↑ RESOLUTION = .5V												
SOURCE 3 BULB W/ ENVELOPE VOLTAGE (S083V0) 0V ↓ 5V ↑ RESOLUTION = .5V												

TIME →

PART 2 - STARTING SECTION 912

ORIGINAL PAGE IS
OF POOR QUALITY

TEST SECTION	CAL												
	923	924	925	926	927	928	929	930	931	932	934	935	936
LARGE AREA SOURCE TEMP (509TSE) 0°K ↓ 10°K ↑ RESOLUTION = .528°K													
BEAM SAMPLE MIRROR TEMP (ARWSE) 0°K ↓ 10°K ↑ RESOLUTION = .528°K													
PRIMARY MIRROR TEMP (PRMISE) 0°K ↓ 5°K ↑ RESOLUTION = .558°K													
AR MODULE TEMP (ARWSE) 0°K ↓ 5°K ↑ RESOLUTION = .558°K													
POINTING MIRROR TEMP (POWSE) 0°K ↓ 5°K ↑ RESOLUTION = .558°K													
INT. SPHERE MODULE TEMP (ISWSE) 0°K ↓ 5°K ↑ RESOLUTION = .558°K													
AR BOLOMETER TEMP (ARBSE) 0°K ↓ 5°K ↑ RESOLUTION = .558°K													
FTM BOLOMETER TEMP (FTBSE) 0°K ↓ 5°K ↑ RESOLUTION = .558°K													
BASE PLATE P3 TEMP (BP3SE) 0°K ↓ 5°K ↑ RESOLUTION = .558°K													
BASE PLATE P2 TEMP (BP2SE) 0°K ↓ 5°K ↑ RESOLUTION = .558°K													
BASE PLATE P1 TEMP (BP1SE) 0°K ↓ 5°K ↑ RESOLUTION = .558°K													
FTM BOLOMETER DC VOLTAGE (REF7B00C) 0V ↓ 10V ↑ RESOLUTION = 2V													
AR BOLOMETER DC VOLTAGE (REARB00C) 0V ↓ 10V ↑ RESOLUTION = 2V													
SOURCE 5 BULB W/O ENVELOPE VOLTAGE (S095V0) 0V ↓ 5V ↑ RESOLUTION = .5V													
SOURCE 4 BULB W/O ENVELOPE VOLTAGE (S084V0) 0V ↓ 5V ↑ RESOLUTION = .5V													
SOURCE 3 BULB W/ ENVELOPE VOLTAGE (S083V0) 0V ↓ 5V ↑ RESOLUTION = .5V													

TIME →

PART 2 - STARTING SECTION 923

ORIGINAL PAGE IS
OF POOR QUALITY

TEST SECTION	TIME													
	937	938	939	940	941	942	943	944	945	947	948	949	950	CAL
SOURCE 2 DRIVE VOLTAGE (SOBZVD) OV ↓ 5V ↑ RESOLUTION = .5V														
LAS DRIVE VOLTAGE (SOBIVO) OV ↓ 5V ↑ RESOLUTION = .5V														
FTM CHOPPER OFF ↓ ON ↑														
AR CHOPPER OFF ↓ ON ↑														
FTM PREAMP OFF ↓ ON ↑														
AR PREAMP OFF ↓ ON ↑														
FTM BIAS OFF ↓ ON ↑														
AR BIAS OFF ↓ ON ↑														
FTM RECT. SIGNAL (REFTBDS) OV ↓ 10V ↑ RESOLUTION = 1V														
AR RECT. SIGNAL (REARBDS) OV ↓ 10V ↑ RESOLUTION = 1V														
POINTING MIRROR Y-AXIS (REPOHIAZPO) -4.5° ↓ - +4.5° ↑ RESOLUTION = 1.125°														
POINTING MIRROR X-AXIS (REPOHIELPO) -4.5° ↓ - +4.5° ↑ RESOLUTION = 1.125°														
AR MIRROR POSITION (REARMPO) 0 ↓ -4° ↑ RESOLUTION = 1 POSITION														
AR FILTER WHEEL (ARFIPPO) POSITION 0 ↓ - 18 ↑ RESOLUTION = 1 POSITION														
INT. SPHERE FILTER WHEEL FPO POSITION 0 ↓ - 18 ↑ RESOLUTION = 1 POSITION														
MODE SELECT WHEEL MOPPO POSITION 0 ↓ - 18 ↑ RESOLUTION = 1 POSITION														
APERTURE WHEEL APPO POSITION 0 ↓ - 18 ↑ RESOLUTION = 1 POSITION														

STARTING SECTION 937

TEST SECTION

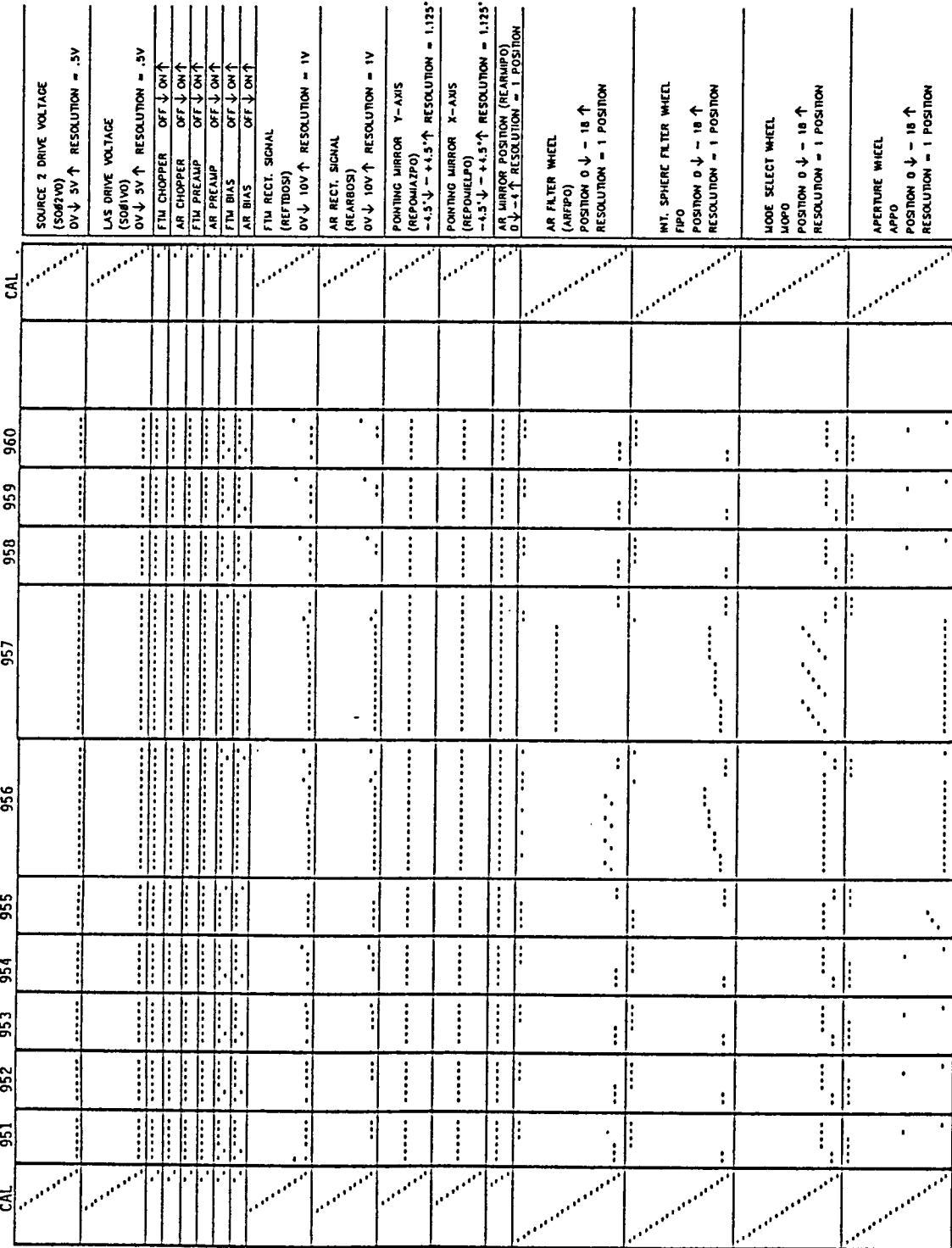
	CAL	937	938	939	940	941	942	943	944	945	947	948	949	950	CAL
LARGE AREA SOURCE TEMP (5091SE) 0°K ↓ 10°K ↑ RESOLUTION = .558°K															
BEAM SAMPLE MIRROR TEMP (AR1MSE) 0°K ↓ 10°K ↑ RESOLUTION = .558°K															
PRIMARY MIRROR TEMP (PR1MSE) 0°K ↓ 5°K ↑ RESOLUTION = .558°K															
AR MODULE TEMP (AR1MSE) 0°K ↓ 5°K ↑ RESOLUTION = .558°K															
POINTING MIRROR TEMP (PM1MSE) 0°K ↓ 5°K ↑ RESOLUTION = .558°K															
INT. SPHERE MODULE TEMP (IS1MSE) 0°K ↓ 5°K ↑ RESOLUTION = .558°K															
AR BOLOMETER TEMP (AR1MSE) 0°K ↓ 5°K ↑ RESOLUTION = .558°K															
FTM BOLOMETER TEMP (FT1MSE) 0°K ↓ 5°K ↑ RESOLUTION = .558°K															
BASE PLATE J3 TEMP (BP1MSE) 0°K ↓ 5°K ↑ RESOLUTION = .558°K															
BASE PLATE J2 TEMP (BP2MSE) 0°K ↓ 5°K ↑ RESOLUTION = .558°K															
BASE PLATE J1 TEMP (BP1MSE) 0°K ↓ 5°K ↑ RESOLUTION = .558°K															
FTM BOLOMETER DC VOLTAGE (REF7B00C) 0V ↓ 10V ↑ RESOLUTION = 2V															
AR BOLOMETER DC VOLTAGE (REAR800C) 0V ↓ 10V ↑ RESOLUTION = 2V															
SOURCE 5 BULB W/O ENVELOPE VOLTAGE (S05V0) 0V ↓ 5V ↑ RESOLUTION = .5V															
SOURCE 4 BULB W/O ENVELOPE VOLTAGE (S04V0) 0V ↓ 5V ↑ RESOLUTION = .5V															
SOURCE 3 BULB W/ ENVELOPE VOLTAGE (S03V0) 0V ↓ 5V ↑ RESOLUTION = .5V															

TIME →

PART 2 - STARTING SECTION 937

ORIGINAL PAGE IS
OF POOR QUALITY

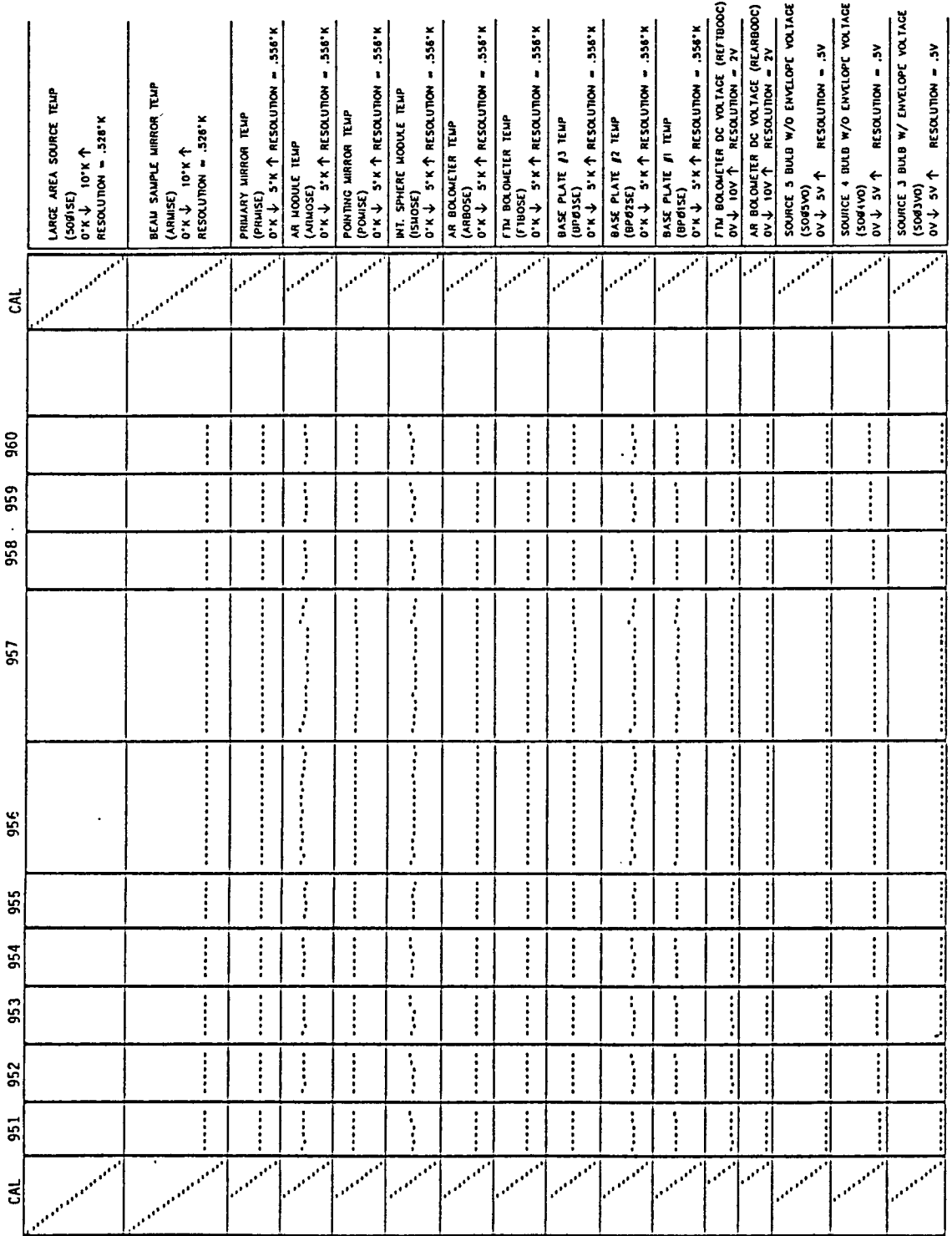
TEST SECTION



TIME →

STARTING SECTION 951

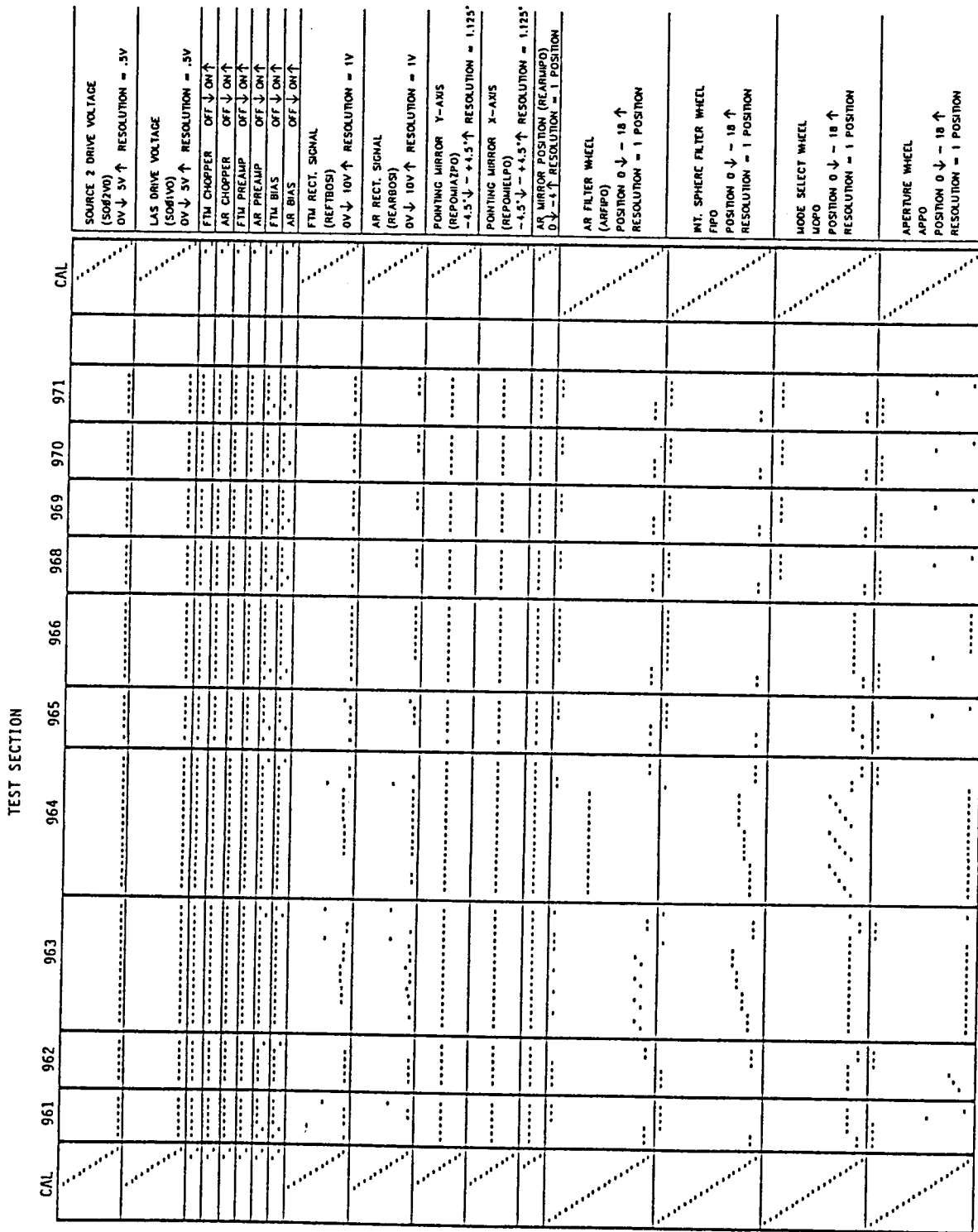
TEST SECTION



TIME →

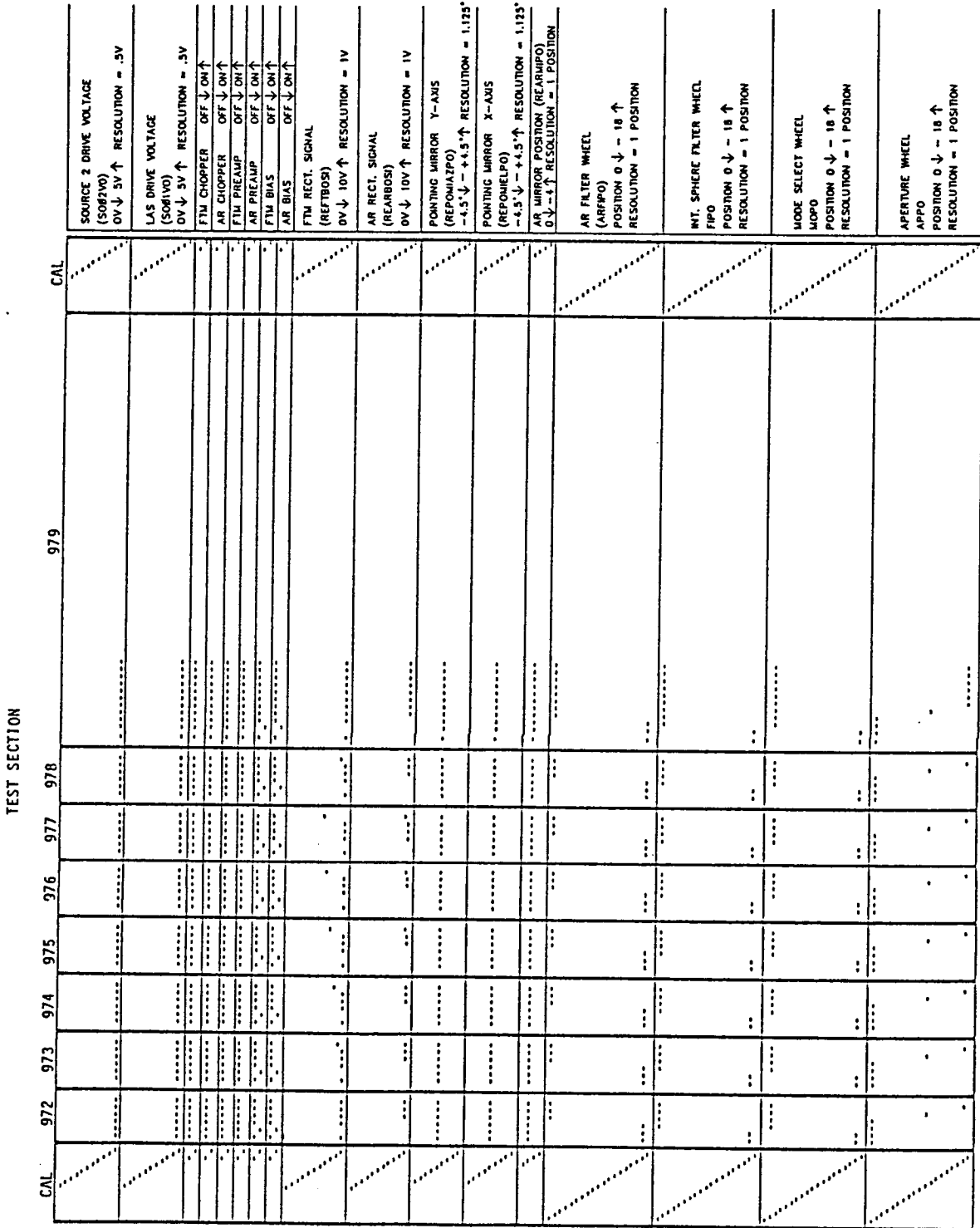
PART 2 - STARTING SECTION 951

ORIGINAL PAGE IS
 OE POOR QUALITY



STARTING SECTION 961

ORIGINAL PAGE IS
OF POOR QUALITY



SOURCE 2 DRIVE VOLTAGE
(S062V0)
0V ↓ 5V ↑ RESOLUTION = .5V

LAS DRIVE VOLTAGE
(S061V0)
0V ↓ 5V ↑ RESOLUTION = .5V

FTM CHOPPER OFF ↓ ON ↑

AR CHOPPER OFF ↓ ON ↑

FTM PREAMP OFF ↓ ON ↑

AR PREAMP OFF ↓ ON ↑

FTM BIAS OFF ↓ ON ↑

AR BIAS OFF ↓ ON ↑

FTM RECT. SIGNAL
(REFTB05)
0V ↓ 10V ↑ RESOLUTION = 1V

AR RECT. SIGNAL
(REARB05)
0V ↓ 10V ↑ RESOLUTION = 1V

POINTING MIRROR Y-AXIS
(REPM02P0)
-4.5 ↓ - +4.5 ↑ RESOLUTION = 1.125'

POINTING MIRROR X-AXIS
(REPM01P0)
-4.5 ↓ - +4.5 ↑ RESOLUTION = 1.125'

AR MIRROR POSITION (REAMP0)
0 ↓ -1 ↑ RESOLUTION = 1 POSITION

AR FILTER WHEEL
(ARF0P0)
POSITION 0 ↓ - 18 ↑
RESOLUTION = 1 POSITION

INT. SPHERE FILTER WHEEL
FIPO
POSITION 0 ↓ - 18 ↑
RESOLUTION = 1 POSITION

MODE SELECT WHEEL
M0P0
POSITION 0 ↓ - 18 ↑
RESOLUTION = 1 POSITION

APERTURE WHEEL
APPO
POSITION 0 ↓ - 18 ↑
RESOLUTION = 1 POSITION

STARTING SECTION 972

TEST SECTION

972	973	974	975	976	977	978	979	CAL
CAL								LARGE AREA SOURCE TEMP (S091SE) 0°K ↓ 10°K ↑ RESOLUTION = .528°K
								BEAM SAMPLE MIRROR TEMP (AR11SE) 0°K ↓ 10°K ↑ RESOLUTION = .528°K
								PRIMARY MIRROR TEMP (PR11SE) 0°K ↓ 5°K ↑ RESOLUTION = .556°K
								AR MODULE TEMP (AR10SE) 0°K ↓ 5°K ↑ RESOLUTION = .556°K
								POINTING MIRROR TEMP (PM11SE) 0°K ↓ 5°K ↑ RESOLUTION = .556°K
								INT. SPHERE MODULE TEMP (IS10SE) 0°K ↓ 5°K ↑ RESOLUTION = .556°K
								AR BOLOMETER TEMP (AR00SE) 0°K ↓ 5°K ↑ RESOLUTION = .556°K
								FTM BOLOMETER TEMP (FT00SE) 0°K ↓ 5°K ↑ RESOLUTION = .556°K
								BASE PLATE P3 TEMP (BP03SE) 0°K ↓ 5°K ↑ RESOLUTION = .556°K
								BASE PLATE P7 TEMP (BP07SE) 0°K ↓ 5°K ↑ RESOLUTION = .556°K
								BASE PLATE P1 TEMP (BP01SE) 0°K ↓ 5°K ↑ RESOLUTION = .556°K
								FTM BOLOMETER DC VOLTAGE (REF1800C) 0V ↓ 10V ↑ RESOLUTION = 2V
								AR BOLOMETER DC VOLTAGE (REAR00C) 0V ↓ 10V ↑ RESOLUTION = 2V
								SOURCE 5 BULB W/O ENVELOPE VOLTAGE (S095V0) 0V ↓ 5V ↑ RESOLUTION = .5V
								SOURCE 4 BULB W/O ENVELOPE VOLTAGE (S084V0) 0V ↓ 5V ↑ RESOLUTION = .5V
								SOURCE 3 BULB W/ ENVELOPE VOLTAGE (S083V0) 0V ↓ 5V ↑ RESOLUTION = .5V

TIME →

PART 2 - STARTING SECTION 972

ORIGINAL PAGE IS
OF POOR QUALITY

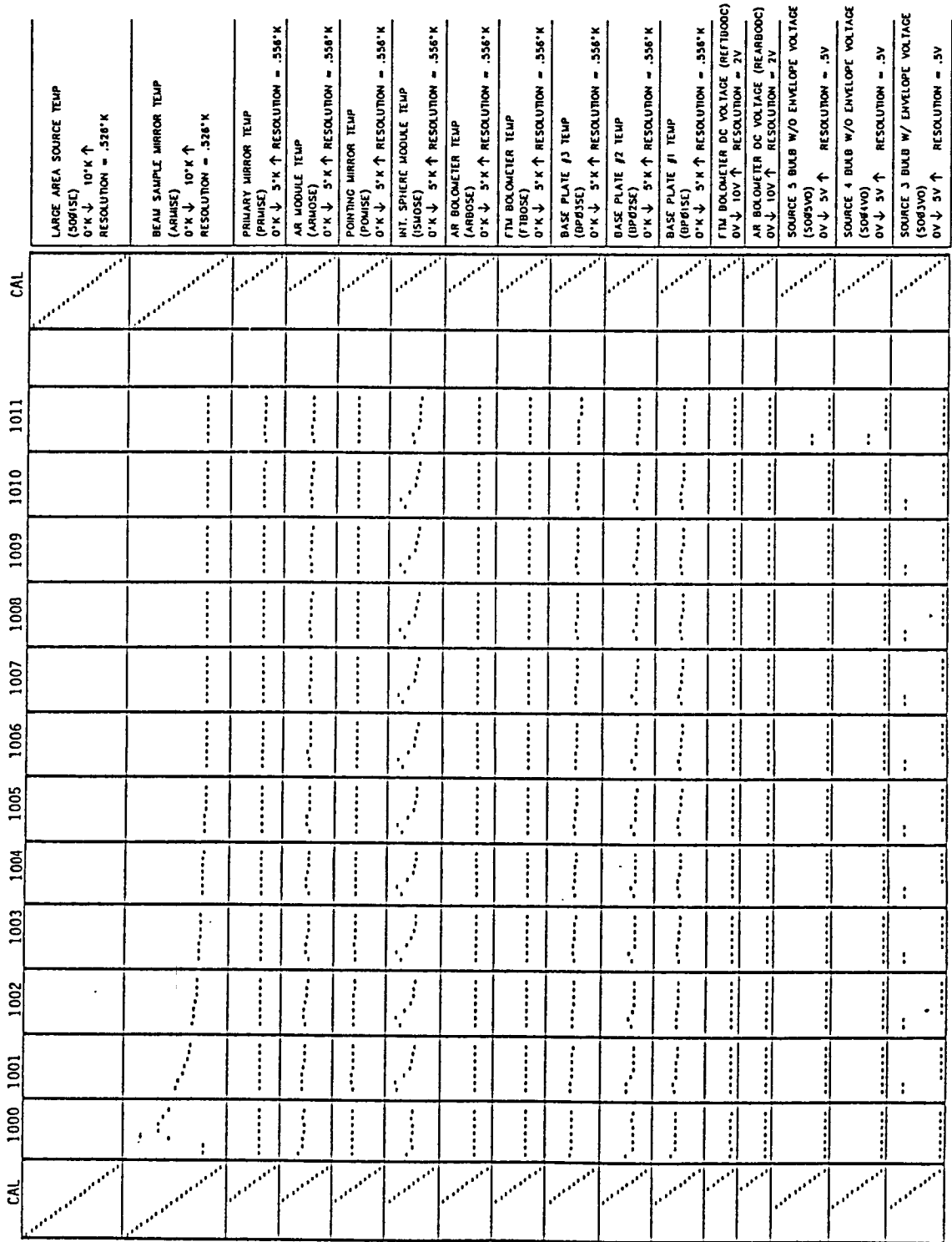
TEST SECTION

	CAL	1000	1001	1002	1003	1004	1005	1006	1007	1008	1009	1010	1011	CAL
SOURCE 2 DRIVE VOLTAGE (SD2V0) 0V ↓ 5V ↑ RESOLUTION = .5V														
LAS DRIVE VOLTAGE (SD1V0) 0V ↓ 5V ↑ RESOLUTION = .5V														
FTM CHOPPER OFF ↓ ON ↑														
AR CHOPPER OFF ↓ ON ↑														
FTM PREAMP OFF ↓ ON ↑														
AR PREAMP OFF ↓ ON ↑														
FTM BIAS OFF ↓ ON ↑														
AR BIAS OFF ↓ ON ↑														
FTM RECT. SIGNAL (REFTBOS) 0V ↓ 10V ↑ RESOLUTION = 1V														
AR RECT. SIGNAL (REARBOS) 0V ↓ 10V ↑ RESOLUTION = 1V														
PONING MIRROR Y-AXIS (REFOYALPO) -4.5 ↓ - +4.5 ↑ RESOLUTION = 1.125°														
PONING MIRROR X-AXIS (REFOXALPO) -4.5 ↓ - +4.5 ↑ RESOLUTION = 1.125°														
AR MIRROR POSITION (REARMIPO) 0 ↓ -4 ↑ RESOLUTION = 1 POSITION														
AR FILTER WHEEL (ARFIPO) POSITION 0 ↓ - 18 ↑ RESOLUTION = 1 POSITION														
INT. SPHERE FILTER WHEEL (FIPO) POSITION 0 ↓ - 18 ↑ RESOLUTION = 1 POSITION														
MODE SELECT WHEEL (MOPO) POSITION 0 ↓ - 18 ↑ RESOLUTION = 1 POSITION														
APERTURE WHEEL (APPO) POSITION 0 ↓ - 18 ↑ RESOLUTION = 1 POSITION														

TIME →

STARTING SECTION 1000

TEST SECTION



TIME →

PART 2 - STARTING SECTION 1000

TEST SECTION

	1020	1019	1018	1017	1016	1015	1014	1013	1012	CAL
SOURCE 2 DRIVE VOLTAGE (SOB2V0) 0V ↓ 5V ↑ RESOLUTION = .5V										
LAS DRIVE VOLTAGE (SOB1V0) 0V ↓ 5V ↑ RESOLUTION = .5V										
FTM CHOPPER OFF ↓ ON ↑										
AR CHOPPER OFF ↓ ON ↑										
FTM PREAMP OFF ↓ ON ↑										
AR PREAMP OFF ↓ ON ↑										
FTM BIAS OFF ↓ ON ↑										
AR BIAS OFF ↓ ON ↑										
FTM RECT. SIGNAL (REFTBOS) 0V ↓ 10V ↑ RESOLUTION = 1V										
AR RECT. SIGNAL (REARBOS) 0V ↓ 10V ↑ RESOLUTION = 1V										
POINTING MIRROR Y-AXIS (REPOHATPO) -4.5° ↓ - +4.5° ↑ RESOLUTION = 1.125°										
POINTING MIRROR X-AXIS (REPOHELPO) -4.5° ↓ - +4.5° ↑ RESOLUTION = 1.125°										
AR MIRROR POSITION (REARMPD) 0 ↓ -1 ↑ RESOLUTION = 1 POSITION										
AR FILTER WHEEL (ARFPO) POSITION 0 ↓ - 18 ↑ RESOLUTION = 1 POSITION										
INT. SPHERE FILTER WHEEL (IPD) POSITION 0 ↓ - 18 ↑ RESOLUTION = 1 POSITION										
MODE SELECT WHEEL (MOPD) POSITION 0 ↓ - 18 ↑ RESOLUTION = 1 POSITION										
APERTURE WHEEL (APD) POSITION 0 ↓ - 18 ↑ RESOLUTION = 1 POSITION										

TIME →

STARTING SECTION 1012

TEST SECTION

TEST SECTION	1012	1013	1014	1015	1016	1017	1018	1019	1020	CAL
LARGE AREA SOURCE TEMP (S091SE) 0°K ↓ 10°K ↑ RESOLUTION = .328°K
BEAM SAMPLE MIRROR TEMP (A91MSE) 0°K ↓ 10°K ↑ RESOLUTION = .328°K
PRIMARY MIRROR TEMP (P91MSE) 0°K ↓ 5°K ↑ RESOLUTION = .556°K
AN MODULE TEMP (A91MOSE) 0°K ↓ 5°K ↑ RESOLUTION = .556°K
POINTING MIRROR TEMP (P01MSE) 0°K ↓ 5°K ↑ RESOLUTION = .556°K
INT. SPHERE MODULE TEMP (S01MSE) 0°K ↓ 5°K ↑ RESOLUTION = .556°K
AR BOLOMETER TEMP (A91BOSE) 0°K ↓ 5°K ↑ RESOLUTION = .556°K
FTM BOLOMETER TEMP (F71BOSE) 0°K ↓ 5°K ↑ RESOLUTION = .556°K
BASE PLATE #3 TEMP (B01P3SE) 0°K ↓ 5°K ↑ RESOLUTION = .556°K
BASE PLATE #2 TEMP (B01P2SE) 0°K ↓ 5°K ↑ RESOLUTION = .556°K
BASE PLATE #1 TEMP (B01P1SE) 0°K ↓ 5°K ↑ RESOLUTION = .556°K
FTM BOLOMETER DC VOLTAGE (REF1000C) 0V ↓ 10V ↑ RESOLUTION = 2V
AR BOLOMETER DC VOLTAGE (REAR000C) 0V ↓ 10V ↑ RESOLUTION = 2V
SOURCE 5 BULB W/O ENVELOPE VOLTAGE (S065V0) 0V ↓ 5V ↑ RESOLUTION = .5V
SOURCE 4 BULB W/O ENVELOPE VOLTAGE (S064V0) 0V ↓ 5V ↑ RESOLUTION = .5V
SOURCE 3 BULB W/ ENVELOPE VOLTAGE (S063V0) 0V ↓ 5V ↑ RESOLUTION = .5V

TIME →

PART 2 - STARTING SECTION 1012

OPTIONAL PAGE IS
OF POOR QUALITY

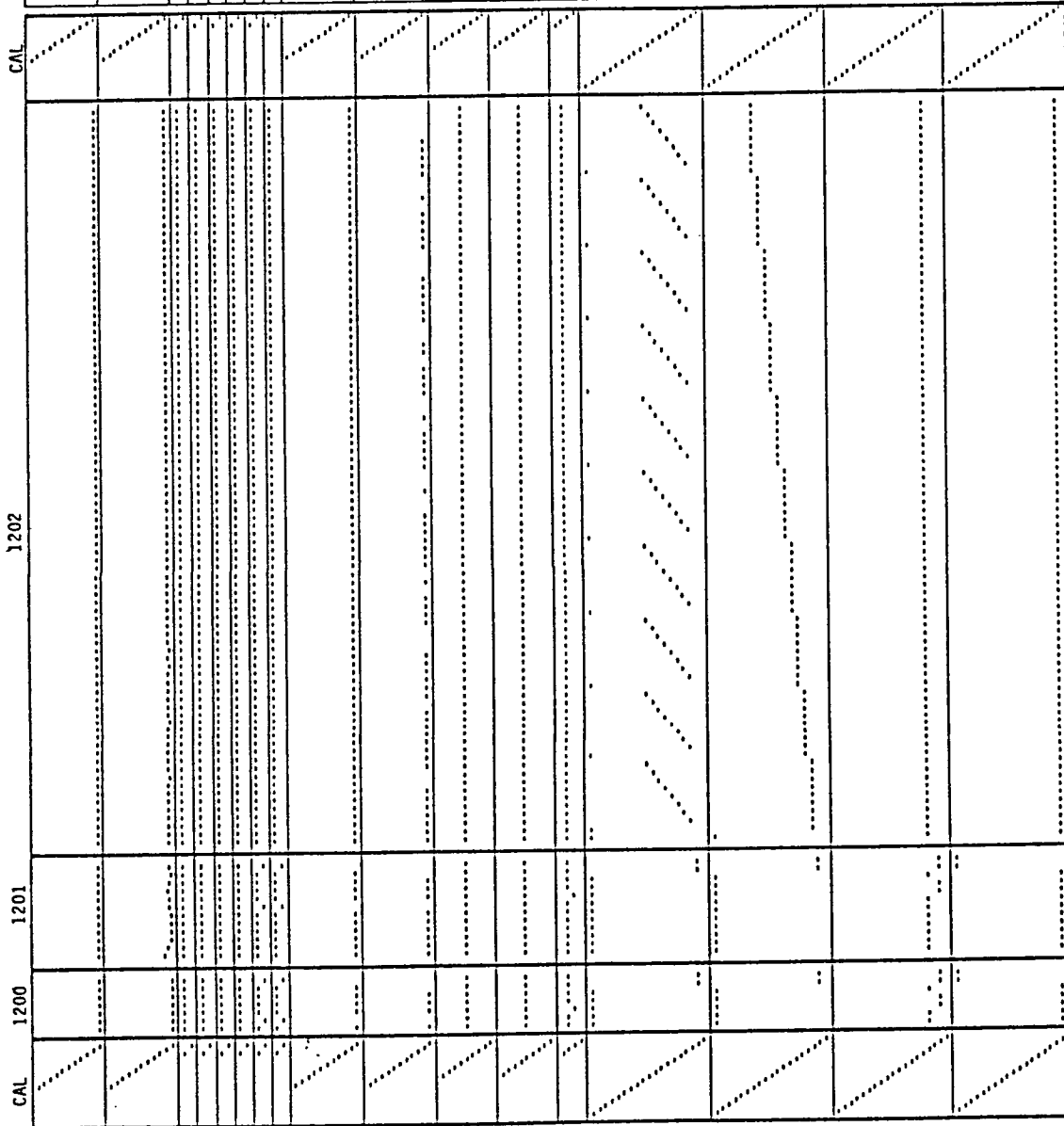
TEST SECTION

CAL	1100	1101	CAL	CAL
LARGE AREA SOURCE TEMP (509TSE) 0°K ↓ 10°K ↑ RESOLUTION = .528°K				
BEAM SAMPLE MIRROR TEMP (ARMISE) 0°K ↓ 10°K ↑ RESOLUTION = .528°K				
PRIMARY MIRROR TEMP (PRMISE) 0°K ↓ 5°K ↑ RESOLUTION = .558°K				
AR MODULE TEMP (ARMOSE) 0°K ↓ 5°K ↑ RESOLUTION = .558°K				
POINTING MIRROR TEMP (POMISE) 0°K ↓ 5°K ↑ RESOLUTION = .558°K				
INT. SPHERE MODULE TEMP (ISSOSE) 0°K ↓ 5°K ↑ RESOLUTION = .558°K				
AR BLOMETER TEMP (ARBOSE) 0°K ↓ 5°K ↑ RESOLUTION = .558°K				
FTM BLOMETER TEMP (FTBOSE) 0°K ↓ 5°K ↑ RESOLUTION = .558°K				
BASE PLATE #3 TEMP (BP#3SE) 0°K ↓ 5°K ↑ RESOLUTION = .558°K				
BASE PLATE #2 TEMP (BP#2SE) 0°K ↓ 5°K ↑ RESOLUTION = .558°K				
BASE PLATE #1 TEMP (BP#1SE) 0°K ↓ 5°K ↑ RESOLUTION = .558°K				
FTM BLOMETER DC VOLTAGE (RFT7B00C) 0V ↓ 10V ↑ RESOLUTION = 2V				
AR BLOMETER DC VOLTAGE (REARB00C) 0V ↓ 10V ↑ RESOLUTION = 2V				
SOURCE 5 BULB W/O ENVELOPE VOLTAGE (S095V0) 0V ↓ 5V ↑ RESOLUTION = .5V				
SOURCE 4 BULB W/O ENVELOPE VOLTAGE (S094V0) 0V ↓ 5V ↑ RESOLUTION = .5V				
SOURCE 3 BULB W/ ENVELOPE VOLTAGE (S093V0) 0V ↓ 5V ↑ RESOLUTION = .5V				

TIME →

PART 2 - STARTING SECTION 1100

TEST SECTION



STARTING SECTION 1200

TIME →

SOURCE 2 DRIVE VOLTAGE (S082V0) 0V ↓ 5V ↑ RESOLUTION = .5V
LAS DRIVE VOLTAGE (S081V0) 0V ↓ 5V ↑ RESOLUTION = .5V
FTM CHOPPER OFF ↓ ON ↑
AR CHOPPER OFF ↓ ON ↑
FTM PREAMP OFF ↓ ON ↑
AR PREAMP OFF ↓ ON ↑
FTM BIAS OFF ↓ ON ↑
AR BIAS OFF ↓ ON ↑
FTM RECT. SIGNAL (R0FTB0S) 0V ↓ 10V ↑ RESOLUTION = 1V
AR RECT. SIGNAL (R0ARB0S) 0V ↓ 10V ↑ RESOLUTION = 1V
PONTING MIRROR Y-AXIS (R0P0M1AZP0) -4.5° ↓ - +4.5° ↑ RESOLUTION = 1.125°
PONTING MIRROR X-AXIS (R0P0M1ELP0) -4.5° ↓ - +4.5° ↑ RESOLUTION = 1.125°
AR MIRROR POSITION (R0ARMP0) 0 ↓ -1 ↑ RESOLUTION = 1 POSITION
AR FILTER WHEEL (ARFP0) POSITION 0 ↓ - 18 ↑ RESOLUTION = 1 POSITION
INT. SPHERE FILTER WHEEL FIPO POSITION 0 ↓ - 18 ↑ RESOLUTION = 1 POSITION
H00S SELECT WHEEL H00S0 POSITION 0 ↓ - 18 ↑ RESOLUTION = 1 POSITION
APERTURE WHEEL APPO POSITION 0 ↓ - 18 ↑ RESOLUTION = 1 POSITION

TEST SECTION

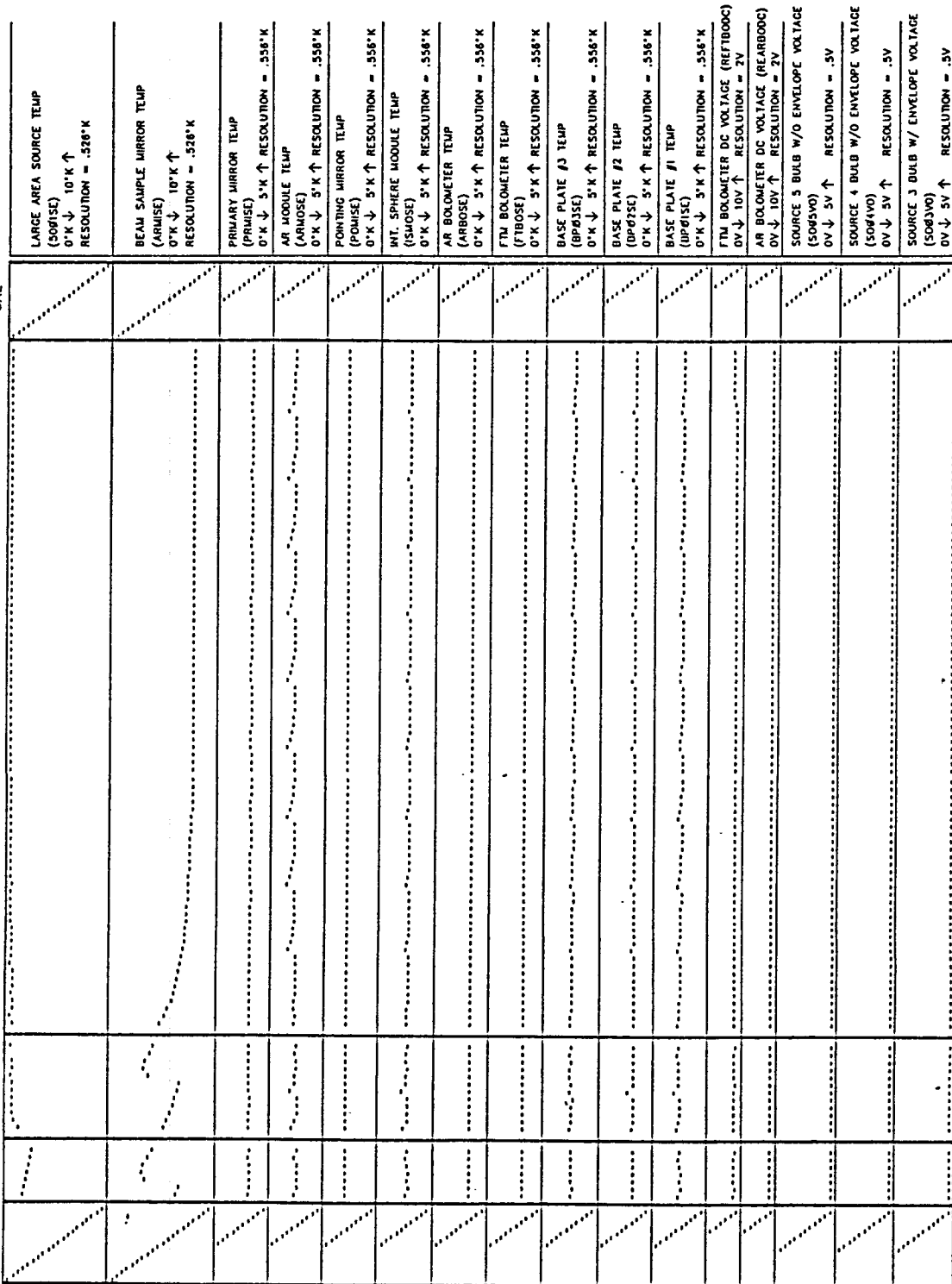
1202

1201

1200

CAL

CAL



TIME →

PART 2 - STARTING SECTION 1200

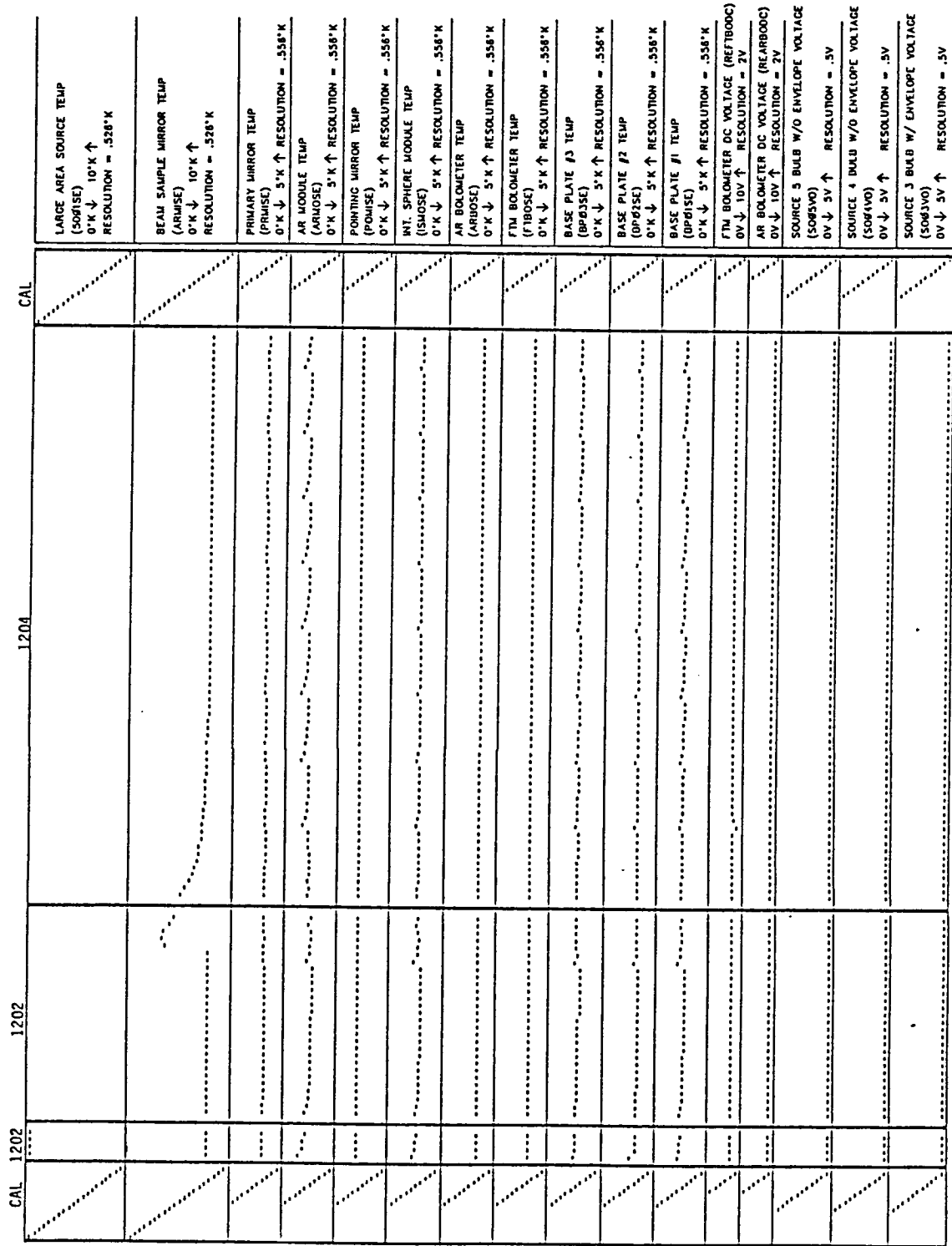
TEST SECTION

TEST SECTION	1202	1203	1204	CAL
SOURCE 2 DRIVE VOLTAGE (SOE2V0)				
0V ↓ 5V ↑ RESOLUTION = .5V				
LAS DRIVE VOLTAGE (SOE1V0)				
0V ↓ 5V ↑ RESOLUTION = .5V				
FTM CHOPPER OFF ↓ ON ↑				
AR CHOPPER OFF ↓ ON ↑				
FTM PREAMP OFF ↓ ON ↑				
AR PREAMP OFF ↓ ON ↑				
FTM BIAS OFF ↓ ON ↑				
AR BIAS OFF ↓ ON ↑				
FTM RECT. SIGNAL (REF1B05)				
0V ↓ 10V ↑ RESOLUTION = 1V				
AR RECT. SIGNAL (REAR1B05)				
0V ↓ 10V ↑ RESOLUTION = 1V				
PONTING MIRROR Y-AXIS (REPOMIAZPO)				
-4.5 ↓ +4.5 ↑ RESOLUTION = 1.125°				
PONTING MIRROR X-AXIS (REPOMIELPO)				
-4.5 ↓ +4.5 ↑ RESOLUTION = 1.125°				
AR MIRROR POSITION (REARMIPO)				
0 ↓ -1 ↑ RESOLUTION = 1 POSITION				
AR FILTER WHEEL (ARFIPO)				
POSITION 0 ↓ - 16 ↑				
RESOLUTION = 1 POSITION				
INT. SPHERE FILTER WHEEL (FIPO)				
POSITION 0 ↓ - 16 ↑				
RESOLUTION = 1 POSITION				
MODE SELECT WHEEL (MOPO)				
POSITION 0 ↓ - 16 ↑				
RESOLUTION = 1 POSITION				
APERTURE WHEEL (APPO)				
POSITION 0 ↓ - 16 ↑				
RESOLUTION = 1 POSITION				

TIME →

STARTING SECTION 1202

TEST SECTION

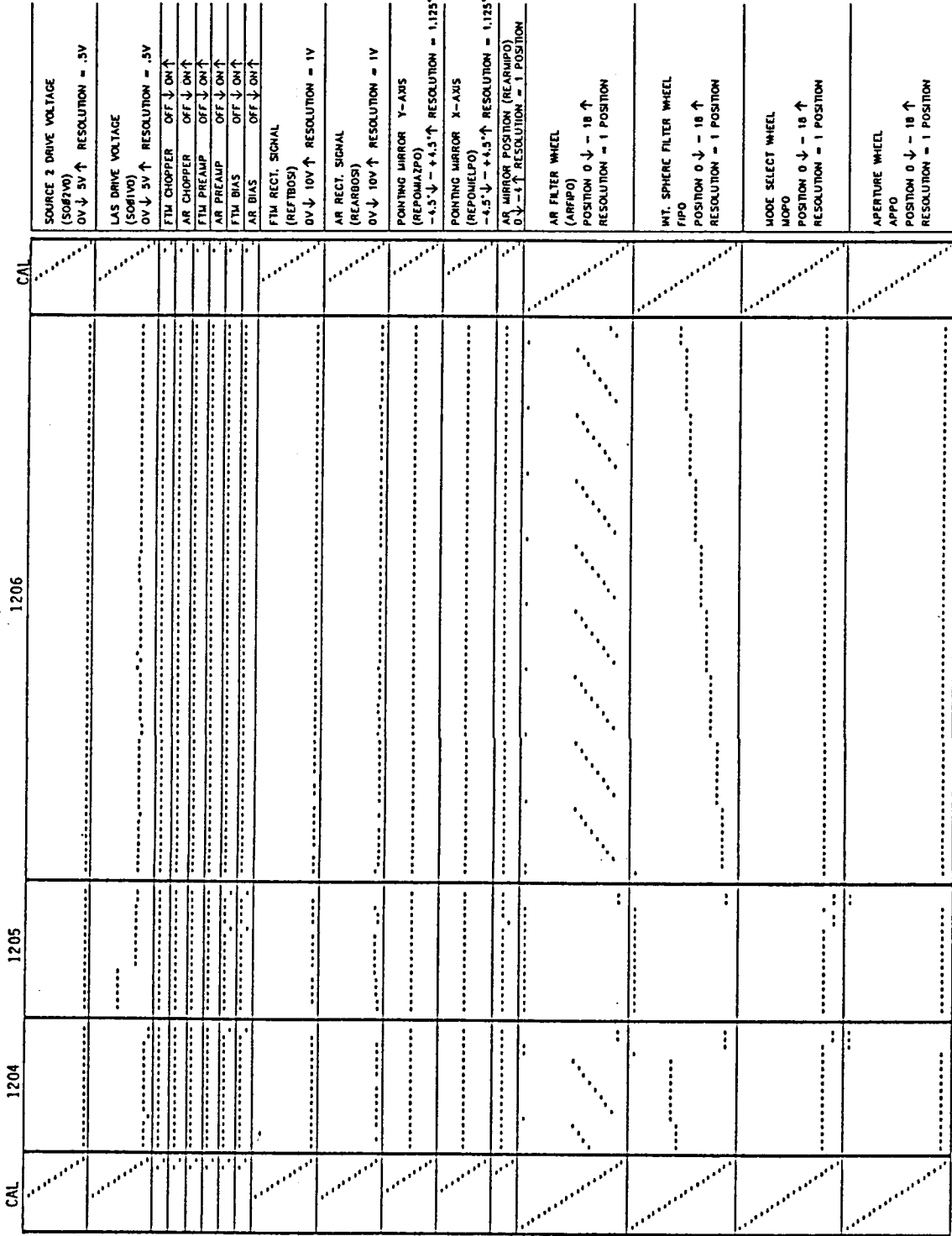


PART 2 - STARTING SECTION 1202

TIME →

ORIGINAL PAGE IS
OF POOR QUALITY

TEST SECTION



SOURCE 2 DRIVE VOLTAGE (SOB2V0)
0V ↓ 5V ↑ RESOLUTION = .5V

LAS DRIVE VOLTAGE (SOB1V0)
0V ↓ 5V ↑ RESOLUTION = .5V

FTM CHOPPER OFF ↓ ON ↑

AR CHOPPER OFF ↓ ON ↑

FTM PREAMP OFF ↓ ON ↑

AR PREAMP OFF ↓ ON ↑

FTM BIAS OFF ↓ ON ↑

AR BIAS OFF ↓ ON ↑

FTM RECT. SIGNAL (REFTB05)
0V ↓ 10V ↑ RESOLUTION = 1V

AR RECT. SIGNAL (REARB05)
0V ↓ 10V ↑ RESOLUTION = 1V

POINTING MIRROR Y-AXIS (REPOMATPO)
-4.5° ↓ - +4.5° ↑ RESOLUTION = 1.125°

POINTING MIRROR X-AXIS (REPOHELPO)
-4.5° ↓ - +4.5° ↑ RESOLUTION = 1.125°

AR MIRROR POSITION (REARMAP0)
0 ↓ 1 ↑ RESOLUTION = 1 POSITION

AR FILTER WHEEL (ARFIPO)
POSITION 0 ↓ - 18 ↑ RESOLUTION = 1 POSITION

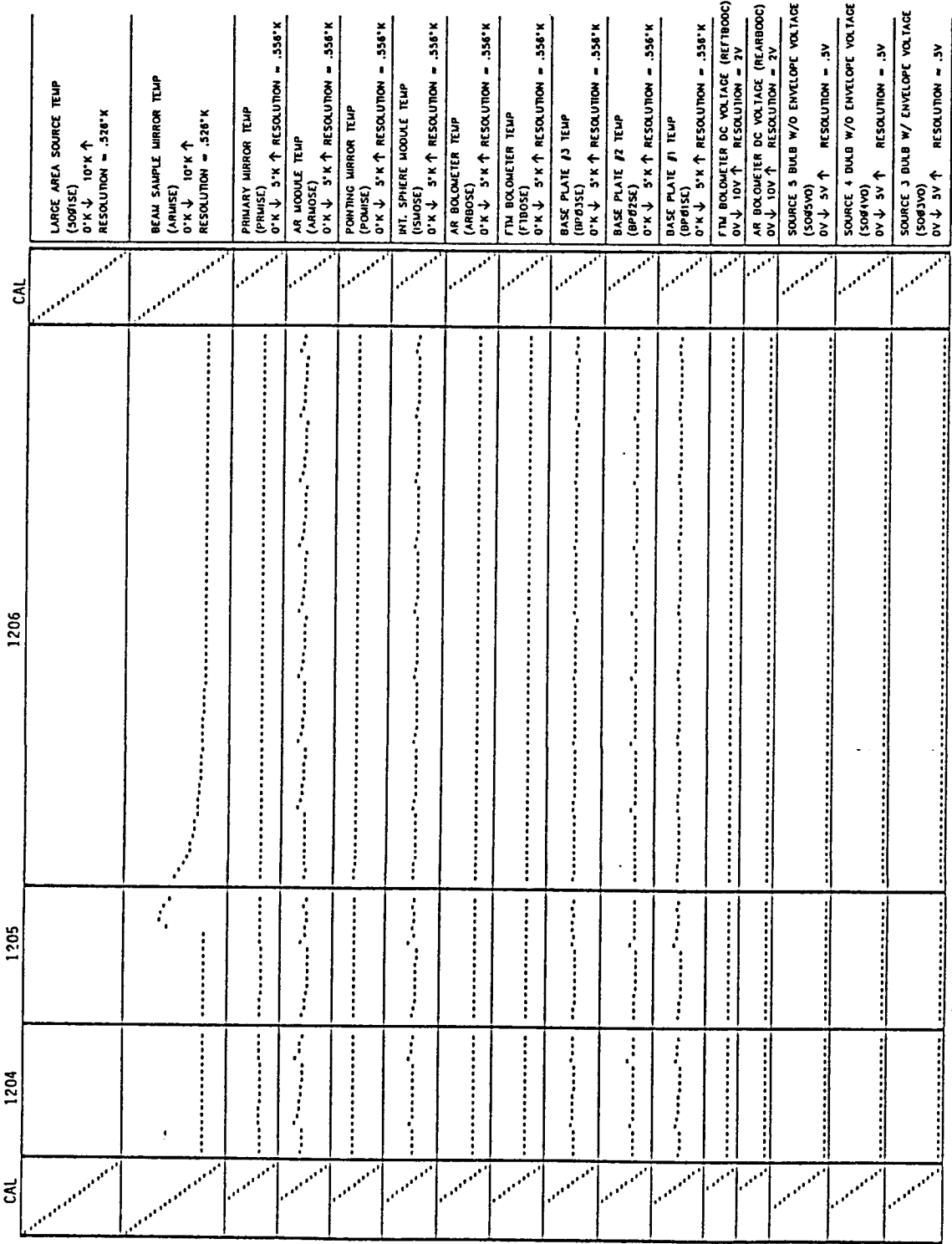
WT. SPHERIC FILTER WHEEL (FIPO)
POSITION 0 ↓ - 18 ↑ RESOLUTION = 1 POSITION

MODE SELECT WHEEL (MOPO)
POSITION 0 ↓ - 18 ↑ RESOLUTION = 1 POSITION

APERTURE WHEEL (APPO)
POSITION 0 ↓ - 18 ↑ RESOLUTION = 1 POSITION

STARTING SECTION 1204

TEST SECTION

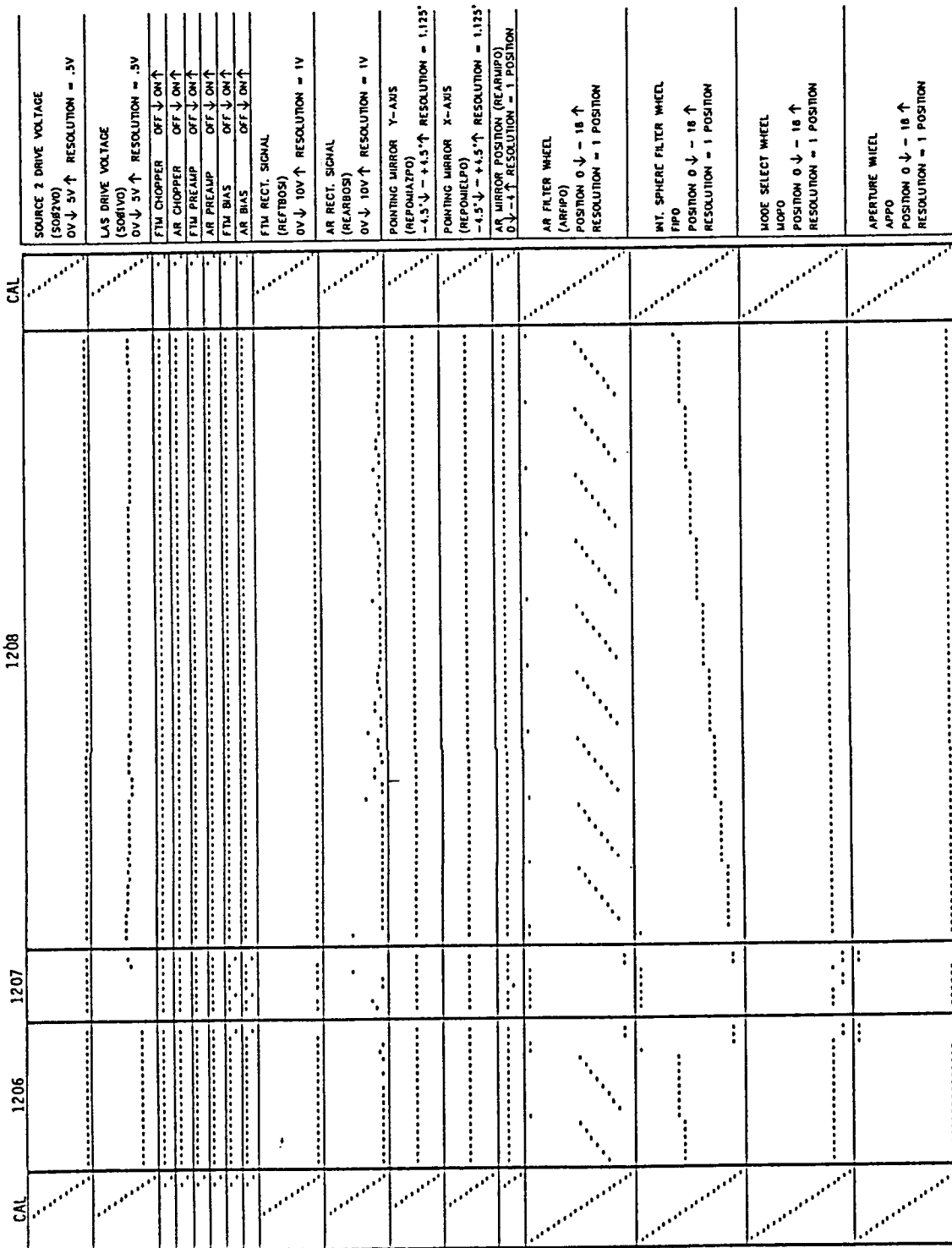


TIME →

PART 2 - STARTING SECTION 1204

ORIGINAL PAGE IS
OF POOR QUALITY

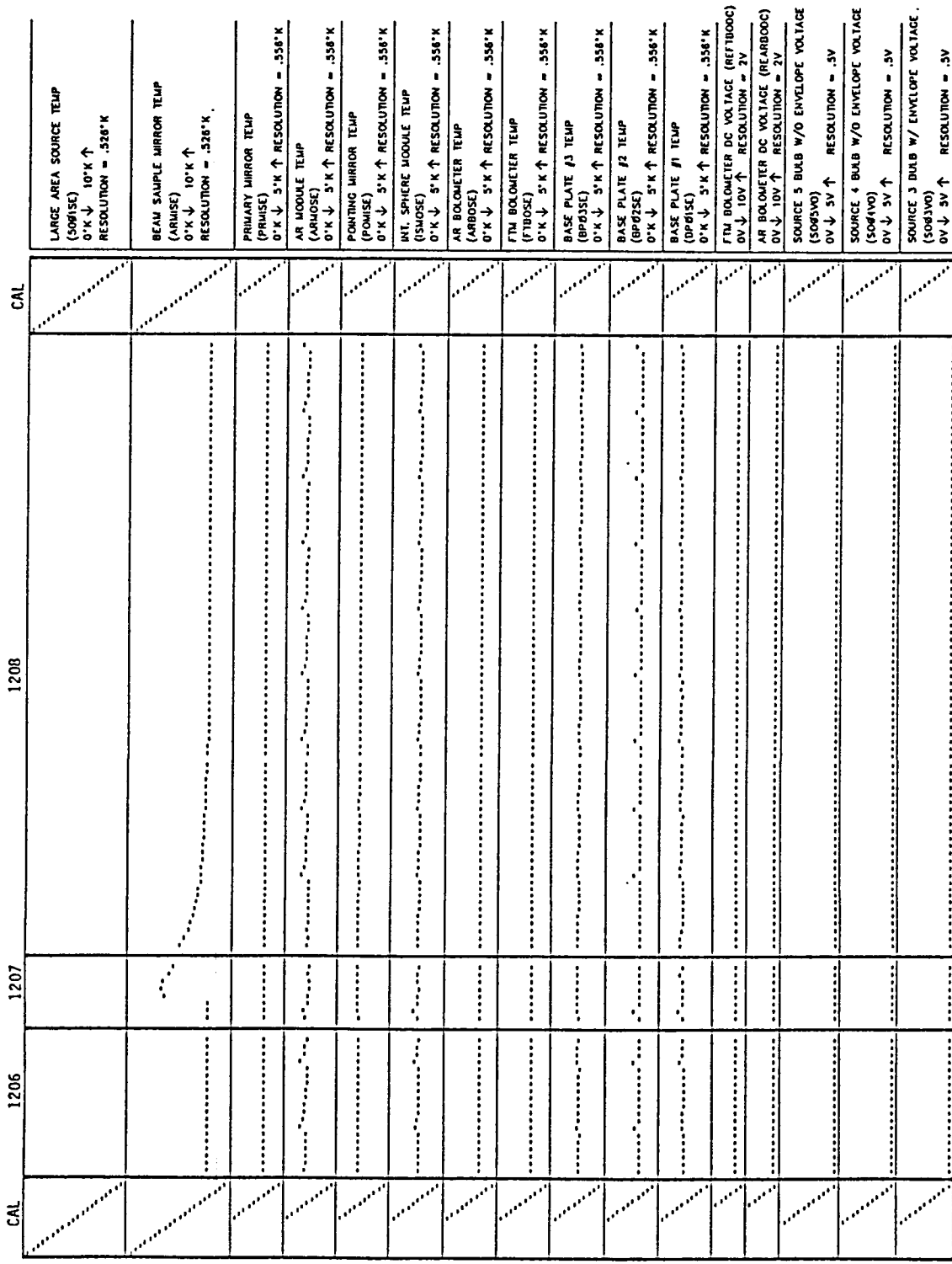
TEST SECTION



TIME →

STARTING SECTION 1206

TEST SECTION



TIME →

PART 2 - STARTING SECTION 1206

ORIGINAL PAGE IS
OF POOR QUALITY

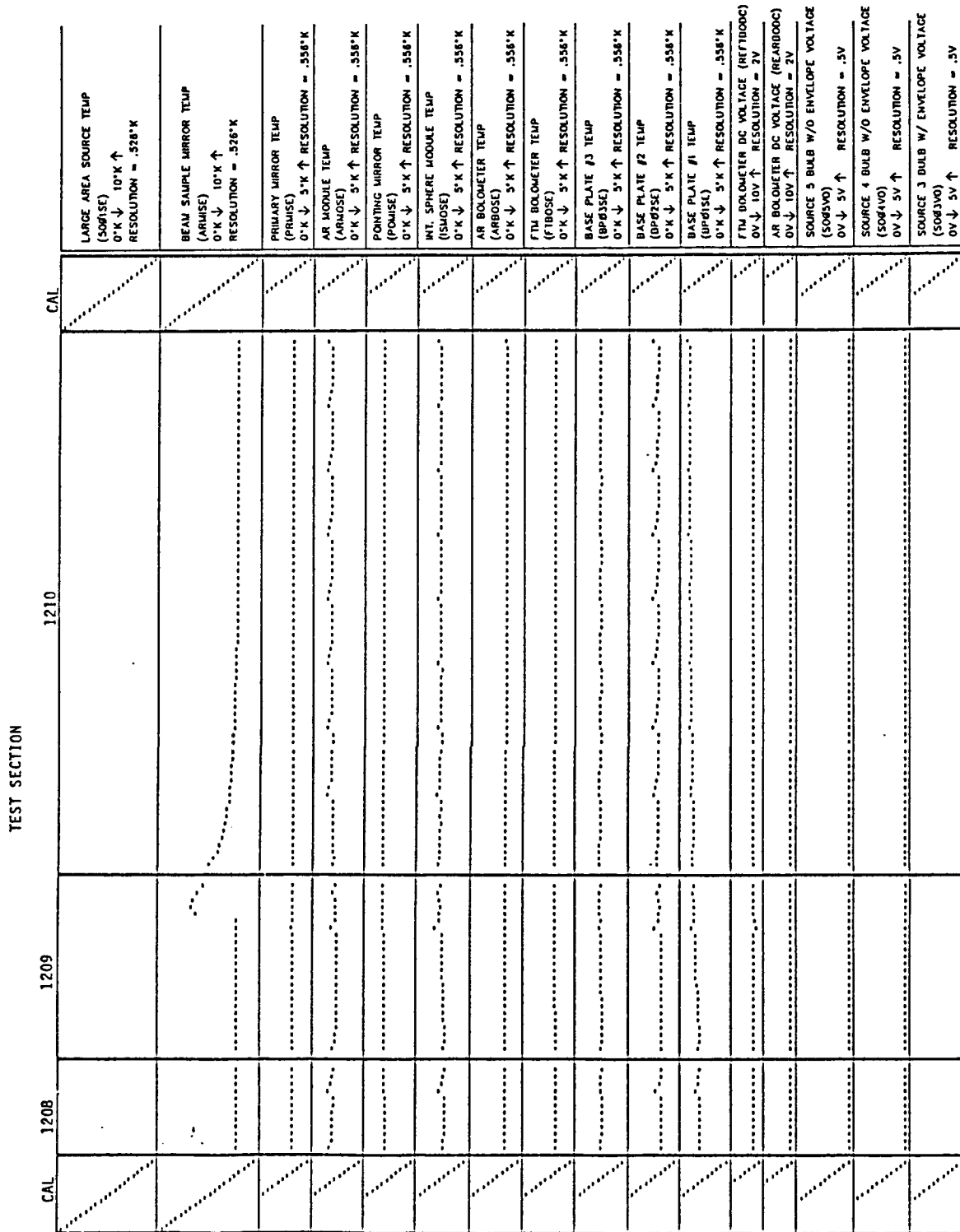
ORIGINAL PAGE IS
OF POOR QUALITY

TEST SECTION		1210	1209	1208	CAL
SOURCE 2 DRIVE VOLTAGE (SOB2V0) OV ↓ 5V ↑ RESOLUTION = .5V					
LAS DRIVE VOLTAGE (SOB1V0) OV ↓ 5V ↑ RESOLUTION = .5V					
FTM CHOPPER OFF ↓ ON ↑					
AR CHOPPER OFF ↓ ON ↑					
FTM PREAMP OFF ↓ ON ↑					
AR PREAMP OFF ↓ ON ↑					
FTM BIAS OFF ↓ ON ↑					
AR BIAS OFF ↓ ON ↑					
FTM RECT. SIGNAL (REF1B05) OV ↓ 10V ↑ RESOLUTION = 1V					
AR RECT. SIGNAL (REF2B05) OV ↓ 10V ↑ RESOLUTION = 1V					
PONTING MIRROR Y-AXIS (REPOHAZPO) -4.5 ↓ - +4.5 ↑ RESOLUTION = 1.125°					
PONTING MIRROR X-AXIS (REPOHELPO) -4.5 ↓ - +4.5 ↑ RESOLUTION = 1.125°					
AR MIRROR POSITION (REARMP0) 0 ↓ -4 ↑ RESOLUTION = 1 POSITION					
AR FILTER WHEEL (AREFPO) POSITION 0 ↓ - 18 ↑ RESOLUTION = 1 POSITION					
INT. SPHERIC FILTER WHEEL FIPO POSITION 0 ↓ - 18 ↑ RESOLUTION = 1 POSITION					
MODE SELECT WHEEL MOP0 POSITION 0 ↓ - 18 ↑ RESOLUTION = 1 POSITION					
APERTURE WHEEL APPO POSITION 0 ↓ - 18 ↑ RESOLUTION = 1 POSITION					

TIME →

STARTING SECTION 1208

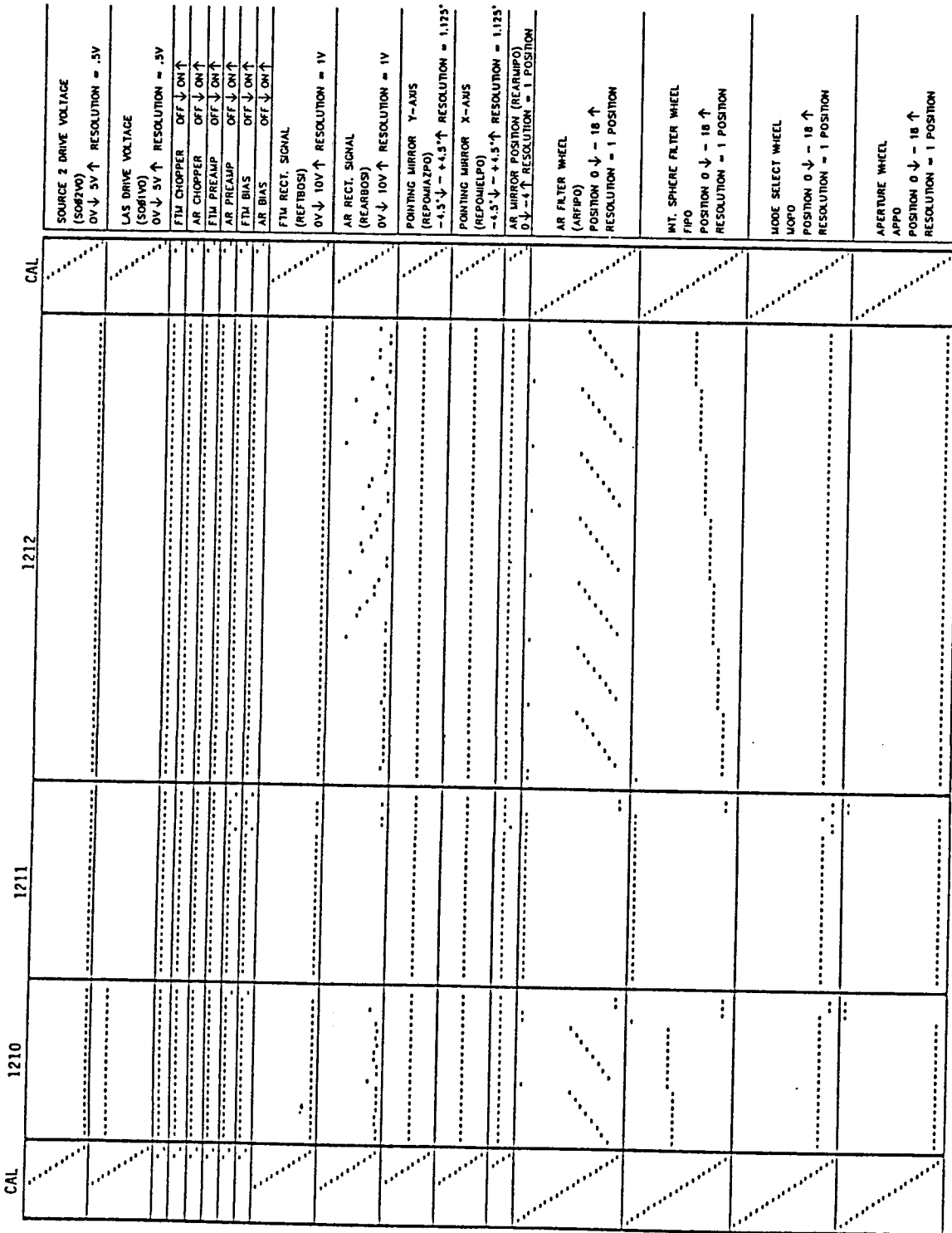
ORIGINAL PAGE IS
 OF POOR QUALITY



PART 2 - STARTING SECTION 1208

STARTING SECTION 1210

TEST SECTION



SOURCE 2 DRIVE VOLTAGE (SOM2V0)
 0V ↓ 5V ↑ RESOLUTION = .5V

LAS DRIVE VOLTAGE (SOM1V0)
 0V ↓ 5V ↑ RESOLUTION = .5V

FTM CHOPPER OFF ↓ ON ↑

FTM CHOPPER OFF ↓ ON ↑

FTM PREAMP OFF ↓ ON ↑

FTM PREAMP OFF ↓ ON ↑

FTM BIAS OFF ↓ ON ↑

FTM BIAS OFF ↓ ON ↑

FTM RECT. SIGNAL (REFTBOS)
 0V ↓ 10V ↑ RESOLUTION = 1V

AR RECT. SIGNAL (REARBOS)
 0V ↓ 10V ↑ RESOLUTION = 1V

PONTING MIRROR Y-AXIS (REPOHAZPO)
 -4.5° ↓ - +4.5° ↑ RESOLUTION = 1.125°

PONTING MIRROR X-AXIS (REPOHLEPO)
 -4.5° ↓ - +4.5° ↑ RESOLUTION = 1.125°

AR MIRROR POSITION (REARUPO)
 0 ↓ -1 ↑ RESOLUTION = 1 POSITION

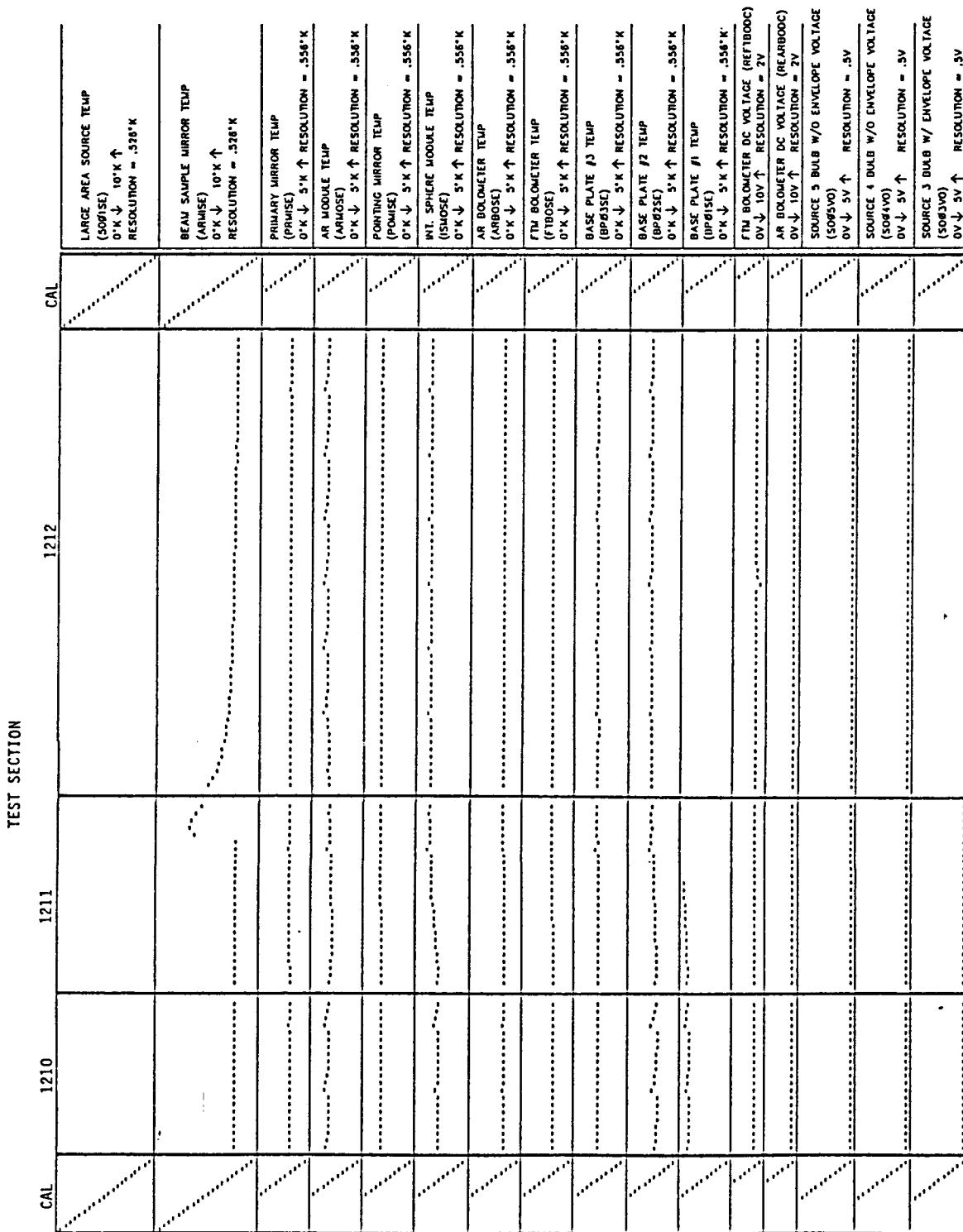
AR FILTER WHEEL (AREFPO)
 POSITION 0 ↓ - 18 ↑ RESOLUTION = 1 POSITION

INT. SPHERE FILTER WHEEL (IFPO)
 POSITION 0 ↓ - 18 ↑ RESOLUTION = 1 POSITION

MODE SELECT WHEEL (MUPO)
 POSITION 0 ↓ - 18 ↑ RESOLUTION = 1 POSITION

APERTURE WHEEL (APPO)
 POSITION 0 ↓ - 18 ↑ RESOLUTION = 1 POSITION

ORIGINAL PAGE IS
OF POOR QUALITY



PART 2 - STARTING SECTION 1210

TIME →

TEST SECTION			
1212	1213	1214	CAL

STARTING SECTION 1212

TIME →

PART 2 - STARTING SECTION 1212

TEST SECTION	1212			1213			1214			CAL
	CAL									
LARGE AREA SOURCE TEMP (5091SE) 0°K ↓ 10°K ↑ RESOLUTION = .528°K										
BEAM SAMPLE MIRROR TEMP (AR19SE) 0°K ↓ 10°K ↑ RESOLUTION = .528°K										
PRIMARY MIRROR TEMP (PR19SE) 0°K ↓ 5°K ↑ RESOLUTION = .558°K										
AR MODULE TEMP (AR10SE) 0°K ↓ 5°K ↑ RESOLUTION = .558°K										
POINTING MIRROR TEMP (PM19SE) 0°K ↓ 5°K ↑ RESOLUTION = .558°K										
INT. SPHERE MODULE TEMP (SM10SE) 0°K ↓ 5°K ↑ RESOLUTION = .558°K										
AR BOLOMETER TEMP (AR10SE) 0°K ↓ 5°K ↑ RESOLUTION = .558°K										
FTM BOLOMETER TEMP (FT10SE) 0°K ↓ 5°K ↑ RESOLUTION = .558°K										
BASE PLATE #3 TEMP (BP10SE) 0°K ↓ 5°K ↑ RESOLUTION = .558°K										
BASE PLATE #2 TEMP (BP10SE) 0°K ↓ 5°K ↑ RESOLUTION = .558°K										
BASE PLATE #1 TEMP (BP10SE) 0°K ↓ 5°K ↑ RESOLUTION = .558°K										
FTM BOLOMETER DC VOLTAGE (REF100DC) 0V ↓ 10V ↑ RESOLUTION = 2V										
AR BOLOMETER DC VOLTAGE (REAR100DC) 0V ↓ 10V ↑ RESOLUTION = 2V										
SOURCE 5 BULB W/O ENVELOPE VOLTAGE (S095V0) 0V ↓ 5V ↑ RESOLUTION = .5V										
SOURCE 4 BULB W/O ENVELOPE VOLTAGE (S084V0) 0V ↓ 5V ↑ RESOLUTION = .5V										
SOURCE 3 BULB W/ ENVELOPE VOLTAGE (S083V0) 0V ↓ 5V ↑ RESOLUTION = .5V										

TIME →

ORIGINAL PAGE IS
OF POOR QUALITY

TEST SECTION

1214

CAL

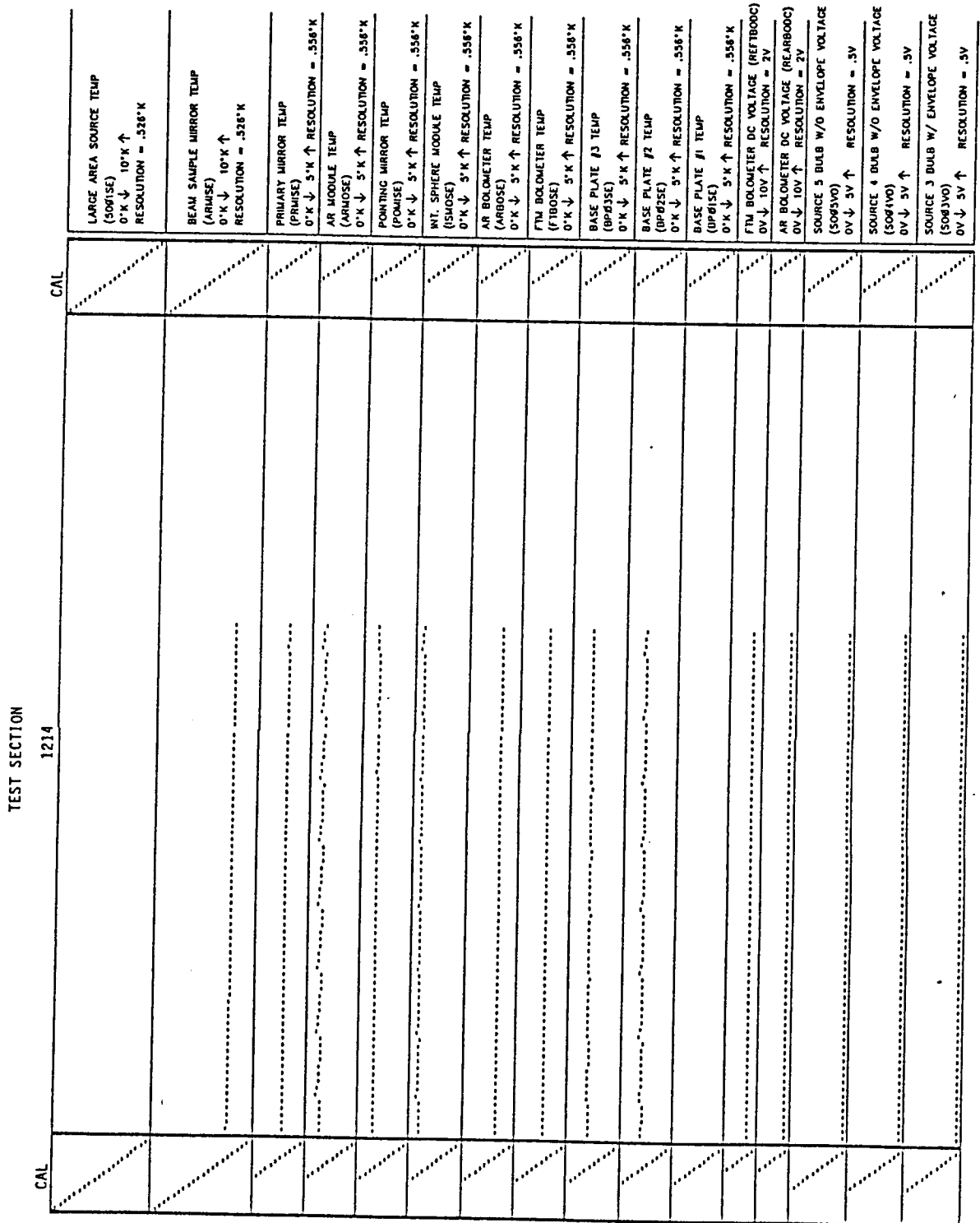
CAL

SOURCE 2 DRIVE VOLTAGE (SOP2V0) OV ↓ 5V ↑ RESOLUTION = .5V			
LAS DRIVE VOLTAGE (SOP1V0) OV ↓ 5V ↑ RESOLUTION = .5V			
FTM CHOPPER OFF ↓ ON ↑			
AR CHOPPER OFF ↓ ON ↑			
FTM PREAMP OFF ↓ ON ↑			
AR PREAMP OFF ↓ ON ↑			
FTM BIAS OFF ↓ ON ↑			
AR BIAS OFF ↓ ON ↑			
FTM RECT. SIGNAL (REFTBOS) OV ↓ 10V ↑ RESOLUTION = 1V			
AR RECT. SIGNAL (REARBOS) OV ↓ 10V ↑ RESOLUTION = 1V			
POINTING MIRROR Y-AXIS (REPOHYZPO) ** -4.5 ↓ - +4.5 ↑ RESOLUTION = 1.125'			
POINTING MIRROR X-AXIS (REPOHXLPO) ** -4.5 ↓ - +4.5 ↑ RESOLUTION = 1.125'			
AR MIRROR POSITION (REARMP0) 0 ↓ -4 ↑ RESOLUTION = 1 POSITION			
AR FILTER WHEEL (ARFIPO) POSITION 0 ↓ - 18 ↑ RESOLUTION = 1 POSITION			
INT. SPHERE FILTER WHEEL FIPO POSITION 0 ↓ - 18 ↑ RESOLUTION = 1 POSITION			
MODE SELECT WHEEL MOP0 POSITION 0 ↓ - 18 ↑ RESOLUTION = 1 POSITION			
APERTURE WHEEL APPO POSITION 0 ↓ - 18 ↑ RESOLUTION = 1 POSITION			

TIME →

STARTING SECTION 1214

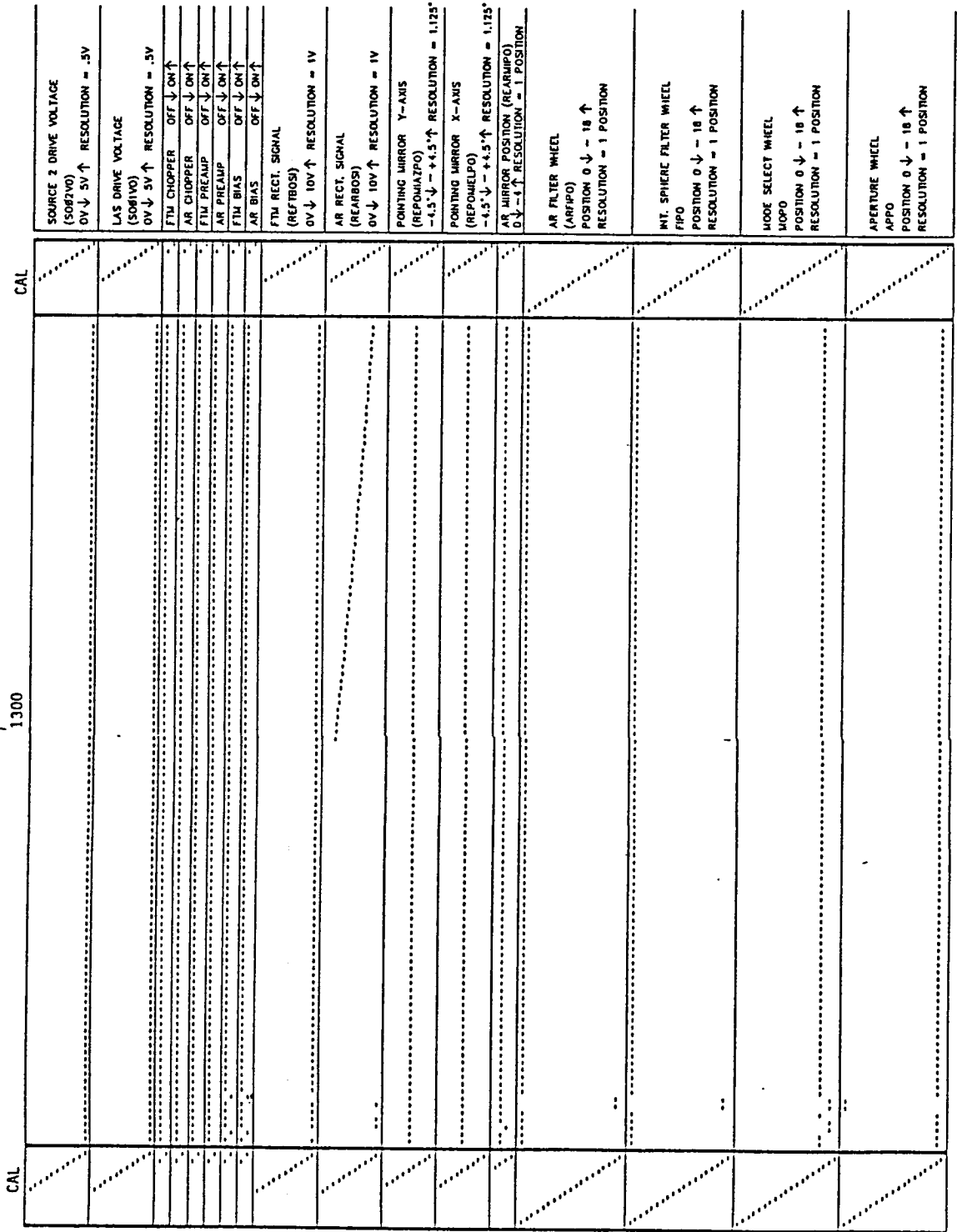
PART 2 - STARTING SECTION 1214



TIME →

ORIGINAL PAGE IS
OF POOR QUALITY

TEST SECTION
1300



TIME →

STARTING SECTION 1300

ORIGINAL PAGE IS
 OF POOR QUALITY

TEST SECTION

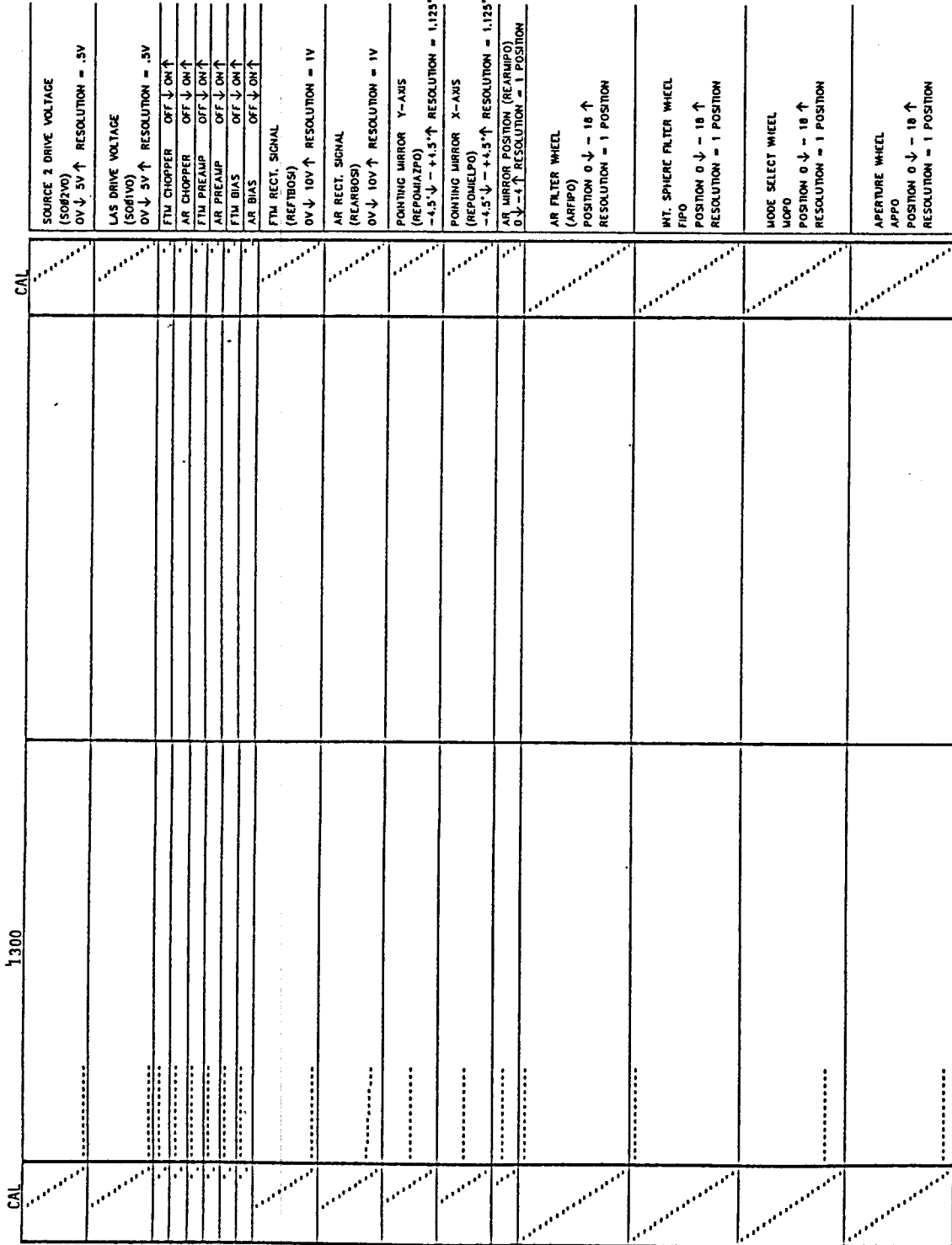
1300

CAL	CAL		
			LARGE AREA SOURCE TEMP (S061SE) 0°K ↓ 10°K ↑ RESOLUTION = .328°K
			BEAM SAMPLE MIRROR TEMP (ARMSSE) 0°K ↓ 10°K ↑ RESOLUTION = .328°K
			PRIMARY MIRROR TEMP (PRMSSE) 0°K ↓ 5°K ↑ RESOLUTION = .558°K
			AR MODULE TEMP (ARMSSE) 0°K ↓ 5°K ↑ RESOLUTION = .558°K
			POINTING MIRROR TEMP (POMISE) 0°K ↓ 5°K ↑ RESOLUTION = .558°K
			INT. SPHERE MODULE TEMP (SMOSE) 0°K ↓ 5°K ↑ RESOLUTION = .558°K
			AR BOLOMETER TEMP (ARBOSSE) 0°K ↓ 5°K ↑ RESOLUTION = .558°K
			FTM BOLOMETER TEMP (FTBOSE) 0°K ↓ 5°K ↑ RESOLUTION = .558°K
			BASE PLATE #3 TEMP (BP#3SE) 0°K ↓ 5°K ↑ RESOLUTION = .558°K
			BASE PLATE #2 TEMP (BP#2SE) 0°K ↓ 5°K ↑ RESOLUTION = .558°K
			BASE PLATE #1 TEMP (BP#1SE) 0°K ↓ 5°K ↑ RESOLUTION = .558°K
			FTM BOLOMETER DC VOLTAGE (REF7B00C) 0V ↓ 10V ↑ RESOLUTION = 2V
			AR BOLOMETER DC VOLTAGE (REARB00C) 0V ↓ 10V ↑ RESOLUTION = 2V
			SOURCE 5 BULB W/O ENVELOPE VOLTAGE (S065V0) 0V ↓ 5V ↑ RESOLUTION = .5V
			SOURCE 4 BULB W/O ENVELOPE VOLTAGE (S064V0) 0V ↓ 5V ↑ RESOLUTION = .5V
			SOURCE 3 BULB W/ ENVELOPE VOLTAGE (S063V0) 0V ↓ 5V ↑ RESOLUTION = .5V

TIME →

PART 2 - STARTING SECTION 1300

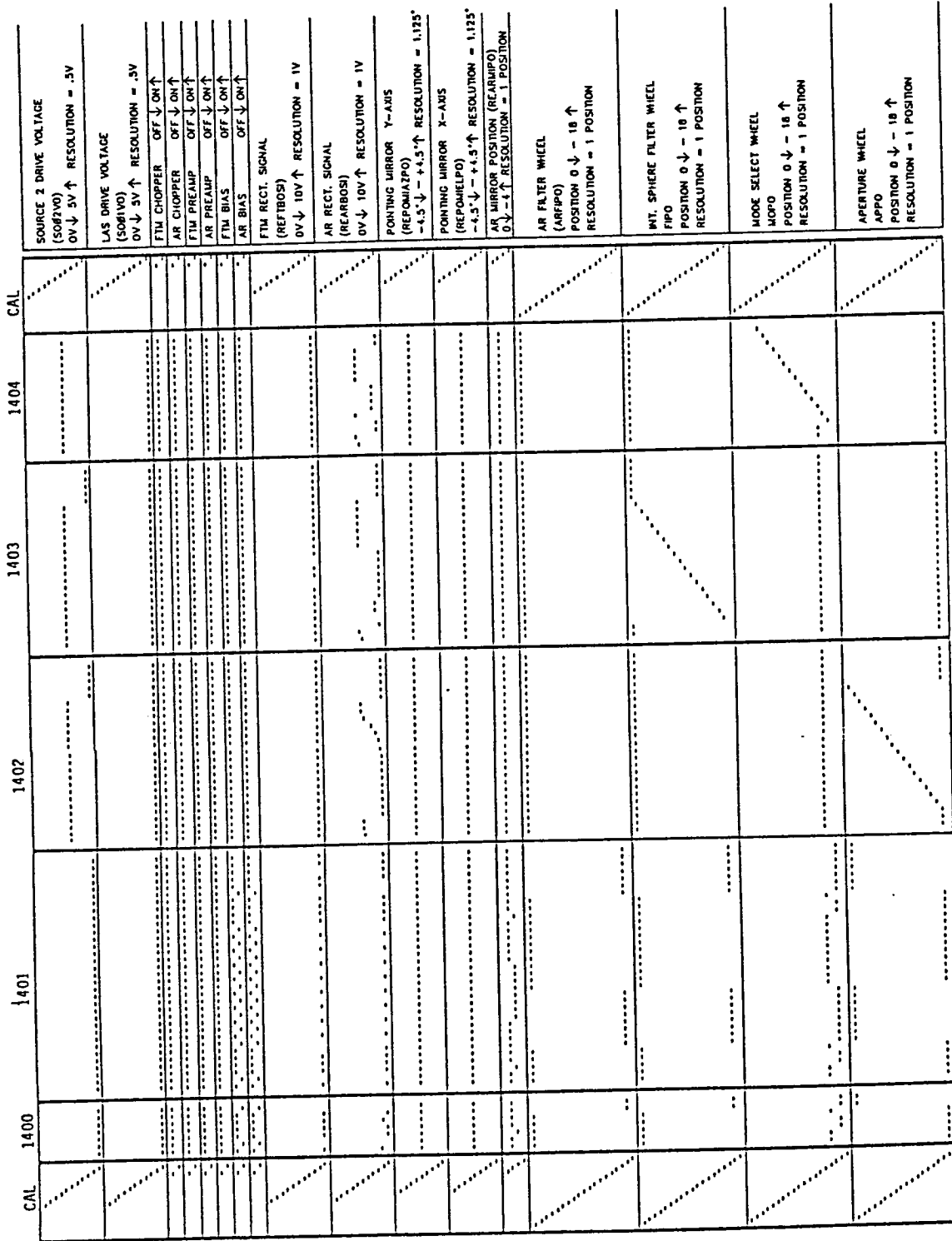
TEST SECTION



STARTING SECTION 1300

STARTING SECTION 1400

TEST SECTION



SOURCE 2 DRIVE VOLTAGE (SOP2V0)
 0V ↓ 5V ↑ RESOLUTION = .5V

LAS DRIVE VOLTAGE (SOP1V0)
 0V ↓ 5V ↑ RESOLUTION = .5V

FTM CHOPPER OFF ↓ ON ↑

AR CHOPPER OFF ↓ ON ↑

FTM PREAMP OFF ↓ ON ↑

AR PREAMP OFF ↓ ON ↑

FTM BIAS OFF ↓ ON ↑

AR BIAS OFF ↓ ON ↑

FTM RECT. SIGNAL (REFTBOS)
 0V ↓ 10V ↑ RESOLUTION = 1V

AR RECT. SIGNAL (REARBOS)
 0V ↓ 10V ↑ RESOLUTION = 1V

PONTING MIRROR Y-AXIS (REQUHAZPO)
 -4.5 ↓ -+4.5 ↑ RESOLUTION = 1.125°

PONTING MIRROR X-AXIS (REQUHELPO)
 -4.5 ↓ -+4.5 ↑ RESOLUTION = 1.125°

AR MIRROR POSITION (REARMPO)
 0 ↓ -4 ↑ RESOLUTION = 1 POSITION

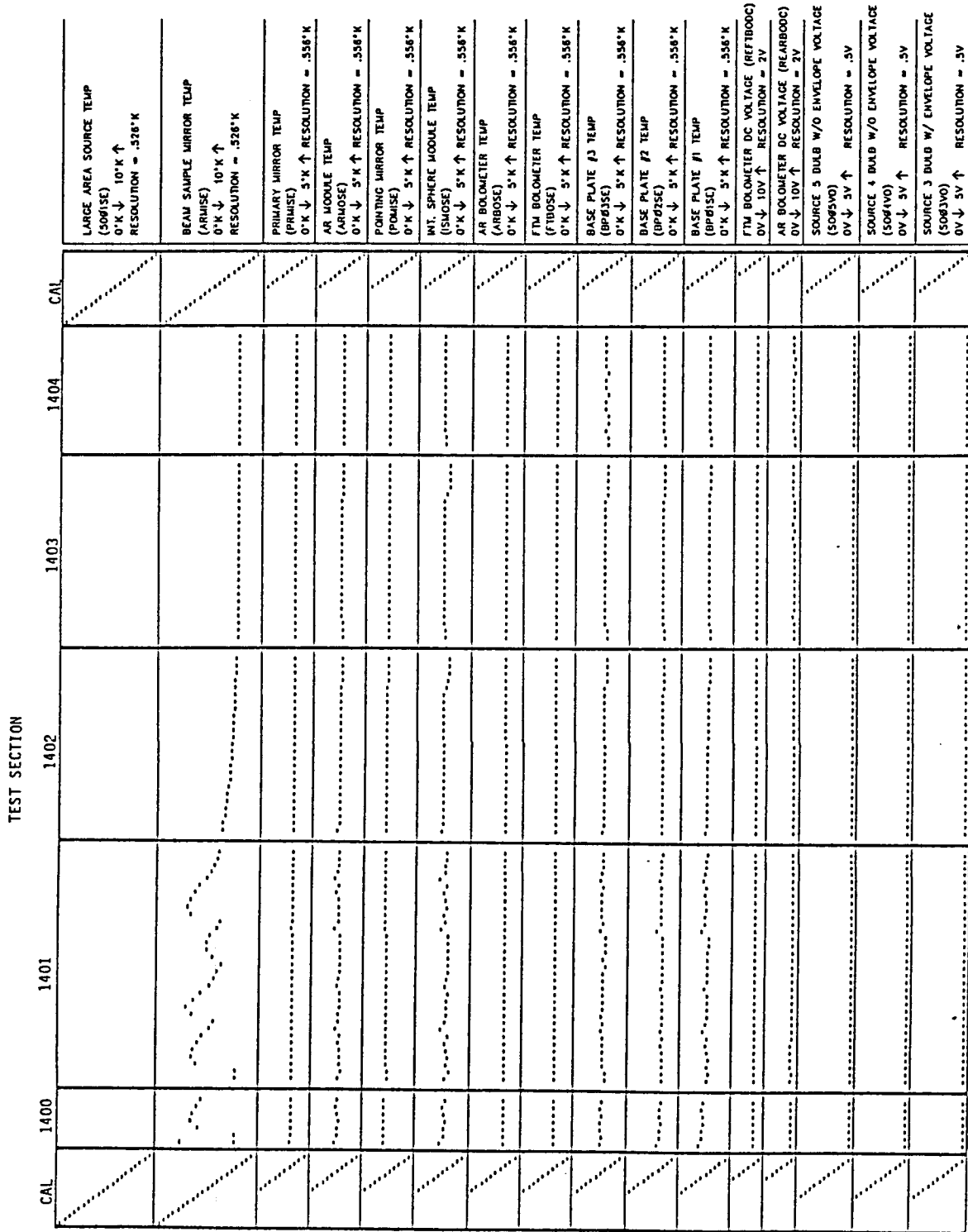
AR FILTER WHEEL (AREFPO)
 POSITION 0 ↓ - 18 ↑
 RESOLUTION = 1 POSITION

INT. SPHERE FILTER WHEEL (IFPO)
 POSITION 0 ↓ - 18 ↑
 RESOLUTION = 1 POSITION

MODE SELECT WHEEL (MOP0)
 POSITION 0 ↓ - 18 ↑
 RESOLUTION = 1 POSITION

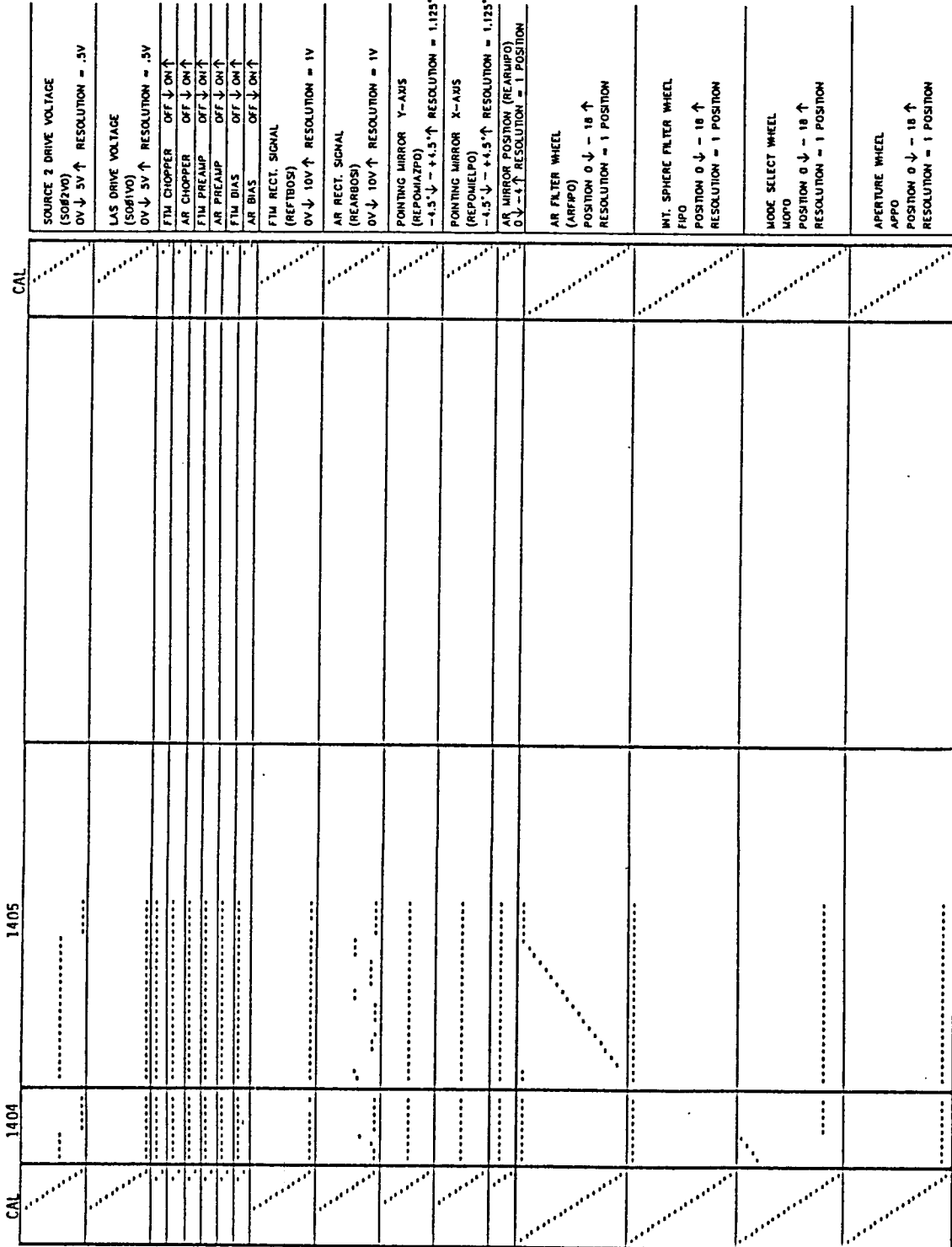
APERTURE WHEEL (APPO)
 POSITION 0 ↓ - 18 ↑
 RESOLUTION = 1 POSITION

ORIGINAL PAGE IS
OF POOR QUALITY



PART 2 - STARTING SECTION 1400

TEST SECTION



STARTING SECTION 1484

TEST SECTION

	1404	1405		CAL
LARGE AREA SOURCE TEMP (SOP15C) 0°K ↓ 10°K ↑ RESOLUTION = .528°K				
BEAM SAMPLE MIRROR TEMP (ARM15E) 0°K ↓ 10°K ↑ RESOLUTION = .528°K				
PRIMARY MIRROR TEMP (PRM15E) 0°K ↓ 5°K ↑ RESOLUTION = .558°K				
AR MODULE TEMP (ARM105E) 0°K ↓ 5°K ↑ RESOLUTION = .558°K				
POINTING MIRROR TEMP (POM15E) 0°K ↓ 5°K ↑ RESOLUTION = .558°K				
INT. SPHERE MODULE TEMP (ISM05E) 0°K ↓ 5°K ↑ RESOLUTION = .558°K				
AR BOLOMETER TEMP (ARB05E) 0°K ↓ 5°K ↑ RESOLUTION = .558°K				
F1M BOLOMETER TEMP (F1B05E) 0°K ↓ 5°K ↑ RESOLUTION = .558°K				
BASE PLATE J3 TEMP (BPJ3E) 0°K ↓ 5°K ↑ RESOLUTION = .558°K				
BASE PLATE J2 TEMP (BPJ2E) 0°K ↓ 5°K ↑ RESOLUTION = .558°K				
BASE PLATE J1 TEMP (BPJ1E) 0°K ↓ 5°K ↑ RESOLUTION = .558°K				
F1M BOLOMETER DC VOLTAGE (REF1B00C) 0V ↓ 10V ↑ RESOLUTION = 2V				
AR BOLOMETER DC VOLTAGE (REARB00C) 0V ↓ 10V ↑ RESOLUTION = 2V				
SOURCE 5 BULB W/O ENVELOPE VOLTAGE (S053V0) 0V ↓ 5V ↑ RESOLUTION = .5V				
SOURCE 4 BULB W/O ENVELOPE VOLTAGE (S043V0) 0V ↓ 5V ↑ RESOLUTION = .5V				
SOURCE 3 BULB W/ ENVELOPE VOLTAGE (S033V0) 0V ↓ 5V ↑ RESOLUTION = .5V				

PART 2 - STARTING SECTION 1404

TIME →

This page intentionally left blank.

APPENDIX G
Bolometer Data

This page intentionally left blank.

Full-time Monitor Bolometer Data

PRECEDING PAGE BLANK NOT FILMED

This page intentionally left blank.

FTM BOLOMETER

INFRARED LABORATORIES, INC.

1808 EAST 17TH STREET
TUCSON, ARIZONA 85718
PHONE: (602) 822-7074
TLX 364412 INTR

UTAH STATE UNIVERSITY

BOLOMETER NOTES

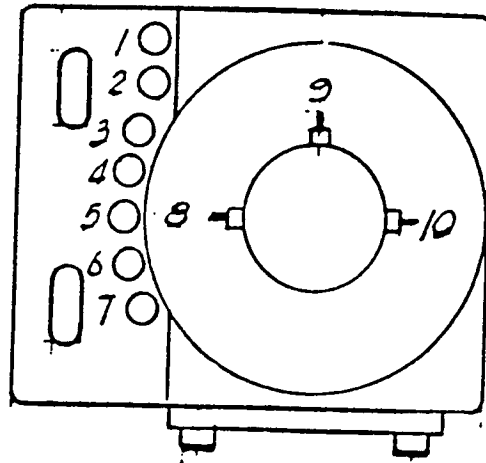
The germanium bolometer, Unit #904, has been mounted in conjunction with a parabolic cone optic in accordance with Utah State University specifications. The bolometer itself is of the composite type and features a 1.75 mm octagonal absorber with nichrome absorbing material mounted within a specially-shaped cavity at the exit aperture of a F/3.0 cone condenser. This cone condenser features an entrance aperture of 6.0 mm and an exit aperture of 1.0 mm.

A nominal 10.0 megohm load resistor has been integrated into the substrate with an input terminal on the side of the substrate. Both detector leads have been brought out to standoff terminals mounted on the side of the substrate. Wiring of the entire module is shown on Utah State DEC Bolometer Preamp Drwg. No. B4-2133 and Fig. I

Exercise great caution not to accidentally over bias the detector. Never allow more than 10 microamps of current to flow through the bolometer itself. Always use high impedance measuring devices when working with the bolometer circuit.

The personnel of Infrared Laboratories, Inc. stand ready to assist you. Please do not hesitate to call on us.


Arnold W. Davidson, Manager



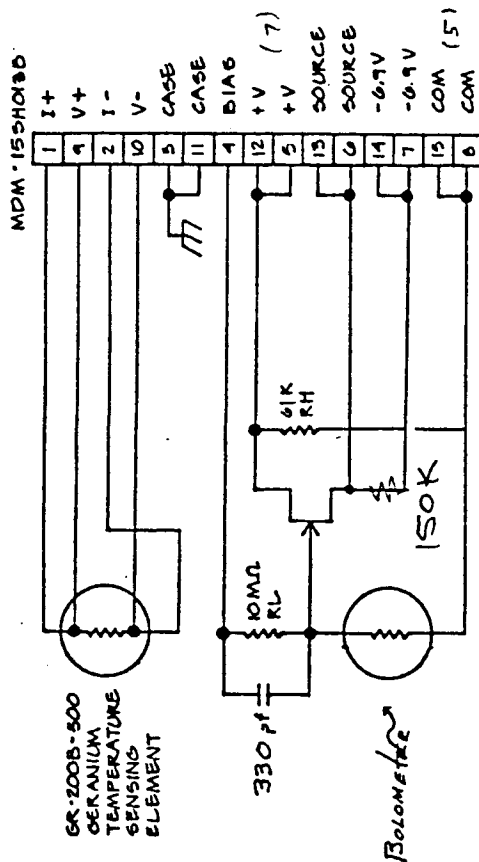
- 1 - I +
- 2 - V +
- 3 - I -
- 4 - V -
- 5 - COMMON
- 6 - SOURCE
- 7 - + V DRAIN
- 8 - LOAD RESISTOR
- 9 - BOLOMETER COMMON
- 10 - BOLOMETER OUTPUT

FIG. I

Figure G-1. Wiring diagram for DEC bolometer module.

0 1 2 3 4 5 6 7 8 9

ORIGINAL PAGE IS
OF POOR QUALITY



8 7 6 5 4 3 2 1
0 0 0 0 0 0 0 0
15 14 13 12 11 10 9

PIN CONFIGURATION
FRONT OF MDM-155H013B

ITEM	QTY.	PART NO.	DESCRIPTION	SPECIFICATIONS
DEC BOLOMETER PREAMP				
DRAWN BY: SJD CHECKED: DATE: SCALE: .001 & .005 .001 & .01 FRACTIONS IN ANGLES & TOLERANCES				
SPACE DYNAMICS LABORATORIES UTAH STATE UNIVERSITY UMC 41 LOGAN, UTAH 84322 (801) 780-2905				
ENGR. APPV. _____ SHEET _____ OF _____ DRAWING NUMBER D4-2133			REV.	
NO.	BY	DATE	DESCRIPTION	REVISIONS
			NEXT ASSY.	
			DWG. NO.	
			DWG. NO.	
			DRAWINGS USED IN	

Figure G-2. DEC Bolometer Preampifier Schematic.

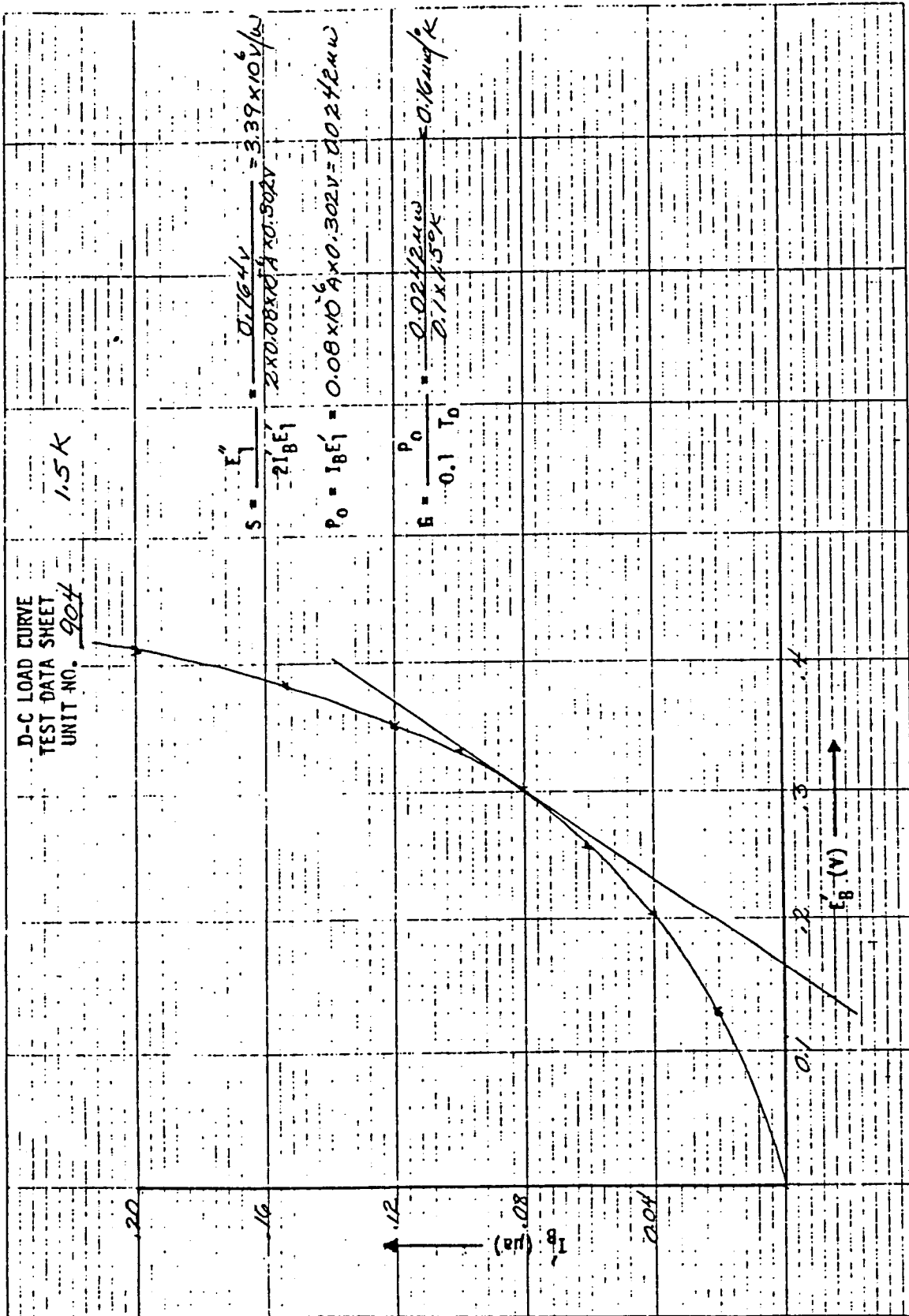


Figure G-3. DC Load Curve, 1.5K, Unit No. 904.

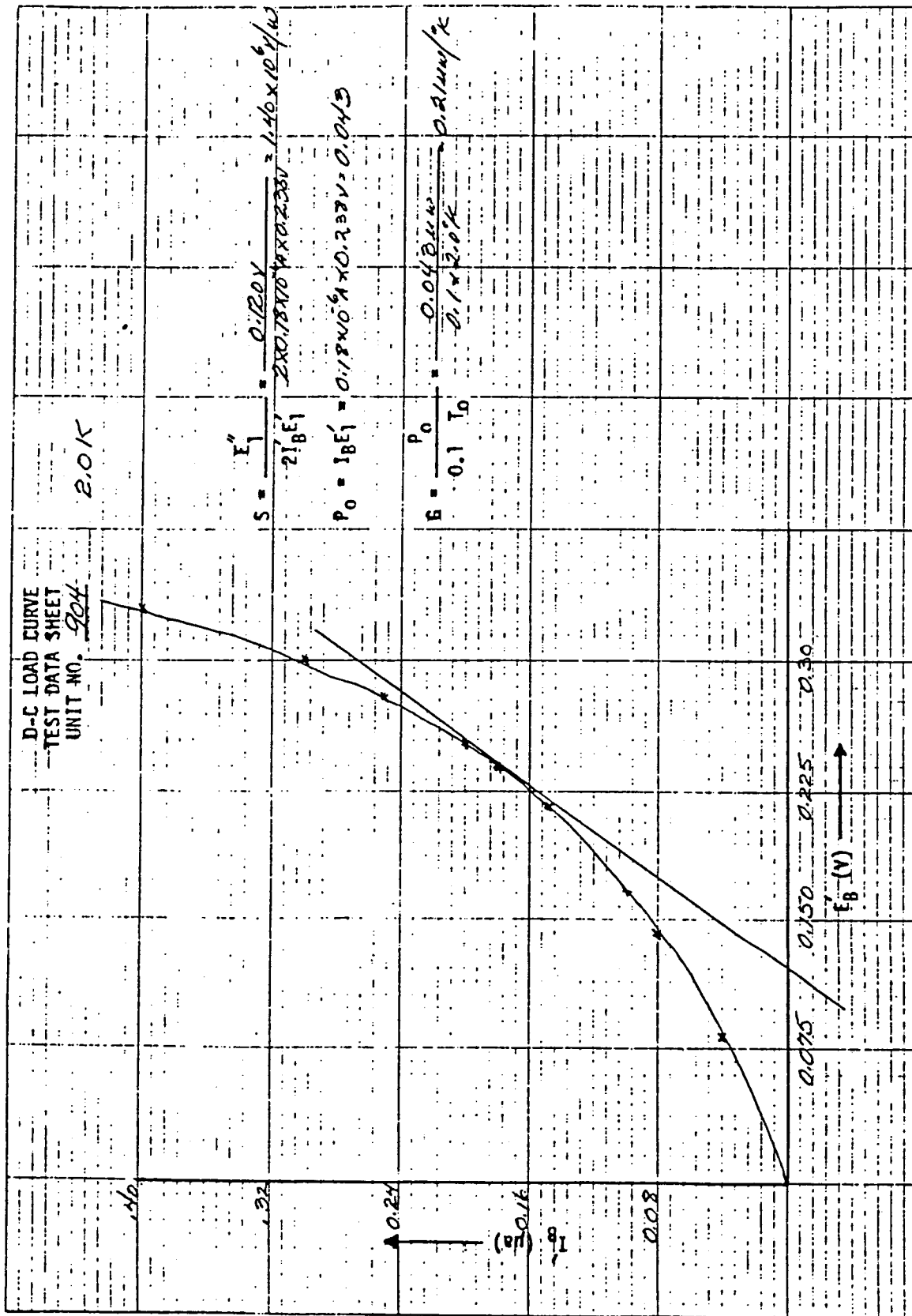


Figure G-4. DC Load Curve, 2.0K, Unit No. 904.

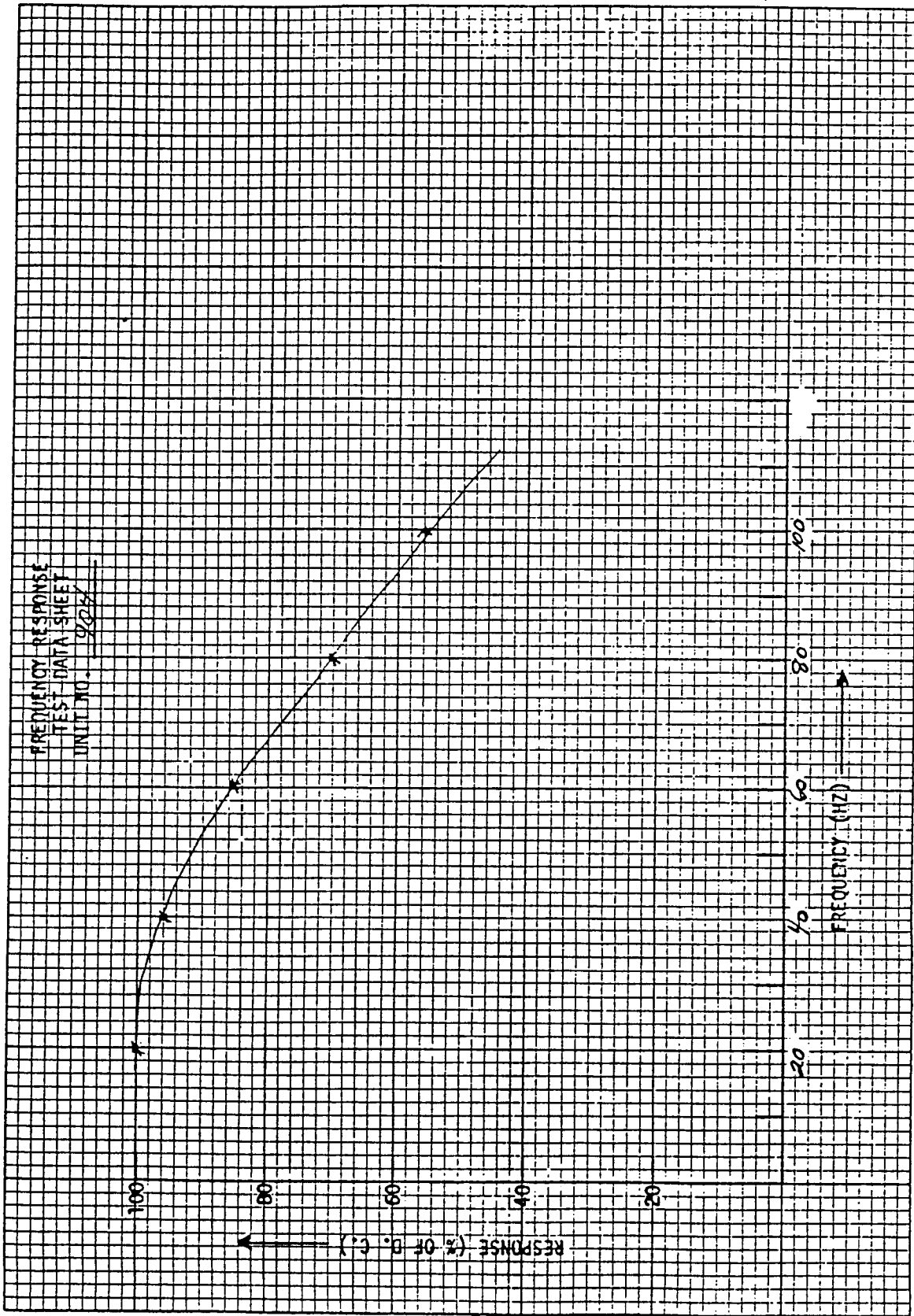


Figure G-5. Frequency response, Unit No. 904.

ORIGINAL PAGE IS
OF POOR QUALITY

UTAH STATE UNIVERSITY

NOTE: The JFet module can be operated up to +12 volts on the drain and -12 volts on the source. A small reduction in noise may be obtained by running the drain at +3 volts and the source at -9 volts. The source resistor which will be external should be chosen to operate the module at approximately 300 μ W of power. It is recommended that a metal film resistor be used as the source resistor.

The wires leading to the germanium temperature sensing element were not fastened down to allow you to install your cold strap first. These wires should be heat sunk to the substrate after installing the cold strap.

Leads #17 and #14 on MDM-155H013B connector are not used because of external source resistor and were left unused in case you wish to use them for something else, or, they may be cut off.

WARNING - IF JFET SOURCE RESISTOR IS SHORTED, DESTRUCTION OF MODULE COULD RESULT.

GENERAL DESCRIPTION

A complete detector system consists of three main parts: The detector mounted on a copper substrate, the liquid helium dewar, and the preamplifier. The preamplifier is bolted directly to the side of the dewar case and is powered by an external supply. This system is mechanically rugged and can be operated under a wide range of environmental conditions and in any attitude within a few degrees horizontal. The usual precautions for handling cryogenic liquids should be followed.* The case of the dewar is evacuated to forepump pressure before use. After periods of several weeks, it may be necessary to reevacuate the bottom plate of the dewar, which is sealed with a rubber O-ring, and then by removing the bottom plate of the radiation shield. A system of internal supports is provided to allow accurate alignment of the cooled surface with respect to the outer case. These supports are the most fragile components in the system. Excessive mechanical shock may fracture one or more of the supports. In order to minimize the possibility of such damage in shipment, the following precautions have been taken. The two bottom plates have been removed and a rigid clamp attached in their place with the internal supports partially loosened. It is necessary to remove the clamp and tighten the internal supports to produce the desired alignment. The two bottom plates may then be replaced according to the enclosed instructions. The case can then be evacuated to forepump pressure and the dewar cooled for operation.

*One of several standard textbooks on this subject is Cryogenic Engineering, by Russell B. Scott, published by D. Van Nostrand Co., Inc., Princeton, New Jersey, Copyright 1959.

COOLING THE DEWAR

After evacuation of the case to forepump pressure, the dewar should be precooled with liquid N₂ or liquid air. A minimum precooling of 5 minutes should be used. Precooling for several hours reduces the consumption of helium.

Before transferring liquid helium, all precoolant must be removed, either by pouring out the liquid or by transferring it. The helium transfer tube should be flushed with helium gas and slowly inserted into the storage dewar. Sealing the top of the storage dewar traps the evolving helium gas and starts to build up pressure which vents through the transfer tube. When tube is touching bottom of storage dewar, an overpressure of about 1/4 psi of helium should be maintained. As the transfer tube cools, it should be inserted into the experimental dewar until it almost touches bottom. Rapid efflux of cold vapor continues for several minutes until liquid begins to collect. A sudden drop in blow-off signals that the liquid is collecting. At a pressure of 1/4 psi, the 1.2 liter dewar should fill in about 2 minutes. When liquid reaches the restricted neck, a sudden jet of very cold gas signals that the transfer is complete. The pressure applied to the storage dewar is released and the tube withdrawn. Do not fail to cap the storage dewar or to turn off the supply of helium gas.

A normal transfer will consume about 2.5 liters of liquid helium and will last about 5 minutes. It is normal for the initial boil-off to be readily visible. As the radiation shield cools, this visible plume will gradually disappear.

PUMPING THE DEWAR

At sea level liquid helium boils at 4.2°K. Most bolometers will be operated below the lambda point of liquid helium at 2.17°K. In the superfluid state, liquid helium is quite stable.

By reducing the vapor pressure above the liquid, temperatures down to 1°K may be attained. 2°K corresponds to a vapor pressure of about 20mm Hg, a very desirable operating point. Figure G-6 shows the pumping system used for this purpose.

A slow pump-down conserves helium. a good indicator is the temperature of the pumping fitting. If ice forms on the outside, you are going a bit fast. After about 45 minutes the lambda point at 38mm Hg should be reached. Once through the transition, the throttle valve can be opened and equilibrium can be reached in about 15 minutes. This recommended period of 1 hour can be shortened to perhaps 30 minutes, but going too fast may simply pump all the helium out of the dewar.

In some pumping systems thermo-mechanical oscillations may occur and rapidly consume the liquid helium. This problem is always solvable by increasing or decreasing the diameter of various sections of the system. This is an annoyance which fortunately is not too common.

A word of caution about air leaks in the pumping system: if air leaks in, it will freeze in the neck tube. If the neck tube becomes blocked, the dewar will rupture! Test for air leaks beforehand and always use the safety feature built into the pumping fitting. The reentrant tube prevents complete blockage of the neck should an air leak be present.

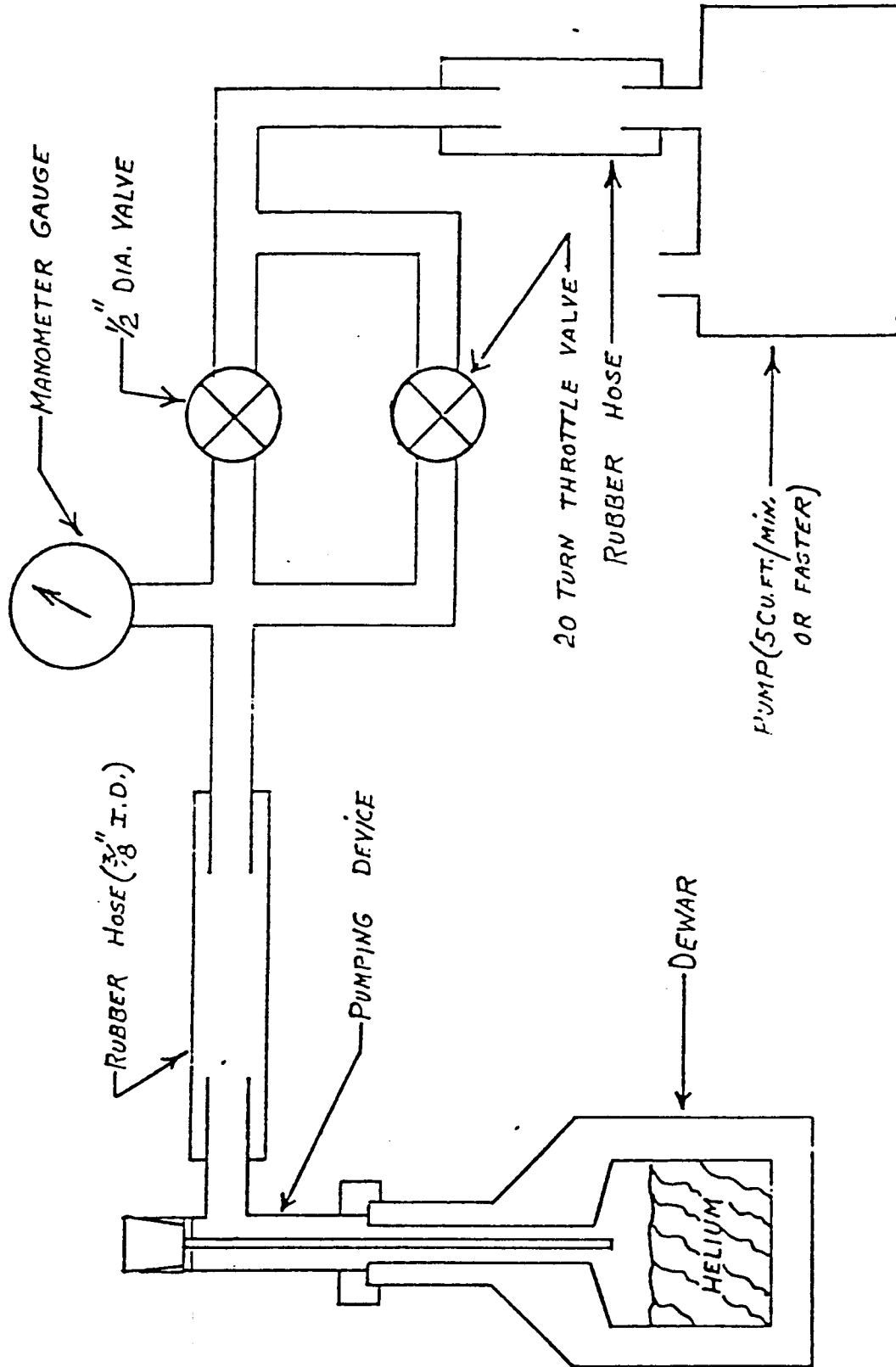
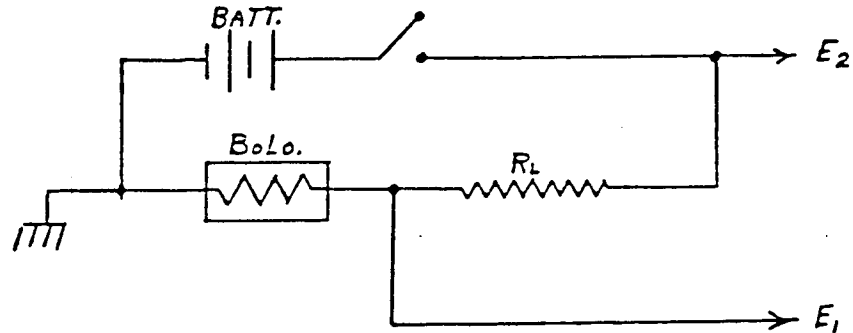


Figure G-6. Pumping system.

RECOMMENDED TEST PROCEDURES

DC Load Curve:

With the bath stabilized at operating temperature and instruments connected as shown in Figure G-7, the E. I. characteristic may be measured. The input impedance of the voltmeter used to measure E_1 should be more than 10 times R_o , the bolometer resistance. The current, I_B , is simply, $(E_2 - E_1)/R_L$. A typical load curve is shown in Figure G-8.



Note: E_2 varied from 0 to R_L/I_B (Max.)

E_1 is measured by high impedance voltmeter.

Figure G-7. Load Curve Setup.

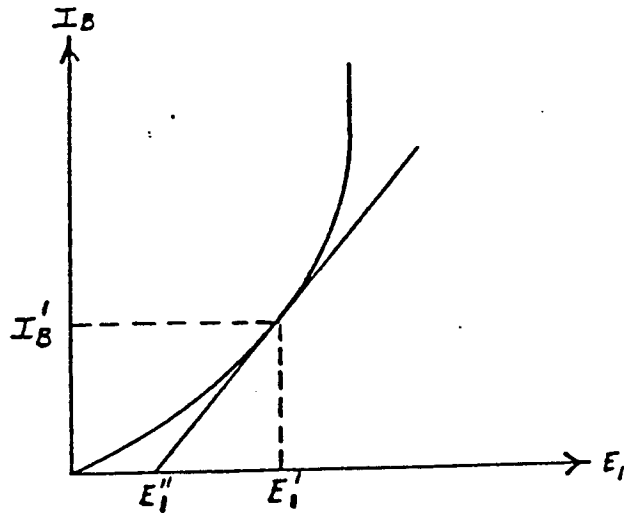


Figure G-8. Load Curve.

Frequency Response:

If a bright source can be placed close enough to the window, the arrangement of Figure G-9 may be used where the oscilloscope responds to d.c. If higher gain is needed, a.c. coupling must be used. The preamplifier, for example, could be utilized with a low gain oscilloscope. In any case, it is necessary to be certain that the true d.c. signal level has been measured, i.e., the a.c. response must be low enough to allow extrapolation to zero frequency. If the bolometer is properly constructed, it will have a single time constant and its frequency response will be as illustrated in Figure G-10a. If, however, there are two time constants, with one very long, the result may resemble Figure G-10b.

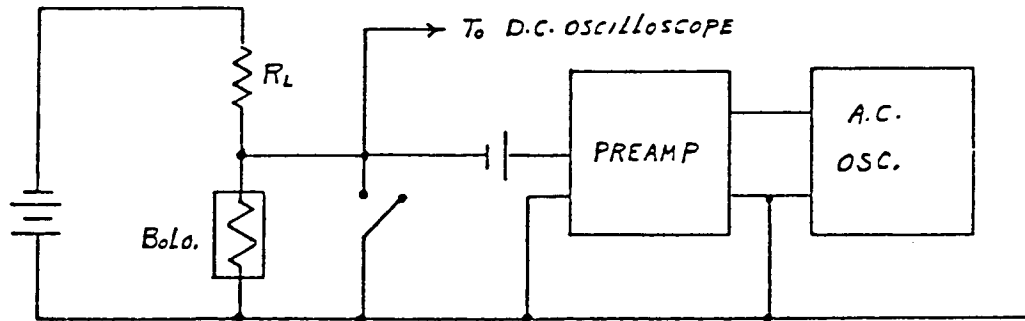


Figure G-9. Frequency Response Setup.

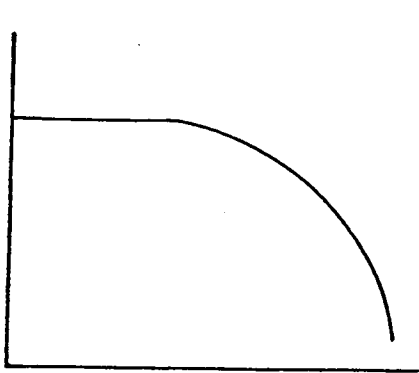


Figure G-10a. Frequency Response, Single τ .

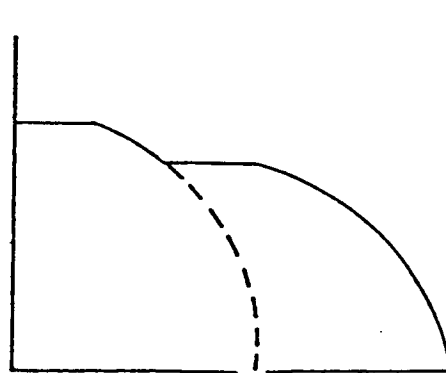


Figure G-10b. Frequency Response, Double τ .

Response Versus Bias Current:

The a.c. output should be measured for various bias currents up to the highest used in the load curve and well beyond the value which produces maximum output.

Absolute Noise Measurement:

This is the most important measurement to be undertaken here. It verifies that the bolometer is working properly and that no serious degradations are occurring in the detector or associated equipment. A number of difficulties may arise, although the following procedures are intended to avoid most of the common problems encountered in noise measurements.

- (a) In the frequency range of interest, 10 to 1000 Hz, a number of narrowband filter systems are available. Any filter may be used here if its effective $Q \approx \Delta f/f \geq 10$. Narrow bandwidths are undesirable since if $\Delta < 1$ cps, inconveniently long measuring times become necessary. An inexpensive filter may be constructed using the circuit supplied upon request. In choosing the frequencies to be used the power line fundamental and its harmonics should be avoided. We usually employ the following set of frequencies: 10, 20, 40, 80, 160, 320, 640 Hz.
- (b) The voltmeter need not be of the true rms variety since we will calibrate it on noise very similar to that we wish to measure. A linear amplifier may be needed between the filter and the voltmeter to increase its sensitivity to about 0.1 mv rms, full scale.
- (c) It is necessary that the preamplifier have performance equivalent to our standard model; the circuit and a brief description are included.
- (d) After connecting the apparatus as shown in Figure G-11, checks must be made to eliminate all interference from power line or other sources. With preamp input shorted or connected to the detector, the waveform on the oscilloscope must be free of ripple or other signals such as partially rectified r.f. coming from nearby transmitters. Ground

loops, lack of a good common, proximity to transformers in oscilloscope or other equipment or poor shielding between detector and preamplifier are common causes of pickup.

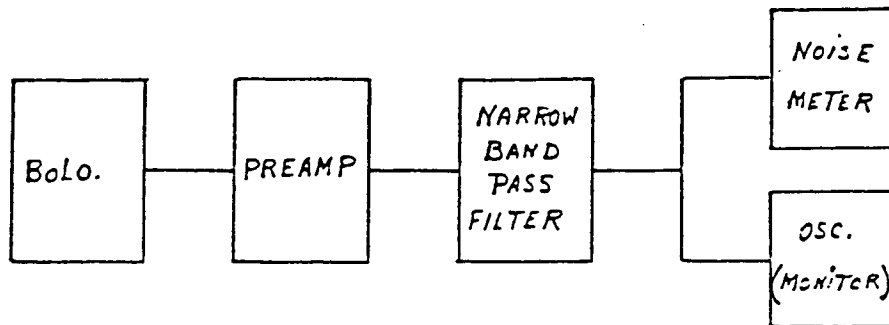


Figure G-11. Noise measurement setup.

- (e) Once the setup is free of interference, it may be calibrated by placing across the input several resistors of known value. The resulting data should be plotted as follows:

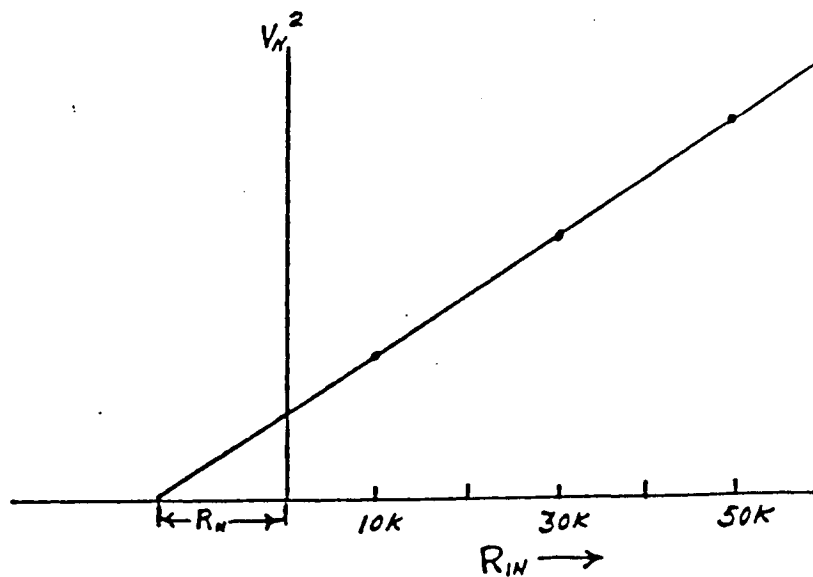


Figure G-12. Noise calibration.

This procedure should be followed for each frequency to be used. In addition to calibrating the noise meter, it determines the value of R_n , the noise equivalent resistance of the preamplifier.

- (f) Detector noise may now be measured as a function of I_B . Values of I_B should be chosen from zero to the highest value on the load curve. Various small batteries can be selected for this purpose. A word of caution on installation of the bias battery is in order: first, we always solder leads to each battery to avoid noisy contacts; second, we must solder with great care to avoid damaging the battery; and last, we usually try more than one battery to be sure the battery is not noisy itself. If all is well, the zero bias noise should just equal the calculated value for R_o and T_o . Optimum value of detector noise will in general be found for large bias currents. This is because the detector impedance is decreasing as the current increases and this can offset the increasing current noise. These measurements should be carried out for various frequencies including the chosen chopping frequency.

Microphonics and pump noise can complicate the problem of ascertaining true detector noise. Even if the window is blocked off, the slightest motion of the inner parts of the dewar can produce a random fluctuation in background. The dewar has been constructed to minimize this problem. Also, our preamplifier is relatively non-microphonic. Pump noise arises when surges in the vapor pressure of the helium bath are large enough to produce temperature fluctuations of the detector. A good test is to suddenly shut off the pump and monitor the noise. Only under rare circumstances have we encountered pump noise.

SYMBOLS, UNITS, AND FORMULAE

T_o (°K)	Bath Temperature
R_o (Ω)	Bolometer Resistance as $I_B \rightarrow 0$
I_B (amp)	Bias Current
E_1 (volt)	Voltage Across Bolometer
R_L (Ω)	Load Resistor, usually cooled
E_2 (volt)	Bias Supply Voltage
S_o (volt/watt)	Maximum Responsivity
$P_o = I_B 'E_1'$ (watt)	Bias power at maximum responsivity
G (watt/°K)	Thermal Conductance
τ (sec)	Thermal time constant
f_o (Hz)	Chopping frequency
V_n (volt)	r.m.s. noise voltage
NEP (watt/Hz ^{1/2})	Noise equivalent power
A (cm ²)	Active area of detector (one surface)
D^* (cm·Hz ^{1/2} /watt)	Detectivity
R_n (Ω)	Noise equivalent resistance

$$S_o = 0.7 (R_o / T_o G)^{1/2}$$

$$NEP = 2 T_o (kG)^{1/2}$$

$$P_o = 0.1 T_o G$$

$$S = E_1^2 / 2 I_B 'E_1'$$

INFRARED LABORATORIES, INC.

1808 EAST 17TH STREET
TUCSON, ARIZONA 85718
PHONE: (602) 822-7074
TLX 364412 INTR

GUARANTEE

GENERAL:

All equipment sold by Infrared Laboratories, Inc. is guaranteed for a period of one year against failure caused by defective materials or workmanship. Defective parts will be repaired or replaced upon return to our Laboratory. Infrared Laboratories, Inc., assumes no liability for the loss of life or property caused by the use or misuse of our products.

DETECTOR:

Each detector is supplied with a set of test data describing its performance. It is strongly recommended that the user repeat the test procedures as described in our operator's manual as soon as possible upon receipt of the detector. Infrared Laboratories, Inc. guarantees that the detector will exhibit the same level of performance described by the test data as furnished. If the detector fails to exhibit this level of performance upon its return to our Laboratory within one year, and if the failure is not caused by misuse or mishandling after delivery, then it will be replaced at no cost.

ARNOLD W. DAVIDSON, MANAGER

This page intentionally left blank.

AR Bolometer Data

PRECEDING PAGE BLANK NOT FILMED

ABSOLUTE RADIOMETER BOLOMETER
INFRARED LABORATORIES, INC.

1808 EAST 17TH STREET
TUCSON, ARIZONA 85718
PHONE: (602) 622-7074
TLX 364412 INTR

UTAH STATE UNIVERSITY

BOLOMETER NOTES

The germanium bolometer, Unit #906, has been mounted in conjunction with a parabolic cone optic in accordance with Utah State University specifications. The bolometer itself is of the composite type and features a 1.75 mm octagonal absorber with nichrome absorbing material mounted within a specially-shaped cavity at the exit aperture of a F/3.0 cone condenser. This cone condenser features an entrance aperture of 6.0 mm and an exit aperture of 1.0 mm.

A nominal 10.0 megohm load resistor has been integrated into the substrate with an input terminal on the side of the substrate. Both detector leads have been brought out to standoff terminals mounted on the side of the substrate. Wiring of the entire module is shown on Utah State DEC Bolometer Preamp Drwg. No. B4-2133 and Fig. I

Exercise great caution not to accidentally over bias the detector. Never allow more than 10 microamps of current to flow through the bolometer itself. Always use high impedance measuring devices when working with the bolometer circuit.

The personnel of Infrared Laboratories, Inc. stand ready to assist you. Please do not hesitate to call on us.


Arnold W. Davidson, Manager

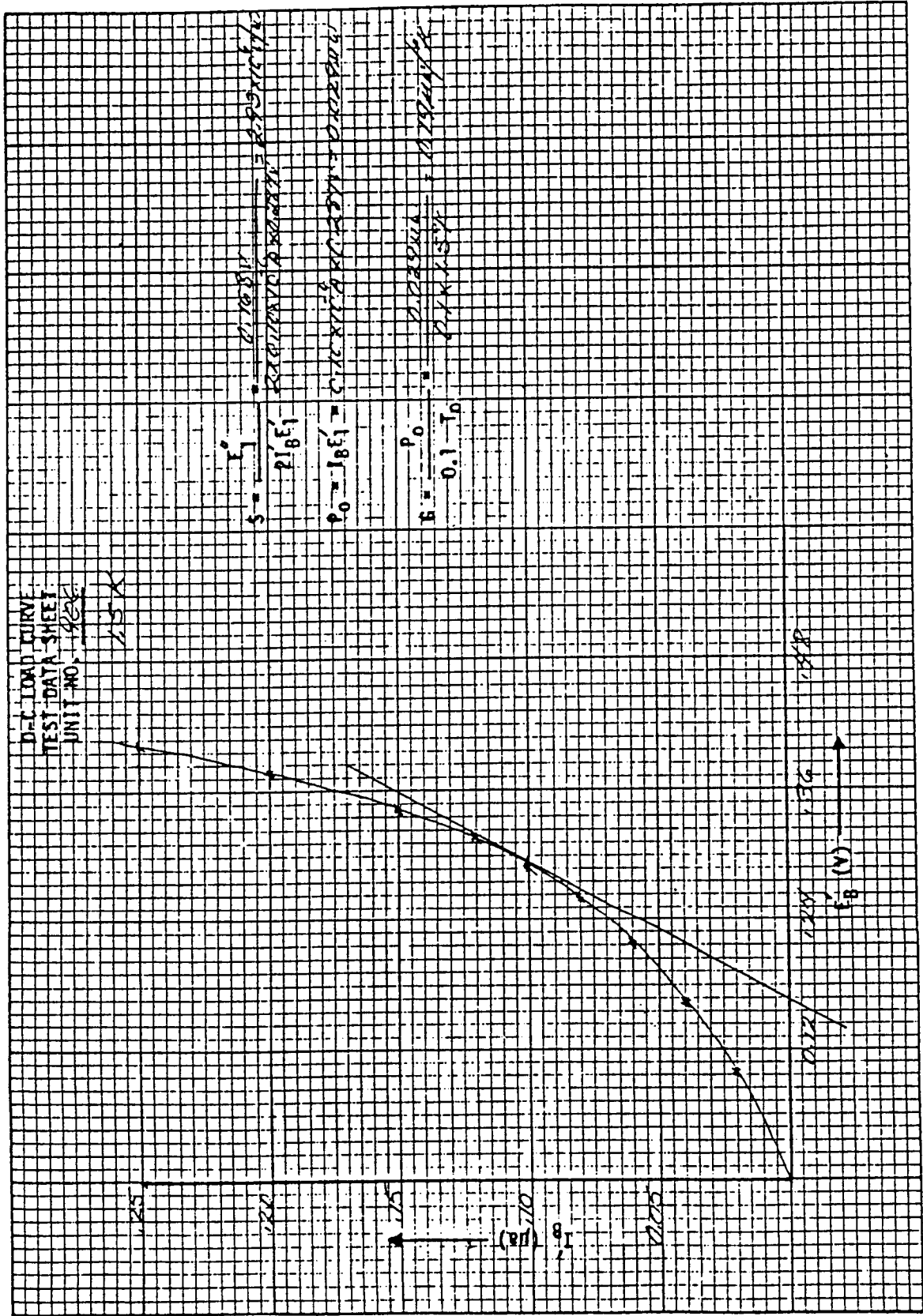


Figure G-13. DC load curve, 1.5K, Unit No. 906.

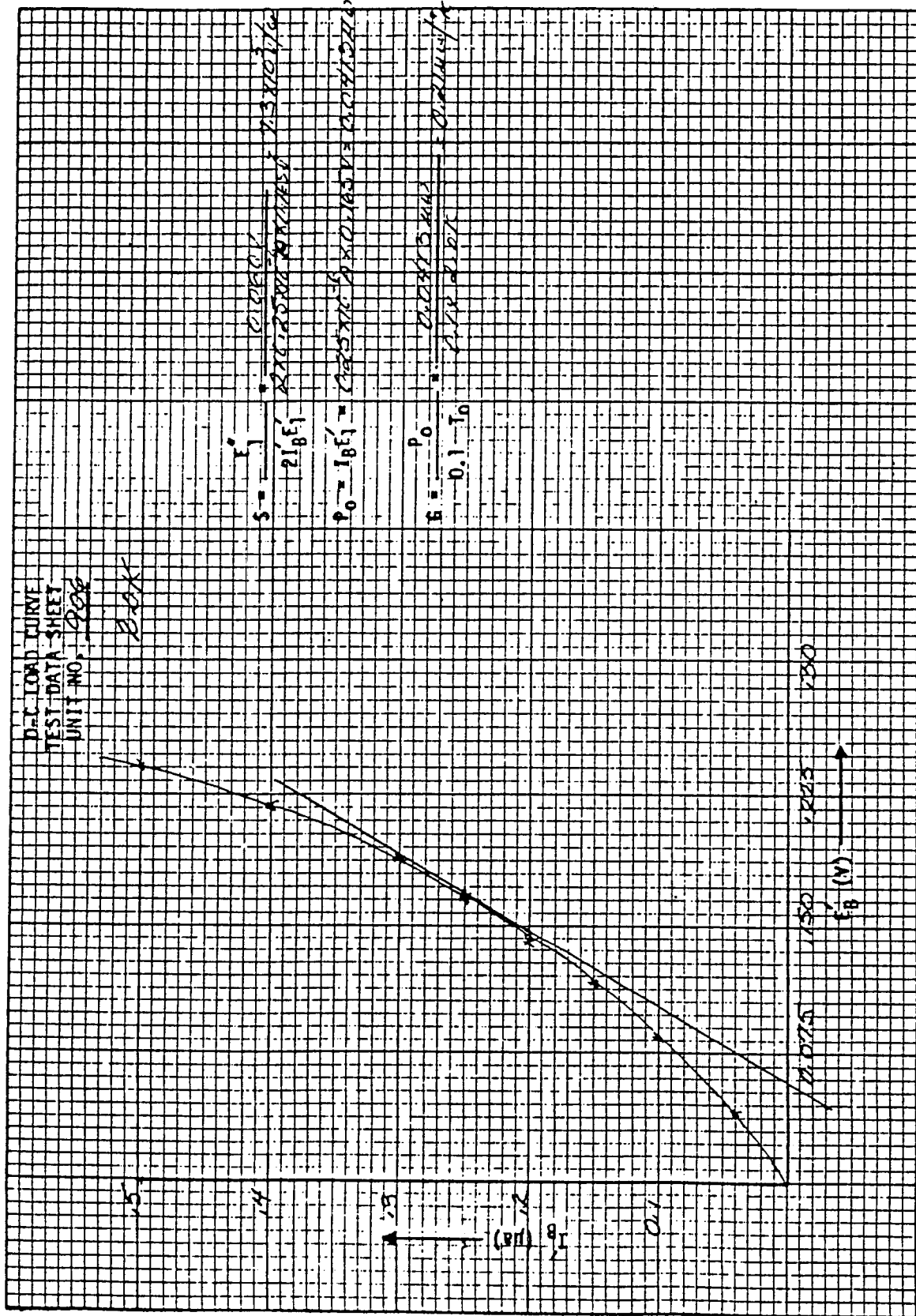


Figure G-14. DC load curve, 2.0K, Unit No. 906.

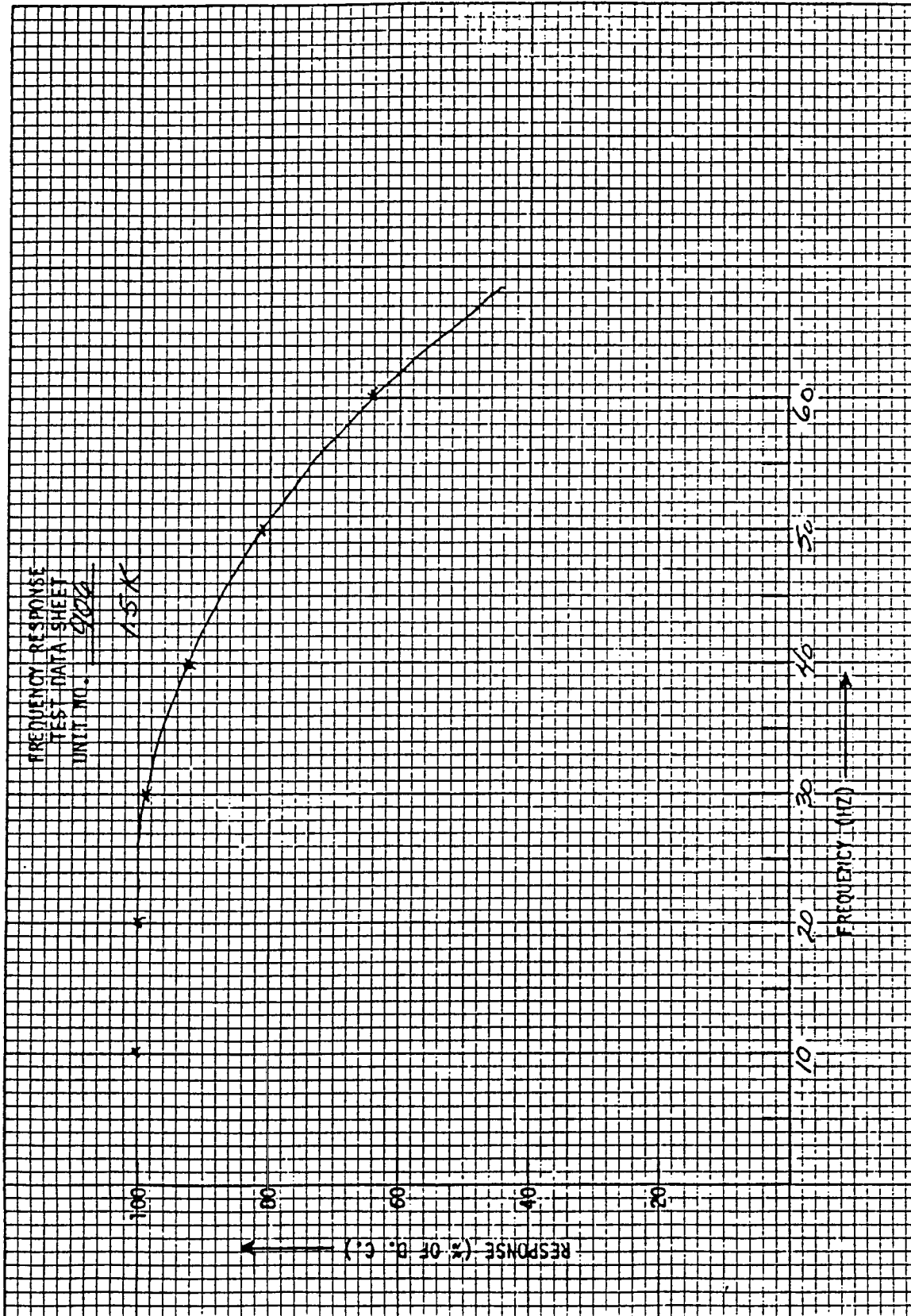


Figure G-15. Frequency response, Unit No. 906.

Spare Bolometer Data

SPARE BOLOMETER

INFRARED LABORATORIES, INC.

1806 EAST 17TH STREET

TUCSON, ARIZONA 85719

PHONE: (602) 622-7074

TLX 384412 INTR

UTAH STATE UNIVERSITY

BOLOMETER NOTES

The germanium bolometer, Unit #905, has been mounted in conjunction with a parabolic cone optic in accordance with Utah State University specifications. The bolometer itself is of the composite type and features a 1.75 mm octagonal absorber with nichrome absorbing material mounted within a specially-shaped cavity at the exit aperture of a F/3.0 cone condenser. This cone condenser features an entrance aperture of 6.0 mm and an exit aperture of 1.0 mm.

A nominal 10.0 megohm load resistor has been integrated into the substrate with an input terminal on the side of the substrate. Both detector leads have been brought out to standoff terminals mounted on the side of the substrate. Wiring of the entire module is shown on Utah State DEC Bolometer Preamp Drwg. No. B4-2133 and Fig. I

Exercise great caution not to accidentally over bias the detector. Never allow more than 10 microamps of current to flow through the bolometer itself. Always use high impedance measuring devices when working with the bolometer circuit.

The personnel of Infrared Laboratories, Inc. stand ready to assist you. Please do not hesitate to call on us.


Arnold W. Davidson, Manager

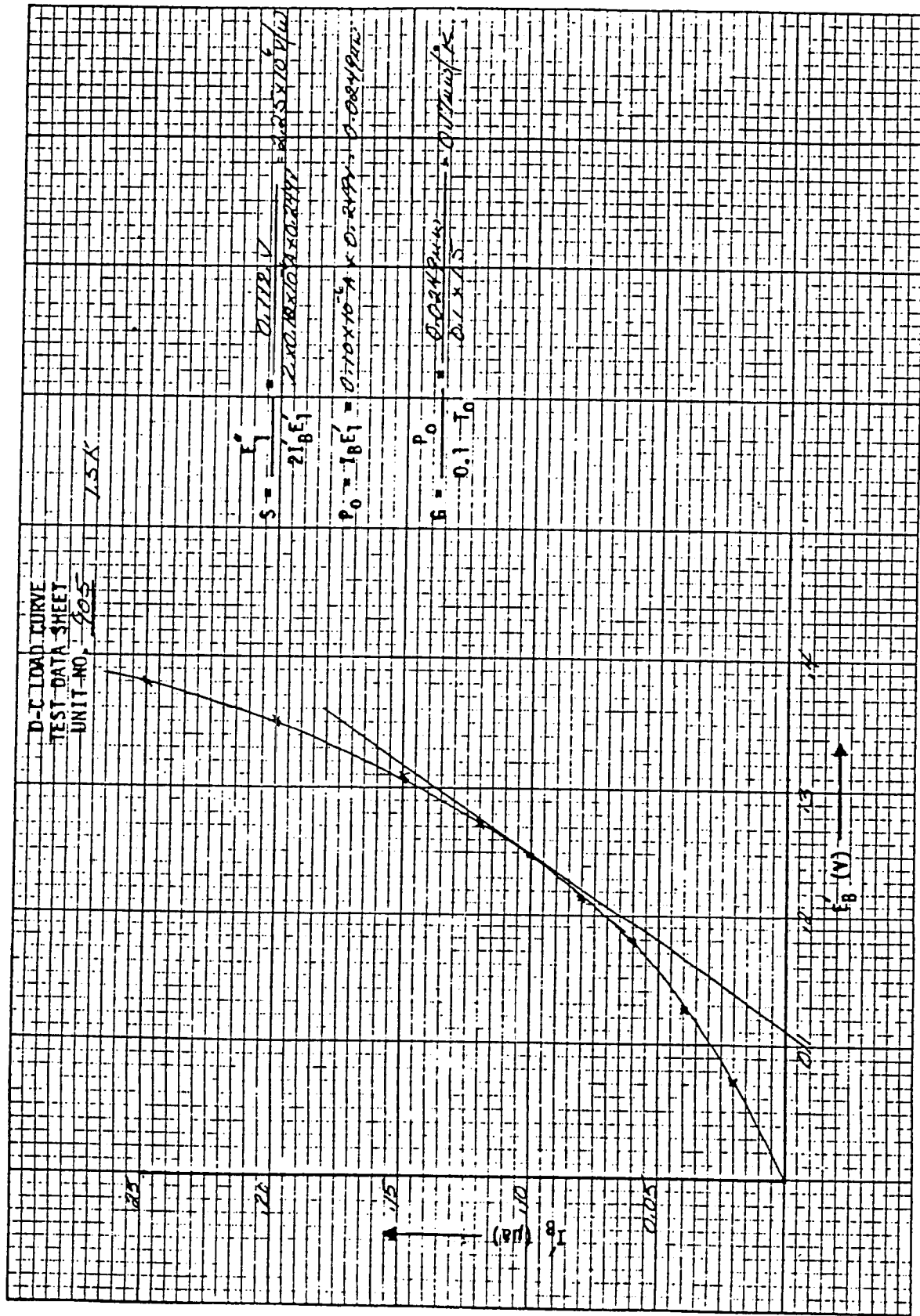


Figure G-16. DC load curve, 1.5K, Unit No. 905.

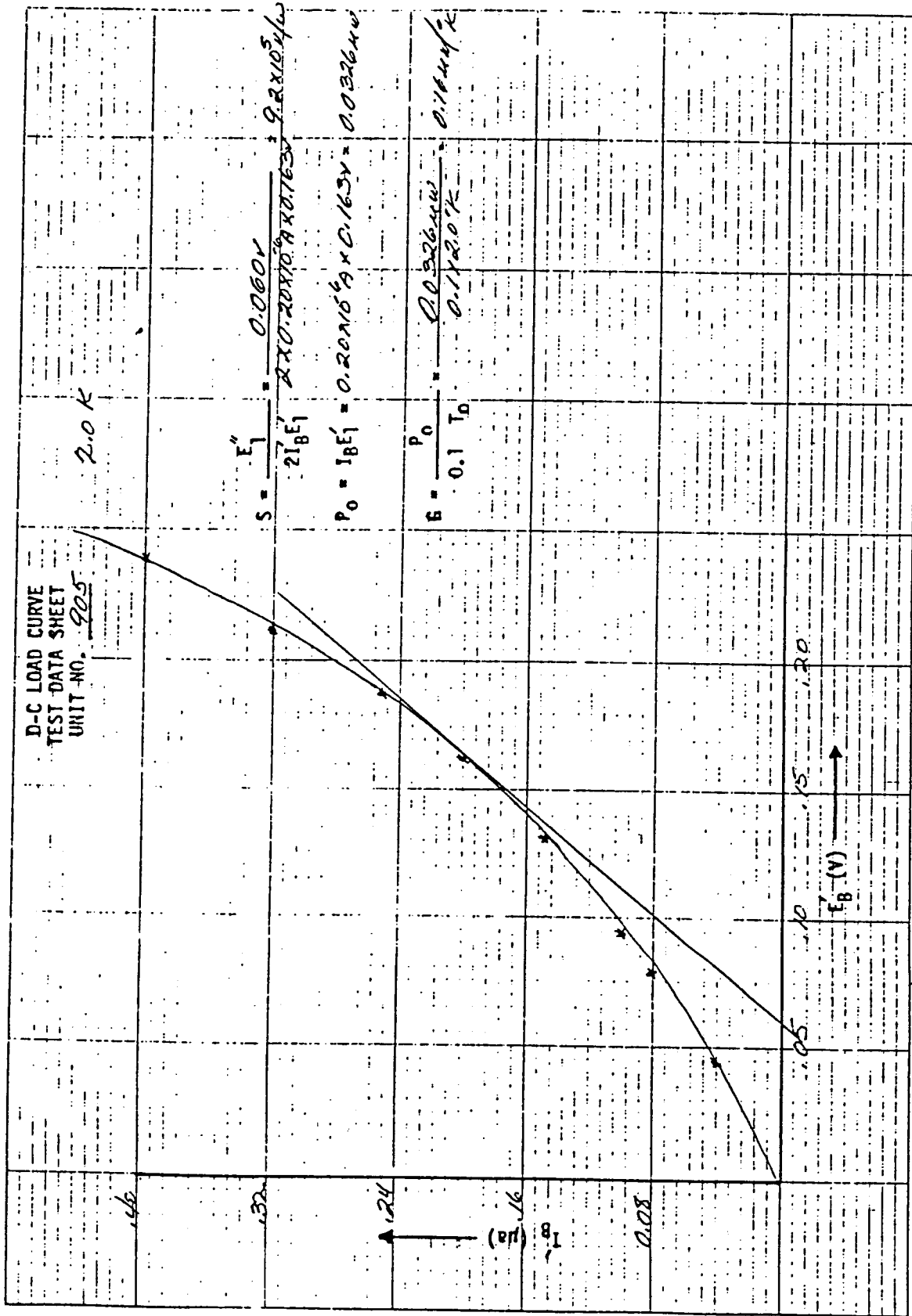


Figure G-17. DC load curve, 2.0K, Unit No. 905.

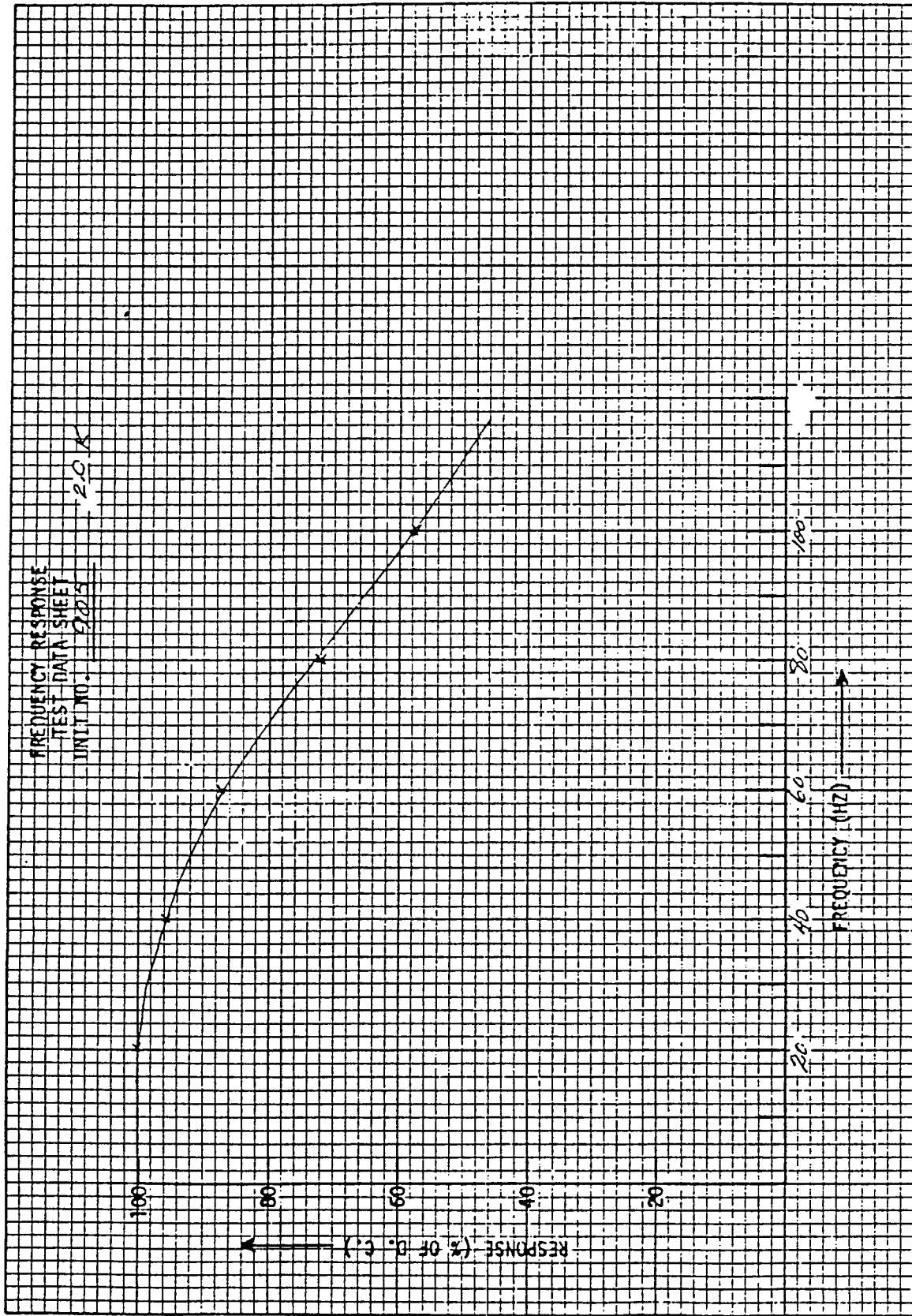


Figure G-18. Frequency response, Unit No. 905.

APPENDIX H
Absolute Calibration Fixtures

This page intentionally left blank.

Absolute Calibration Fixtures

The calibration of the AR was accomplished by making use of a special test Dewar and certain calibration devices normally utilized at USU to calibrate cryogenic IR systems. Each of these units and the corresponding interface fixtures are illustrated in the accompanying drawings.

Figure H-1 illustrates the layout of the special test Dewar fabricated by Infrared Laboratories, Tucson, Arizona, and shipped with the bolometer detectors. This Dewar was used for the calibration of the AR.

Figure H-2 illustrates the layout of the USU Cold Collimator. This device, which can be cooled to 10 to 20°K, contains a precision aperture wheel and a filter wheel. The gimbal mounted mirror can be pointed with the microprocessor controlled motors to produce a raster scan for field-of-view mapping.

Figure H-3 illustrates the optical layout of the USU Cold Collimator.

Figure H-4 illustrates the layout of the filter and aperture wheels, the window, and the source.

Figure H-5 illustrates the coupling, or interfacing technique used to couple the USU Cold Collimator to the special test Dewar containing the AR for calibration. Note that vacuum, radiation shield, and cold shield continuity is maintained through the interface with photon-tight, non-contact baffles.

Figure H-6 illustrates the coupling, or interfacing technique used to couple the USU Extended-area source to the special test Dewar containing the AR for calibration. Note that vacuum, radiation shield, and cold shield continuity is maintained through the interface with photon-tight non-contact baffles.

PRECEDING PAGE BLANK NOT FILMED

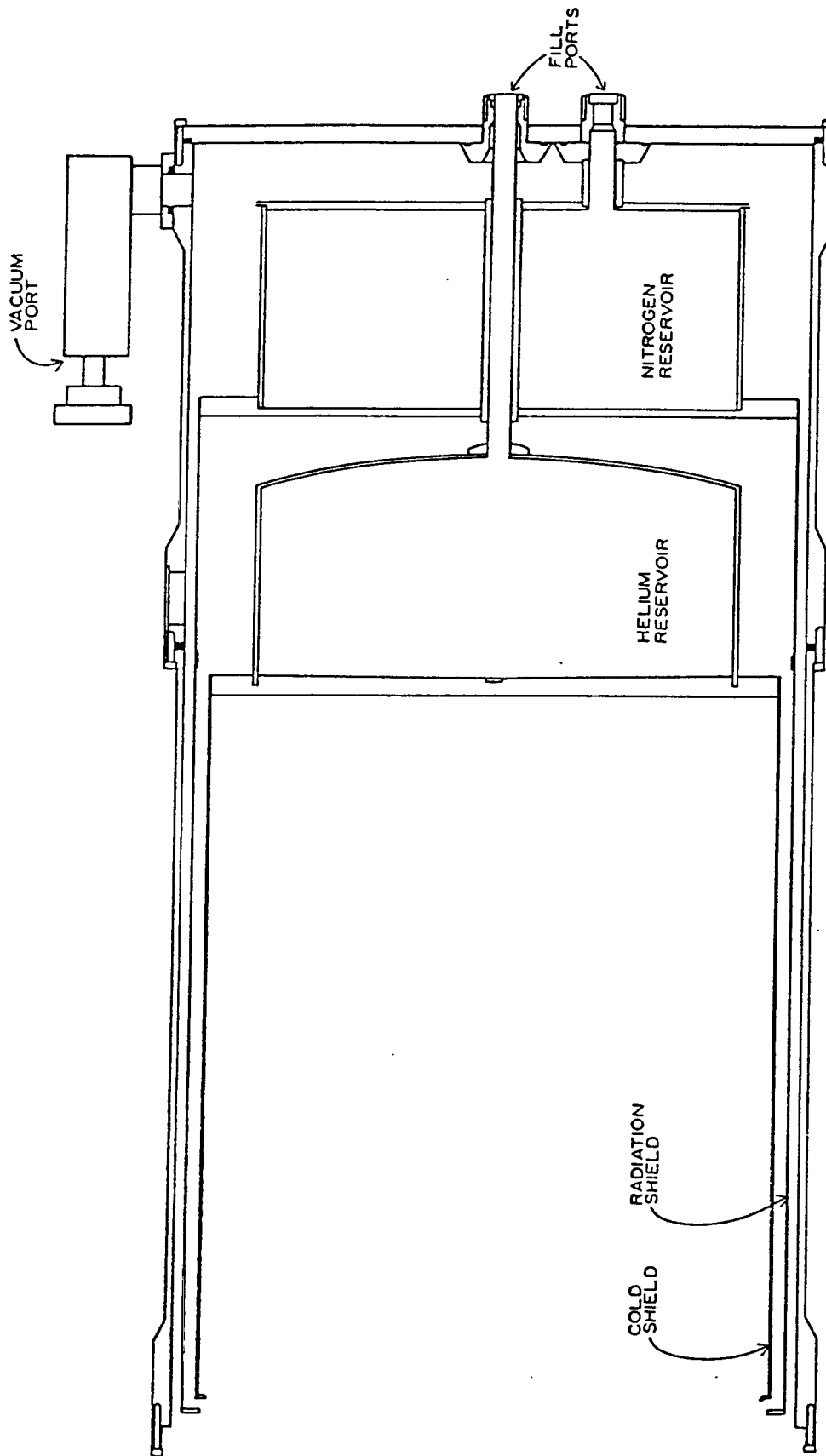


Figure H-1. Layout sketch of the Infrared Laboratories test Dewar. The AR was mounted in this Dewar for calibration.

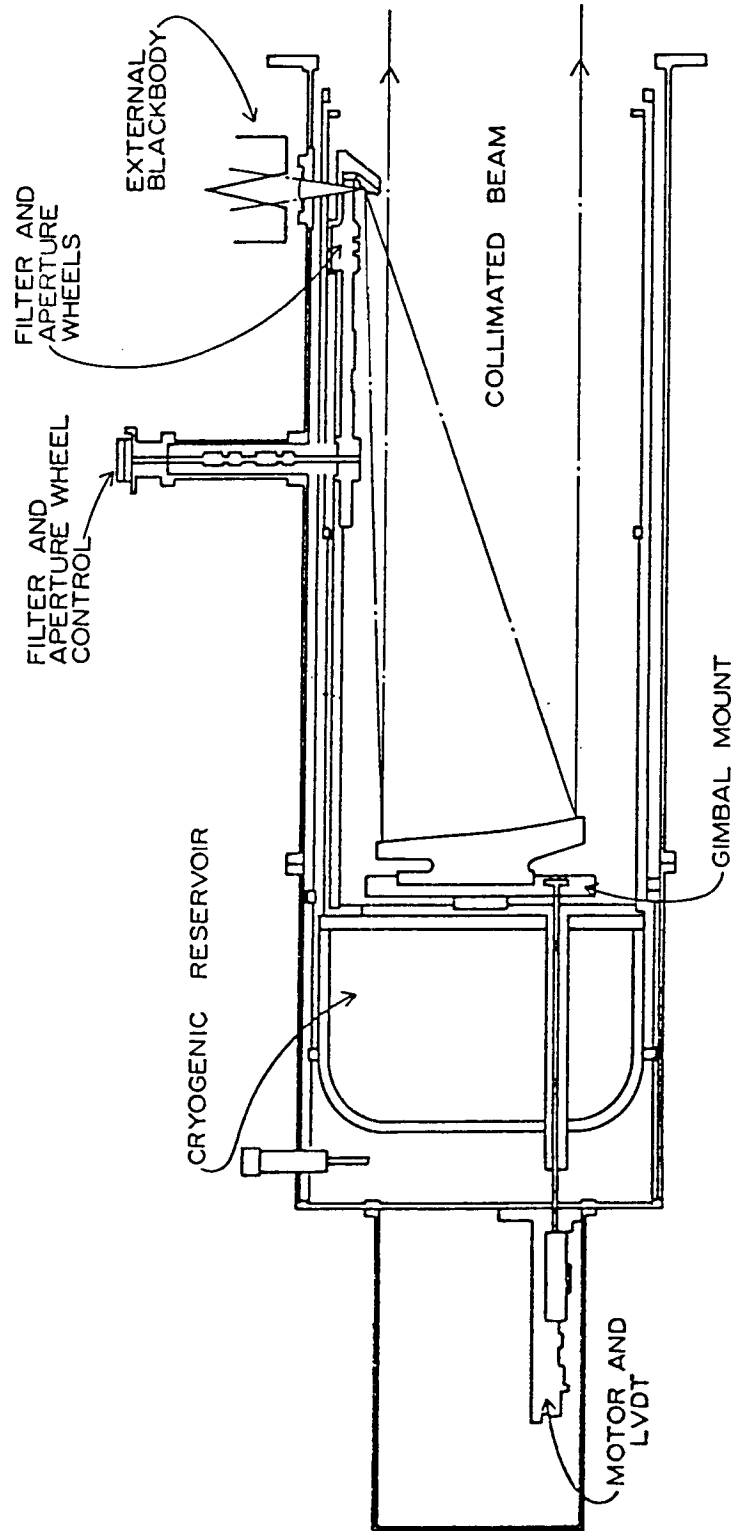


Figure H-2. Layout sketch of the USU Cold Collimator. This cryogenic device contains a precision aperture and a filter wheel, and motors to scan the beam.

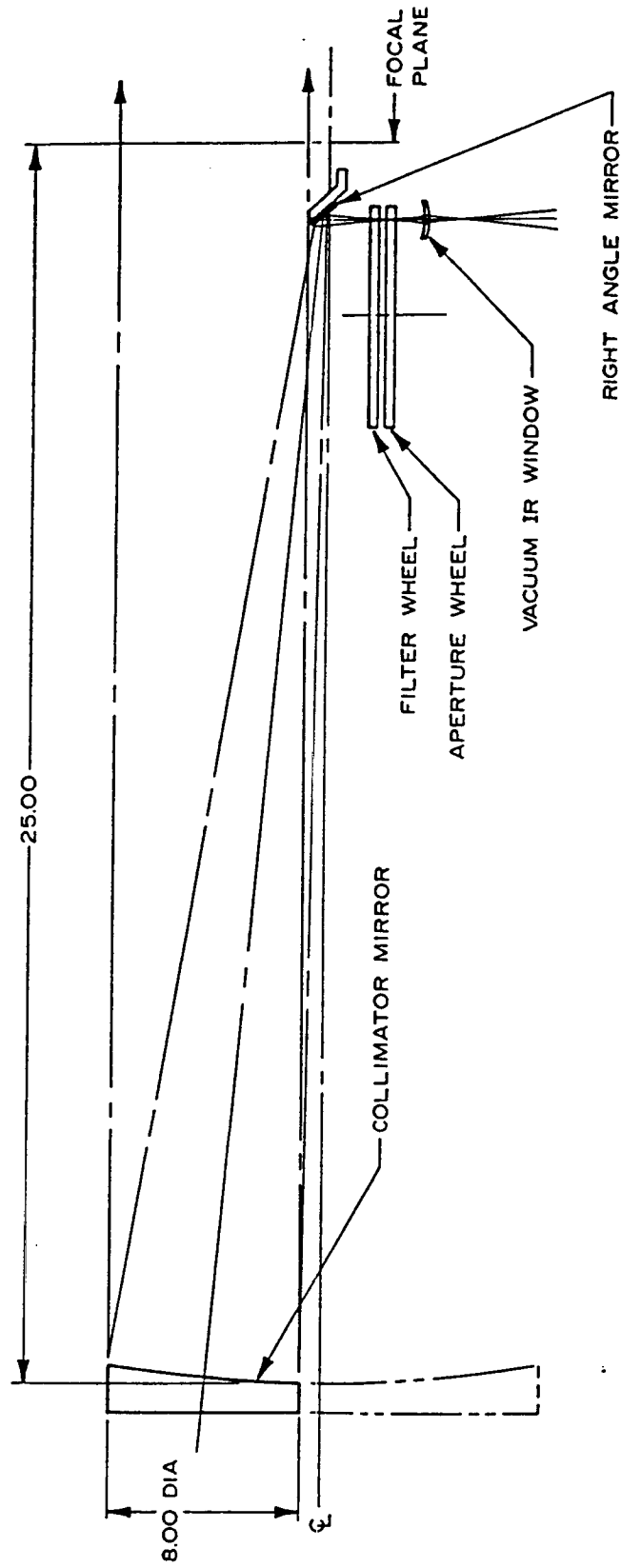


Figure H-3. Optical sketch of the USU Cold Collimator.

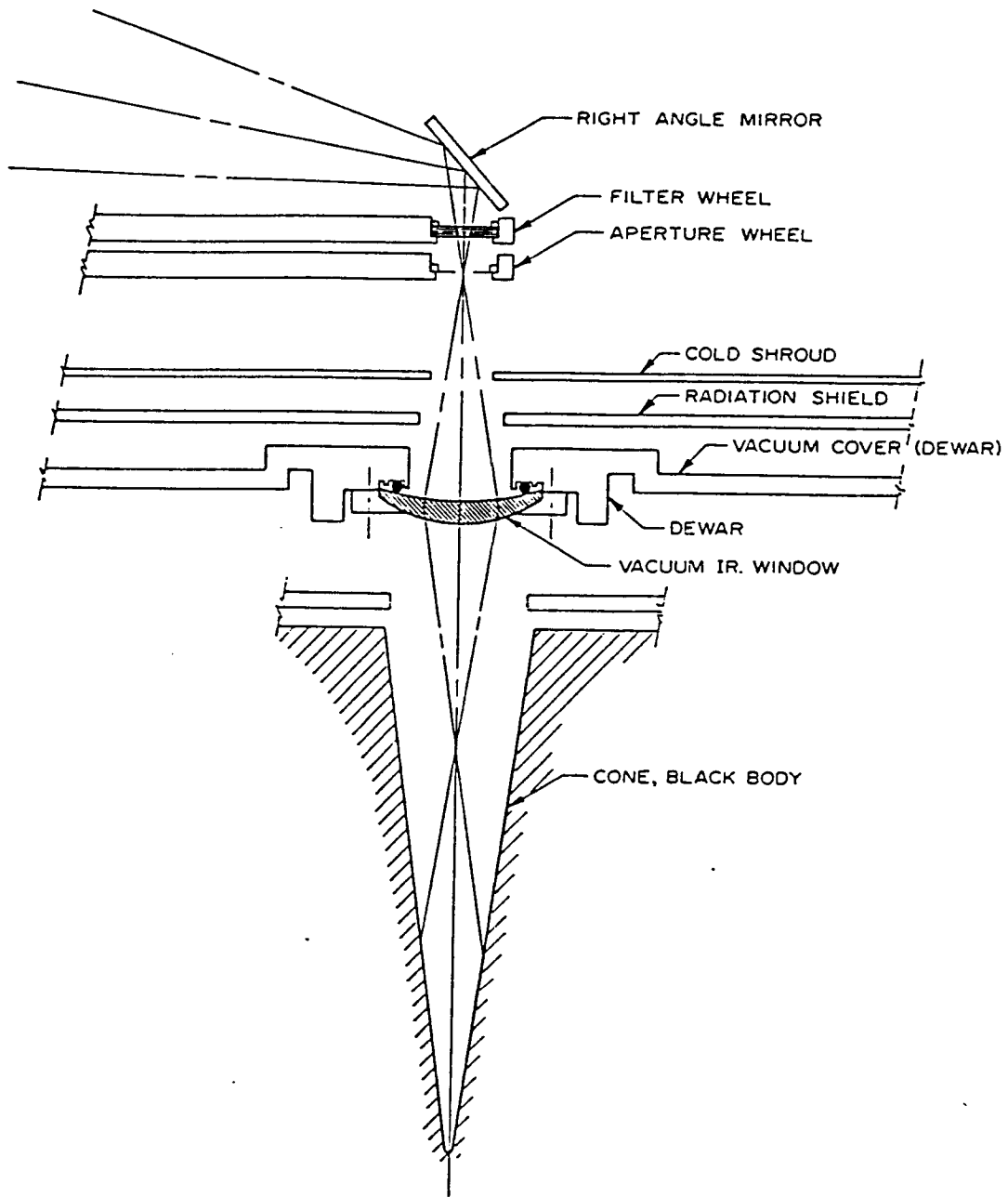


Figure H-4. Optical Schematic of the USU Cold Collimator showing details of the filter and aperture wheels, window, and external blackbody source.

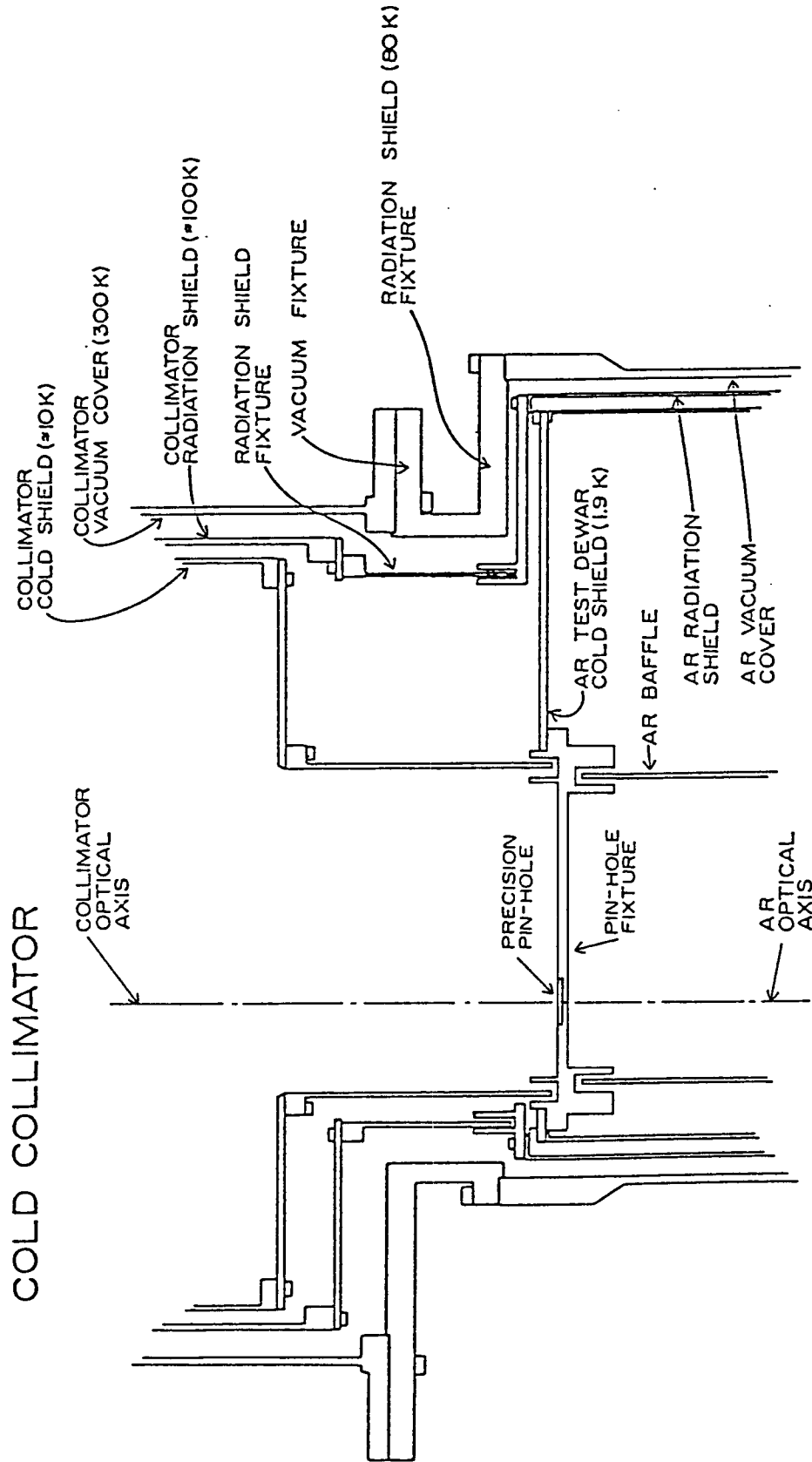


Figure H-5. Layout sketch of the special test Dewar interfaced to the USU cold collimator. Note that vacuum, radiation shield, and cold shield continuity are maintained in the interface. The AR baffle is fitted with a photon-tight non-contact baffle.

COLD EXTENDED--AREA SOURCE

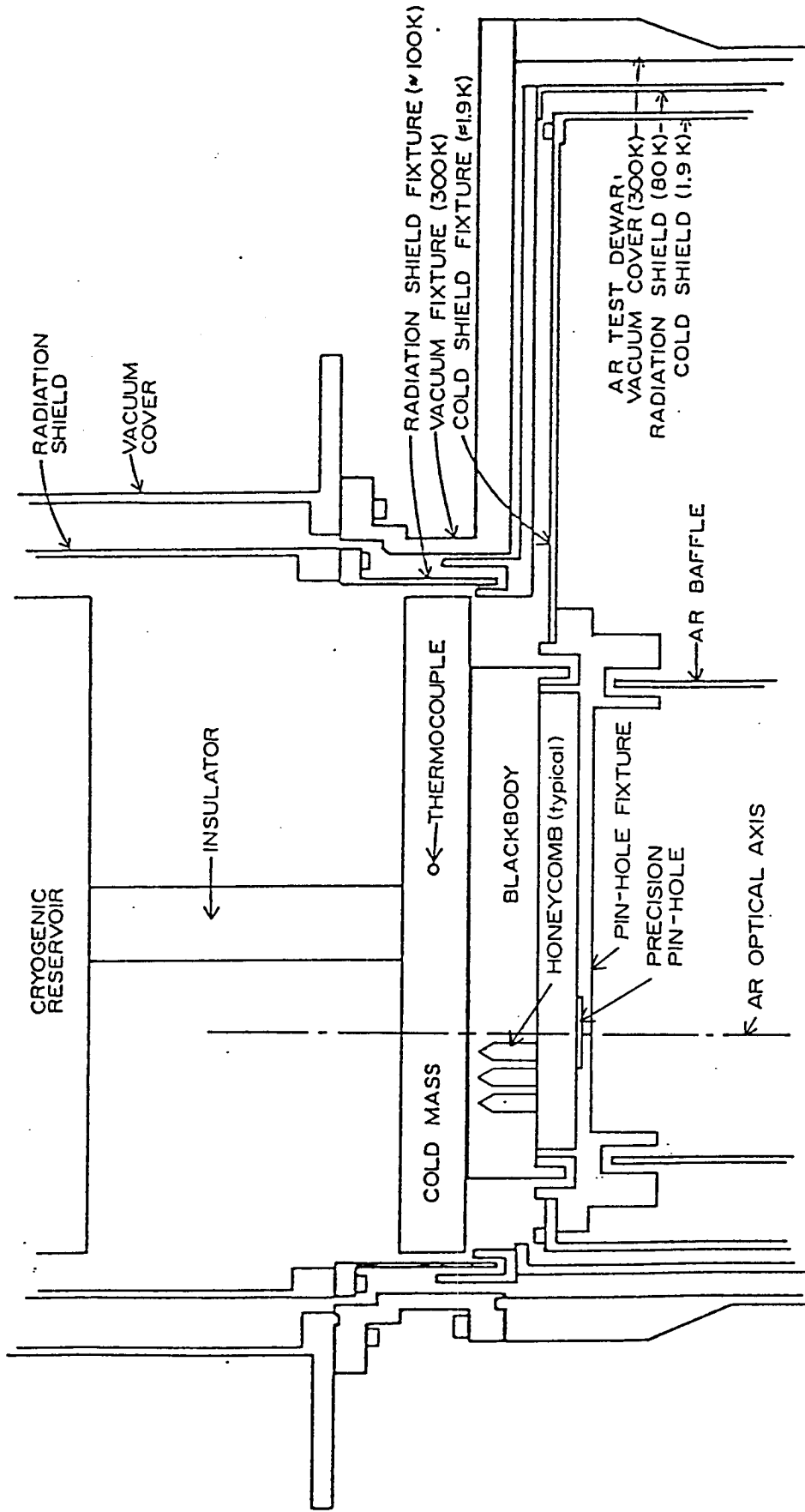


Figure H-6. Layout sketch of the special test Dewar interfaced to the USU cold collimator. Note that vacuum, radiation shield, and cold shield continuity are maintained in the interface. The temperature controlled blackbody simulator is honeycombed, blackened, and coupled to the AR baffle with a photon-tight non-contact baffle.

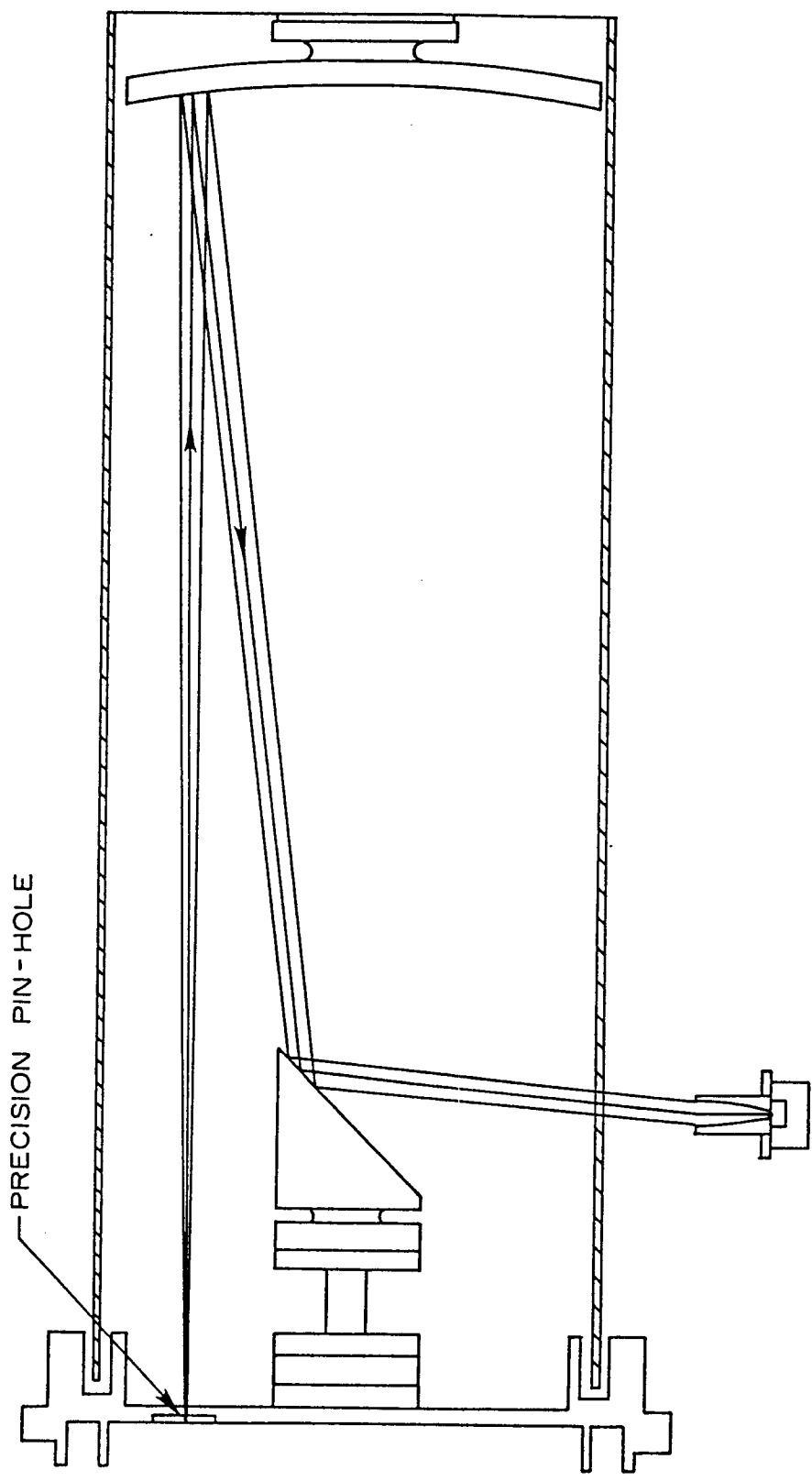


Figure H-7. A diagram of the Absolute Radiometer showing the precision off-axis pinhole used for calibrating the Absolute Radiometer.

APPENDIX J
DEC Beam Uniformity Tests

This page intentionally left blank.

DEC Beam Uniformity Tests

From 8 September 1986 through 20 September 1986, Utah State University personnel worked on-site at NASA GSFC to measure the DEC output beam uniformity. These measurements were in response to contract NAS5-28185, Modification No. 5. The modification provided for verification of uniformity of illumination by utilizing an X-Y scanning device with a stepping resolution of 5mm or less and a sampling diameter of 2 cm or less. Measurements were to be made with a silicon photodiode detector (peak response at approximately 0.90 μm) and a quartz halogen lamp with a color temperature of approximately 1800°K as the source.

During most of the first week equipment was recleaned and checked prior to entering the clean room with the DEC instrument. Preliminary objectives were to replace the DEC large area source with the quartz halogen lamp, and mount an X-Y plotter such that its axes (with detector attached) could be maneuvered to monitor and record the output beam's uniformity of illumination.

When clean room operations began, USU removed the top cover and skin from around the outside of the DEC. Next we removed the integrating sphere module from the DEC baseplate. The large area source was removed from the first integrating sphere and the quartz halogen lamp and its mounting fixture were installed in its place. The light from this high intensity lamp would be used for mapping the DEC output beam uniformity. The mounting fixture for the lamp was equipped such that it would allow nitrogen gas to circulate around the bulb to help dissipate heat. The integrating sphere module was then mounted back onto the DEC baseplate, and the skin and top cover were reinstalled. The DEC was mounted on three legs which held its base approximately 15 inches above the test baseplate. The test baseplate supported the X-Y plotter with its detector. Figure J-1 shows the setup which was used to make the measurements.

The detector and baffle assembly are shown in Figure J-2. The detector assembly consists of 4 main parts as follows: 1.) The front end of the assembly acts as a baffle to prevent energy from large off-axis angles from getting to the detector. Energy from $\pm 8^\circ$ will illuminate the detector without being blocked at all. 2.) A shutter mechanism is built into the detector assembly. The shutter uses a flat plate mounted on the shaft of a DC motor. When the motor runs in one direction, the plate is placed over the detector to block the light. Rotation in the opposite direction moves the plate from in front of the detector and allows the light to impinge upon it. The shutter allows the measurement of DC offset drift in order that it may be subtracted from the data. 3.) The detector is an EG&G Model UV444BQ. Its responsivity curve is shown in Figure J-3. The detector has an active area of approximately 1 cm^2 (round, 11.8 mm diameter). 4.) A preamplifier is mounted under the detector. A schematic of the preamp circuit is shown in Figure J-4.

Prior to departure for NASA GSFC, the field of view of the assembly and linearity of the system were checked at USU. The response to energy along the X-, and Y-axis of the assembly is given in Figures J-5 and J-6, respectively. The linearity looked very good. At GSFC, with the high intensity lamp installed, examination of the DEC beam indicated that a low enough background existed that the gain of the system could be increased and the lamp could be operated somewhat cooler to avoid excessive heating problems. This was accomplished and the beam uniformity data were taken and recorded. Subsequently, after returning to USU, further testing was accomplished at the increased gain level. During this testing we found a definite nonlinearity, which occurs in the gain stage of the amplifier. This nonlinearity results in the following calibration equation:

$$\text{Flux} = 0.05483 \times V^2 + 3.71V \quad (\text{Eq. } -1)$$

where: V = Voltage from detector

Figure J-7 shows the measured response versus a straight line. We took data from a lower gain and verified that the detector was linear and that it was the higher gain amplifier that was introducing the nonlinearity. The amplifier electronics schematic is shown in Figure J-8. The low-pass filter shown after the gain stage has a corner frequency of 1 Hz.

The detector assembly was mounted in place of the pen on a Tektronix plotter. The Tektronics computer controlled the test by repeating the following sequence:

1. At an initial detector (plotter) position, with the shutter open, the computer takes 20 samples of signal data from the A/D converter.
2. Shutter closed.
3. Average the 20 samples and display a point on the computer screen to show the averaged value.
4. Place averaged value into an array to be saved on tape. During this period the signal has stabilized after closing the shutter.
5. Take 20 samples with shutter closed.
6. Move plotter to next position.
7. Open shutter.
8. Average 20 samples taken with shutter closed and display point on the computer screen.
9. Place averaged value into array to be saved on tape.
10. Repeat from No. 1.

Scanning of the beam was accomplished by moving the detector through the X, Y coordinate system in the following manner, coordinates are measured in cm from $X = 0.0$, $Y = 0.0$:

1. Initially set to coordinates $X = 0.0$, $Y = 0.0$
2. Obtain readings as detailed above with 0.5 cm increment movements in Y axis until coordinates $X = 0$, $Y = 24.5$ are

reached.

3. Set coordinates to $X = 0.5$, $Y = 0.0$,
4. Obtain readings as detailed above with 0.5 cm increment movements in Y axis until coordinates $X = 0.5$, $Y = 24.5$ are reached.
5. Set coordinates to $X = 1.0$, $Y = 0.0$, etc, etc,
6. Continue in this manner until coordinates $X = 38$, $Y = 24.5$ are reached. This will map the entire field.

NOTE: In the text and plots that follow, the X- and Y-axes of the plotter are also referred to as Azimuth and Elevation, respectively, i.e., $X = \text{Azimuth}$, $Y = \text{Elevation}$. These terms are used because they match NASA-used terms and help orient the plots with regard to DEC and DIRBE. The plots of beam uniformity are shown as they would be seen from inside DEC looking out.

The complete mapping took approximately 4 hours to perform. The nitrogen cylinders used to cool the high intensity lamp lasted approximately 3 hours, so each test had to be interrupted once to turn off the lamp and change the nitrogen cylinder. When this was accomplished and the lamp was turned back on, it was allowed to stabilize for a few minutes before continuing the mapping.

Five complete sets of data were taken as described above. The data from the various tests are referred to by file number, i.e., File 1 through File 5.

The data in File #1 were taken with the high intensity lamp set to 26 volts. This saturated the detector during the center of the scan where the beam was most intense. The data have been processed and plotted, but should be used cautiously.

File #2 data were taken on 15 September 1986 with the bulb voltage reduced to 23.1 volts. The nitrogen cylinder was changed at the end of the scan when the X-axis (azimuth) equaled 28 cm. No effects are noted in the data from changing the cylinder.

File #3 data were taken on 16 September 1986. This data set

was taken with the high intensity bulb voltage set at 23.1 volts as in File #2, but the Mode Select wheel in the DEC was moved to the opaque position. This test was accomplished to measure any light leaks getting to the detector, but not coming through the normal optical path. This data set shows the energy around X (azimuth) = 2, Y (elevation) = 2, which was coming from an LED in the plotter. The rest of the map shows essentially no light leaks.

File #4 data were taken 16 September 1986. This data set is a repeat of the test conditions during file #2. This test was performed to check the repeatability of the data. The Nitrogen bottle was changed during this test at the end of the 16 cm X (azimuth)-axis scan. Again, no effect is apparent in the data.

File #5 data were recorded on 17 September 1986. It is also a repeat of the test conditions in Files #2 and #4. The nitrogen cylinder was changed during the test, but the scan coordinates were not recorded when the change was made. In the data from this test there is a low area during the 21.5 cm X (azimuth)-axis scan. It is very possible that this could have resulted from changing the nitrogen cylinder if the lamp was not allowed to heat back up and stabilize completely before the test was continued. Different personnel changed the cylinder during this test.

The data presented in the following pages have been processed in the following manner:

1. The shutter closed data were subtracted from the shutter open data for each position.
2. These data were examined to eliminate any large spikes. There were a few points with approximately -3V excursions, these points were forced to -0.5V. The point X (azimuth) = 0.0, Y (elevation) = 0.0, was also forced to -0.5V to give the same value to the lower end of the plots.
3. The data were entered into a plotting package which would accept 3000 data points. This included all points

from a particular file, up through and including points
X (azimuth) = 30 cm, Y (elevation) = 24.5 cm.

4. Contour plots were made with a contour every 0.2V with every 1.0V line labeled. We tried labeling lines more frequently than the 1V intervals, but the resulting plots were not as easily read. Contour plots are shown in Figures J-9, J-16, J-23, J-25, and J-32 for Files 1 through 5, respectively.

5. We produced side views of the plots looking along the X (azimuth)- and Y (elevation)-axes. These plots are shown in Figures J-10 and J-11, J-17 and J-18, J-26 and J-27, and J-33 and J-34, for Files 1, 2, 4, and 5, respectively.

6. We also produced plots showing three dimensional views of the data from 4 angles. These plots are shown in Figures J-12 through J-15, J-19 through J-22, J-24, J-28 through J-31, and J-35 through J-38 for Files 1 through 5 respectively.

All of the plots in Figures J-9 through J-38 show voltage measured versus position. They have not been corrected for the detector nonlinearity.

We took the data from File #2 and corrected it for the detector response by using equation #1. This data was then normalized to the largest value in the file. The point X (azimuth) = 0.0, Y (elevation) = 0.0 was forced to -0.05 to give the same minimum as the earlier plots of uncorrected data. The corrected data set is shown in Figures J-39 through J-45. The effect on the data from the correction is more pronounced on the larger data values. Thus, the correction tends to make the central peak a little larger with respect to the plateau which surrounds it than it would otherwise appear.

The corrected and normalized data from File #2 will be provided on floppy disc to Mr. Bill Stabnow at GSFC. The data is formatted as follows:

No file header is in file (Filename is D2N.DAT)

Azimuth Elevation Amplitude (CR) (LF)

The data set contains data for Azimuths 0 through 38 and elevations 0 through 24.5. The first point (0,0) has been forced to -0.05. The data plotted in Figures J-43 through J-49 were taken from this set. The plotting package again can only handle 3000 data points, so every data point from azimuth 0 through 30 cm was used to generate the plots.

Figures J-46 and J-47 are provided to demonstrate the capabilities of the plotting software. Both plots have been made of the same test data set. They have been processed the same way as the data presented in this report. The data set was constructed to show the results of a single point which is much greater or smaller in value than the surrounding points, and a group of points which are greater or smaller than the surrounding points. The data set was made up of the following points: For Azimuth (X) = 0 through 15, all points = 0, except the following, which are all equal to 10.0:

(6,16.5) through (6,19.5), (6.5,16.5) through (6.5,19.5),
(7,16.5) through (7,19.5), (7.5,16.5) through (7.5,19.5),
(8,16.5) through (8,19.5), (8.5,16.5) through (8.5,19.5),
(9,16.5) through (9,19.5), (9.5,16.5) through (9.5,19.5), and
(7.5,6).

For Azimuth (X) = 15.5 through 30, all points = 10, except the following, which are all equal to 0:

(21,16.5) through (21,19.5), (21.5,16.5) through
(21.5,19.5),
(22,16.5) through (22,19.5), (22.5,16.5) through
(22.5,19.5),
(23,16.5) through (23,19.5), (23.5,16.5) through
(23.5,19.5),
(24,16.5) through (24,19.5), (24.5,16.5) through
(24.5,19.5), and (22.5,6).

Figure J-47 shows how the software handles a step function. There are many contour lines placed very close together, not just a single contour line. The contours are placed so close together in fact, that the labels cannot be read. The program does not put dashed lines where there is a lower spot to distinguish it from higher spots. We can be sure when we see a single contour line, that there is not a large hill or valley or the line would be darker than a single line.

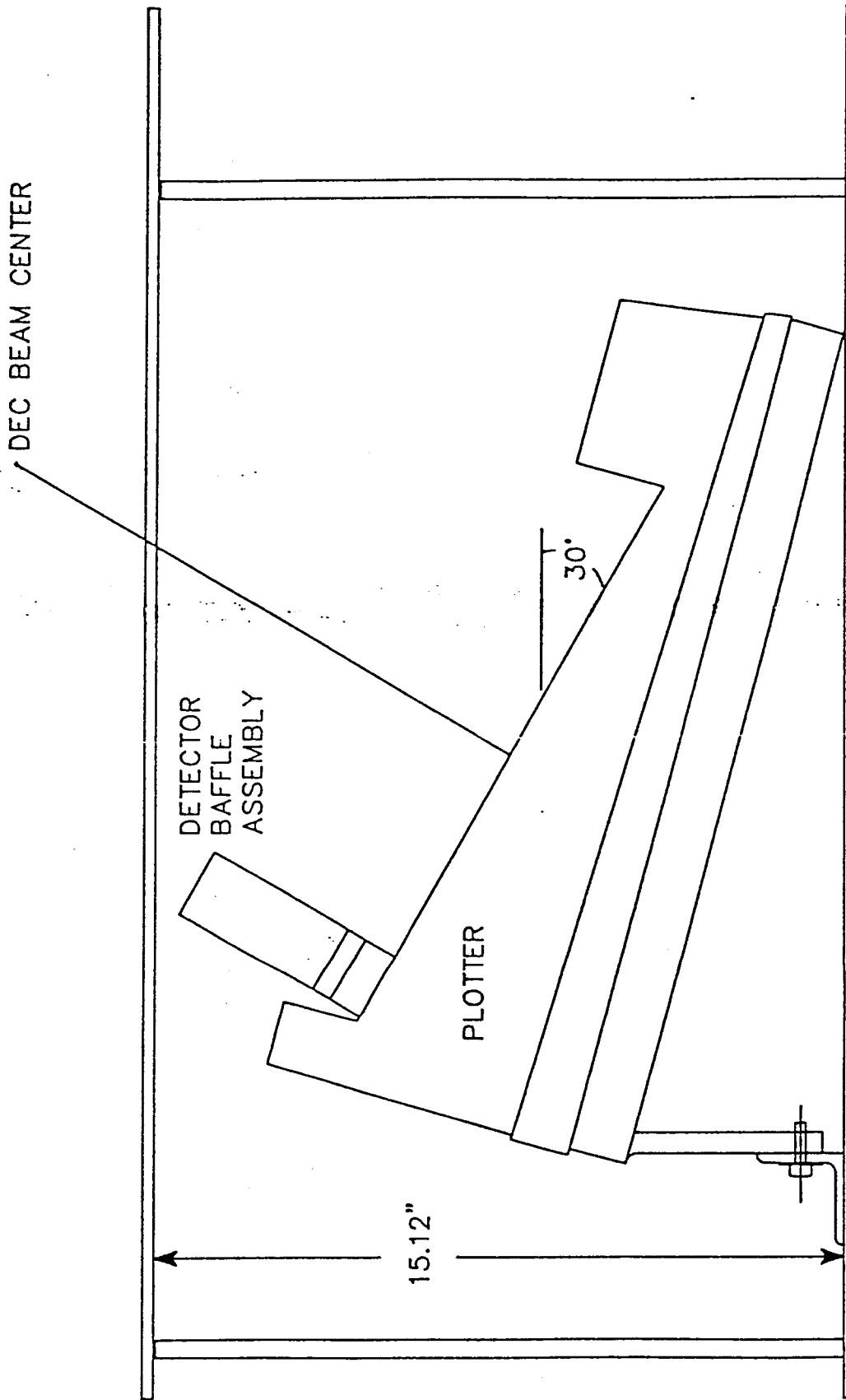


Figure J-1. DEC beam uniformity test setup.

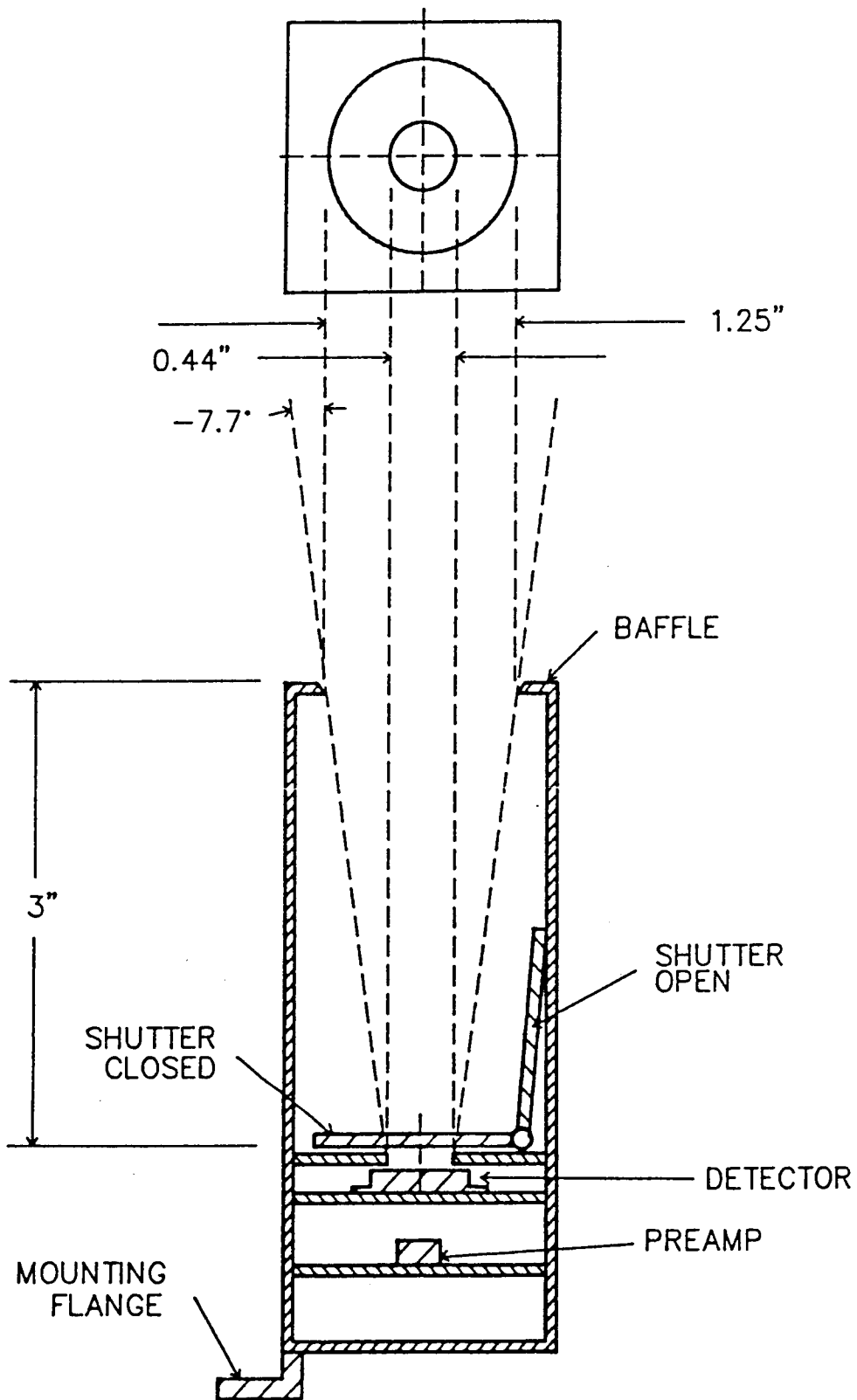


Figure J-2. Cutaway view of DEC beam uniformity detector/baffle assembly.

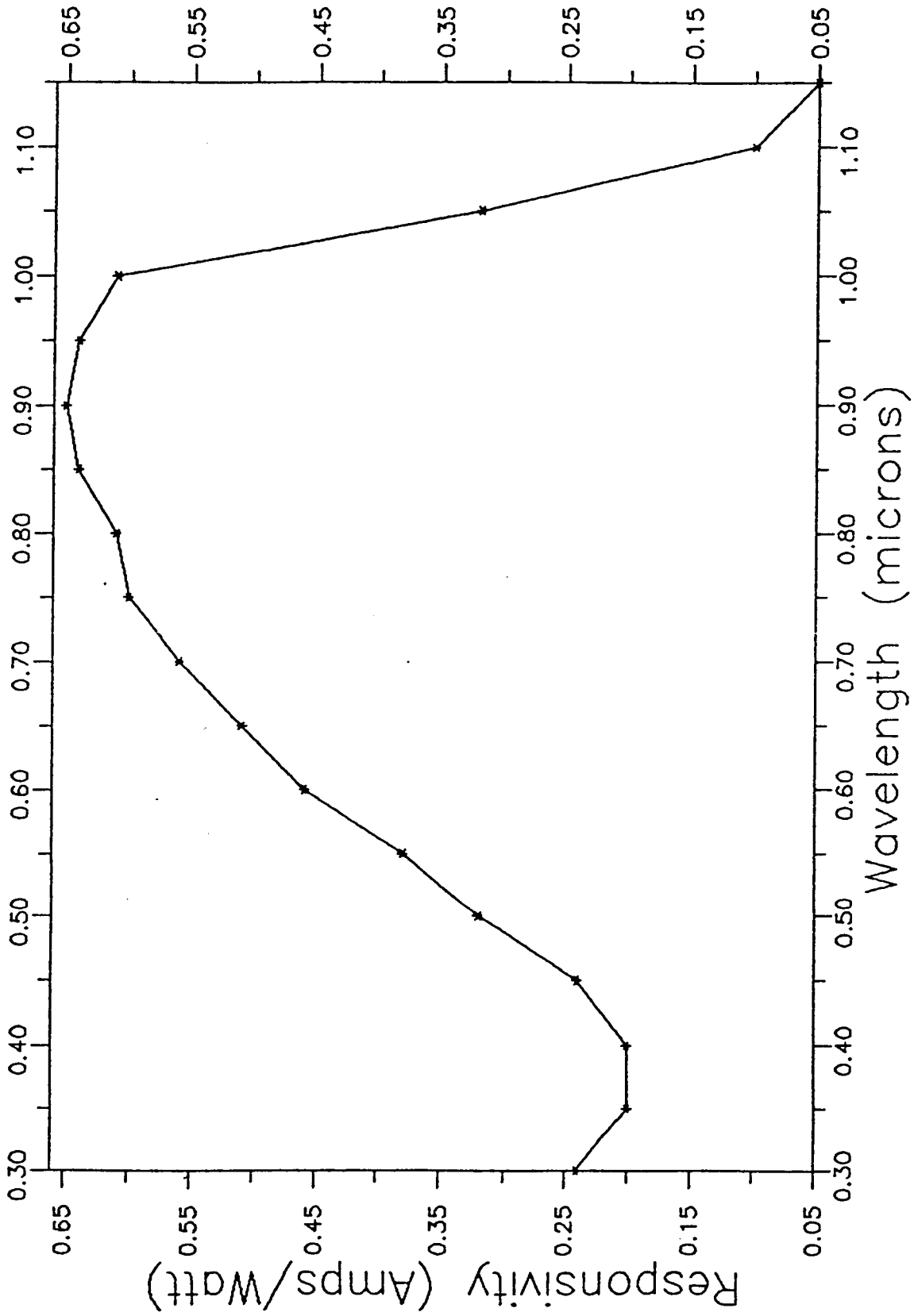


Figure J-3. DEC beam detector response.

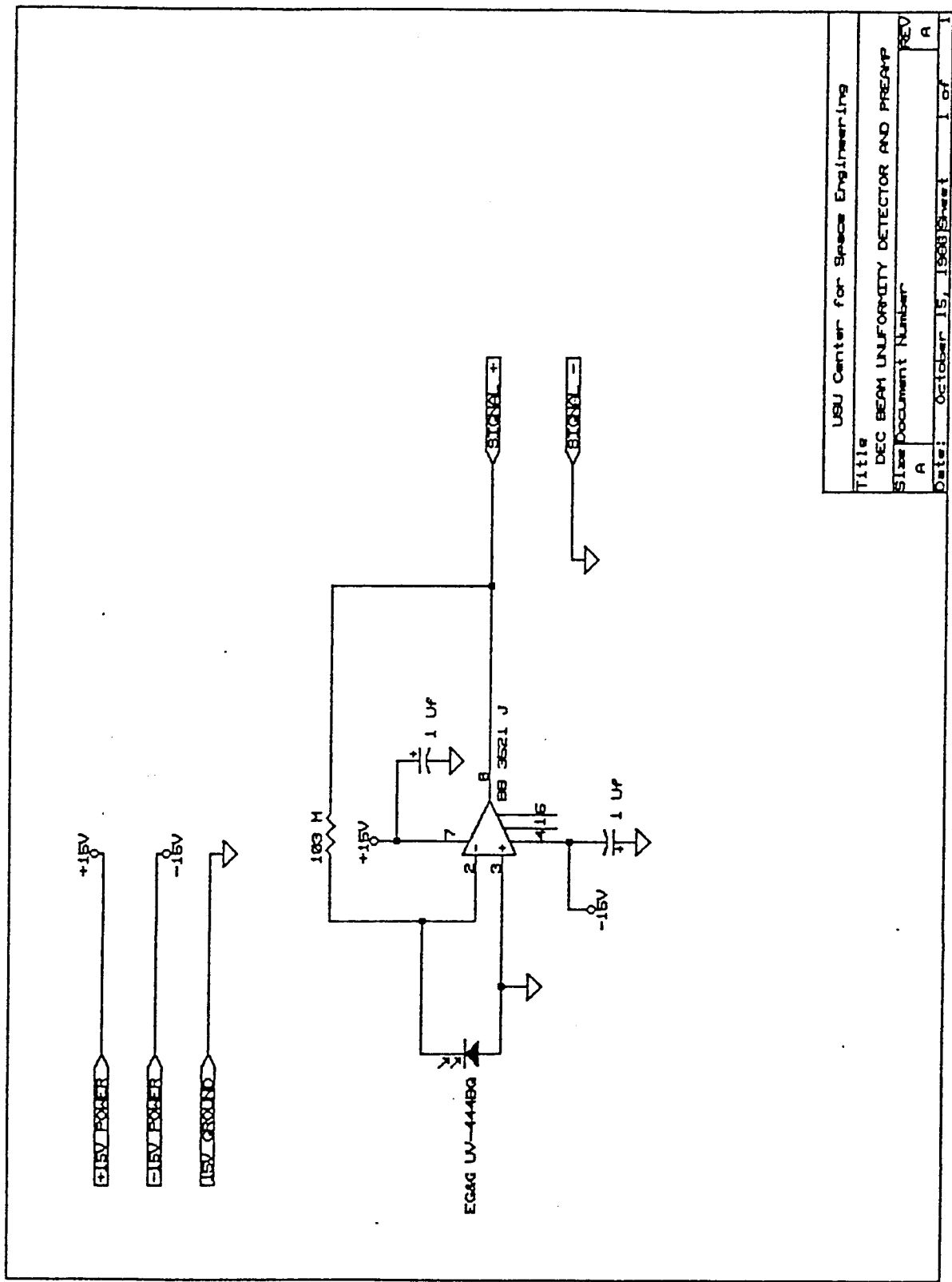


Figure J-4. DEC beam uniformity detector preamp schematic.

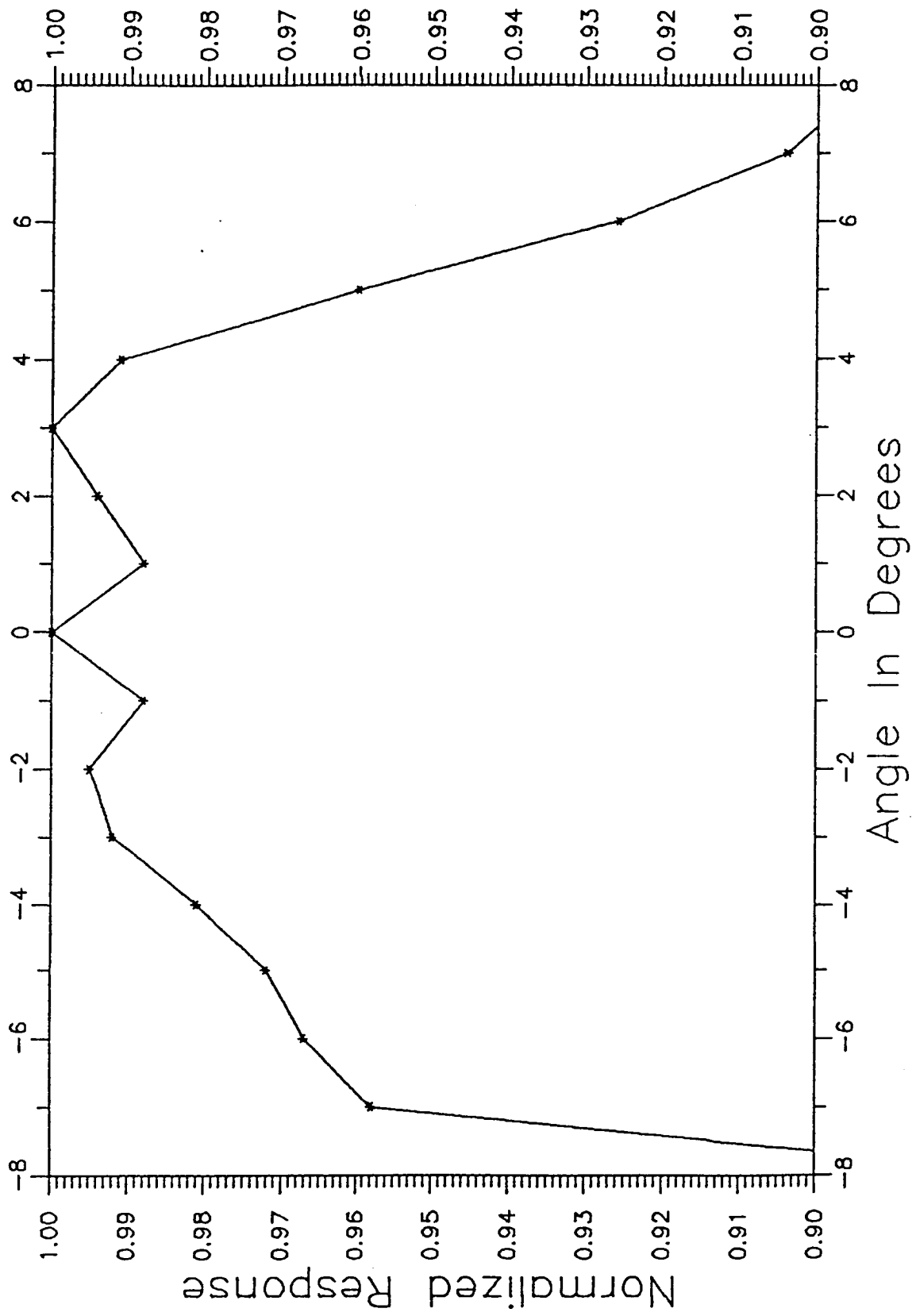


Figure J-5. DEC beam uniformity X-axis field-of-view.

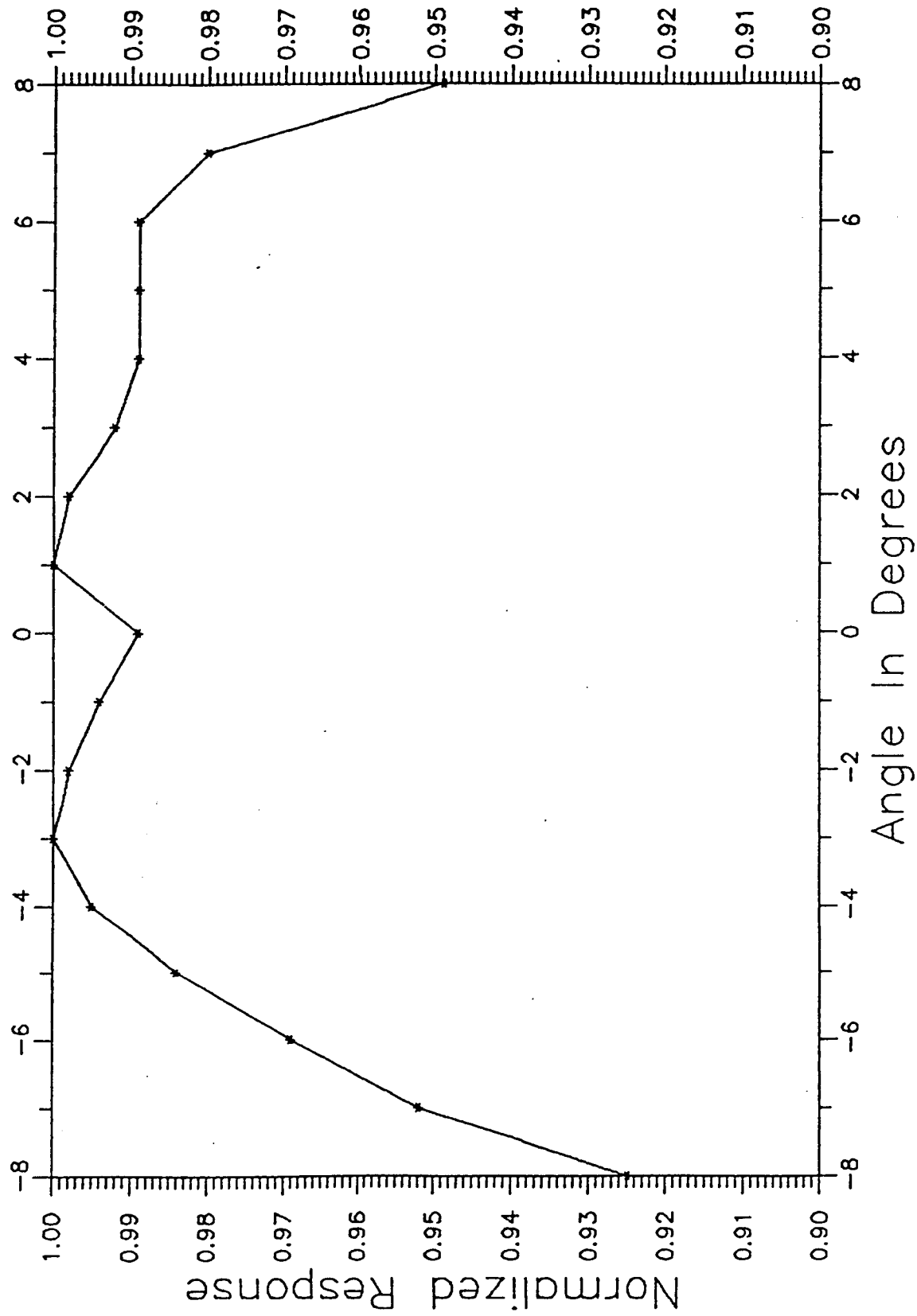


Figure J-6. DEC beam uniformity Y-axis field-of-view.

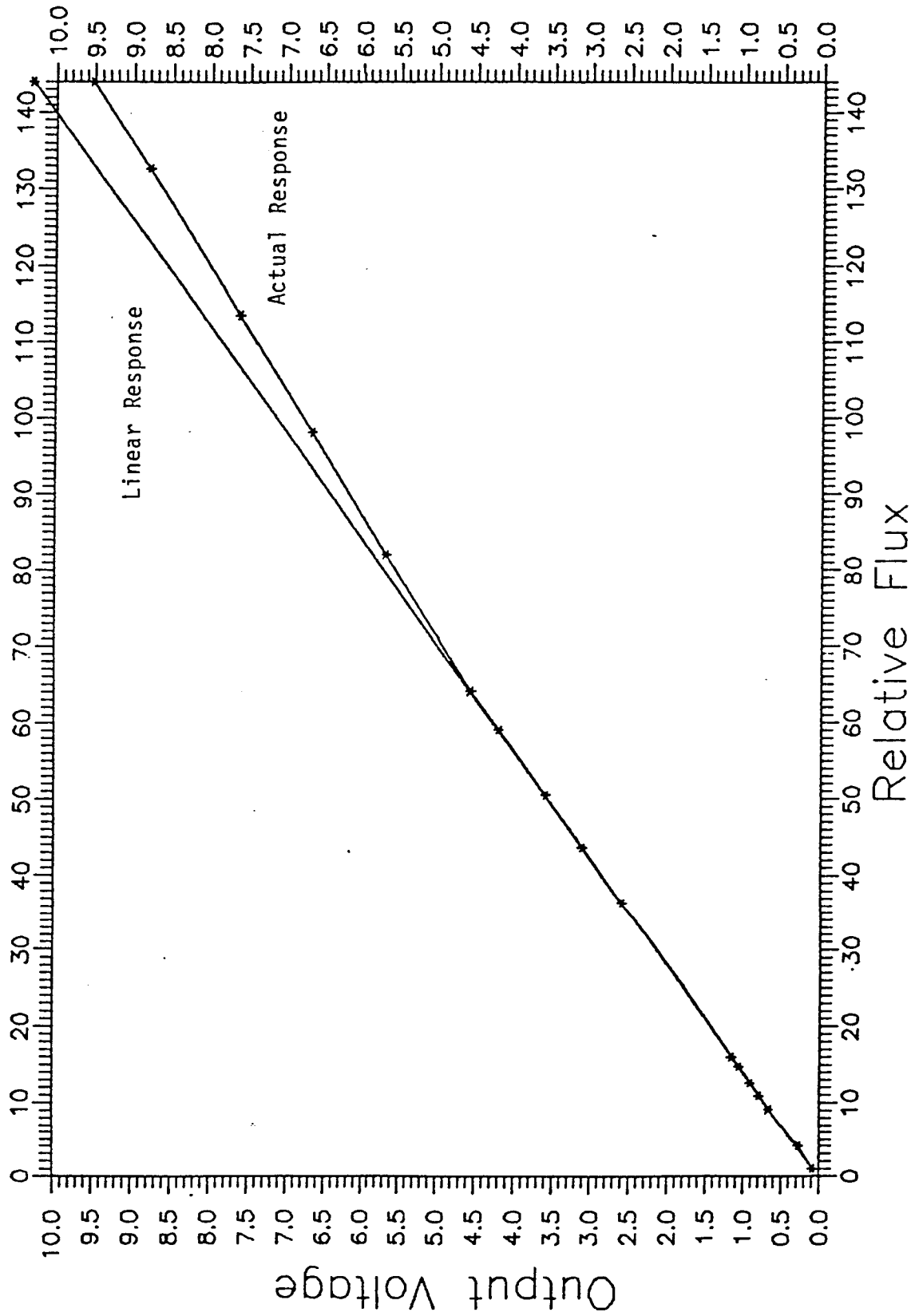


Figure J-7. Linear response versus actual response.

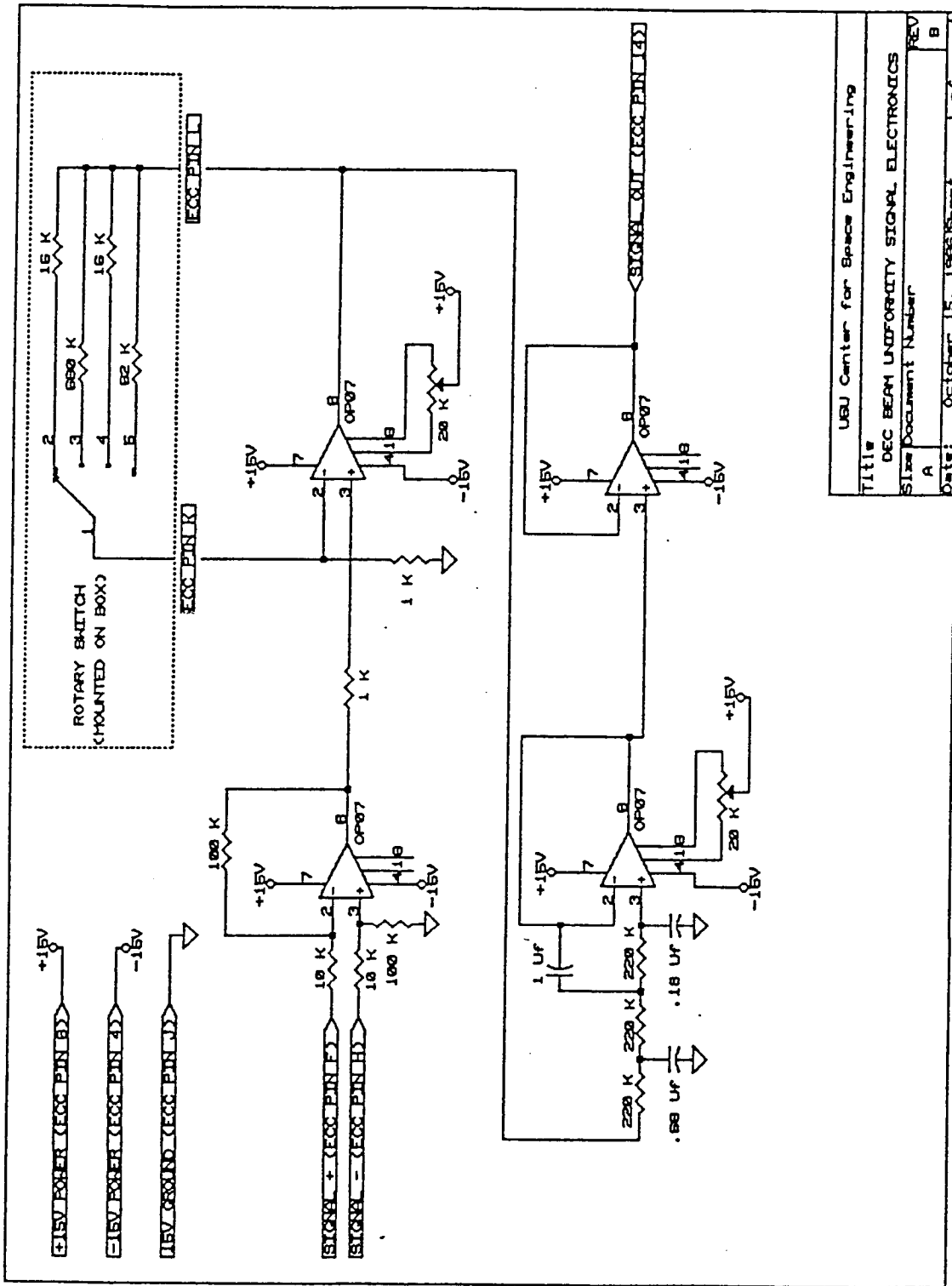


Figure J-8. DEC beam uniformity amplifier schematic.

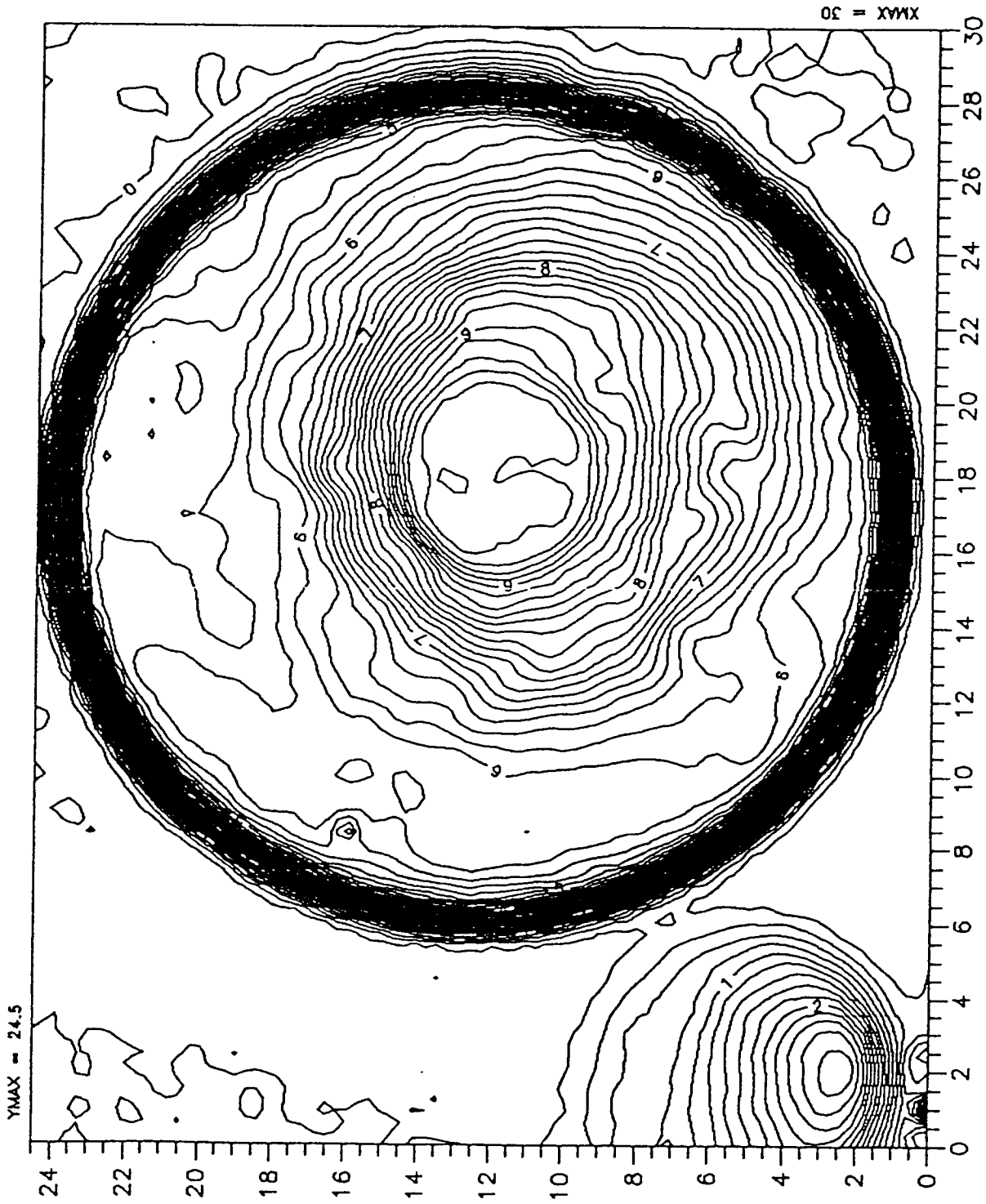


Figure J-9. DEC beam mapping file #1 - contour every 0.2V.

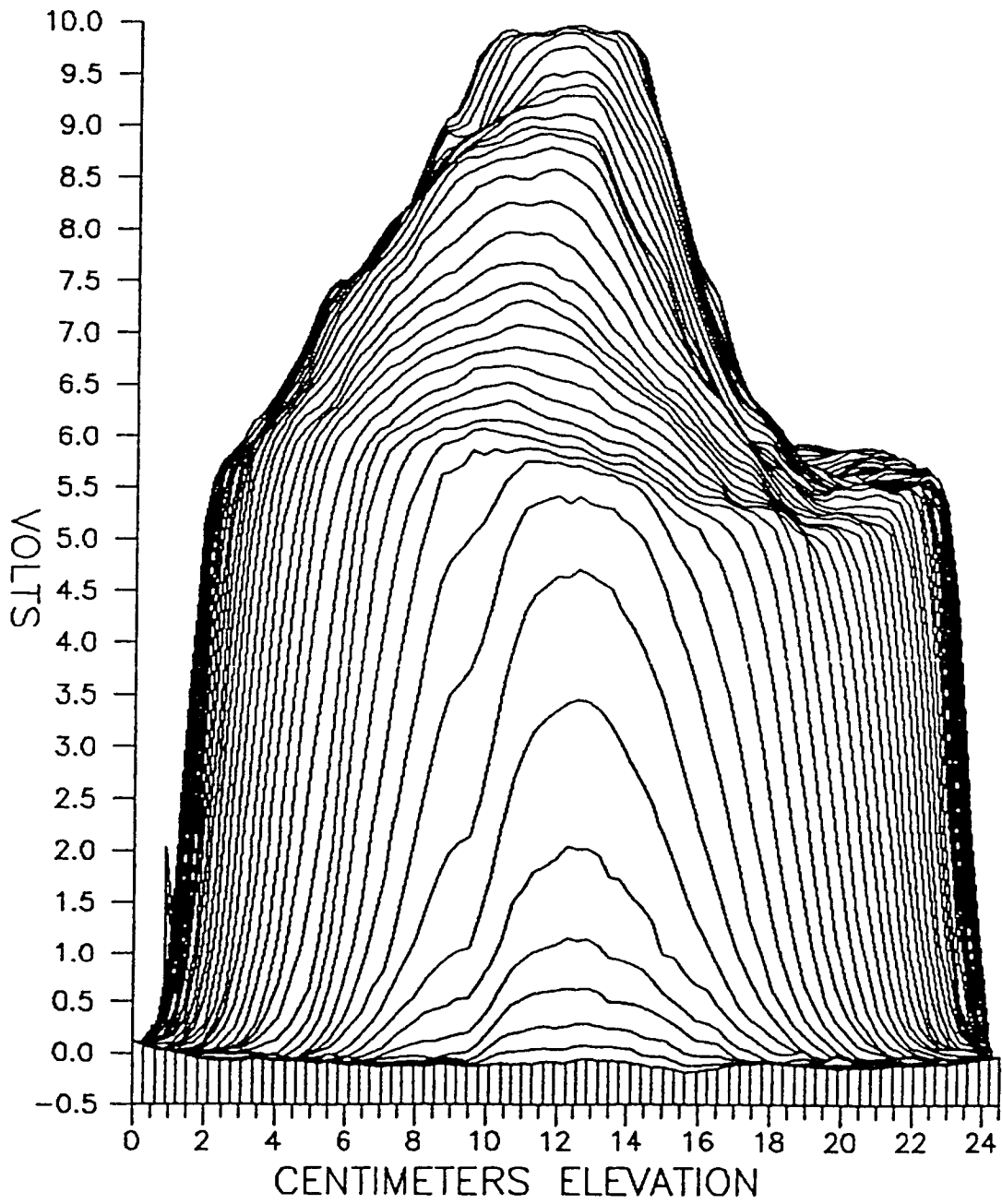


Figure J-10. DEC beam mapping file #1 - Tilt: 0 - Rotation: 0.

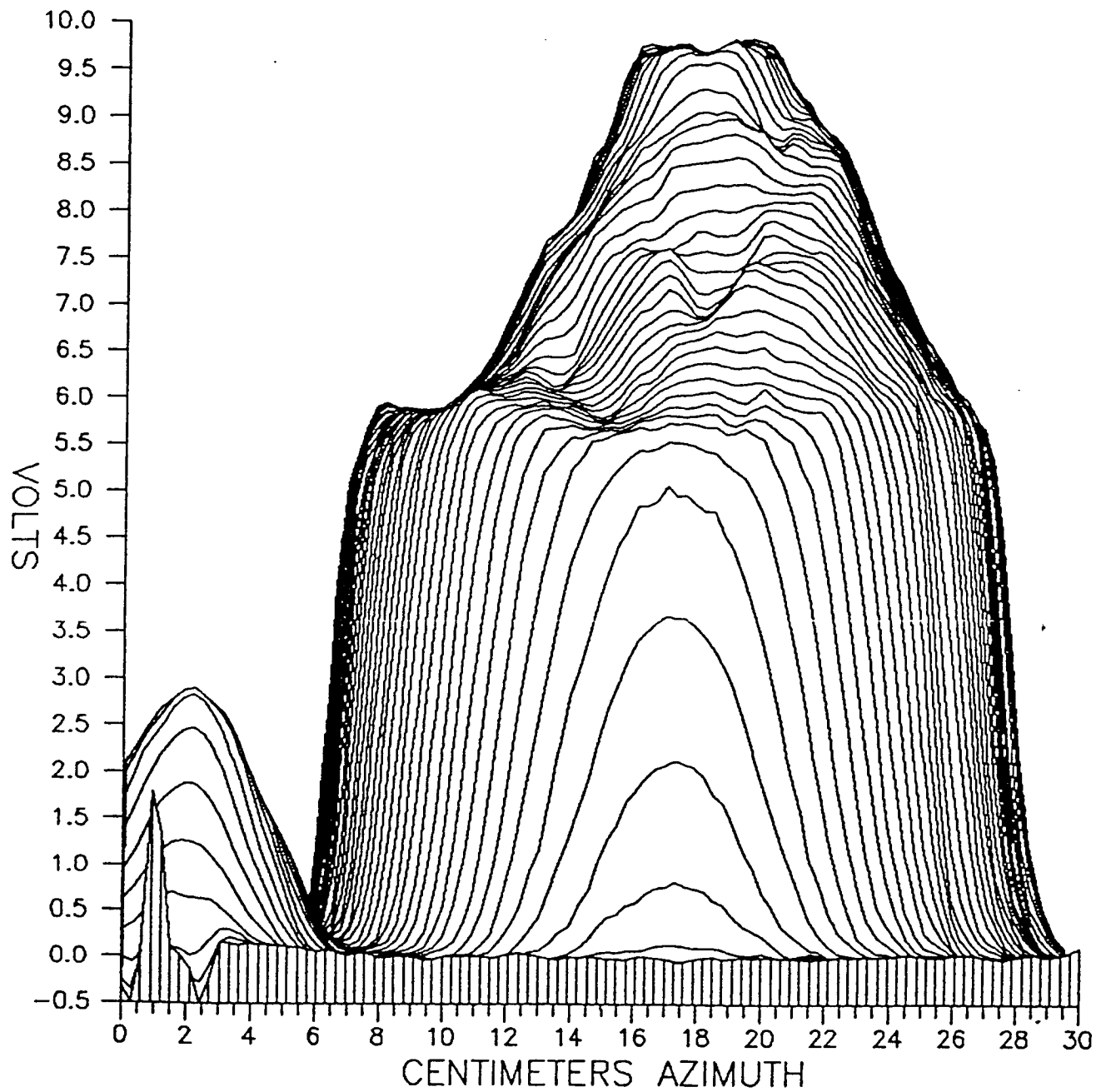


Figure J-11. DEC beam mapping file #1 - Tilt: 0 - Rotation: 270.

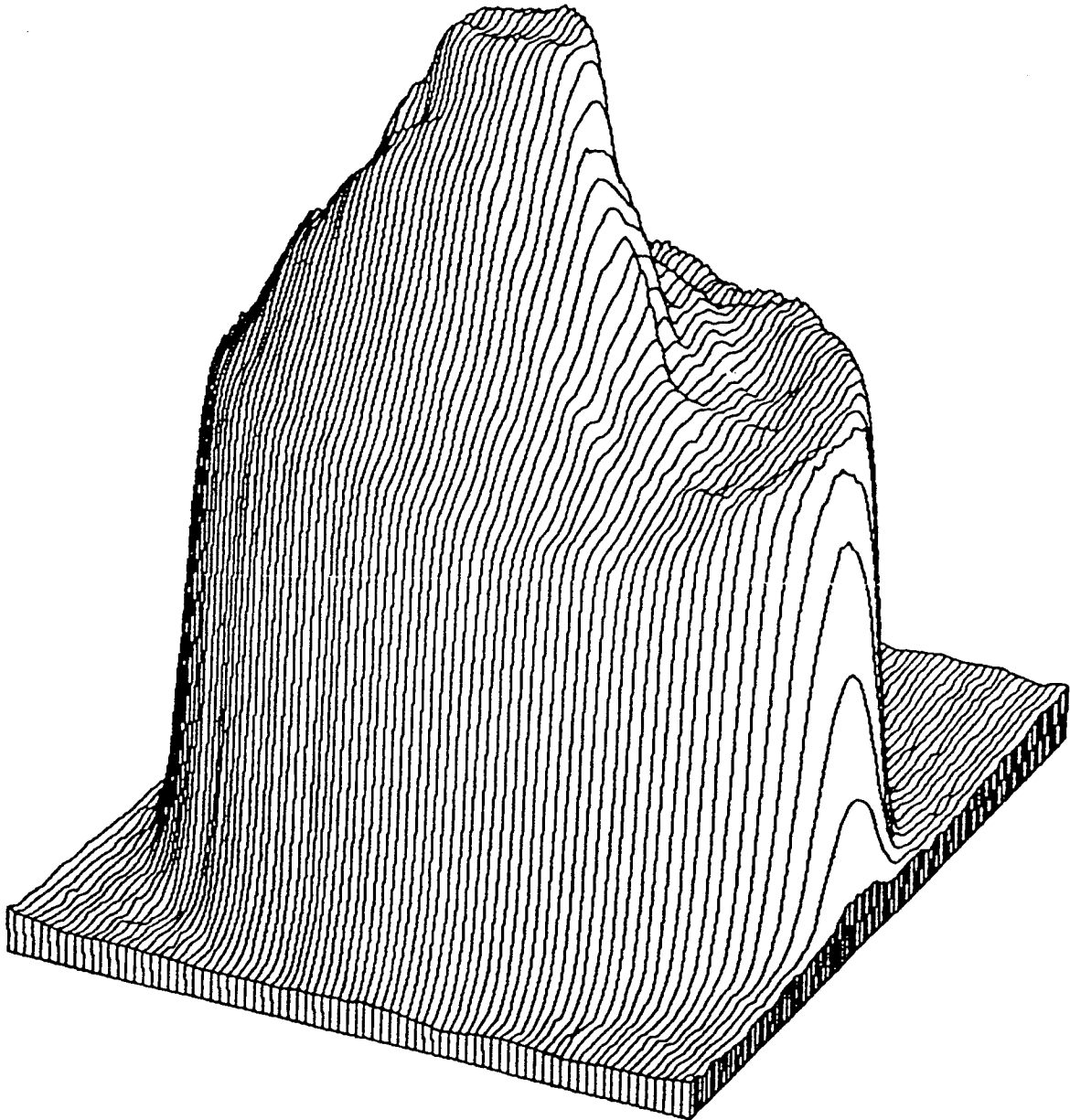


Figure J-12. DEC beam mapping file #1 - Tilt: 25 - Rotation: 25.

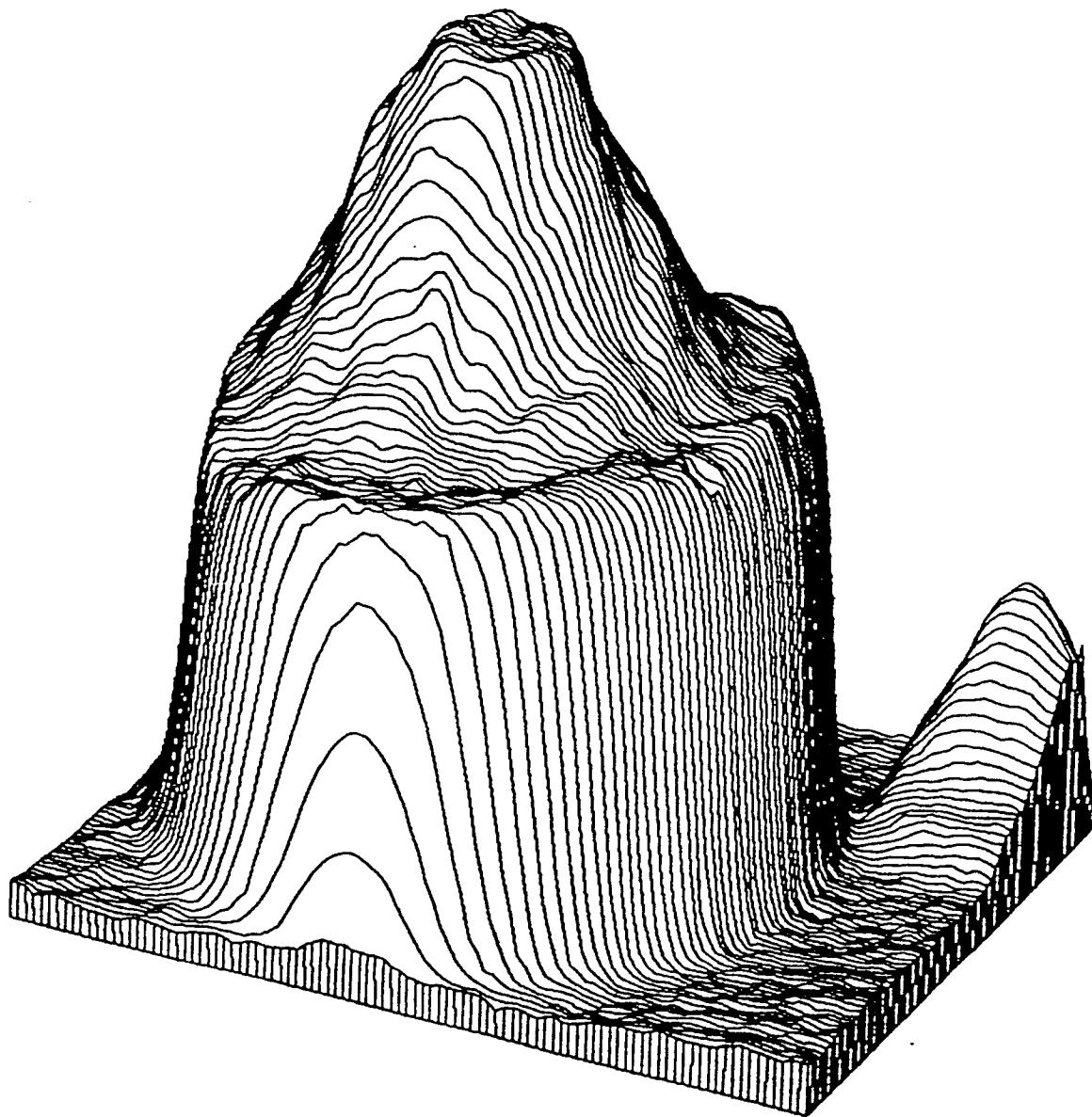


Figure J-13. DEC beam mapping file #1 - Tilt: 25 - Rotation: 115.

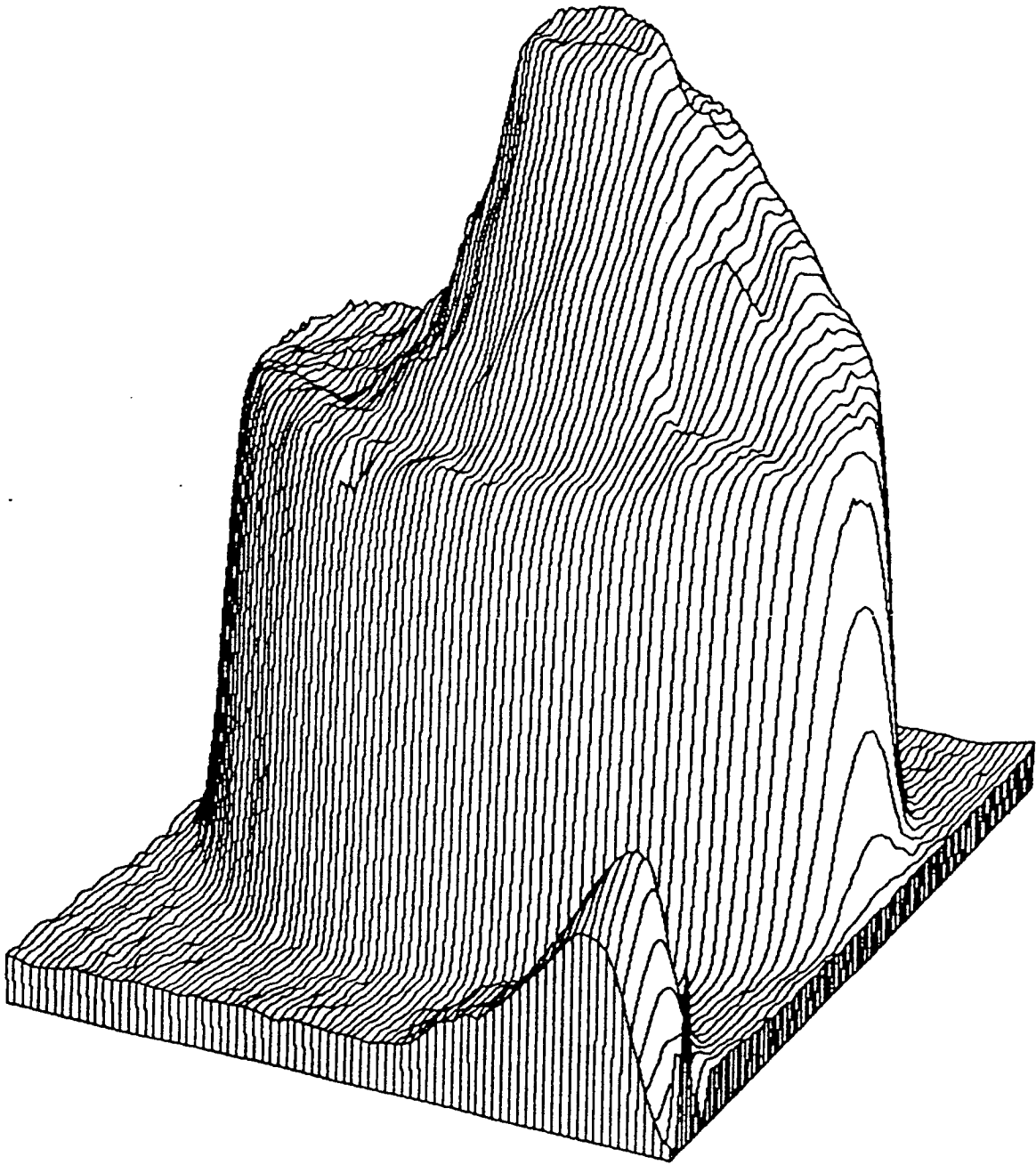


Figure J-14. DEC beam mapping file #1 - Tilt: 25 - Rotation: 205.

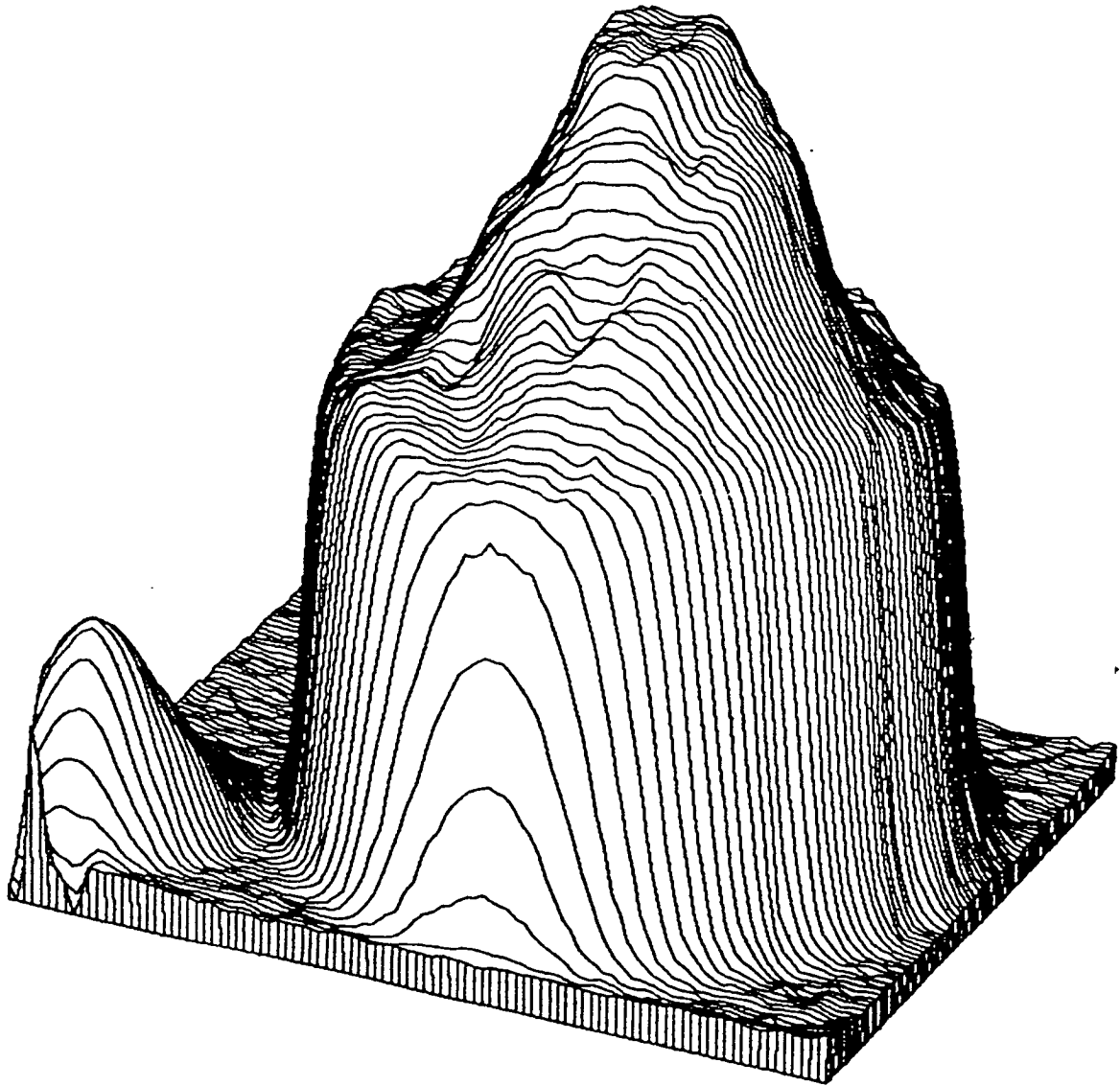


Figure J-15. DEC beam mapping file #1 - Tilt: 25 - Rotation: 205.

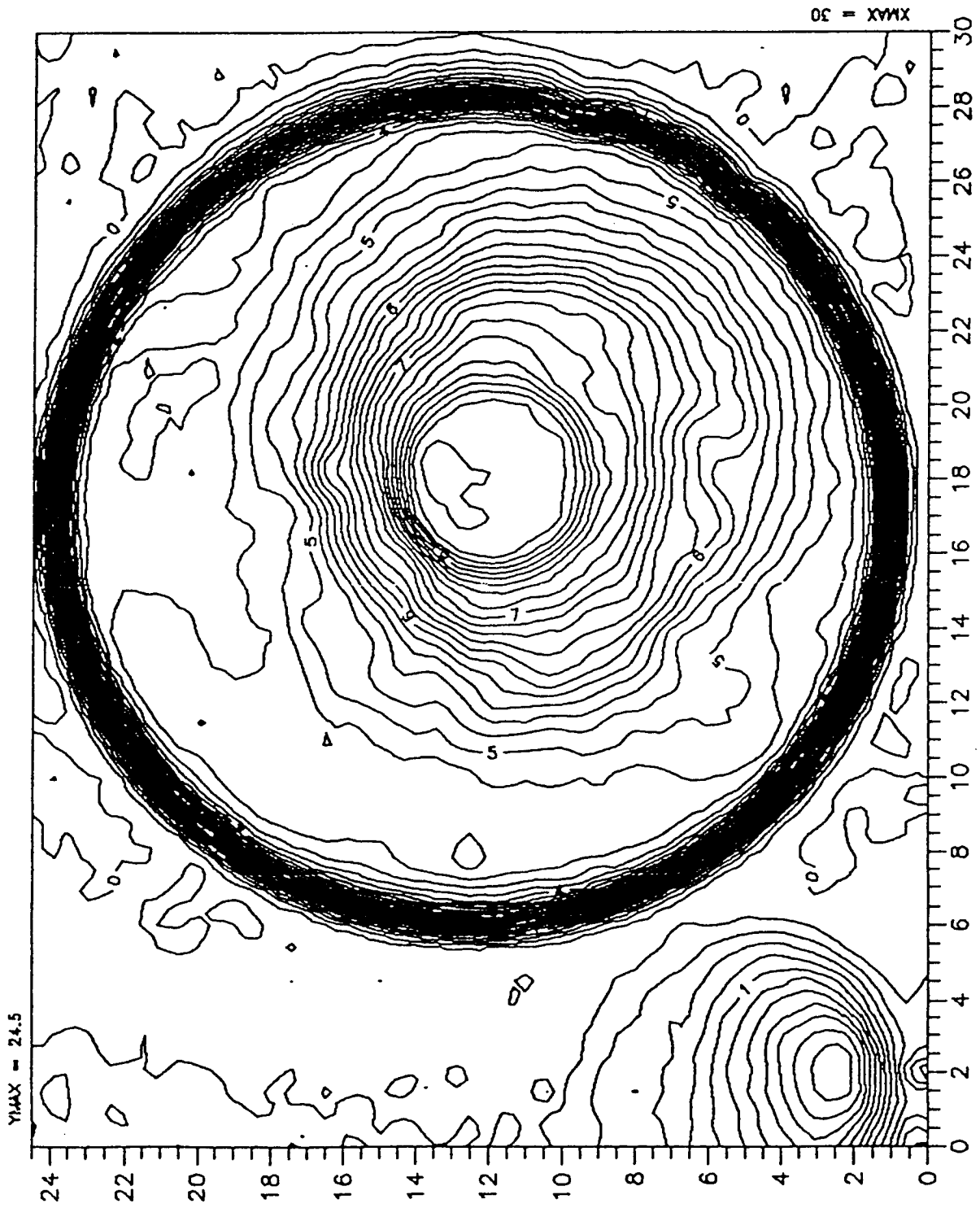


Figure J-16. DEC beam mapping file #2 - contour every 0.2V.

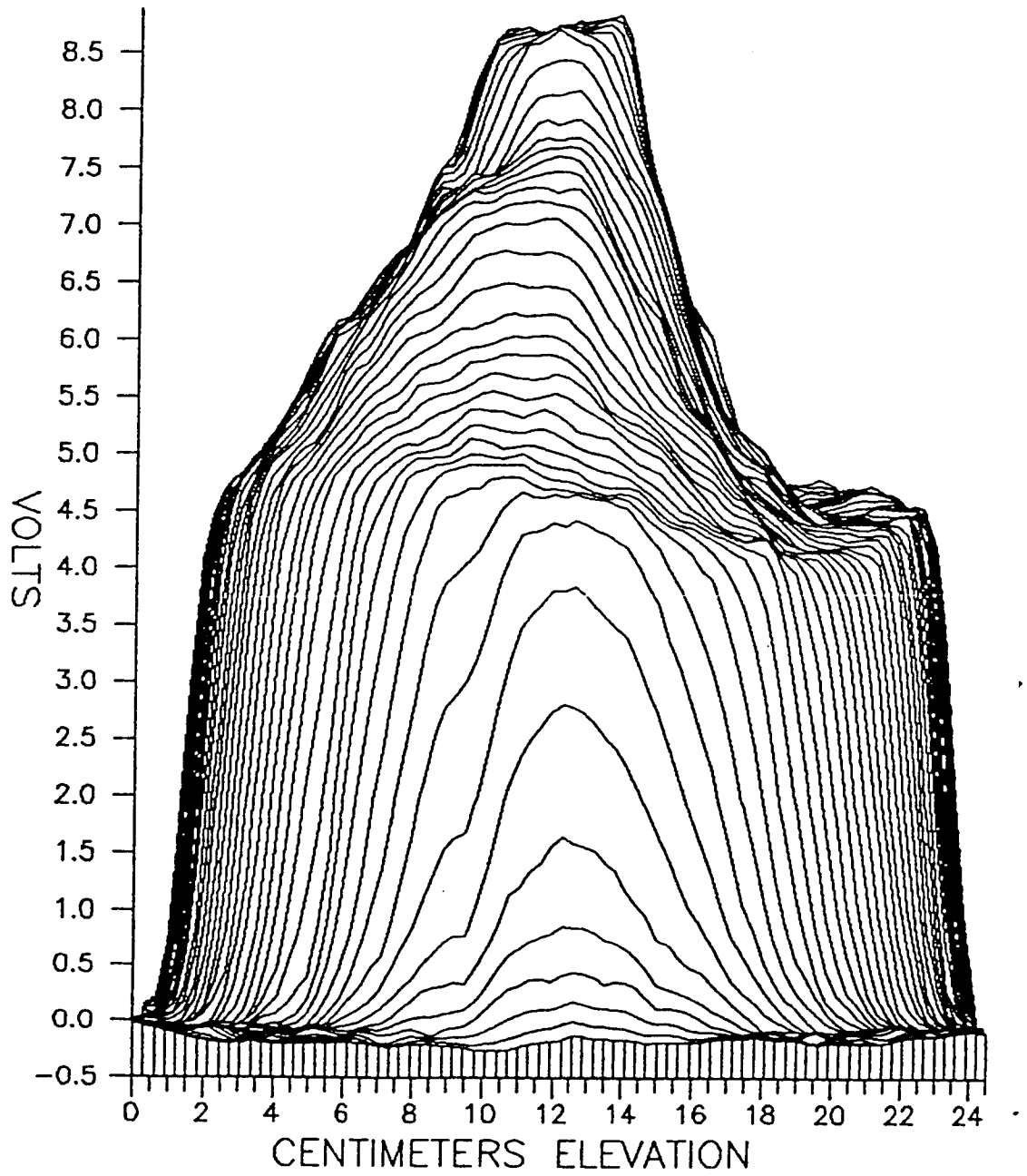


Figure J-17. DEC beam mapping file #2 - Tilt: 0 - Rotation: 0.

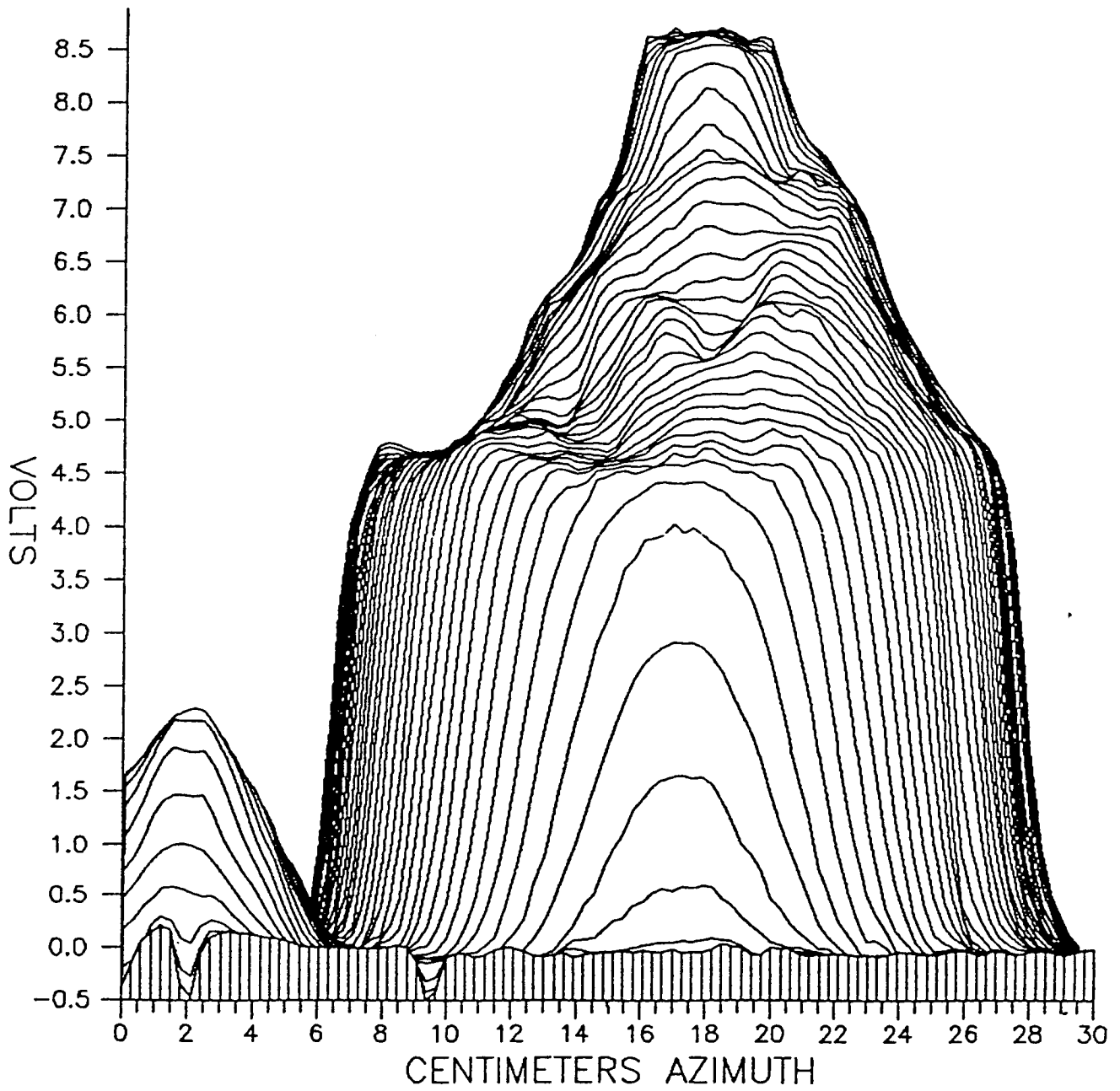


Figure J-18. DEC beam mapping file #2 - Tilt: 0 - Rotation: 270.

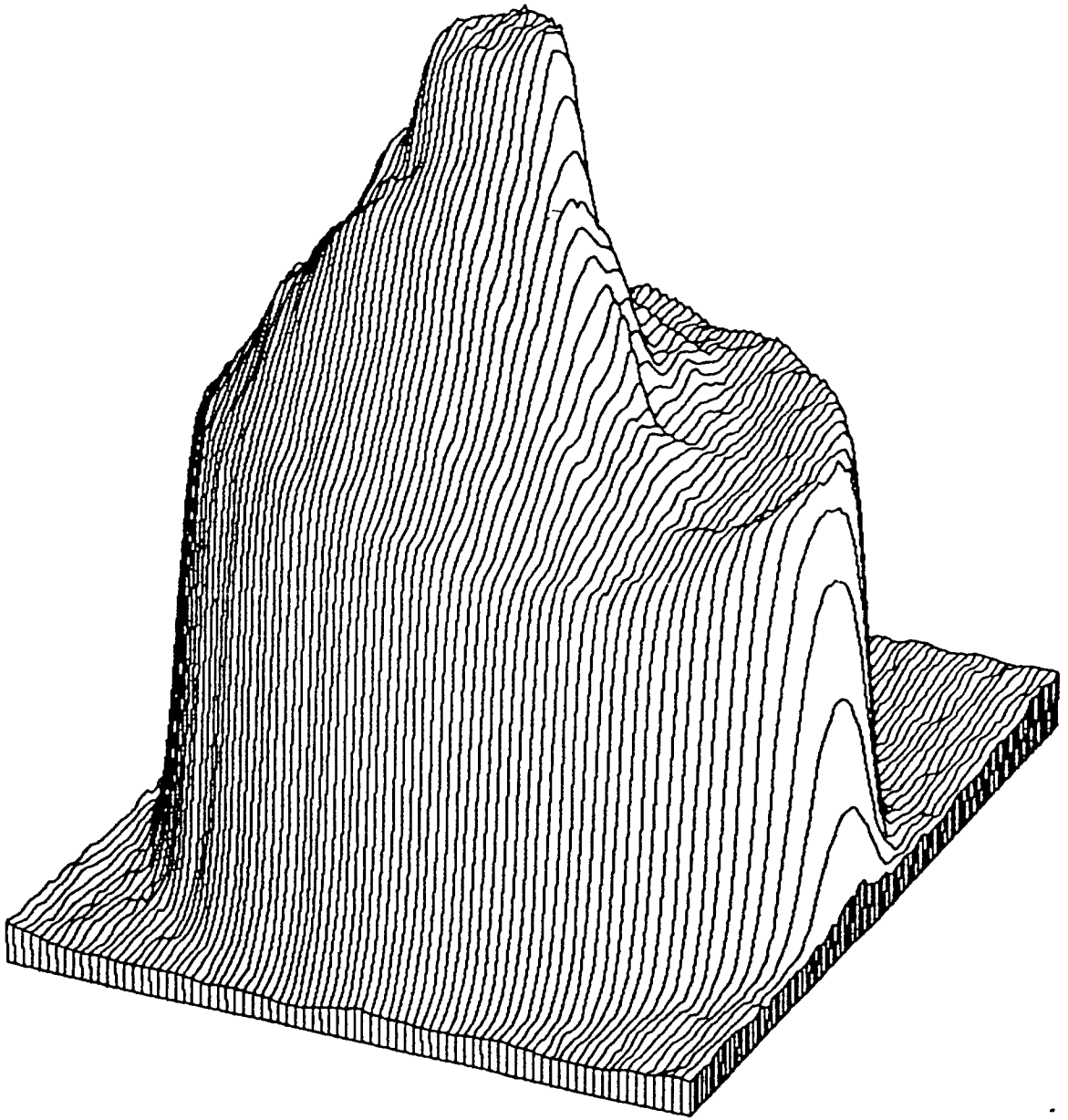


Figure J-19. DEC beam mapping file #2 - Tilt: 25 - Rotation: 25.

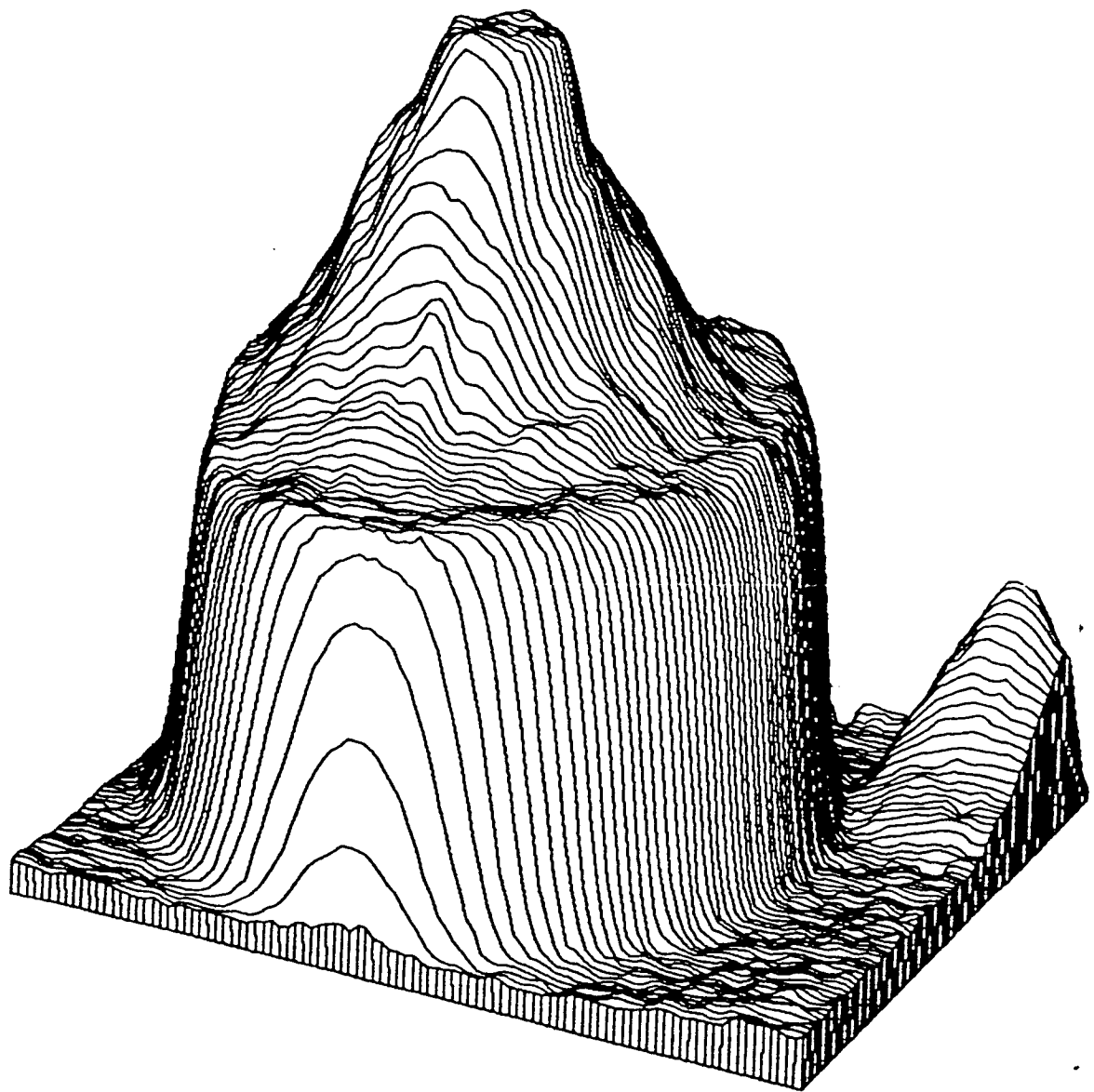


Figure J-20. DEC beam mapping file #2 - Tilt: 25 - Rotation: 115.

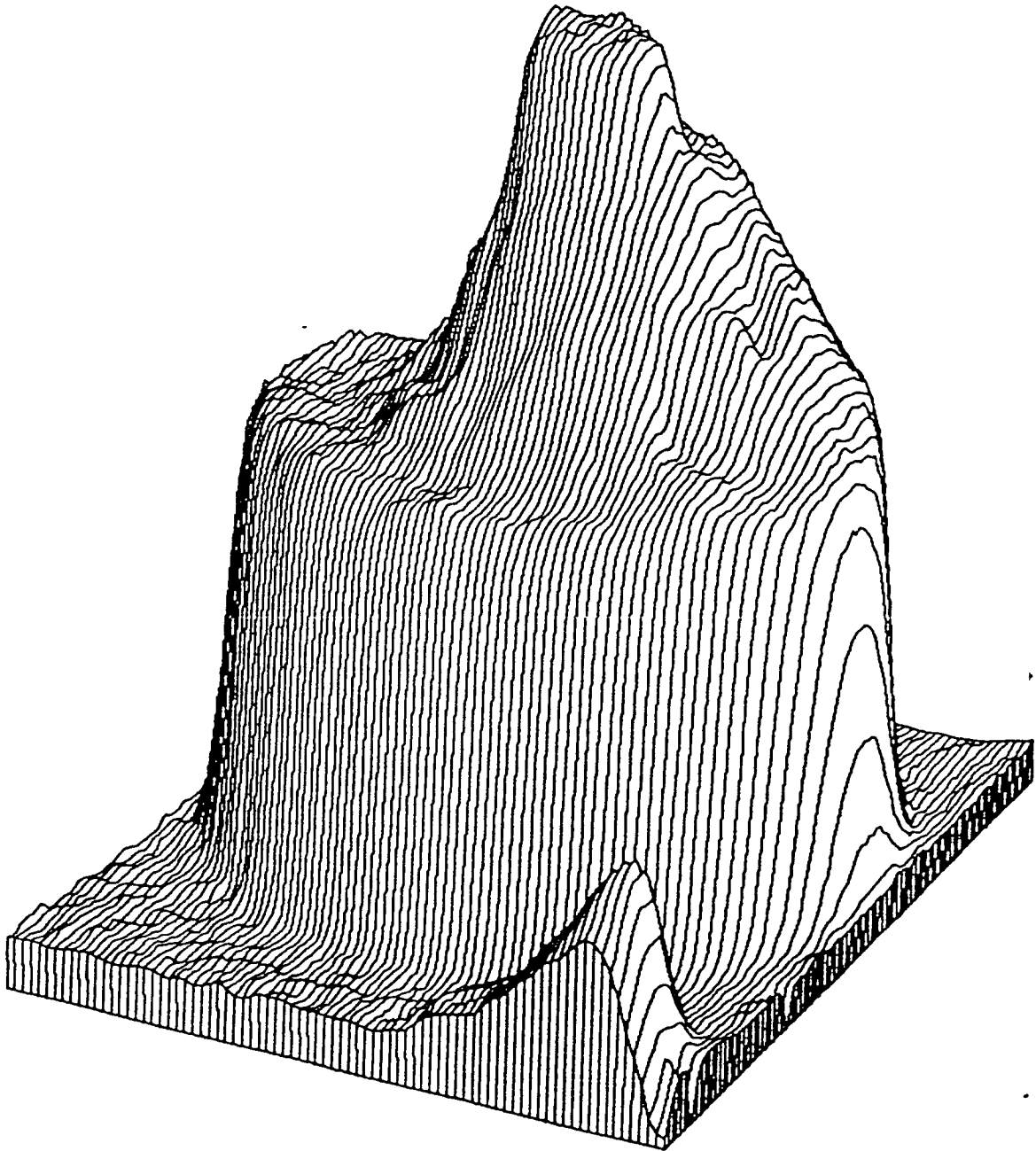


Figure J-21. DEC beam mapping file #2 - Tilt: 25 - Rotation: 205.

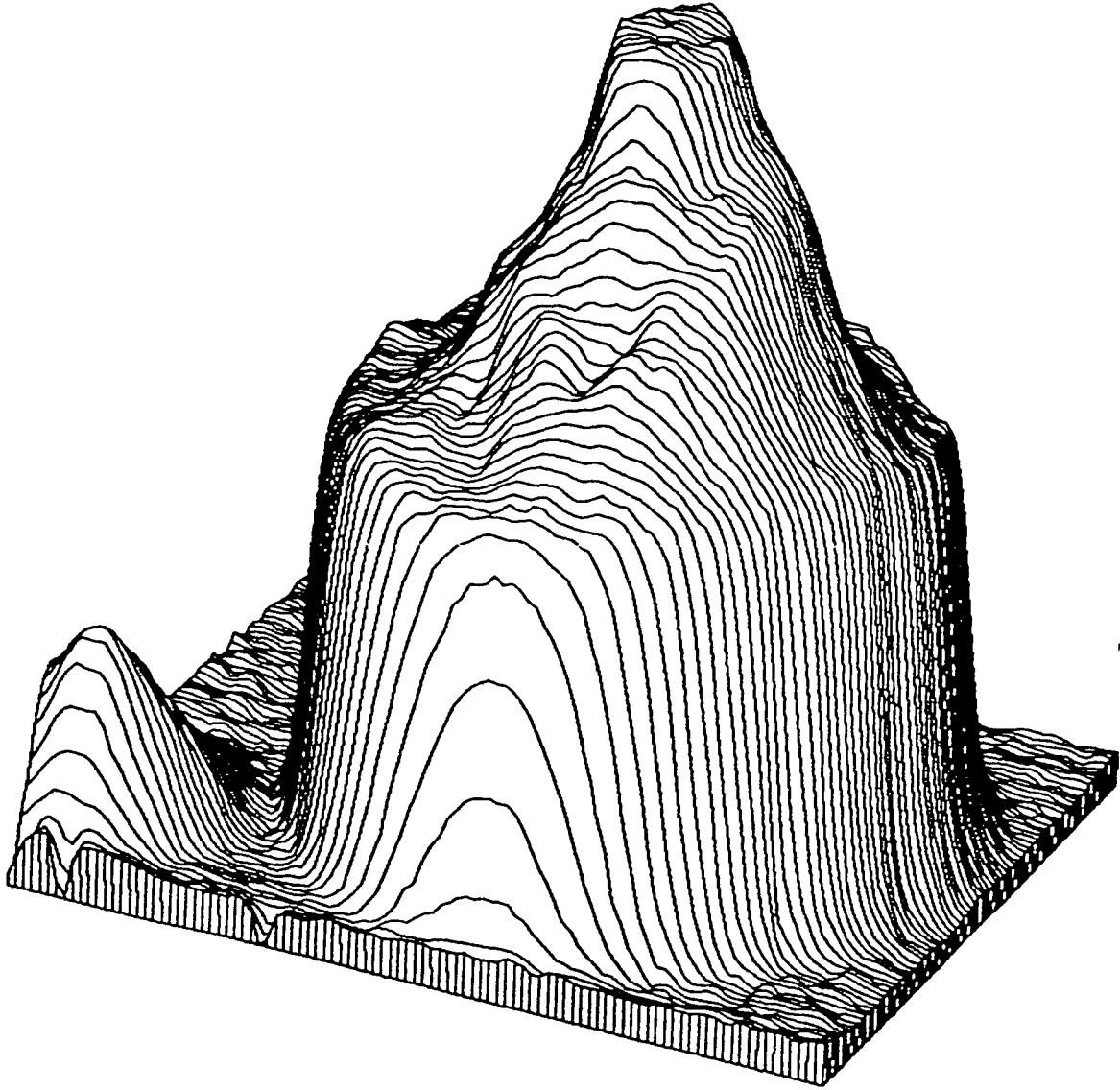


Figure J-22. DEC beam mapping file #2 - Tilt: 25 - Rotation: 295.

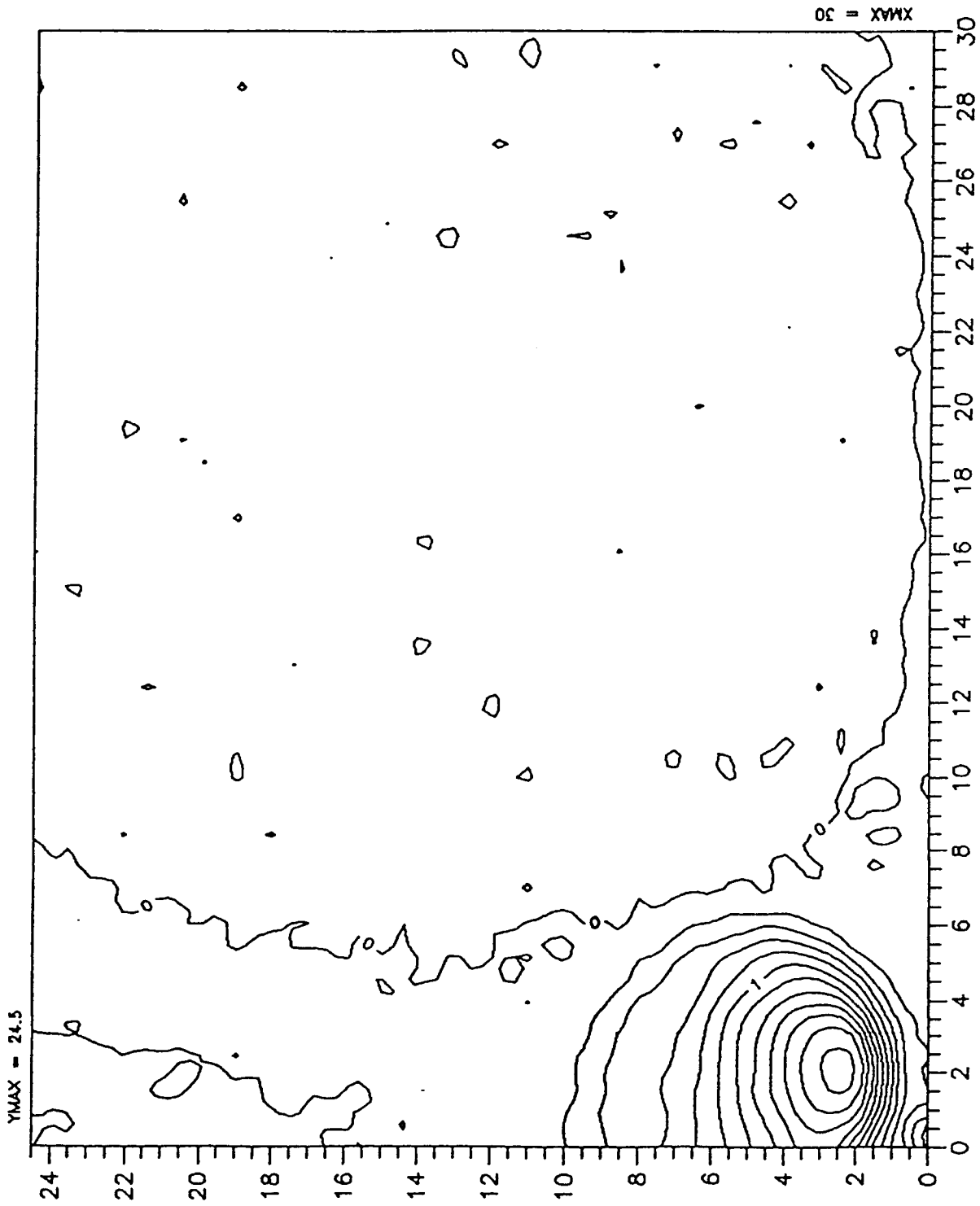


Figure J-23. DEC beam mapping file #3 - contour every 0.2V.

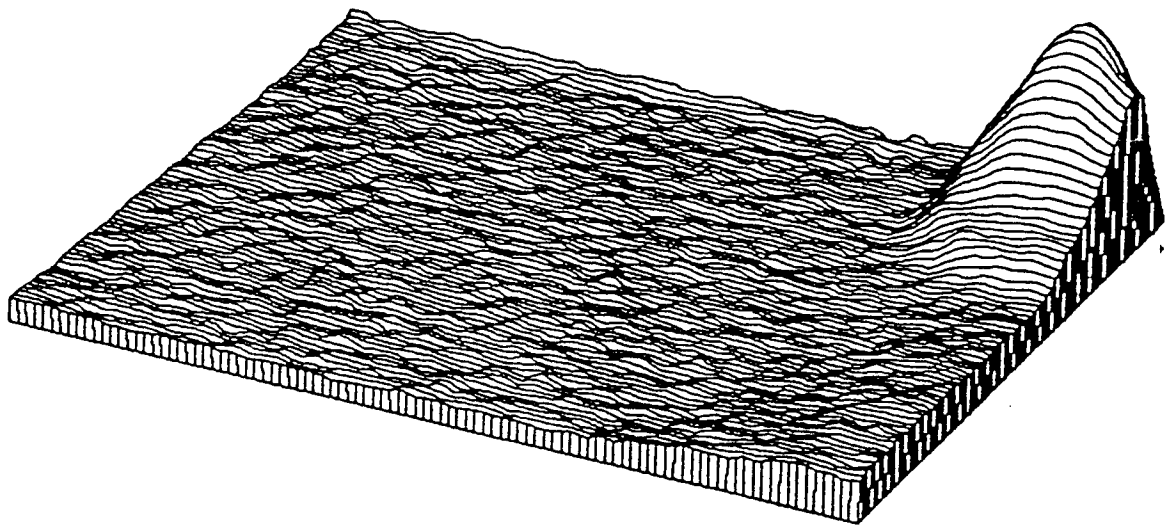


Figure J-24. DEC beam mapping file #3 - Tilt: 25 - Rotation: 115.

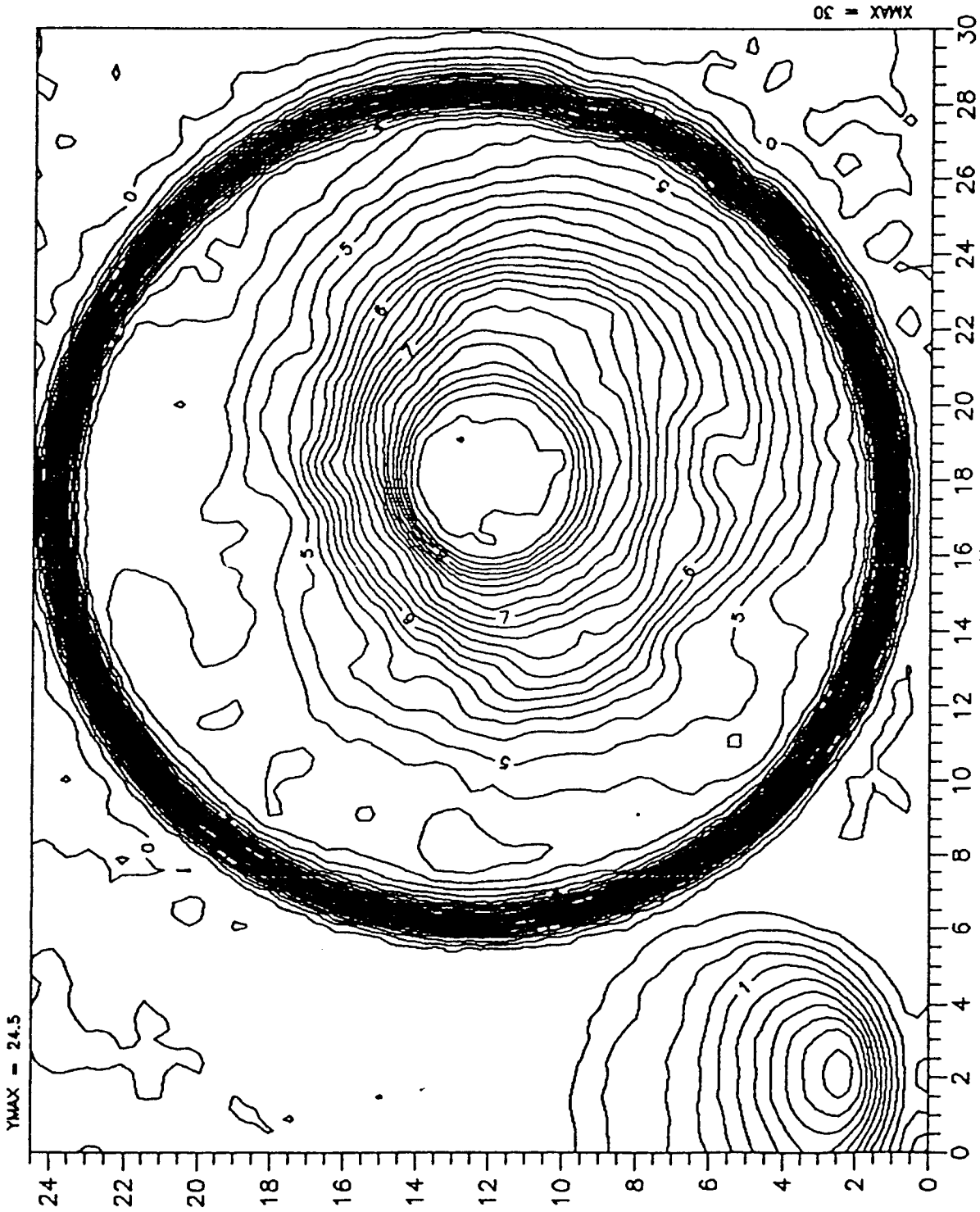


Figure J-25. DEC beam mapping file #4 - contour every 0.2V.

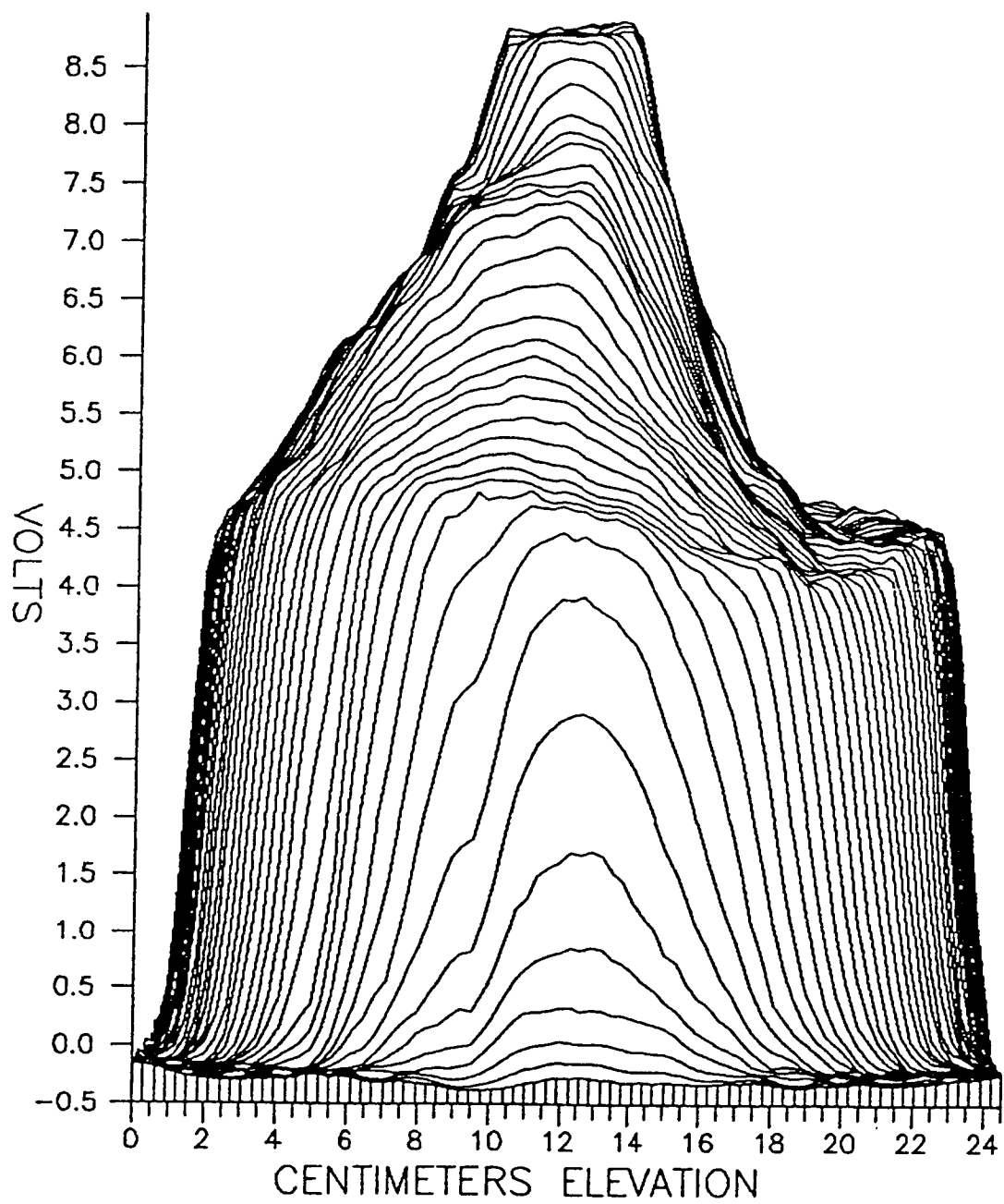


Figure J-26. DEC beam mapping file #4 - Tilt: 0 - Rotation: 0.

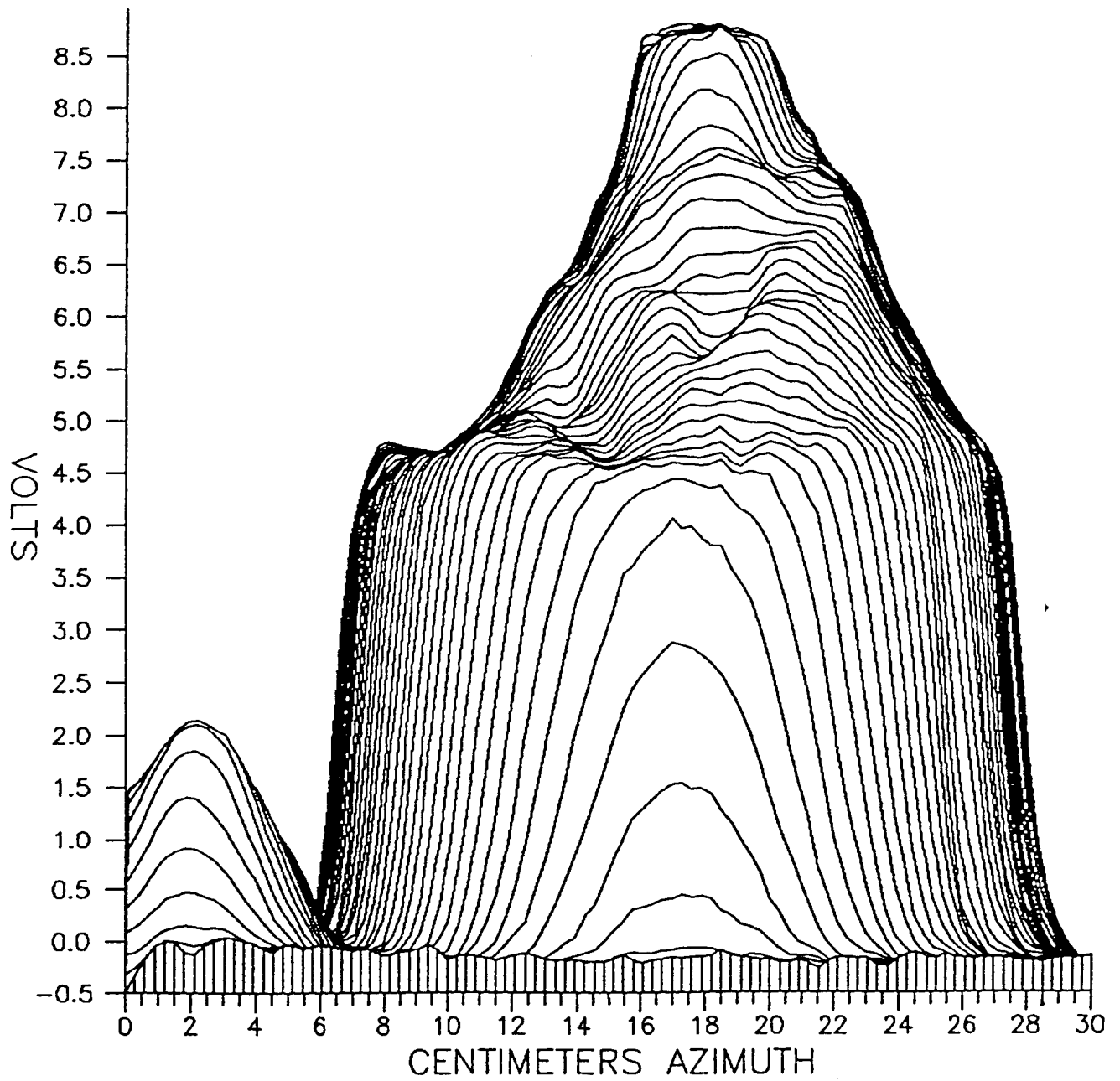


Figure J-27. DEC beam mapping file #4 - Tilt: 0 - Rotation: 270.

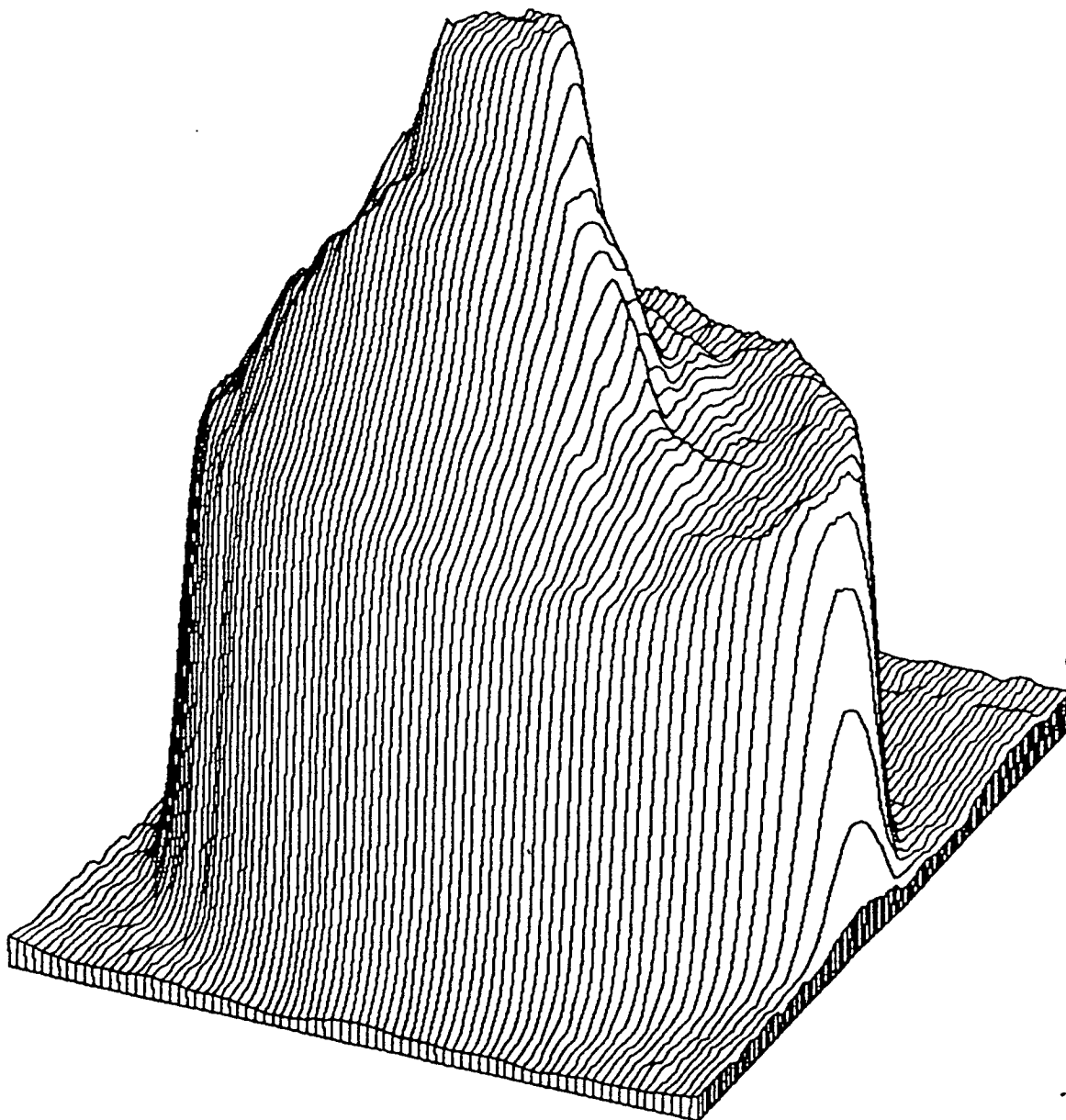


Figure J-28. DEC beam mapping file #4 - Tilt: 25 - Rotation: 25.

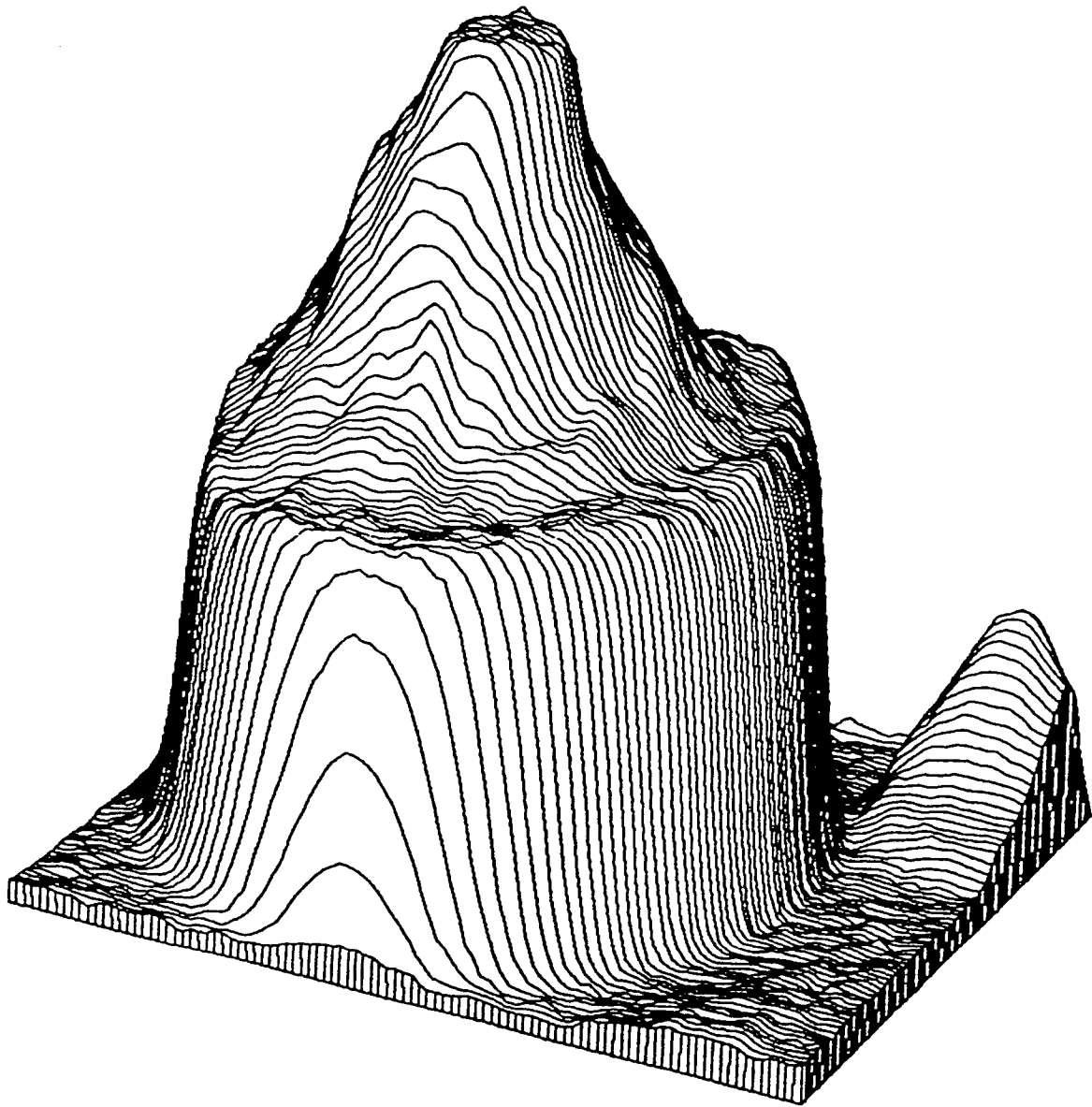


Figure J-29. DEC beam mapping file #4 - Tilt: 25 - Rotation: 115.

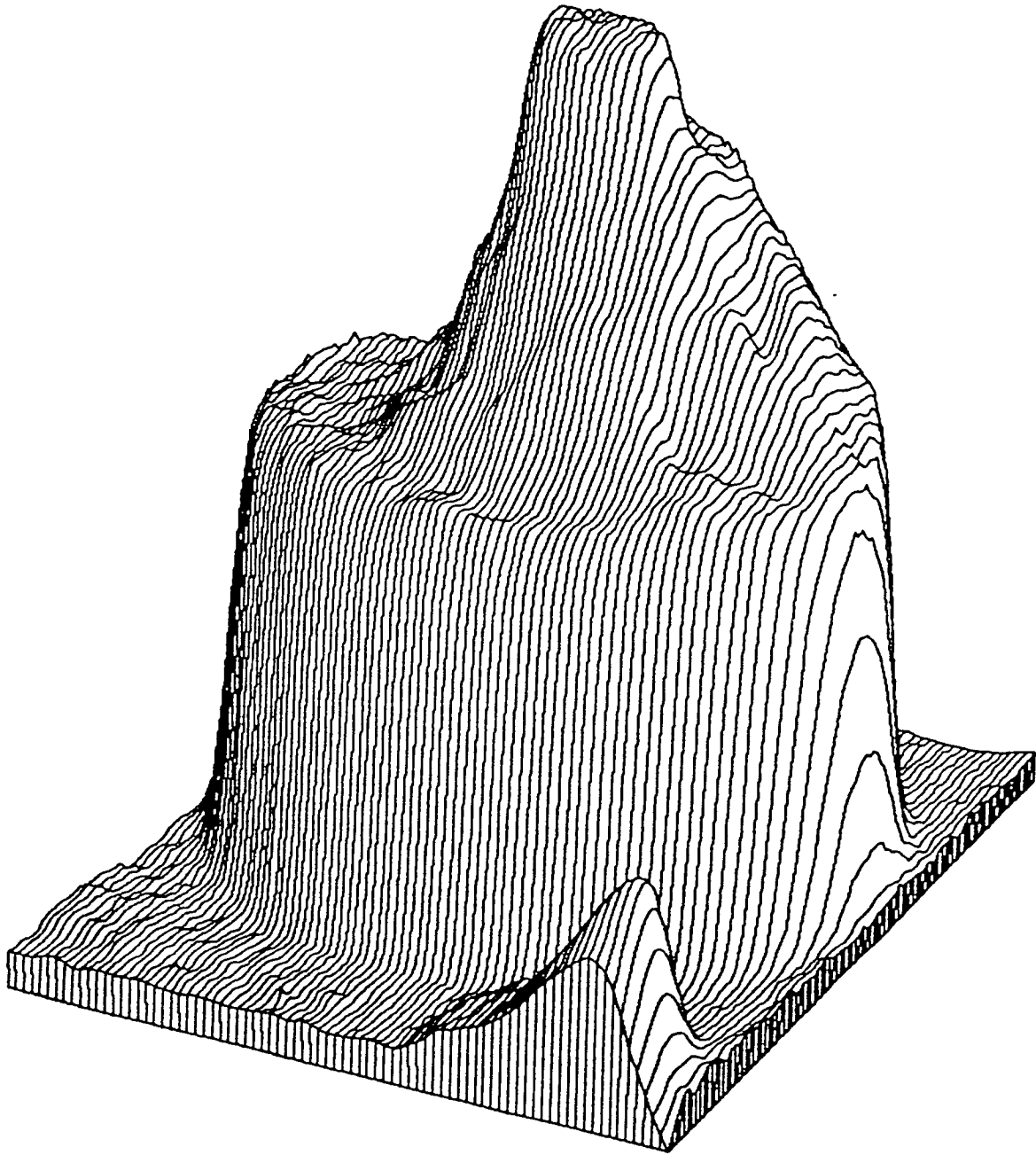


Figure J-30. DEC beam mapping file #4 - Tilt: 25 - Rotation: 205.

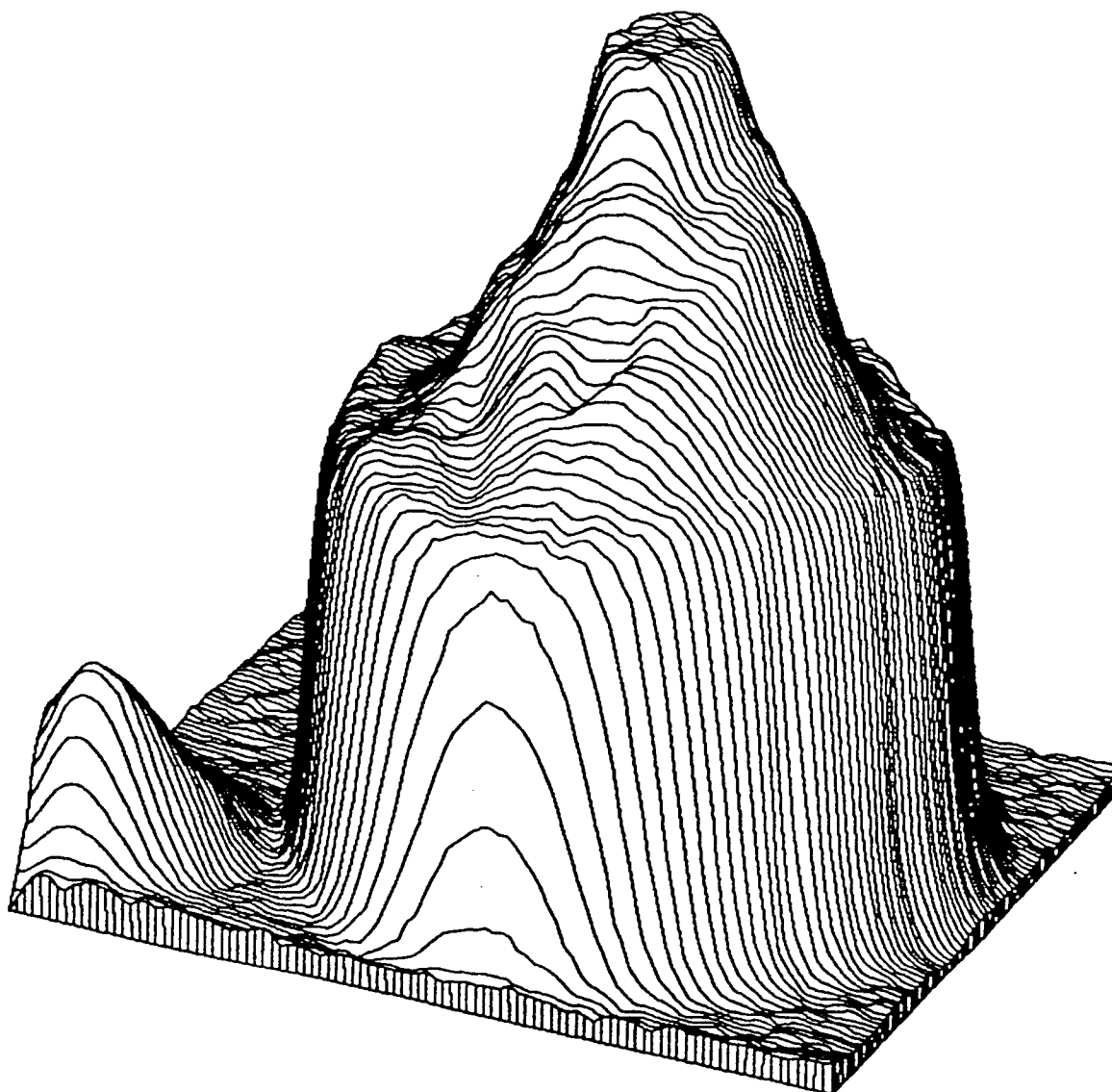


Figure J-31. DEC beam mapping file #4 - Tilt: 25 - Rotation: 295.

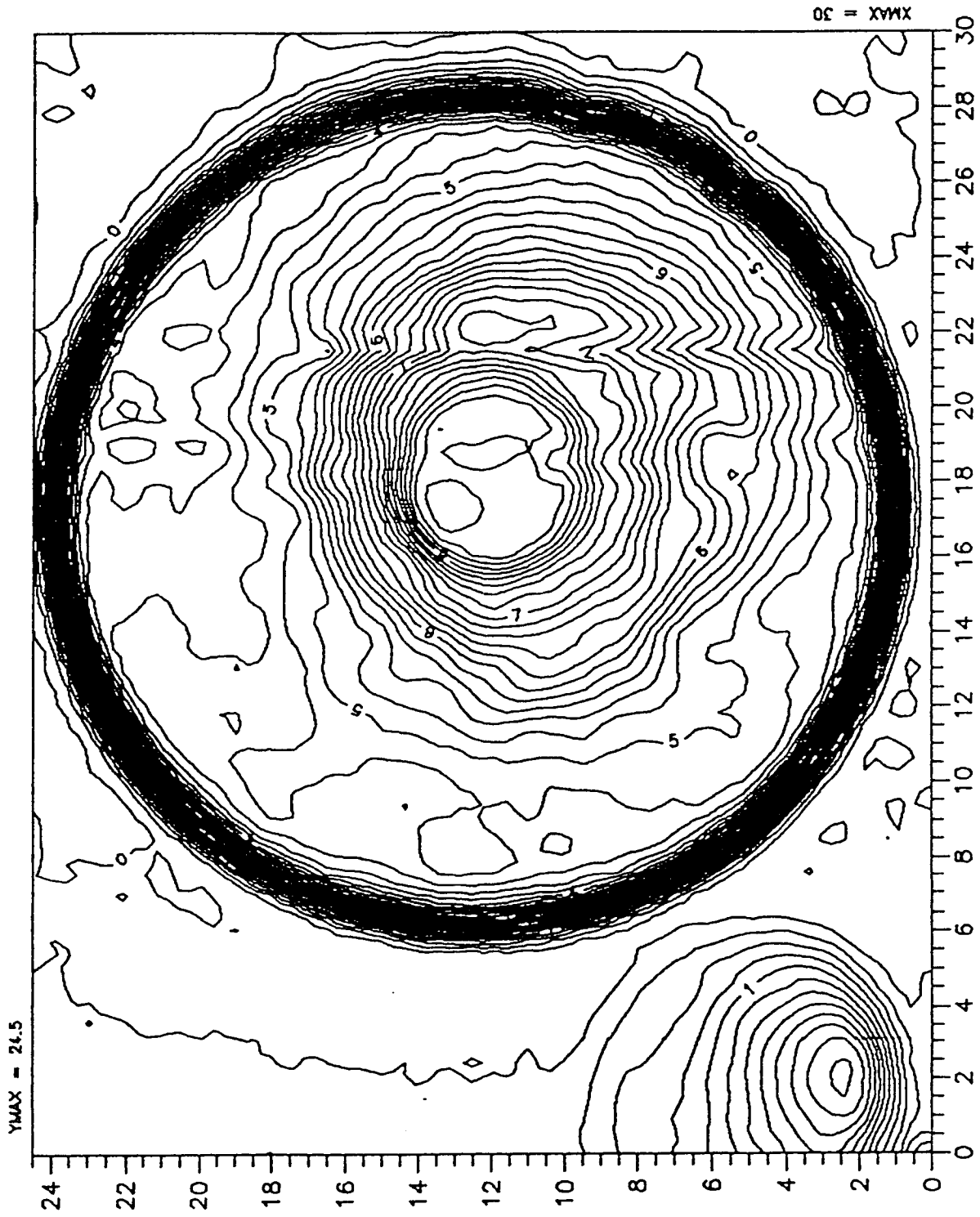


Figure J-32. DEC beam mapping file #5 - contour every 0.2V.

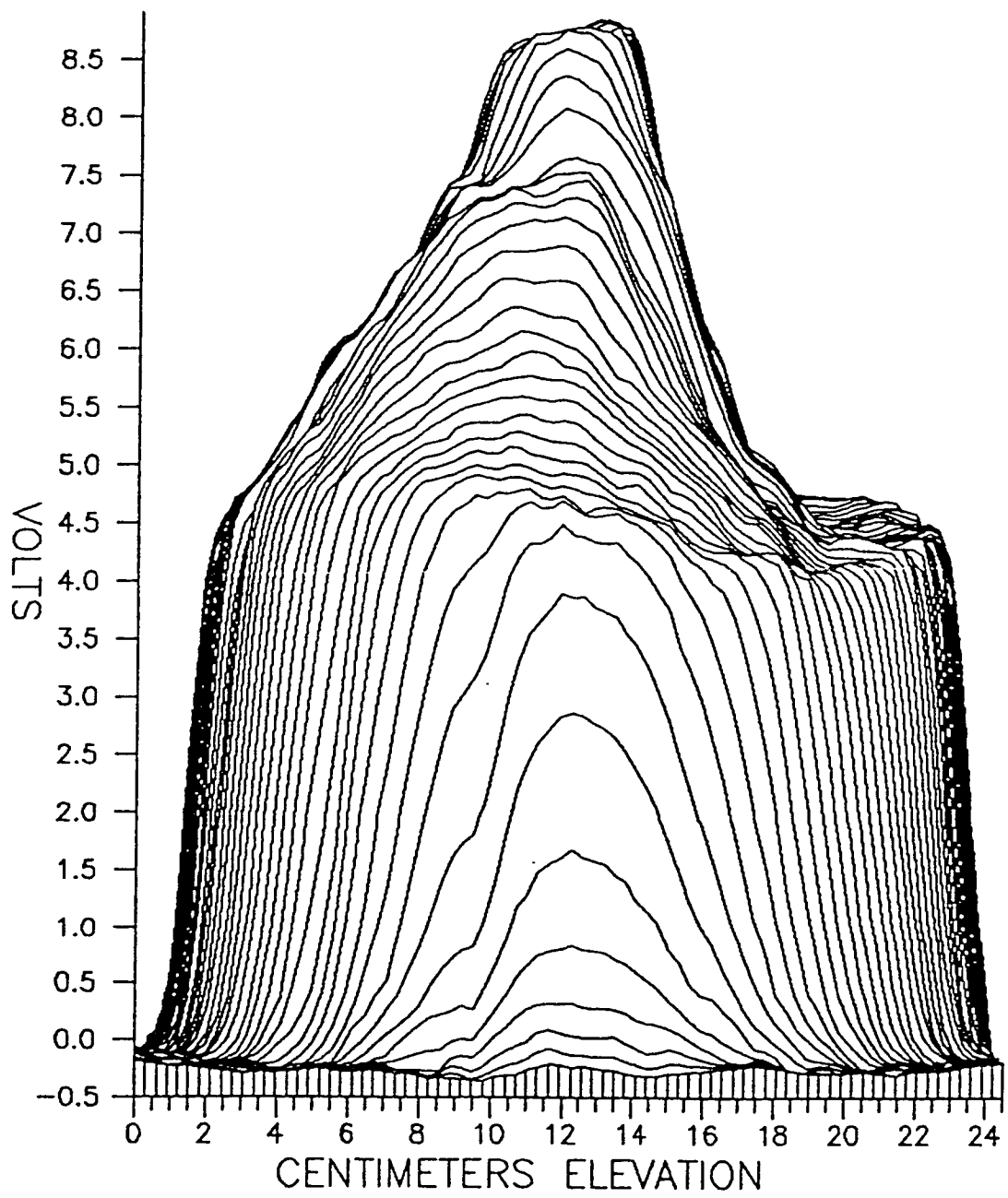


Figure J-33. DEC beam mapping file #5 - Tilt: 0 - Rotation: 0.

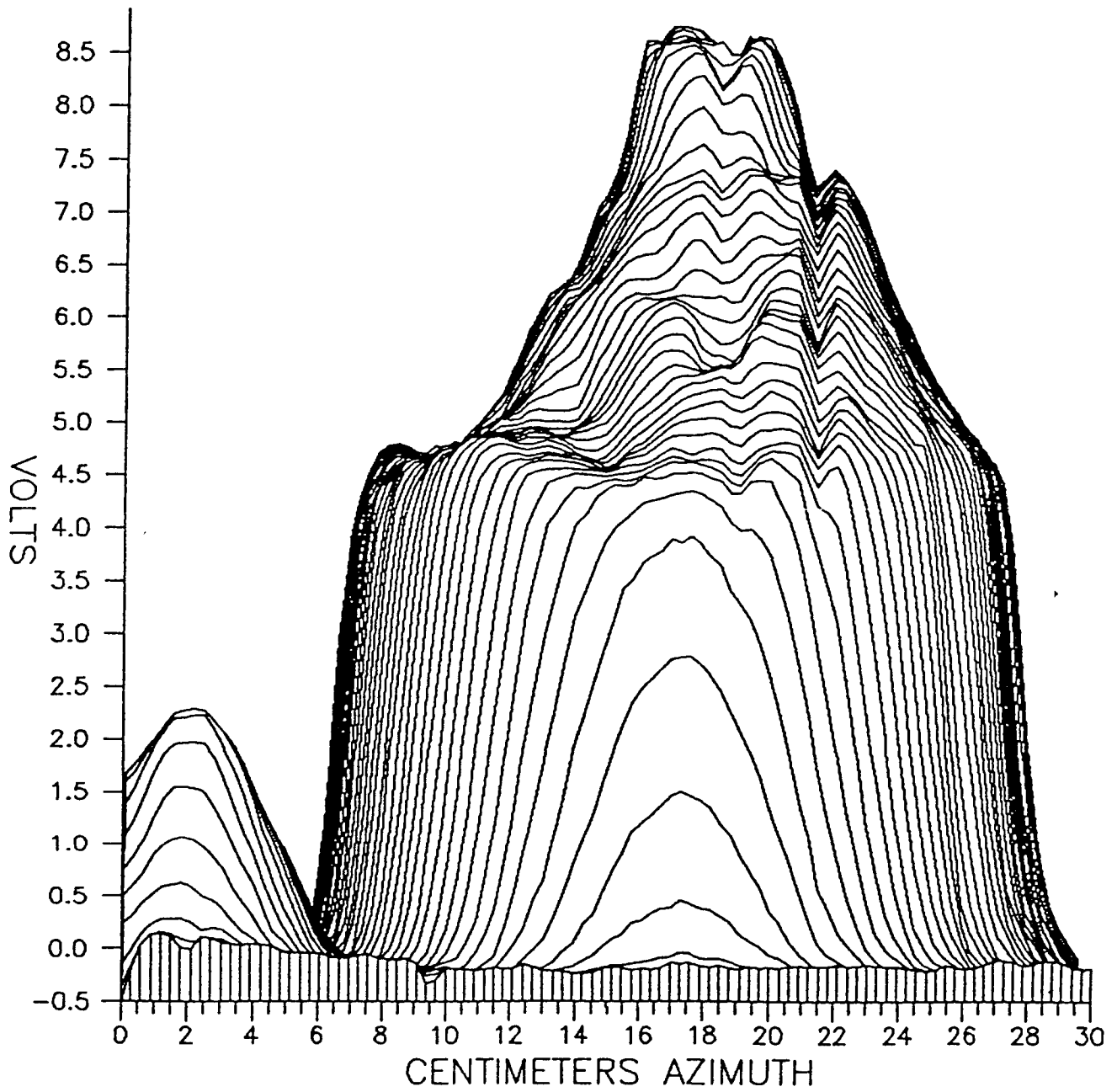


Figure J-34. DEC beam mapping file #5 - Tilt: 0 - Rotation: 270.

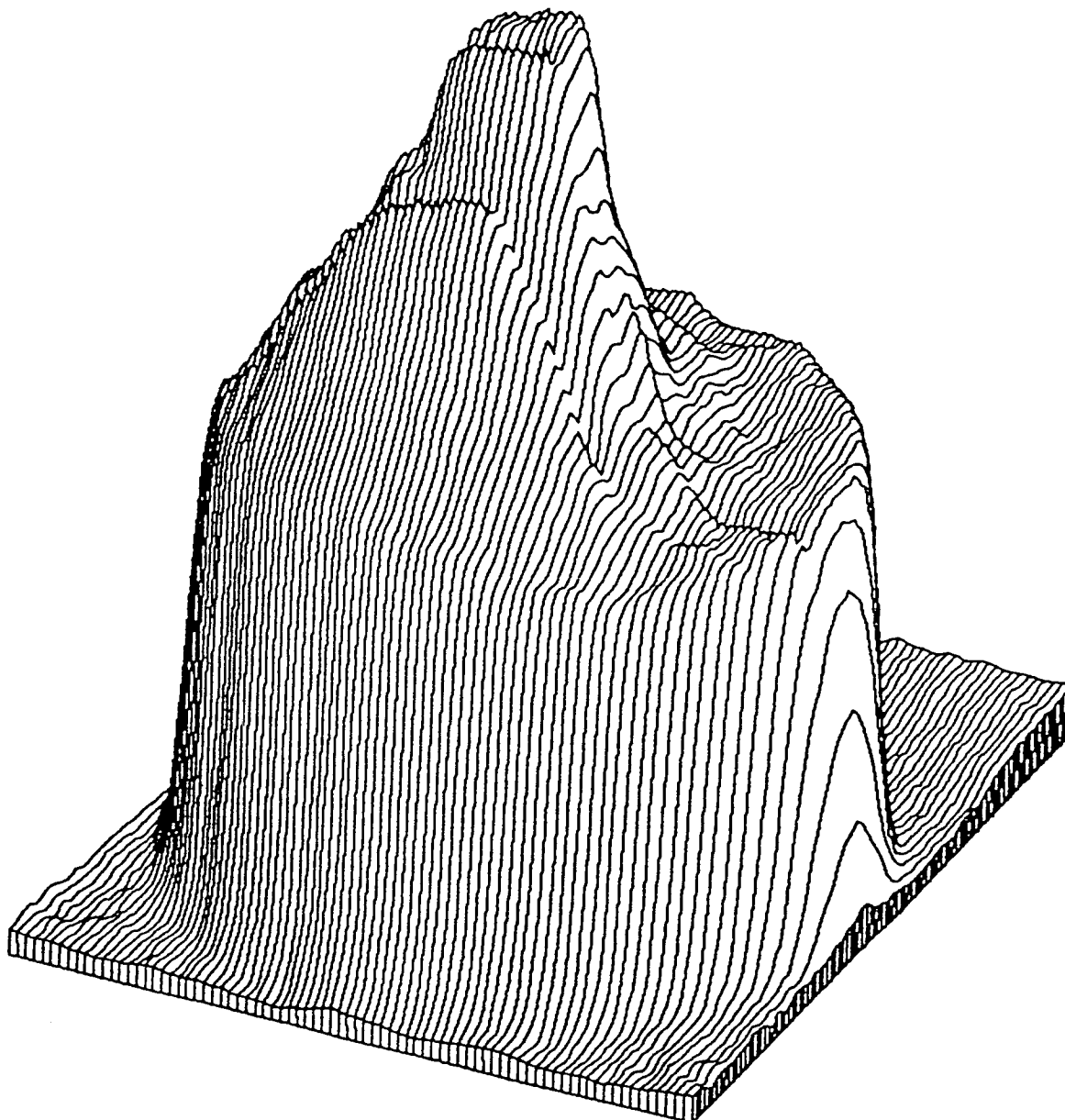


Figure J-35. DEC beam mapping file #5 - Tilt: 25 - Rotation: 25.

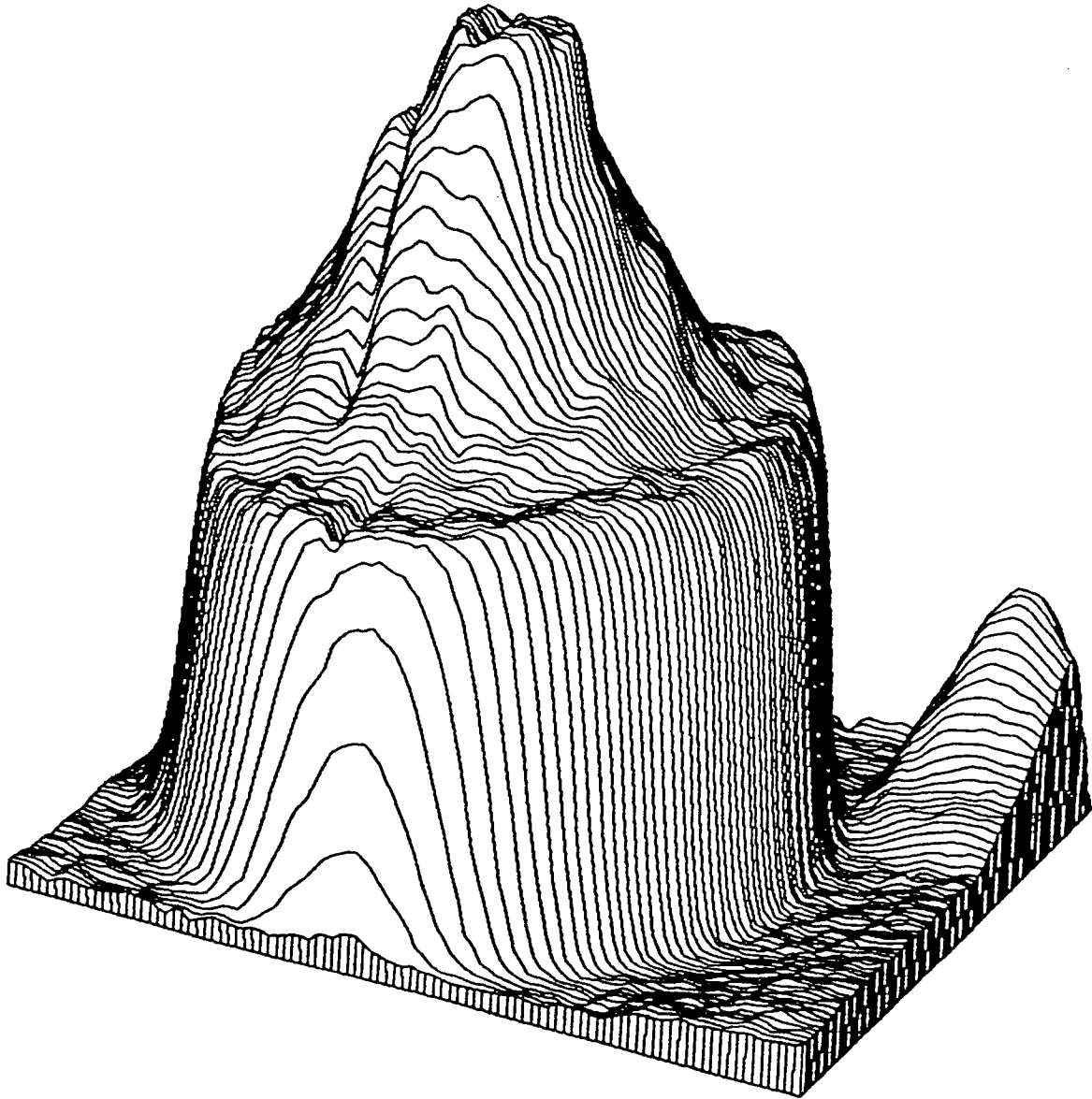


Figure J-36. DEC beam mapping file #5 - Tilt: 25 - Rotation: 115.

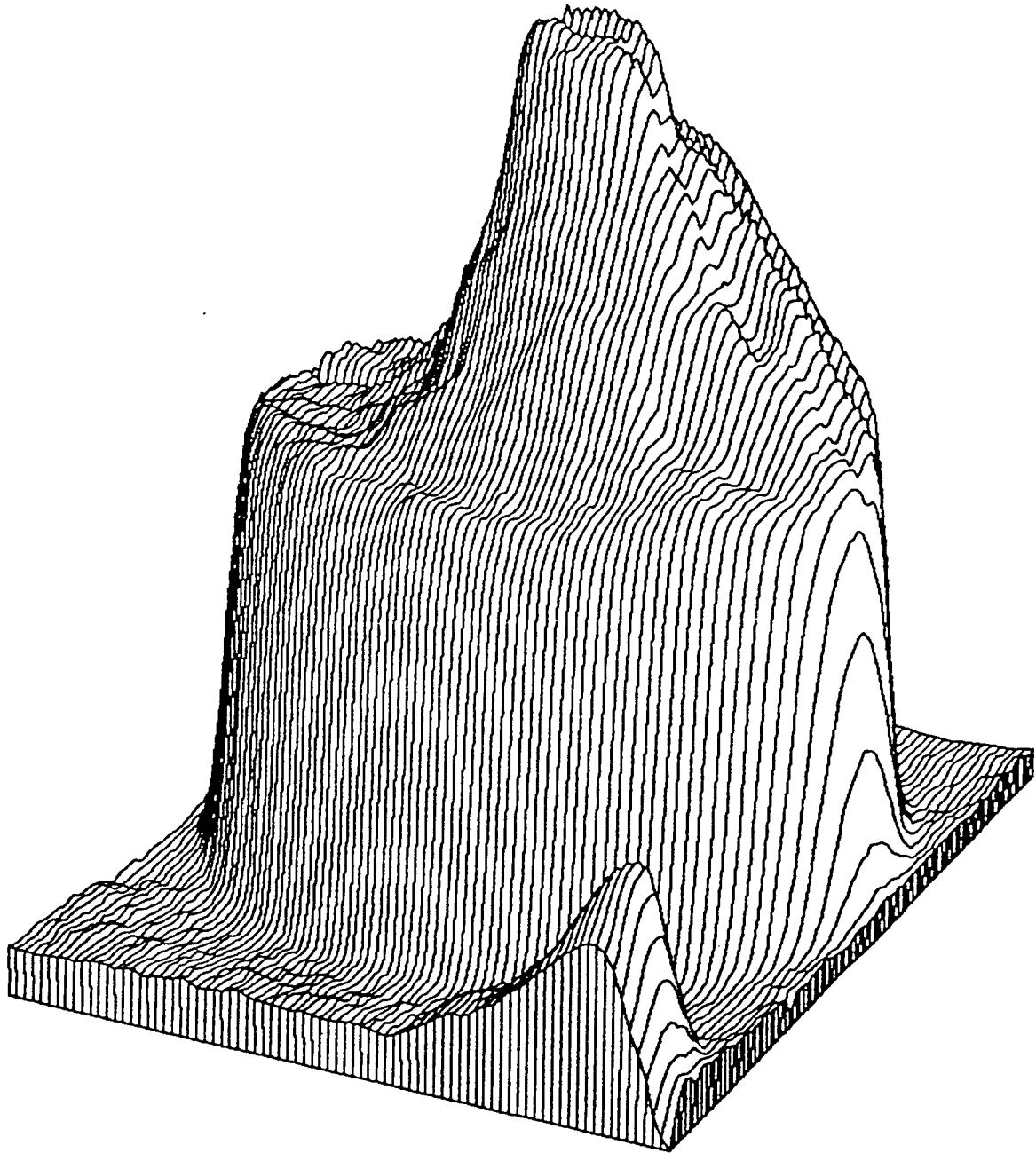


Figure J-37. DEC beam mapping file #5 - Tilt: 25 - Rotation: 205.

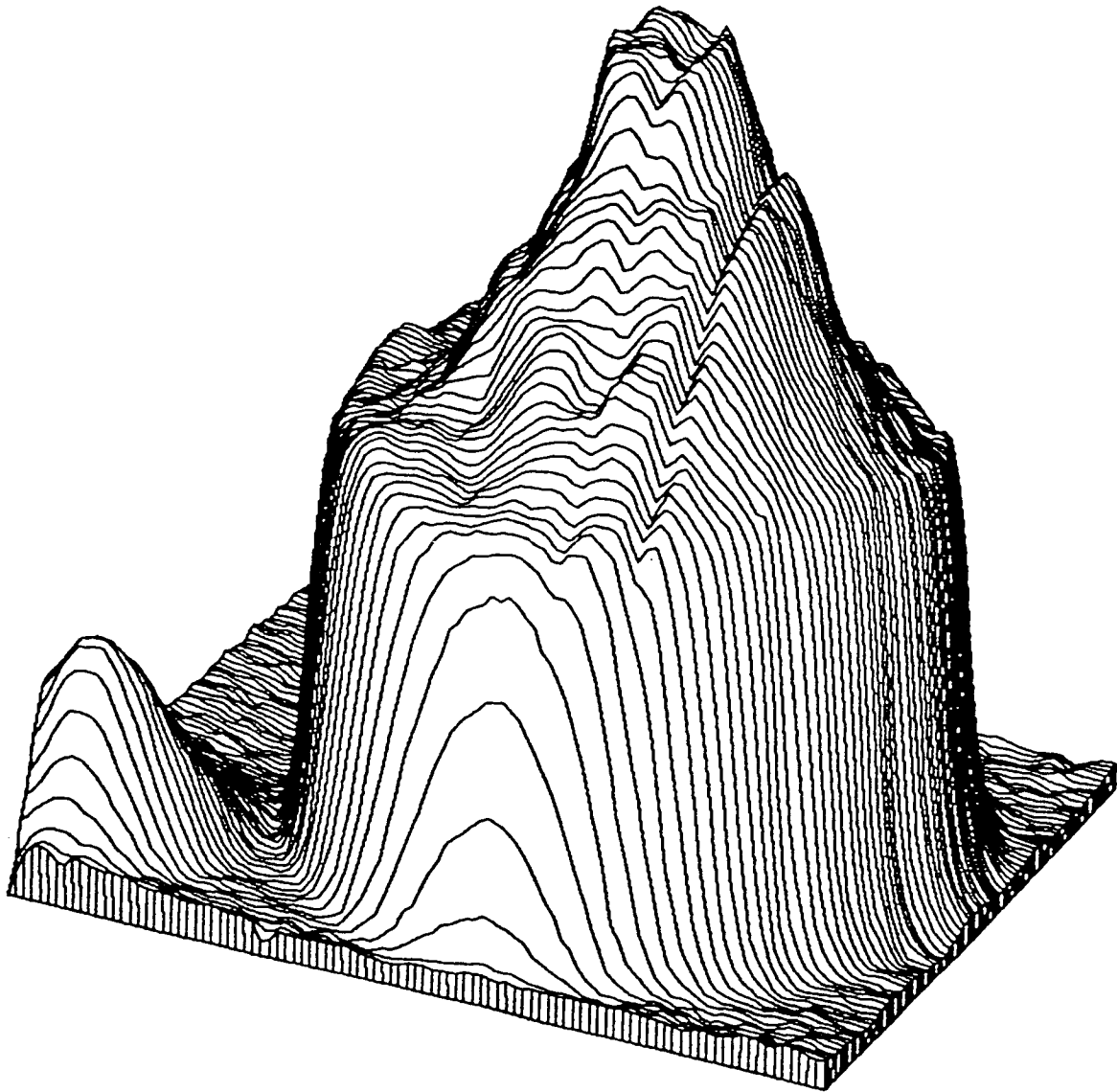


Figure J-38. DEC beam mapping file #5 - Tilt: 25 - Rotation: 295.

ORIGINAL PAGE IS
OF POOR QUALITY

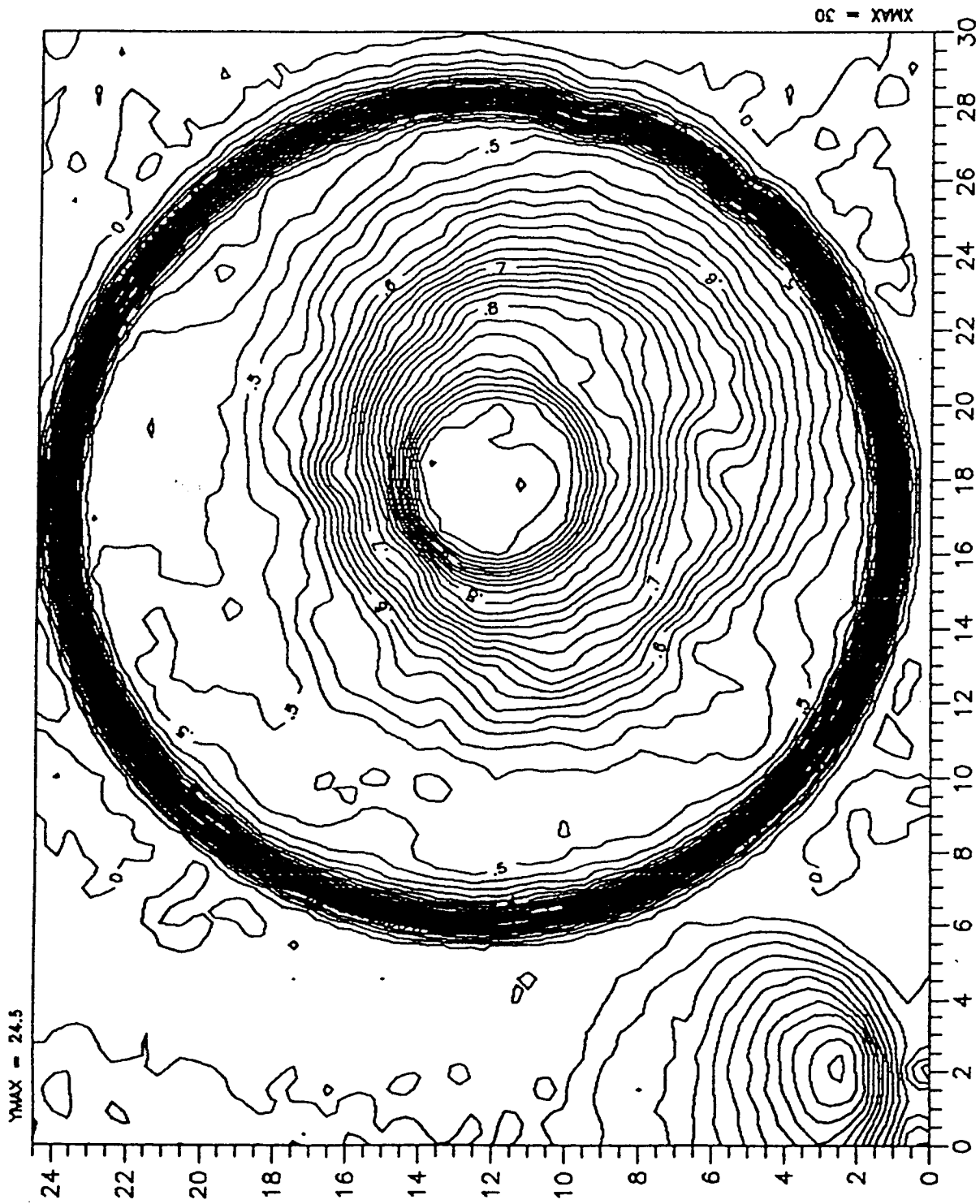


Figure J-39. DEC beam mapping file #2 - contour every 0.02 - corrected and normalized.

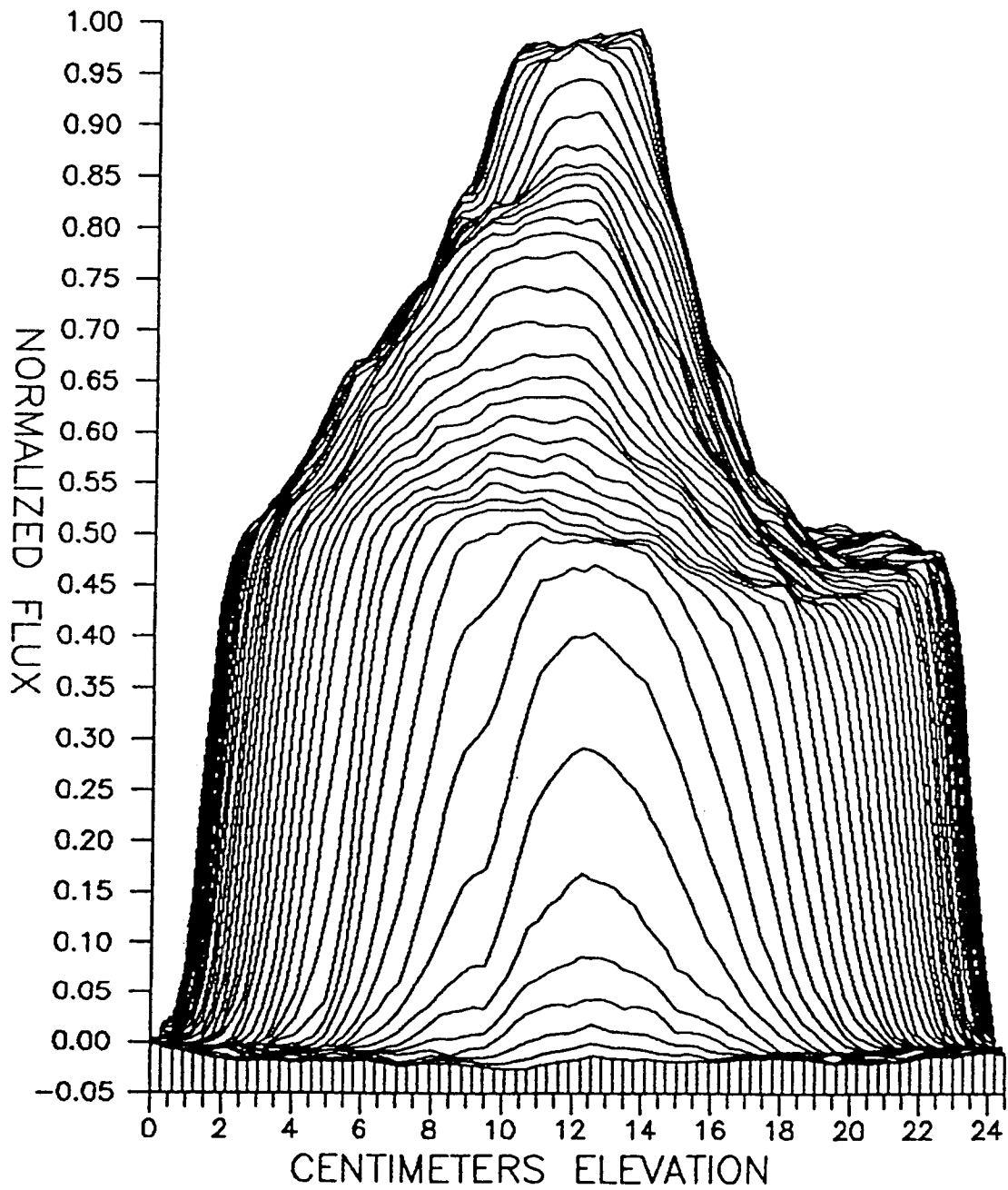


Figure J-40. DEC beam mapping file #2 - Tilt: 0 - Rotation: 0.
Normalized and corrected.

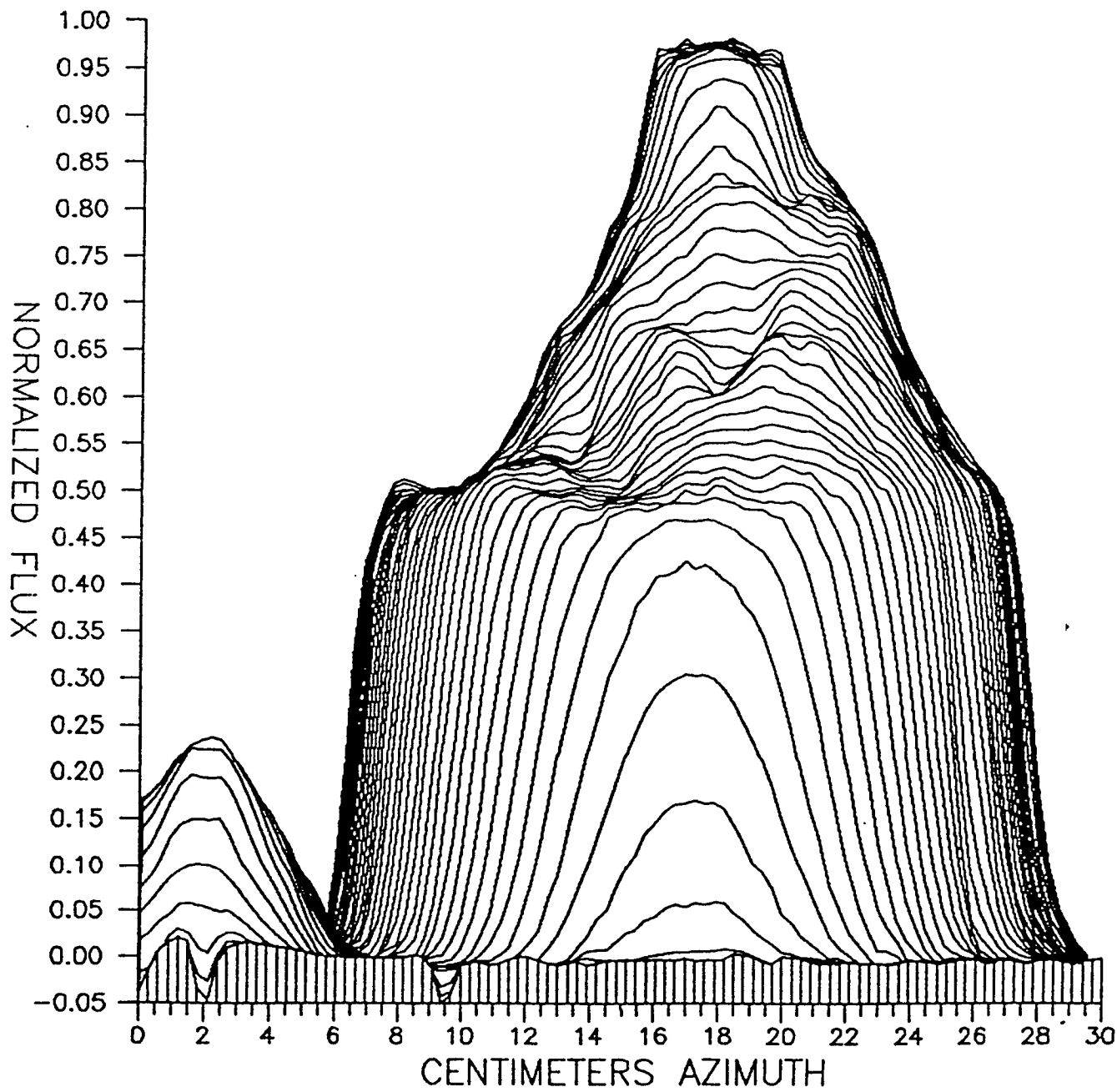


Figure J-41. DEC beam mapping file #2 - Tilt: 0 - Rotation: 270.
Normalized and corrected.

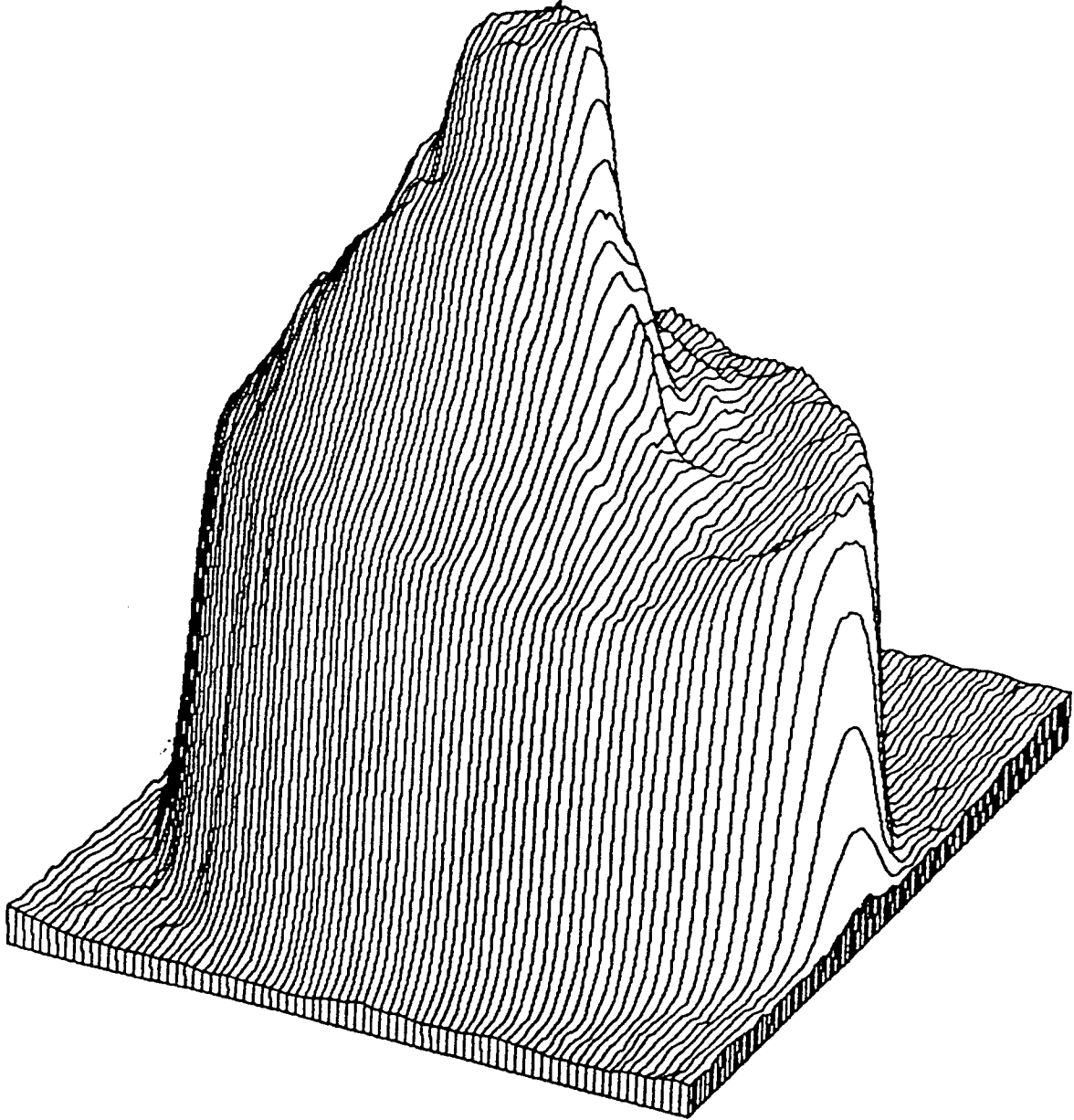


Figure J-42. DEC beam mapping file #2 - Tilt: 25 - Rotation: 25.
Normalized and corrected.

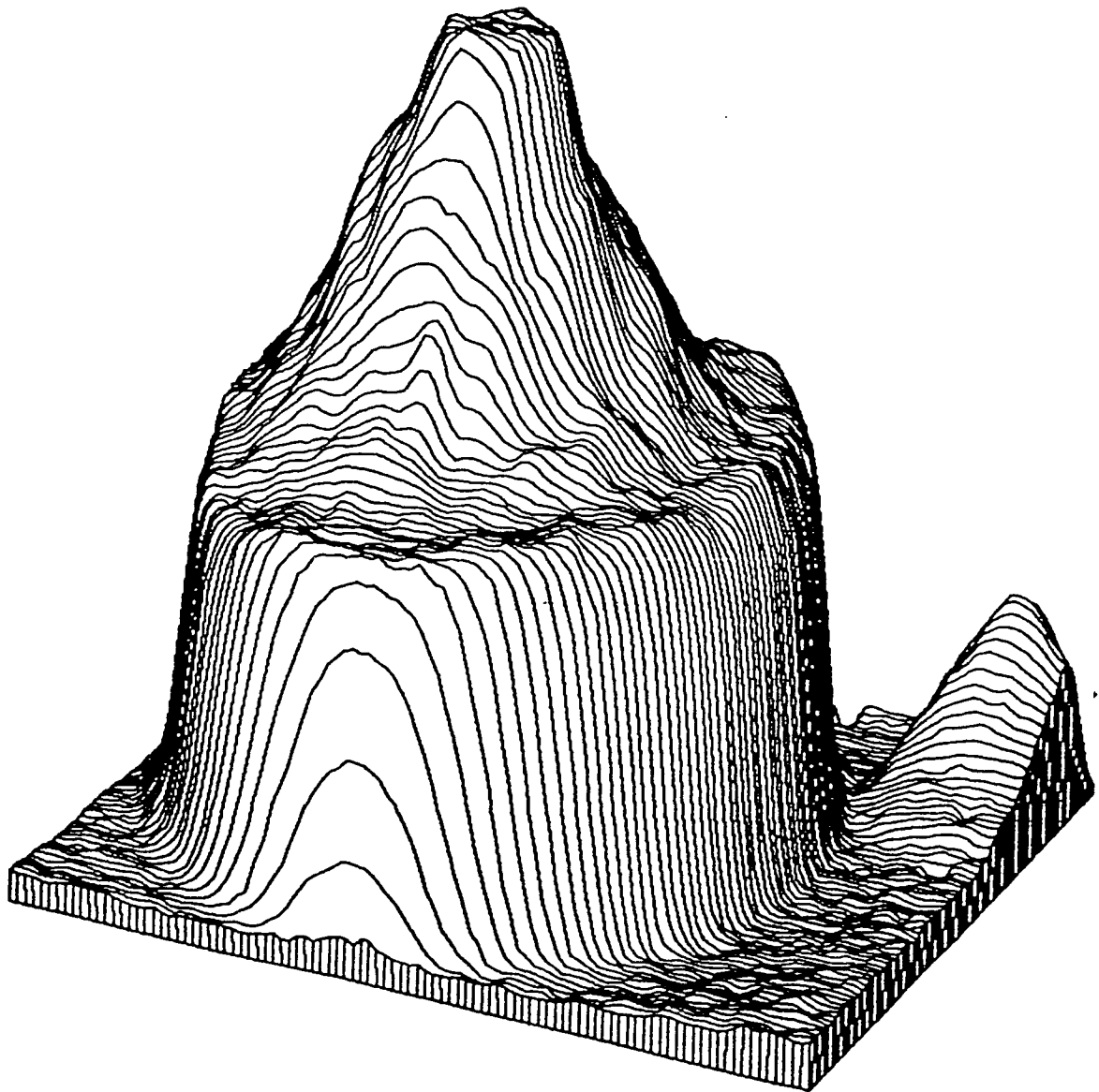


Figure J-43. DEC beam mapping file #2 - Tilt: 25 - Rotation: 115.
Normalized and corrected.

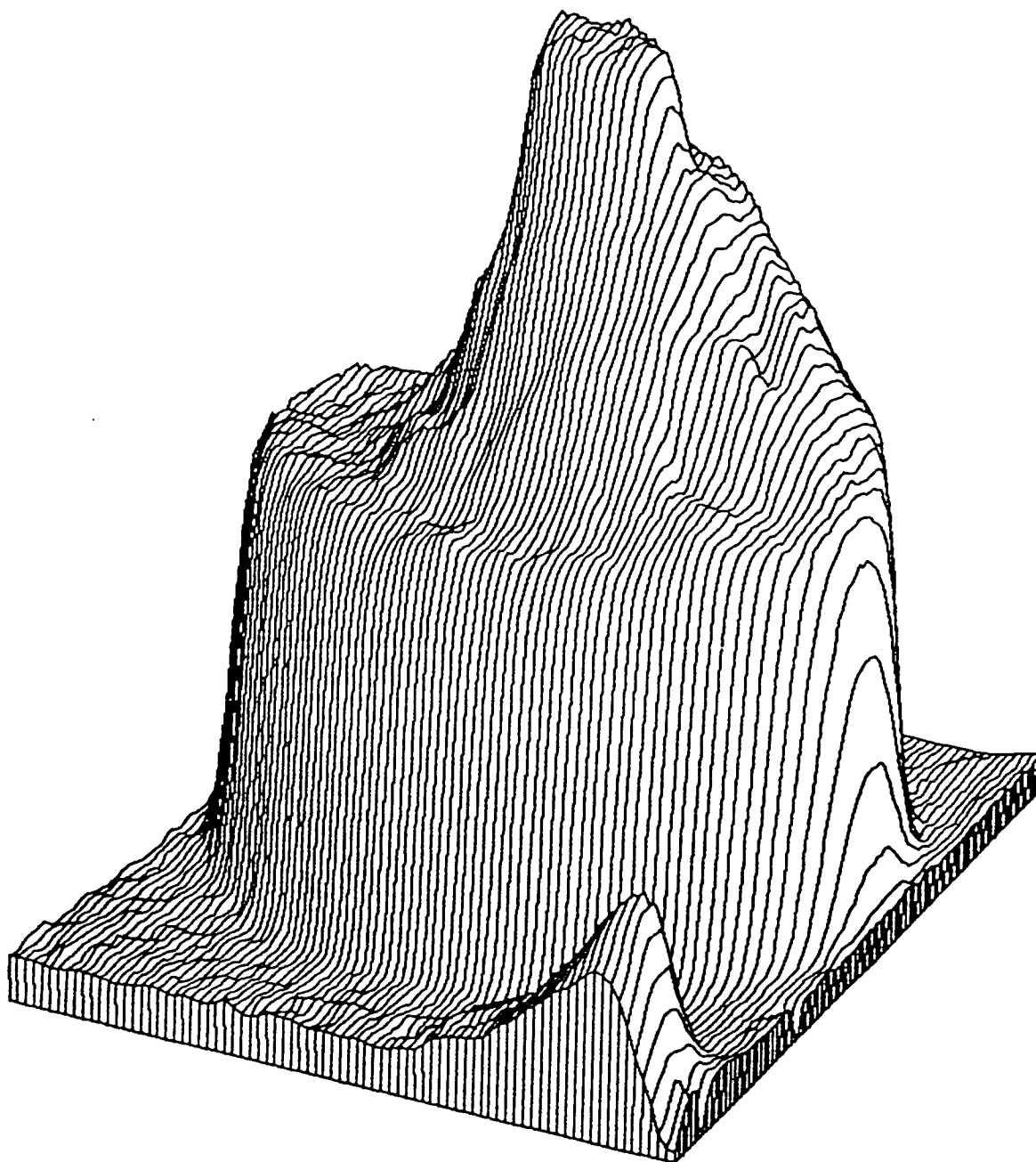


Figure J-44. DEC beam mapping file #2 - Tilt: 25 - Rotation: 205
Normalized and corrected.

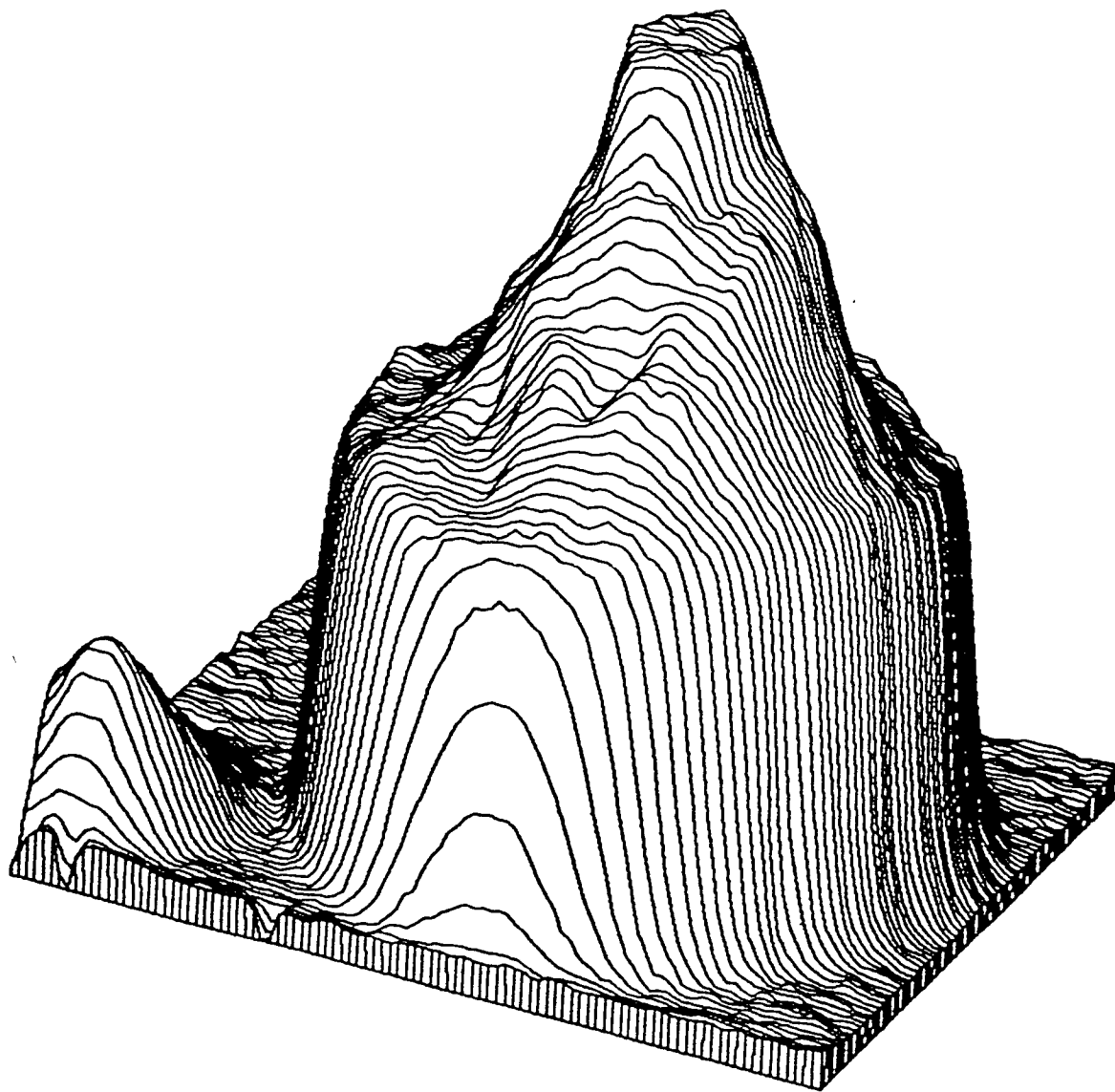


Figure J-45. DEC beam mapping file #2 - Tilt: 25 - Rotation: 295.
Normalized and corrected.

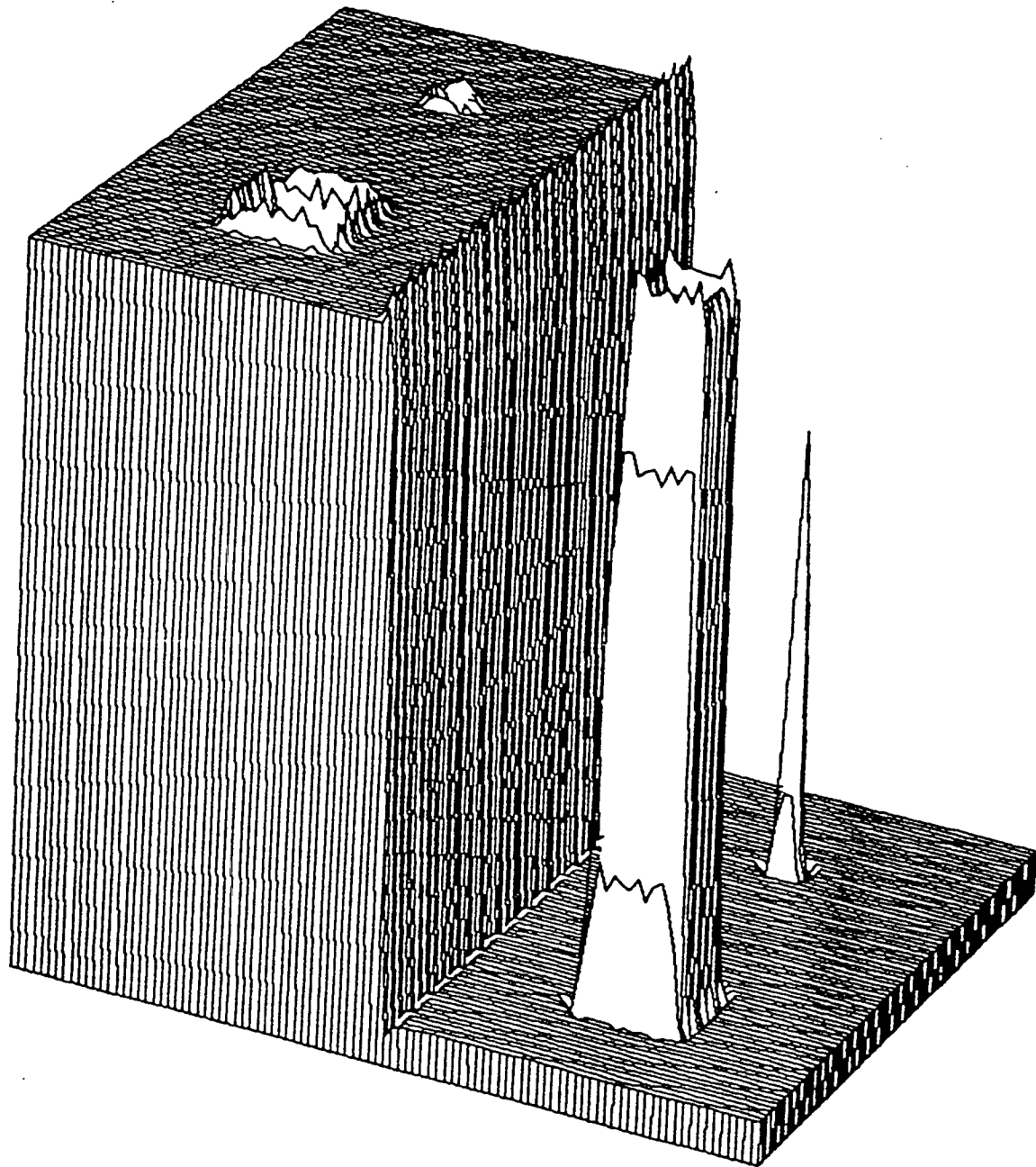


Figure J-46. DEC software demonstration - Tilt: 25 -
Rotation: 115.

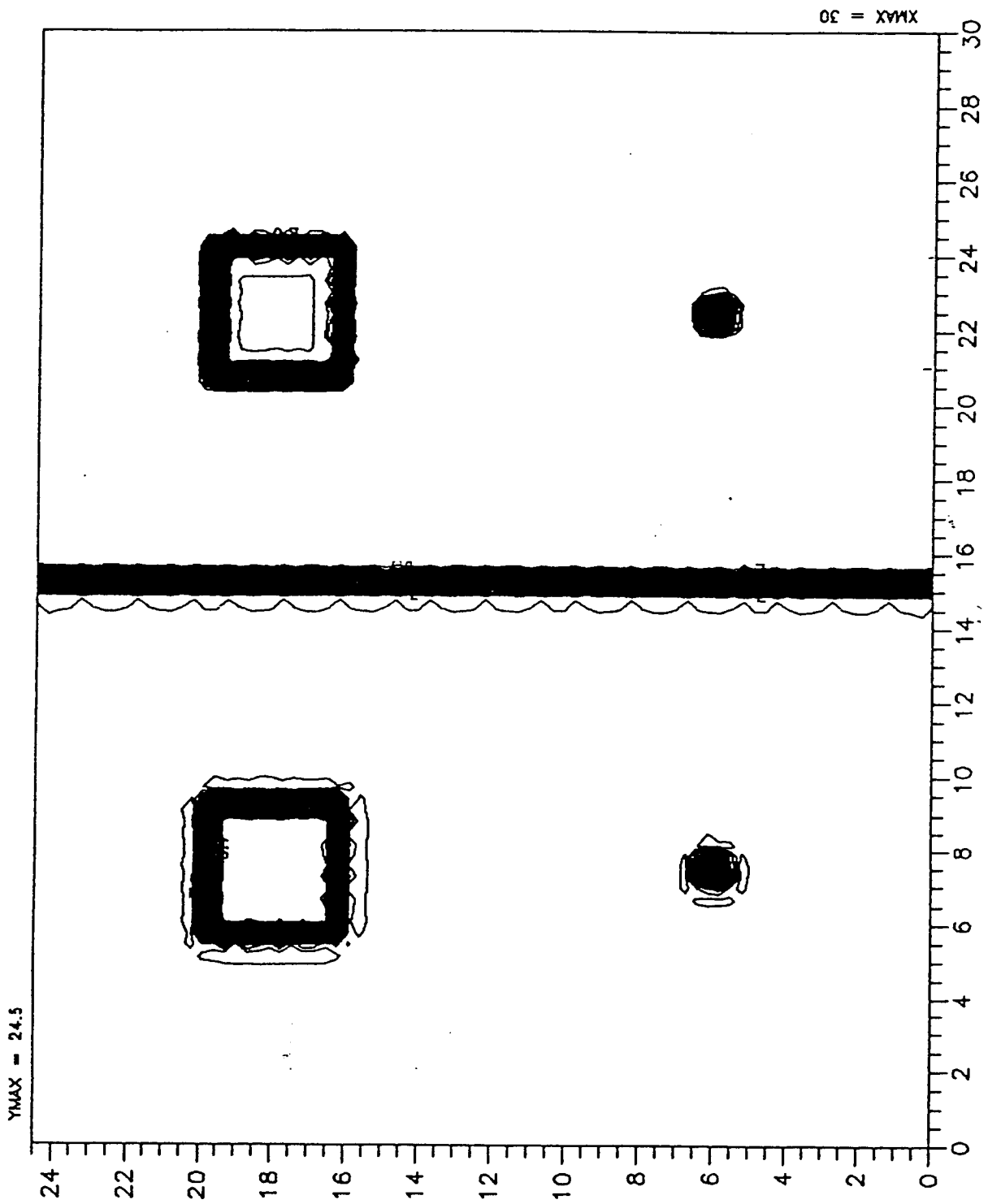


Figure J-47. DEC software demonstration - contour every 0.2V.